eman ta zabal zazu

Universidad del País Vasco

Euskal Herriko Unibertsitatea

Departamento de Química Orgánica I

Facultad de Farmacia

Development of novel hybrid phosphorated quinoline derivatives as topoisomerase 1B inhibitors with antiproliferative activity

Memoria presentada por

Asier Selas Lanseros

Para optar al grado de doctor con mención “doctor internacional”

Vitoria-Gasteiz, 2022

Acknowledgements/agradecimientos

El trabajo recogido en la presente memoria no hubiera podido llevarse a cabo sin la asistencia, colaboración y orientación de un gran número de personas que de una forma u otra no solo estuvieron presentes, sino que contribuyeron para la finalización y presentación del mismo.

En primer lugar, me gustaría agradecer a la Dra. Concepción Alonso y al profesor Francisco Palacios por abrirme las puertas del departamento de Química Orgánica I y darme la oportunidad de formar parte de su grupo de investigación, por su apoyo inquebrantable y (sobretodo) su paciencia. Aprovecho la ocasión para mostrar mi más sincero reconocimiento a su trabajo y trayectoria, logrando dar el salto a proyectos de química terapéutica de alto nivel y formar a jóvenes investigadores en el campo. También quisiera agradecer al resto de compañeros de línea de investigación (Dr. Martín, Dra. Fuertes, Dra. Rubiales y Ángela) por su dedicación y buen hacer en el mundo de las topoisomerasas. Ha sido un verdadero placer formar parte de este grupo.

También me gustaría recordar y agradecer al resto de compañeros del grupo de investigación que han ido pasando por más o menos tiempo, pero que todos ellos han dejado su huella (espero no dejarme a nadie). Adrián, Alba, Aitor, Carla, Gonzalo, Ishraq, Julene, Kassia, Kharim, Leire, Maider, Saverio, Xabi, Xabi Jr, Víctor Zuriñe, Zouhair, ha sido una suerte compartir laboratorio y cafetería con vosotros, me llevo un gran recuerdo. Y no quisiera olvidarme de los profesores: Ana, Begoña, Carme, Delos, Edorta, Javi, Mirari, Yurre, por demostrar cada día que la química orgánica no es aburrida en absoluto. Sois un ejemplo y un gran equipo.

And now, I may move to English for a while to express my utmost gratitude to Dr. Birgitta R. Knudsen (Department of Molecular Biology and Genetics, Aarhus University) and Dr. Cinzia Tesauro (VPCIR Biosciences), it has been such an honour to collaborate with your research groups that I had to do it twice. It has been a challenging adventure into Molecular Biology (a baptism of fire) with a happy ending and I really enjoy all the good times in the lab, cake-days, beer-days and breakfast-meetings. I will never forget all the support that I received from all the members of the group, I really needed it to hurdle all the obstacles on the way. I specially want to thank to all the amazing lab mates in Aarhus: Josephine, Kamilla, Karol, Kathrine Kirstine, Maria, Noriko and of course, Adam. This PhD memory has a strong Danish accent.

Y por supuesto, muchísimas gracias a la familia y amigos por todo el cariño y la ayuda que me han dado en todo momento. Esta Aventura hubiera sido imposible sin ellos. Muchas gracias a mis padres por creer en mí y exigirme para que llegue a ser lo que puedo ser. A mis abuelos, por toda su ternura y apoyarme hasta en las peores decisiones. A Pili, por preocuparse siempre por mí. A todos mis amigos, que han sufrido mis ausencias y han prometido brindar cuando recupere parte de mi libertad.

Por último, quisiera guardar unas últimas líneas para agradecer a Andrea todo su apoyo y paciencia conmigo (ella sí que se las ha ganado). Muchas gracias por tu dulzura, por estar siempre ahí, por cuidarme cuando se me olvida y por suministrarme café y comida en los malos momentos. Al final vas a acabar cogiéndole cariño a las topoisomerasas tú también.

"*We can speak and think only of what exists. And what exists is uncreated and imperishable for it is whole and unchanging and complete. It was not or nor shall be different since it is now, all at once, one and continuous.*"

Attributed to ***Parmenides of Elea***

"*The investigation of the truth is in one way hard, in another easy. An indication of this is found in the fact that no one is able to attain the truth adequately, while, on the other hand, no one fails entirely, but everyone says something true about the nature of all things, and while individually they contribute little or nothing to the truth, by the union of all a considerable amount is amassed.*"

***Aristotle**, Metaphysics, book 2 (α), chapter I*

Index

Abbreviations, acronyms and symbols

List of abbreviations, acronyms and symbols used in the work:

σ*1*R	sigma-1 receptor
δ	chemical shift
λ	wavelength
^{o}C	Celsius degree
5-HT2B	serotonin receptor 2B
Å	Armstrong
A	adenine
aa	amino acid
ACE	angiotensin converting enzyme
ACHE	acetylcholinesterase
ADC	antibody-drug conjugate
ADP	adenosine diphosphate
Ag	antigen
ALK	anaplastic lymphoma kinase
AmB	amphotericin B
LAmB	liposomal amphotericin B
API	active pharmaceutical ingredient
ATP	adenosine triphosphate
ATR	ataxia-telangiectasia-mutated-and-Rad3-related
BALB/c	Bagg Albino mouse
Br	bromine
BSA	bovine serum albumin
C (atom)	carbon
C (nt)	cytosine
Ca	calcium
CAN	cerium ammonium nitrate
CAT A	cathepsin
CCD	charge-coupled device
CCK-8	cell counting kit 8
CES	carboxylesterase
CFDA-AM	carboxyfluorescein-based assay
CHK-1	checkpoint kinase 1
Cl	chlorine
CL	cutaneous leishmaniasis
CNS	central nervous system
COPD	chronic obstructive pulmonary disease
CPT	camptothecin
hCPT	homocamptotecin
CTAOH	(cetyltrimethyl-ammonium hydroxide
CTL	control
CY3	cyanine 3
CysLT1R	cysteinyl leukotriene receptor 1
DA	Diels Alder
Da	dalton
kDa	kilodalton
Aza-DA	aza-Diels Alder
DC	dendritic cell
d	doublet
dd	doublet of doublets

ddd	doublet of doublets of doublets
DABCO	1,4-diazabicyclo[2.2.2]octane
dAMP	deoxyadenosine monophosphate
DCP	dicumyl peroxide
DDQ	dichloro dicyano benzoquinone
DDR	DNA-damage response
DEAE	diethylaminoethyl cellulose
DEPT	distortionless enhancement of polarization transfer
DMEM	Dulbecco's modified Eagle medium
DMF	dimethylformamide
DMSO	dimethylsulfoxide
DNA	deoxyribonucleic acid
dsDNA	double-stranded DNA
ssDNA	single-stranded DNA
dNTPs	deoxynucleotide triphosphates
DPDC	di-isopropyl peroxydicarbonate
DSB	double-stranded breaks
DX	dexamethasone
EDTA	ethylenediaminetetraacetic acid
e.e.	enantiomeric excess
ELISA	enzyme-linked immunoassay
EMA	European Medicines Agency
EMEM	Eagle's minimum essential medium
equiv.	equivalent
Et	ethyl
EtBr	ethidium bromide
EWG	electron-witdrawing group
F	fluorine
FBS	fetal bovine serum
FDA	Food and Drug Administration of the United States of America
G	guanine
g	gram
μg	microgram
ng	nanogram
GABA	γ-aminobutiric acid
GM-CSF	granulocyte-macrophage colony-stimulating factor
GF-AFC	aminofluorocoumarin based assay
GI_{50}	growth inhibition 50%
Glu	glutamate
iGluR	ionotropic glutamate receptor
mGluR	metabotropic glutamate receptor
GLOBOCAN	global cancer incidence, mortality and prevalence
H	proton/hydrogen
h	hour
H_2O	water
ddH_2O	double distilled water
HBV	hepatitis B virus
HbR	haemoglobin receptor
HCV	hepatitis C virus
HD	high density
HER2	human epidermal growth factor receptor 2
HIV	human immunodeficiency virus

HMBC	heteronuclear multiple bond correlation
HMG-Co-A	3-hydroxy-3-methylglutaryl coenzyme A
HMQC	heteronuclear multiple quantum coherence
HRMS	high-resolution mass spectrometry
HRP	Horseradish peroxidase
Hz	hertz
MHz	megahertz
IFN	interferon
Ig	immunoglobulin
ILs	ionic liquids
IL	interleukin
iRFP	infrared fluorescent protein
^{i}Pr	isopropyl
J	coupling-constant
KD	knockdown
L	litre
mL	millilitre
μL	microliter
LA	Lewis-acid
LDL-C	low-density lipoprotein cholesterol
Lk	linking number
M	molar
mM	milimolar
μM	micromolar
nM	nanomolar
m (RMN)	multiplet
m (length unit)	meter
mm	milimeter
nm	nanometer
M^{+}	molecular ion
m/z	mass/charge number ratio
MCR	multicomponent reaction
Me	methyl
Mg	magnesium
min	minute
Mn	manganese
mol	mol
mmol	mmol
nmol	nanomol
pmol	picomol
fmol	femtomol
mp	melting point
MS	molecular sieves
MTT	3-(4,5-dimethylthaizol-2-yl)-2,5-diphenyltetrazolium bromide
Mur A	UDP-N-acetylglucosamine enolpyruvyltransferase
MW	microwave
N	nitrogen
NAD	Nicotinamide adenine dinucleotide
NaI	nanoliposomal irinotecan
Nick	nicked DNA
NMR	nuclear magnetic resonance
1D-NMR	monodimensional NMR

2D-NMR	bidimensional NMR
NOE	nuclear Overhausser spectroscopy
1D-NOESY	NOE difference spectroscopy
NP	nanoparticle
nt	nucleotide
O	oxygen
OAc	Ethyl acetate
Ox.	oxidation
P	phosphorus
PAD	plasmid
PAM	polyacrylamide
PARP	poly (ADP-ribose) polymerase
PBS	phosphate buffered saline
PEG	polyethylene glycol
PEP	phosphoenolpyruvate
Ph	phenyl
PK	pharmacokinetic
PLGA	poly(lactic-co-glycolic acid)
PMS	5-methylphenazinium methyl sulfate
ppm	part per million
ProTide	nucleotide prodrug
Psi	pounds per square inch
q	quadruplet
QUIN	quinoline
REEAD	Rolling-circle Enhanced Enzyme Activity Detection
C/L REEAD	Cleavage/Ligation REEAD
RCA	rolling-circle amplification
RCP	rolling-circle product
Rel	relaxed DNA
Rf	retention factor
RISC	RNA induced silencing complex
RNA	ribonucleic acid
siRNA	small interfering RNA
mRNA	messenger RNA
dsRNA	double-stranded DNA
s	singlet
SAR	structure-activity relationship
SARS-CoV-2	severe acute respiratory syndrome coronavirus 2
Sb	antimony
Sc	supercoiled DNA
SD	standard deviation
SDS	sodium dodecyl sulphate
sec	second
S_NAr	nucleophilic aromatic substitution
SSB	single-strand breaks
T	thymine
T-ALL	T-cell-derived acute lymphoblastic leukaemia
TAF	tenofovir alafenamide fumarate
TBAB	tetrabutylammonium bromide
TBE	tris-borate-EDTA
TBP	TATA-binding protein
TBST	tris-buffered saline Tween 20

TDM	α,α'-trehalose dimycolate
TDP	tyrosyl-DNA phosphodiesterase
TDM	α,α'-trehalose dimycolate
TE	tris-EDTA
TEA	trimethylamine
TFA	trifluoroacetic acid
THQ	tetrahydroquinoline
TLC	thin layer chromatography
TMM	α,α'-trehalose monomycolate
TNF	tumor necrosis factor
TOP1	topoisomerase 1
hTOP1B	human topoisomerase 1B
LTOP1B	*Leishmania* topoisomerase 1B
pfTopo1	*Plasmodium falciparum* TOP1
TOP2	topoisomerase 2
TOP1CC	topoisomerase 1-DNA cleavage-complex
TOP2CC	topoisomerase 2-DNA cleavage-complex
TOPCC	topoisomerase-DNA cleavage complex
Tris	tris(hydroxymethyl)aminomethane
Ts	tosyl
TsOH	*p*-toluensulfonic acid
Tyr	tyrosine
U	uracil
UDP	uracil diphosphate
USA	United States of America
UV	ultraviolet
V	volts
v	volume
VL	visceral leishmaniasis
WB	western blot
WST-8	2-(2-methoxy-4-nitrophenyl)-3-(4-nitrophenyl)-5-(2,4-disulfophenyl)-2H-tetrazolium sodium salt

Introduction and objectives

1. Topoisomerase I as a target in anticancer drug research

Cancer is a major healthcare problem and a global death leading cause. According to its latest report, GLOBOCAN (the World Health Organization's International Agency for Research on Cancer Global Cancer Observatory) estimated an incidence of 19 million new cancer cases, more than 50 million prevalent cases and around 10 million deaths directly associated to cancer in 2020 worldwide [1]. Furthermore, GLOBOCAN predicts that there will be 28.9 new cancer cases by 2040 based on the actual trend and expected demographical changes, primarily associated to the contemplated improvement of socioeconomic conditions in developing countries and the related population growth and enlargement of life expectancy.

The major purpose of cancer therapy is to specifically inhibit the growth and spread cancer cells and in this regard, therapies involving conventional chemotherapy, radiotherapy, immunotherapy and surgery are applied, along with the emerging precision medicine approaches[2]. Even though, chemotherapeutic drugs remain playing a key role in the oncologic treatment alone or as an essential part of a targeted cancer therapy and hence, the development of selective, safer and more pharmacologically active compounds represents an active area of research in drug discovery and medicinal chemistry[3]. Accordingly, human DNA topoisomerase I (TOP1) constitutes a broadly explored validated therapeutic target and therefore, TOP1 inhibitor drugs have emerged as potential anticancer agents, highlighting the fact that some TOP1 inhibitors have reached to the clinical approval and are currently administered alone or as a payload of a pharmaceutical composition[4].

1.1. DNA topoisomerases

Historical perspective: the discovery of topoisomerases, DNA topology-modulating enzymes essential for genome stability and DNA metabolism.

The double helical structure of DNA is supercoiled as a means of compacting the genome for a stable and secure storing of the genetic information. Maintaining an appropriate topological

[1] a) Sung H, Ferlay J, Siegel RL, *et al.* Global Cancer Statistics 2020: GLOBOCAN Estimates of Incidence and Mortality Worldwide for 36 Cancers in 185 Countries. *CA Cancer J Clin*. 2021;71(3):209-249. doi:10.3322/caac.21660 b) GLOBOCAN 2020 database. Accessed May 3, 2022 at https://gco.iarc.fr/

[2] Mollaei M, Hassan ZM, Khorshidi F, Langroudi L. Chemotherapeutic drugs: Cell death- and resistance-related signaling pathways. Are they really as smart as the tumor cells?. *Transl Oncol*. 2021;14(5):101056. doi:10.1016/j.tranon.2021.101056

[3] Kumar B, Singh S, Skvortsova I, Kumar V. Promising Targets in Anti-cancer Drug Development: Recent Updates. *Curr Med Chem*. 2017;24(42):4729-4752. doi:10.2174/0929867324666170331123648

[4] Thomas A, Pommier Y. Targeting Topoisomerase I in the Era of Precision Medicine. *Clin Cancer Res*. 2019;25(22):6581-6589. doi:10.1158/1078-0432.CCR-19-1089

state of DNA was assumed to be essential even before DNA topoisomerases were discovered, either by DNA winding when genes have to be stored or by DNA unwinding when strand separation is required to access the genetic information[5]. In this regard, understanding the coiling and tangling of the DNA during its metabolic manipulation entailed an issue since the deciphering of the double helical architecture of the genomic DNA molecule[6].

The first indications of a supercoiled state in the DNA were reported by Vinograd and collaborators in 1965 while working with double-stranded DNA (dsDNA) polyoma tumour viruses[7]. During DNA-sedimentation analysis, Vinograd found two forms of circular dsDNA with different compactness-degree. The most compact form of dsDNA reported a higher resistance to denaturation by heating or exposure to elevated pH. Surprisingly, electron-microscopy analysis demonstrated that the unique structural difference between the two forms of dsDNA was the presence of a single-stranded breakage in the less compact form, presumably by the endonuclease activity of a DNase I enzyme. In light of these findings, Vinograd and collaborators firstly suggested the existence of two circular dsDNA with the same chemical formula and stereochemistry but varying in how the double-helix of DNA is wounded around itself in the three-dimensional space (topology), *i.e.* the presence of DNA topoisomers differentiated by their supercoiling state. One year later, Vinograd and Lebowitz proposed the theory of DNA supercoiling and established the basis of the quantitative measure for the DNA supercoiling state[8], namely the *Linking number* or *Lk* (the number of the double-helical turns in the linear molecule of a circular dsDNA), which is defined as the sum of the twist (coiling of individual strands of DNA around the axis of DNA helix) and the writhe (coiling of the axis of DNA helix itself in the space)[9].

At that time, it was thought that the relaxation activity of supercoiled DNA was produced by a sequence of endonuclease (DNase I)-DNA ligase activity of two independent enzymes. However, in the late 1960s Wang purified an *E. coli* cell lysate reporting the putative endonuclease-ligase activity in a positively charged DEAE (diethylaminoethyl cellulose) column and he obtained a single enzyme responsible for the removal of negative supercoils (Figure 1) in a circular dsDNA

[5] a) Watson JD, Crick FH. The structure of DNA. *Cold Spring Harb Symp Quant Biol*. 1953;18:123-131. doi:10.1101/sqb.1953.018.01.020

[6] a) Delbrück M. On the replication of desoxyribonucleic acid (DNA). *Proc Natl Acad Sci U S A*. 1954;40(9):783-788. doi:10.1073/pnas.40.9.783

[7] Vinograd J, Lebowitz J, Radloff R, Watson R, Laipis P. The twisted circular form of polyoma viral DNA. *Proc Natl Acad Sci U S A*. 1965;53(5):1104-1111. doi:10.1073/pnas.53.5.1104

[8] Vinograd J, Lebowitz J. Physical and topological properties of circular DNA. *J Gen Physiol*. 1966;49(6):103-125. doi:10.1085/jgp.49.6.103

[9] White JH. Self-linking and the gauss integral in higher dimensions. *Am J Math*. 1969;91(3):693-728. doi: 10.2307/2373348

by a combination of both endonuclease activity (which allows the swivel of the parental DNA strands) and DNA ligase activity that seals the breakage in the phosphate backbone[10]. Wang and collaborators named the enzyme as "ω protein" (ω being the symbol used to refer to the angular velocity of the centrifuge, as at that time the DNA relaxation activity was usually evaluated by ultracentrifugation) and published the work in 1971, resulting this *E.coli* "ω protein" the first topoisomerase to be discovered[11].

Likewise, in 1972 Champoux and coworkers published the finding of an enzyme isolated from mouse embryonic cells with DNase I-DNA ligase sequential activity, which reported not only to relax negatively supercoiled DNA, but also to resolve positively supercoiled dsDNA substrates[12] (Figure 1). Initially, the enzyme was called "swivelase" and represents the discovery of the first eukaryotic topoisomerase.

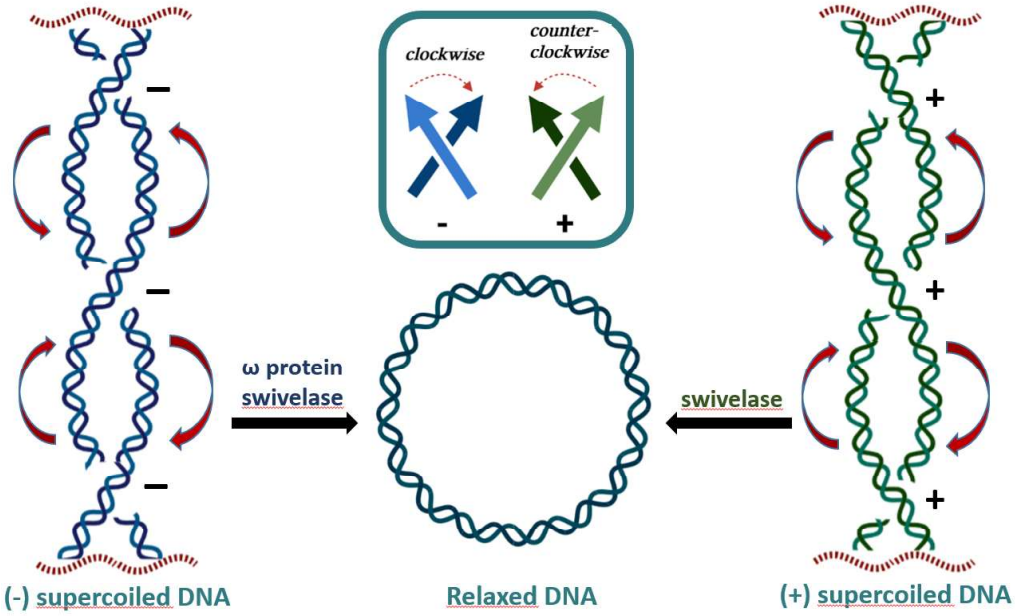

Figure 1. General overview of negatively (left side, in blue) and positively (right side, in green) supercoiled dsDNA, along with the corresponding relaxed form of circular dsDNA in between. In the middle of the figure (above) the two possible plectonemic supercoils are illustrated: by consensus, in a bidimensional plane, ***negative plectonemic supercoils*** *present a clockwise crossover, while* ***positive plectonemic supercoils*** *are drawn showing a counter-clockwise crossover.*

In the later years, more "swivelases" were isolated from many both eukaryotic and prokaryotic sources (human, monkey, rat, frog, duck, chicken, *Drosophila* flies, *Bacillus* bacteria and yeasts,

[10] Wang JC. A journey in the world of DNA rings and beyond. *Annu Rev Biochem*. 2009;78:31-54. doi:10.1146/annurev.biochem.78.030107.090101

[11] Wang JC. Interaction between DNA and an Escherichia coli protein omega. *J Mol Biol*. 1971;55(3):523-533. doi:10.1016/0022-2836(71)90334-2

[12] Champoux JJ, Dulbecco R. An activity from mammalian cells that untwists superhelical DNA--a possible swivel for DNA replication (polyoma-ethidium bromide-mouse-embryo cells-dye binding assay). *Proc Natl Acad Sci U S A*. 1972;69(1):143-146. doi:10.1073/pnas.69.1.143

among others), but this enzyme family did not have yet a systematic name to describe their enzymatic mode of action[13]. Nevertheless, studies with these enzymes led to the disclosure of their catalytic mechanism, which comprises the introduction of a transient break in the dsDNA phosphate backbone that allows the swivel of the DNA chains around the gap and a subsequent resealing of the breakage. Once disclosed the catalytic mechanism, the enzymes previously known as "ω protein" and "swivelases", were finally named as topoisomerases[14], a term that accurately defines their selective function in modulating the DNA topology. Since then, topoisomerases have been described in all three cellular domains of life (Archaea, Bacteria and Eucarya) and were further classified according to their catalytic mechanism and domain organization.

DNA topoisomerases: structure, mechanism and classification

DNA topoisomerases are ubiquitous enzymes that resolve DNA topological tension in the genome during essential cellular processes as DNA replication, transcription, chromosome segregation and recombination. The general mechanism of DNA topoisomerases involves a cleavage of the dsDNA phosphate backbone by the catalytic Tyr (Tyrosine) residue of the topoisomerase, resulting in a covalent phosphodiester linkage between the Tyr and the terminus of the cleaved strand (TOPCC, topoisomerase cleavage complex). The scission in the dsDNA permits the DNA to swivel around the nick and then the enzyme reseals the gap, leaving the dsDNA intact and relaxing negative or/and positive supercoils[15]. Moreover, bacterial DNA gyrase (type II topoisomerase) and reverse gyrase (type I topoisomerase) are topoisomerases present in bacteria with the ability to introduce negative or positive supercoils into the DNA, respectively[16].

There are three different nomenclatures used in the classification of DNA topoisomerases, *i.e.* historical (I-VI), mechanistic and evolutionary nomenclatures. This fact may lead to confusion but fortunately, the phylogenetic features that allow the evolutionary classification[17] are in concordance and further support the characteristics used for the mechanistic categorization[15].

---

[13] Champoux JJ. Proteins that affect DNA conformation. *Annu Rev Biochem*. 1978;47:449-479. doi:10.1146/annurev.bi.47.070178.002313

[14] Kirkegaard K, Wang JC. Escherichia coli DNA topoisomerase I catalyzed linking of single-stranded rings of complementary base sequences. *Nucleic Acids Res*. 1978;5(10):3811-3820. doi:10.1093/nar/5.10.3811

[15] Schoeffler AJ, Berger JM. DNA topoisomerases: harnessing and constraining energy to govern chromosome topology. *Q Rev Biophys*. 2008;41(1):41-101. doi:10.1017/S003358350800468X

[16] Champoux JJ. DNA topoisomerases: structure, function, and mechanism. *Annu Rev Biochem*. 2001;70:369-413. doi:10.1146/annurev.biochem.70.1.369

[17] Forterre P, Gadelle D. Phylogenomics of DNA topoisomerases: Their origin and putative roles in the emergence of modern organisms. *Nucleic Acids Res*. 2009;37(3):679-692. doi: 10.1093/nar/gkp032

Accordingly, based on the *Lk* number alteration and the number of cleaved strands, DNA topoisomerases can be classified into type I and type II subfamilies. Type I topoisomerases (TOP1) are ATP-independent DNA modulating enzymes that relax supercoil tension by introducing transient single-strand breaks (SSB) in dsDNA substrates and change the *Lk* by units of 1 ($\Delta Lk = \pm 1$), while type II topoisomerases (TOP2) require Mg^{2+} and coupled ATP-hydrolysis in order to relax supercoils (and also decatenate/unknot) dsDNA by introducing double-stranded breaks (DSB) and altering the *Lk* number by units of 2 ($\Delta Lk = \pm 2$)[16].

Type I topoisomerases (TOP1)

According to their catalytic mechanism, sequence and domain organization, type I topoisomerases are further divided into three groups: IA, IB and IC. In the cleavage step of enzymatic catalysis, type IA topoisomerases form a TOP1CC (TOP1 cleavage complex) in which the catalytic Tyr residue of the enzyme remains covalently bounded (posphotyrosine linkage) to the 5' end of the cleaved strand. Afterwards, a second DNA strand passes by an enzyme-bridged strand passage mechanism through the transient nick (the strand passes without swivelling across the enzyme-bridged gate, as depicted in Figure 2) and finally the enzyme religates the cleaved strand leaving the DNA duplex relaxed and intact[18]. At this point, it has to be mentioned that divalent metallic cations (mainly Mg^{2+}) are necessary cofactors for TOP1A catalysis, in particular to orient the free hydroxyl group of the cleaved strand to the phosphotyrosine bound and favour the religation[19]. On the contrary, in IB and IC subfamilies the Tyr residue remains covalently linked to the 3' terminus of the cleaved strand and the supercoil is relaxed by means of a controlled strand rotation mechanism in which the second strand rotates (swivels) around the transient nick, as illustrated in the Figure 2[20]. TOP1B and TOP1C do not need Mg^{2+} cations to be active, even though it is reported that bivalent metallic cations as Mg^{2+}, Mn^{2+} and Ca^{2+} could stimulate TOP1B activity as much as 25-fold[21].

[18] Dekker NH, Rybenkov VV, Duguet M, *et al.* The mechanism of type IA topoisomerases. *Proc Natl Acad Sci U S A*. 2002;99(19):12126-12131. doi:10.1073/pnas.132378799

[19] Corbett KD, Berger JM. Structure, molecular mechanisms, and evolutionary relationships in DNA topoisomerases. *Annu Rev Biophys Biomol Struct*. 2004;33:95-118. doi:10.1146/annurev.biophys.33.110502.140357

[20] Capranico G, Marinello J, Chillemi G. Type I DNA Topoisomerases. *J Med Chem*. 2017;60(6):2169-2192. doi:10.1021/acs.jmedchem.6b00966

[21] Stewart L, Ireton GC, Parker LH, Madden KR, Champoux JJ. Biochemical and biophysical analyses of recombinant forms of human topoisomerase I. *J Biol Chem*. 1996;271(13):7593-7601. doi:10.1074/jbc.271.13.7593

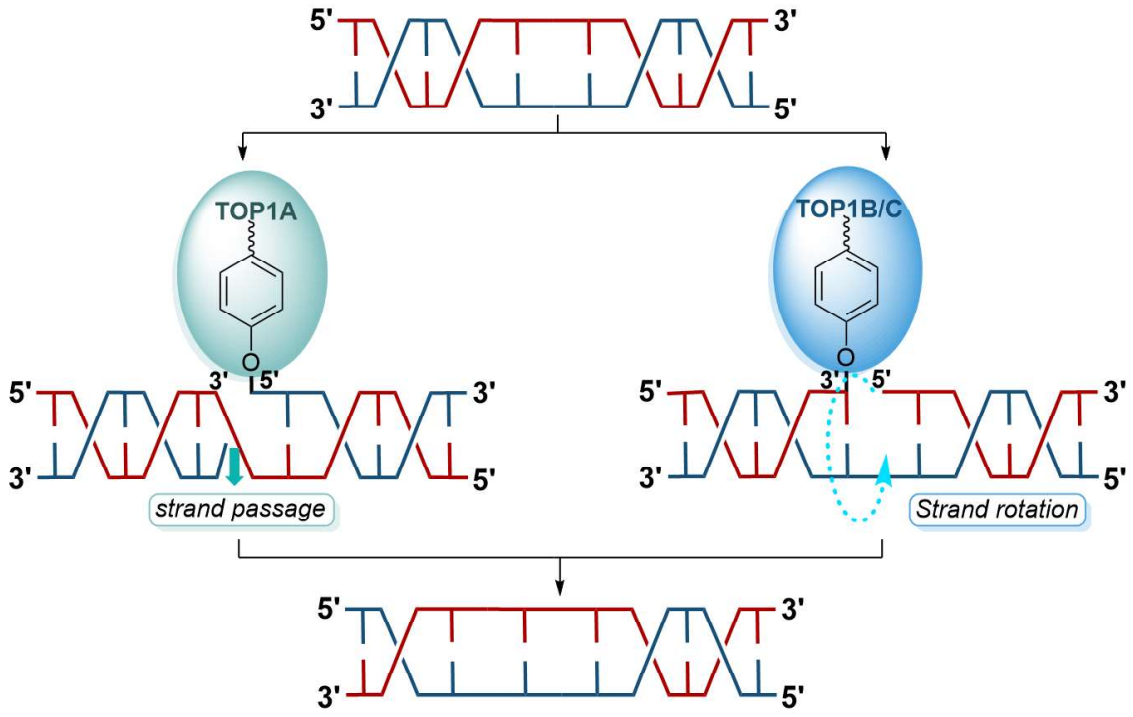

*Figure 2. Catalytic mechanism of TOP1 enzymes: type IA topoisomerases resolve positive/negative supercoils by a **strand passage** mechanism, while type IB/C topoisomerases effect controlled **strand rotation**.*

Type II topoisomerases (TOP2)

Type II topoisomerases share the mode of relaxing supercoils by forming an enzyme-bridged DSB in the DNA duplex and effecting a strand passage of another dsDNA segment through the nick, which is subsequently resealed[16]. Type II topoisomerases are further divided into IIA (TOP2A) and IIB (TOP2B) subclasses according to their sequence and domain structure. The type IIA topoisomerase family comprises the eukaryotic TOP2 (including the human TOP2α and TOP2β isoforms), viral/bacteriophage TOP2 and bacterial DNA gyrase and TopoIV. On the other hand, the presence of type IIB topoisomerases is restricted to *Archaea* organisms, plants and algae[15].

1.2. Targeting human type IB topoisomerase (hTOP1B)

Targeting topoisomerases in drug research

The human genome encodes six DNA topoisomerases: two type IB (nuclear TOP1B and mitochondrial TOP1B), two type IIA (TOP2α, TOP2β) and two type IA topoisomerases (TOP3α

and TOP3β)[22]. Among human topoisomerases, nuclear TOP1 and TOP2 are well-established and validated therapeutic targets of anticancer drugs. Regarding TOP2, the chemotherapeutic drugs etoposide, doxorubicin and mitoxantrone are interfacial inhibitors (*poisons*) of TOP2 that act by stabilizing TOP2CC (TOP2 cleavage complexes), whereas the TOP2 catalytic inhibitor dexrazoxane is used as an adjuvant to decrease the cardiotoxicity induced by doxorubicin[23]. Besides human topoisomerases, eukaryotic TOP1B of *Leishmania* genus is reported as an emerging druggable target for the development of antileishmanial agents with therapeutic potential[24]. In like manner, moving on to prokaryotic topoisomerases, bacterial DNA gyrase (a type IIA topoisomerase) is the biomolecular target of current antibiotics quinolones and coumarin. Furthermore, type IA bacterial topoisomerase has been identified as a biological target and consequently, selective bacterial TOP1A inhibitors are under investigation for the development of new antibiotics against *Mycobacterium tuberculosis, Helicobacter pylori, Pseudomonas aeruginosa and Streptococcus pneumoniae* infective agents[25]. Within the context of this introduction, the present section will focus mainly on human TOP1B inhibitors, since human (nuclear) TOP1 has been the most widely studied DNA topoisomerase as a biological target in medicinal chemistry[26].

TOP1B catalytic cycle

Among type IB topoisomerases in eukaryotic cells, human nuclear topoisomerase 1 (hTOP1) is a broadly studied biological target in anticancer drug discovery. Eukaryotic TOP1B remove negative and positive supercoils in dsDNA by means of a catalytic cycle comprising 5 steps, as depicted in Figure 3: (**A**) **Binding:** the enzyme binds to the DNA duplex. (**B**) **Cleavage:** Nucleophilic attack by the catalytic tyrosine residue (located at the position 723 in humans) to a DNA phosphodiester group (transesterification reaction) to introduce a SSB. The reaction results in a covalent TOP1-DNA cleavage complex (TOP1CC) that allows the **controlled strand rotation**

[22] Pommier Y, Nussenzweig A, Takeda S, Austin C. Human topoisomerases and their roles in genome stability and organization [published online ahead of print, 2022 Feb 28]. *Nat Rev Mol Cell Biol*. 2022;1-21. doi:10.1038/s41580-022-00452-3

[23] Delgado JL, Hsieh CM, Chan NL, Hiasa H. Topoisomerases as anticancer targets. *Biochem J*. 2018;475(2):373-398. Published 2018 Jan 23. doi:10.1042/BCJ20160583

[24] Reguera RM, Elmahallawy EK, García-Estrada C, Carbajo-Andrés R, Balaña-Fouce R. DNA Topoisomerases of Leishmania Parasites; Druggable Targets for Drug Discovery. *Curr Med Chem*. 2019;26(32):5900-5923. doi:10.2174/0929867325666180518074959

[25] Seddek A, Annamalai T, Tse-Dinh YC. Type IA Topoisomerases as Targets for Infectious Disease Treatments. *Microorganisms*. 2021;9(1):86. Published 2021 Jan 1. doi:10.3390/microorganisms9010086

[26] Martín-Encinas E, Selas A, Palacios F, Alonso C. The design and discovery of topoisomerase I inhibitors as anticancer therapies [published online ahead of print, 2022 Mar 23]. *Expert Opin Drug Discov*. 2022;1-21. doi:10.1080/17460441.2022.2055545

(**C**) of the cleaved strand. (**D**) **Religation**: the transesterification reaction is reversible and the transient DNA nick formed in the cleavage step is religated by TOP1 through the nucleopilic attack of the free hydroxyl (OH-) group at the cleaved 5'-end to the phosphotyrosine bond at 3' terminus. (**E**) **Unbinding:** finally, the enzyme leaves the DNA intact and relaxed.

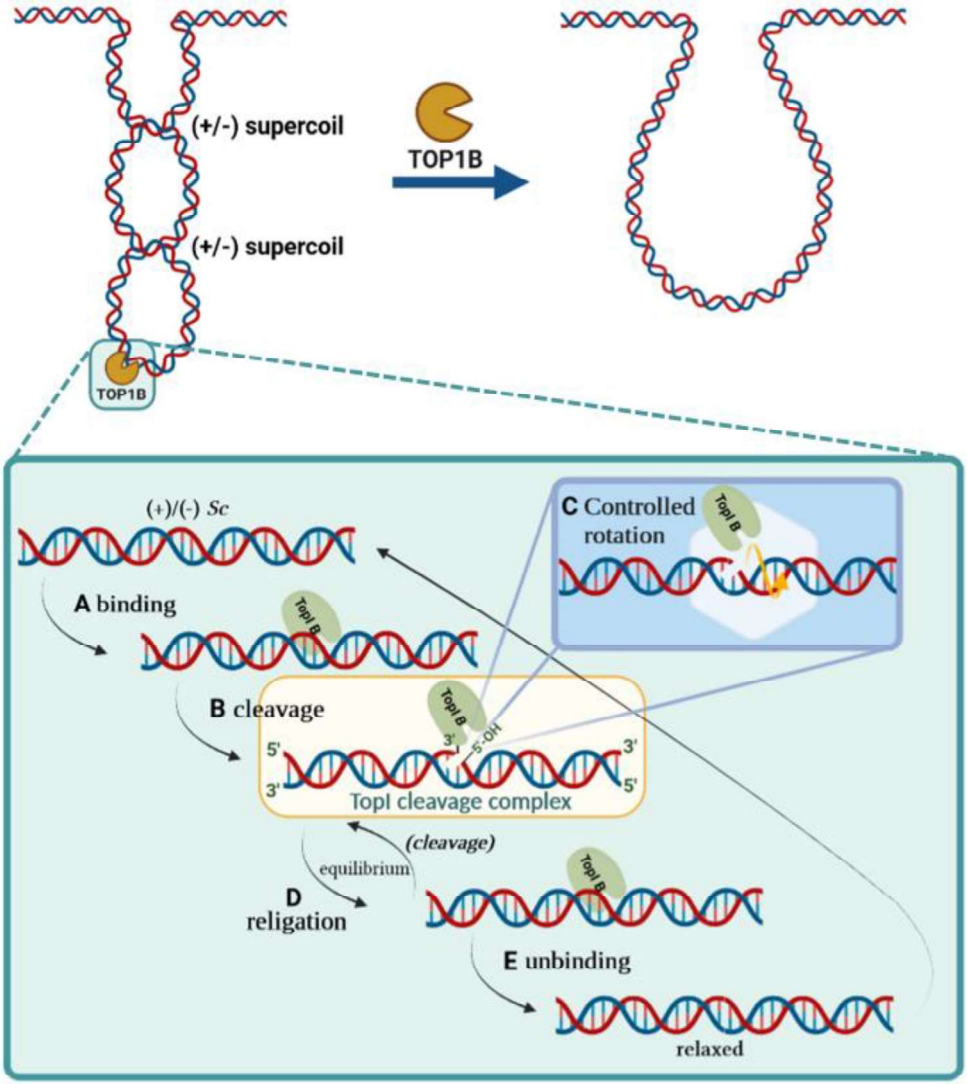

Figure 3. Catalytic cycle of TOP1B.

TOP1 inhibitors: poisons or suppressors

The crystallization of human TOP1CC stabilized by the exogenous ligand camptothecin (CPT, a natural alkaloid compound with a selective TOP1B inhibitory activity) allowed its characterization by X-ray diffraction (Figure 4, 1T8I PDB). The study of the CPT-TOP1B-dsDNA ternary complex revealed the mode of action of the natural TOP1B inhibitor CPT and its synthetic derivatives topotecan and SN-38, which actually are clinically relevant anticancer drugs.

Accordingly, based on their mode of action TOP1 inhibitors are mainly classified into TOP1 *poisons* (or interfacial inhibitors) and TOP1 *suppressors*[27].

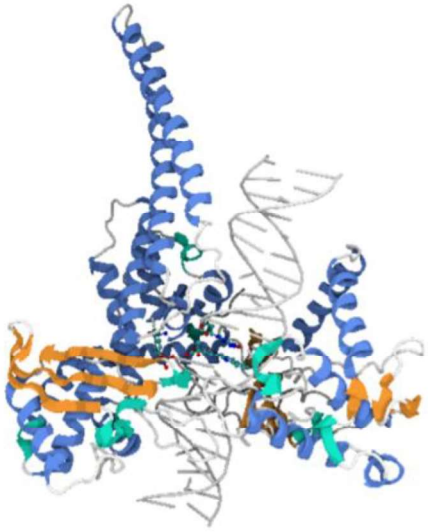

Figure 4. 1T8I PDB crystal structure of human TOP1-CPT-DNA ternary complex in 3D obtained by X-ray diffraction.

Instead of inhibiting the enzyme in a direct manner, TOP1 interfacial inhibitors target the macromolecular interface of catalytic intermediates when TOP1 is covalently bounded to DNA (hence the name). TOP1 interfacial inhibitors are also known as *poisons*, as they stabilize the TOP1CC to "poison" the cell, avoiding specifically the religation step of the TOP1 catalytic cycle[28]. As depicted in the Figure 5, cleavage and religation steps of TOP1B catalytic cycle are in equilibrium (displaced toward religation in order to finish the cycle) as the transesterification reaction catalyzed by the Tyr residue is a reversible process that may turn backwards (by the nucleophilic attack of the free hydroxyl group of the 5' end to the 3´phosphotyrosine linkage). From a pharmacodynamic point of view, *poison*-like TOP1 inhibitors target the catalytic intermediates TOP1CCs, whereas *suppressor*-like TOP1 inhibitors act by interfering in any other catalytic step of TOP1 cycle without trapping TOP1CCs (*e.g.* impeding the binding/unbinding of the enzyme or hindering the cleavage step)[20] and are also referred as catalytic inhibitors in the scientific literature.

[27] Pommier Y. DNA topoisomerase I inhibitors: chemistry, biology, and interfacial inhibition. *Chem Rev*. 2009;109(7):2894-2902. doi:10.1021/cr900097c

[28] Pommier Y, Kiselev E, Marchand C. Interfacial inhibitors. *Bioorg Med Chem Lett*. 2015;25(18):3961-3965. doi:10.1016/j.bmcl.2015.07.032

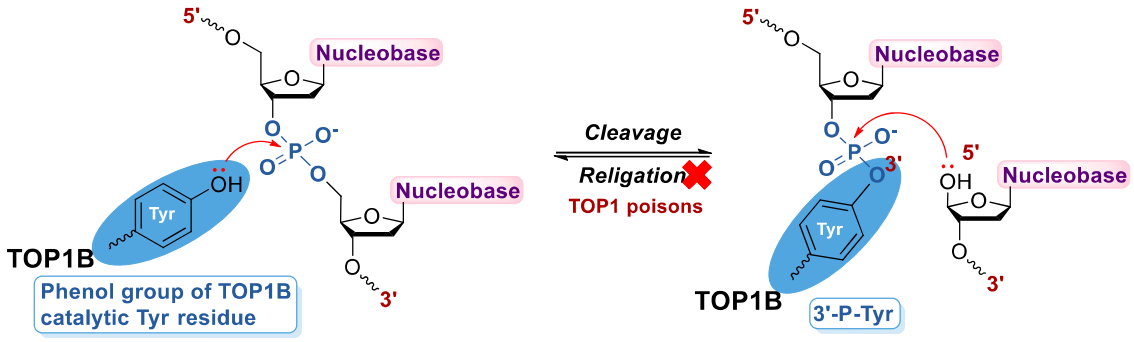

Figure 5. A schematic overview of the cleavage-religation equilibrium in TOP1B.

In regard to *poison*-like TOP1 inhibitors, the accumulation of trapped TOP1CCs results in DNA damage by collision with replication forks or transcription machinery, and subsequent apoptosis of the cell[4]. Consequently, the cytotoxic effect of *poisons* such as CPT correlates directly with the level of intracellular activity of TOP1. This fact has convert TOP1 *poisons* into suitable chemotherapeutic drugs since cancer cells show an increased TOP1 activity and a higher replication rate than non-cancer cells[29].

1.3. Development of human TOP1B (hTOP1) inhibitors as cancer chemotherapeutic drugs in medicinal chemistry

In the present section, the most relevant human TOP1B inhibitors reported in the scientific literature are going to be classified, analysing first those ones derived from natural sources and then semisynthetic/synthetic TOP1 inhibitors developed as cancer chemotherapeutic drugs or drug candidates.

1.3.1. Natural compounds targeting hTOP1B

Natural products represent an important source of anticancer drugs, highlighting the fact that more than the half of the drugs used in cancer chemotherapy are based on natural compounds[30]. Regarding natural anticancer drugs targeting TOP1, the most representative example is camptothecin (CPT, 1, Figure 6). Camptothecin is a natural alkaloid firstly isolated in 1963 from the bark and wood of the Chinese tree *Camptoteca acuminata,* which presented a strong and a wide-spectrum anticancer activity in several cytotoxicity *in vitro* screenings as well as in a mouse

[29] Postma C, Koopman M, Buffart TE, *et al.* DNA copy number profiles of primary tumors as predictors of response to chemotherapy in advanced colorectal cancer. *Ann Oncol*. 2009;20(6):1048-1056. doi:10.1093/annonc/mdn738

[30] Newman DJ, Cragg GM. Natural Products as Sources of New Drugs over the Nearly Four Decades from 01/1981 to 09/2019. *J Nat Prod*. 2020;83(3):770-803. doi:10.1021/acs.jnatprod.9b01285

leukaemia model[31]. Despite the fact that its mode of action was unknown, clinical trials were started in which CPT showed a promising antitumor activity, even though clinical studies had to be cancelled in 1972 due to severe and unpredictable side effects including diarrhoea, vomiting, myelosuppression and haemorrhages[32]. In 1971, Wang published the discovery of the first topoisomerase[11] and in the late 1980s TOP1 was unravelled to be the biological target of CPT[33]. CPT was found to be the first TOP1 inhibitor to be discovered and since then, TOP1 became a widely studied cancer chemotherapeutic target[26].

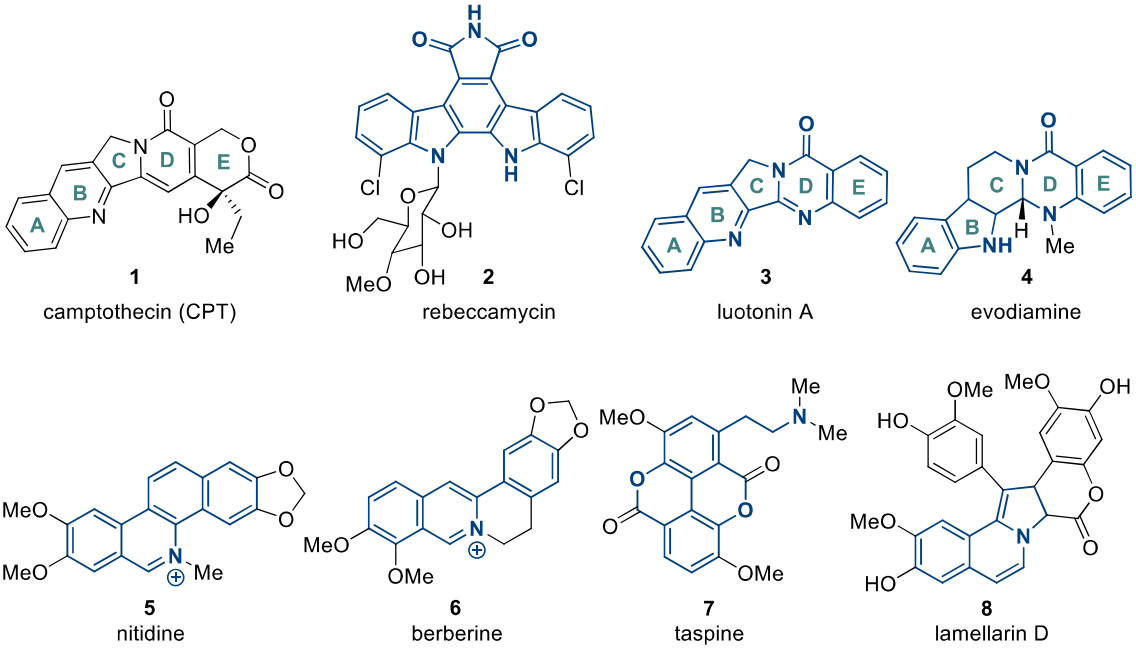

Figure 6. Chemical structures of natural alkaloids targeting human TOP1B.

Succeeding CPT, some other natural drugs were studied as TOP1 inhibitors. One of the earliest natural derivatives studied as TOP1 *poisons* were the indolocarbazole alkaloids such as rebeccamycin (**2**, Figure 6), isolated from *Lechevaliera aerocolonigenes*[34]. Given the absence of the lactone ring in its structure, rebeccamycin results more stable at physiological pH than CPT.

[31] Wall ME, Wani MC, Cook CE, Palmer KH, McPhail AT, Sim GA. Plant antitumor agents. I. the isolation and structure of camptothecin, a novel alkaloidal leukemia and tumor inhibitor from camptotheca acuminata1,2. *J Am Chem Soc*. 1966;88(16):3888-3890. doi: 10.1021/ja00968a057

[32] Muggia FM, Creaven PJ, Hansen HH, Cohen MH, Selawry OS. Phase I clinical trial of weekly and daily treatment with camptothecin (NSC-100880): correlation with preclinical studies. *Cancer Chemother Rep*. 1972;56(4):515-521.

[33] a) Hsiang YH, Hertzberg R, Hecht S, Liu LF. Camptothecin induces protein-linked DNA breaks via mammalian DNA topoisomerase I. *J Biol Chem*. 1985;260(27):14873-14878. doi:10.1016/S0021-9258(17)38654-4. b) Kjeldsen E, Mollerup S, Thomsen B, Bonven BJ, Bolund L, Westergaard O. Sequence-dependent effect of camptothecin on human topoisomerase I DNA cleavage. *J Mol Biol*. 1988;202(2):333-342. doi:10.1016/0022-2836(88)90462-7

[34] a) Sánchez C, Méndez C, Salas JA. Indolocarbazole natural products: occurrence, biosynthesis, and biological activity. *Nat Prod Rep*. 2006;23(6):1007-1045. doi:10.1039/b601930g. b)

In addition, mechanistic studies revealed that indolocarbazoles act not only by stabilizing the cleavage complex TOP1-DNA, they also behave as DNA intercalators[35].

Among other alkaloids as TOP1 inhibitors, it is noteworthy to mention the family of pyrroloquinazolinoquinolines such as luotonins[36]. Luotonins are structurally similar to CPT, with one more nitrogen in the fused backbone and lacking the lactone function in the E-ring. Luotonin A (**3**, Figure 6), isolated from the Chinese herbal medicinal plant *Peganum nigeiastum*, is a *poison*-like TOP1 inhibitor that shares its mode of action with CPT.

Evodiamine (**4**, Figure 6) is an indoloquinazoline alkaloid isolated from the Chinese plant *Tetradium ruticarpum* (previously named as *Evodia rutaecarpa*) and the fruits of *Euonymus europaeus* that exhibits a broad range of biological applications, including antiproliferative, anti-inflammatory, anti-nociceptive, antimicrobial and anti-neurodegenerative activities[37]. Evodiamine was firstly described as a TOP1 poison[38], but later on was reclassified as a TOP1 and TOP2 dual catalytic inhibitor[39]. In this regard, nicking assays showed that evodiamine is not trapping TOP1CCs as no TOP1-mediated nicked plasmid was observed in presence of evodiamine in an ethidium bromide-containing agarose gel.

The benzo[*c*]phenantridine scaffold-containing alkaloids were revealed as effective TOP1 inhibitors *in vitro*. Such is the case of nitidine (**5**, Figure 6), which was isolated from the Chinese plant *Zanthoxylum nitidum* and Kenyan plant *Asian toddalia,* was found to be a dual TOP1/TOP2 inhibitor with the ability to stabilize TOP1CCs[40]. Nitidine and its benzophenanthridinium salts have high toxicity levels due to the presence of a positively charged iminium group in the molecule (even in the form of chlorinated salts)[41]. However, the finding of nitidine as a TOP1 *poison* has brought the preparation of semisynthetic derivatives reported as selective TOP1 inhibitors (exposed in section 3.2.2., *vide infra*). In like manner, benzylisoquinoline alkaloids such

[35] Meng LH, Liao ZY, Pommier Y. Non-camptothecin DNA topoisomerase I inhibitors in cancer therapy. *Curr Top Med Chem*. 2003;3(3):305-320. doi:10.2174/1568026033452546

[36] Cagir A, Jones SH, Gao R, Eisenhauer BM, Hecht SM. Luotonin A. A naturally occurring human DNA topoisomerase I poison. *J Am Chem Soc*. 2003;125(45):13628-13629. doi:10.1021/ja0368857

[37] Sun Q, Xie L, Song J, Li X. Evodiamine: A review of its pharmacology, toxicity, pharmacokinetics and preparation researches. *J Ethnopharmacol*. 2020;262:113164. doi:10.1016/j.jep.2020.113164

[38] Chan AL, Chang WS, Chen LM, *et al.* Evodiamine stabilizes topoisomerase I-DNA cleavable complex to inhibit topoisomerase I activity. *Molecules*. 2009;14(4):1342-1352. doi:10.3390/molecules14041342

[39] Pan X, Hartley JM, Hartley JA, White KN, Wang Z, Bligh SW. Evodiamine, a dual catalytic inhibitor of type I and II topoisomerases, exhibits enhanced inhibition against camptothecin resistant cells. *Phytomedicine*. 2012;19(7):618-624. doi:10.1016/j.phymed.2012.02.003

[40] Fang SD, Wang LK, Hecht SM. Inhibitors of DNA topoisomerase I isolated from the roots of zanthoxylum nitidum. *J Org Chem*. 1993;58(19):5025-5027. doi: 10.1021/jo00071a001

[41] Janin YL, Croisy A, Riou JF, Bisagni E. Synthesis and evaluation of new 6-amino-substituted benzo[c]phenanthridine derivatives. *J Med Chem*. 1993;36(23):3686-3692. doi:10.1021/jm00075a025

as berberine (**6**, Figure 6), isolated from plants belonging to the *Berberis* genus, reported an inhibitory effect against the catalytic activity of TOP1 instead of acting as the *poison*-like inhibitor CPT does. Moreover, it was observed a synergistic combination of berberine and CPT, which would increase the effectivity in targeting human cancer cells[42].

The aporphine alkaloid taspine (**7**, Figure 6), isolated from the bark of the South American tree *Croton lechleri*[43] was reported as a selective TOP1 inhibitor that acts by inhibiting both cleavage and religation steps of the catalytic cycle of the enzyme[44]. Likewise, the pyrrole alkaloid lamellarin D (**8**, Figure 2) isolated from a *Lamellaria sp*. mollusk was found to inhibit TOP1 by stabilizing the TOP1CC *in vitro*, although it is around five-fold less active than CPT[45].

Besides alkaloids, some other natural compounds have been described as TOP1 inhibitors. During a drug screening of natural anthraquinones extracted from *Rubia cordifolia sp.*, compounds **9** and **10** (Figure 7) presented a notable *in vitro* antiproliferative activity in four human cancer cell lines (A-549, SK-OV-3, Hep-G2, HT-29) with IC_{50} values in the micromolar range (41-89 µM). The cytotoxicity was further explained by a dual inhibition of TOP1/TOP2 reported at 100 µM by DNA relaxation assays[46].

The polyphenolic compound gossypol (**11**, Figure 7), derived from the cotton plant *belonging to the Gossypium* genus, was reported as a dual TOP1/TOP2 catalytic inhibitor, interfering with the catalytic activity of both enzymes in DNA relaxation assays and decatenation assays *in vitro*, respectively[47]. Likewise, the natural monocyclic compound 2-methoxycinnamaldehyde (2-MCA, **12**, Figure 7) isolated from the bark of the Chinese plant *Cinnamomum verum* was reported to inhibit the cell proliferation and to induce apoptosis *in vitro* in the human cancer cell line Hep-

[42] Inoue N, Terabayashi T, Takiguchi-Kawashima Y, *et al.* The benzylisoquinoline alkaloids, berberine and coptisine, act against camptothecin-resistant topoisomerase I mutants. *Sci. Rep*. 2021;11(1):7718. doi: 10.1038/s41598-021-87344-2

[43] Rollinger JM, Schuster D, Baier E, Ellmerer EP, Langer T, Stuppner H. Taspine: bioactivity-guided isolation and molecular ligand-target insight of a potent acetylcholinesterase inhibitor from Magnolia x soulangiana. *J Nat Prod*. 2006;69(9):1341-1346. doi:10.1021/np060268p

[44] Castelli S, Katkar P, Vassallo O, Falconi M, Linder S, Desideri A. A natural anticancer agent thaspine targets human topoisomerase IB. *Anticancer Agents Med Chem*. 2013;13(2):356-363. doi:10.2174/1871520611313020021

[45] a) Marco E, Laine W, Tardy C, *et al.* Molecular determinants of topoisomerase I poisoning by lamellarins: comparison with camptothecin and structure-activity relationships. *J Med Chem*. 2005;48(11):3796-3807. doi:10.1021/jm049060w. b) Facompré M, Tardy C, Bal-Mahieu C, *et al.* Lamellarin D: a novel potent inhibitor of topoisomerase I. *Cancer Res*. 2003;63(21):7392-739

[46] Jeong SY, Zhao BT, Lee CS, Son JK, Min BS, Woo MH. Constituents with DNA topoisomerases I and II inhibitory activity and cytotoxicity from the roots of Rubia cordifolia. *Planta Med*. 2012;78(2):177-181. doi:10.1055/s-0031-1280265

[47] Senarisoy M, Canturk P, Zencir S, Baran Y, Topcu Z. Gossypol interferes with both type I and type II topoisomerase activities without generating strand breaks. *Cell Biochem Biophys*. 2013;66(1):199-204. doi:10.1007/s12013-012-9468-5

3B. Furthermore, 2-MCA was revealed to inhibit TOP1 and TOP2 catalytic activity *in vitro* and to reduce the volume of a tumor in an *in vivo* tumor xenograft mice model[48].

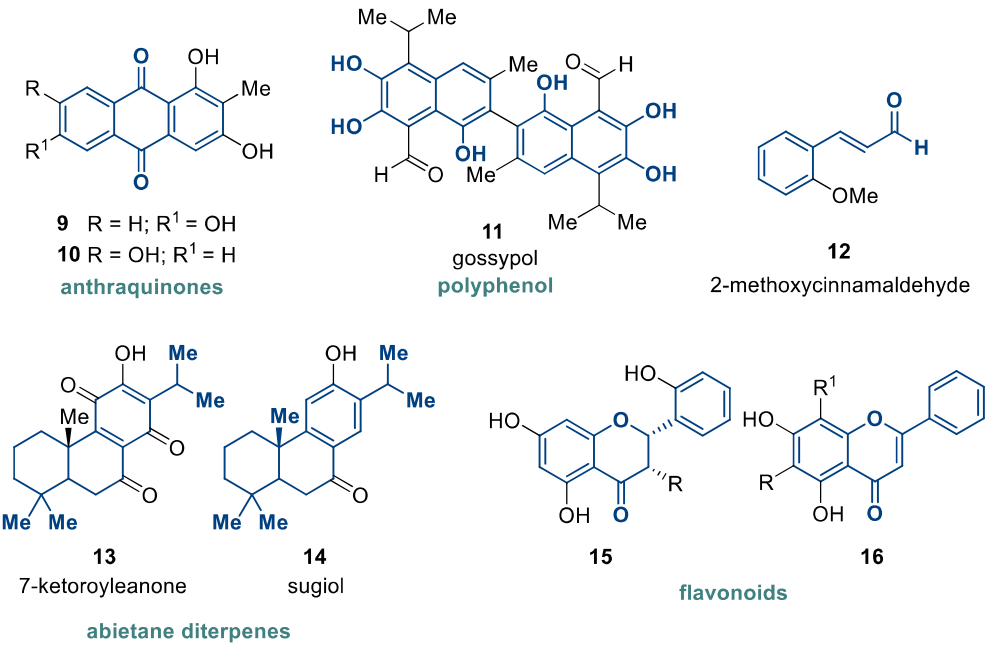

Figure 7. Chemical structures of natural anthraquinones, polyphenol, 2-MCA, abietane diterpenes and flavonoids targeting human TOP1B.

Diterpenes with *in vitro* antiproliferative activity such as abietane diterpenes 7-ketoroyleanone (**13**, Figure 7) and sugiol (**14**, Figure 7) were reported as dual TOP1/TOP2 inhibitors, interacting preferably against TOP1. These diterpenes exposed lower IC_{50} values on TOP1 mediated DNA relaxation assay than the reference compound CPT[49]. Likewise, flavonoids **15** and **16** (Figure 7), extracted from *Scutellaria amoena*, were revealed as antiproliferative agents with TOP1 inhibitory activity, presenting TOP1 IC_{50} values of 20.0 and 16.4 µM respectively[50].

Some other products extracted from natural sources have been recently documented in patents comprising TOP1 inhibitors with antiproliferative applications[51]. For example, monocyclic phenol derivatives (**17**, **18** and **19** in Figure 8) with TOP1 inhibitory activity extracted from the fungus

[48] Perng DS, Tsai YH, Cherng J, Kuo CW, Shiao CC, Cherng JM. Discovery of a novel anti-cancer agent targeting both topoisomerase I and II in hepatocellular carcinoma Hep 3B cells in vitro and in vivo: Cinnamomum verum component 2-methoxycinnamaldehyde. *J Drug Target*. 2016;24(7):624-634. doi:10.3109/1061186X.2015.1132221

[49] Fronza M, Lamy E, Günther S, Heinzmann B, Laufer S, Merfort I. Abietane diterpenes induce cytotoxic effects in human pancreatic cancer cell line MIA PaCa-2 through different modes of action. *Phytochemistry*. 2012;78:107-119. doi:10.1016/j.phytochem.2012.02.015

[50] Han HJ, Tan NH, Zeng GZ, *et al.* Natural inhibitors of DNA topoisomerase I with cytotoxicities. *Chem Biodivers*. 2008;5(7):1364-1368. doi:10.1002/cbdv.200890124

[51] Selas A, Martin-Encinas E, Fuertes M, *et al.* A patent review of topoisomerase I inhibitors (2016-present). *Expert Opin Ther Pat*. 2021;31(6):473-508. doi:10.1080/13543776.2021.1879051

Peniillium purpurogenum were published in two respective patents[52,53]. In like manner, flavonol derivatives (**20**, Figure 8) extracted from *Phyllodium pulchellum* were reported in a patent describing the extraction method and the application as TOP1 inhibitors with anticancer activity[54]. The terpenoid globulusal A (**21**, Figure 8), which was extracted from the fruits of the eucalyptus tree (*Eucalyptus globulus*)[55], was reported in a communication describing TOP1 inhibitory, antiproliferative activities and a related proapoptotic effect. Likewise, a glycosylated quinoid chalcone derivative (**22**, Figure 8) was described reporting TOP1 inhibitory activity and cytotoxic effect in a panel of several cancer cell lines[56].

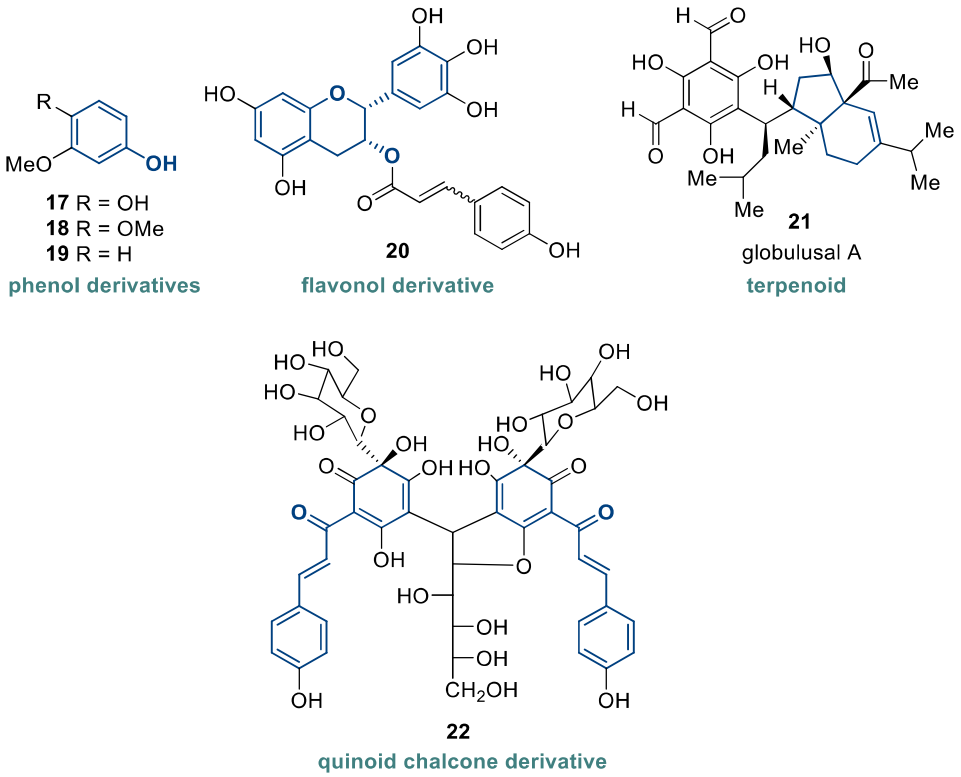

Figure 8. Chemical structures of recently patented natural compounds targeting human TOP1B.

[52] Wang C, Shao C, Wang M, *et al.* Application of phenol derivatives in preparation of topoisomerase I inhibitor. *Faming Zhuanli Shenqing*. CN 108938605, 2018

[53] Wang C, Shao C, Wang M, *et al.* Marine fungus separated from gorgonian and its application in preparing topoisomerase I inhibitor. *Faming Zhuanli Shenqing*. CN 108929857, 2018

[54] Wang C, Shao C, Xin L, *et al.* Application of flavonoid compound in preparation of topoisomerase I inhibitor. *Faming Zhuanli Shenqing*. CN 108926553, 2018

[55] Liu N, Ni W, Jin L, Yu Y, Liu H. Novel topoisomerase I inhibitor, and its pharmaceutical composition, preparation method and application in preparing drugs for treating cancer and complications and preparing functional health-care product. *Faming Zhuanli Shenqing*. CN 107986951, 2018

[56] Tang Y, Duan, J, Le, S. Quinoid chalcone-C-glycoside dimer compound having antitumor and antiinflammatory activity. *PCT Int. Appl*. WO 2017219510, 2017

1.3.2. Semisynthetic and synthetic *N*-heterocyclic compounds targeting hTOP1B

1.3.2.1. CPT derivatives (CPTs)

We previously described the CPT as the reference TOP1 inhibitor that induces a potent antiproliferative effect through a *poison*-like mode of action. However, the antitumor activity of CPT decreases rapidly in physiological conditions (pH 7.4, 37ºC) due to the hydrolysis of the lactone group, causing the ring opening and the transformation into the inactive carboxylate form[57]. Providing the fact that CPT is mainly administered intravenously, its poor water solubility represents a pharmacokinetic drawback that limits the application in clinics.

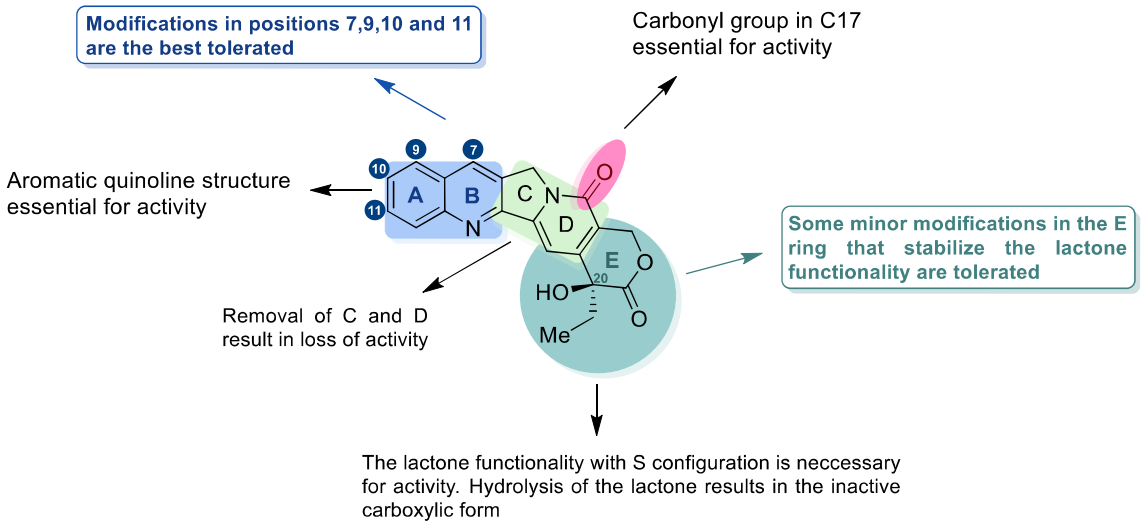

Figure 9. Chemical structure of CPT accompanied by a general overview of the SAR study thereof.

As it can be observed in the Figure 9, the pentacyclic structure of the camptothecin comprises an aromatic quinoline framework (rings A and B) linked to an indolizine moiety bearing a carbonyl group (rings C and D) and a δ-lactone ring containing a hydroxyl group and an ethyl substituent in the *S* configuration (E ring). A quasi-planar structure accompanied by a lack of hydrophilic moieties in the molecule hinders a suitable hydrosolubility. Furthermore, the chemical instability derived from the transformation of the lactone ring into the open and inactive carboxylate form limits the bioavailability of the drug, leading to difficulties to maintain appropriate levels of the active lactone-form in the organism, which may cause a lack of efficacy or the appearance of toxicities[58]. In addition, a continuous exposure to the CPT while

[57] Hatefi A, Amsden B. Camptothecin delivery methods. *Pharm Res*. 2002;19(10):1389-1399. doi:10.1023/a:1020427227285

[58] Martino E, Della Volpe S, Terribile E, *et al.* The long story of camptothecin: From traditional medicine to drugs. *Bioorg Med Chem Lett*. 2017;27(4):701-707. doi:10.1016/j.bmcl.2016.12.085

chemotherapeutic treatments triggers the emerging of resistance toward CPT[59]. In light of the aforementioned drawbacks and taking into account the high anticancer potential of CPT due to a TOP1-*poison* mode of action, scientific efforts were initiated focusing in the SAR (structure-activity relationship) optimization of the CPT structure in order to improve the pharmacokinetic profile and clinical efficacy of the natural parental compound.

The main points to introduce modifications in the CPT scaffolds are A and B rings (Figure 9). The insertion of hydrophilic substituents in positions C9, C10 and C11 increases the water solubility of the drug, while B ring functionalization at C7 with lipophilic substituents enhances the biological activity and the lactone stability[58].

Some minor modifications in the E ring are well tolerated in order to stabilize the lactone without decreasing the biological activity (Figure 9), while modifications in C and D rings (including the carbonyl group of the pyridine ring) lead to the loss of the biological effect[60].

A-ring modifications

The introduction of a *N*-alkyl chain at C9 results in the improvement of biological activity and water solubility. Following this strategy, the insertion of side alkyl chains with tertiary amines at C9 led to the development of drugs as topotecan (**23**, Figure 10), a clinically used TOP1 poison with enhanced hydrophilic properties as the tertiary amine is charged at physiological pH[61]. In the same way, belotecan (**24**, Figure 10) is another CPT derivative with a secondary amino group at C9 that increases even more the water solubility[62].

Similarly, the insertion of a nitro group in C9 gave place to the development of the water insoluble CPT derivative rubitecan (**25**, Figure 10), a strong antiproliferative TOP1 poison which was initially oriented to be orally administrated. The equilibrium between 9-nitrocamptothecin (inactive form) and its metabolite 9-aminocamptothecin (active and hydrosoluble form) was

[59] Tesauro C, Morozzo della Rocca B, Ottaviani A, *et al.* Molecular mechanism of the camptothecin resistance of Glu710Gly topoisomerase IB mutant analyzed in vitro and in silico. *Mol Cancer*. 2013;12(1):100. doi:10.1186/1476-4598-12-100

[60] Huang Q, Wang L, Lu W. Evolution in medicinal chemistry of E-ring-modified Camptothecin analogs as anticancer agents. *Eur J Med Chem*. 2013;63:746-757. doi:10.1016/j.ejmech.2013.01.058

[61] Jaxel C, Kohn KW, Wani MC, Wall ME, Pommier Y. Structure-activity study of the actions of camptothecin derivatives on mammalian topoisomerase I: evidence for a specific receptor site and a relation to antitumor activity. *Cancer Res*. 1989;49(6):1465-1469

[62] Kim JH, Lee SK, Lim JL, Shin HJ, Hong CI. Preformulation studies of a novel camptothecin anticancer agent, CKD-602: physicochemical characterization and hydrolytic equilibrium kinetics. *Int J Pharm*. 2002;239(1-2):207-211. doi:10.1016/s0378-5173(02)00099-6

predicted to be displaced towards the amino form, but clinical trials were finally interrupted due to a limited antitumor activity[63].

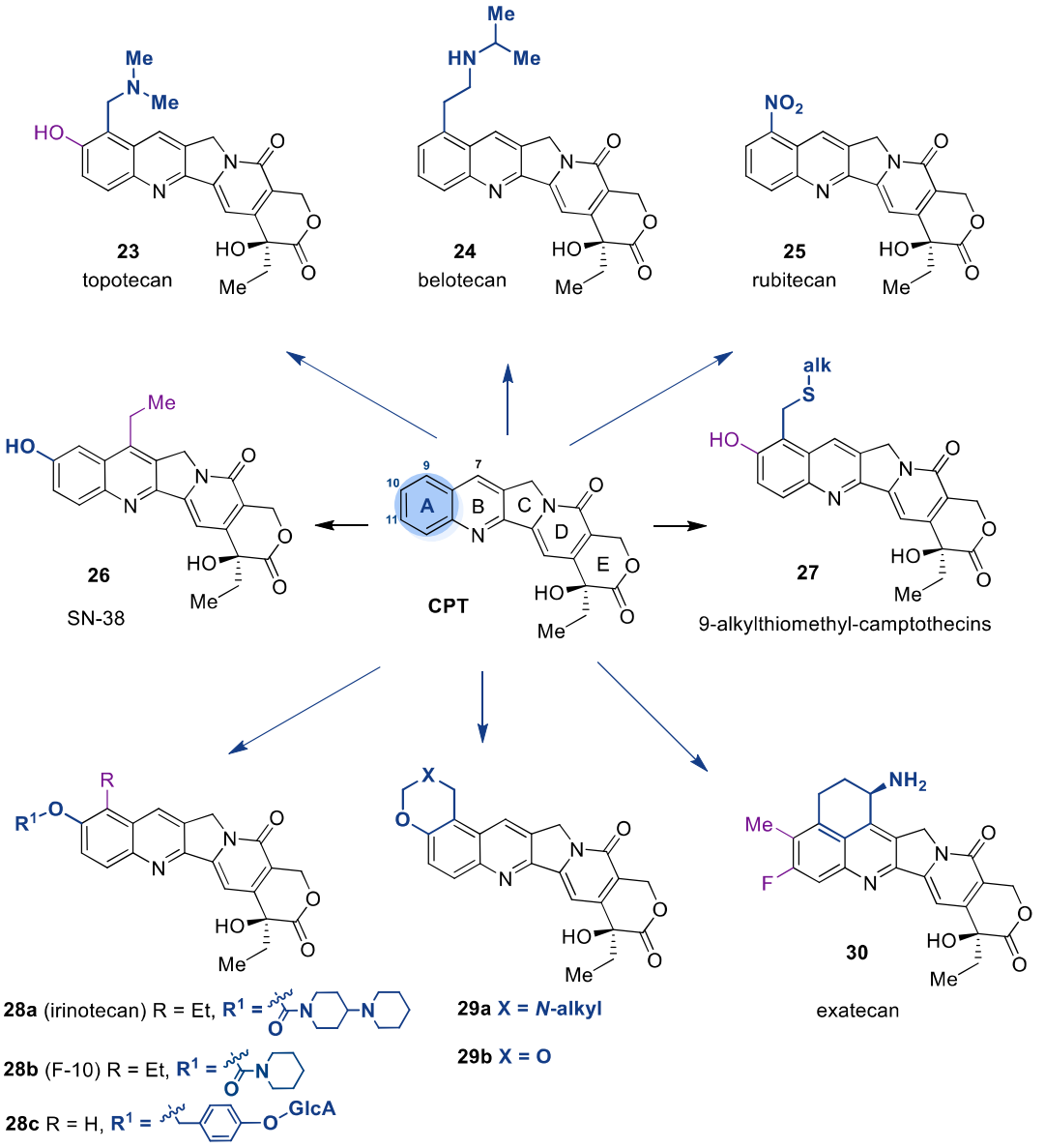

Figure 10. A-ring modifications in the CPT scaffold.

10-Hydroxycamptothecin (10-OH-CPT) is a natural alkaloid that also occurs naturally in *Camptotheca acuminata*. The presence of a hydroxyl group in C10 was demonstrated to improve the biological activity *in vivo*[64]. This hydroxyl group in position C10 has been maintained in some CPT semisynthetic analogues such as topotecan (**23**, Figure 10) and SN-38 (**26**, Figure 10), while

[63] Clark JW. Rubitecan. *Expert Opin Investig Drugs*. 2006;15(1):71-79. doi:10.1517/13543784.15.1.71
[64] Das B, Madhusudhan P, Reddy PV, Anitha Y. Natural camptothecins. Ind J Chem. 2001;40b:453-464

10-OH-CPT derivatives (**27**, Figure 6) were prepared by the transformation of the tertiary amine of topotecan hydrochloride into alkylthiomethyl functionalities in the presence of thiols[65].

Derivatization of the 10-OH substituent has led to the preparation of prodrugs (compounds **28**, Figure 10) that preserve the alcohol group. In this regard, irinotecan (**28a**) is a broadly studied and clinically used drug formed by a dipiperidino moiety linked through an ester bond to the C10 position of 7-ethyl-10-hydroxycamptothecin, which is hydrolyzed *in vivo* to obtain the parent drug SN-38 (**4**, Figure 10) after intravenous administration[66]. More recently, a 10-OH-CPT prodrug (F-10, **28b**, Figure 6) protected with a piperidin-1-yl moiety reported promising antiproliferative effect and TOP1 inhibition *in vitro*, as well as an improved antitumor effect in a xenograft model comparing to the reference SN-38[67]. Another remarkable example is the compound **28c**, a prodrug of 10-OH-CPT which was found to be 80 times more soluble than the parental drug, even though it was significantly less cytotoxic than the unprotected compound *in vitro*[68].

Inspired by the strategy of protecting 10-OH in CPT derivatives, some groups have focused in the preparation of CPT derivatives combining subsitutions in C9 and C10 (compounds **29**, Figure 10). In this context, 1,3-oxazine-fused camptothecins (**29a**) were found to present improved *in vitro* cytotoxicities compared to the references CPT and topotecan[69], while 9,10-[1,3]-dioxocamptothecin **29b** showed similar biological behaviour with an enhanced pharmacokinetic profile[70]. Regarding hexacyclic analogues of CPT, the insertion of halogenated substituents and an extra alicyclic ring to the AB quinoline ring system led to the development of exatecan (**30**,

[65] Tan H, Wang G, Li J, *et al.* Synthesis of novel 10-hydroxycamptothecin derivatives utilizing topotecan hydrochloride as ortho-quinonemethide precursor. *Bioorg Med Chem*. 2015;23(1):118-125. doi:10.1016/j.bmc.2014.11.020

[66] Bailly C. Irinotecan: 25 years of cancer treatment. *Pharmacol Res*. 2019;148:104398. doi:10.1016/j.phrs.2019.104398

[67] Fan S, Cao YX, Li GY, *et al.* F10, a new camptothecin derivative, was identified as a new orally-bioavailable, potent antitumor agent. *Eur J Med Chem*. 2020;202:112528. doi:10.1016/j.ejmech.2020.112528

[68] Leu YL, Chen CS, Wu YJ, Chern JW. Benzyl ether-linked glucuronide derivative of 10-hydroxycamptothecin designed for selective camptothecin-based anticancer therapy. *J Med Chem*. 2008;51(6):1740-1746. doi:10.1021/jm701151c

[69] Wang S, Li Y, Liu Y, Lu A, You Q. Novel hexacyclic camptothecin derivatives. Part 1: synthesis and cytotoxicity of camptothecins with an A-ring fused 1,3-oxazine ring. *Bioorg Med Chem Lett*. 2008;18(14):4095-4097. doi:10.1016/j.bmcl.2008.05.103

[70] Rodríguez-Berna G, Mangas-Sanjuán V, Gonzalez-Alvarez M, *et al.* A promising camptothecin derivative: Semisynthesis, antitumor activity and intestinal permeability. *Eur J Med Chem*. 2014;83:366-373. doi:10.1016/j.ejmech.2014.06.050

Figure 10)[71], a highly water soluble CPT derivative found to be more active than CPT, topotecan and SN-38 *in vitro* and *in vivo*[72].

B-ring modifications

The insertion of lipophilic side chains in C7 as alkyl groups has been demonstrated to enhance the biological activity of TOP1. Accordingly, longer and bulkier alkyl chains increases the lipid solubility of the molecule, leading to favourable lipophilic interactions with the TOP1-DNA cleavage complex, which correlates with a higher activity[73].

Silyl-substituted CPT analogues (**31**, Figure 11) were described as a novel class of TOP1 inhibitors[74]. Among them, the 7-silyl substituted derivatives cositecan (**31a**) and silatecan (**31b**) were reported as potent TOP1 poisons with improved pharmacokinetic profile.

[71] Mitsui I, Kumazawa E, Hirota Y, Aonuma M, Sugimori M, Ohsuki S, Uoto K, Ejima A, Terasawa H, Sato K. A new water-soluble camptothecin derivative, DX-8951f, exhibits potent antitumor activity against human tumors in vitro and in vivo. *Jpn J Cancer Res.* 1995;86:776-782

[72] a) Kumazawa E, Tohgo A. Antitumour activity of DX-8951f: a new camptothecin derivative. *Expert Opin Investig Drugs*. 1998;7(4):625-632. doi:10.1517/13543784.7.4.625. b) Li F, Jiang T, Li Q, Ling X. Camptothecin (CPT) and its derivatives are known to target topoisomerase I (Top1) as their mechanism of action: did we miss something in CPT analogue molecular targets for treating human disease such as cancer?. *Am J Cancer Res*. 2017;7(12):2350-2394

[73] Liang X, Wu Q, Luan S, *et al.* A comprehensive review of topoisomerase inhibitors as anticancer agents in the past decade. *Eur J Med Chem*. 2019;171:129-168. doi:10.1016/j.ejmech.2019.03.034

[74] Josien H, Bom D, Curran DP, Zheng Y, Chou T. 7-silylcamptothecins (silatecans): A new family of camptothecin antitumor agents. *Bioorg Med Chem Lett*. 1997;7(24):3189-3194. doi: 10.1016/S0960-894X(97)10181-0

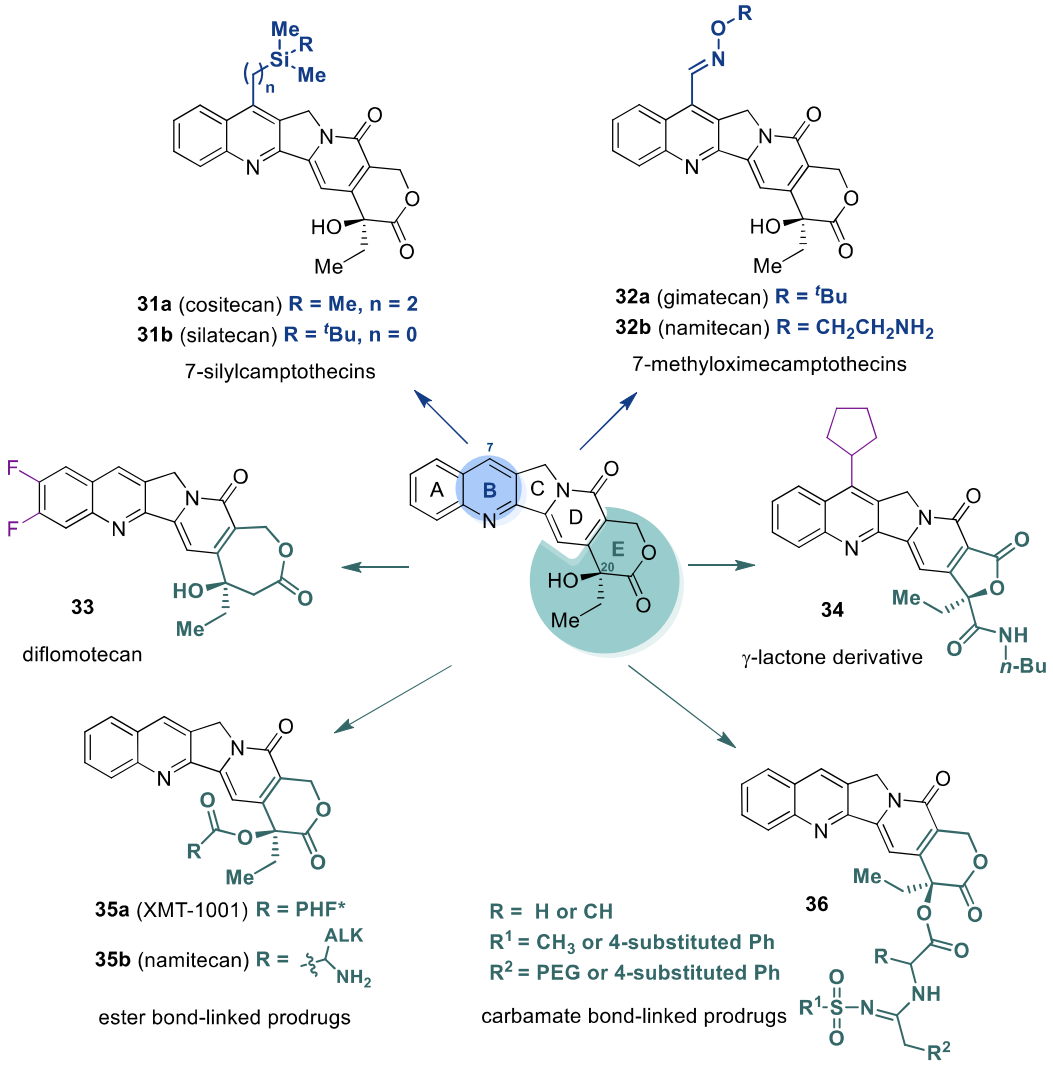

Figure 11. B-ring and E-ring modifications in the CPT scaffold.

In like manner, the functionalization with *O*-substituted oxime substituents at C7 (**32**, Figure 11) led to the development of the lipophilic derivative gimatecan (**32a**), an *O*-*tert*-butyl oxime substituted analogue that reported an increased biological activity on human tumor xenograft model *in vivo*[75]. Nevertheless, not only lipophilic replacements resulted in successful modifications, but also namitecan (**32b**), an *O*-(2-aminoethyl)-substituted oxime derivative, resulted in an enhanced pharmacokinetic profile with a maintained biological activity[76].

[75] DE Cesare M. High Efficacy of Intravenous Gimatecan on Human Tumor Xenografts. *Anticancer Res*. 2018;38(10):5783-5790. doi:10.21873/anticanres.12917

[76] Beretta GL, Zuco V, De Cesare M, Perego P, Zaffaroni N. Namitecan: a hydrophilic camptothecin with a promising preclinical profile. *Curr Med Chem*. 2012;19(21):3488-3501. doi:10.2174/092986712801323252

E-ring modifications

The most limiting drawback of CPTs is its poor chemical stability due to the opening of the δ-lactone ring. Hydrolysis of the lactone results in the opening of the six membered ring, generating a water-soluble carboxylate (Scheme 1)[77]. Hence, the displacement of the lactone (active form) towards the carboxylate (inactive form) hinders the plasma stability. Moreover, the inactive carboxylate form binds readily to human serum albumin, making it inaccessible for cellular uptake and decreasing even more the bioavailability of the drug[78].

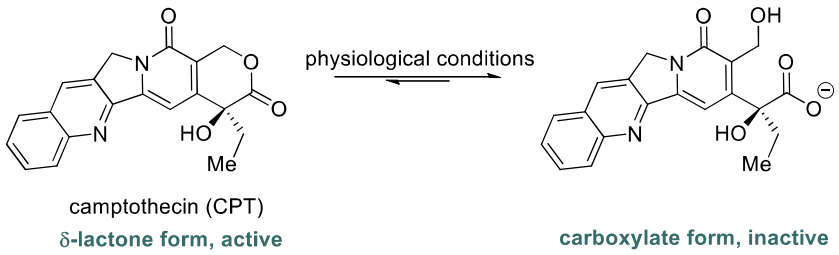

Scmeme 1. Hydrolysis of the δ-lactone ring of CPT at physiological conditions.

In this regard, the expansion of the lactone ring to a 7-membered system has led to the discovery of the more active family of homocamptothecins (hCPT). The insertion of a methylene group between the C20 and the carboxyl group increases the chemical stability by avoiding the conversion of the lactone into carboxylate[79]. The first hCTP selected for clinical studies was diflomotecan (**33**, Figure 11). Oral diflomotecan showed a favourable pharmacokinetic profile and a maintained biological activity, even though the urinary excretion was very low. This drug candidate exposed a high bioavailability but considerably variability between the patients[80].

The lactone function in the *S* conformation was believed to be crucial for the TOP1 inhibitory activity. Surprisingly, the reduction of the E ring size has been explored[81], which led to a series

[77] Fassberg J, Stella VJ. A kinetic and mechanistic study of the hydrolysis of camptothecin and some analogues. *J Pharm Sci*. 1992;81(7):676-684. doi:10.1002/jps.2600810718

[78] Burke TG, Mi Z. Preferential binding of the carboxylate form of camptothecin by human serum albumin. *Anal Biochem*. 1993;212(1):285-287. doi:10.1006/abio.1993.1325

[79] a) Lavergne O, Demarquay D, Bailly C, *et al.* Topoisomerase I-mediated antiproliferative activity of enantiomerically pure fluorinated homocamptothecins. *J Med Chem*. 2000;43(11):2285-2289. doi:10.1021/jm000129j. b) Tangirala RS, Antony S, Agama K, *et al.* Synthesis and biological assays of E-ring analogs of camptothecin and homocamptothecin. *Bioorg Med Chem*. 2006;14(18):6202-6212. doi:10.1016/j.bmc.2006.05.073

[80] Gelderblom H, Salazar R, Verweij J, *et al.* Phase I pharmacological and bioavailability study of oral diflomotecan (BN80915), a novel E-ring-modified camptothecin analogue in adults with solid tumors. *Clin Cancer Res*. 2003;9(11):4101-4107

[81] a) Hautefaye P, Cimetière B, Pierré A, *et al.* Synthesis and pharmacological evaluation of novel non-lactone analogues of camptothecin. *Bioorg Med Chem Lett*. 2003;13(16):2731-2735. doi:10.1016/s0960-894x(03)00534-1. b) Li M, Tang W, Zeng F, Lou L, You T. Semi-synthesis and biological activity of gamma-

of biologically active CPT derivatives with a 5-membered ketone ring. Among this family of γ-lactones, compound **34** (Figure 11) presented a strong *in vitro* TOP1 activity, comparable to topotecan and SN-38.

In order to avoid the transformation of the lactone into the inactive carboxylic acid, several other strategies have been further developed focusing on the protection of the hydroxyl group present in the C20 of the CPT structure. Such is the case of XMT-1001 (**35a**, Figure 11), a CPT prodrug functionalized with a PHF polyacetal polymer (poly-1-hydroxymethylethylene hydroxymethylformal), was developed *via* esterification of the hydroxyl group of the lactone[82]. XMT-1001 showed a wider therapeutic window and an improved drug exposure than CPT in human tumor xenograft models. Likewise, the formation of α-amino acid ester prodrugs of CPT (**35b**, Figure 11) was succesfully explored obtaining a predictable and suitable hydrolysis of the ester bond and the consequent release of CPT in physiological conditions, which resulted to be pH dependant and proportional to the R side chain length.[83]. Furthermore, CPT prodrugs with voluminous substituents linked to the CPT scaffold in C20 by carbamate functionalities (compounds **36**, Figure 11) were investigated. Accordingly, a family of pegylated sulfonilamidines[84] and a second set of sulfonilamidines functionalized with phenyl substituents[85] were found to present more potent *in vitro* antiproliferative effect than the reference drugs CPT and topotecan.

1.3.2.2. Non-CPT derivatives

Aside from CPT derivatives, there are other relevant families of synthetic compounds described as TOP1 inhibitors, which in some cases have been developed starting from natural drugs obtaining selective, potent and chemically stable synthetic derivatives. In the present section,

lactones analogs of camptothecin. *Bioorg Med Chem Lett*. 2008;18(24):6441-6443. doi:10.1016/j.bmcl.2008.10.074

[82] Yurkovetskiy AV, Fram RJ. XMT-1001, a novel polymeric camptothecin pro-drug in clinical development for patients with advanced cancer. *Adv Drug Deliv Rev*. 2009;61(13):1193-1202. doi:10.1016/j.addr.2009.01.007

[83] Deshmukh M, Chao P, Kutscher HL, Gao D, Sinko PJ. A series of alpha-amino acid ester prodrugs of camptothecin: in vitro hydrolysis and A549 human lung carcinoma cell cytotoxicity. *J Med Chem*. 2010;53(3):1038-1047. doi:10.1021/jm901029n

[84] Song ZL, Chen HL, Wang YH, *et al.* Design and synthesis of novel PEG-conjugated 20(S)-camptothecin sulfonylamidine derivatives with potent in vitro antitumor activity via Cu-catalyzed three-component reaction. *Bioorg Med Chem Lett*. 2015;25(13):2690-2693. doi:10.1016/j.bmcl.2015.04.060

[85] Song ZL, Wang MJ, Li L, *et al.* Design, synthesis, cytotoxic activity and molecular docking studies of new 20(S)-sulfonylamidine camptothecin derivatives. *Eur J Med Chem*. 2016;115:109-120. doi:10.1016/j.ejmech.2016.02.070

the most representative families of semisynthetic/synthetic TOP1 inhibitors will be slightly exposed, attending to a classification based on the central core of the chemical structure.

Indenoisoquinolines

Pommier, Cushman and collaborators developed indeno[1,2-*c*]isoquinoline derivatives as strong TOP1 inhibitors[86]. These indenoisoquinolines are probably the most remarkable examples of non-CPT like TOP1 poisons, which retain better the biological response toward CPT- (and CPT derivatives-) resistant mutant forms of TOP1[87]. Among this family of indenoisoquinolines, the experimental drugs indotecan (LMP400), indimitecan (LMP776) and LMP744 (Figure 12) headed to phase I and II clinical trials for the treatment of solid tumors as they are chemically more stable, stabilize TOP1CCs more persistently and present an enlarged plasma-life than CPT and CPT derivatives[86].

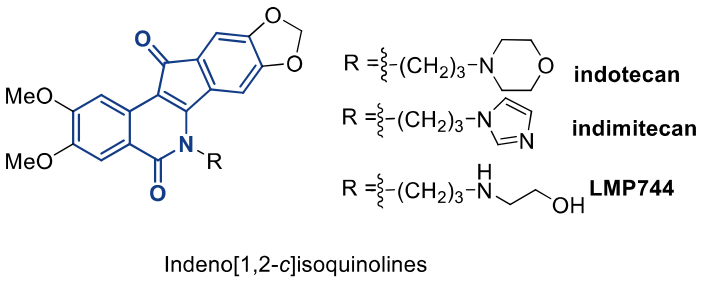

Figure 12. Indenoisoquinoline scaffold containing TOP1 inhibitors.

Aromathecins

In like manner, Pommier and coworkers developed the so-called aromathecins (Figure 13), a set of stable molecules that were outlined as formal composites of CPT and indenoisoquinolines[88]. These compounds possess a remarkable inhibition of TOP1 via stabilizing TOP1CCs and a related anticancer potential. The structure of aromathecins comprises a benzo[6,7]indolizine framework fused to a quinolinone motif, where substitutions in position 14 are well tolerated

[86] Cinelli MA, Reddy PV, Lv PC, *et al.* Identification, synthesis, and biological evaluation of metabolites of the experimental cancer treatment drugs indotecan (LMP400) and indimitecan (LMP776) and investigation of isomerically hydroxylated indenoisoquinoline analogues as topoisomerase I poisons. *J Med Chem*. 2012;55(24):10844-10862. doi:10.1021/jm300519w

[87] Antony S, Jayaraman M, Laco G, *et al.* Differential induction of topoisomerase I-DNA cleavage complexes by the indenoisoquinoline MJ-III-65 (NSC 706744) and camptothecin: base sequence analysis and activity against camptothecin-resistant topoisomerases I. *Cancer Res*. 2003;63(21):7428-7435.

[88] Cinelli MA, Morrell AE, Dexheimer TS, *et al.* The structure-activity relationships of A-ring-substituted aromathecin topoisomerase I inhibitors strongly support a camptothecin-like binding mode. *Bioorg Med Chem*. 2010;18(15):5535-5552. doi:10.1016/j.bmc.2010.06.040

and allow the insertion of hydrophilic substituents to enhance the water solubility with a maintained or improved biological activity[89].

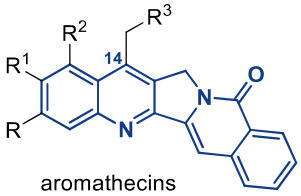

Figure 13. General structure of aromathecins, a family of TOP1 inhibitors.

Benzophenanthridines

We previously presented nitidine as a natural quaternary-ammonium alkaloid with several toxicities that limit clinical studies (in section 3.1, *vide supra*). In order to overcome these chemical drawbacks, La Voie *et al*. successfully developed neutral benzo[*i*]phenanthridine derivatives that inhibit only TOP1 or both enzymes TOP1 and TOP2. In this regard, further investigations proved that 2,3-methylenedioxy and 8,9-dimethoxy substitution patterns (**1**, Figure 14) result crucial for dual TOP1/TOP2 inhibition, while 2,3-dimethoxy- and 8,9-methylenedioxy- substituted benzo[*i*]phenanthridine derivative **2** is a selective TOP1 inibitor[90].

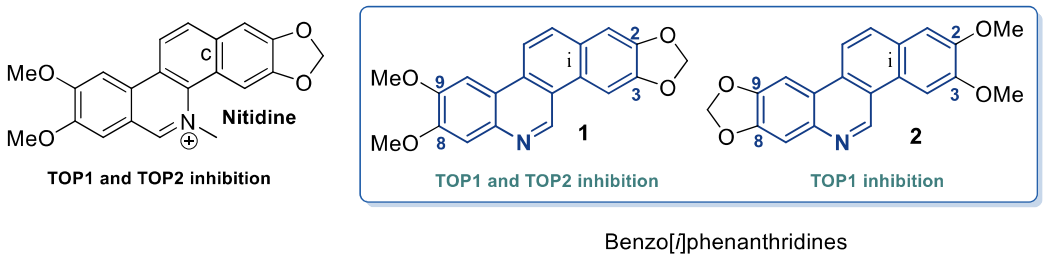

Figure 14. Benzophenanthridine scaffold containing TOP1 inhibitors.

Naphthyridines

SAR studies for the optimization of the *N*-heterocyclic core of the previous mentioned family of dibenzo[*i*]phenantridines led to La Voie´s group to develop a set of fused dibenzonaphthyridines as TOP1 *poisons*. Among these, the dibenzo[*c,h*][1,6]naphthyridine analog Genz-644282 (**37**,

[89] Cinelli MA, Morrell A, Dexheimer TS, Scher ES, Pommier Y, Cushman M. Design, synthesis, and biological evaluation of 14-substituted aromathecins as topoisomerase I inhibitors. *J Med Chem*. 2008;51(15):4609-4619. doi:10.1021/jm800259e

[90] Makhey D, Li D, Zhao B, *et al.* Substituted benzo[i]phenanthridines as mammalian topoisomerase-targeting agents. *Bioorg Med Chem*. 2003;11(8):1809-1820. doi:10.1016/s0968-0896(03)00053-1

Figure 15) resulted a promising drug candidate which arrived to clinical studies[91]. In regard to the dibenzonaphthyridine core, Cushman and collaborators successfully explored dibenzo[*c,h*][1,6]naphthyridinones (**38**, Figure 15) as anticancer agents and TOP1 inhibitors that act by trapping TOP1CCs[92].

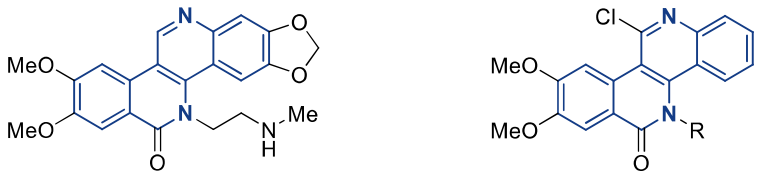

37
Genz-644282

38

Figure 15. 1,6-Naphthyridine scaffold containing TOP1 inhibitors.

Besides the dibenzonaphthyridine family, naphthyridine-based scaffolds have been broadly studied as topoisomerase I inhibitors. For instance 2,4-disubstituted 1,5-naphthyridines[93] (**39**, Figure 16) and fused 7*H*-indeno[2,1-*c*][1,5]naphthyridines[94] (**40**) were reported as TOP1 catalytic inhibitors with *in vitro* antiproliferative effect toward human cancer cell lines. During the development of a nanosensor for measuring TOP1 activity in a novel drug-screening system, these fused indenonaphthyridines were found to interfere in the TOP1 activity by blocking the TOP1 enzyme–DNA complex dissociation, inhibiting the post-ligation step of catalysis[95]. In an attempt to expand on the previous work, the preparation of a new generation of novel fused naphthyridine derivatives was investigated, broadening the size of the polyheterocyclic central

[91] Ruchelman AL, Houghton PJ, Zhou N, Liu A, Liu LF, LaVoie EJ. 5-(2-aminoethyl)dibenzo[*c,h*][1,6]naphthyridin-6-ones: variation of n-alkyl substituents modulates sensitivity to efflux transporters associated with multidrug resistance. *J Med Chem*. 2005;48(3):792-804. doi:10.1021/jm049447z

[92] Kiselev E, Dexheimer TS, Pommier Y, Cushman M. Design, synthesis, and evaluation of dibenzo[c,h][1,6]naphthyridines as topoisomerase I inhibitors and potential anticancer agents. *J Med Chem*. 2010;53(24):8716-8726. doi:10.1021/jm101048k

[93] Alonso C, Fuertes M, González M, Rodríguez-Gascón A, Rubiales G, Palacios F. Synthesis and biological evaluation of 1,5-naphthyridines as topoisomerase I inhibitors. A new family of antiproliferative agents. *Curr Top Med Chem*. 2014;14(23):2722-2728. doi:10.2174/1568026614666141215152441

[94] Alonso C, Fuertes M, González M, *et al.* Synthesis and biological evaluation of indeno[1,5]naphthyridines as topoisomerase I (TopI) inhibitors with antiproliferative activity. *Eur J Med Chem*. 2016;115:179-190. doi:10.1016/j.ejmech.2016.03.031

[95] Andersen MB, Tesauro C, Gonzalez M, *et al.* Advantages of an optical nanosensor system for the mechanistic analysis of a novel topoisomerase I targeting drug: a case study. *Nanoscale*. 2017;9(5):1886-1895. doi:10.1039/c6nr06848k

core by incorporating chromene[96] and quinoline[97] moieties into the 1,5-naphthyridine scaffold. The molecular hybridization of two (or more) biologically active pharmacophoric scaffolds into a new chemical entity represents a highly convenient strategy to explore rational structural modifications yielding to more complex central cores[98]. In this regard, the hybridization of 1,5-naphthyridines with chromene/quinoline frameworks enhanced the biological response and, furthermore, the quinolino[4,3-*b*][1,5]naphthyridine derivatives **41a** and **41b** (Figure 16) were revealed as *poison*-like TOP1 inhibitors with enhanced *in vitro* antiproliferative activity.

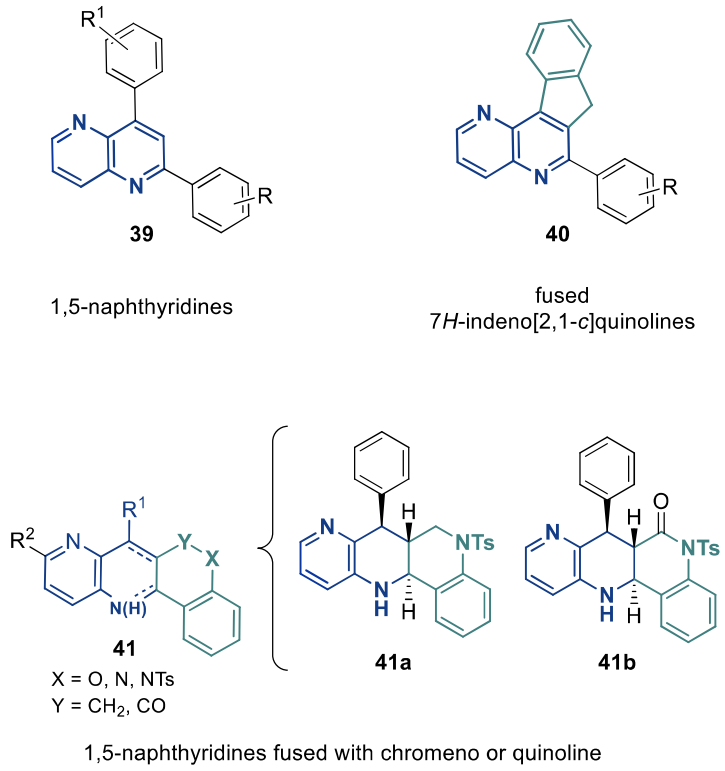

Figure 16. 1,5-Naphthyridine scaffold containing TOP1 inhibitors.

[96] Martín-Encinas E, Rubiales G, Knudssen BR, Palacios F, Alonso C. Straightforward synthesis and biological evaluation as topoisomerase I inhibitors and antiproliferative agents of hybrid Chromeno[4,3-b][1,5]Naphthyridines and Chromeno[4,3-b][1,5]Naphthyridin-6-ones. *Eur J Med Chem*. 2019;178:752-766. doi:10.1016/j.ejmech.2019.06.032

[97] Martín-Encinas E, Selas A, Tesauro C, *et al.* Synthesis of novel hybrid quinolino[4,3-b][1,5]naphthyridines and quinolino[4,3-b][1,5]naphthyridin-6(5H)-one derivatives and biological evaluation as topoisomerase I inhibitors and antiproliferatives. *Eur J Med Chem*. 2020;195:112292. doi:10.1016/j.ejmech.2020.112292

[98] a) Bérubé G. An overview of molecular hybrids in drug discovery. *Expert Opin Drug Discov*. 2016;11(3):281-305. doi:10.1517/17460441.2016.1135125. b) Ivasiv V, Albertini C, Gonçalves AE, Rossi M, Bolognesi ML. Molecular Hybridization as a Tool for Designing Multitarget Drug Candidates for Complex Diseases. *Curr Top Med Chem*. 2019;19(19):1694-1711. doi:10.2174/1568026619666190619115735

Indoloquinazolines

The development of novel evodiamine and rutaecarpine analogs has led to indoloquinazoline derivatives with dual topoisomerase I and II inhibitory activity. Among these compounds, evodiamine derivatives **42a-d** (Figure 17) were revealed to inhibit TOP1/TOP2 at 50 µM and further mechanistic experiments demonstrated their ability to stabilize TOP1CCs but not TOP2CC, concluding that they act as dual TOP1 poisons and *suppressor*-like TOP2 inhibitors[99].

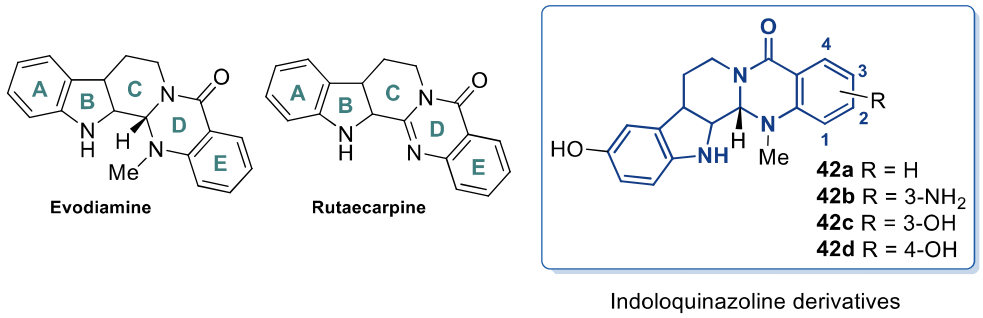

Figure 17. Indoloquinazoline scaffold containing TOP1 inhibitors.

Indolocarbazoles

In the early 1990's, synthetic derivatives of the natural indolocarbazole antibiotic K252a were revealed as *poison*-like TOP1 inhibitors presenting a promising antiproliferative activity *in vitro*[100]. Several synthetic glycosylated derivatives were developed by introducing β-linked sugars (rather than α-sugars, which were considerably less active) in the *N*-glycosyl moiety (mono or di-substituted indolocarbazoles), highlighting the β-glucose linked derivatives NB-506 (**43**, Figure 18) and edotecarin (**44**), which were prescribed for clinical trials[35,101]. From a mechanistic point of view, the mode of action of indolocarbazoles differs from the CPT. Despite both are TOP1 poisons, indolocarbazoles further act as DNA intercalators with the ability to bind to triplex DNA[35].

[99] Dong G, Wang S, Miao Z, *et al.* New tricks for an old natural product: discovery of highly potent evodiamine derivatives as novel antitumor agents by systemic structure-activity relationship analysis and biological evaluations. *J Med Chem*. 2012;55(17):7593-7613. doi:10.1021/jm300605m

[100] Yamashita Y, Fujii N, Murakata C, Ashizawa T, Okabe M, Nakano H. Induction of mammalian DNA topoisomerase I mediated DNA cleavage by antitumor indolocarbazole derivatives. *Biochemistry*. 1992;31(48):12069-12075. doi:10.1021/bi00163a015

[101] Basili S, Moro S. Novel camptothecin derivatives as topoisomerase I inhibitors. *Expert Opin Ther Pat*. 2009;19(5):555-574. doi:10.1517/13543770902773437

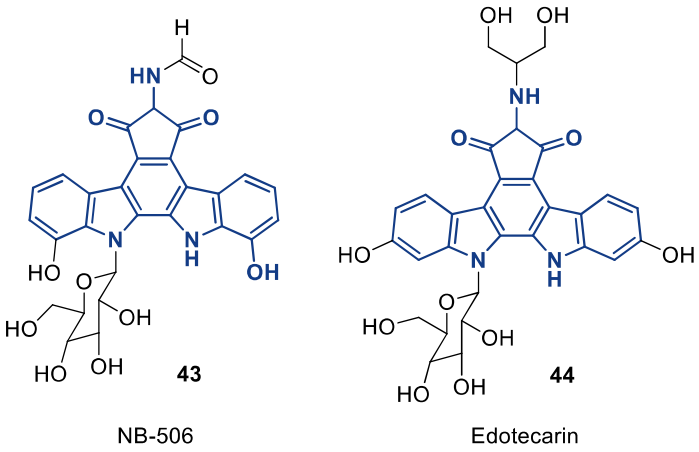

Figure 18. Indolocarbazole scaffold containing TOP1 inhibitors.

Arylpyridines

2,4,6-Trisubstituted aryl pyridines, a family of small molecules bearing a monocyclic pyridine scaffold, were investigated as dual TOP1/TOP2 inhibitors and *in vitro* antiproliferative agents. Among them, the arylpyridine derivative **45** (Figure 20) was found to strongly inhibit TOP1 in DNA relaxation assays[102]. Later on, a new family based on a tricyclic scaffold composed of arylpyrydine fused with benzofuran was developed, where the derivative **46** (Figure 19) was reported as a dual TOP1/TOP2 catalytic inhibitor presenting GI_{50} values between 0.2-5.9 µM in HCT-15, T47D and HeLa cancer cell lines *in vitro*[103].

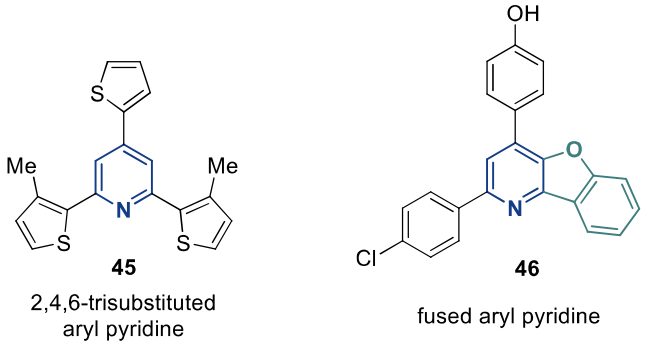

Figure 19. Arylpyridine scaffold containing TOP1 inhibitors.

[102] Basnet A, Thapa P, Karki R, *et al.* 2,6-Dithienyl-4-furyl pyridines: Synthesis, topoisomerase I and II inhibition, cytotoxicity, structure-activity relationship, and docking study. *Bioorg Med Chem Lett*. 2010;20(1):42-47. doi:10.1016/j.bmcl.2009.11.041

[103] Park S, Thapa Magar TB, Kadayat TM, *et al.* Rational design, synthesis, and evaluation of novel 2,4-Chloro- and Hydroxy-Substituted diphenyl Benzofuro[3,2-b]Pyridines: Non-intercalative catalytic topoisomerase I and II dual inhibitor. *Eur J Med Chem*. 2017;127:318-333. doi:10.1016/j.ejmech.2017.01.003

Quinolines

Likewise, a set of 3,4,6-trisubstituted quinoline scaffold-based compounds were studied as TOP1 inhibitors. A substitution pattern including 1,3,4-oxadiazol-2-yl substituent in C3, aminoalkyl morpholine/imidazole moiety in C4 and phenyl group in C6 of the quinoline core revealed a new series of TOP1 inhibitors (compounds **47**, Figure 20). Among these compounds, the quinoline derivative **47a** was identified as a potent TOP1 inhibitor (IC_{50} values of 0.029 ± 0.004 µM *in vitro* and 2.74 ± 0.314 µM *ex vivo*) that acts by stabilizing TOP1CCs[104]. Subsequently, a lead compound optimization was carried out by means of chemical modifications in 1,3,4-oxadiazol-2-yl 6-phenylquinoline derivative **47c**. Replacement of the 4-methoxy substituent by a 4-amino group in the phenyl ring located in position C6 of the quinoline scaffold resulted in an improvement in the metabolic stability (**47c** was found to have a high clearance in human liver microsomes while compound **47d** showed lower intrinsic clearance, increasing the half-life of the drug), while the TOP1 inhibitory activity is maintained[105].

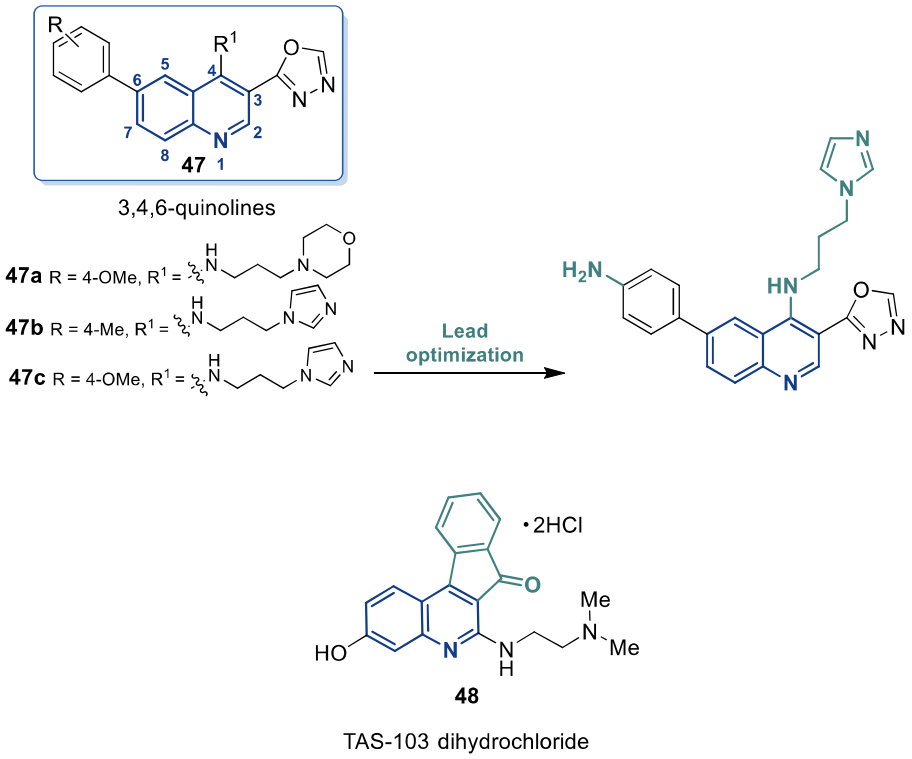

Figure 20. Quinoline scaffold containing TOP1 inhibitors.

[104] Kundu B, Das SK, Paul Chowdhuri S, *et al.* Discovery and Mechanistic Study of Tailor-Made Quinoline Derivatives as Topoisomerase 1 Poison with Potent Anticancer Activity. *J Med Chem*. 2019;62(7):3428-3446. doi:10.1021/acs.jmedchem.8b01938

[105] Kundu B, Sarkar D, Chowdhuri SP, *et al.* Development of a metabolically stable topoisomerase I poison as anticancer agent. *Eur J Med Chem*. 2020;202:112551. doi:10.1016/j.ejmech.2020.112551

Furthermore, TAS-103, a hybrid of quinoline and indene forming a 7*H*-indeno[2,1-*c*]quinolin-7-one central core (**48**, Figure 20), was developed as a broad spectrum antiproliferative agent that reported dual TOP1/TOP2 inhibitory activity[106]. During mechanistic studies *in vitro*, TAS-103 was found capable to trap both TOP1CCs and TOP2CCs, even though its ability to stabilize TOP1CCs is lower in comparison with the reference drugs CPT and CPT derivatives (specially at high concentrations), suggesting a different manner to interfere in the TOP1 catalytic cycle[107].

[106] Aoyagi Y, Kobunai T, Utsugi T, Oh-hara T, Yamada Y. In vitro antitumor activity of TAS-103, a novel quinoline derivative that targets topoisomerases I and II. *Jpn J Cancer Res*. 1999;90(5):578-587. doi:10.1111/j.1349-7006.1999.tb00786.x

[107] Minderman H, Wrzosek C, Cao S, *et al.* Mechanism of action of the dual topoisomerase-I and -II inhibitor TAS-103 and activity against (multi)drug resistant cells. *Cancer Chemother Pharmacol*. 2000;45(1):78-84. doi:10.1007/PL00006747

2. Synthesis of quinolines

The quinoline ring-system

Heterocycles are molecules formed by one or more rings composed (at least) of two elements, one of which being usually carbon[108]. Heterocyclic compounds are ubiquitously present in nature and hence play a pivotal role in organic chemistry, which enables the development and optimization of synthetic routes for their preparation/modification and guides their synthesis to diverse applications (industry, agriculture, materials, therapeutic agents, etc.)[109]. The relevance of heterocycles is not only because of their natural abundance, but also due to the biochemical significance of heterocyclic-containing biomolecules, which result essential to life. In this regard, heterocyclic compounds are present in numerous indispensable biomolecules and precursors thereof, such as nucleobases (and consequently, are part of structures with higher complexity degree *e.g.* nucleotides, coenzymes or nucleic acids), essential amino acids (histidine, tryptophan, proline), sugars or lipids[110].

Quinoline **49** (benzo[*b*]pyridine, illustrated in the Figure 21) is an aromatic nitrogen-containing heterocycle constituted by a benzene and a pyridine fused at two adjacent carbons. F.F. Runge firstly extracted an impure fraction containing large quantities of quinoline from coal tars in 1834, who initially named the compound as "leukol" (*leukos* meaning white in Greek + *ol*)[111]. Later in 1842, C. Gerhardt isolated a pure portion of the same compound by dry-distillation of cinchona alkaloids (*Cinchona* spp.)[112] and renamed the molecule as "quinoline"[113].

[108] Moss GP, Smith PAS, Tavernier D. Glossary of class names of organic compounds and reactivity intermediates based on structure (IUPAC recommendations 1995). *Pure Appl Chem*. 1995;67(8-9):1307-1375. doi: 10.1351/pac199567081307

[109] Matada BS, Pattanashettar R, Yernale NG. A comprehensive review on the biological interest of quinoline and its derivatives. *Bioorg Med Chem*. 2021;32:115973. doi: https://doi.org/10.1016/j.bmc.2020.115973

[110] a) Watson JD, CRick FHC. Molecular structure of nucleic acids: A structure for deoxyribose nucleic acid. *Nature*. 1953;171(4356):737-738. doi: 10.1038/171737a0. b) Wu G. Amino acids: metabolism, functions, and nutrition. *Amino Acids*. 2009;37(1):1-17. doi:10.1007/s00726-009-0269-0 c) Dashty M. A quick look at biochemistry: carbohydrate metabolism. *Clin Biochem*. 2013;46(15):1339-1352. doi:10.1016/j.clinbiochem.2013.04.027. d) Griffin BA. Lipid metabolism. *Surgery (Oxford)*. 2013;31(6):267-272. doi: https://doi.org/10.1016/j.mpsur.2013.04.006

[111] Runge FF. Ueber einige produkte der steinkohlendestillation. *Ann Phys*. 1834;107(5):65-78. https://doi.org/10.1002/andp.18341070502

[112] Gerhardt Ch. Untersuchungen über die organischen Basen. *Ann Chem Pharm*. 1842; 42:310-313

[113] Gerhardt Ch. Chinolein oder Chinoilin. *Ann Chem Pharm*. 1842; 44:279-280

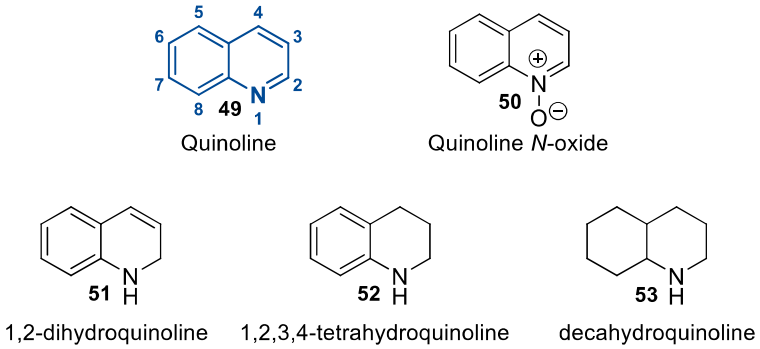

*Figure 21. Frameworks of quinoline (**1**) and oxidized (**2**) or reduced forms (**3,4,5**) thereof.*

Along with the fully aromatic and neutral quinoline structure **49**, the frameworks corresponding to oxidized (**50**) or reduced forms (**51**, **52**, **53**) are collected in the Figure 21. These alternative reduced hydroquinolines are common motifs present in many bioactive compounds[114], while quinoline *N*-oxides are revealed as useful precursors for synthetic modifications of quinolines[115]. Furthermore, the closely related quinolones (quinolinones, *i.e.* derivatives with a carbonyl group in the quinoline scaffold) also occur in natural products and result essential for the biological activity of numerous compounds[116] (Figure 22, see the quinolinones **54**, **55**, **56** and **57**). The main quinolones are the 2-quinolone **54** (Figure 22) and 4-quinolone **55**, and both maintain a keto-enol tautomery with the corresponding hydroxiquinoline, being the quinolone form the major tautomer.

[114] Muthukrishnan I, Sridharan V, Menéndez JC. Progress in the chemistry of tetrahydroquinolines. *Chem Rev*. 2019;119(8):5057-5191. doi: 10.1021/acs.chemrev.8b00567

[115] Gribble GW, Kishbaugh TLS. Chapter 6.1 - six-membered ring systems: Pyridine and benzo derivatives. *Adv Heterocycl Chem*. 2016;28:391-437. doi: https://doi.org/10.1016/B978-0-08-100755-6.00012-0

[116] a) Winter RW, Kelly JX, Smilkstein MJ, Dodean R, Hinrichs D, Riscoe MK. Antimalarial quinolones: synthesis, potency, and mechanistic studies. *Exp Parasitol*. 2008;118(4):487-497. doi:10.1016/j.exppara.2007.10.016. b) Pham TDM, Ziora ZM, Blaskovich MAT. Quinolone antibiotics. *Med Chem Commun*. 2019;10(10):1719-1739. http://dx.doi.org/10.1039/C9MD00120D. doi: 10.1039/C9MD00120D. c) Aly AA, El-Sheref EM, Mourad AE, Bakheet MEM, Bräse S. 4-Hydroxy-2-quinolones: syntheses, reactions and fused heterocycles. *Mol Divers*. 2020;24(2):477-524. doi:10.1007/s11030-019-09952-5

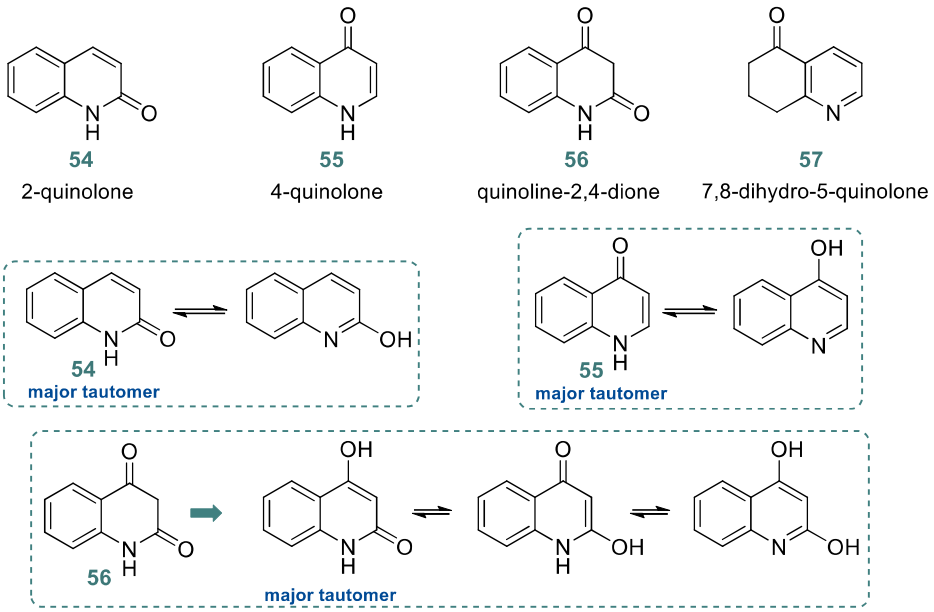

Figure 22. Framework of quinolones and tautomeric equilibrium with hydroxyquinolines.

Quinoline: natural sources, chemical applications and bioactive compounds

Quinoline is considered a privileged scaffold due to its natural abundance, biological significance and wide range of applications. Thus, the quinoline core is present in many different natural sources, such as the antimalarial quinine alkaloids (**58**, Figure 23) obtained from *Cinchona* spp.[117] Remarkably, Cinchona alkaloids quinine and quinidine are also reported as the first organocatalysts used in asymmetric organic synthesis in 1912[118]. In like manner, the indoloquinoline alkaloid cryptolepine (**60**), obtained from the African plant *Cryptolepis sanguinolenta*, has shown antimalarial and antiproliferative activity *in vitro*. The neurotoxin gephirotoxin (**61**) is a decahydroquinoline alkaloid isolated from the skin of *Dendrobates histrionicus* frogs (native from Colombia)[119]. Veranamine (**62**), a β-carboline alkaloid isolated from the marine sponge *Verongula rigida* (Florida, USA), showed both *in vivo* and *in vitro* antidepressant activity *via* inhibition of serotonin receptor 2B (5-HT2B) and sigma-1 receptor (σ*1*R)[120]. Likewise, the previously mentioned camptothecin (**1**), a pentacyclic alkaloid isolated

[117] Shang XF, Morris-Natschke SL, Liu YQ, *et al.* Biologically active quinoline and quinazoline alkaloids part I. *Med Res Rev*. 2018;38(3):775-828. doi:10.1002/med.21466

[118] Bredig G, Fiske WS. Beiträge zur chemischen Physiologie und Pathologie. *Biochem Z*. 1912;46:7

[119] Wijnsma R, Verpoorte R. CHAPTER 19 - Quinoline alkaloids of cinchona. In: CONSTABEL F, VASIL IK, eds. *Phytochemicals in plant cell cultures.* Academic Press; 1988:335-355. https://doi.org/10.1016/B978-0-12-715005-5.50026-1

[120] Kochanowska-Karamyan A, Araujo HC, Zhang X, *et al.* Isolation and synthesis of veranamine, an antidepressant lead from the marine sponge verongula rigida. *J Nat Prod*. 2020;83(4):1092-1098. doi: 10.1021/acs.jnatprod.9b01107

from *Camptotheca acuminata*, is a broadly studied anticancer agent *via* interfacial inhibition of TOP1[4].

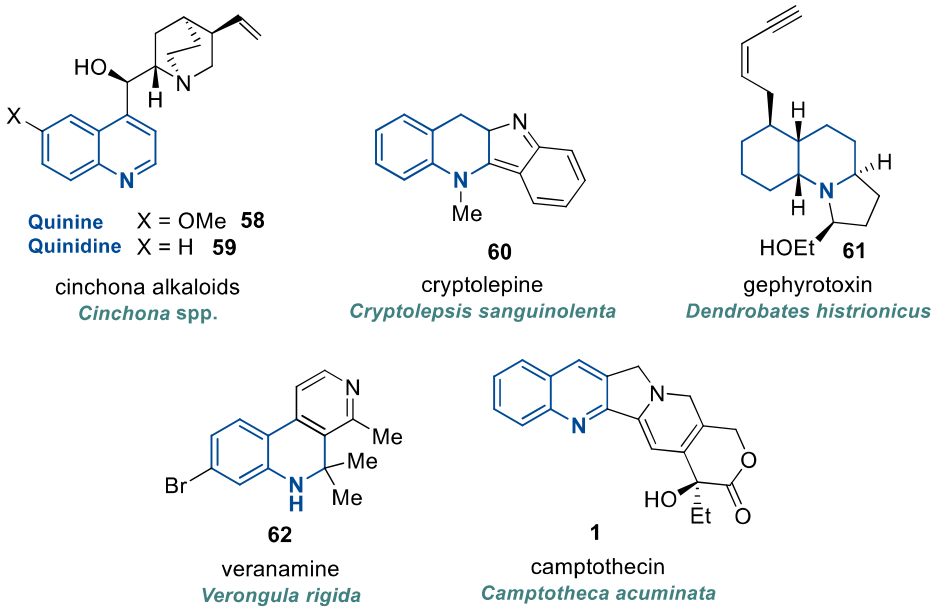

Figure 23. Natural bioactive compounds containing a quinoline-based central core.

Besides natural occurring quinolines, they can be found in many synthetic compounds with various chemical and industrial applications, as shown in the Figure 24. Quinoline scaffolds are commonly used as ligands[121] for metallic catalysts in cross-coupling reactions and asymmetric synthesis, such is the case for the so-called APAC ligand (**63**, Figure 24). Moreover, quinoline-containing dyes have been oriented to various applications. The water-soluble colorant **64** (E-104 in Europe, D&C yellow no. 10 in USA) is mainly applied as a colorant in food industry[122], whereas the water insoluble dye **65** (D&C yellow no. 11 in USA) is used as colouring agent in cosmetics[123]. Likewise, photovoltaic dyes (such as the compound **66**) with quinoline skeletons represent a significant class of chemical materials to produce photovoltaic cells[124]. Furthermore,

[121] Romero EA, Chen G, Gembicky M, Jazzar R, Yu J, Bertrand G. Understanding the activity and enantioselectivity of acetyl-protected aminoethyl quinoline ligands in palladium-catalyzed β-C(sp3)–H bond arylation reactions. *J Am Chem Soc*. 2019;141(42):16726-16733. https://doi.org/10.1021/jacs.9b06746. doi: 10.1021/jacs.9b06746

[122] Weisz A, James IC, Mazzola EP, Ridge CD, Ijames CF, Markey SP. Identification of 1',5'-naphthyridinophthalone and its quantification in the color additive D&C Yellow No. 10 (Quinoline Yellow) using high-performance liquid chromatography. *Food Addit Contam Part A Chem Anal Control Expo Risk Assess*. 2018;35(3):439-447. doi:10.1080/19440049.2017.1416183

[123] Chequer FM, Venâncio Vde P, de Souza Prado MR, *et al.* The cosmetic dye quinoline yellow causes DNA damage in vitro. *Mutat Res Genet Toxicol Environ Mutagen*. 2015;777:54-61. doi:10.1016/j.mrgentox.2014.11.003

[124] Lewinska G, Sanetra J, Marszalek KW. Application of quinoline derivatives in third-generation photovoltaics. *J Mater Sci : Mater Electron*. 2021;32(14):18451-18465. https://doi.org/10.1007/s10854-021-06225-6. doi: 10.1007/s10854-021-06225-6

a red fluorescent biosensor based on a BODIPY (4,4-difluoro-4-bora-3a,4a-diaza-*s*-indacene) skeleton **67**[125] has been developed for the detection of iridium(III) in biological systems, as a sensitive bioimaging tool with medical applications.

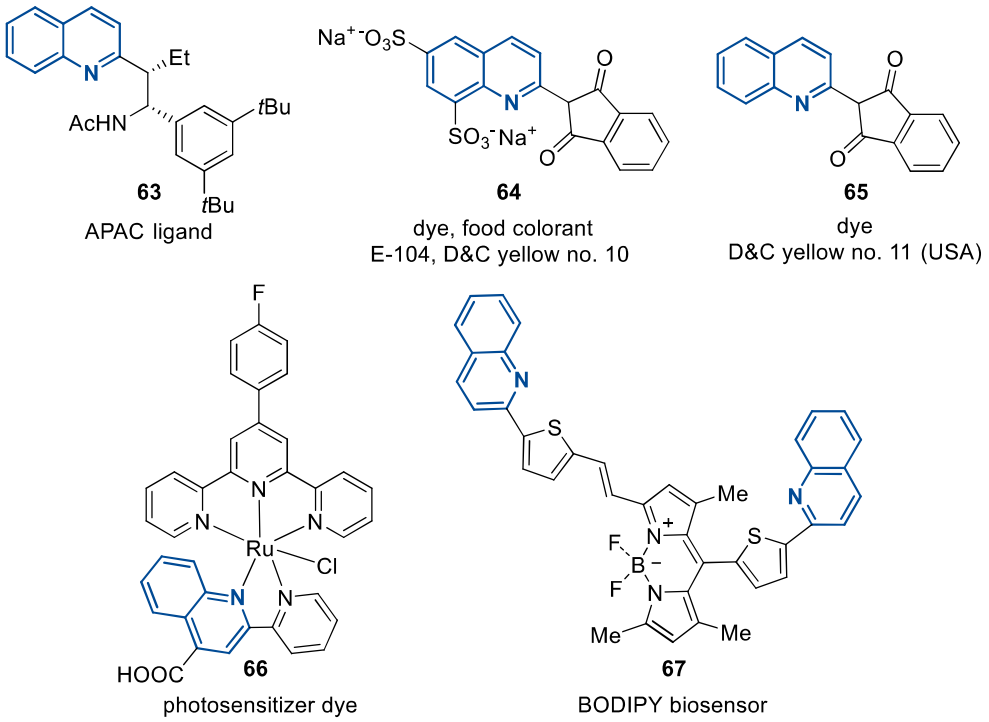

Figure 24.Representative examples of quinoline-containing compounds with chemical and industrial significance.

The quinoline scaffold in medicinal chemistry and pharmacology

Quinolines are structures of particular significance in the area of medicinal chemistry. In this sense, quinine (**58**, Figure 25) is the oldest known drug based on a quinoline scaffold and curiously, it is the origin of the name "quinoline". The first written reference of quinine dates from the XVII century, when in 1630 Spanish Jesuit missionaries established in South America reported the use of powdered cinchona bark to treat paludal fever. Historically, the native Indian population had used infusions of cinchona bark powder as an antimalarial medicine and they transferred this knowledge to the Spaniards to the extent that the Countess of Chinchón (Francisca Enríquez de Rivera), the wife of the Viceroy of Peru, was cured with cinchona. Later in 1640, she introduced the cinchone bark in Europe and in 1742, Linnaeus named the tree "*Cinchona officinalis*" and the whole genus thereof "*Cinchona*" in her honour (note the small misspelling by Linnaeus)[126]. Quinine alkaloid was firstly isolated in 1820 by J. Pelletier and J.B.

[125] Qu X, Bian Y, Li J, Pan Y, Bai Y. A red fluorescent BODIPY probe for iridium (III) ion and its application in living cells. *R Soc Open Sci*. 2019;6(1):181090. doi:10.1098/rsos.181090

[126] Bruce-Chwatt LJ. Three hundred and fifty years of the Peruvian fever bark. *Br Med J (Clin Res Ed)*. 1988;296(6635):1486-1487. doi:10.1136/bmj.296.6635.1486

Caventou from *Cinchona* spp. trees and aforementioned purified quinine replaced the classic bark powder. Quinine has been the only effective antimalarial agent until the 1920´s, when a new generation of synthetic quinine derivatives were developed, highlighting the launch of chloroquine **68** (Figure 25) in the 1940's and related analogues (*e.g.* hydroxychloroquine **69**, piperaquine **70**, mefloquine **71**, and primaquine **72**).

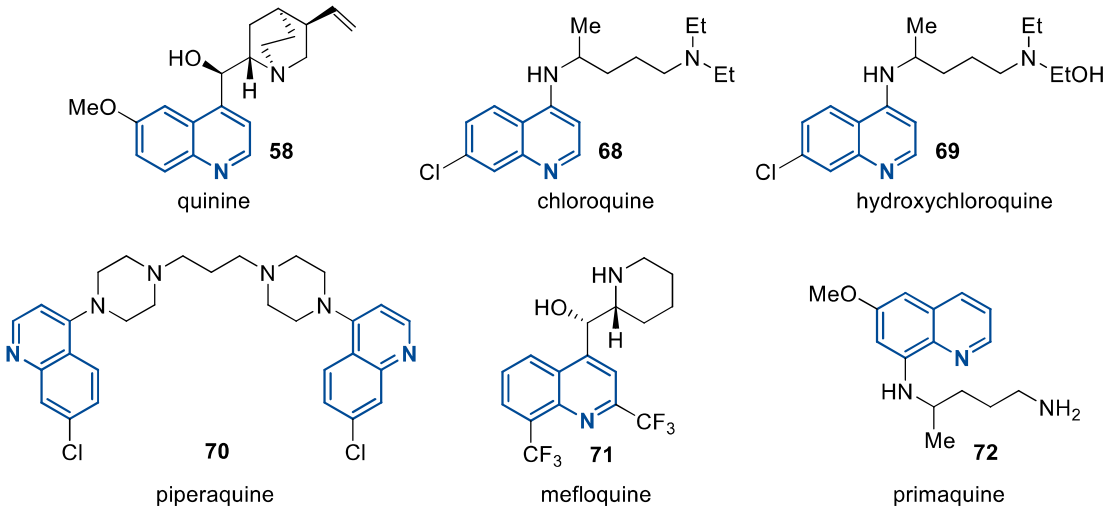

Figure 25. Quinoline core-based antimalarial agents.

It is noteworthy to mention that the pharmacological use of quinine remains nowadays, almost 400 years after the first proved historical evidence. At present, the main first line drugs for the treatment of malaria are chloroquine and artemisin derivatives, but quinine and chloroquine are indicated in some clinical situations such as drug resistance scenarios or pregnancy[127]. The mechanism of action of quinoline-based antimalarial drugs (quinine and synthetic derivatives) remains unclear, but is accepted that they accumulate into the food vacuoles and act by inhibiting the digestion of haemoglobin during the blood stages of malaria parasites, leading to parasite death[128]. Furthermore, chloroquine was revealed as an anti-inflammatory agent and is currently used in inflammatory rheumatic diseases such as rheumatoid arthritis or lupus erythematosus[129], and more recently has been tried as an antiviral agent to treat acute infections with SARS-CoV-2[130].

[127] WHO Guidelines for malaria. https://www.who.int/publications/i/item/guidelines-for-malaria. Accessed December 28, 2021

[128] Tse EG, Korsik M, Todd MH. The past, present and future of anti-malarial medicines. *Malar J*. 2019;18(1):93. doi:10.1186/s12936-019-2724-z

[129] Schrezenmeier E, Dörner T. Mechanisms of action of hydroxychloroquine and chloroquine: implications for rheumatology. *Nat Rev Rheumatol*. 2020;16(3):155-166. doi:10.1038/s41584-020-0372-x

[130] Touret F, de Lamballerie X. Of chloroquine and COVID-19. *Antiviral Res*. 2020;177:104762. doi:10.1016/j.antiviral.2020.104762

Besides antimalarial agents, the quinoline ring system is present in several other clinically approved drugs and the most representative examples are described herein (the chemical structures are collected in the Figure 26):

Pitavastatin (**73**, Figure 26) belongs to the drug class called statins, which act decreasing low-density lipoprotein cholesterol (LDL-C) levels *via* competitive inhibition of 3-hydroxy-3-methylglutaryl coenzyme A (HMG-Co-A)[131]. Pitavastatin was the latest statin launched to the market.

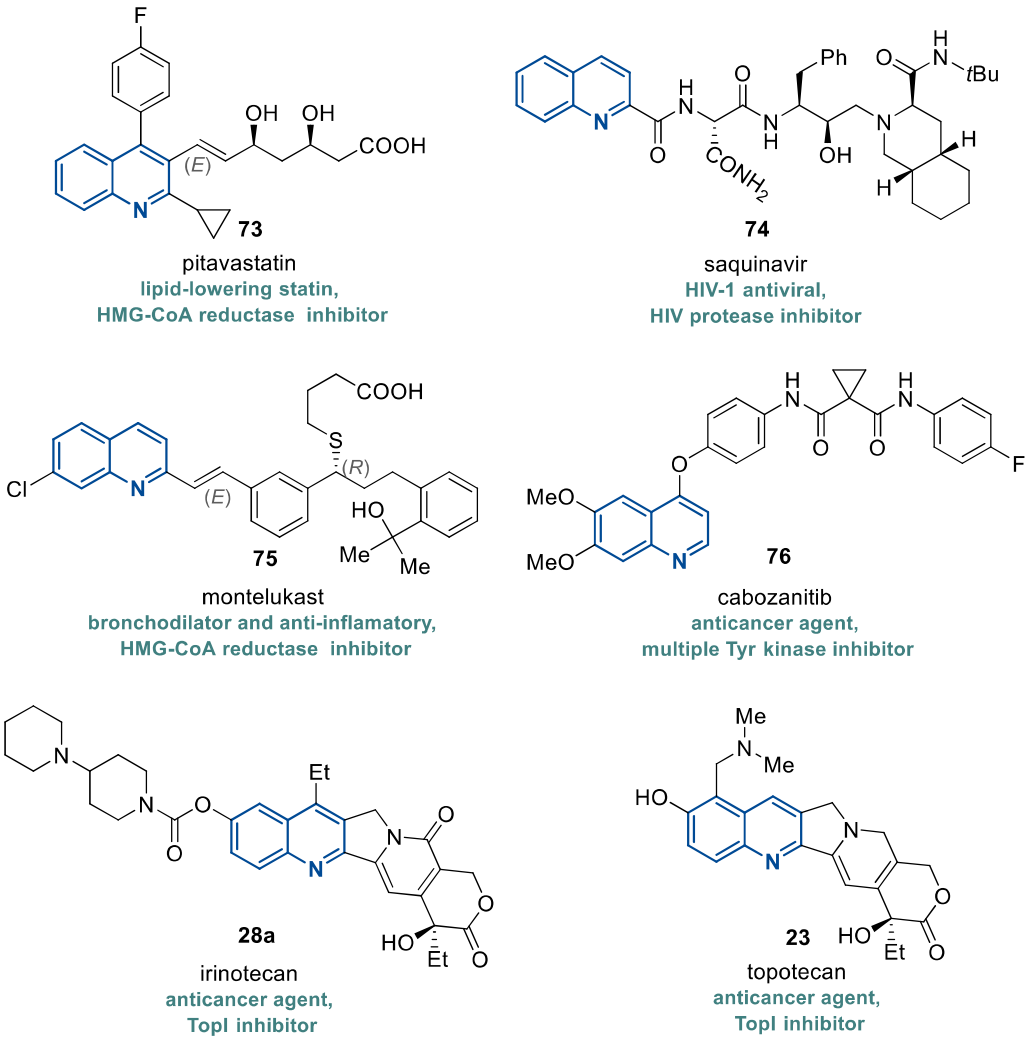

Figure 26. Clinically approved drugs based on a quinoline scaffold.

[131] Chan P, Shao L, Tomlinson B, Zhang Y, Liu ZM. An evaluation of pitavastatin for the treatment of hypercholesterolemia. *Expert Opin Pharmacother*. 2019;20(1):103-113. doi:10.1080/14656566.2018.1544243

Saquinavir (**74**) has been the first protease inhibitor approved for the treatment of HIV infection in 1995, acting as an inhibitor of HIV protease. Saquinavir showed a high affinity towards the HIV virus protease, with limited effect on human structurally related proteases[132].

Montelukast (**75**) is a cysteinyl leukotriene receptor 1 (CysLT1R) reversible antagonist[133], which has been widely used in asthma as a complementary drug in therapies involving inhalated corticosteroids or β-2 adrenergic agonists.

Cabozanitib (**76**) is a multikinase inhibitor used in metastatic renal cell carcinoma and medullary thyroid cancer[134]. More recently, it has been approved as a second line treatment for hepatocellular carcinoma by European Medicines Agency (EMA) and FDA in 2018 and 2019 respectively[135].

Irinotecan (**28a**) and topotecan (**23**) are TOP1 inhibitors currently used as a second-line chemotherapeutic agents in advanced cancers[4] (previously shown in section 1.3.2.1. of the introduction, Figure 10).

Besides clinically approved drugs including fully aromatic quinoline cores in their pharmacophore, there are some other therapeutic agents containing closely related quinoline derivative-scaffolds, mainly quinolones or hydrogenated forms of quinoline (Figure 27). This is the case of fluoroquinolones, a class of broad-spectrum bactericidal antibiotics currently used in respiratory, ocular and urinary tract infections (ciprofloxacin, levofloxacin and moxifloxacin, structures **77**, **78** and **79** in the Figure 27). Fluoroquinolones are selective inhibitors of the bacterial type II topoisomerases TopIV and DNA gyrase, causing the interruption of the DNA synthesis[136].

[132] la Porte CJ. Saquinavir, the pioneer antiretroviral protease inhibitor. *Expert Opin Drug Metab Toxicol*. 2009;5(10):1313-1322. doi:10.1517/17425250903273160

[133] Diamant Z, Mantzouranis E, Bjermer L. Montelukast in the treatment of asthma and beyond. *Expert Rev Clin Immunol*. 2009;5(6):639-658. doi:10.1586/eci.09.62

[134] Martínez Chanzá N, Xie W, Asim Bilen M, *et al.* Cabozantinib in advanced non-clear-cell renal cell carcinoma: a multicentre, retrospective, cohort study. *Lancet Oncol*. 2019;20(4):581-590. doi:10.1016/S1470-2045(18)30907-0

[135] Personeni N, Rimassa L, Pressiani T, Smiroldo V, Santoro A. Cabozantinib for the treatment of hepatocellular carcinoma. *Expert Rev Anticancer Ther*. 2019;19(10):847-855. doi:10.1080/14737140.2019.1674141

[136] Luan G, Drlica K. Fluoroquinolone-gyrase-DNA cleaved complexes. In: Drolet M, ed. *DNA topoisomerases: Methods and protocols.* New York, NY: Springer New York; 2018:269-281. https://doi.org/10.1007/978-1-4939-7459-7_19

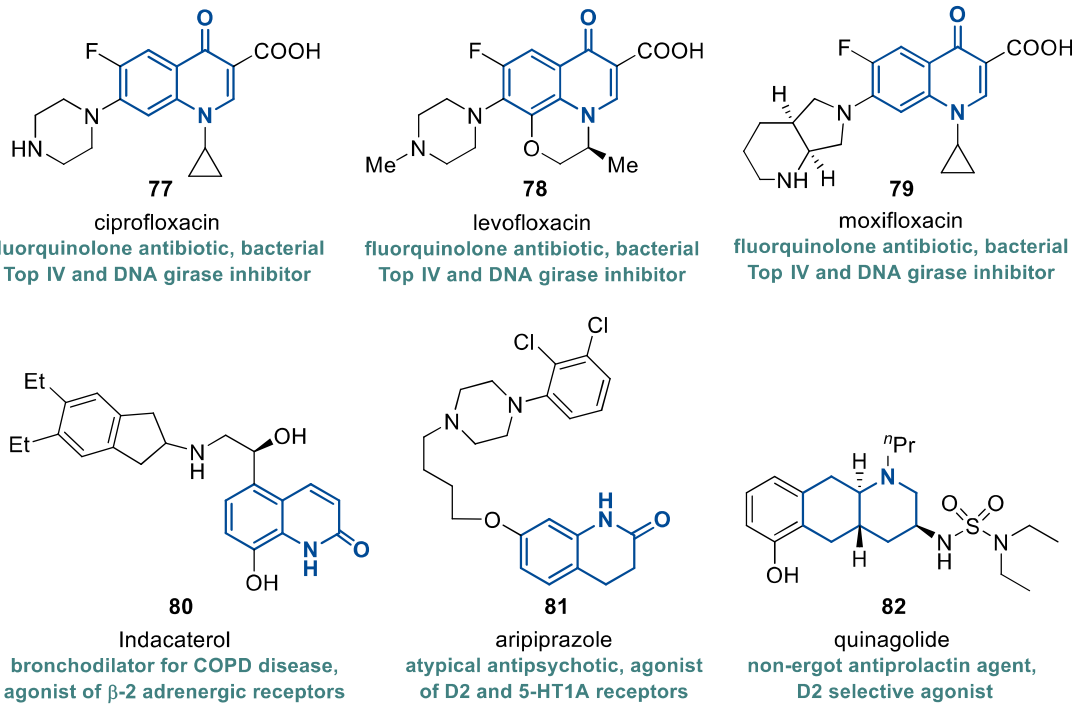

Figure 27. Other quinoline-derived scaffolds in clinically approved drugs.

Accordingly, indacaterol (**80**) is a 2-quinolone containing bronchodilator used for the treatment of COPD (Chronic Obstrucive Pulmonary Disease). Indacaterol acts as a ultralong-acting agonist of β-2 adrenergic receptors in the smooth muscle, allowing a daily administration regime[137].

Aripiprazole (**81**) is an atypical antipsychotic used in the treatment of schizophrenia, bipolar disorder, Tourette´s disorder, bipolar mania and depression. The antipsychotic effect of aripiprazole is due to the agonism of dopamine receptor D2 and serotonin type 1 receptor 5-HT1[138].

Quinagolide (**82**) is a non-ergot (non ergoline derivative) used in hyperprolactinemia therapy, acting as a selective agonist of dopamine D2 receptors at pharmaceutical concentrations[139].

[137] Rossi A, Polese G. Indacaterol: a comprehensive review. *Int J Chron Obstruct Pulmon Dis*. 2013;8:353-363. doi:10.2147/COPD.S21625

[138] Kinghorn WA, McEvoy JP. Aripiprazole: pharmacology, efficacy, safety and tolerability. *Expert Rev Neurother*. 2005;5(3):297-307. doi:10.1586/14737175.5.3.297

[139] Barlier A, Jaquet P. Quinagolide--a valuable treatment option for hyperprolactinaemia. *Eur J Endocrinol*. 2006;154(2):187-195. doi:10.1530/eje.1.02075

2.1. Major methods for the synthesis of quinolines

2.1.1. Metal-free synthesis of quinolines

2.1.1.1. Aniline-based conventional syntheses of quinolines

Conventional syntheses include the oldest and well established methods for the preparation of quinolines, from Skraup (1880) to Povarov (1963). These synthetic strategies revolve around nucleophile additions of primary (and in some cases secondary) amines to diverse electrophilic species (carbonyls, electron deficient alkenes such as β-carbon of α,β-unsaturated carbonyls etc.). In most of the conventional methods the synthesis is conducted by an aniline and an annulation partner which acts as electrophilic target (Scheme 2). The reaction undergoes a cyclization to yield the quinoline, but in some cases the annulation product is the non-aromatic dihydro/tetrahydroquinoline. These semi-hydrogenated derivatives can be further subjected to oxidation, which allows the formation of the corresponding aromatic quinoline.

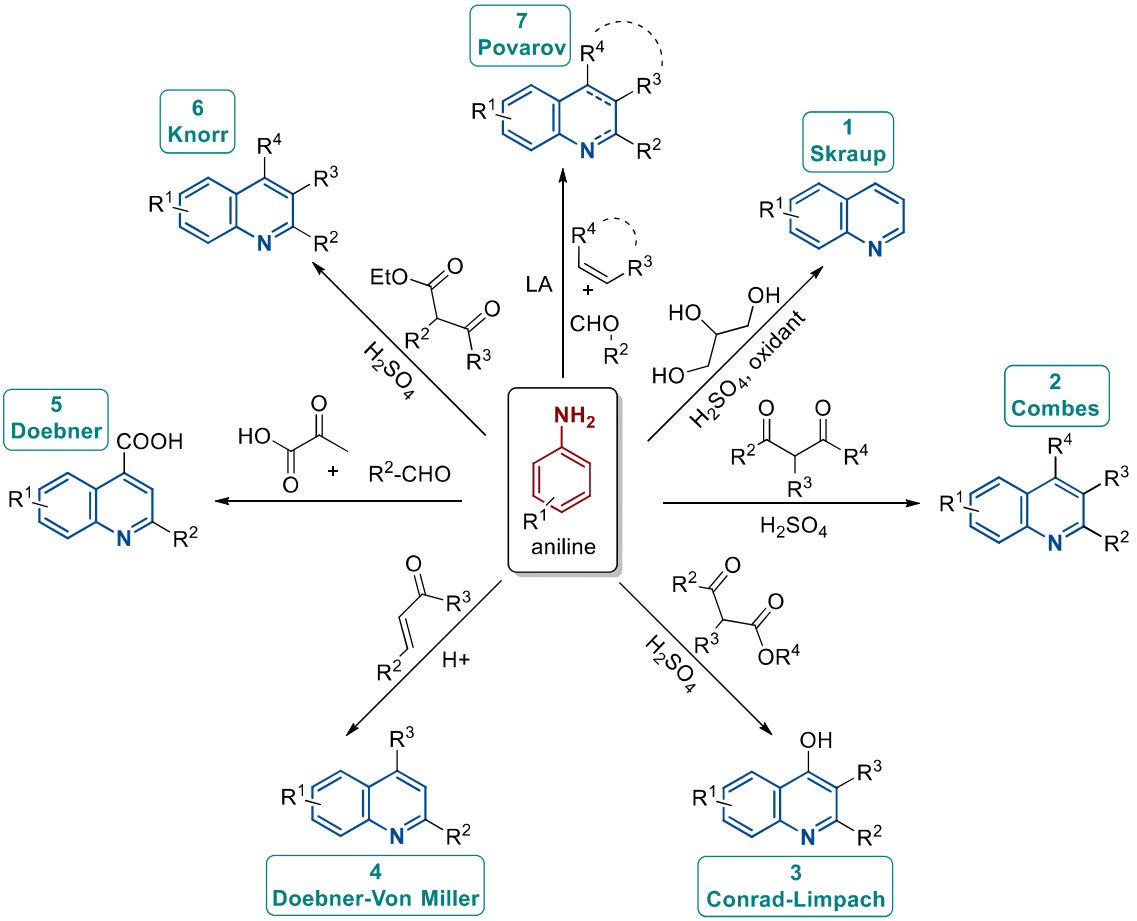

Scheme 2. Aniline-based conventional syntheses of quinolines.

Skraup (1) -1880-

In the Skraup synthesis of quinolines (route **1**, Scheme 2), primary anilines are heated with glycerol (even substituted glycerols) and a strong acid in the presence of an oxidant[140]. Acid-catalyzed dehydration of glycerol produces acroleine *in situ*, which receives a nucleophilic 1,4 addition of the aniline and cyclizates to form a hydroquinoline. In the last step, the hydroquinoline is converted to the quinoline by oxidation. Skraup´s route requires the use of a strong acid that may difficult the isolation of the final products from the crude and have to deal with low yields[141].

Combes (2) -1888-

Combes reported the synthesis of quinolines involving the acid-catalyzed condensation of β-diketones and aniline to form an enamine intermediate followed by a cyclization[142] (**2**, Scheme 2). The use of unsymetric β-diketones gives a mixture of regioisomers and it may complicate the separation process of the reaction products.

Conrad-Limpach (3) -1887-

Conrad and Limpach disclosed a straightforward route to afford quinolines substituted with a hydroxyl group in C4, *via* acid-catalyzed condensation of anilines with β-ketoesters followed by ring closure of the enamine intermediate[143] (**3**, Scheme 2). When the reaction is performed at high temperatures, it may derive to the Conrad-Limpach-Knorr quinolone synthesis obtaining the consequent quinol-4-one[144].

Doebner-Von Miller (4) -1881-

In 1881 Doebner and Von Miller disclosed an alternative method for the Skraup´s synthesis. In this procedure, anilines undergo annulation with α,β-unsaturated ketones or aldehydes in the

[140] 1. Manske RHF, Kulka M. The skraup synthesis of quinolines. *Org React*. 2011:59-98. https://doi.org/10.1002/0471264180.or007.02

[141] AlMarzouq DS, Elnagdi NMH. Glycerol and Q-Tubes: Green Catalyst and Technique for Synthesis of Polyfunctionally Substituted Heteroaromatics and Anilines. *Molecules*. 2019; 24(9):1806. https://doi.org/10.3390/molecules24091806

[142] Bergstrom FW. Heterocyclic nitrogen compounds. part IIA. hexacyclic compounds: Pyridine, quinoline, and isoquinoline. *Chem Rev*. 1944;35(2):77-277. https://doi.org/10.1021/cr60111a001

[143] Conrad M, Limpach L. Synthesen von chinolinderivaten mittelst acetessigester. *Chem Ber.* 1891; 24:2990. https://doi.org/10.1002/cber.188702001215

[144] Heindel ND, Bechara IS, Lemke TF, Fish VB. Cyclization of aniline-acetylenedicarboxylate adducts. improved synthesis of 8-nitro-2-carbomethoxy-4(1H)-quinolones. *J Org Chem*. 1967;32(12):4155-4157. https://doi.org/10.1021/jo01287a127

presence of an acid catalyst or iodine to afford the desired quinolines[145] (**4**, Scheme 2). More recent approaches involving Lewis acid catalysts, microwave (MW) irradiation and solvent free methods have led to a better scalability, higher yields and a considerable reduction of hazardous reagents[146].

Doebner (5) -1887-

Doebner synthesis involves the reaction of anilines with aldehydes and pyruvic acid under acidic conditions (**5**, Scheme 2), to afford 2-substituted quinolines with carboxylic acids in position 4[147]. Doebner´s method represents the first example of a multicomponent reaction for the synthesis of quinolines.

Knorr (6) -1886-

Knorr synthesis (**6**, Scheme 2) is conducted by condensation of anilines and β-ketoesters to obtain an anilide intermediate. In case of stable anilides, these could be isolated and used as precursors for the preparation of the corresponding quinolines. The reaction proceeds by an acidic dehydrogenation of the anilide and a subsequent cyclization to yield 2-hydroxyquinolines[148].

Povarov (7) -1963-

More recently, in 1963 Povarov disclosed a [4+2] cycloaddition between olefins and imines derived from anilines and aromatic aldehydes, obtaining 1,2,3,4-tetrahydroquinolines which could be dehydrogenated *in situ* to form the desired 2-, 3- and 4-substituted quinolines (**7**, Scheme 2). The Povarov reaction could be carried out in a multicomponent version, starting from aromatic aldehydes, anilines and the corresponding dienophile (usually alkenes, enol ethers or enamines)[149].

---

[145] Denmark SE, Venkatraman S. On the mechanism of the Skraup−Doebner−Von miller quinoline synthesis. *J Org Chem*. 2006;71(4):1668-1676. https://doi.org/10.1021/jo052410h

[146] Ranu BC, Hajra A, Dey SS, Jana U. Efficient microwave-assisted synthesis of quinolines and dihydroquinolines under solvent-free conditions. *Tetrahedron*. 2003;59(6):813-819. doi: https://doi.org/10.1016/S0040-4020(02)01587-9

[147] Nitidandhaprabhas O. Doebner's reaction with 6-methyl-2-amino pyridine. *Nature*. 1966;212(5061):504-505. https://doi.org/10.1038/212504b0

[148] Knorr L. Synthetische Versuche mit dem Acetessigester. *Justus Liebigs Ann Chem*. 1886;236:69-115. https://doi.org/10.1002/jlac.18862360105

[149] Povarov LS. αβ-Unsaturated ethers and their analogues in reactions of diene synthesis. *Russ Chem Rev*. 2007;36(9):656-670. doi: 10.1070/RC1967v036n09ABEH001680

2.1.1.2. Aniline derivatives-based conventional syntheses of quinolines

There are some other established methods based on aniline derivatives, mainly by using *o*-substituted anilines or 2,3-indolediones as precursors of anilines as presented in the Scheme 3:

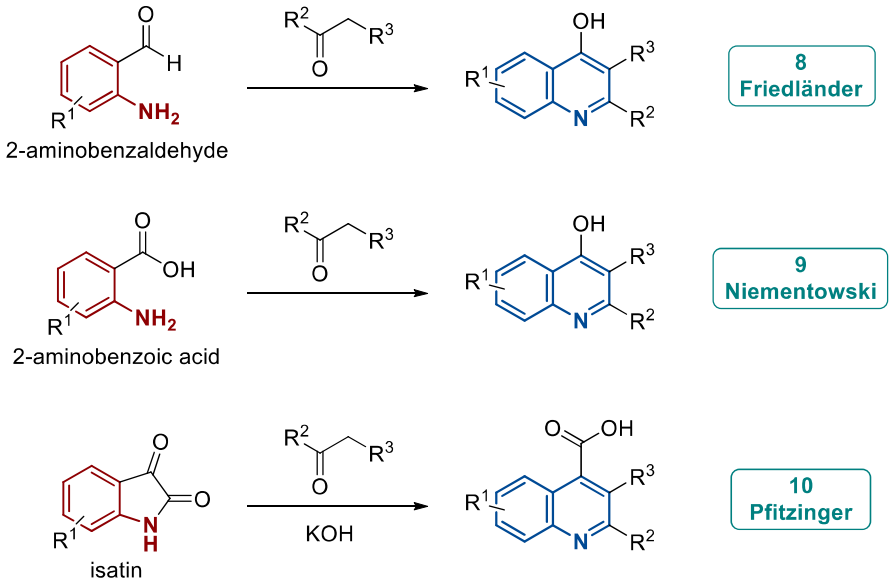

Scheme 3. Aniline derivatives-based conventional syntheses of quinolines.

Friedländer (8) -1882-

Friedlander reaction (**8**, Scheme 3) is a straightforward, simple and widely used method for the synthesis of quinolines in one step, and consists of an heteroannulation between 2-aminobenzaldehyde and carbonyl derivatives (mainly an aldehyde or a ketone) with at least one activated (electron deficient) α-methylene, upon aldolic condensation and subsequent cyclodehydration of the intermediate under both acidic or basic conditions[150].

Niementowski (9) -1894-

In 1894, Niementowski presented an extension of the Friedländer method involving a condensation of anthranilic acid derivatives (2-aminobenzoic acid) and carbonyls, affording 2- and 3- substituted 4-hydroxiquinoline derivatives[151] (**9**, Scheme 3).

[150] a) Friedländer P. Ueber o-Amidobenzaldehyd. *Ber Dtsch Chem Ges*. 1882;15:2572 b) Marco-Contelles J, Pérez-Mayoral E, Samadi A, Carreiras Mdo C, Soriano E. Recent advances in the Friedländer reaction. *Chem Rev*. 2009;109(6):2652-2671. doi:10.1021/cr800482c

[151] Niementowski S. Synthesen der Chinolinderivate. *Chem Ber*. 1894;27(2):1394–1403. doi:10.1002/cber.18940270242

Pfitzinger (10) -1886-

Pfitzinger´s method (**10**, Scheme 3) comprises a reaction between isatin (1*H*-Indole-2,3-dione) and a carbonyl derivatives with an activated α-carbon under strong basic conditions (mostly KOH or NaOH) to obtain quinoline -4-carboxilic acids (chinchoninic acids) substituted in positions 3 and 4. The base converts the isatin into isatinic acid, which condenses with the carbonyl, followed by an intramolecular cyclization to finally obtain the corresponding quinoline[152].

2.1.1.3. Catalyzed synthesis of quinolines

Until the very end of the XX century, only 2 main types of catalysts were available for organic synthesis, namely transition-metal catalysts and enzymes. It was then when B. List and D. MacMillan (Figure 28) independently disclosed a third class of catalysis: organocatalysis, *i.e*. the use of organic molecules to catalyse organic transformations and in particular, asymmetric synthesis. Technically, the use of organocatalysts dates back over a century when G. Bredig and W.S. Fiske used cinchona alkaloids to conduct an entioselective addition of hydrogen cyanide to aldehydes[118], but it was coined by List and MacMillan in the 1990´s. This discovery implied a chemical innovation and relaunched the field of enantioselective catalysis, providing to the chemists a precise, robust and environmentally friendly new approach for molecular construction beyond the metal-catalyzed chemistry. In 2021, List and MacMillan were awarded with the Nobel Prize in Chemistry "for the development of asymmetric organocatalysis" in recognition for their contribution to a more effective and sustainable organic chemistry[153]. Nowdays List and Macmillan still being references in asymmetric organocatalysis.

Figure 28. Benjamin List and David W.C. MacMillan

[152] Buu-Hoi N, Royer R, Xuong ND, Jacquignon P. The Pfitzinger reaction in the synthesis of quinoline derivatives. *J Org Chem*. 1953;18(9):1209-1224. https://doi.org/10.1021/jo50015a019

[153] The Nobel Prize. https://www.nobelprize.org/prizes/chemistry/2021/summary/ Accessed December 24, 2021

A selection of representative organocatalyzed syntheses of quinolines are shown thereupon, including organoacids (Lewis acids, *Brønsted acids), organobases (Lewis bases, Brønsted bases), chiral catalysts, atroposelective catalysts, aminoacids, triflates and ionic liquids.*

Acid-catalysts mediated synthesis of quinolines

The aforementioned conventional Skraup method for the synthesis of quinolines has to deal with the use of hazardous acids/oxidants, strong reaction environment and low to moderate yields. Several optimizations have been studied to improve the reaction rate and conditions. In 2014, Len *et al.* carried out an upgraded Skraup synthesis, which uses MW irradiation as source of heat[154]. In the same year, Hasan and collaborators developed an alternative Skraup procedure employing MW irradiation and ionic liquids as mild and environmentally friendly acidic organocatalysts to achieve 2,4-quinolines (Scheme 4). Ionic liquids (ILs) are systems of charged particles composed only by ions with melting point below 100ºC, and in this case, ILs allowed the Skraup synthesis of quinolines in the absence of any oxidant agent[155].

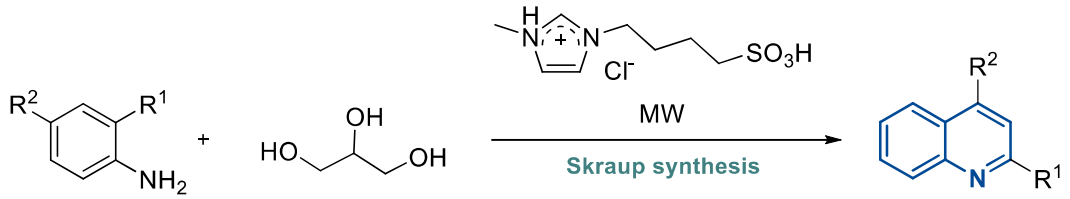

Scheme 4. Optimized Skraup method using MW irradiation and ionic liquids disclosed by Len et al.

The Friedländer reaction has been widely used for the simple and straightforward preparation of highly functionalized quinolines. In the last 2 decades, several optimizations have been studied in order to use mild conditions and components (specially non hazardous acids), solvent-free methodologies and recyclable organocatalysts, while rapid reaction rates and high yields are maintained. In 2010, Zhu *et al*. presented an indirect Friedländer synthesis of quinolines, employing 2-alkylvinyl anilines as precursors of 2-aminophenylketones[156]. *In situ* catalytic

[154] Saggadi H, Luart D, Thiebault N, Polaert I, Estel L, Len C. Quinoline and phenanthroline preparation starting from glycerol via improved microwave-assisted modified skraup reaction. *RSC Adv*. 2014;4(41):21456-21464. doi: 10.1039/C4RA00758A

[155] Amarasekara AS, Hasan MA. 1-(1-alkylsulfonic)-3-methylimidazolium chloride Brönsted acidic ionic liquid catalyzed skraup synthesis of quinolines under microwave heating. *Tetrahedron Lett*. 2014;55(22):3319-3321. doi: https://doi.org/10.1016/j.tetlet.2014.04.047

[156] Peng C, Wang Y, Liu L, Wang H, Zhao J, Zhu Q. P-toluenesulfonic acid promoted annulation of 2-alkynylanilines with activated ketones: Efficient synthesis of 4-alkyl-2,3-disubstituted quinolines. *Eur J Org Chem*. 2010;2010(5):818-822. https://doi.org/10.1002/ejoc.200901257

hydration of 2-alkylvinyl anilines with *p*-toluensulfonic acid (TsOH) and the following heteroannulation with activated ketones under acidic conditions provided the corresponding 2-, 3- and 4-substituted quinolines, as illustrated in the Scheme 5.

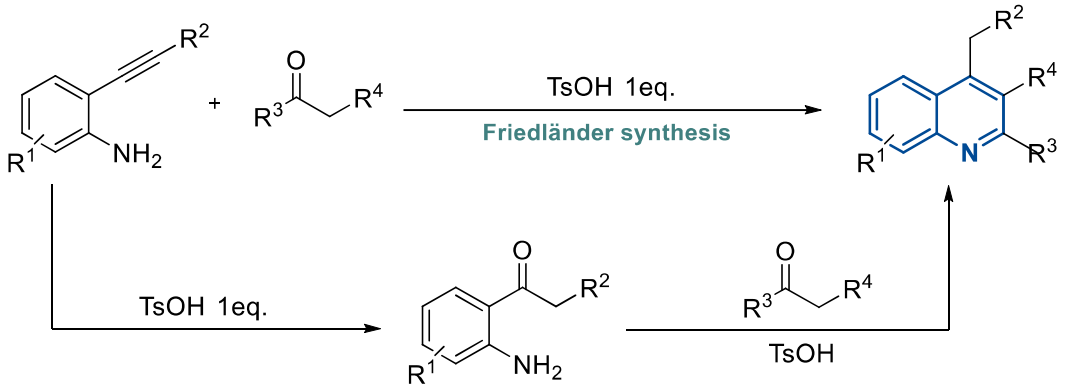

Scheme 5. Indirect Friedländer reaction presented by Zhu et al.

In the same year, Dughera and collaborators disclosed a Brønsted acid catalyzed version of the Friedländer reaction between 2-aminobenzophenones and activated carbonyls (Scheme 6)[157]. *o*-Benzenedisulfonimide was successfully employed as organocatalyst, which is additionally easily recoverable and it can be used in the following reactions.

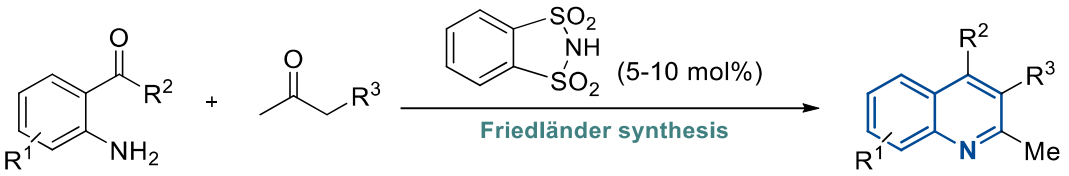

Scheme 6. Benzenedisulfonimide-catalyzed Friedländer reaction presented by Dughera et al.

Likewise, a solvent-free Friedländer approach for the preparation polysubstituted (2-, 3-, and 4-substituted) quinolines was presented by Singh and collaborators in 2017 (Scheme 7). The reactions were conducted by mildly heating 2-aminobenzophenones and carbonyls with an electron deficient α-methylene, under the presence of malic acid as organoacid catalyst[158].

[157] Barbero M, Bazzi S, Cadamuro S, Dughera S. O-benzenedisulfonimide as a reusable brønsted acid catalyst for an efficient and facile synthesis of quinolines via friedländer annulation. *Tetrahedron Lett*. 2010;51(17):2342-2344. doi: 10.1016/j.tetlet.2010.02.139

[158] Tufail F, Saquib M, Singh S, *et al.* Bioorganopromoted green Friedländer synthesis: A versatile new malic acid promoted solvent free approach to multisubstituted quinolines. *New J Chem*. 2017;41(4):1618-1624. doi: 10.1039/C6NJ03907C

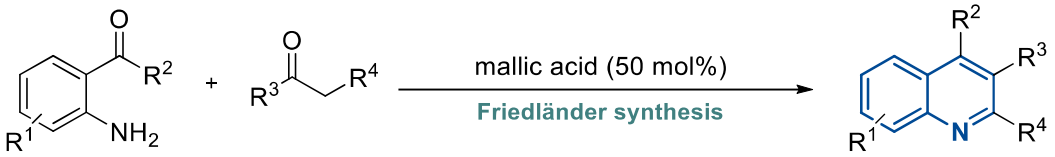

Scheme 7. Solvent-free Friedländer reaction disclosed by Singh et al.

Base-catalysts mediated synthesis of quinolines

In 2010, Zhu and collaborators disclosed a method for the preparation of 2-alcoxy-3-substituted quinolines by an intramolecular cyclization of *o*-alkynylaryl isocyanides catalyzed by DABCO (1,4-diazabicyclo[2.2.2]octane) (Scheme 8). The reaction undergoes by the dehydration of the corresponding *N*-formylamide precursor to yield *o*-alkynylaryl isocyanides, which are readily cyclizated in the presence of DABCO and oxygenated nucleophiles[159].

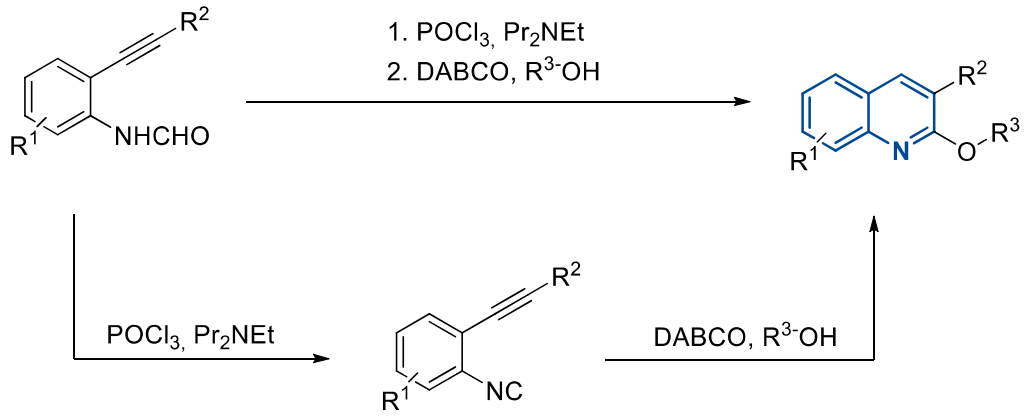

Scheme 8. DABCO catalyzed intramolecular cyclization of o*-alkynylaryl isocyanides presented by Zhu et al.*

Kwon and colleagues published a one-pot procedure to obtain 3-monosubstituted quinolines (Scheme 9), conducted by a triphenylphosphine catalyzed reaction of *N*-tosylated 2-aminobenzaldehydes and activated acetylenes (substituted with EWGs), followed by an aromatization of the dihydroquinoline intermediates by detosylation in aqueous HCl[160].

[159] Zhao J, Peng C, Liu L, Wang Y, Zhu Q. Synthesis of 2-alkoxy(aroxy)-3-substituted quinolines by DABCO-promoted cyclization of o-alkynylaryl isocyanides. *J Org Chem*. 2010;75(21):7502-7504. https://doi.org/10.1021/jo1017525

[160] Khong S, Kwon O. One-pot phosphine-catalyzed syntheses of quinolines. *J Org Chem*. 2012;77(18):8257-8267. doi: 10.1021/jo3015825

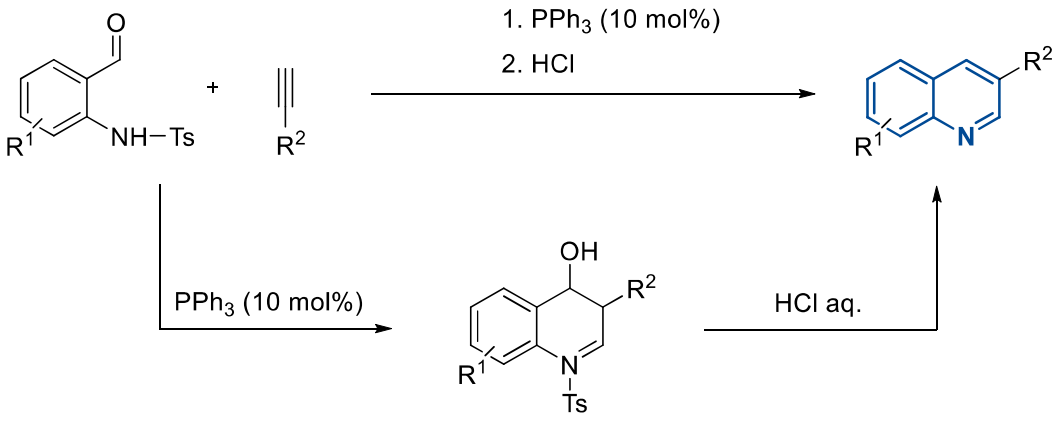

Scheme 9. Triphenylphosphine catalyzed heteroannulation between N-tosylated 2-aminobenzaldehydes and acetylenes outlined by Kwon et al.

In 2017, an alternative method for the Pfitzinger reaction organocatalyzed by CTAOH (cetyltrimethyl-ammonium hydroxide) was developed by Shankarling *et al*., involving the heteroannulation of isatins and ketones under mild basic and ultrasonic conditions[161] (Scheme 10). The combination of CTAOH and ultrasonic irradiation led to the formation of 2-substituted 4-carboxyl quinolines in high yields and fast reaction rates. Additionally, the surfactant character of CTAOH allows the use of water as the solvent as the reactants are solubilized in micelles.

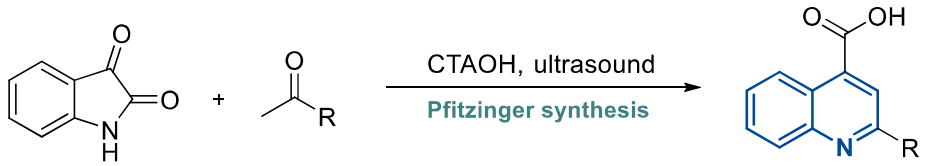

Scheme 10. CTAOH catalyzed Pfizinger reaction disclosed by Shankarling et al.

Organocatalysts mediated synthesis of quinolines

Besides catalysts based on their acidic/basic nature, there are some other strategies involving organocatalysis with natural occurring aminoacids as L-proline or organocatalyzed one-pot approaches of sequential/cascade reactions to afford the quinoline framework. In the present section, some representative examples will be exposed.

The study of L-proline in organocatalysis is an active area of research, either playing the role of the catalyst *per se* or acting as a ligand of a transition-metal catalyst. Proline is an accessible aminoacid available in both enantiomeric forms (L or R) and consequently, it has been widely

[161] More PA, Shankarling GS. Energy efficient Pfitzinger reaction: A novel strategy using a surfactant catalyst. *New J Chem*. 2017;41(21):12380-12383. http://dx.doi.org/10.1039/C7NJ01937H

used in asymmetric synthesis. Moreover, it is also considered a bifunctional organocatalyst as is composed of both acidic (carboxylate) and basic (secondary amine) moieties[162]. In 2012, Panahi and coworkers presented a L-proline-catalyzed multicomponent method for the synthesis of 2-amino-3-cyano-4-arylquinoline derivatives, involving a heteroannulation reaction between anilines, benzaldehydes and malononitrile (Scheme 11)[163].

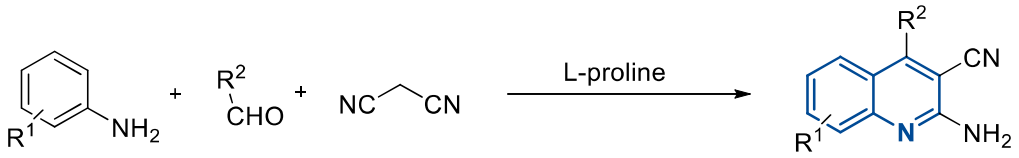

Scheme 11. L-Proline catalyzed multicomponent reaction disclosed by Panahi et al.

Likewise, one-pot cascade reactions stablish highly efficient straightforward synthetic methodologies. In this regard, Shi and collaborators presented a one-pot synthesis of 2- and 3-(di)substituted quinolines through a sequential Michael/Staudinger/aza-Wittig reaction[164] (Scheme 12). The process starts with a Michael addition of carbonyl derivatives to *o*-azido-β-nitrostyrenes, which is followed by a Staudinger reaction with triphenylphosphine and a subsequent intramolecular aza-Wittig reaction to yield the corresponding quinolines, upon dehydrogenation by releasement of nitromethane.

[162] Jarvo ER, Miller SJ. Amino acids and peptides as asymmetric organocatalysts. *Tetrahedron*. 2002;58(13):2481-2495. doi: https://doi.org/10.1016/S0040-4020(02)00122-9

[163] Khalafi-Nezhad A, Sarikhani S, Shahidzadeh ES, Panahi F. L-proline-promoted three-component reaction of anilines, aldehydes and barbituric acids/malononitrile: Regioselective synthesis of 5-arylpyrimido[4,5-b]quinoline-diones and 2-amino-4-arylquinoline-3-carbonitriles in water. *Green Chem*. 2012;14(10):2876-2884. doi: 10.1039/C2GC35765H

[164] Yu Z, Zheng H, Yuan W, Tang Z, Zhang A, Shi D. An unexpected one-pot synthesis of multi-substituted quinolines via a cascade reaction of Michael/Staudinger/aza-Wittig/aromatization of ortho-azido-β-nitro-styrenes with various carbonyl compounds. *Tetrahedron Lett*. 2013;69(38):8137-8141. doi: https://doi.org/10.1016/j.tet.2013.07.050

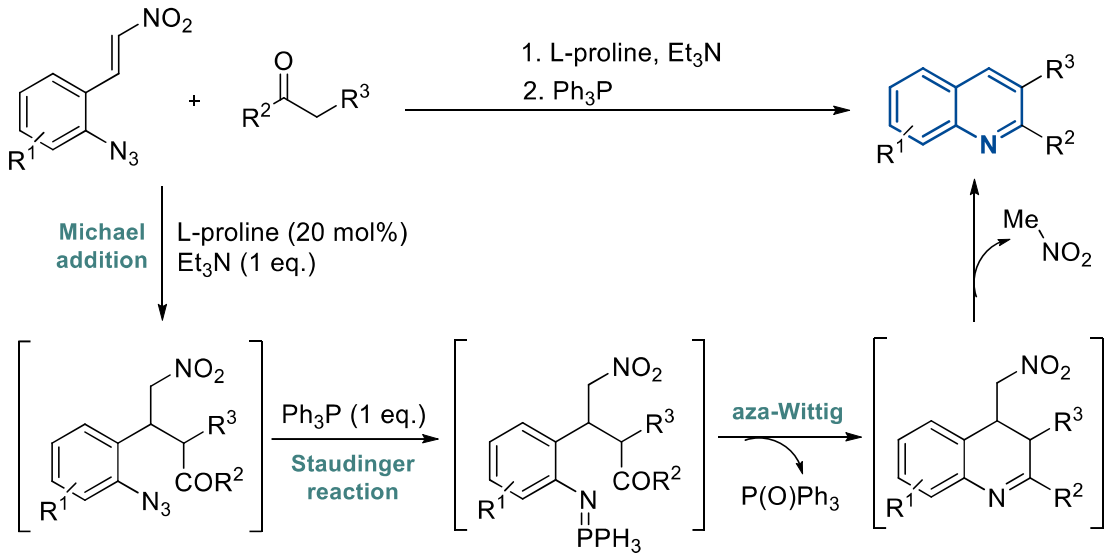

Scheme 12. L-Proline catalyzed Michael/Staudinger/aza-Wittig cascade reaction disclosed by Shi et al.

In 2019, Cheng and collaborators disclosed a one-pot atroposelective Friedländer synthesis of quinolines by annulation of α-aminoaryl ketones and β-dicarbonyl derivatives catalyzed by CPA (Chiral Phosphoric Acid), as illustrated in the Scheme 13. Axially chiral 4-arylquinolines were obtained in high yields and enantioselectivities (more than 90% in both cases), representing a remarkable application for the development of novel asymmetric catalysts[165].

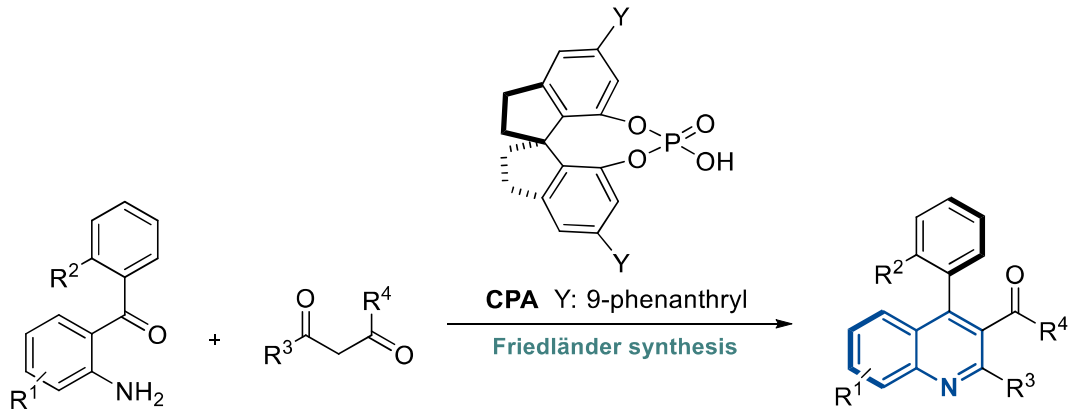

Scheme 13. CPA catalyzed one-pot atroposelective Friedländer reaction disclosed *by Cheng et al.*

[165] Shao Y, Dong M, Wang Y, Cheng P, Wang T, Cheng D. Organocatalytic atroposelective Friedländer quinoline heteroannulation. *Org Lett*. 2019;21(12):4831-4836. https://doi.org/10.1021/acs.orglett.9b01731

2.1.2. Metal catalyzed synthesis of quinolines

Transition-metal catalyzed coupling reactions provides rapid and robust tools to create or destroy single or multiple bonds in a unique synthetic operation. Accordingly, in the present section representative examples will be briefly exposed, involving transition metal salts or complexes to achieve highly functionalized quinolines by simple, quick and straightforward methodologies.

Transition-metal catalyzed Friedländer reactions

As shown in the previous section (2.2.1.), the development of modified Friedländer variations is thereby attracting increasing attention, and metal-catalyzed organic synthesis is not an exception. Two main strategies have been reported in the scientific literature:

A) Conventional Friedländer heteroannulation of 2-aminophenyl carbonyls with activated carbonyl derivatives (aldehydes or ketones) catalyzed by metals. Hence, an yttrium(III) triflate catalyzed Friedländer reaction at room temperature was described by Gibbs and collaborators in 2005[166] (Scheme 14, route **A**).

B) Oxidative and/or reductive Fiedländer approaches of unreactive Friedländer precursors (*e.g.* nitro groups that need to be converted into amino moieties by hydrogen transfer or alcohols that are oxidized to carbonyls). The metal catalyst plays a dual role: acts as an oxidant/reductant to transform the precursor into the reactive substrate, and additionally catalyzes the Friedländer reaction. This represents an interesting strategy due to a higher chemical stability of the precursors, which may be directly converted into quinolines in one unique action. In this regard, Miller *et al*. described a reductive Friedländer reaction between 2-nitrobenzaldehydes and enolizable carbonyls catalyzed by tin(II) chloride and zinc(II) chloride (Scheme 14, route **B**), which involves the reduction of the nitro derivative followed by a condensation in a single operation[167]. In the same way, Vander Mierde and collaborators disclosed an oxidative Friedländer variant of 2-aminobenzyl alcohol (which requires to be oxidized to the corresponding aldehyde form) with activated ketones, catalyzed by a second generation Grubbs catalyst and KO*t*Bu[168] (Scheme 14, route **C**). Wu *et al.* presented an oxidative/reductive Friedländer synthesis catalyzed by

[166] De SK, Gibbs RA. A mild and efficient one-step synthesis of quinolines. *Tetrahedron Lett*. 2005;46(10):1647-1649. doi: https://doi.org/10.1016/j.tetlet.2005.01.075

[167] McNaughton BR, Miller BL. A mild and efficient one-step synthesis of quinolines. *Org Lett*. 2003;5(23):4257-4259. doi:10.1021/ol035333q

[168] Vander Mierde H, Van Der Voort P, De Vos D, Verpoort F. A ruthenium-catalyzed approach to the Friedländer quinoline synthesis. *Eur J Org Chem*. 2008;2008(9):1625-1631. doi: https://doi.org/10.1002/ejoc.200701001

$Ru(PPh_3)_3Cl_2$ (Scheme 14, route **D**), in which the catalyst reduces the 2-nitrobenzaldehyde to 2-aminobenzaldehyde and also oxidizes the 2-aminobenzyl alcohol to the carbonyl form. Finally, Friedländer annulation leads to the desired quinolines[169].

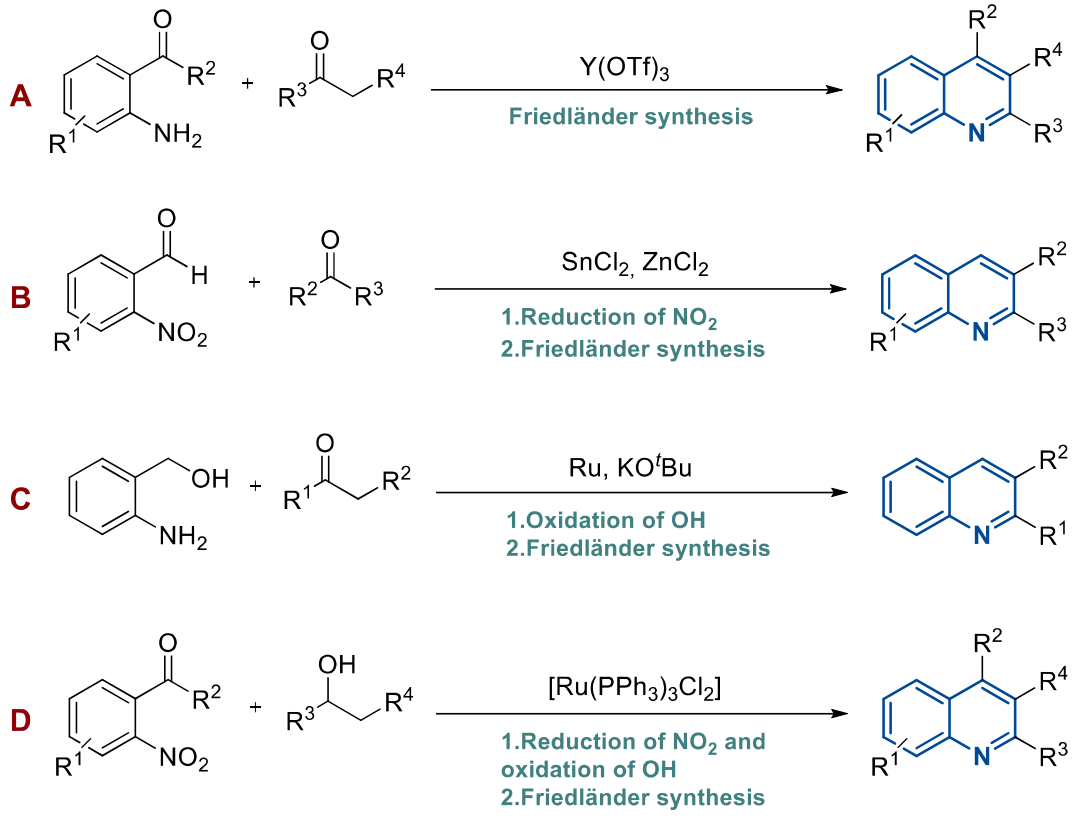

Scheme 14. Transition-metal catalyzed Fiedländer reactions.

Palladium(II), iron(III), zinc(II) and CuBr-ZnI₂ transition-metal catalyzed reactions

In 2014, Orellana *et al*. described a one-pot protocol to afford a series of 2- and 3-quinoline derivatives. Palladium catalyzed condensation between 2-bromoanilines and cyclopropanols and the subsequent oxidation of the cross-coupling products lead to the formation of the corresponding quinolines (Scheme 15, route **A**). Furthermore, 2-bromoaniline acts as the oxidant agent in the Pd catalyzed condensation-oxidation sequence and accordingly 2 equivalents thereof are required[170].

[169] Li H, Wang C, Zhu S, Dai C, Wu Y. Ruthenium(II)-catalyzed hydrogen transfer/annulation cascade processes between alcohols and 2-nitrobenzaldehydes. *Adv Synth Catal*. 2015;357(2-3):583-588. doi: https://doi.org/10.1002/adsc.201400898

[170] Nikolaev A, Nithiy N, Orellana A. One-step synthesis of quinolines via palladium-catalyzed cross-coupling of cyclopropanols with unprotected ortho-bromoanilines. *Synlett*. 2014;25(16):2301-2305. doi: 10.1055/s-0034-1378613

In the same way, Sun and co-workers reported an efficient one-pot quinoline synthesis *via* $Pd(OAc)_2$ catalyzed oxidative cyclization between anilines and aryl allyl alcohols[171] (Scheme 15, route **B**).

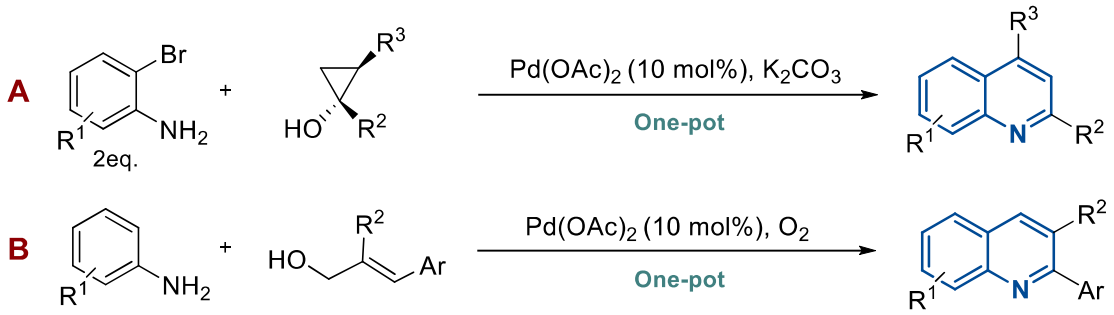

Scheme 15. Palladium(II) catalyzed synthesis of quinolines.

Liu and co-workers developed an iron(III) catalyzed oxidative cross coupling reaction of *N*-alkyl anilines with styrenes/acetylenes in the presence of di-tert-butyl peroxide [$(t\text{BuO})_2$] to generate 2,4-disubstituted quinolines[172] (Scheme 16).

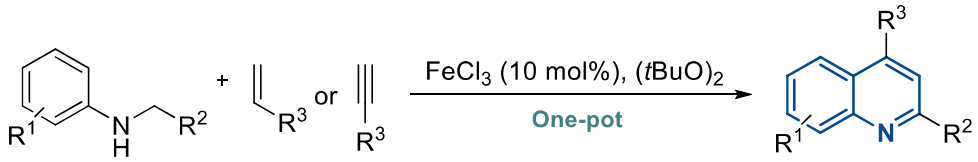

Scheme 16. Iron(III) catalyzed synthesis of quinolines disclosed by Liu et al.

A simple, efficient and solvent-free zinc(II) triflate catalyzed MCR method was disclosed by Chandak *et al*. in 2016. Anilines, aldehydes and acetylenes underwent a tandem condensation-cyclization reaction *via* $Zn(OTf)_2$ induced C-H activation to afford 2,4-disubstituted quinolines [173], as shown in the Scheme 17.

[171] Xu J, Sun J, Zhao J, Huang B, Li X, Sun Y. Palladium-catalyzed synthesis of quinolines from allyl alcohols and anilines. *RSC Adv*. 2017;7(58):36242-36245. doi: 10.1039/C7RA06425J

[172] Liu P, Li Y, Wang H, Wang Z, Hu X. Synthesis of substituted quinolines by iron-catalyzed oxidative coupling reactions. *Tetrahedron Lett*. 2012;53(49):6654-6656. doi: https://doi.org10.1016/j.tetlet.2012.09.090

[173] Sarode PB, Bahekar SP, Chandak HS. Zn(OTf)2-mediated CH activation: An expeditious and solvent-free synthesis of aryl/alkyl substituted quinolines. *Tetrahedron Lett*. 2016;57(51):5753-5756. doi: https://doi.org/10.1016/j.tetlet.2016.10.113

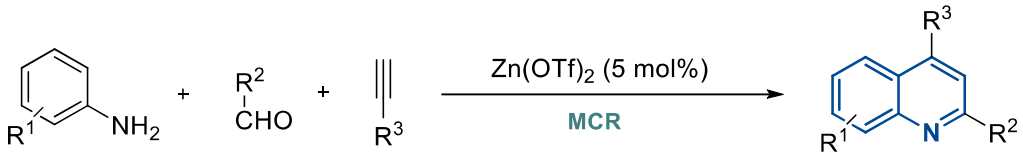

Scheme 17. Zinc(II) cayalyzed synthesis of quinoline presented by Chandak et al.

In 2016, Maiti and co-workers presented a solvent-free MCR approach *via* Zn(II)-Cu(I) combo-catalyzed oxidative cyclization of anilines, aldehydes and acetylenes to obtain 2,4-quinoline derivatives in moderate to high yields (61-82 %)[174] (Scheme 18).

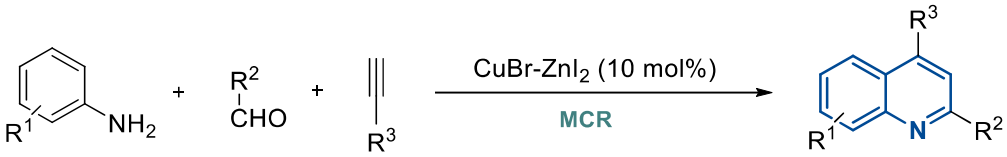

Scheme 18. Zinc-copper catalyzed oxidative MCR reaction disclosed by Maiti et al.

[174] Mondal RR, Khamarui S, Maiti DK. CuBr–ZnI2 combo-catalysis for mild CuI–CuIII switching and sp2 C–H activated rapid cyclization to quinolines and their sugar-based chiral analogues: A UV–Vis and XPS study. *ACS Omega*. 2016;1(2):251-263. doi: 10.1021/acsomega.6b00185

2.1.3. Miscellaneous methods for the synthesis of quinolines

Besides the expounded methods for the preparation of quinolines, there are some approaches that were not classified into the aforementioned categorization (namely conventional methods, acid/base/aminoacid catalyzed approaches and metal-catalyzed reactions) and some of the most representative examples are going to be exposed.

Halogen-catalyzed synthesis of quinolines

A solvent-free and bromodimethylsulfonium bromide (BDMS) catalyzed Fiedländer synthesis was published by Vittal Rao and collaborators in 2012. Heteroannulation of 2-aminoaryl ketones with enolizable ketones in the presence of 10 mol% BDMS (as bromine source) led to the formation of 2-, 3- and 4-substituted quinolines[175] (Scheme 19).

Scheme 19. Bromine catalyzed Fiedländer reaction disclosed by Vittal Rao et al.

Accordingly, Cheon and collaborators developed an iodide (I_2) catalyzed direct approach for the preparation of 2-quinoline derivatives[176]. Tetrabutylammonium iodide (TBAI) is used as source of I_2 and plays the role of a nucleophilic catalyst. The reaction proceeds *via* nucleophilic iodination to the electrophilic β-carbon of 2-aminostyryl ketones, leading to the formation of s-trans β-iodoketones, which undergo conformational change and sequential condensation-elimination of HI to yield the corresponding quinolines (Scheme 20).

[175] Venkatesham R, Manjula A, Vittal Rao B. (Bromodimethyl)sulfonium bromide catalyzed solvent-free Friedlander synthesis of substituted quinolines. *J Heteroc Chem*. 2012;49(4):833-838. doi: https://doi.org/10.1002/jhet.873

[176] Lee SY, Jeon J, Cheon C. Synthesis of 2-substituted quinolines from 2-aminostyryl ketones using iodide as a catalyst. *J Org Chem*. 2018;83(9):5177-5186. doi: 10.1021/acs.joc.8b00552

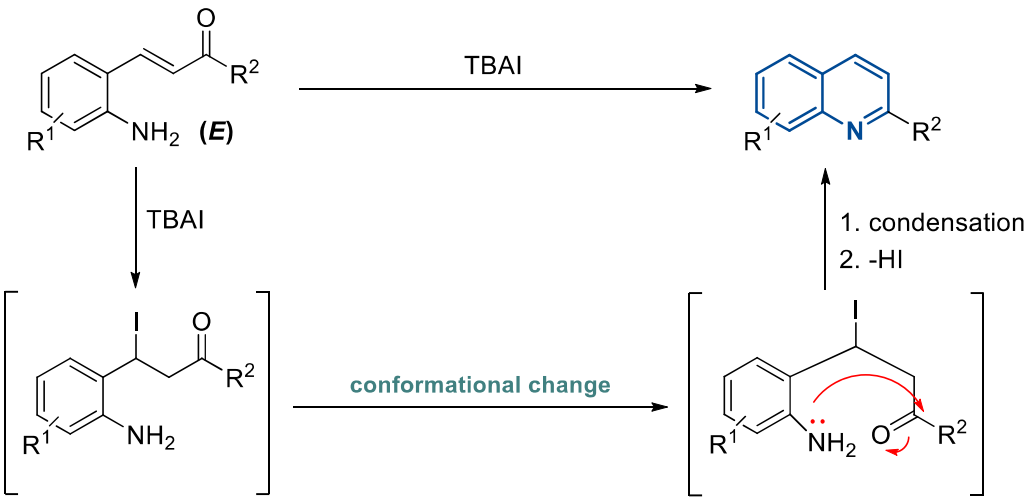

Scheme 20. Iodine catalyzed methodology presented by Cheon et al.

Radical-mediated synthesis of quinolines

Alternatively, radical-mediated heteroannulations suppose a straightforward approach to obtain quinolines with high atom (and step) economy. These transient and highly reactive radical intermediates are usually *is situ* generated by removing a hydrogen from the substrate with strong bases, peroxides or by switching the transition state of a metallic catalyst.

In 1984, Tundo and collaborators disclosed a direct method for the preparation of 2,4-disubstituted quinolines through a heteroannulation reaction between aryliminyl radicals and alkynes[177]. Aryliminium radicals were generated *in situ* from diaryl imines in the presence of DPDC (di-isopropyl peroxydicarbonate), which underwent a sequence of alkylation and cyclization to obtain the desired quinolines (Scheme 21). This represents a relatively ancient example that employs a highly explosive and hazardous peroxide (DPDC), but results illustrative of the radical-mediated approach. As time went on, safer methodologies with mild reaction conditions were disclosed and hence, some recent syntheses are going to be exposed.

[177] Leardini R, Pedulli GF, Tundo A, Zanardi G. Aromatic annelation by reaction of arylimidoyl radicals with alkynes: A new synthesis of quinolines. *J Chem Soc Chem Commun*. 1984(20):1320-1321. doi: 10.1039/C39840001320

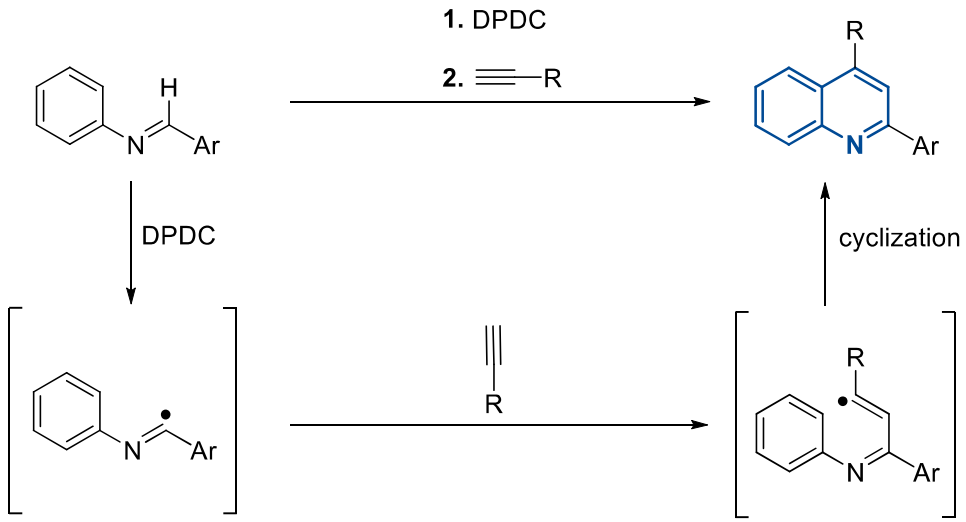

Scheme 21. Heteroannulation reaction between aryliminyl radicals and alkynes disclosed by Tundo et al.

In 2016, Li and co-workers developed an intramolecular oxidative radical heteroannulation of *o*-cyanoarylacrylamides and α-keto acids, using silver(I) nitrate (Scheme 22, route **A**) or potassium persulfate (route **B**) as oxidant agent. The reaction proceeds *via* an addition/cyclization cascade to obtain 3-carboxyl-2,4-quinolines in moderate to high yields[178].

Likewise, in 2020 Mei, Zhu, Han and collaborators presented an oxidative radical reaction between *o*-cyanoarylacrylamide and aromatic thiols in the presence of DCP (dicumyl peroxide), to afford 3-thiomethylated 2,4-quinolones (Scheme 22, route **C**) [179].

[178] Wang S, Fu H, Shen Y, Sun M, Li Y. Oxidative radical addition/cyclization cascade for the construction of carbonyl-containing quinoline-2,4(1H,3H)-diones. *J Org Chem*. 2016;81(7):2920-2929. doi: 10.1021/acs.joc.6b00210

[179] Yin Z, Yu Y, Li C, Mei H, Zhu K, Han J. Sulfuration-triggered radical cyclization of o-cyanoarylacrylamides to 3-thiomethylated quinoline-2,4-dione. *ChemistrySelect*. 2020;5(46):14534-14537. https://doi.org/10.1002/slct.202003999

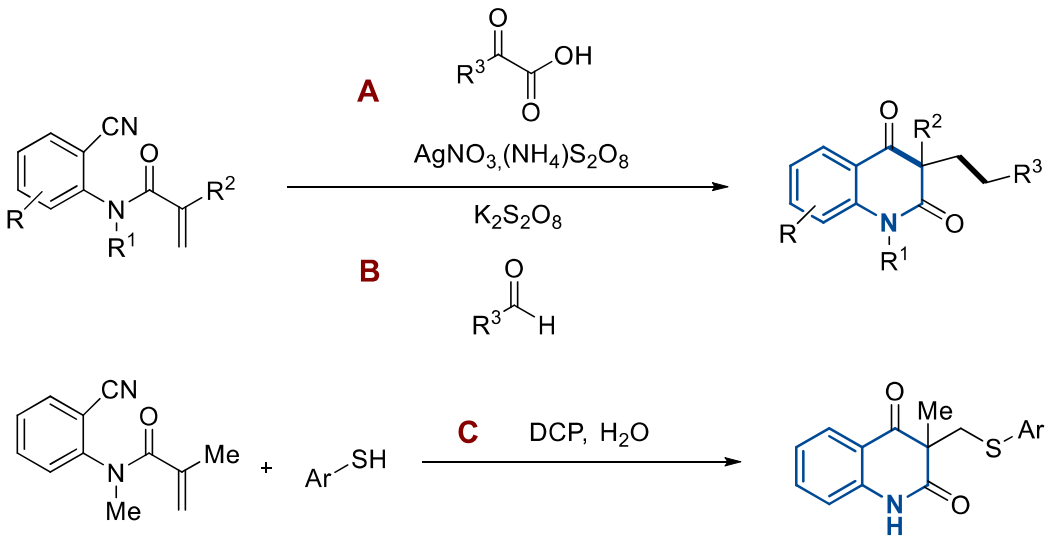

Scheme 22. Oxidative radical heteroannulation reactions for the synthesis of quinolines.

In 2013, Zhou and collaborators disclosed a method for the preparation of 2,4-quinolines *via* visible light induced radical cyclization of trifluoroacetimidoyl chlorides with acetylenes, in the presence of tris(bipyridine)ruthenium(II) chloride as a photocatalyst (Scheme 23, above)[180]. Likewise, in 2018 Yu *et al.* described a reaction for the preparation of quinolines. A visible light photocatalyzed intramolecular reaction of aryliminyl radicals leads to the formation of 2-quinolines and fused derivatives (Scheme 23, below)[181].

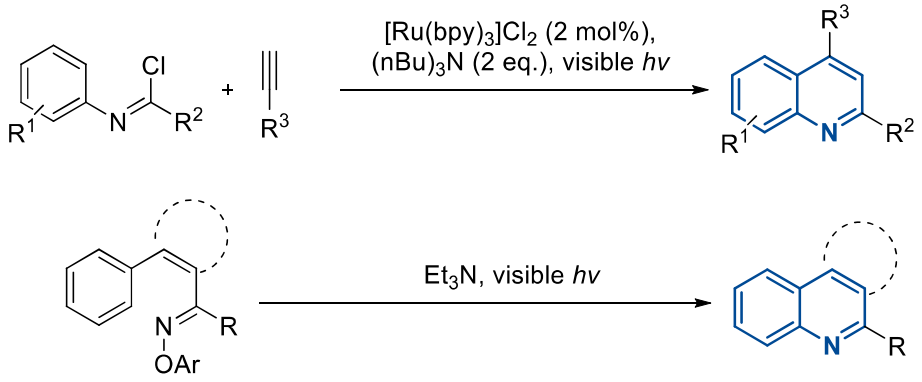

Scheme 23. Visible light-catalyzed methods for the synthesis of quinolines.

[180] Dong X, Xu Y, Liu JJ, Hu Y, Xiao T, Zhou L. Visible-light-induced radical cyclization of trifluoroacetimidoyl chlorides with alkynes: Catalytic synthesis of 2-trifluoromethyl quinolines. *Chem Eur J*. 2013;19(50):16928-16933. https://doi.org/10.1002/chem.201303149

[181] Sun J, He Y, An X, Zhang X, Yu L, Yu S. Visible-light-induced iminyl radical formation via electron-donor–acceptor complexes: A photocatalyst-free approach to phenanthridines and quinolines. *Org Chem Front*. 2018;5(6):977-981. doi: 10.1039/C7QO00992E

3. Objectives

Herein are collected the main objectives of the present work:

-Synthesis of hybrids of quinoline derivatives and pentavalent organophosphorus moieties as candidates for small-molecule-like TOP1 inhibitors with potential applications as antiproliferative and antileishmanial agents.

-Study of the Povarov reaction for the obtainment of a small compound library of hybrid phosphorated quinoline derivatives with pharmacologically interest/potential: based on the retrosynthetic pathway shown in the Figure X, both step-by step and MCR one-pot methodologies are going to be investigated for the Povarov reaction between phosphorated aldimines (derived from phosphoated aldimines and benzaldehydes) and styrene/acetylene. Furthermore, the versatility of the Povarov reaction is going to be exploited for the access to the quinoline framework fused with indene (indeno[2,1-*c*]quinoline core) with a higher molecular complexity by using indene as the dienophile.

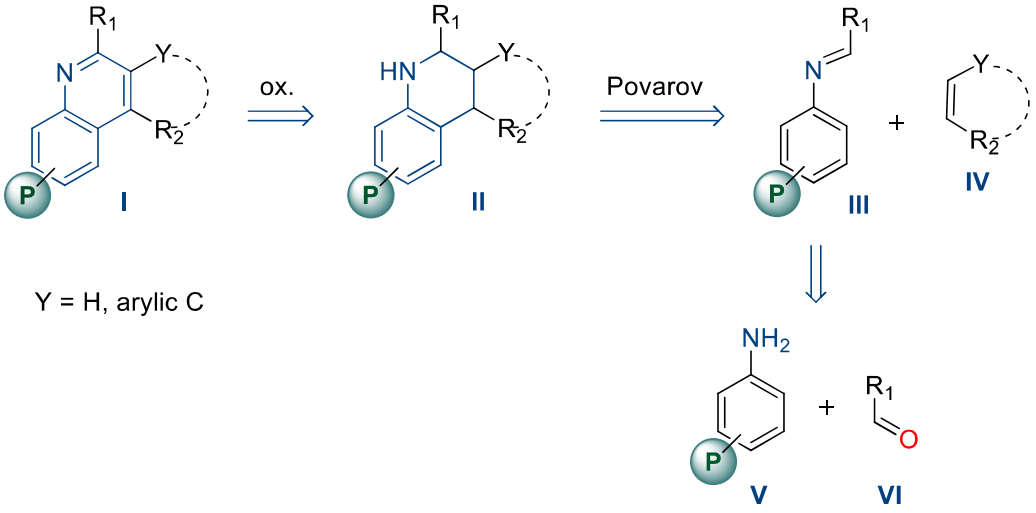

Proposed retrosynthetic analysis of the hybrid phosphorated quinoline (I) and tetrahydroquinoline (II) derivatives.

-Biological evaluation of the newly synthesized hybrid phosphorated quinoline derivatives as hTOP1B inhibitors *in vitro* and further mechanistic studies to elucidate the mode of action of the potential TOP1 inhibitory activity (essentially, discern between *poison*-like or *suppressor*-like TOP1 inhibitors).

-Development of novel quantitative and reliable *in vitro* drug-screening methods in order to evaluate the TOP1 inhibitory activity and further study which steps of the TOP1 catalytic cycle are affected by the potential drug.

-Biological evaluation of the novel hybrid phosphorated quinoline derivatives as antiproliferative agents in human cancer cell lines *in vitro* (and a non-cancer cell line as a control).

-Biological evaluation of the novel phosphorated quinolines as antileishmanial agents and leishmanial TOP1B (LTOP1B) inhibitors.

Chapter I. Synthesis of phosphorated quinoline derivatives by the [4+2] Povarov reaction

I-1. The role of phosphorus in medicinal chemistry and drug discovery

Phosphorus (P) is categorized into the "CHNOPS" group as one of the six vital elements for life, being the phosphate group the most representative form in biology. Phosphate is indispensable in all the (modern) forms of live. Phosphates are present in nucleotides and consequently in nucleic acids, being part of the phosphate backbone that provides structural support to DNA and RNA. Phospholipids play a key role in cell structure, cell-signalling and as a reservoir of biomolecules. Likewise, phosphorus results fundamental in coenzymes such as adenosine triphosphate (ATP, Figure 29), the primary carrier of energy in cells, in which the energy needed for biochemical reactions is stored in the phosphodiester bonds of the triphosphate nucleotide[182]. A substantial part of biochemical reactions involves transformations with phosphate (and its corresponding esters) as substrates or ligands**,** including the biosynthetic pathways of nucleotides, oligonucleotides, proteins, carbohydrates or lipids, along with others[183].

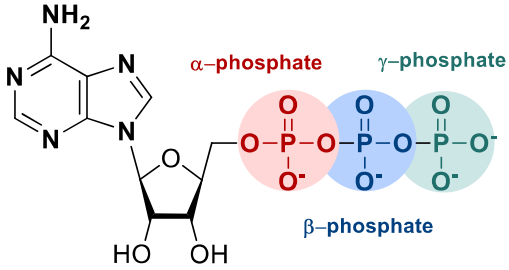

Figure 29. Structure of the ATP molecule.

Besides its relevance in biochemistry, applications of P-containing molecules have been broadly studied in many different fields such as agriculture (insecticides), ecology (fertilizers), food industry, metallurgy or pharmaceutical research (drugs)[182].

Phosphorus in medicinal chemistry and drug discovery

Phosphorus-containing drug discovery constitutes an attractive area of research in medicinal chemistry. On the one hand, phosphorus(III) containing moieties (see Table 1) possess a lone electron pair in the P atom, which confers a high reactivity and a strong coordination capacity, and therefore, the research of organophosphorus drugs is mainly focused on more stable

[182] Pasek M. A role for phosphorus redox in emerging and modern biochemistry. *Curr Opin Chem Biol*. 2019;49:53-58. doi:10.1016/j.cbpa.2018.09.018

[183] Knouse KW, Flood DT, Vantourout JC, *et al.* Nature Chose Phosphates and Chemists Should Too: How Emerging P(V) Methods Can Augment Existing Strategies. *ACS Cent Sci*. 2021;7(9):1473-1485. doi:10.1021/acscentsci.1c00487

phosphorus(V) containing functional groups. Thus, the vast majority of clinically accepted drugs contain pentavalent P functionalities (see Table 2) such as phosphate/phosphonate, phosphinate/phosphine oxides, the corresponding esters and amides, and even S or halogen containing analogues[184].

Table 1. Principal P(III)-based organophosphorus functionalities.

Phosphite 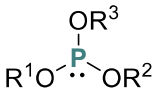	**Posphoramidite** 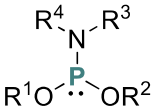	**Phosphorothioite** 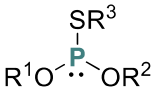
Phosphonite 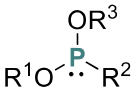	**Posphonamidite** 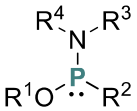	**Phosphonothioate** 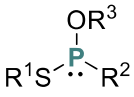
Phosphinite 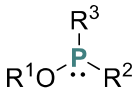	**Posphinamidite** 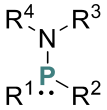	**Thiophosphine** 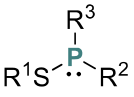
Phosphine (3ary) 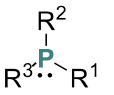	**Phosphine (3ary)** 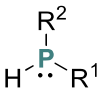	**Phosphine (3ary)** 

[184] Yu H, Yang H, Shi E, Tang W. Development and Clinical Application of Phosphorus-Containing Drugs. *Med Drug Discov*. 2020;8:100063. doi:10.1016/j.medidd.2020.100063

Table 2. Principal P(V)-based organophosphorus functionalities.

Phosphate 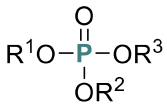	**Posphoroamidate** 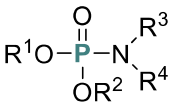	**Phosphorothiate** 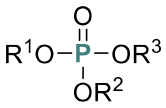	**Tiophosphate** 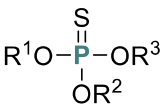
Phosphonate 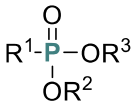	**Posphonamidate** 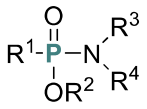	**Phosphonothioate** 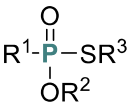	**Thiophosphonate** 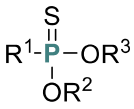
Phosphinate 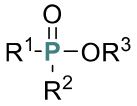	**Posphinamidate** 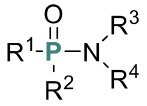	**Phosphonothioate** 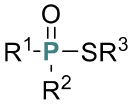	**Thiophosphinate** 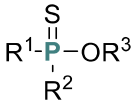
Phosphine oxide 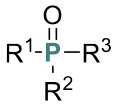	**Phosphine sulfide** 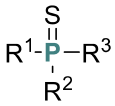	**Phosphonium ylide** 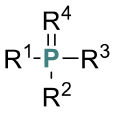	**Phosphorane** 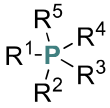

Phosphorus containing isosteres may be used to replace a similar moiety of an active molecule and modify the biological activity. For instance, isosters of neurotransmitters γ-aminobutiric acid (GABA) and glutamic acid bearing phosphonic/phosphinic acid instead of carboxylic acid resulted in a substantial modification of pharmacodynamic properties: even the affinity was generally maintained, intrinsic activity and selectivity varied considerably. In this regard, the natural ligand GABA (**83**, Figure 30) is a well-known agonist for $GABA_A$ and $GABA_B$ receptors, but the replacement of the carboxylate by mono/di-alkylphosphine moieties **84** gave place to a potent and selective agonist effect towards $GABA_B$ metabotropic receptors[185]. Likewise, L-glutamic acid (**85**, Figure 30) is an endogenous agonist for both metabotropic (mGluR) and ionotropic (iGluR) receptors while the corresponding phosphonate isostere **86** selectively activates group III mGluRs[186].

[185] Froestl W, Mickel SJ, Hall RG, *et al.* Phosphinic acid analogues of GABA. 1. New potent and selective GABAB agonists. *J Med Chem*. 1995;38(17):3297-3312. doi:10.1021/jm00017a015

[186] Watkins JC, Krogsgaard-Larsen P, Honoré T. Structure-activity relationships in the development of excitatory amino acid receptor agonists and competitive antagonists. *Trends Pharmacol Sci*. 1990;11(1):25-33. doi:10.1016/0165-6147(90)90038-a

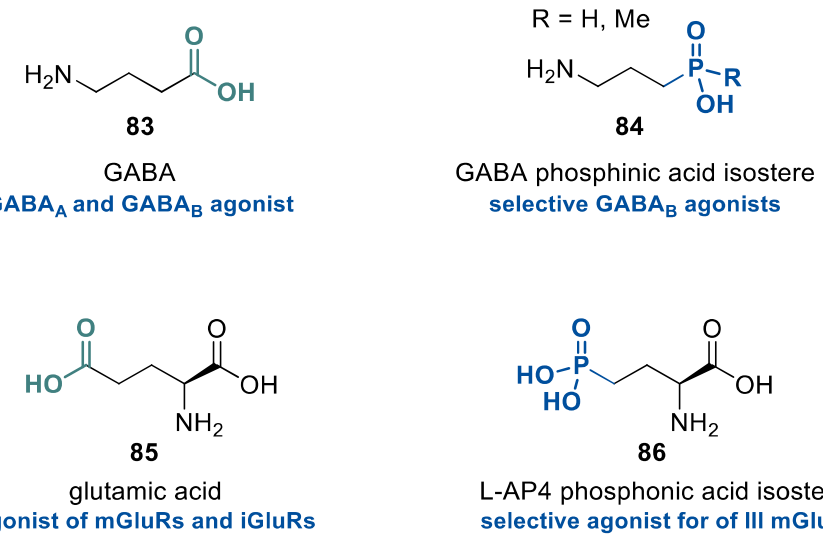

Figure 30. Structures of the neurotransmitters GABA and glutamic acid, along with their corresponding phosphinic/phosphonic acid isosteres.

I-1.1. Phosphorus-based transition state intermediate analogues

From a biochemical perspective, enzymes are proteins that catalyze specific chemical reactions in living organisms by substantially accelerating the conversion of substrates (S) into products (P) without being themselves consumed or permanently altered. Catalysis mediated increment of the reaction rate arises from a decrease in the activation energy of the reaction, and this fact can be explained by the transition-state theory postulated by Pauling[187]. During the progress of a reaction, the transition-state represents a temporary and short-living configuration with the highest value of free-energy[188]. Pauling proposed that the reaction rate of an enzymatic activity is determined by the degree of the enzyme-transition-state complex stability (a higher stability leads to a faster reaction), and in this regard, enzymes act by stabilizing these transition-state complexes (see the diagram depicted in Figure 31)[189]. Accordingly, surrogates that stabilize the transition-state complex with a higher affinity than intrinsic ligands are known as transition-state analogues that present a higher affinity towards the enzyme, resulting in A) potent enzymatic inhibitors (drug candidates) or B) robust tools for structural, mechanistic and kinetic studies of the respective enzymatic activity.

[187] Pauling L. Nature of forces between large molecules of biological interest. *Nature*. 1948;161(4097):707-709. doi:10.1038/161707a0

[188] Schramm VL. Enzymatic transition state theory and transition state analogue design. *J Biol Chem*. 2007;282(39):28297-28300. doi:10.1074/jbc.R700018200

[189] Pauling L. Molecular Architecture and Biological Reactions. *Chem Eng News*. 1946;24:1375

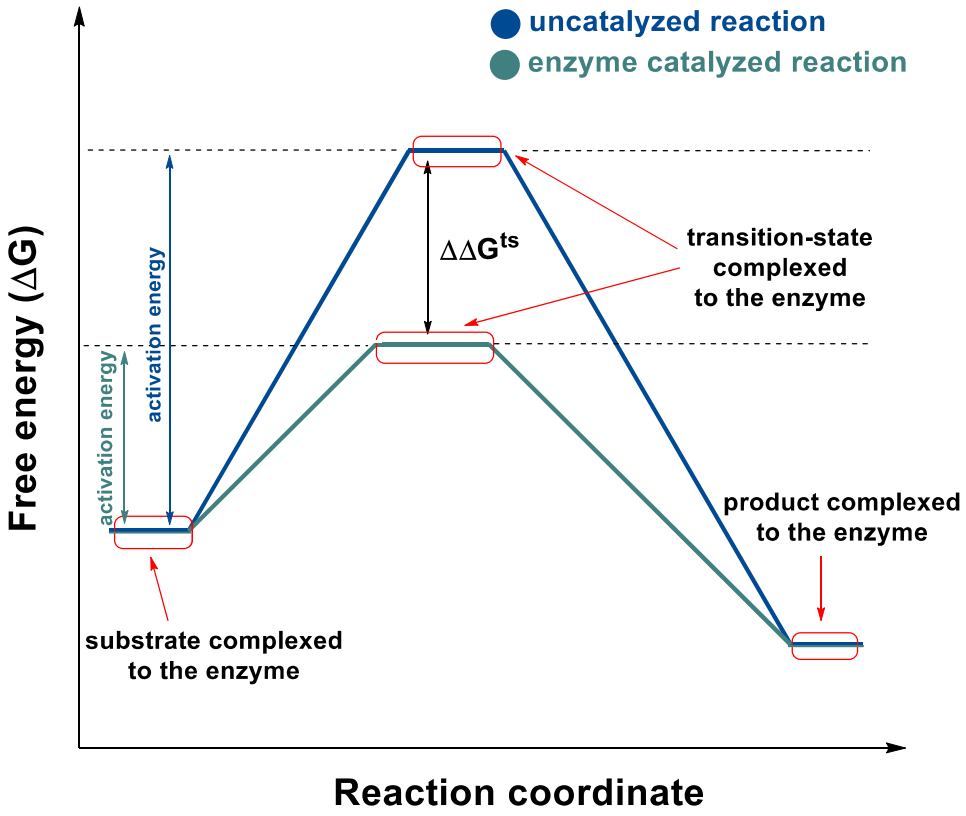

Figure 31. Energy diagram showing how the activation energy needed for a chemical reaction (conversion of the substrate/s into a product) is reduced when an enzyme stabilizes the transition-state intermediate.

Over the last 50 years phosphorated transition-state analogues have been successfully explored in medicinal chemistry. For instance, Gobec and collaborators presented a set of phosphonate containing transition-state analogues of antigen 85C, an enzyme of *Mycobacterium Tuberculosis* with mycolyltransferase activity (Figure 32)[190]. Antigen 85C is a protein complex that catalyzes the transfer of mycolic acid from one molecule of α,α'-trehalose monomycolate (TMM) to another TMM, leading to the formation of α,α'-trehalose dimycolate (TDM), essential step for the cell wall synthesis[191]. The tetrahedral phosphonate transition-state analogue shown in Figure 32 was found to stabilize more efficiently the transition-state of the reaction catalysed by antigen 85 C than the intrinsic trehalose, therefore resulting in a high affinity and strong inhibition of the enzyme *via* a phosphate-based transition-state-complex.

[190] Gobec S, Plantan I, Mravljak J, *et al.* Design, synthesis, biochemical evaluation and antimycobacterial action of phosphonate inhibitors of antigen 85C, a crucial enzyme involved in biosynthesis of the mycobacterial cell wall. *Eur J Med Chem*. 2007;42(1):54-63. doi:10.1016/j.ejmech.2006.08.007

[191] Jackson M, Raynaud C, Lanéelle MA, *et al.* Inactivation of the antigen 85C gene profoundly affects the mycolate content and alters the permeability of the Mycobacterium tuberculosis cell envelope. *Mol Microbiol*. 1999;31(5):1573-1587. doi:10.1046/j.1365-2958.1999.01310.x

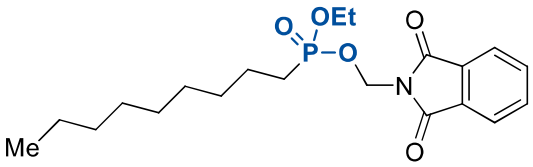

tetrahedral phosphonate **TS analogue**
for *Mycobacterium tuberculosis* 85C antigen

Figure 32. A transition-state analogue bearing a phosphonate functionality.

I-1.2. Phosphorus-containing drugs

In regards to drug discovery, the phosphorus moiety can be integrated into the pharmacophore structure, or contrarily the *P*-group can play its role as the pro-moiety of a prodrug that gives place to the corresponding parent drug after *in vivo* bioactivation. There are some exceptions that do not fit fully within this classification, for instance, in nucleo(s)tide analogues as the ProTide approach the P-group emerges masked as a phosphate surrogate which is part of the pharmacophore, but at the same time acts as a pro-moiety-like group involved in the metabolic activation of the prodrug (see the ProTides, reference). In this section, a representative selection of phosphorated drugs will be briefly exposed, along with P-containing inorganic molecules as counter-ions and excipients in drug formulations.

I-1.2.1. Phosphorus as part of the pharmacophore

Herein, we focus our attention on pharmacologically relevant drugs containing a phosphorated functionality as part of the pharmacophore.

(Phosphonate)-Fosfomycin

Fosfomycin (**87**, Figure 33) is a broad-spectrum antibiotic effective towards both Gram-positive and Gram-negative bacteria. Fosfomycin acts as a bactericidal analogue of phosphoenolpyruvate (PEP) that irreversibly inhibits the UDP-*N*-acetylglucosamine enolpyruvyltransferase (Mur A), resulting in a blockade of the biosynthesis of peptidoglycan[192]. Fosfomycin is currently formulated in salt forms for oral (with calcium or trimethamine counter-ions) and intravenous (with sodium counter-ions) administration[193].

[192] Kwan ACF, Beahm NP. Fosfomycin for bacterial prostatitis: a review. *Int J Antimicrob Agents*. 2020;56(4):106106. doi:10.1016/j.ijantimicag.2020.106106

[193] Arteche-Eguizabal L, Domingo-Echaburu S, Urrutia-Losada A, Grau-Cerrato S. Fosfomycin: Salt is what really matters. *Enferm Infecc Microbiol Clin (Engl Ed)*. 2021;39(4):206-207. doi:10.1016/j.eimc.2020.06.006

(Phosphine oxide)-Brigatinib

Out of phosphine oxide containing drugs, brigatinib (**88**, Figure 33) is a second generation anaplastic lymphoma kinase (ALK) inhibitor approved by the FDA in 2017 for ALK+ non-small cell lung cancer[194]. Brigatinib presents an enhanced CNS penetration and consequently an improved anti-tumor effect on brain metastasis, a promising advantage considering that lung cancers tend to spread by metastasis since are located in a highly vascularized tissue[195].

(Phosphinate)-Fosinopril

Fosinopril (**89**, Figure 33) is an angiotensin converting enzyme (ACE) inhibitor used in the treatment of hypertension and chronic heart failure. Fosinopril is the only ACE inhibitor containing a phosphorated moiety, which is in fact a phosphinate ester prodrug which is activated *in vivo* to give place to the corresponding active phosphinic acid derivative fosinoprilat (**90**)[196].

(S and F containing phosphates)-Dyflos and ecothiopate iodide

Dyflos (**91**, Figure 33) and ecothiopate iodide (**92**) are both acetylcholinesterase (ACHE) inhibitors based on fluorine/sulphur containing phosphates (phosphorofluoridate for dyflos and phosphorothiate for ecothiopate iodide), which are currently used in chronic ocular hypertension (initially were used in humans and later in veterinary medicine)[184].

[194] FDA resources page. https://www.fda.gov/drugs/resources-information-approved-drugs/brigatinib. Accessed December 28, 2021.

[195] Rigaud C, Dourthe M. Chapter 4 - management of ALK positive patients with tumors other than lung cancer. In: Friboulet L, ed. *Therapeutic strategies to overcome ALK resistance in cancer.* Vol 13. Academic Press; 2021:71-86. doi:10.1016/B978-0-12-821774-0.00008-5

[196] Davis R, Coukell A, McTavish D. Fosinopril. A review of its pharmacology and clinical efficacy in the management of heart failure. *Drugs*. 1997;54(1):103-116. doi:10.2165/00003495-199754010-00012

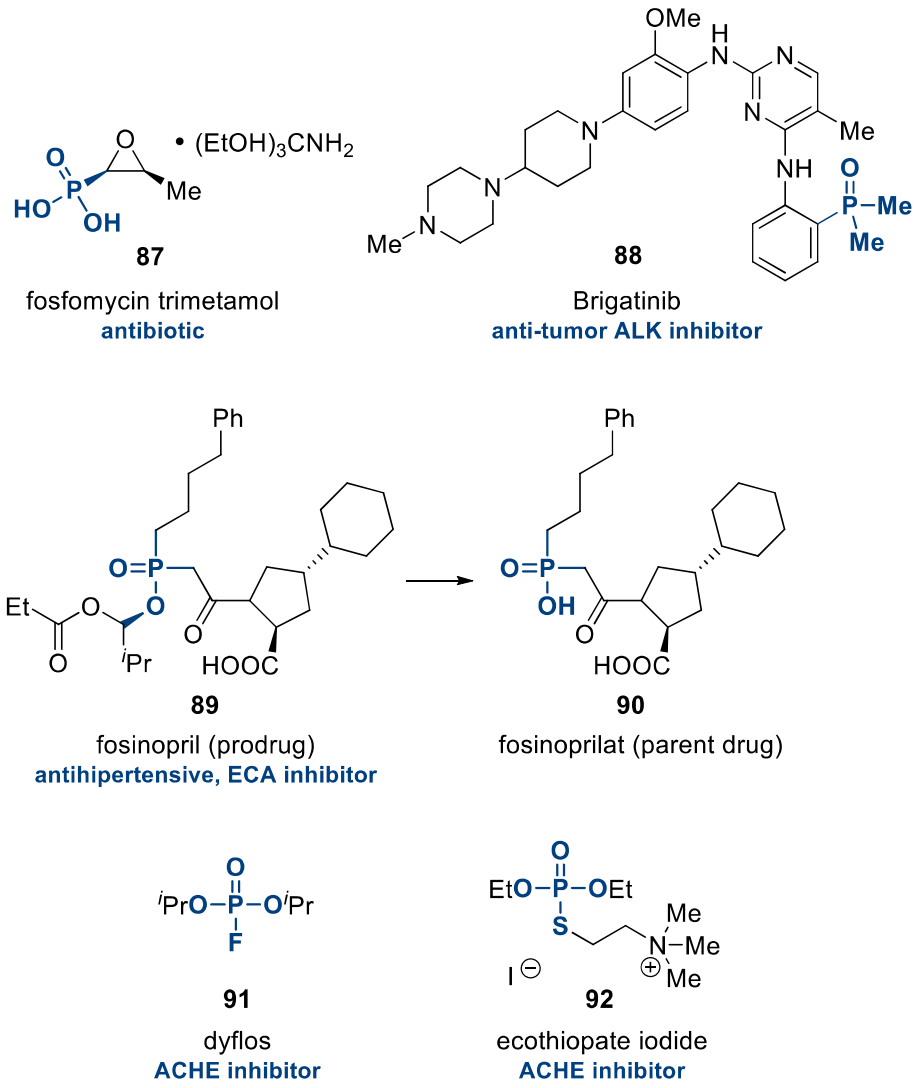

Figure 33. Drugs bearing a phosphorated group in the pharmacophore.

(Phosphate)-Nucleo(s)tide phosphate/phosphonate prodrugs

Nucleo(s)tide prodrugs are pharmacologically inactive but pharmacokinetically suitable drugs that are metabolically activated *in vivo*. Out of this category, is noteworthy to highlight the nucleotide prodrugs (ProTides, prodrugs of nucleotides) introduced by McGuigan and collaborators in the 1990's[197].

In the ProTide approach (Figure 34), the phosphorus moiety is not part of the protective group. Contrarily, the phosphorus is part of an enmasked phosphate of a nucleo(s)tide as a aryloxyphosphor(n)amidate form, which plays a primary role in the bioactivation by consecutive

[197] McGuigan C, Tsang HW, Sutton PW, De Clercq E, Balzarini J. Synthesis and anti-HIV activity of some novel chain-extended phosphoramidate derivatives of d4T (stavudine): esterase hydrolysis as a rapid predictive test for antiviral potency. *Antivir Chem Chemother*. 1998;9(2):109-115. doi:10.1177/095632029800900202

action of intrinsic metabolic enzymes. After releasing the two masking protective groups (the aryloxy ester first and the amino acid moiety later), the resulting monophosphate nucleo(s)tide is phosphorylated (twice) to obtain the active nucleo(s)tide triphosphate[198].

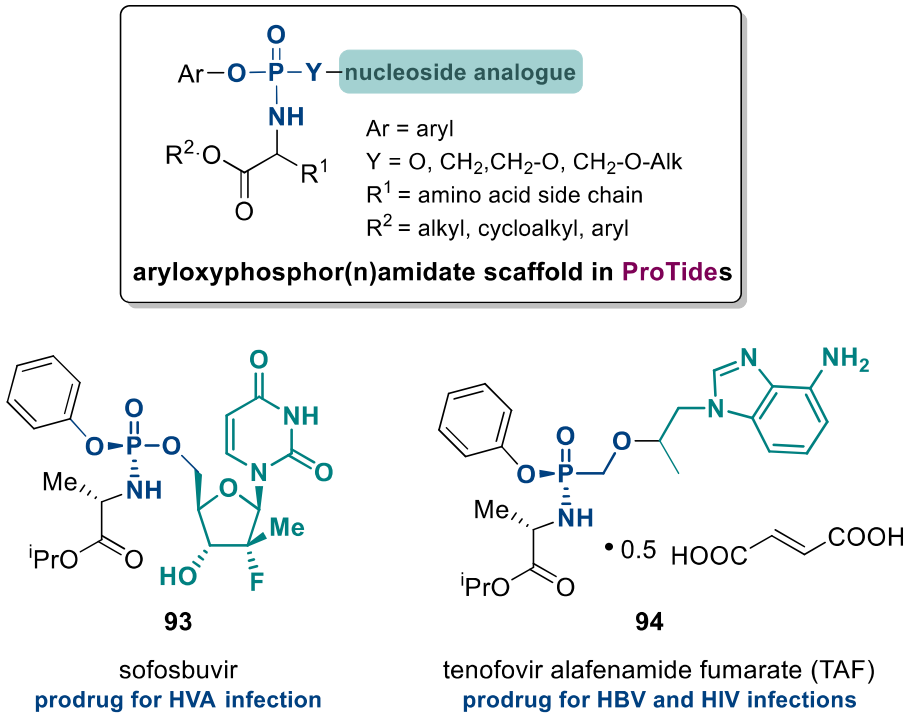

Figure 34. ProTide drugs containing an aryloxyphosphor(n)amidate scaffold.

Phosphate ProTide: Sofosbuvir

Sofosbuvir (**93**, Figure 34) in a guanosine analogue prodrug, composed of a guanosine monophosphate derivative protected with a phenol ether and a L-alanine residue in the phosphate moiety. Sofosbuvir is activated in the liver by means of sequential steps involving the combination of various enzymes as shown in Scheme 24: hydrolysis of carboxyl esters by cathepsin A (Cat A) and carboxylesterase 1 (CES 1), phosphoraminidase activity of hHint 1 hydrolase, and finally phosphorylation reaction by both UMP-CMPK and NDPK kinases[199]. The corresponding active guanosine triphosphate analogue (**94**) is a direct antiviral used to treat the hepatitis C virus (HCV) *via* inhibition of HCV polymerase.

[198] Slusarczyk M, Serpi M, Pertusati F. Phosphoramidates and phosphonamidates (ProTides) with antiviral activity. *Antivir Chem Chemother*. 2018;26:2040206618775243. doi:10.1177/2040206618775243
[199] Dousson CB. Current and future use of nucleo(s)tide prodrugs in the treatment of hepatitis C virus infection. *Antivir Chem Chemother*. 2018;26:2040206618756430. doi:10.1177/2040206618756430

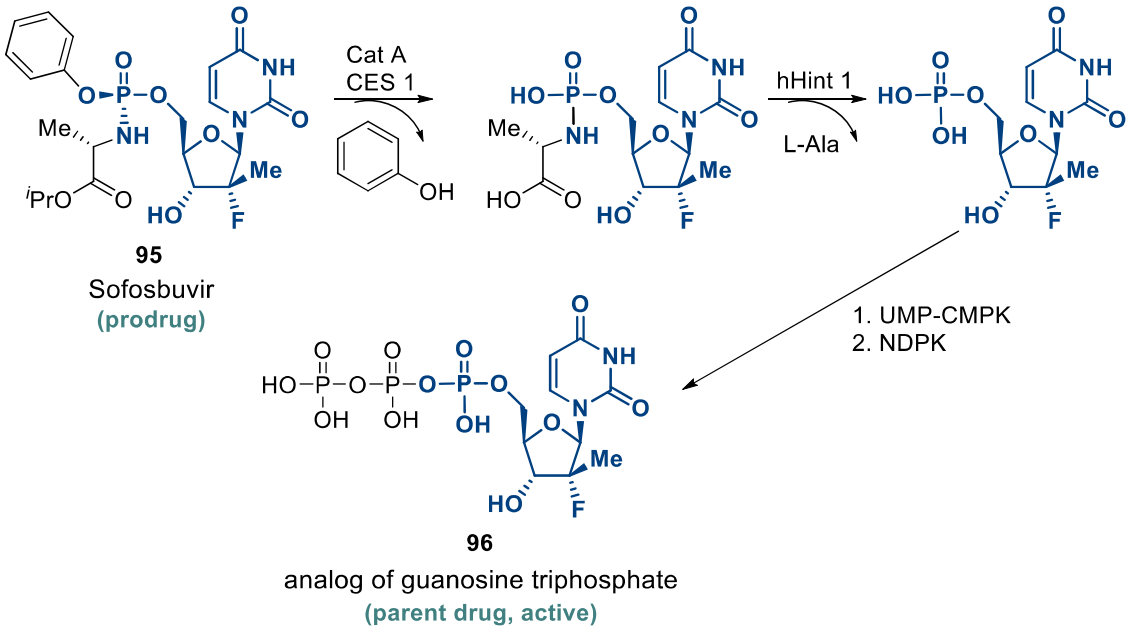

Scheme 24. In vivo bioactivation of sofosbuvir.

Phosphonate ProTide: Tenofovir alafenamide

Tenofovir alafenamide fumarate (TAF, chemical structure **97** in Figure 34, *vide supra*) is formed by an aryloxyfosfonamidate of alanine linked to an adenosine derivative which lacks the ribose moiety. The metabolic bioactivation of TAF gives place to tenofovir, a dAMP analogue with antirretroviral activity. TAF is currently used for the treatment of infections with hepatitis B virus (HBV) and human immunodeficiency virus (HIV)[198].

Bisphosphonates

Bisphosphonates are bone seeking agents clinically used in diseases involving bone loss such as osteoporosis or Paget´s disease, and are structurally composed of two phosphonate groups ($P(O)(OH)_2$) linked to a central C atom (**A**, Figure 35; *e.g.* sodium risendronate **97**)[200]. Bisphosphonates are analogues of pyrophosphate (**B**, Figure 35; *e.g.* etiodronate disodium **98**) with an improved chemical stability provided by the C atom in between, which confers resistance to the activity of intestinal phosphatases, therefore bisphosphonates are suitable drugs for oral administration[201].

[200] Cawthray J, Wasan E, Wasan K. Bone-seeking agents for the treatment of bone disorders. *Drug Deliv Transl Res*. 2017;7(4):466-481. doi:10.1007/s13346-017-0394-3

[201] Buchet R, Millán JL, Magne D. Multisystemic functions of alkaline phosphatases. *Methods Mol Biol*. 2013;1053:27-51. doi:10.1007/978-1-62703-562-0_3

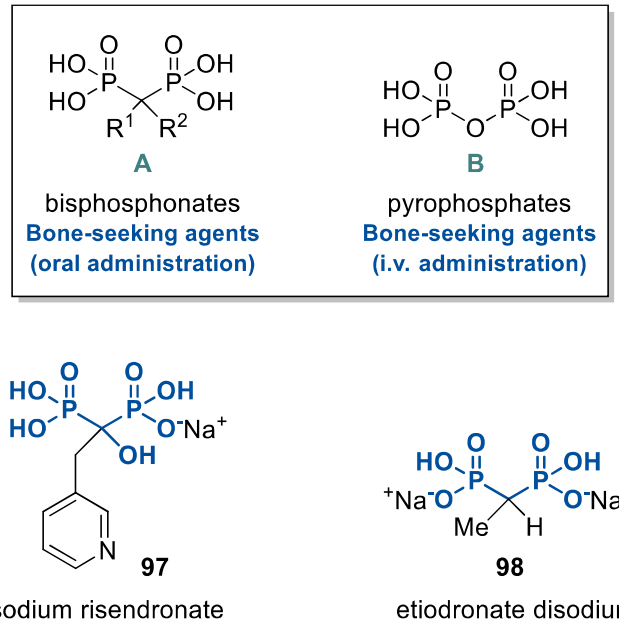

Figure 35. Comparison between the main structures of bisphosphonates and pyrophosphates with an example of each.

Bisphosphonates preferably bind to Ca^{2+} ions with high affinity and hence, once absorbed they are accumulated in high concentrations in the bone tissue. When osteoclasts destroy the bone, bisphosphonates are released and selectively internalized by the same osteoclasts, resulting in the induction of osteoclast apoptosis by following different molecular pathways (depending on the structure of the bisphosphonate). The final pharmacological result is a reduction of the osteoclastic bone resorption[200].

I-1.2.2. Phosphorus as part of the pro-moiety

As mentioned before, a considerable part of metabolism involves biotransformation of phosphate esters. Hence, unprotected phosphate-containing compounds are likely to be quickly transformed *in vivo* and this may explain their wide use as pro-moieties in the preparation of ester prodrugs to improve the water solubility of orally and intravenously administered drugs. Phosphate prodrugs are activated by phosphatases such as alkaline phosphatases present in plasma and enterocytes of the intestinal barrier *via* hydrolysis of the phosphate esters[202], among others.

[202] Huttunen KM, Raunio H, Rautio J. Prodrugs--from serendipity to rational design. *Pharmacol Rev*. 2011;63(3):750-771. doi:10.1124/pr.110.003459

Steroid-derived sodium phosphates

Dexamethasone (DXM) is a long acting glucocorticoid used in inflammatory/allergic disorders, cerebral edema and in the management of circulatory shock such as septic shock[203]. Dexamethasone sodium phosphate is a prodrug of the active DXM protected with a phosphate group and formulated in a sodium salt form in order to allow intravenous administration. The employment of (disodium) phosphate as the protective group comparing with other pro-moieties (as hemisuccinates) confers to DXM a high degree of solubility and chemical stability in aqueous environment, as well as a faster bioconversion by alkaline phosphatases of the water soluble prodrug into the active form (free DXM)[204]. Besides DXM, there are other corticosteroid ester phosphates used in clinics as prednisolone sodium phosphate[202] and hydrocortisone sodium phosphate[205]. The structures of dexamethasone/prednisolone/hydrocortisone (**99**, **100**, **101**) sodium phosphate are depicted in Figure 36.

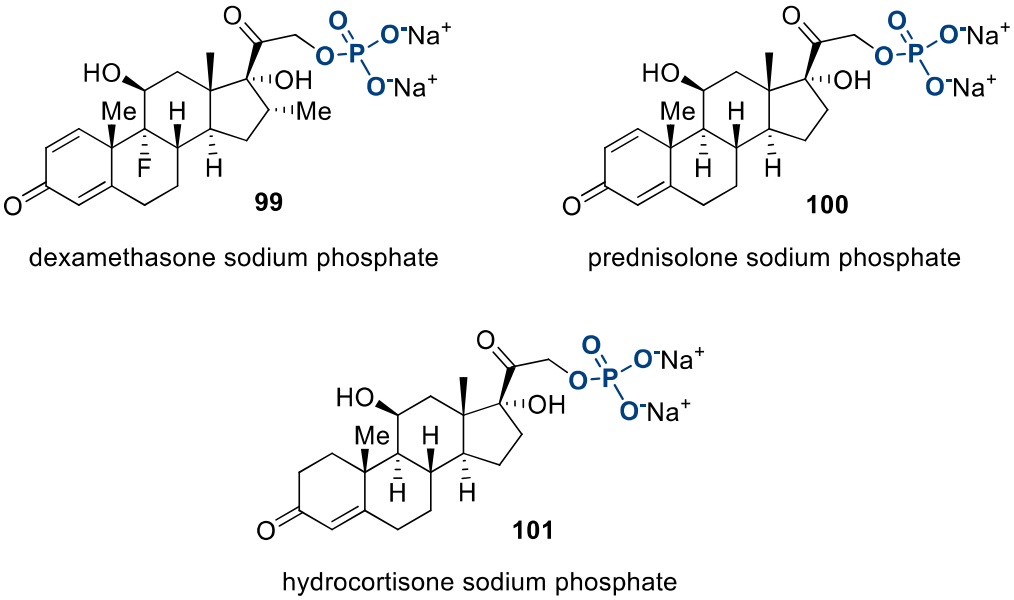

Figure 36. Structures of dexamethasone, prednisolone and hydrocortisone formulated in their sodium phosphate salt form.

[203] 1. Flower RJ, Gavins F. Dexamethasone. In: Enna SJ, Bylund DB, eds. *xPharm: The comprehensive pharmacology reference.* New York: Elsevier; 2008:1-6. doi:10.1016/B978-008055232-3.61572-7

[204] Rohdewald P, Möllmann H, Barth J, Rehder J, Derendorf H. Pharmacokinetics of dexamethasone and its phosphate ester. *Biopharm Drug Dispos*. 1987;8(3):205-212. doi:10.1002/bdd.2510080302

[205] Shankar-Hari M, Santhakumaran S, Prevost AT, *et al. Defining phenotypes and treatment effect heterogeneity to inform acute respiratory distress syndrome and sepsis trials: secondary analyses of three RCTs*. Southampton (UK): NIHR Journals Library; July 2021.

I-1.2.3. Phosphorus in counter-ions of active pharmaceutical ingredients (APIs)

APIs formulated in the salt form are conveniently used to overcome physicochemical limitations of the API (mainly poor water solubility, but also low thermic stability, high hygroscopicity or difficulties to crystallize the compound)[206]. Chloride is the most common counter-anion for the salt formation of basic ionizable groups, although there is a wide range of pharmacologically well tolerated anions as sulphate, bromide, maleate or phosphate, among others[207]. In particular, phosphate is currently used as a counter-ion to form salts of APIs with chloroquine (**102**, Figure 37), codeine (**103**) and carvedilol (**104**) in their correspondent pharmaceutical compositions.

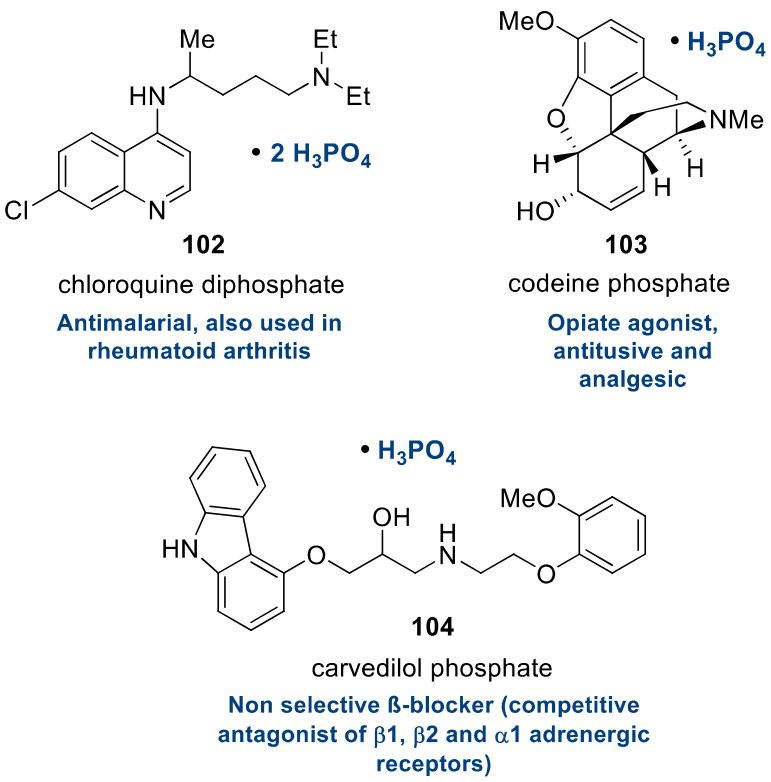

Figure 37. Drugs formulated as salts of APIs with phosphate counter-ions.

I-1.2.4. Inorganic phosphorus-containing excipients in drug formulations

Inorganic phosphorous compounds are also used in close relation with APIs as excipients in pharmaceutical formulations (Figure 38). This is the case of calcium phosphates, widely used as

[206] Serajuddin AT. Salt formation to improve drug solubility. *Adv Drug Deliv Rev*. 2007;59(7):603-616. doi:10.1016/j.addr.2007.05.010

[207] Di L, Kerns EH. Chapter 7 - solubility. In: Di L, Kerns EH, eds. *Drug-like properties (second edition).* Boston: Academic Press; 2016:61-93. doi:10.1016/B978-0-12-801076-1.00007-1.

diluents in orally administered solid dosage forms[208]. In the same way, phosphoric acid is employed as an excipient to adjust the pH and stabilize the pharmaceutic composition[209], as well as its corresponding sodium salts.

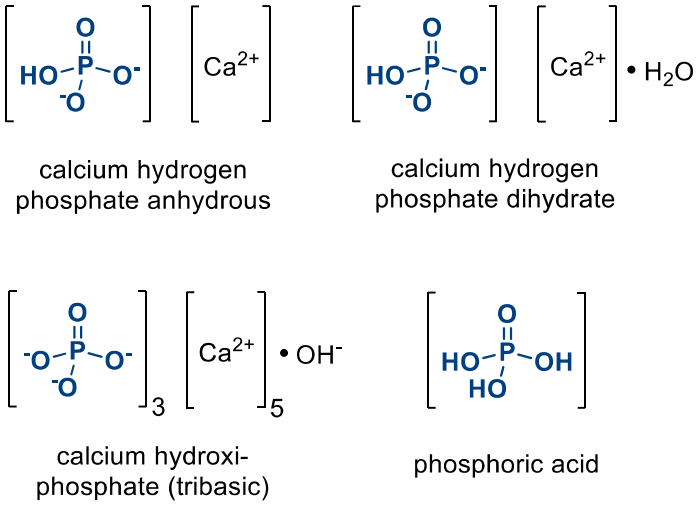

Figure 38. Phosphorus-containing inorganic excipients commonly used in pharmaceutical compositions.

[208] Wagner M, Hess T, Zakowiecki D. Studies on the pH-dependent solubility of various grades of calcium phosphate-based pharmaceutical excipients. *J Pharm Sci*. 2021;S0022-3549(21)00656-0. doi:10.1016/j.xphs.2021.12.005

[209] Drugs.com. Accessed December 6, 2021 at https://www.drugs.com/inactive/phosphoric-acid-95.html

I-2. The Povarov reaction

N-containing heterocycles are among the most significant class of compounds in the fields of biochemistry and medicinal chemistry. Natural occurring *N*-heterocyclic compounds are present in the structure of essential biomolecules and play a key role in organic reactions that arise in all living organisms at molecular level. Furthermore, the vast majority of biologically active organic compounds contain a *N*-heterocyclic moiety and among them, the quinoline scaffold is an ubiquitous pharmacophore as previously described.

Among those methodologic strategies described for the preparation of the quinoline scaffold, the aza-Diels Alder (aza-DA) reaction represent a powerful and versatile synthetic tool from a chemical point of view, which gives access to the formation of 2 new C-C bonds and generates one six-membered ring bearing a nitrogen with an exceptional atom economy. In this regard, aza-DA reactions have been widely explored for the formation of six-membered nitrogen rings.

In 1963, Povarov and Mikhailov firstly discovered the aza-DA reaction between *N*-aryl imines **105** (Scheme 25) and ethyl vinyl ether/tioether **106** in the presence of $BF_3.Et_2O$ (boron trifluoride diethyl etherate) as a Lewis acid catalyst, obtaining tetrahydroquinoline adducts **107**, which were dehydrogenated with *p*-toluensulfonic acid to yield quinolines **108**[149].

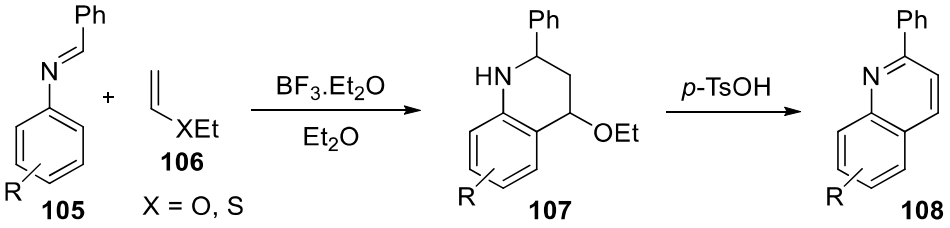

Scheme 25. Original aza-Diels Alder reaction described by Povarov in 1963.

The standard Povarov reaction involves an acid promoted [4+2]-cycloaddition between a *N*-aryl imines (which act as formal aza-dienes) and electron rich dienophiles, acceding to a broad variety of tetrahydroquinolines (and consequently to their corresponding dehydrogenated quinolines). Hence, the Povarov cycloaddition gives place to tetrahydroquinoline adducts containing three stereogenic centers (even the stereoselectivity is quite ambiguous and depends on the reagents and reaction conditions) with an excellent control of the regiochemistry. Moreover, the Povarov reaction introduces up to three points of diversity (as it can be observed in the Scheme 26) and tolerates a wide range of dienophiles, allowing the exploration of

structurally diverse *N*-heterocyclic structures[210]. The control of the regio- and stereochemistry makes the Povarov reaction an advantageous synthetic methodology.

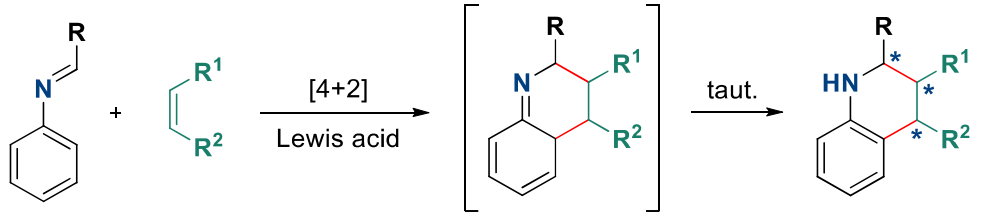

Scheme 26. Standard Lewis-acid catalyzed Povarov reaction

One-pot and MCR approaches of the Povarov reaction

In 1964 Povarov and Mikhailov described a [4+2] imino-DA cycloaddition between anilines **109** (Scheme 27) and 2 equivalents of vinyl ether **110**, in the presence of $BF_3.Et_2O$. The first equivalent of vinyl ether condensates with the aniline to form the corresponding imine, which undergoes cyclization through the Povarov reaction with the second equivalent of vinyl ether to form tetrahydroquinoline **111**[149]. Finally, further dehydrogenation of adducts **111** with *p*-TsOH allowed the obtainment of quinolines **112**. This cascade synthesis was the first one-pot version of the Povarov reaction.

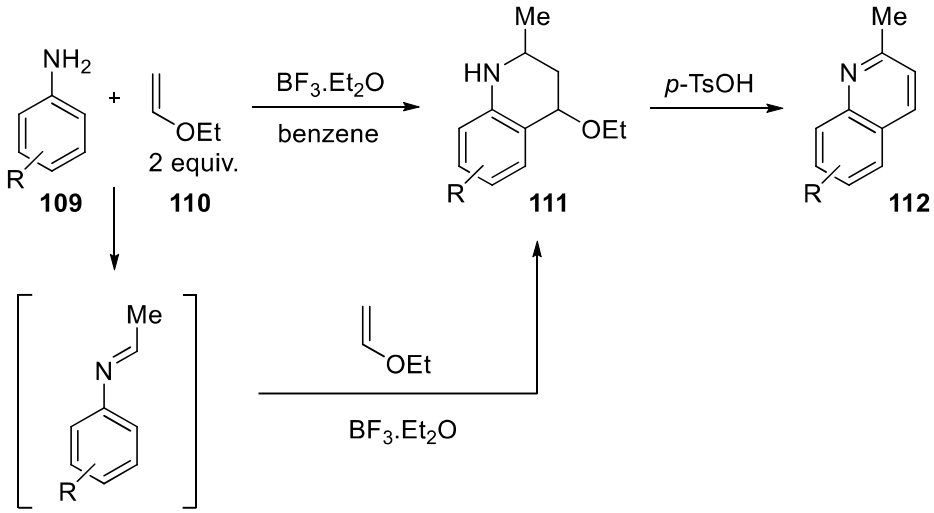

Scheme 27. The first (cascade) one-pot approach described for the Povarov reaction by Povarov and Mikhailov in 1964.

[210] Bello Forero J,S., Jones Junior J, da Silva F,M. The Povarov reaction as a versatile strategy for the preparation of 1, 2, 3, 4-tetrahydroquinoline derivatives: An overview. *Curr Org Synth*. 2016;13(2):157-175. doi:10.2174/1570179412666150706183906

The versatility of the Povarov reaction confers to this synthetic methodology the accessibility to be performed in either one-pot or MCR manner[114]. The one-pot Povarov approach allows the *in situ* formation of the aza-diene that undergo cyclization reaction upon the addition of the corresponding dienophile, while the MCR Povarov goes one step forward and enables the straightforward synthesis upon reaction of the starting materials (the aniline, the carbonyl compound and the dienophile), which results specially convenient in terms of atom-economy and step-efficiency[211].

In 1993 Narasaka and collaborators reported the first Povarov MCR approach between aniline (**113**, Scheme 28), aldehydes **114** and vinyl sulphides **115**, in the presence of stoichometric amounts of $BF_3.Et_2O$[212]. Narasaka observed that *in situ* preparation of imines **116** by a sequential MCR protocol improves the reactivity, obtaining tetrahydroquinoline derivatives **117** in high yields (70-83 %).

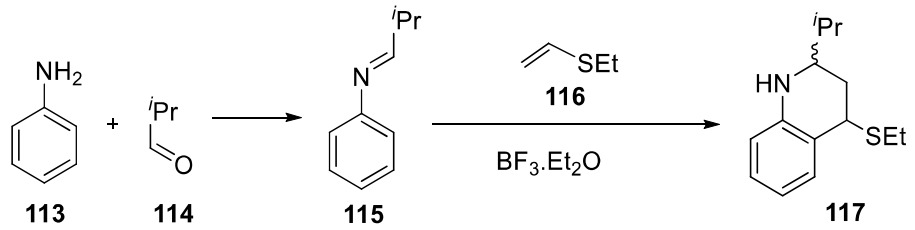

Scheme 28. The first (sequential) MCR Povarov reaction described by Narasaka et al.

I-2.1. The mechanism of the Povarov reaction

The mechanistic features of the Povarov reaction are still subject of active research and debate. On the one hand, some authors like Jacobsen[213] defend a concerted imino-DA reaction (through the intermediate **I**, Scheme 29). In this sense, Palacios and Cossío[214] reported an *endo* asynchronous concerted process in a reaction between double LA-activated (with BF_3Et_2O) *N*-(pyridine-3-yl)aldimines and olefins, supported on experimental and computational mechanistic

[211] Ghashghaei O, Masdeu C, Alonso C, Palacios F, Lavilla R. Recent advances of the Povarov reaction in medicinal chemistry. *Drug Discov Today Technol*. 2018;29:71-79. doi:10.1016/j.ddtec.2018.08.004

[212] Narasaka K, Shibata T. BF3.OEt2 Catalyzed [4+2] Cycloaddition Reactions of N-Aryl Schiff's Bases with 1-Alkenyl, 1,2-Propadienyl, and 1-Alkynyl Sulfides. *Heterocycles*. 1993;35:1039-1053. doi:10.3987/com-92-s(t)98

[213] Xu H, Zuend SJ, Woll MG, Tao Y, Jacobsen EN. Asymmetric cooperative catalysis of strong Brønsted acid-promoted reactions using chiral ureas. *Science*. 2010;327(5968):986-990. doi:10.1126/science.1182826

[214] Palacios F, Alonso C, Arrieta A, *et al.* Lewis acid activated aza-Diels–Alder reaction of N-(3-pyridyl)aldimines: An experimental and computational study. *Eur J Org Chem*. 2010;2010(11):2091-2099. doi:10.1002/ejoc.200901325

studies. On the contrary, some other authors like Lavilla[215] and Zhu[216] conceive the Povarov reaction as a stepwise process (following the route **B** collected in the Scheme 29). Lavilla observed clear evidence of a stepwise mechanism (a Mannich-intramolecular cyclization sequence) in the Povarov reaction between aldimines and polar olefins, where the more polar is the nature of the olefin, more clearly seems the reaction to proceed through a cationic intermediate[217]. Overall, from a mechanistic perspective, the Povarov process is not totally clear yet and it may be explained by both approaches, in which the predominant mechanism seems to depend on the nature of the reagents, the solvent, the catalyst and the reaction conditions.

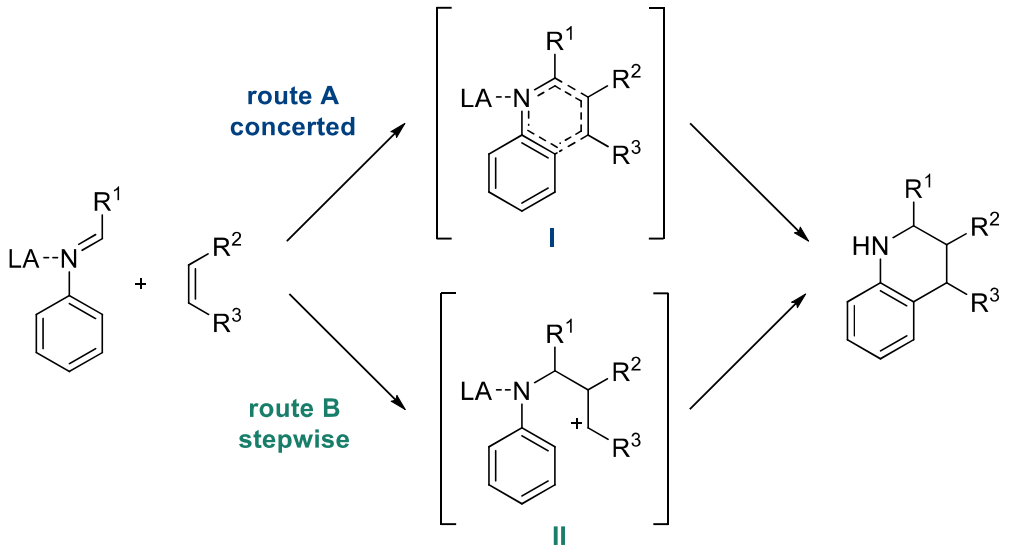

Scheme 29. Concerted and stepwise mechanistic pathways of the Povarov reaction

I-2.2. Electrophilic activation of the diene by Lewis-acid (LA) and Brønsted-acid (BA) catalysts

In the Povarov reaction, the diene and the dienophile usually present opposite electrophilicity within an inverse electron-demand [4+2]-cycloaddition, where electron-poor *N*-aryl imines react with electron-rich dienophiles. *N*-aryl imines are stable Schiff bases due to the aryl group linked to the iminic nitrogen, but in like manner, they commonly result poorly reactive. Moreover, the electrodonating nature of the substituents of the dienophile could not be strong enough to

[215] Lavilla R, Bernabeu MC, Carranco I, Díaz JL. Dihydropyridine-based multicomponent reactions. Efficient entry into new tetrahydroquinoline systems through Lewis acid-catalyzed formal [4 + 2] cycloadditions. *Org Lett*. 2003;5(5):717-720. doi:10.1021/ol027545d

[216] Dagousset G, Zhu J, Masson G. Chiral phosphoric acid-catalyzed enantioselective three-component povarov reaction using enecarbamates as dienophiles: Highly diastereo- and enantioselective synthesis of substituted 4-aminotetrahydroquinolines. *J Am Chem Soc*. 2011;133(37):14804-14813. doi:10.1021/ja205891m

[217] Bello D, Ramon R, Lavilla R. Mechanistic variations of the Povarov multicomponent reaction and related processes. *Curr Org Chem*. 2010;14(4):332-356. doi:10.2174/138527210790231883

activate the ethylene. These two scenarios require the electrophilic activation of the imine by coordinating a Lewis-acid catalyst to the nitrogen atom, which removes electronic density from the iminic carbon to promote the Povarov reaction[218]. A wide range of LA have been described as convenient catalyst in the Povarov cycloaddition, *e.g.* $BF_3.Et_2O$, lanthanide triflates, lanthanide salts such as cerium ammonium nitrate (CAN)[219] or indium salts[220]. In 1988, Grieco and co-workers found that Brønsted-acids, which are able to protonate the iminic nitrogen, could be conveniently used to catalyze the Povarov reaction. Accordingly, during DA cycloaddition between cyclopentadiene and aldimines in the presence of trifluoroacetic acid (TFA), Grieco and collaborators expected a formal [4+2] Diels-Alder reaction (pathway **A**, Scheme 30), but they found that *N*-aryl imines were acting as the dienophile in an inverse electron-demand [4+2]-cycloaddition after electrophilic activation by TFA, obtaining adducts **118** derived from the Povarov reaction (pathway **B**, Scheme 30) instead of the expected DA products[221].

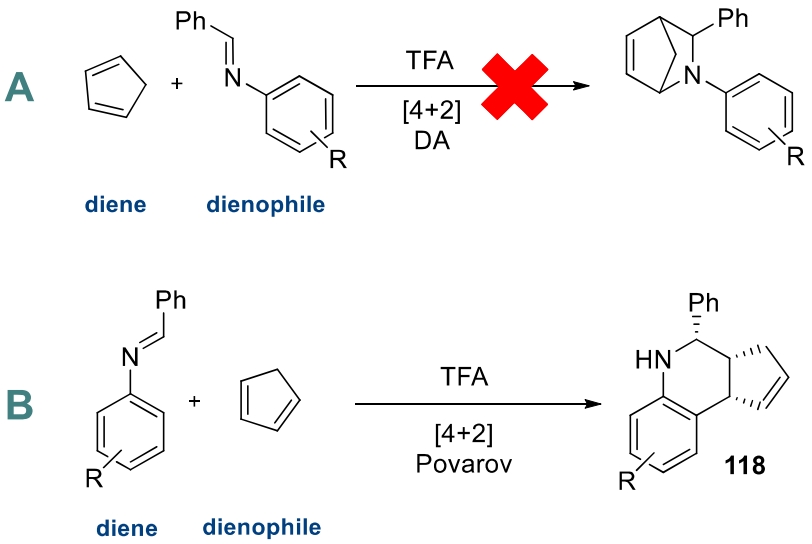

Scheme 30. Inverse electron-demand [4+2]-cycloaddition obtained by Grieco and coworkers between cyclopentadiene and aldimines activated by TFA.

[218] Kouznetsov VV. Recent synthetic developments in a powerful imino Diels–Alder reaction (Povarov reaction): Application to the synthesis of N-polyheterocycles and related alkaloids. *Tetrahedron*. 2009;65(14):2721-2750. doi:10.1016/j.tet.2008.12.059

[219] Sridharan V, Menéndez JC. Cerium(IV) ammonium nitrate as a catalyst in organic synthesis. *Chem Rev*. 2010;110(6):3805-3849. doi: 10.1021/cr100004p

[220] Manian, Rathna Durga R. S., Jayashankaran J, Ramesh R, Raghunathan R. Rapid synthesis of tetrahydroquinolines by indium trichloride catalyzed mono- and bis-intramolecular imino Diels—Alder reactions. *ChemInform*. 2007;38(6). doi:10.1002/chin.200706139

[221] Grieco PA, Bahsas A. Role reversal in the cyclocondensation of cyclopentadiene with heterodienophiles derived from aryl amines and aldehydes: Synthesis of novel tetrahydroquinolines. *Tetrahedron Lett*. 1988;29(46):5855-5858. doi:10.1016/S0040-4039(00)82208-X

Key advances in the discovery of efficient catalysts for the Povarov reaction

In 1995 Kobayashi *et al.* reported the Povarov reaction of olefins with aldimines electronicallly activated by 10 mol% of lanthanide triflates, obtaining tetrahydroquinoline adducts in high yields[222]. Kobayashi´s discovery opened the door to the development of highly efficient Lewis-acid (*e.g.* lanthanide triflates and chlorides) and metal-free Brønsted-acid catalysts[223], which allowed to move from stoichiometric to catalytic amounts of catalyst. Nowadays, a wide variety of powerful catalysts are used to promote the Povarov reaction, including Lewis-acids ($BF_3.Et_2O$, $(Yb(OTf)_3$, $Sc(OTf)_3$, CAN, $SnCl_4$, $FeCl_3$, $ZnCl_2$, $CuBr_2$, $BiCl_3$, $InCl_3$, phosphoric acids), Brønsted-acids (*p*-TSOH, TFA, HCl, TfOH, Tf_2NH), or molecular iodine (I_2), among others. One year Later, Kobayashi and co-workers disclosed the first asymmetric Povarov reaction between hydroxy-aldimines **119** (Scheme 31) and non-chiral vinyl ether/2,3-dihyfrofurane/ciclopentadiene **120** using a chiral lanthanide triflate complex as LA catalyst in the presence of a base, to obtain *cis*-tetrahydroquinoline adducts **121** with high enantiomeric excesses[224]. The discoveries of MCR and enantioselective versions and specially the development of highly efficient catalysts initiated by Kobayashi re-attracted the attention of synthetic organic chemists towards the Povarov reaction.

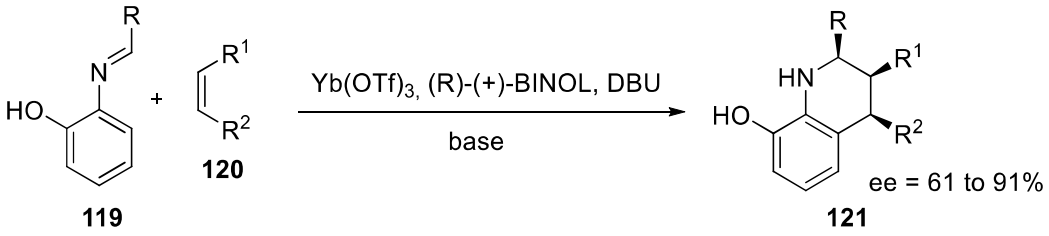

Scheme 31. Asymetric Povarov reaction catalyzed by a lanthanide triflate-complex as a Lewis-acid catalyst.

I-2.3. Dienophiles in the Povarov reaction

The Povarov reaction tolerates a wide range on dienophiles, acceding to many different tetrahydroquinoline-derived scaffolds.

[222] Kobayashi S, Ishitani H, Nagayama S. Lanthanide Triflate Catalyzed Imino Diels-Alder Reactions; Convenient Syntheses of Pyridine and Quinoline Derivatives. *Synthesis.* 1995;1995(9):1195-1202

[223] Akiyama T, Morita H, Fuchibe K. Chiral brønsted acid-catalyzed inverse electron-demand aza Diels−Alder reaction. *J Am Chem Soc*. 2006;128(40):13070-13071. doi: 10.1021/ja064676r

[224] Ishitani H, Kobayashi S. Catalytic asymmetric aza diels-alder reactions using a chiral lanthanide lewis acid. enantioselective synthesis of tetrahydroquinoline derivatives using a catalytic amount of a chiral source. *Tetrahedron Lett*. 1996;37(41):7357-7360. doi: https://doi.org/10.1016/0040-4039(96)01655-3

Alkenes and alkynes as dienophiles

Our research group presented styrenes **124a** (Scheme 32)[93] and the cyclic derivative indene **124b**[94] as dienophiles in a $BF_3.Et_2O$ promoted Povarov MCR (with imines derived from 3-aminopyridine **122** and aldehydes **123**) for the synthesis of highly functionalized tetrahydroquinoline/quinoline derivatives **125a/126a** or indenotetrahydroquinoline/indenoiquinolines **125b/126b**. Likewise, our group also presented acetylenes **124c** as suitable dienophile in the Povarov reaction to yield directly quinoline derivatives **126a**[225], a strategy oriented to avoid the final oxidation step.

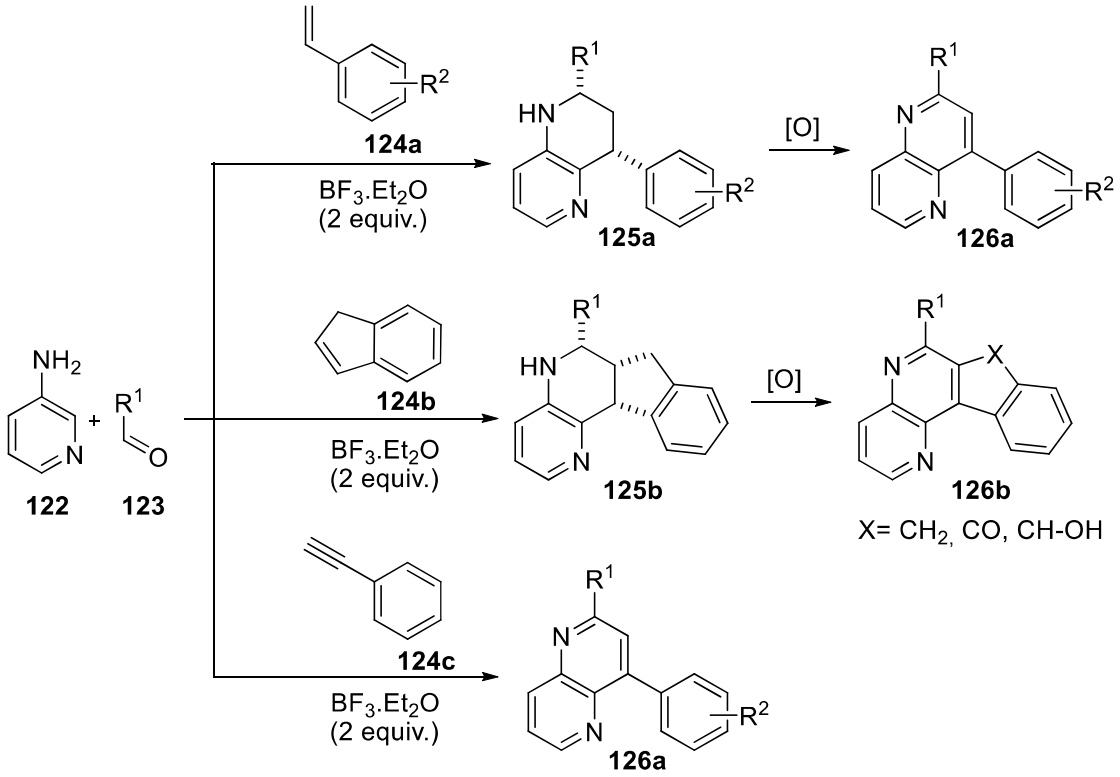

Scheme 32. Styrenes, indene and acetylenes as dienophiles in the Povarov reaction.

Vynil/enol ethers/enamin(d)es and cyclic derivatives as dienophiles

Povarov performed the first imino-DA [4+2]-cycloaddition employing vinyl ethers and vinyl thioethers as dienophiles. In the same way enol ethers and cyclic derivatives have been broadly explored, including their analogues vinyl enamides/enamines (and cyclic derivatives thereof). As an example, in 2012 Jacobsen, Marcurelle and collaborators disclosed an asymmetric Povarov

[225] Alonso C, González M, Palacios F, Rubiales G. Study of the hetero-[4+2]-cycloaddition reaction of aldimines and alkynes. synthesis of 1,5-naphthyridine and isoindolone derivatives. *J Org Chem*. 2017;82(12):6379-6387. doi: 10.1021/acs.joc.7b00977

reaction of imine glyoxalate **127** (Scheme 33) and 2,3-dihydro-1*H*-pyrrole **128** as dienophiles, in the presence of a chiral urea Brønsted-acid catalyst, obtaining tetrahydroquinoline adducts **129** which were the precursors of derivatives **130** (a whole library of >2000 derivatives)[226].

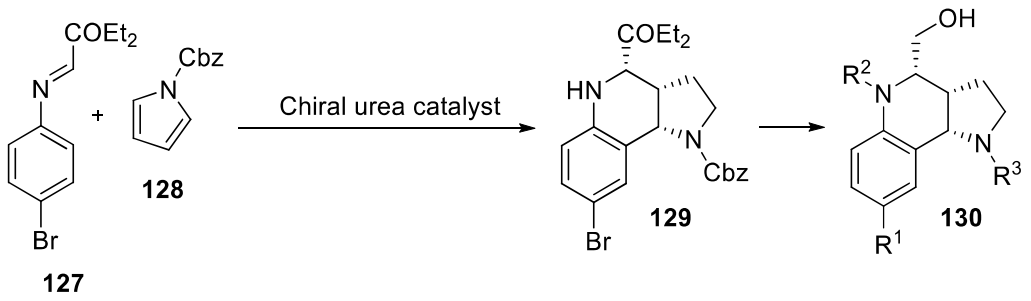

Scheme 33. Asymetric Povarov reaction described by Jacobsen and collaborators

Intramolecular Povarov reaction

Besides the standard Povarov reaction, if the diene and the dienophile are present in the same molecule, the Povarov reaction can occur intramolecularly to achieve fused *N*-containing polycyclic structures of high complexity. For instance, in our group, Martín-Encinas disclosed a smart intramolecular Povarov reaction (described in the Scheme 34) to yield fused quinolino[4,3-*b*][1,5]naphthyridine scaffolds **131**, acceding to *N*-polyheterocycles with elevated biological interest as TOP1 inhibitors[97].

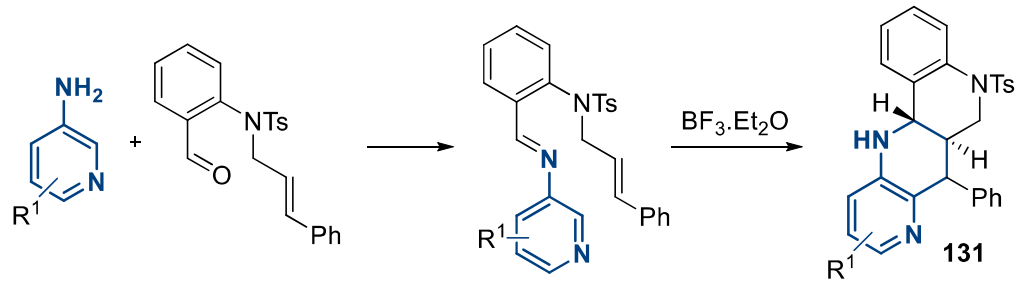

Scheme 34. Intramolecular Povarov reaction described by Martín-Encinas.

I-2.4. Dehydrogenation of tetrahydroquinoline adducts obtained by the Povarov reaction to achieve fully aromatic quinolines

The formation of tetrahydroquinoline adducts provided by the Povarov reaction may be subjected to selective dehydrogenation with oxidizing agents to obtain the corresponding

[226] Gerard B, O'Shea MW, Donckele E, *et al.* Application of a catalytic asymmetric Povarov reaction using chiral ureas to the synthesis of a tetrahydroquinoline library. *ACS Comb Sci*. 2012;14(11):621-630. doi:10.1021/co300098v

aromatic quinolines. The process comprises the formal removal of 4 hydrogen atoms and further implies the loss of the stereoselectivity obtained during the Povarov reaction. Several oxidants have been successfully explored for the dehydrogenation of tetrahydroquinoline adducts, such as DDQ, CAN, manganese acetate, molecular sulphur and nitrobenzene[227]. It must be mentioned that during the oxidation step undesired side-elimination reactions can occur (specially with non-aromatic N-C and O-C bonds), reducing the yield of the process. Accordingly, Lavilla and coworkers presented a method for the selective oxidation of lactam-fused tetrahydroquinoline derivatives with manganese oxide in the presence of stoichiometric amounts of pyridine, which yields to the corresponding quinoline **132** derivatives avoiding side elimination reactions driving to undesired opened derivatives **133** (the process is described in the Scheme 35).

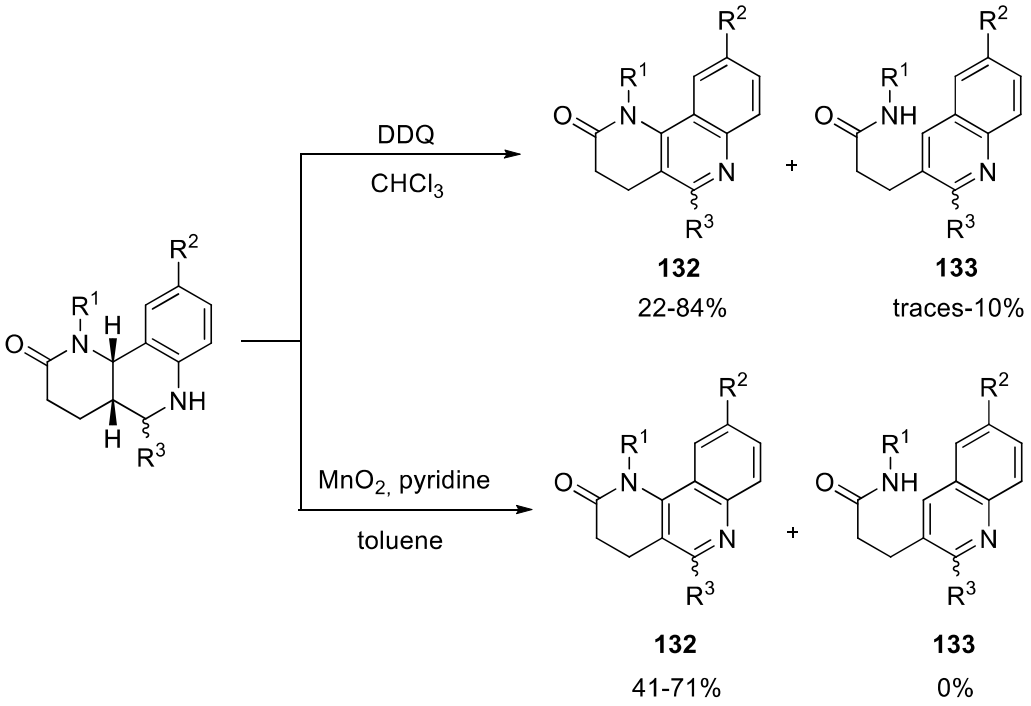

Scheme 35. Selective oxidation of tetrahydroquinoline adducts disclosed by Lavilla and collaborators.

[227] Vicente-García E, Ramón R, Preciado S, Lavilla R. Multicomponent reaction access to complex quinolines via oxidation of the Povarov adducts. *Beilstein J Org Chem*. 2011;7:980-987. doi:10.3762/bjoc.7.110

I-2.5. Summary, a historical approach of the Povarov reaction

We have described the mechanism and synthetic applicability of the Povarov reaction, along with the key advances achieved since its discovery by Povarov and Mikhailov in 1963 until the late 1990s, when the interest of the Povarov reaction grew considerably and nowadays is still a broadly used synthetic method. These key findings are collected in the timeline depicted in the Figure 39, in where the main advances are placed into a historical frame.

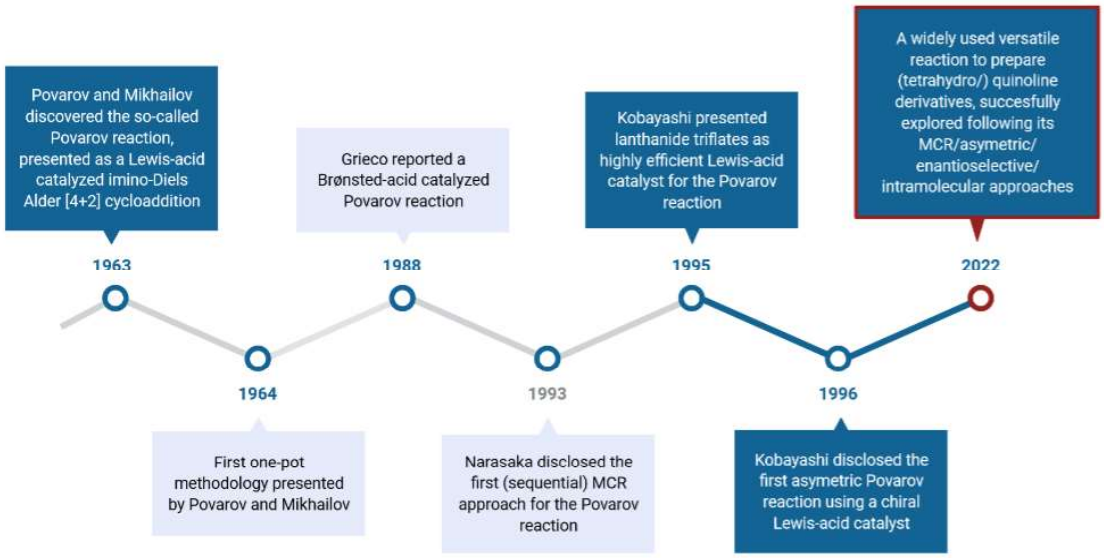

Figure 39. Schematic timeline covering the discovery and main advances of the Povarov reaction.

I-3. Synthesis of quinolinylphosphine oxide derivatives

**Note: from this point on, compounds, schemes, figures and tables will be enumerated starting from the number 1. This numerical order will be maintained to reference the compounds herein synthesized in the following chapters dedicated to their biological evaluation.*

Continuing with our research group´s previous work focused in the development of small *N*-containing heterocycles as TOP1 inhibitors[93,94], we designed a set of 2,4-diarylsubstituted 1,2,3,4-tetrahydroquinolines and quinolines bearing a pentavalent diphenylphosphine oxide moiety which may be conveniently prepared by the Povarov reaction which involves a Lewis acid promoted [4+2] cycloaddition reaction. For the preparation of 8-quinolinylphosphine oxide derivatives **III**, this reaction could be performed between *N*-aryl imines **II** (obtained by condensation between anilines **I** and aldehydes) and electron rich dienophiles, acceding to a broad variety of tetrahydroquinolines **III** (Scheme 1).

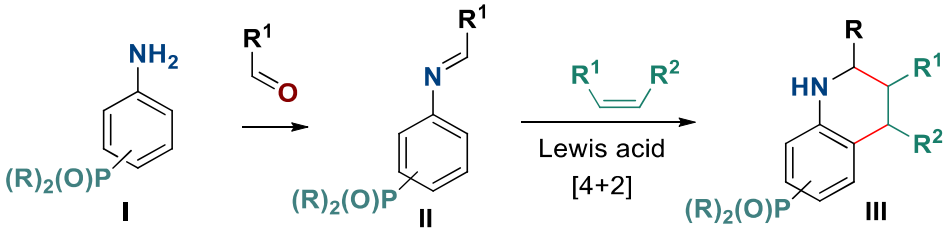

Scheme 1. Lewis-acid catalyzed Povarov reaction

I-3.1. Synthesis of (2-aminophenyl)diphenylphosphine oxide 1a

In order to accomplish the synthesis of quinoline derivatives through the Povarov reaction, firstly we had to prepare the corresponding *o*-phosphine oxide aniline **1a** (Figure 1) as long as this initial substrate is not commercially available.

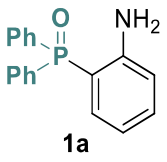

*Figure 1. Structure of (2-aminophenyl)diphenylphosphine oxide **1a**.*

Based on the existing bibliography, apparently the most reliable method for the preparation of *o*-phosphine oxide aniline **1a** (Figure 2) implies a 2 step procedure involving a nucleophilic

aromatic substitution reaction (S_NAr) of 1,2-dinitrobenzenes with trivalent organophosphorus reagents (Scheme 2).

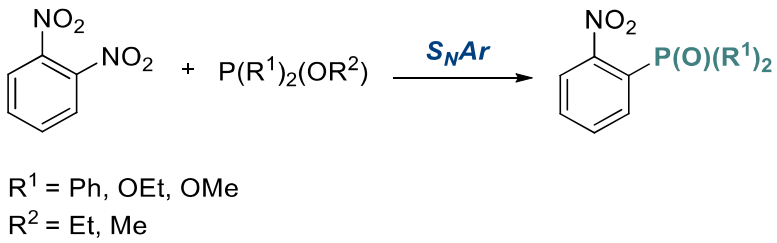

Scheme 2. S_NAr of 1,2-dinitrobenzenes and nucleophilic trivalent phosphorus reagents outlined by Cardogan and collaborators.

The present S_NAr methodology was disclosed by Cardogan and collaborators in 1969[228] but is still being used in recent publications[229]. Cardogan´s group described the displacement of a nitro group by nucleophilic phosphorus reagents through a Michaelis-Arbuzov-like mechanism. The reaction involves the nucleophilic addition of a trivalent phosphite/phosphinite to 1,2-dinitrobenzenes and a subsequent nucleophilic displacement of the activated nitro group to form a phosphonium salt intermediate. Finally, a dealkylation reaction mediated by the displaced nitro anion leads to the corresponding 2-nitrodiphenyl pentavalent phosphine oxide derivative (Scheme 2).

The aniline **1a** was prepared following the synthetic route depicted in scheme 3, which comprises a nucleophilic displacement of a nitro group of 1,2-dinitrobenzene with ethyl diphenylphosphinite and a subsequent selective hydrogenation of the nitro functionality.

[228] Cadogan JIG, Sears DJ, Smith DM. The reactivity of organophosphorus compounds. part XXV. displacement of activated aromatic nitro-groups by tervalent phosphorus reagents. *J Chem Soc C*. 1969(10):1314-1318. doi:10.1039/J39690001314

[229] a) Rad'kova NY, Tolpygin AO, Rad'kov VY, *et al.* Bis(alkyl) rare-earth complexes coordinated by bulky tridentate amidinate ligands bearing pendant Ph2P=O and Ph2P=NR groups. Synthesis, structures and catalytic activity in stereospecific isoprene polymerization. *Dalton Trans*. 2016;45(46):18572-18584. doi: 10.1039/C6DT03074B b) Navarro Y, García López J, Iglesias MJ, López Ortiz F. Chelation-assisted interrupted copper(I)-catalyzed Azide–Alkyne–Azide domino reactions: Synthesis of fully substituted 5-triazenyl-1,2,3-triazoles. *Org Lett*. 2021;23(2):334-339. doi: 10.1021/acs.orglett.0c03838.

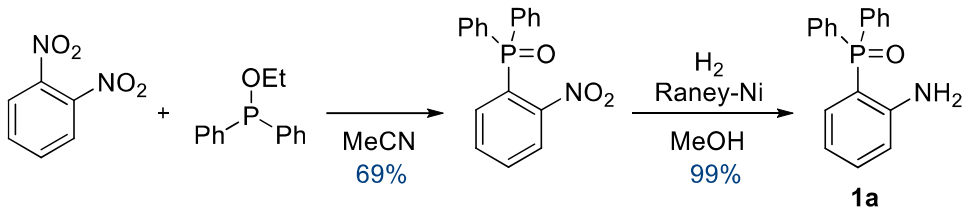

*Scheme 3. Synthesis of the starting substrate **1a**.*

Reaction monitoring by ^{31}P-NMR spectroscopy revealed that the ethyl diphenylphosphinite was not totally converted into (2-nitrophenyl)diphenylphosphine oxide, even though after purification of the crude reaction, (2-nitrophenyl)diphenylphosphine oxide was obtained in a good yield (69%). Moreover, the present S_NAr prodecure allows an easy recovery of the starting 1,2-dinitrobenzene, which can be re-used in future reactions. After the insertion of the pentavalent phosphorous functionalities in the benzene ring, the nitro group was easily reduced into amino functionality in a quantitative yield (shown as 99 %) by selective catalytic hydrogenation in the presence of Raney nickel, obtaining the desired (2-aminophenyl)diphenylphosphine oxide **1a** (Scheme 3).

I-3.2. Synthesis of hybrid diphenylphosphine oxide substituted 1,2,3,4-tetrahydroquinolines by the Povarov reaction

I-3.2.1. One-pot step-by-step reaction with olefins (*route A*)

Once the starting substrate **1a** was prepared, we proceeded to use it in the subsequent steps. Phosphine oxide derived aldimines **4** can be easily prepared by the condensation of phosphorated aniline **1a** and aromatic aldehydes **2** in refluxing chloroform (Scheme 4). In order to protect the imines from hydrolysis, reactions were conducted under inert nitrogen atmosphere (N_2 gas) and molecular sieves were added to the reaction media.

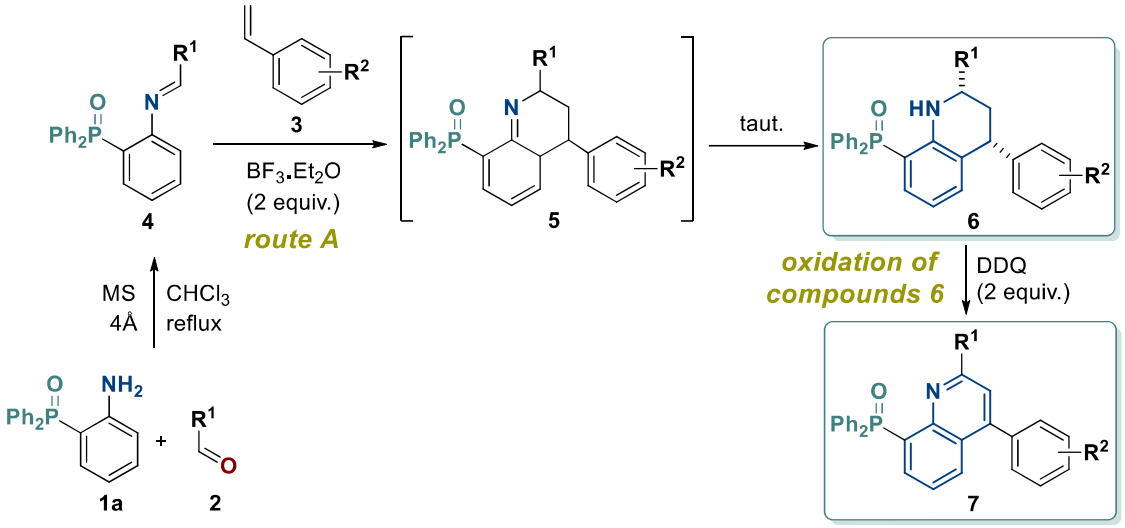

*Scheme 4. Synthetic **route A** (stepwise Povarov) for the preparation of 1,2,3,4-tetrahydroquinolin-8-yl phosphine oxides **6**.*

The formation of aldimines **4** was monitored by ^{1}H and ^{31}P-NMR spectroscopy. Despite their chemical instability, conversion of aniline **1a** into the corresponding aldimine **4** can be observed to a certain extent by NMR if the reaction is performed in deuterated chloroform and aliquots are taken under inert N_2 atmosphere (in the case of ^{31}P-NMR, the reaction can be made in $CHCl_3$ and then dilute the sample in $CDCl_3$). The reaction conditions for the formation of aldimines **4** are collected in the Table 1.

Table 1. Preparation of 2-(diphenylphosphine oxide) aldimines **4**.

Entry	Compound		Reaction time
	Nº	R^1	
1	**4a**	2-MeO-C_6H_4	12h
2	**4b**	4-$(EtO)_2P(O)O$- C_6H_4	24h
3	**4c**	1-naphthyl	24h
4	**4i**	3,4-F_2-C_6H_3	24h

Unfortunately, aldimines **4** result sensitive to hydrolysis, and therefore they were prepared *in situ* for the subsequent cycloaddition reactions, without previous isolation. After completion of imine formation in refluxing chloroform, the reaction was cooled down and phosphorated *N*-aryl imines **4** were used in the subsequent conventional Povarov approach comprised a Lewis acid (LA) catalyzed aza-Diels Alder reaction with electron rich olefins **3,** in the presence of boron trifluoride diethyl etherate ($BF_3.Et_2O$) as a Lewis acid catalyst (Scheme 4, ***route A***). In order to protect imines from hydrolysis, Povarov reactions were conducted under an inert nitrogen atmosphere (N_2 gas) and molecular sieves (4 Å) were added to the reaction media. The reaction

was heated at reflux and monitored by thin layer chromatography, ^{1}H and ^{31}P NMR spectroscopy.

As an example, ^{31}P-NMR monitoring for the preparation of aldimine **4a** (R^1 = 2-MeO; R^2 = H; Table 1, entry 1) and subsequent Povarov reaction of this imine with phenylstyrene **3a** (R^2 = H) is shown in the Figure 2. In this regard, due to the reaction between diphenylphosphine oxide aniline **1a** and 2-methoxybenzaldehyde **2a** (R^1 = 2-MeO), the ^{31}P-NMR signal of aniline **1a** (δ = 37.12 ppm) disappears, while a new signal (at δ = 29.42 ppm) corresponding to the formation of the aldimine 2-(2-methoxybenzylideneaminophenyl)diphenylphosphine oxide **4a** (R^1 = 2-MeO) is observed. After 2 h of reaction, the starting aniline has not been consumed and at 12 h the formation of the imine **4a** is completed. Then, the conversion of the aldimine **4a** into the corresponding tetrahydroquinoline **6a** through the Povarov reaction is completed in 36 h upon addition of $BF_3.Et_2O$ and phenylstyrene **3** (R^2 = H).

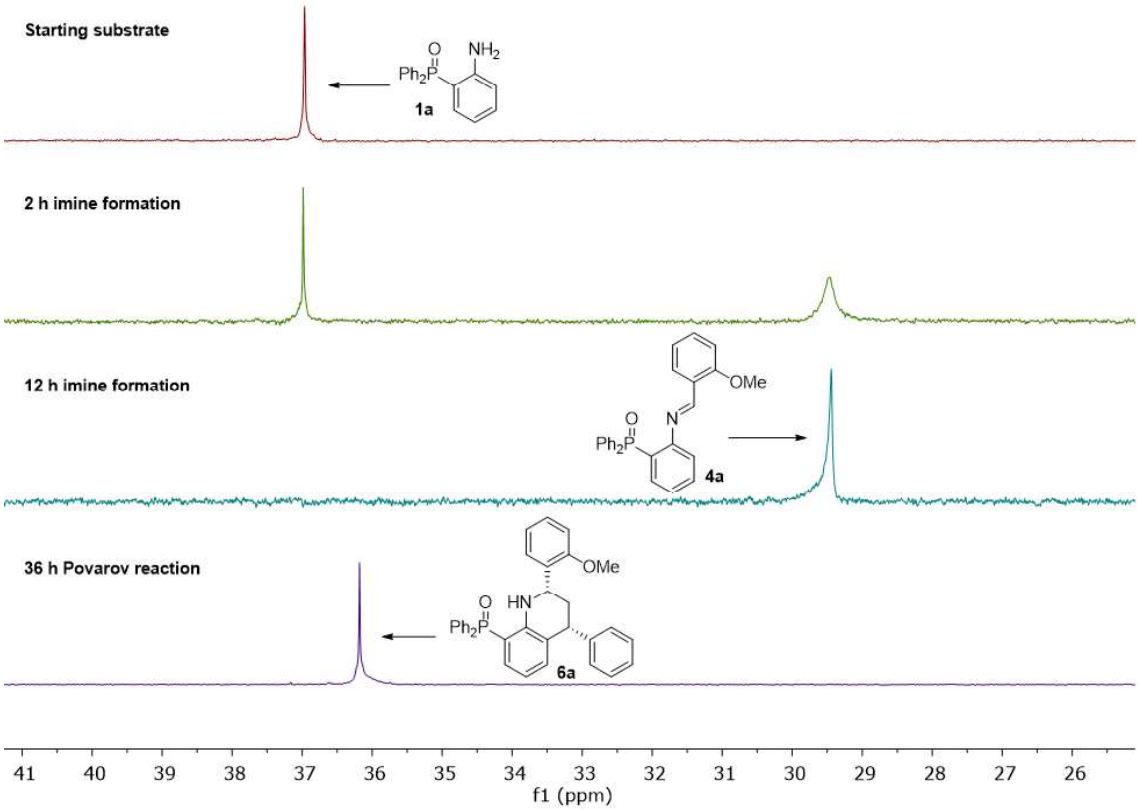

*Figure 2. Formation of imine **4a** and the subsequent Povarov reaction to yield compound **6a** monitored by ^{31}P-NMR.*

The structures of the newly synthesized 1,2,3,4-tetrahydroquinolines **6** were afterwards determined by 1D- and 2D-NMR spectroscopy and mass spectrometry experiments. Hence, in the ^{1}H-NMR spectrum of compound **6a,** there can be clearly observed the signals corresponding

to the four aliphatic hydrogens of the tetrahydropyridinyl moiety (positions 2, 3 and 4 thereof), as shown in the Figure 3.

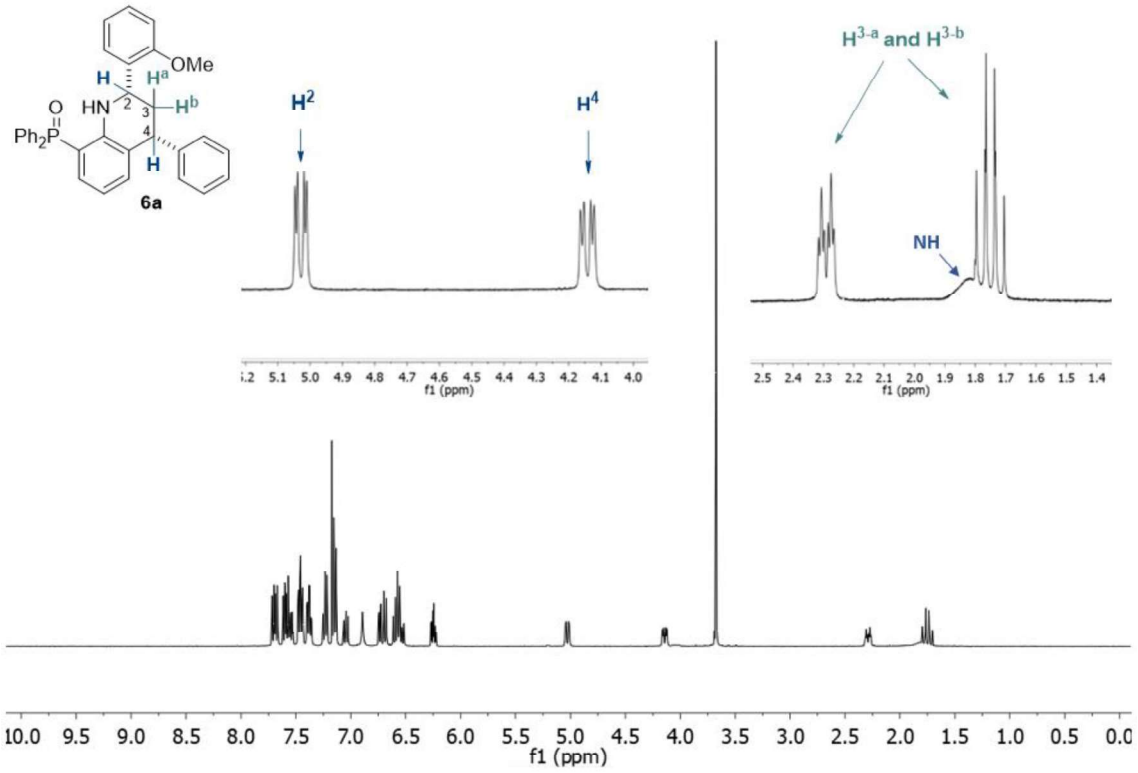

*Figure 3. ^{1}H-NMR spectrum of 1,2,3,4-tetrahydroquinolin-8-yl phosphine oxide **6a**.*

In the ^{1}H-NMR spectrum of compound **6a** (Figure 3), the low-field regions containing the characteristic aliphatic protons of the tetrahydroquinoline core (protons in positions 2, 3-a, 3-b and 4, respectively) are highlighted. Representative signals of this spectrum are a doublet at δ_H = 5.11 ppm with coupling constants of $^{3}J_{HH}$ = 12.3 Hz and $^{3}J_{HH}$ = 4.3 Hz corresponding to the proton at position 2 and a doublet at δ_H = 4.23 ppm with coupling constants of $^{3}J_{HH}$ = 12.3 Hz and $^{3}J_{HH}$ = 4.3 Hz corresponding to the 4-H proton. In addition, the two protons of the methylenic carbon (CH_2, located in position 3 of the tetrahydroquinoline) namely 3a-H and 3b-H are in fact diastereotopic protons, so we can observe them as two signals at low chemical shifts, one signal for each proton. One of the methylenic protons is observed as a multiplet at δ_H = 2.36 - 2.41 ppm, while the other methylenic proton is observed at δ_H = 1.80 ppm as a doublet of doublets of doublets (ddd) with coupling constants of $^{3}J_{HH}$ = 12.3 Hz, $^{3}J_{HH}$ = 11.1 Hz and $^{2}J_{HH}$ = 12.5 Hz. Moreover, the signal corresponding to methoxy group was observed at 3.68 ppm as a singlet. Finally, at δ = 1.82 ppm a wide signal is assigned to the proton of the NH group of the tetrahydroquinoline core, which disappears upon treatment of the sample with deuterated H_2O (D_2O).

The structural elucidation by ^{13}C-NMR spectroscopy (Figure 4) supports the proposed structure of compound **6a** and is in concordance with the results observed in the previously exposed ^{1}H-NMR experiment. Thus, at 50.0 ppm and 44.8 ppm two signals are observed assigned to the aliphatic carbons at positions C-2 and C-4 respectively. The methylenic carbon (CH_2) is visualized as a signal at 38.0 ppm, whose nature was confirmed by the DEPT-135 ^{13}C-NMR experiment and the methoxy group is observed as a signal at 55.4 ppm.

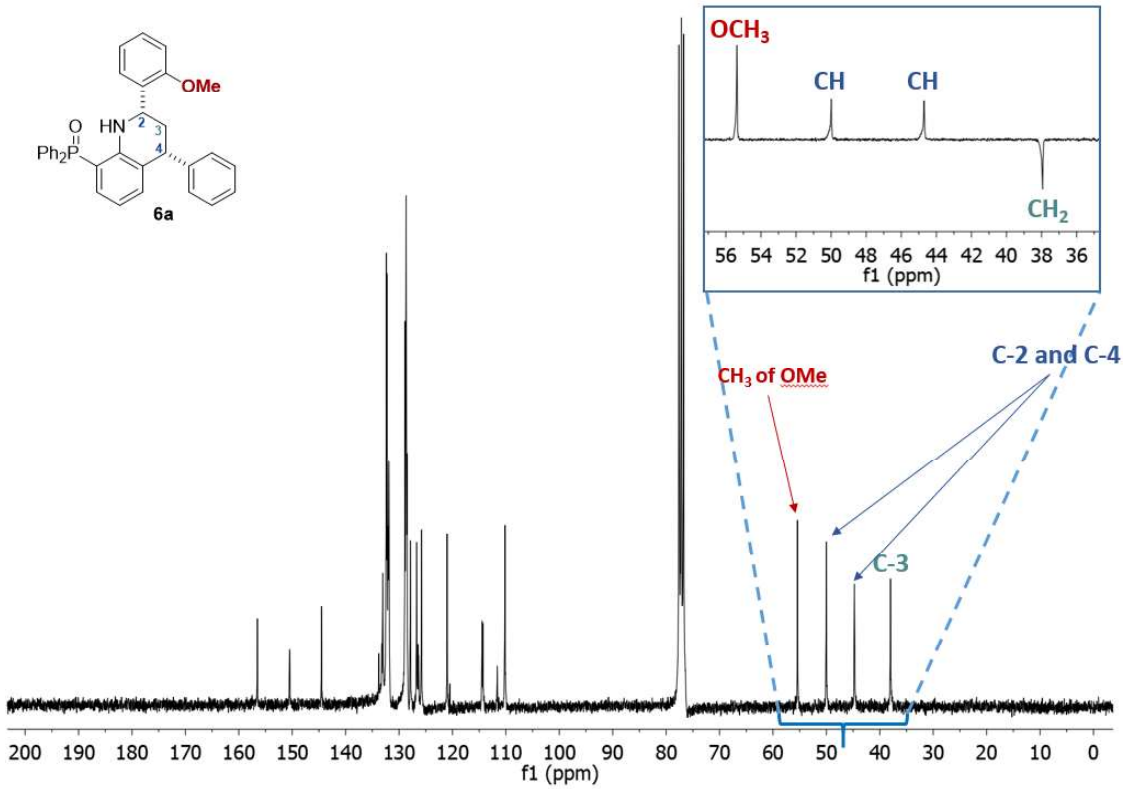

*Figure 4. ^{13}C-NMR spectrum of 1,2,3,4-tetrahydroquinolin-8-yl phosphine oxide **6a**.*

The regiochemistry of the process could be determined by 2D HMQC (C-H 1-bond correlation) and HMBC (C-H 2,3-bonds correlation) experiments of compound **6a**. Unfortunately, one of the signals needed to determine the configuration corresponds to the NH group, which appears overlapped with the aromatic signals. Consequently, in this case the regiochemistry was determined by NOESY (Nuclear Overhauser Effect SpectroscopY) NMR experiments. Precisely, due to the presence of a 2-methoxyphenyl substituent at position 2 of the tetrahydroquinoline ring, NOE effect is observed between the methyl of the methoxy substituent and the methylenic group of the tetrahydroquinoline ring (Figure 5). The selective saturation of the methyl protons has a positive NOE effect on the methylenic protons of 2.85% and 0.75% respectively.

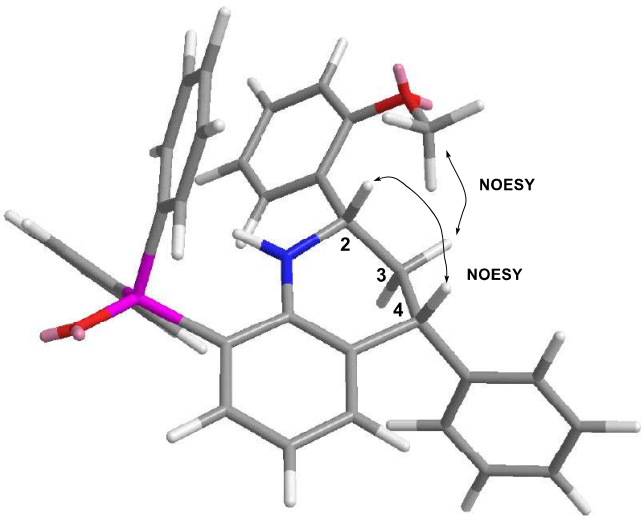

*Figure 5. Relative configuration for the compound **6a** assigned by 1D-NOESY -NMR.*

Furthermore, the stereoselectivity of the process was also determined by 1D-NOESY experiments. The selective saturation of the 2-H proton presents a positive NOESY effect on the 4-H proton (3.70%), showing a relative cis-configuration between the protons located in position 2 and 4 and therefore suggesting that the cycloaddition reaction between phosphorated imines and dienophiles occurs through an *endo* transition state (Figure 5).

In view of the results obtained in NOESY NMR spectroscopy experiments, we can conclude that the process may be explained by a [4+2]-cycloaddition reaction between aldimines **4** and dienophiles **3** that leads to the formation of intermediate adducts **5** (Scheme 4, ***route A*****),** followed by a subsequent prototropic tautomerization to yield the tetrahydroquinolines **6**. The yields obtained after purification by column chromatography and crystallization in hexane:ethyl acetate are collected in the table 2 (see entries with the ***route A***).

Table 2. Synthesis of 1,2,3,4-tetrahydroquinolin-8-yl phosphine oxides **6** by routes **A** and **B**.

Entry	Compound			Route	Yield (%)*
	Nº	R^1	R^2		
1	**6a**	2-MeO-C_6H_4	H	A	91
2	**6b**	4-$(EtO)_2P(O)O$- C_6H_4	H	A/B	44/66
3	**6c**	1-naphthyl	H	A	65
4	**6d**	2-naphthyl	H	B	72
5	**6e**	2-pyridyl	H	B	69
6	**6f**	C_6H_5	4-Me	B	61
7	**6g**	4-F-C_6H_4	4-Me	B	71
8	**6h**	4-F-C_6H_4	4-F	B	44
9	**6i**	3,4-F_2-C_6H_3	4-F	A	49

A variable small fraction (5-20%) of the corresponding quinolines **7 was observed after purification by silica/alumina column chromatography. This fact warned us to consider tetrahydroquinolines **6** sensitive to oxidation, even though once isolated they demonstrated to be stable both in solid/oil state and in dissolution.*

3.2.2. MCR reaction with olefins (*route B*)

Once we achieved the preparation of phosphine oxide-substituted tetrahydroquinolines **6** prepared through the conventional one-pot Povarov reaction, we estimated to explore the MCR Povarov reaction in a single operation approach. In this regard, we consider the Povarov three-component reaction a highly favourable convergent synthetic strategy for the preparation of tetrahydroquinolines **6** with step economy and tolerating a wide range of aromatic aldehydes **2** and styrenes **3** (Scheme 5, ***route B***). Accordingly, aniline **1a**, aromatic aldehydes **2**, styrenes **3** and 2 equivalents of $BF_3.Et_2O$ (in the presence of molecular sieves) were heated in refluxing chloroform until the consumption of starting materials. Total conversion of aniline **1a** into tetrahydroquinolines **6** was observed within 24-48 h, in a regio- and diastereoselective way (the yields after column chromatography purification and crystallization are collected in Table 2 (see entries with the ***route B***).

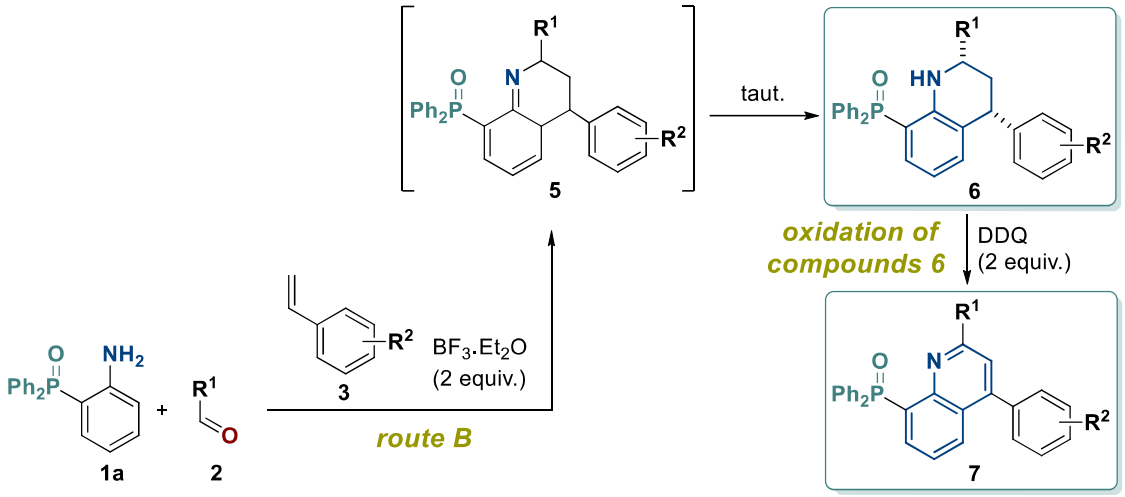

*Scheme 5. Synthetic **route B** (Povarov MCR) for the preparation of 1,2,3,4-tetrahydroquinolin-8-yl phosphine oxides 7.*

In view of the results collected in Table 2, we can conclude that the present methodology (in both step-by-step and MCR versions) tolerates a wide range of electron-donating and electron-withdrawing aromatic aldehydes and styrenes. In particular, the one-pot protocol (***route A***, Scheme 4) allowed the obtainment of the tetrahydroquinoline derivative **6a** (R^1 = 2-MeO-C_6H_4; R^2 = H; Table 2, entry 1) in a high yield (91%), whereas the Povarov MCR approach (***route B***, Schme 5) resulted specially effective for the synthesis of tetrahydroquinoline derivatives **6d** (R^1 = 2-naphthyl; R^2 = H; entry 4) and **6g** (R^1 = 4-F-C_6H_4; R^2 = 4-Me; entry 7) in one single step, with yields of 72% and 71% respectively.

I-3.3. Synthesis of diphenylphosphine oxide substituted quinolines

I-3.3.1. Oxidation of 1,2,3,4-tetrahydroquinolin-8-yl phosphine oxides 6

After the preparation of tetrahydroquinoline primary adducts **6** by the Povarov reaction, we considered the synthesis of the corresponding quinolines **7** by a subsequent dehydrogenation process (Scheme 6). Tetrahydroquinolines **6** are subjected to oxidation to obtain the corresponding quinolines **7**, which involves the removal of four hydrogens by an oxidant agent and leads to the loss of the stereoselectivity. The selective dehydrogenation of THQ frameworks leads to fully aromatic quinolines, and this fact may have a remarkable effect towards inhibition of TOP1 as flat or quasi-flat polyaromatic systems may stablish favourable interactions with TOP1-DNA complexes (mainly π-stacking interactions with DNA base pairs)[230].

DDQ is one of the most used oxidizing agent to dehydrogenate Povarov adducts. Our group had previous experience working with DDQ and in the present oxidations, rapid conversions with no evidences of side reaction products were observed. In this manner, we optimized a standard protocol using tetrahydroquinolines **6** and 2 equivalents of DDQ in refluxing chloroform (Scheme 6). The reaction progress was followed by TLC and NMR spectroscopy (^{1}H, ^{31}P) and, in all cases, reactions were completed after 2 h. The isolation of quinolines **7** from the reaction crudes may result challenging, because of the dirtiness derived from the excess of DDQ and reduced form thereof. Thus, as DDQ and reduced form result partially soluble in water, we realized that a work up comprising washing the organic solution just with water several times (5-10) allows to get rid of the impurities that hinder the purification step.

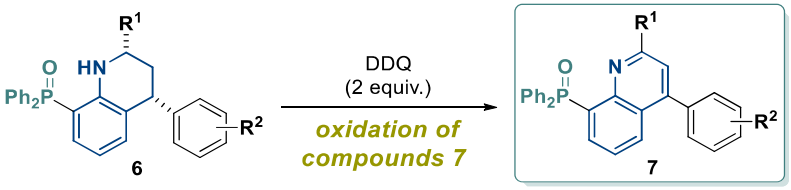

*Scheme 6. Aromatization of 1,2,3,4-tertrahydroquinolin-8-yl phosphine oxides **6** to yield quinoline-8-yl phosphine oxides **7**.*

Following the current DDQ oxidation protocol, we proceeded to the preparation of the quinoline-8-yl derivative **7a** by the selective dehydrogenation of 1,2,3,4-tetrahydroquinolin-8-yl derivative **6a** as a model reaction. The formation of (2-(2-methoxyphenyl)-4-phenylquinolin-8-yl)diphenylphosphine oxide **7a** was confirmed by ^{1}H-NMR spectroscopy. In the ^{1}H-NMR

[230] Pommier Y, Marchand C. Interfacial inhibitors: targeting macromolecular complexes [published correction appears in Nat Rev Drug Discov. 2012 Mar;11(3):250]. *Nat Rev Drug Discov*. 2011;11(1):25-36. Published 2011 Dec 16. doi:10.1038/nrd3404

spectrum of the fully aromatic quinoline derivative **7a**, the characteristic signals corresponding to the aliphatic protons present in the tetrahydroquinoline ring of **6a** disappeared, while a new characteristic signal appears in the aromatic region (at δ = 8-9 ppm) as shown in Figure 6.

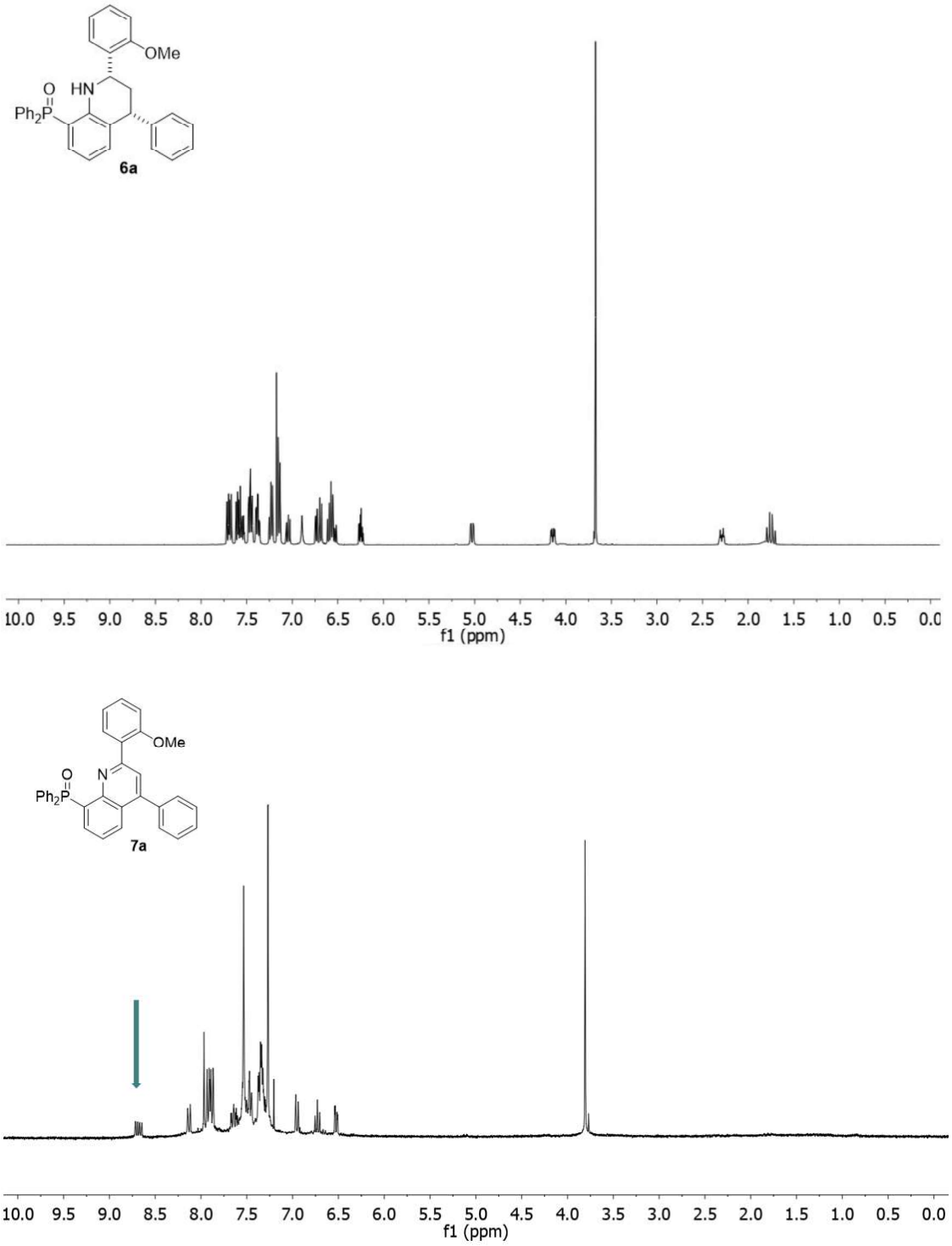

*Figure 6. Comparison between ^{1}H-NMR spectra of tetrahydroquinolin-8-yl phospine oxide **6a** and the corresponding quinolin-8-yl phospine oxide **7a**.*

Once established the reaction conditions, we next studied the scope of the selective dehydrogenation process. Thus, the optimized DDQ protocol was applied to the rest of 1,2,3,4-tetrahydroquinolin-8-yl phosphine oxides **6**. The afforded quinolin-8-yl phosphine oxides **7** were isolated by column chromatography and recrystallyzed in hexane:ethyl acetate. Yields of quinolines **7** prepared by the aforementioned DDQ oxidation approach are summarized in Table 3.

Table 3. Yields of quinoline-8-yl phosphine oxides **7** obtained by ***DDQ oxidation of compounds 6***.

Entry	**Compound**			**Yield (%)**
	Nº	**R^1**	**R^2**	
1	**7a**	2-MeO-C_6H_4	H	74
2	**7b**	4-$(EtO)_2P(O)O$- C_6H_4	H	65
3	**7c**	1-naphthyl	H	72
4	**7d**	2-naphthyl	H	82
5	**7f**	C_6H_5	4-Me	88
6	**7g**	4-F-C_6H_4	4-Me	93
7	**7h**	4-F-C_6H_4	4-F	96
8	**7i**	3,4-F_2-C_6H_3	4-F	99

If we attend to the results listed in the Table 3, we can observe that the DDQ dehydrogenation procedure of tetrahydroquinolines **6** to obtain the fully aromatic quinolinyl phosphine oxides **7** was found to be an efficient method with overall high yields (65-99%). The best yields were obtained with quinoline derivatives **7g** (R^1 = 4-F-C_6H_4; R^2 = 4-Me; entry 6), **7h** (R^1 = 4-F-C_6H_4; R^2 = 4-Me; entry 7), and **7i** (R^1= 3,4-F-C_6H_3; R^2 = 4-F; entry 8), showing excellent yields (between 93-99%).

I-3.3.2. Povarov reaction with acetylenes (*route C*)

Once we obtained quinolines **7a-i** by the oxidation of isolated Povarov tetrahydroquinoline adducts **6** with DDQ, we moved to investigate a straightforward method to obtain directly quinolines **7** involving a Povarov reaction between 2-(diphenylphosphine oxide) aldimines **4** and acetylenes **8** (Scheme 7, ***route C***).

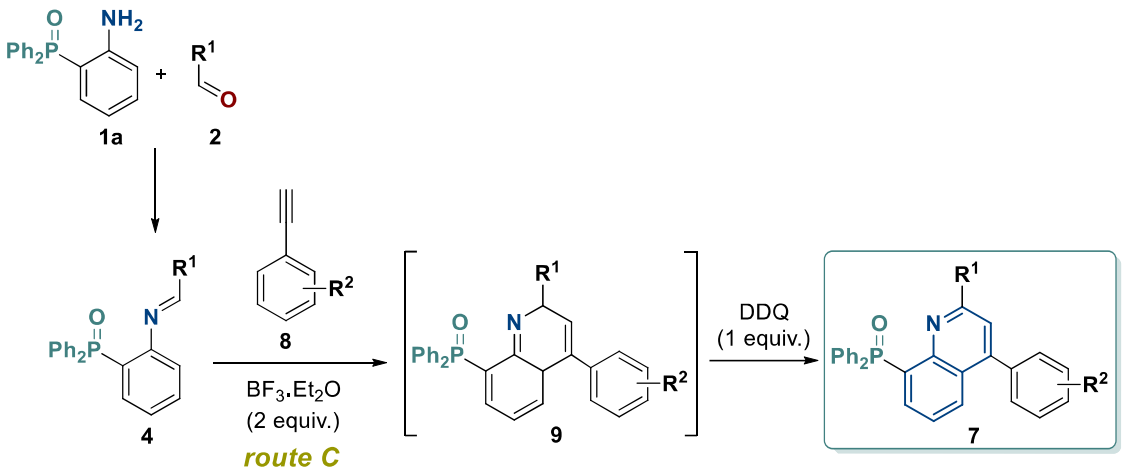

*Scheme 7. Synthetic route for the direct preparation of quinoline-8-yl phosphine oxides **7**.*

To start the investigation, a Povarov approach starting from *in situ* generated imines was explored. In this regard, aldimines **4** were prepared from the condensation of aniline **1a** and aromatic aldehydes **2** in refluxing chloroform within 24 h (we used the same conditions described for the imines prepared in ***route A*** (Scheme 4, *vide supra*). Imines **4** were reacted with acetylenes **8**, 2 equivalents of $BF_3.Et_2O$ and DDQ, to obtain regioselectively quinolines **7** (Scheme 7, Table 4). The structure of the obtained compounds **7** by the ***route C*** (oxidative Povarov reaction) was confirmed by comparison with derivatives **7** obtained by ***oxidation of compounds 6***.

Table 4. Yields of quinoline-8-yl phosphine oxides **7** obtained by ***route C***.

Entry	Compound			Yield (%)
	Nº	R^1	R^2	
1	**7f**	C_6H_5	4-Me	82
2	**7g**	4-F-C_6H_4	4-Me	71
3	**7h**	4-F-C_6H_4	4-F	68
4	**7j**	C_6H_5	4-F	56
5	**7k**	4-F-C_6H_4	H	50

As it can be observed in the table 4, the straightforward preparation of quinolinyl phosphine oxides **7** through the step-by-step Povarov-DDQ oxidation reaction sequence (***route C***) reported moderate to high yields (50-82%) and resulted specially effective for the direct preparation of the compound **7f** ($R^1 = C_6H_5$; R^2 = 4-Me; Table 4, entry 1) in a one-pot approach.

At this point it has to be mentioned that during the Povarov reaction with acetylenes (Scheme 7), in the absence of DDQ evidences of an unexpected side oxidation reaction of intermediates

6 were observed by the *in situ* generated imines **4**, as these imines **4** can act as H acceptors and therefore reduce to the corresponding secondary amine form (isolated from the reaction crudes), resulting in an undesired loss of efficiency[231]. This undesired reduction of imines **4** can be prevented by directly adding DDQ to the Povarov reaction. The formation of quinolines **7** between aldimines and acetylenes in the presence of DDQ can be explained by a step-by-step Povarov reaction[225] that proceeds through the intermediate adducts **9,** whose subsequent tatutomerization-dehydrogenation sequence in the presence of DDQ leads to the formation of quinolines **7** (Scheme 7).

Furthermore, it should be noted that the Povarov MCR with acetylenes is not favoured, as the reaction is reported to undergo a predominant side-reaction between aldehydes and acetylenes. In acidic media, aromatic aldehydes and acetylenic compounds lead to the formation of undesired α,β-unsaturated ketones[232]. For this reason, the development of a MCR approach was discarded and we ruled out the study of the stepwise Povarov-DDQ oxidation one-pot cascade reaction, using acetylenes as dienophiles.

I-3.4. Summary of the synthetic routes employed for the preparation of hybrid quinolin-8-yl phosphine oxide derivatives 6 and 1,2,3,4-tetrahydroquinolin-8-yl phosphine oxide derivatives 7

Initially, quinoline derivatives **7** (Scheme 8) were the main object of research, but preliminary studies with tetrahydroquinolines **6** revealed certain biological activity as antiproliferative/TOP1 inhibitor agents. Based on these inferences, we had to consider the isolation and further evaluation of tetrahydroquinoline adducts along with fully aromatic quinolines. Accordingly, various strategies based on the Povarov reaction were investigated for the synthesis of 2,4-disubstituted 1,2,3,4-tetrahydroquinolines (**6**) and quinoline (**7**) derivatives bearing a diphenyl phosphine oxide functionality in position 8 (namely ***route A***, ***route B***, ***oxidation of compounds 6*** and ***route C***). All the syntetic routes studied in this section are collected in the Scheme 8.

[231] Selas A, Ramírez G, Palacios F, Alonso C. Design, synthesis and cytotoxic evaluation of diphenyl(quinolin-8-yl)phosphine oxides. Tetrahedron Lett. 2021;70:153019. doi:10.1016/j.tetlet.2021.153019

[232] Rueping M, Bootwicha T, Baars H, Sugiono E. *Beilstein J. Org. Chem.* 2011;*7:*1680–1687. doi:10.3762/bjoc.7.198

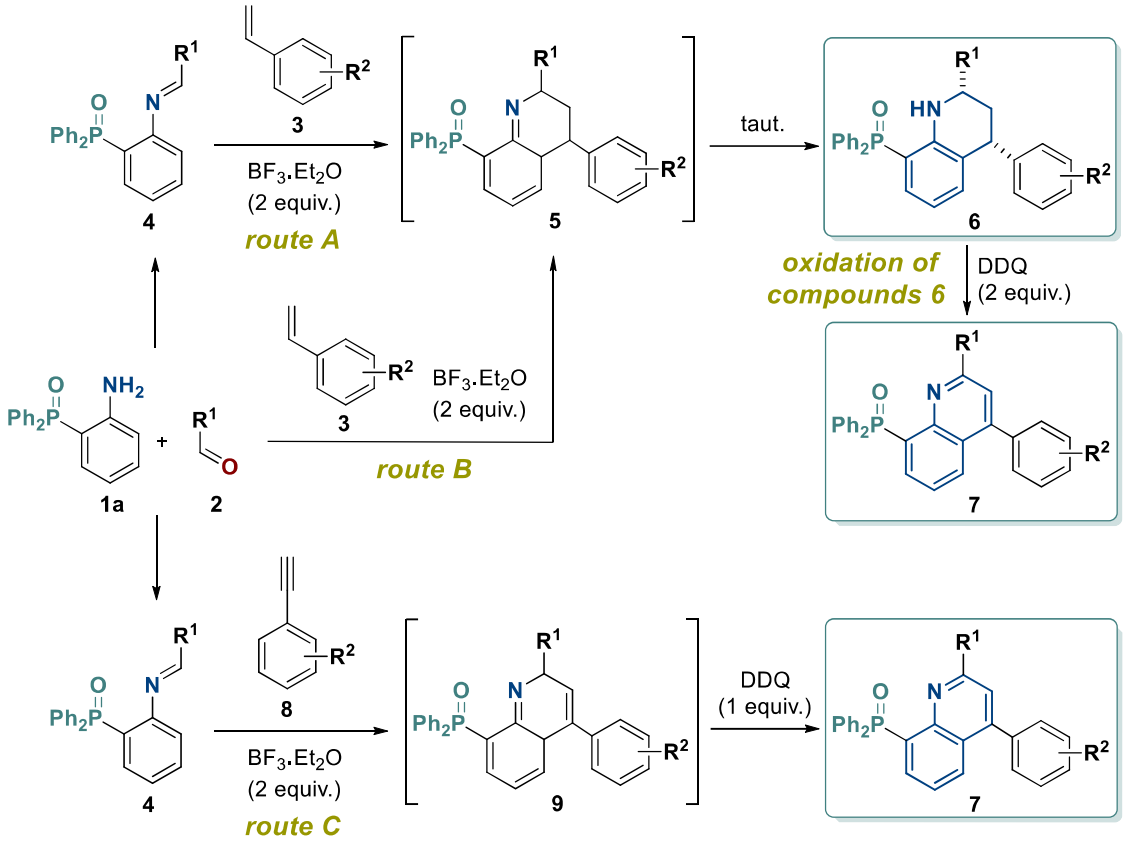

*Scheme 8. Synthetic routes for the preparation of 1,2,3,4-tetrahydroquinolin-8-yl phosphine oxides **6** and quinolin-8-yl phospine oxides **7**. A general overview.*

I-4. Synthesis of hybrid dialkyl 1,2,3,4-tetrahydroquinolinylphosphonates and dialkyl quinolinylphosphonates

Continuing our previous work initiated with the preparation of phosphine oxide substituted quinoline derivatives as candidates for TOP1 inhibitors[233], we decided to expand our research and focus on the preparation of novel phosphonate-functionalized quinolines for a further biological study. Accordingly, we framed the study of novel hybrid 2,4-quinoline derivatives with dialkyl phosphonate functionalities. In light of the experience obtained from the previous work, we estimate to the Povarov reaction a highly convenient procedure to access to the aforementioned hybrid quinolinyl phosphonates.

I-4.1. Synthesis of anilines substituted with dialkyl phosphonate 1b, 1c and 1d

First of all, we started with the preparation of dialkyl phosphonate-substituted anilines **1b**, **1c** and **1d** (Figure 7) as starting material for the Povarov reaction as these compounds are not commercially available.

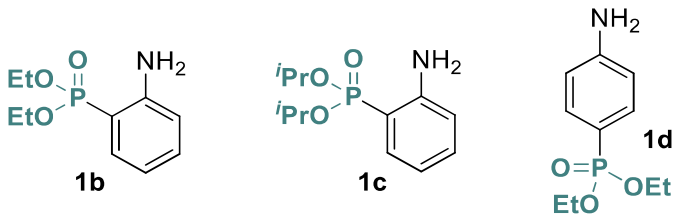

*Figure 7. Structure of dialkyl phosphonate-substituted anilines **1b**, **1c** and **1d**.*

In order to obtain the dialkyl phosphonate-substituted anilines **1b**, **1c** and **1d**, we firstly tried the aforementioned S_NAr of dinitrobenzenes with trivalent organophosphorus reagents described by Cardogan (shown in the section 3.1. *vide supra*). Cardogan described the displacement of a nitro group by nucleophilic trialkyl phosphites that leads to the corresponding dialkylphosphonate derivative (Scheme 9, ***route A***). The ***route A*** has been successfully employed in the preparation of dialkyl phosphonate-substituted anilines **1b** and **1c**. Nevertheless, the reaction did not occur with *p*-dinitrobenzene under the same reaction conditions, at least in a measurable range after 120 hours (this fact was also observed by Cardogan and collaborators). Consequently, when we decided to extend the scope of the Povarov reaction using an aniline bearing a dialkyl phosphonate group in *para*- position (aniline **1d**), alternative methods had to be explored.

[233] Alonso C, Fuertes M, Martín-Encinas E, *et al.* Novel topoisomerase I inhibitors. Syntheses and biological evaluation of phosphorus substituted quinoline derivates with antiproliferative activity. *Eur J Med Chem*. 2018;149:225-237. doi:10.1016/j.ejmech.2018.02.058

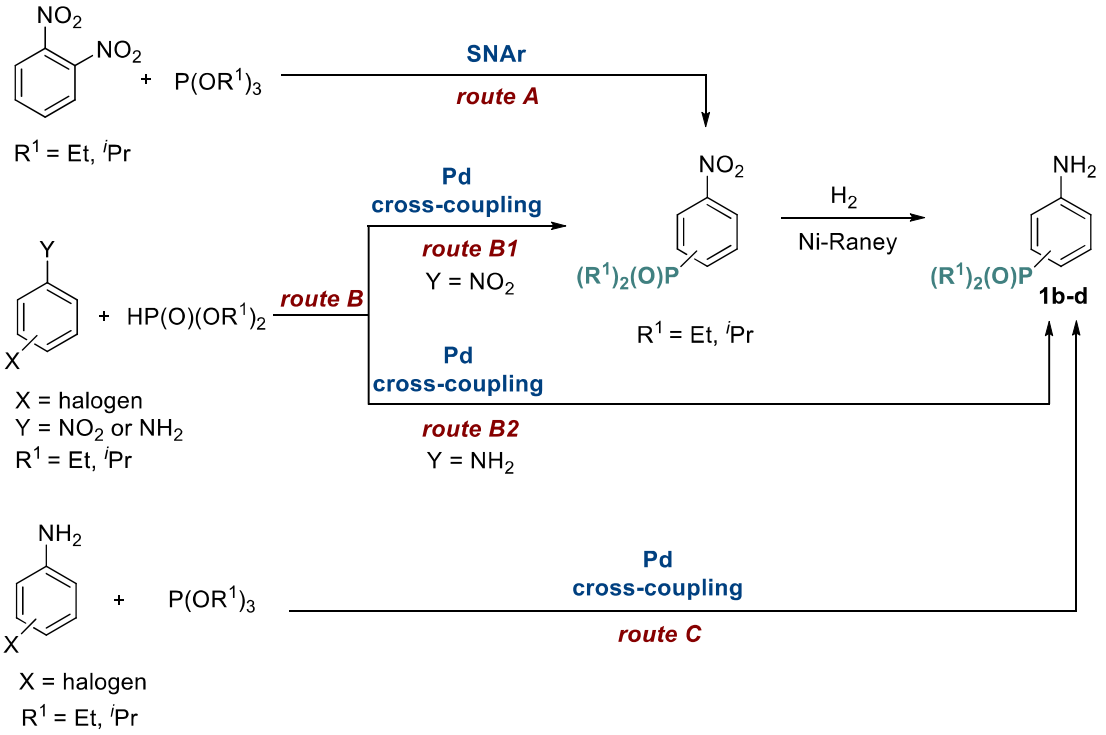

*Scheme 9. Synthetic routes studied for the preparation of dialkyl phosphonate-substituted anilines **1b-d**.*

The S_NAr approach (***route A***, Scheme 9) results to be intrinsically limited to the preparation of ortho phosphorated nitrobenzenes, and therefore we found the Pd-catalyzed cross coupling approach (***route B*** and ***route C***, Scheme 9) a convenient method for the preparation of phosphorylated anilines **1b**, **1c** and **1d**. In this regard, the Pd-catalyzed reaction between aryl halides and dialkyl-*H*-phosphites described by Hirao and co-workers resulted a suitable method[234]. Tetrakis(triphenylphosphine)palladium(0) [$Pd(PPh_3)_4$]-mediated catalysis allows a direct C-P bound formation by inserting dialkyl phosphonate moieties into aromatic systems with a nitro substituent. More recently, Guilard *et al.* disclosed a novel entry to extend the present cross-coupling reaction to aryl halides bearing primary amines[235]. Guilard and collaborators described the *in situ* formation of $Pd(PPh_3)_4$ from $Pd(OAc)_2$ 2 mol% and PPh_3 6 mol%. Based on these works, we elaborated a procedure involving a Pd cross coupling reaction between aryl halides and dialkyl-*H*-phosphites in two ways: 1) a protocol employing nitro-substituted aryl halides, which requires an additional step to transform the nitro group into a

[234] Hirao T, Masunaga T, Yamada N, Ohshiro Y, Agawa T. Palladium-catalyzed new carbon-phosphorus bond formation. *Bull Chem Soc Jpn*. 1982;55(3):909-913. doi:10.1246/bcsj.55.909.
[235] Bessmertnykh A, Douaihy CM, Guilard R. Direct synthesis of amino-substituted aromatic phosphonates via palladium-catalyzed coupling of aromatic mono- and dibromides with diethyl phosphite. *Chem Lett*. 2009;38(7):738-739. doi:10.1246/cl.2009.738.

primary amine (***route B1***) or 2) a straightforward protocol using NH_2-containing aryl halides (***route B2***).

In contrast to the *o*-halogenated anilines, *p*-halogenated aniline proceeded through the cross-coupling reaction with a certainly low yield (***route B2***), so we decided to investigate other methodologies to afford *p*-diethylphosphonate aniline **1d**. We followed the protocol disclosed by Iranpoor *et al.*, which consists of a ligand-free-Pd catalyzed reaction between aryl halides and trialkylphosphites to yield dialkyl arylphosphonates[236]. By following this procedure (***route C***), we obtained the desired *p*-dialkylphosphoryl aniline **1d** in a relatively high yield.

The synthetic routes followed for each dialkyl phosphonate-substituted anilines (**1b**, **1c**, **1d**) are shown below:

Synthesis of diethyl (2-aminophenyl)phosphonate 1b

We proceeded the **routes A**, **B1** and **B2** as depicted in the Scheme 10, and based on the obtained results we considered the ***route B2*** the most appropriate protocol to prepare diethyl (2-aminophenyl)phosphonate **1b** in relatively high yields by a single step methodology.

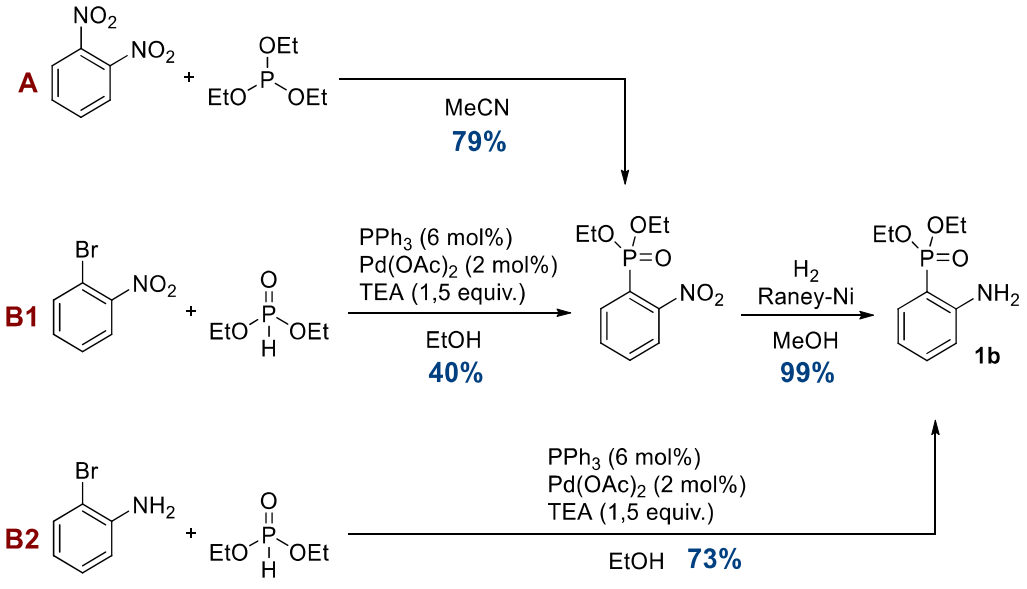

*Scheme 10. Synthetic routes studied for the preparation of the aniline **1b**.*

[236] Iranpoor N, Firouzabadi H, Moghadam KR, Motavalli S. First reusable ligand-free palladium catalyzed C–P bond formation of aryl halides with trialkylphosphites in neat water. *RSC Adv*. 2014;4(99):55732-55737. doi:10.1039/C4RA07680J

Synthesis of diisopropyl (2-aminophenyl)phosphonate 1c

The ***routes A***, ***B1*** and ***B2*** were investigated for the preparation of diisopropyl (2-aminophenyl)phosphonate **1c** (Scheme 11). Attending to the results, it can be noted that the ***route B2*** leads to phosphorylated aniline **1c** in a moderate yield but in a single operation. Nevertheless, the ***route A*** was considered the most appropriate protocol to prepare the compound **1c** in higher yields, resulting also an easily scalable synthetic methodology.

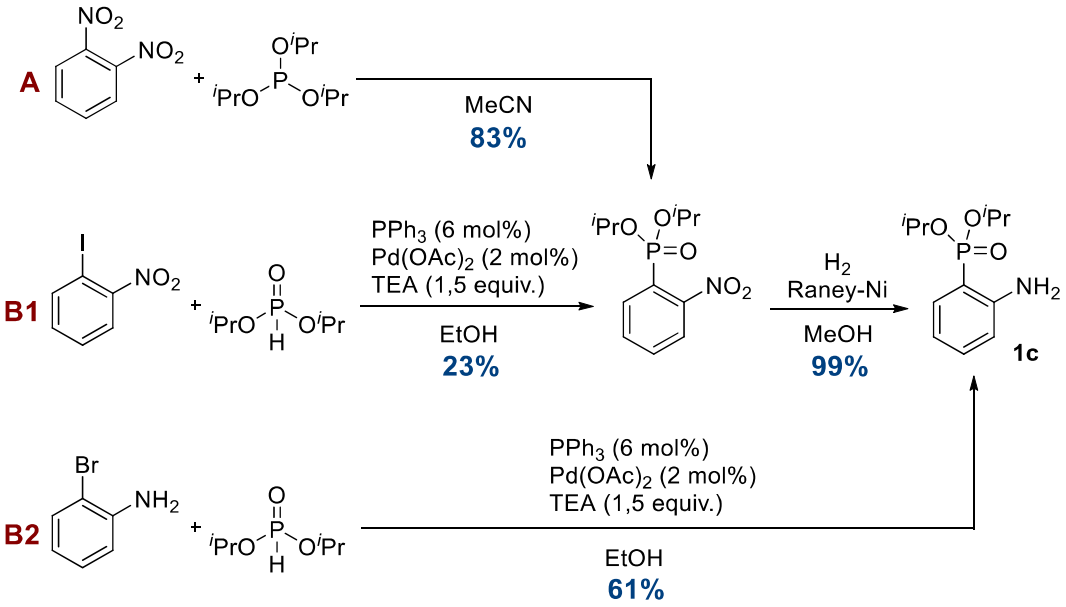

*Scheme 11. Synthetic routes studied for the preparation of the aniline **1c**.*

Synthesis of diethyl (4-aminophenyl)phosphonate 1d

Both ***routes B1*** and ***C*** have demonstrated to be convenient approaches to prepare the aniline **1d** in similar yields (synthetic routes are shown in the Scheme 12), but we lean towards the ***route C*** as it implies a single operation process.

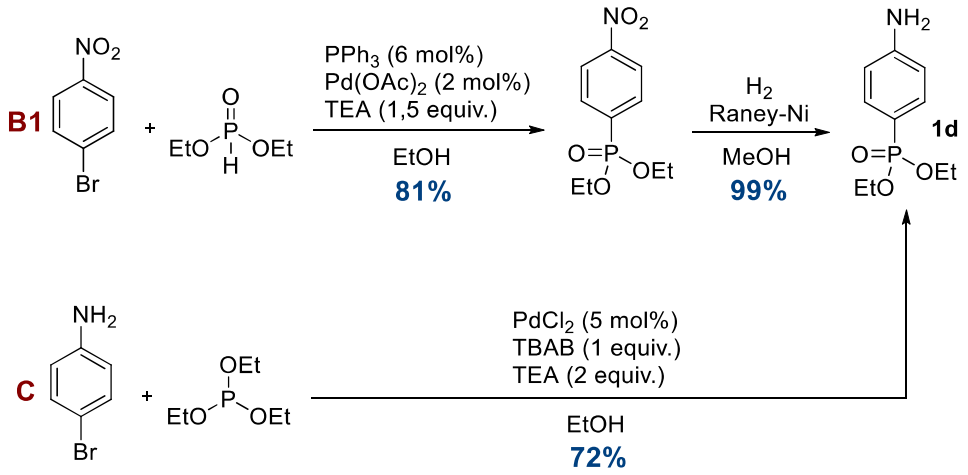

*Scheme 12. Synthetic routes studied for the preparation of the aniline **1d**.*

I-4.2. Synthesis of dialkyl quinolin-8-ylphosphonates

I-4.2.1. One-pot reaction with olefins (*route A*)

We initiated the study by exploring the step-by-step Povarov reaction between imines **10** derived from the condensation of diethyl (2-aminophenyl)phosphonate **1b** and aldehydes **2** with styrenes **3**. Once the imine formation was completed (monitored by $^{1}H/^{31}P$-NMR spectroscopy experiments), imines **10** were electrophilically activated by adding 2 equivalents of $BF_3.Et_2O$ and reacted with styrenes **3** in refluxing chloroform (Scheme 13). A complete formation of adducts **12** was observed by $^{1}H/^{31}P$-NMR spectroscopy in all cases, but we realised that phosphorylated tetrahydroquinolines **12** were quite sensitive to spontaneous oxidation while/after purification by silica/alumina gel chromatography (even if they were manipulated under N_2 atmosphere and conserved at -20ºC), affording a variable mixture of tetrahydroquinolines **12** and corresponding quinolines **13**.

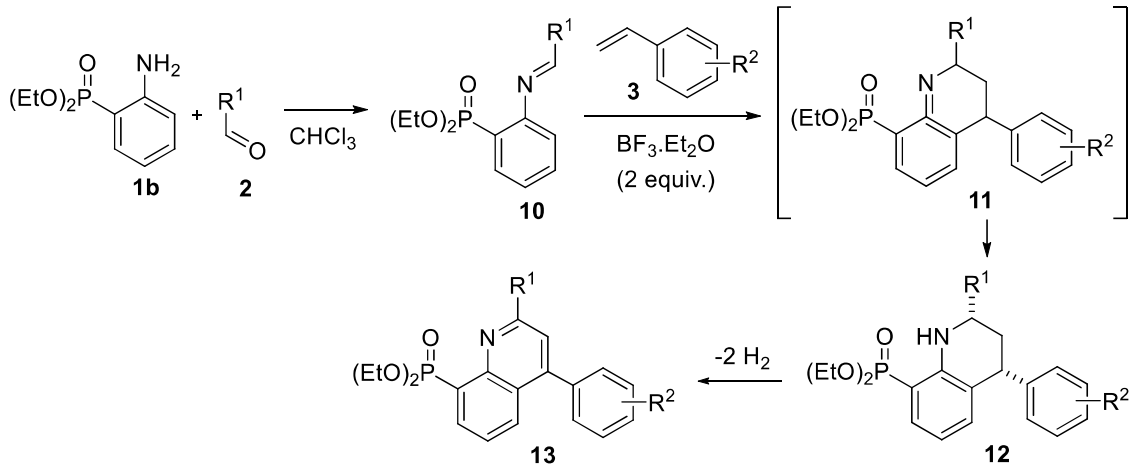

*Scheme 13. Povarov step-by-step approach for the preparation of diethyl 1,2,3,4-tetrahydroquinolin-8-ylphosphonates **12** and quinolin-8-ylphosphonates **13**.*

For instance, in the Figure 8 the ^{31}P-NMR monitoring of the Povarov reaction and the further purification by column chromatography is shown for the tetrahydroquinoline **12h** (R^1 = 3,4-F_2-C_6H_3; R^2 = H). Hence, it can be observed how the starting aniline **1b** (δ = 22.30 ppm) is converted into the corresponding tetrahydroquinoline **12h** (δ = 22.30 ppm) upon a one-pot Povarov reaction. The aniline **1b** was condensed with 3,4-difluorobenzaldehyde to yield the corresponding imine, which was reacted *in situ* with phenylstyrene and 2 equivalents of $BF_3.Et_2O$ for 6 h at refluxing chloroform. After the isolation of the compound **12h** by column chromatography we observed the formation of a small signal at δ = 18.46 ppm corresponding to the fully aromatic quinoline derivative **13h**.

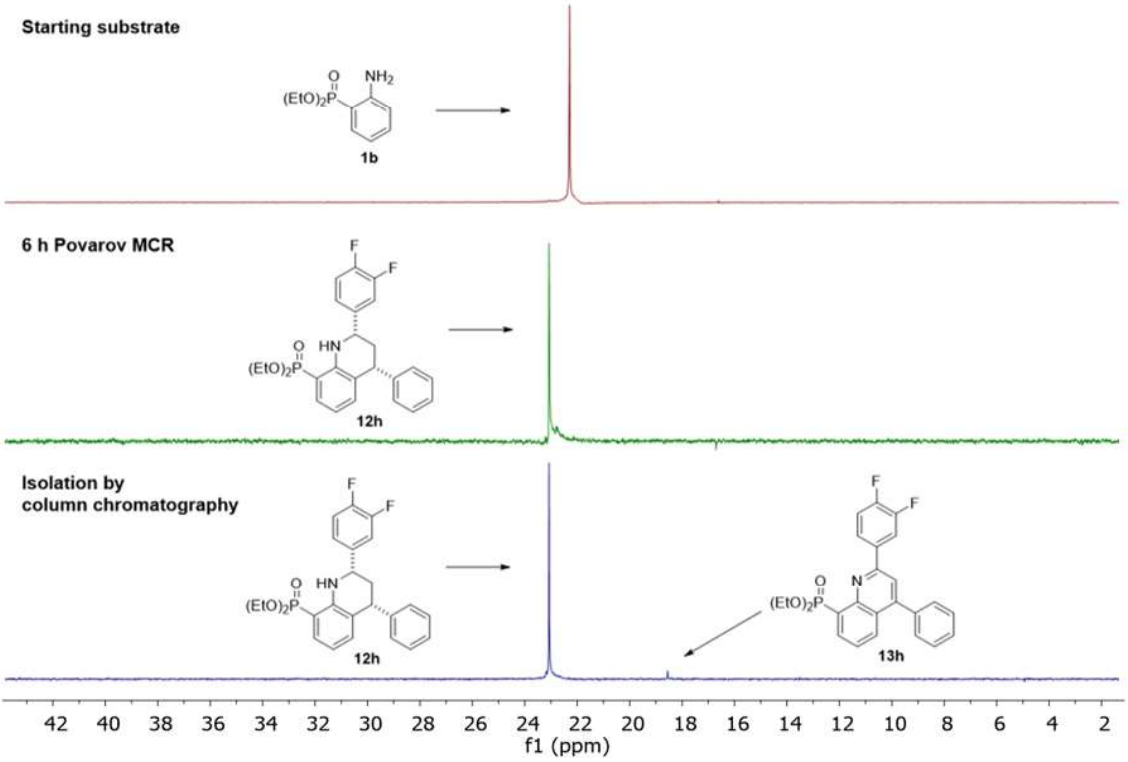

*Figure 8. ^{31}P-NMR monitoring of the Povarov reaction to yield the 1,2,3,4-tetrahydroquinolin-8-yl derivative **12h** and traces of **13h**.*

Furthermore, the compound **12h** was found to be instable in dissolution and attempts to isolate the tetrahydroquinoline **12h** from the mixture of **12h** and **13h** (crystallization, recolumn etc.) resulted in the formation of higher percentage of the aromatized form **13h**, as depicted in the Figure 9.

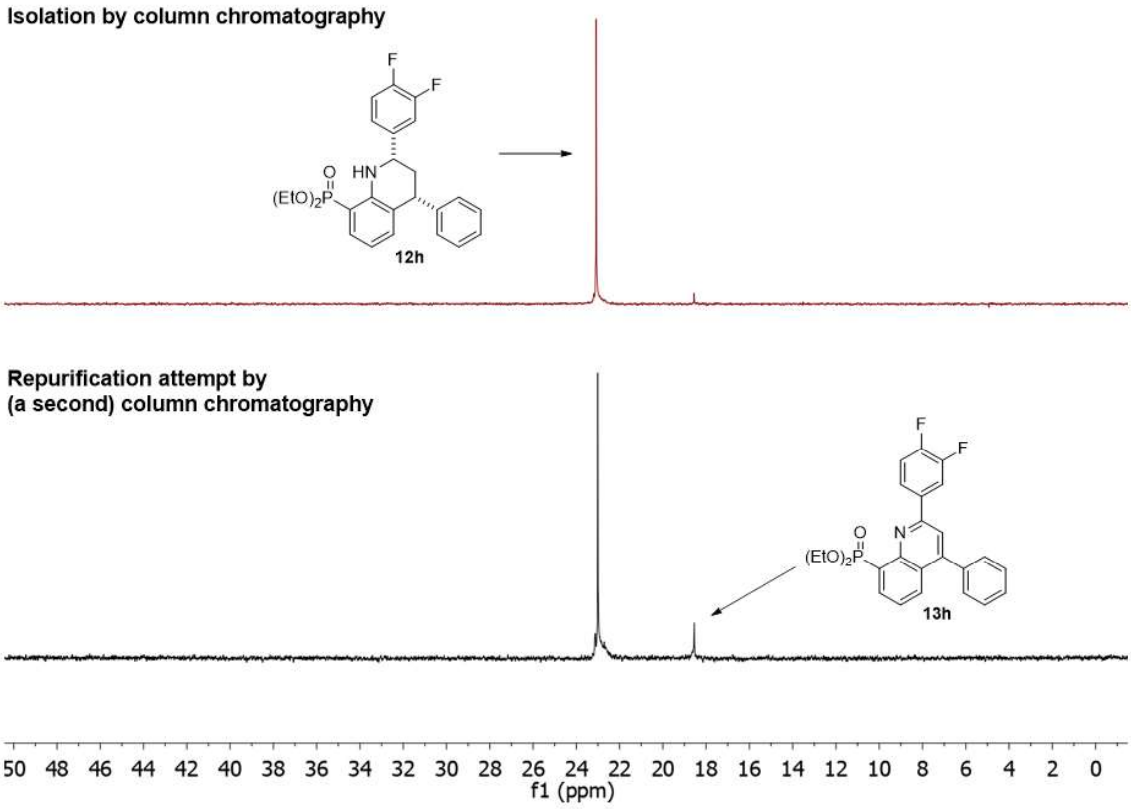

*Figure 9. ^{31}P-NMR monitoring of the purification attempts of the 1,2,3,4-tetrahydroquinolin-8-yl derivative **12h.***

We confirmed the presence of the two compounds **12h** and **13h** by NMR-spectroscopy and high-resolution mass-spectroscopy (HRMS) characterization. For instance, traces of the quinoline structure were detected in the ^{1}H-NMR spectrum of **12h**, as shown in the Figure 10. The presence of characteristic signals corresponding to the quinoline **13h** (marked with an arrow) confirmed what we previously observed in ^{31}P-NMR experiments.

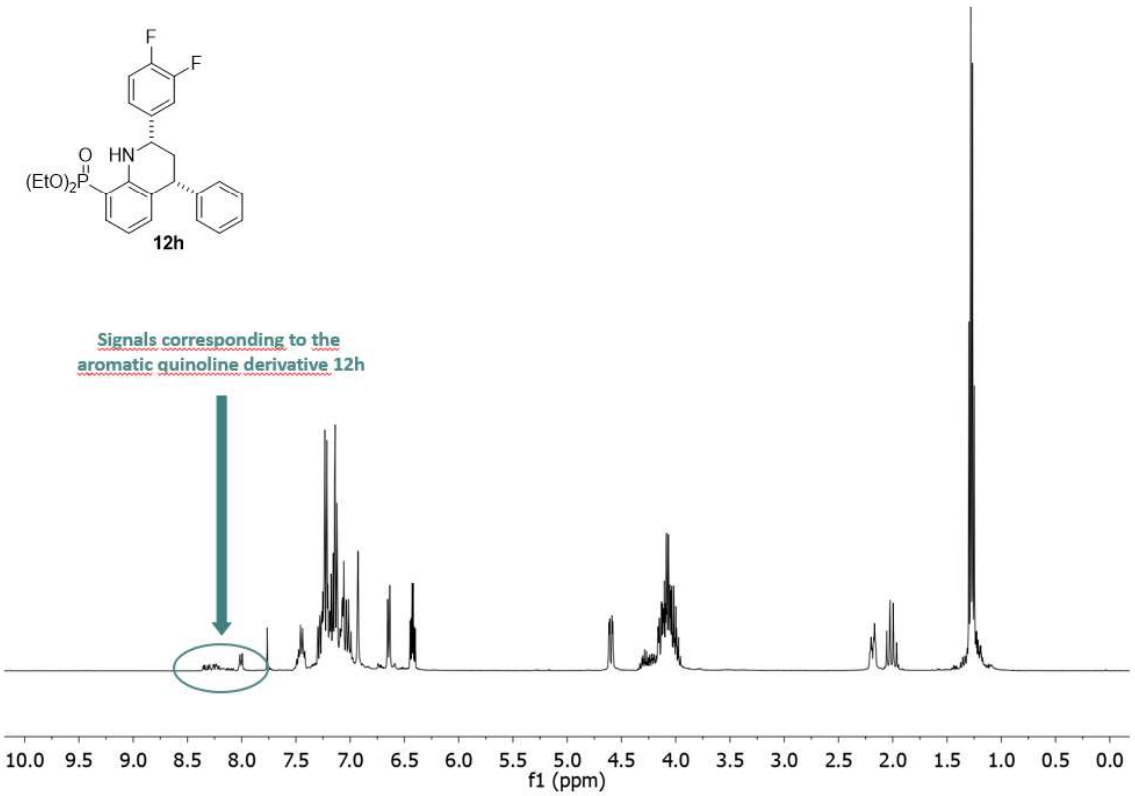

*Figure 10. ^{1}H-NMR spectrum of 1,2,3,4-tertrahydroquinolin-8-yl derivative **12h** showing the presence of traces of the quinolin-8-yl derivative **13h**.*

In view of these results, unfortunately we had to assume that, in our hands, it was no possible to isolate the 1,2,3,4-tetrahydroquinolin-8-yl derivarives **12** as pure molecules due to the reported chemical instability. Accordingly, we decided to focus on the straightforward synthesis of the fully aromatic quinolin-8-yl derivatives **13** and therefore we planned a stepwise Povarov-DDQ dehydrogenation cascade reaction (depicted in the Scheme 14), comprising a one-pot step-by-step Povarov reaction between a readily prepared imines **10** and styrenes **3** (Scheme 14, ***route A***), followed by a DDQ ***oxidation of compounds 12*** to yield the fully aromatic quinolin-8-yl derivarives **13**.

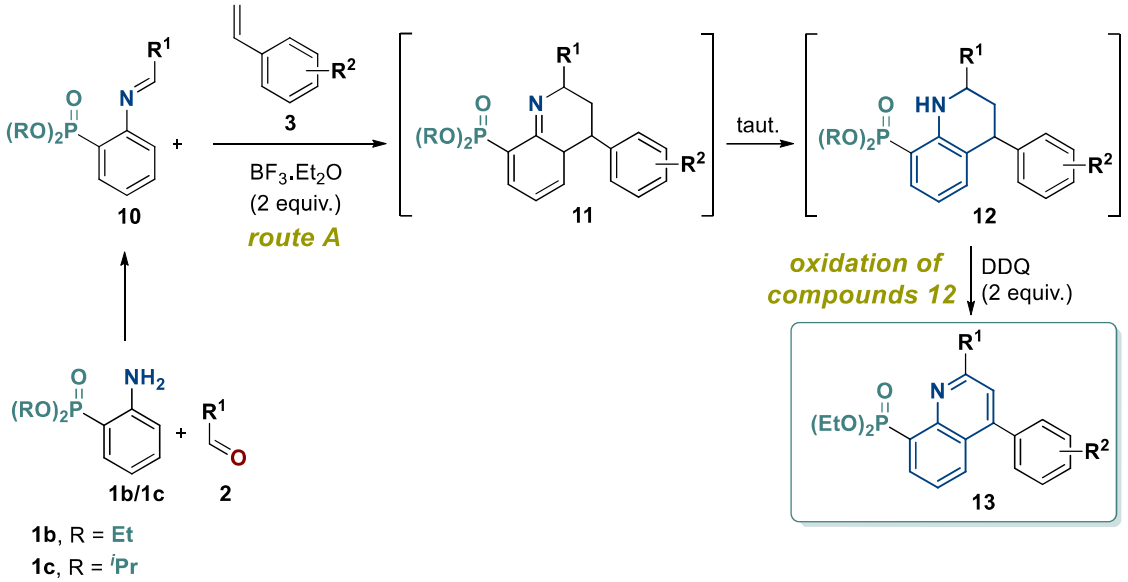

*Scheme 14. Synthetic **route A** (stepwise Povarov reaction) followed by the in situ **oxidation of compounds 12** for the preparation of diethyl quinolin-8-ylphosphonates **13**.*

Having all the previously expounded considerations in mind, we initiated the study of the aforementioned stepwise Povarov-DDQ dehydrogenation cascade approach by the preparation of the compound **13a** (R = Et; R^1 = C_6H_5; R^2 = H; Table 5, entry 1) as a model reaction. First, the diethyl(2-(benzylideneamino)phenyl)phosphonate aldimine **10a** (R^1 = C_6H_5) was generated *in situ* from aniline **1b** (R = Et) and benzaldehyde **2a** (R^1 = C_6H_5) within 16 hours, which was thereupon reacted with phenylstyrene **3a** (R^2 = H) in the presence of 2 equivalents of $BF_3.Et_2O$. The reactions were heated in refluxing chloroform until $^{31}P/^{1}H$-NMR experiments indicated the consumption of imine **10a** and the formation of the 1,2,3,4-tetrahydroquinolin-8-yl derivative **12a** (R = Et; R^1 = C_6H_5; R^2 = H). Subsequently, the tetrahydroquinoline **12a** was *in situ* dehydrogenated by adding 2 equivalents of DDQ. The mixture was stirred and heated to chloroform reflux until TLC and $^{31}P/^{1}H$-NMR spectroscopy analysis indicated the total consumption of the tetrahydroquinoline **12a** and the formation of the fully aromatic quinolin-8-yl derivative **13a** (2 h). Upon purification by column chromatography, diethyl (2,4-diphenylquinolin-8-yl)phosphonate **13a** was afforded in 74% yield.

In the ^{1}H-NMR spectrum of the compound **13a** (Figure 11), it can be clearly appreciated the aromatic zone comprising the protons of the aromatic quinoline system. Furthermore, we can observe a multiplet at δ = 1.32-1.36 ppm corresponding to the six protons of the 2 CH_3 of the diethyl phosphonate moiety and a multiplet at δ = 4.26-4.44 ppm assigned to the four protons the 2 CH_2 of the diethyl phosphonate.

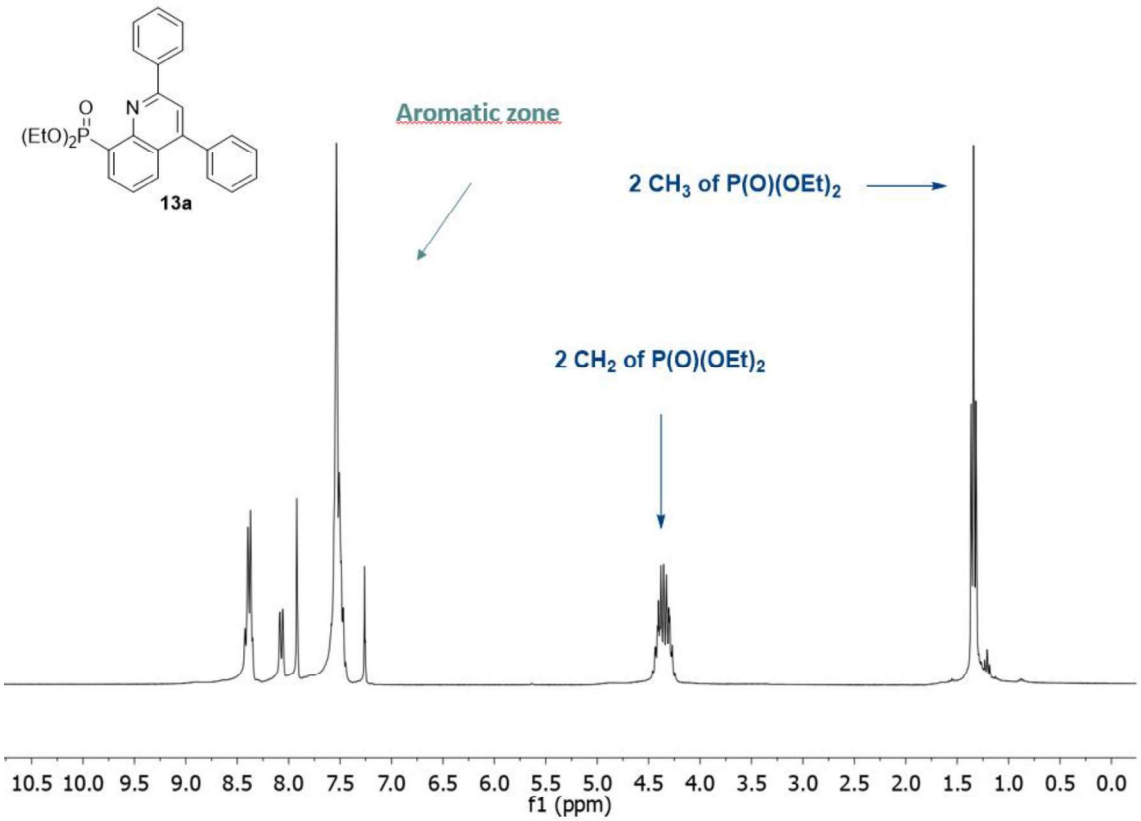

*Figure 11. ^{1}H-NMR spectrum of diethyl (2,4-diphenylquinolin-8-yl)phosphonate **13a**.*

Likewise, the ^{13}C-NMR spectrum of the compound **13a** shows several signals between δ = 119.3-156.6 ppm, corresponding to the carbons of the quinoline core (Figure 12). Moreover, both ^{13}C-NMR and ^{13}C-DEPT 135 NMR experiments confirm the presence of the two carbons of 2 CH_3 of the diethyl phosphonate moiety visualized as a doublet at δ = 16.7 ppm ($^{3}J_{CP}$ = 6.6 Hz) and the two carbons corresponding to the 2 CH_2 of the diethyl phosphonate group that are observed as a doublet at δ = 62.5 ppm ($^{3}J_{CP}$ = 5.7 Hz).

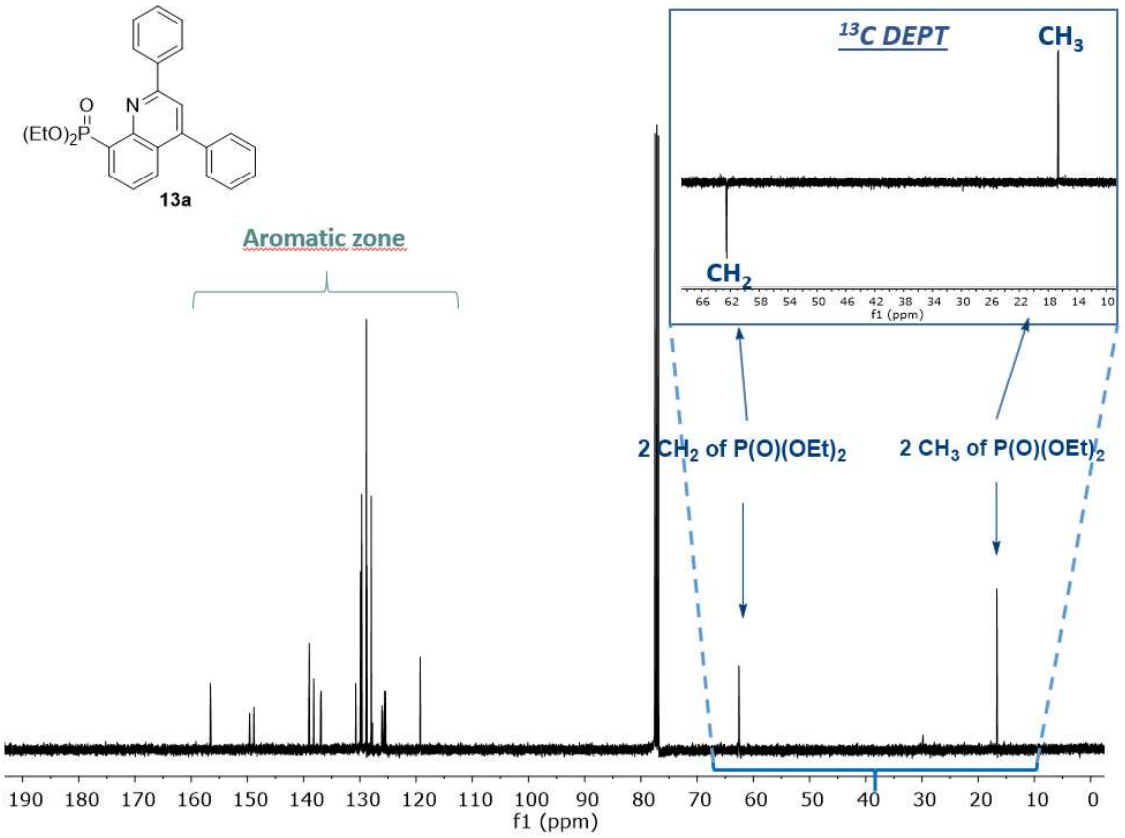

*Figure 12. ^{13}C-NMR spectrum of diethyl (2,4-diphenylquinolin-8-yl)phosphonate **13a**,with a region compared to the ^{13}C DEPT 135 NMR spectrum thereof.*

To further expand the substrate scope of this one-pot methodology, we extended the current stepwise Povarov-DDQ dehydrogenation reaction sequence (Scheme 14, ***route A***) to a wider range of aromatic aldehydes and styrenes with different electron-withdrawing and electron-donating substituents. In the table 5 are collected the yields of diethyl quinolin-8-yl phosphonates (entries 1-14) obtained upon column chromatography and crystallization (see entries with ***route A***).

Table 5. Yields of dialkyl quinolin-8-ylphosphonates **13** obtained by step-by-step Povarov reaction (***route A***) and a subsequent DDQ oxidation or Povarov MCR and a subsequent DDQ oxidation (***route B***) and subsequent DDQ oxidation.

Entry	Compound				Route	Yield (%)
	Nº	R	R^1	R^2		
1	**13a**	Et	C_6H_5	H	A	74
2	**13b**	Et	2-MeO-C_6H_4	H	A	48
3	**13c**	Et	3-MeO- C_6H_4	H	B	89
4	**13d**	Et	4-MeO-C_6H_4	H	A	41
5	**13e**	Et	4-$(EtO)_2P(O)O$- C_6H_4	H	A	64
6	**13f**	Et	1-naphthyl	H	B	60
7	**13g**	Et	2-naphthyl	H	B	83
8	**13h**	Et	3,4-F_2-C_6H_3	H	B	76
9	**13i**	Et	C_6H_5	4-Me	A	54
10	**13j**	Et	4-F-C_6H_4	4-Me	A	52
11	**13k**	Et	3,4-F_2-C_6H_3	4-Me	A	47
12	**13l**	Et	C_6H_5	4-F	A	60
13	**13m**	Et	4-F-C_6H_4	4-F	A	68
14	**13n**	Et	3,4-F_2-C_6H_3	4-F	A	43
15	**13o**	^{i}Pr	4-F-C_6H_4	H	B	34
16	**13p**	^{i}Pr	3,4-F_2-C_6H_4	H	B	38
17	**13q**	^{i}Pr	4-F-C_6H_4	4-Me	B	58
18	**13r**	^{i}Pr	3,4-F_2-C_6H_3	4-Me	B	39
19	**13s**	^{i}Pr	4-F-C_6H_4	4-F	B	68
20	**13t**	^{i}Pr	3,4-F_2-C_6H_3	4-F	B	88

I-4.2.2. MCR reaction with olefins (*route B*)

Afterwards, we planned to study the oxidative Povarov MCR variant for the preparation of quinoline derivatives **13** (the synthetic methodology is depicted in the Scheme 15, *i.e.* the ***route B*** followed by the *in situ* ***oxidation of compounds 12*** with DDQ).

We started our study with the preparation of compound **13f** (R = Et; R^1 = 1-naphthyl; R^2 = H; Table 5, entry 6) following a three-component Povarov reaction between aniline **1b** (R = Et), naphthaldehyde **2** (R^1 = 1-naphthyl) and phenylstyrene **3** (R^2 = H), in the presence of 2 equivalents of $BF_3.Et_2O$. After 12 hours, ^{1}H- and ^{31}P-NMR indicated that the reaction was completed. The procedure was followed by the *in situ* addition of 2 equivalents of DDQ and the mixture was heated to reflux for 2 h (Scheme 15). Diethyl (2-(naphthalen-1-yl)-4-phenylquinolin-8-yl)phosphonate **12f** was obtained upon isolation by column chromatography in a moderate yield (60%).

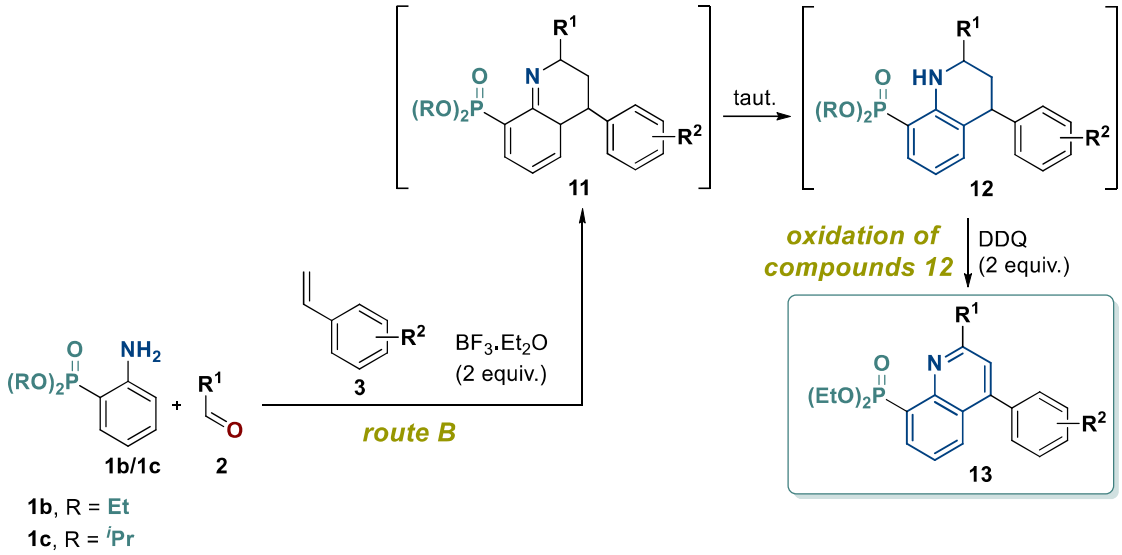

*Scheme 15. Synthetic **route B** (MCR Povarov reaction) followed by the in situ **oxidation of compounds 12** for the preparation of dialkyl quinolin-8-ylphosphonates **13**.*

The ^{1}H-NMR spectrum for the compound **13f** is shown in the Figure 13, where we can observe the aromatic H atoms in a range between 7.51-8.60 ppm and two signals corresponding to the protons of the 2 CH_3 of the diethyl phosphonate (observed as a multiplet at δ = 1.16-1.20 ppm) along with the protons of the 2 CH_2 (observed as a multiplet at δ = 4.19-4.30 ppm).

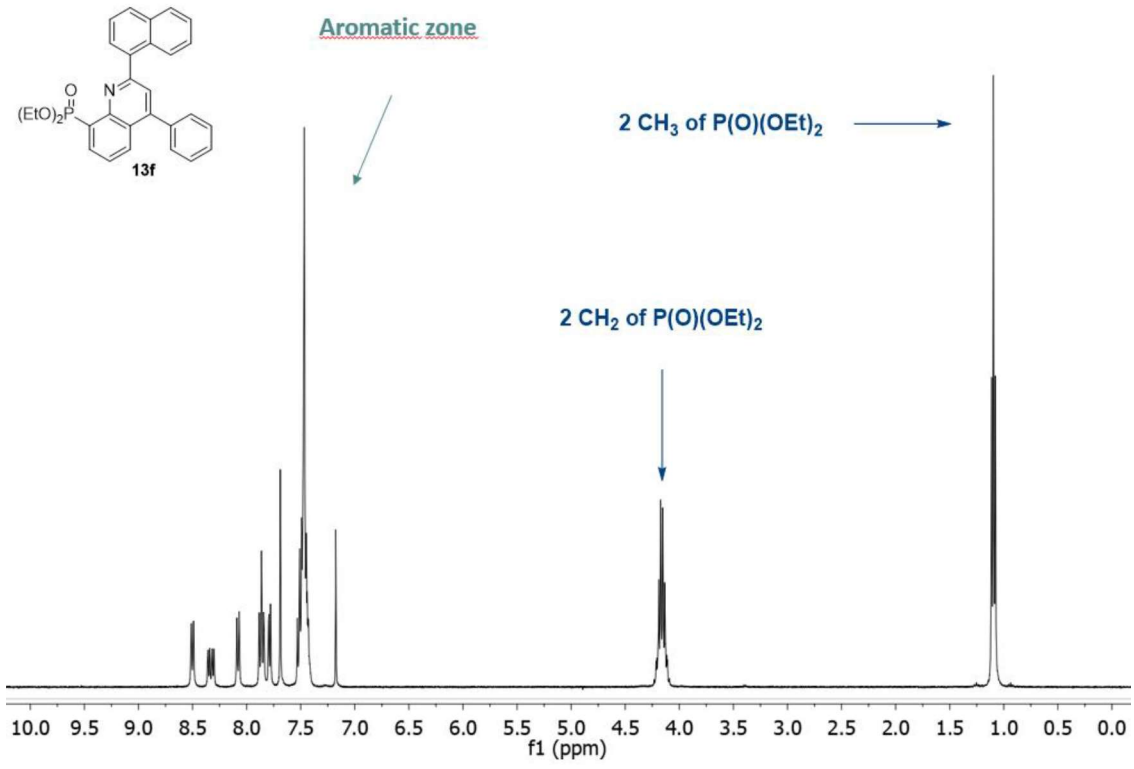

*Figure 13. ^{1}H-NMR spectrum of diethyl (2-(naphthalen-1-yl)-4-phenylquinolin-8-yl)phosphonate **13f**.*

In the Figure 14 (^{13}C-NMR spectrum of the compound **13f**), we can observe the signals corresponding to the aromatic carbons, along with two signals at δ = 16.5 ppm and 62.9 ppm assigned to the CH_3 and CH_2 carbons of the diethyl phosphonate moiety respectively.

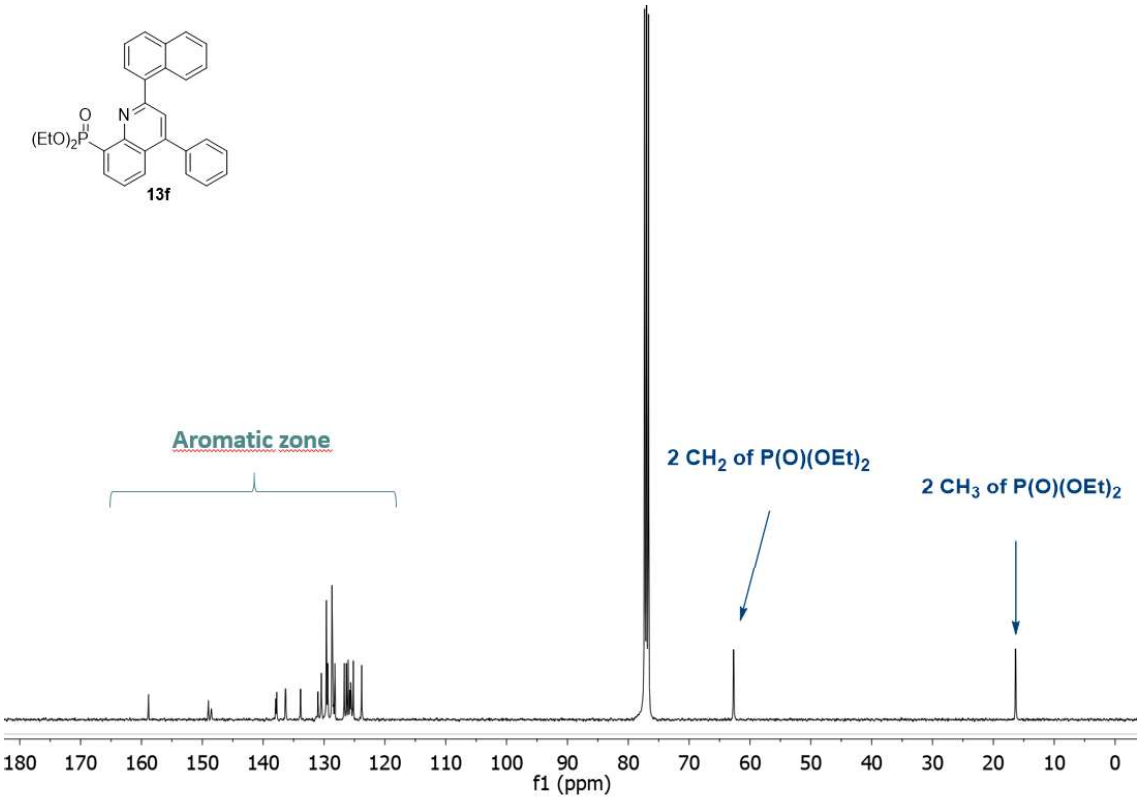

*Figure 14. ^{13}C-NMR spectrum of diethyl (2-(naphthalen-1-yl)-4-phenylquinolin-8-yl)phosphonate **13f**.*

Once we afford the quinolin-8-yl derivative **13f** following the MCR Povarov-DDQ dehydrogenation cascade, we extended the scope of the current methodology comprising the MCR Povarov reaction (***route B***) followed by a ***DDQ oxidation*** of the *in situ* generated Povarov adducts. In this manner, the reactivity of 2-dialkylphosphonate-substituted anilines (**1b** R =Et; **1c** R = ^{i}Pr) and a variety of styrenes and aromatic aldehydes (Scheme 15) was explored. In the table 5 are listed the corresponding yields of quinolines **13** obtained by the current synthetic ***route B*** upon purification by column chromatography and recrystallization (see entries with ***route B***).

Summary of the synthetic routes employed for the preparation of quinolin-8-yl dialkyl phosphonate derivatives 13

Considering the results collected in the Table 5, the presented one-pot Povarov-DDQ dehydrogenation reaction sequence was found to be an appropriate methodology for the preparation of diethyl quinolin-8-yl phosphonates **13a-n** (Table 5, entries 1-13) and diisopropyl quinolin-8-yl phosphonates **13o-t** (entries 14-19) with a wide range of aromatic, electron-

donating and electron-withdrawing substituents. Despite the fact that the tetraydroquinoline adducts **12** were not stable and we had to outline a synthetic approach to directly yield the fully aromatic derivatives, the disclosed one-pot methodologies (Scheme 16, ***route A*** step-by-step; ***route B*** MCR) lead to the obtention of quinolines **13** in a regioselective way and with overall moderate to high yields. The MCR approach allowed a more direct approach with step-economy and resulted specially efficient for the preparation of dialkyl quinolin-8-ylphosphonates **13c** (R = Et; R^1 = 3-MeO- C_6H_4; R^2 = H; Table 5, entry 3), **13g** (R = Et; R^1 = 2-naphthyl; R^2 = H; entry 7) and **13t** (R = ^{i}Pr; R^1 = 3,4-F_2- C_6H_3; R^2 = 4-F; entry 20).

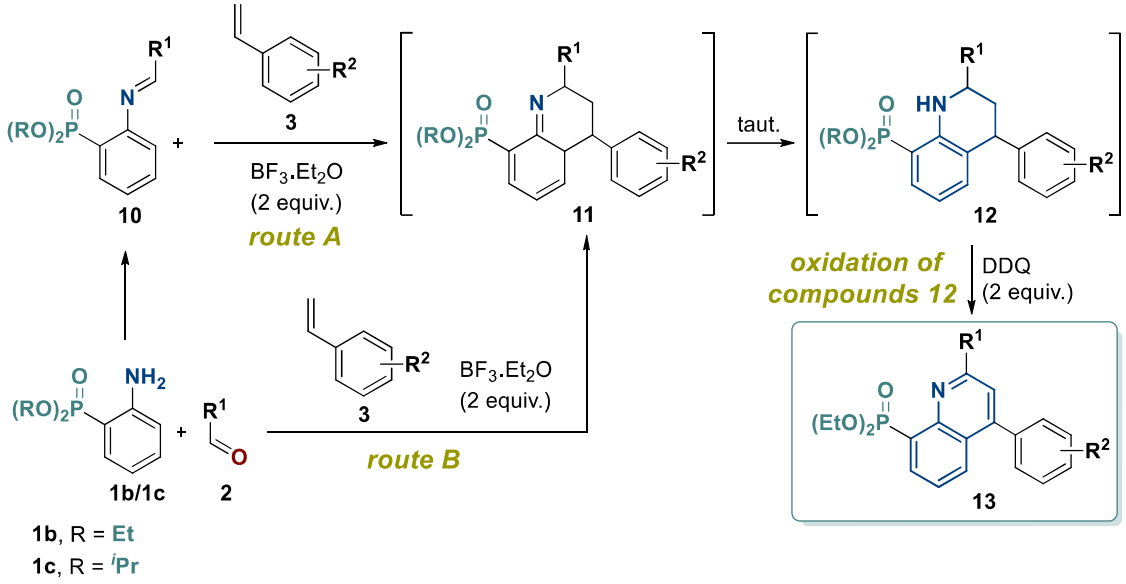

*Scheme 16. Synthetic routes for the preparation of dialkyl quinolin-8-ylphosphonates **13**.*

I-4.3. Synthesis of hybrid diethyl 1,2,3,4-tetrahydroquinolin-6-ylphosphonates and diethyl quinolin-6-ylphosphonates

In order to expand the scope of the reaction and increase the structural diversity in the synthesis of dialkyl phosphonate-substituted quinoline derivatives, we proposed the preparation of 2,4-quinoline derivatives with the diethyl phosphonate functionality in position 6. For this purpose, we started the study of the Povarov MCR reaction with the phosphorylated aniline **1d**.

I-4.3.1. Preparation of diethyl 1,2,3,4-tetrahydroquinolin-6-ylphosphonates by the Povarov MCR approach

We investigated a three-component Povarov reaction between aniline **1d**, aldehydes **2** and styrenes **3**, in the presence of molecular sieves and 2 equivalents of $BF_3.Et_2O$ (***Povarov MCR***, Scheme 17). We started exploring the model reaction between diethyl (4-aminophenyl)phosphonate **1d**, 4-fluorobenzaldehyde **2** (R^1 = 4-F_2-C_6H_5**)** and 4-fluorophenylstyrene **3** (R^2 = 4-F). The reaction was stirred to reflux in chloroform until $^{31}P/^{1}H$-NMR experiments indicated the consumption of starting material (1.5 h) and tetrahydroquinoline **15e** was afforded. Surprisingly, the diethyl (2,4-bis(4-fluorophenyl)-1,2,3,4-tetrahydroquinolin-6-yl)phosphonate **15e** (R^1 = 4-F-C_6H_4; R^2 = 4-F) resulted to be stable under purification conditions and we were able to successfully isolate by column chromatography (86% yield) and further purification by recrystallization in diethyl ether.

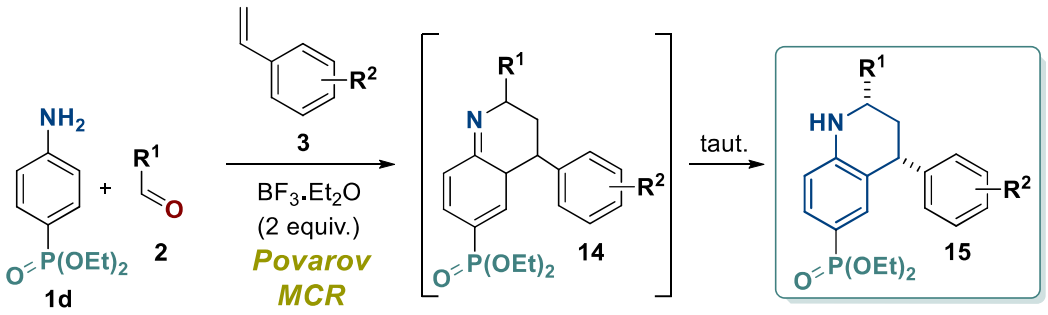

Scheme 17. ***Povarov MCR*** *synthetic route for the preparation of diethyl 1,2,3,4-tetrahydroquinolin-6-ylphosphonates* ***15****.*

The structure of the obtained 1,2,3,4-tetrahydroquinolines **15** was determined by one-dimensional and two-dimensional NMR spectroscopy (*i.e.* 1D-NMR and 2D-NMR) and HRMS experiments. Hence, the ^{1}H-NMR spectrum of tetrahydroquinoline derivative **15e** is shown in the Figure 15, where we can observe the characteristic aliphatic protons corresponding to the non-aromatic piperidine ring of the tetrahydroquinoline moiety. On the one hand, at high field we can observe the signals corresponding to two diastereotopic protons (namely 3a-H and 3b-

H) of the methylene (position 3 of the tetrahydroquinoline core) detected as a doublet of doublets (dd) at δ = 2.11 ppm ($^2J_{HH}$ = 12.3 Hz, $^3J_{HH}$ = 11.3 Hz) and a multiplet at 2.23-2.28 ppm respectively. Moreover, it can be appreciated the presence of two doublet of doublets assigned to the 2-H and 4-H protons at δ = 4.26 ppm ($^3J_{HH}$ = 12.3 Hz, $^3J_{HH}$ = 5.2 Hz) and 4.64 ppm ($^3J_{HH}$ = 11.3 Hz and $^3J_{HH}$ = 2.9 Hz) respectively. Finally, the proton of the NH group is visible as a wide singlet at δ = 4.42 ppm, which disappears upon treatment of the sample with D_2O.

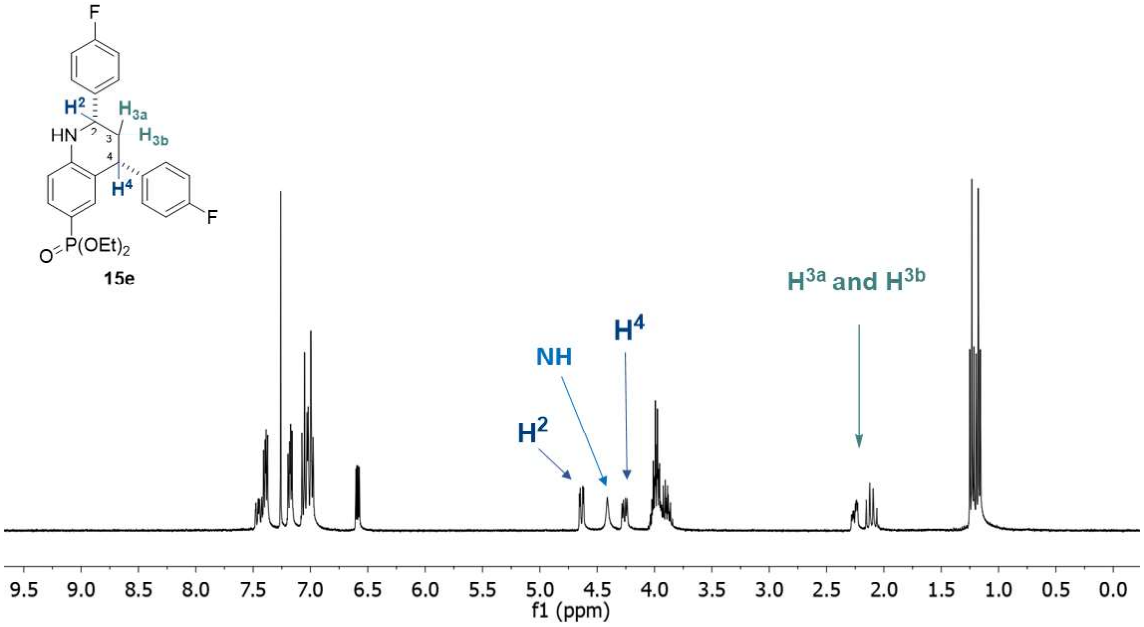

*Figure 15. ^{1}H-NMR spectrum of diethyl (2,4-bis(4-fluorophenyl)-1,2,3,4-tetrahydroquinolin-6-yl)phosphonate **15e**.*

The regiochemistry of the process was determined by a HMBC (Heteronuclear Multiple Bond Correlation) 2D-NMR experiment of the compound **15e** (the spectra of HMBC is shown in Figure 16), where a cross-linking connectivity is observed between the proton of the NH group and the C-3 methylenic carbon. This correlation confirms that the 4-fluorophenyl substituent has been regioselectively introduced in the position 4 of the quinoline moiety and not in the position 3. The other possible regioisomer bearing the 4-fluorophenyl substituent in position 3 was certainly discarded, which would imply a cross-linking connectivity between the proton of the amino group and the carbon attached to the 4-fluorophenyl group instead, and we did not observe this cross-peak pattern.

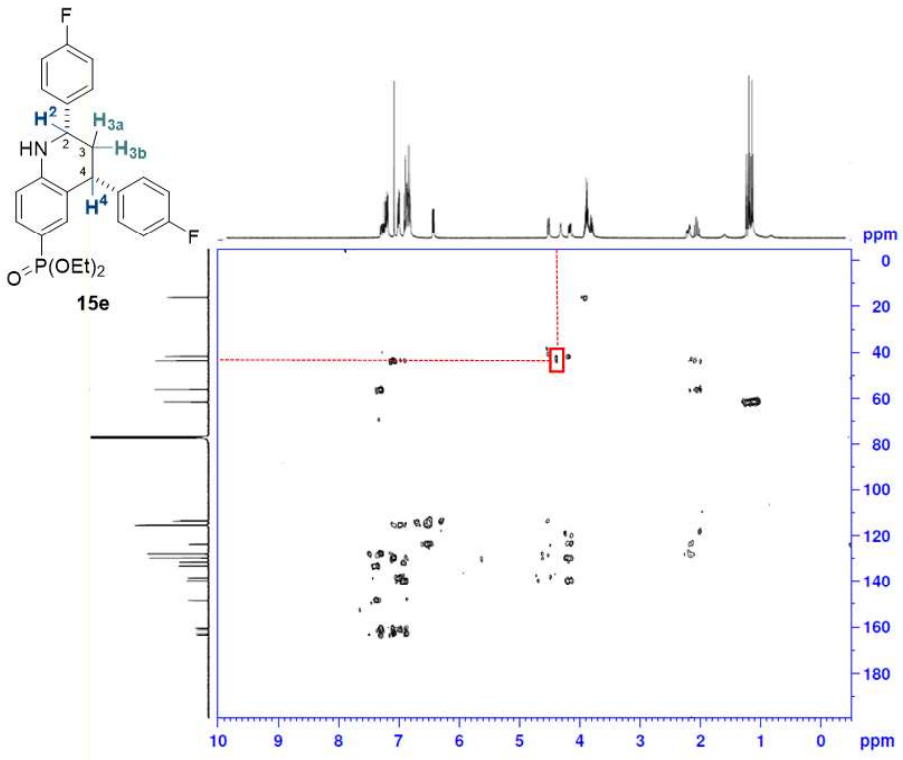

Figure 16. HMBC spectra of of diethyl (2,4-bis(4-fluorophenyl)-1,2,3,4-tetrahydroquinolin-6-yl)phosphonate ***15e.***

Likewise, the stereoselectivity of the process was determined by 1D-NOESY-NMR spectroscopy as depicted in the Figure 17. The selective saturation of the 2-H proton presented a positive NOESY effect on the 4-H proton (3.50%) and the methylenic protons (2.81% and 0.62% respectively). In addition, the selective saturation of the 4-H proton presented positive NOESY effect on the 2-H proton (3.28%) and the methylenic protons (3.74% and 0.75%). The collected results indicate a relative *cis*-configuration between the protons in position 2 and 4 of the quinoline core and therefore suggests that the [4+2] Povarov-like cycloaddition reaction occurs through an *endo* transition state.

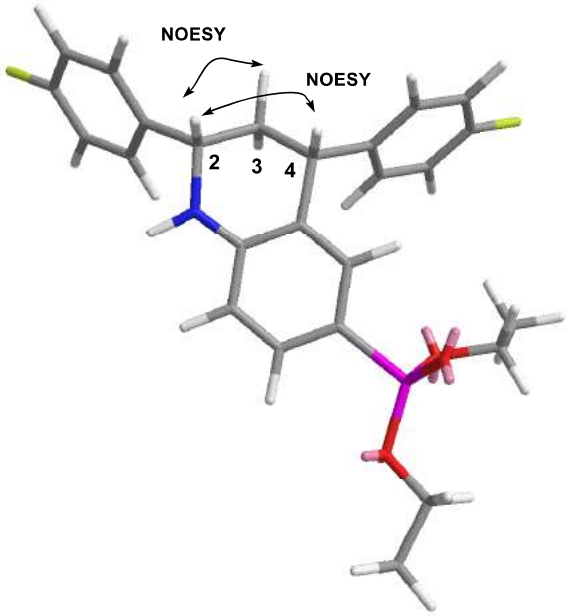

*Figure 17. Relative configuration of diethyl (2,4-bis(4-fluorophenyl)-1,2,3,4-tetrahydroquinolin-6-yl)phosphonate **15e** assigned by 1D-NOESY experiments.*

Once afforded the tetrahydroquinoline **15e** and elucidated its chemical structure, we applied the current optimized Povarov MCR methodology to a variety of diverse aromatic aldehydes and styrenes in order to broaden the scope of the reaction. Accordingly, we obtained a set of 1,2,3,4-tetrahydroquinolin-6ylphosphonates **15** in good to excellent yields as shown in the Table 6.

Table 6. Synthesis of diethyl 1,2,3,4-tetrahydroquinolin-6.ylphosphonates **15** by the Povarov MCR approach.

Entry	**Compound**			**Reaction time (h)**	**Yield (%)**
	Nº	**R^1**	**R^2**		
1	**15a**	4-F-C_6H_4	H	1,5	81
2	**15b**	3,4-F_2-C_6H_3	H	1,5	97
3	**15c**	4-F-C_6H_4	4-Me	2	65
4	**15d**	3,4-F_2-C_6H_3	4-Me	1	79
5	**15e**	4-F-C_6H_4	4-F	1,5	86
6	**15f**	3,4-F_2-C_6H_3	4-F	1,5	65

In contrast to the previously unsuccessfully attempted preparation of diethyl 1,2,3,4-tetrahydroquinolin-8-ylphosphonates **12** (Scheme 16), the Povarov MCR reaction was found to be an exceptionally convenient method for the preparation of diethyl tetrahydroquinolin-6-ylphosphonates **15** in high yields (65-97%). In particular, it is noteworthy to highlight the 97% of yield achieved for the derivative **15b** (R^1 = 3,4-F_2-C_6H_3; R^2 = H; Table 6, entry 2).

I-4.3.2. Preparation of diethyl quinolin-6-ylphosphonates by DDQ oxidation of 1,2,3,4-tetrahydroquinolin-6-yl derivatives 15

Once we achieved the tetrahydroquinolines **15** by the MCR Povarov reaction, we proceeded to their dehydrogenation to yield the corresponding quinolines **16** by oxidation with DDQ (Scheme 18). We started studying the dehydrogenation of 1,2,3,4-tetrahydroquinolin-6yl phosphonate **15a** (R^1 = 4-F-C_6H_4; R^2 = H;) as the model reaction.

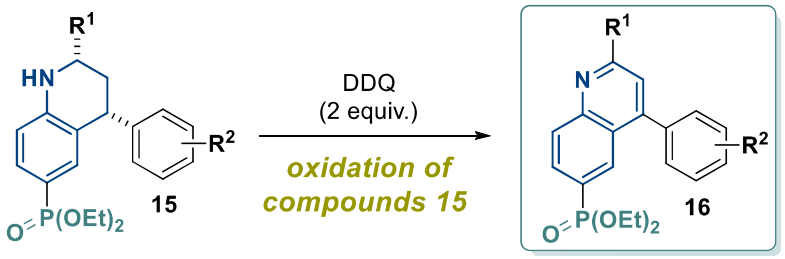

*Scheme 18. Aromatization of diethyl 1,2,3,4-tetrahydroquinolin-6-ylphosphonates **15** to yield diethyl quinoline-6-ylphosphonates **16**.*

Accordingly, the tetrahydroquinolin-6-yl derivative **15a** was reacted with 2 equivalents of DDQ in chloroform at 60 °C and the evolution of the dehydrogenation of the corresponding aromatic quinoline derivative **16a** was monitored by $^{31}P/^{1}H$-NMR spectroscopy. In the Figure 18 we can observe the conversion of tetrahydroquinoline **15a** into dehydrogenated quinoline **16a** in ^{1}H-NMR experiments. After 1 h of dehydrogenation with DDQ, an aliquot was taken and the ^{1}H-NMR spectrum revealed that the reaction was still in progress but not finished yet. In the Figure 18 it can be clearly observed how as the dehydrogenation was proceeding, the signals corresponding to the four aliphatic protons of the tetrahydroquinoline moiety (plus the NH group) disappeared, and new aromatic protons corresponding to the newly formed pyridine ring of **16a** appeared.

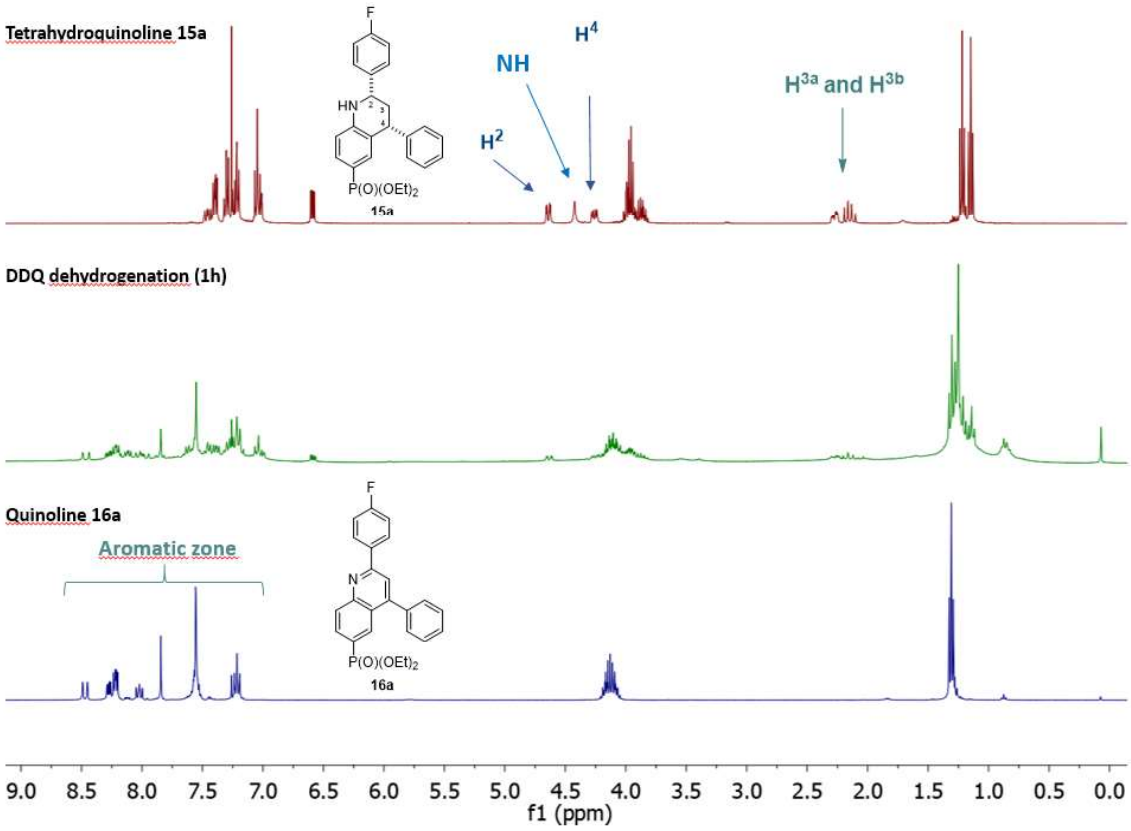

*Figure 18. ^{1}H-NMR spectrum showing the conversion during the dehydrogenation of the diethyl tetrahydroquinolin-6-ylphosphonate **15a** to yield the corresponding quinoline derivative **16a.***

Following this protocol, we assessed the dehydrogenation of all the previously synthesized tetrahydroquinolines **15** to yield the corresponding quinolines **16** (Scheme 18). In all cases, the formation of compounds **16** was confirmed by TLC and ^{1}H/^{31}P-NMR experiments after 2 h. The reaction mixture was chromatographed and the subsequent pure quinolines **16** were obtained in excellent yields, as shown in Table 7.

Table 7. Yields of quinolines **16** obtained by DDQ oxidation of tetrahydroquinolines **15.**

Entry	Compound			Yield (%)
	Nº	R^1	R^2	
1	**16a**	4-F-C_6H_4	H	91
2	**16b**	3,4-F_2-C_6H_3	H	89
3	**16c**	4-F-C_6H_4	4-Me	98
4	**16d**	3,4-F_2-C_6H_3	4-Me	84
5	**16e**	4-F-C_6H_4	4-F	78
6	**16f**	3,4-F_2-C_6H_3	4-F	71

Based on the results collected in the Table 7, we may consider the DDQ oxidation an efficient method for the dehydrogenation of tetrahydroquinolin-6-ylphosphonates **15** to obtain diethyl quinolin-6-yl phosphonates **16** in high yields (71-98%). The higher yield (98%) was obtained for the preparation of quinolin-6-yl derivative **16c** (R^1 = 4-F-C_6H_4; R^2 = 4-Me; Table 7, entry 3).

Summary of the synthetic routes employed for the preparation of 1,2,3,4-tetrahydroquinolin-6-yl diethyl phosphonate derivatives 15 and diethyl quinolin-6-yl phosphonate derivatives 16

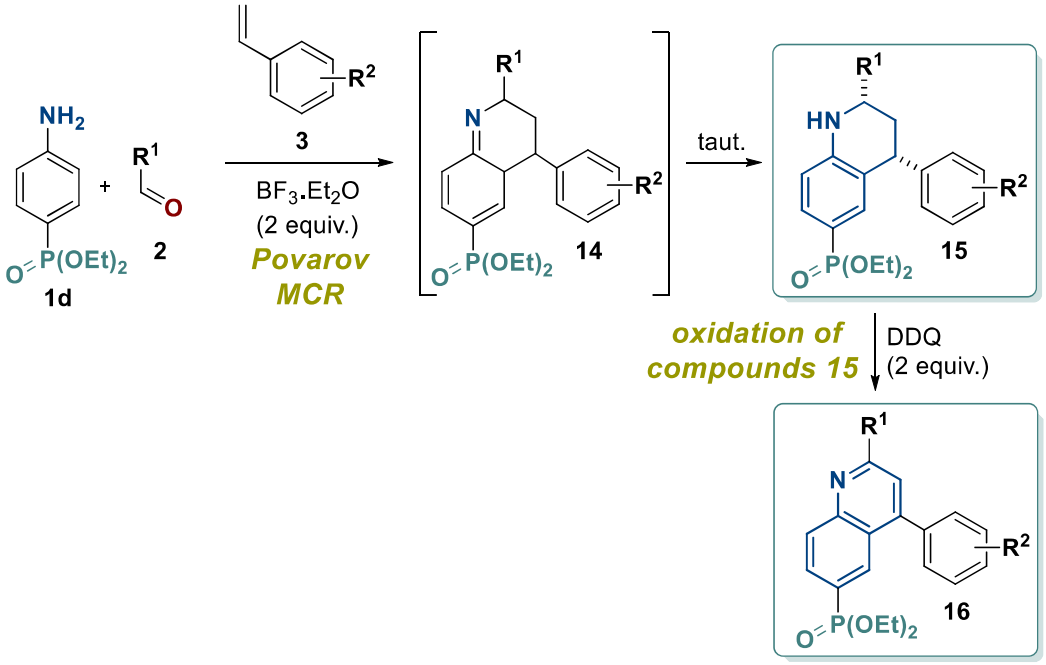

*Scheme 19. Synthetic route for the preparation of diethyl 1,2,3,4-tetrahydroquinolin-6-y phosphonates **15** and diethyl quinolin-6-ylphosphonates **16**.*

In view of the obtained results, we may consider the MCR Povarov reaction a highly efficient methodology for the regio- and stereo-controlled preparation of diethyl 1,2,3,4-tetrahydroquinolin-6-ylphosphonate derivatives **15** (Scheme 19) with a broad variety of substituents. The versatility of the Povarov reaction permitted the insertion of the diethyl phosphonate functionality in the position 6 of the tetrahydroquinoline framework, thus increasing the structural diversity of the obtained phosphorated quinoline derivatives. Furthermore, a subsequent DDQ oxidation protocol allowed the selective dehydrogenation of the tetrahydroquinoline core of derivatives **15** to afford quinolin-6-yl diethyl phosphonate derivatives **16** in excellent yields and short reaction times.

I-5. Synthesis of hybrid dialkyl indeno[2,1-*c*]quinolinylphosphonates

Once we explored the synthesis of phosphorated quinoline derivatives **6**, **7**, **13**, **15** and **16**, the scope of the Povarov reaction was expanded in an attempt to increase the diversity of the quinoline-based central core. Hence, we decided to study the preparation of fused derivatives between quinolines and indenes, bearing a dialkyl phosphonate substituent in the heterocyclic framework. The indenoquinoline (and the indenoisoquinoline analogue) motif is present in the structure of relevant TOP1 inhibitors such as TAS-103, inditecan and indimitecan, and therefore we considered appropriate to include indenoquinoline scaffold-based compounds to our research. In light of these concerns, we outlined the preparation of hybrid dialkyl indeno[2,1-*c*]quinolinylphosphonates as candidates by the Povarov reaction.

I-5.1. Synthesis of dialkyl tetrahydro-*5H*-indeno[2,1-*c*]quinolinylphosphonates

The three component Povarov reaction between anilines **1**, benzaldehydes **2** and indene **17** was performed in the presence of 2 equivalents of $BF_3.Et_2O$ and molecular sieves. First, we started exploring the reaction between diethyl (4-aminophenyl)phosphonate **1d** (R = Et) , 3-methoxybenzaldehyde **2** (R^1 = 3-MeO-C_6H_4) and indene **17,** along with 2 equivalents of $BF_3.Et_2O$ (as shown in the Scheme 20). The reaction mixture was stirred in refluxing chloroform until $^{31}P/^{1}H$-NMR spectroscopy indicated the consumption of staring material, and diethyl (6-(3-methoxyphenyl)-6,6a,7,11b-tetrahydro-*5H*-indeno[2,1-*c*]quinolin-2-yl)phosphonate **19d** (R = 2-P(O)$(OEt)_2$; R^1 = 3-MeO-C_6H_4) was obtained (yield = 65% upon isolation by column chromatography).

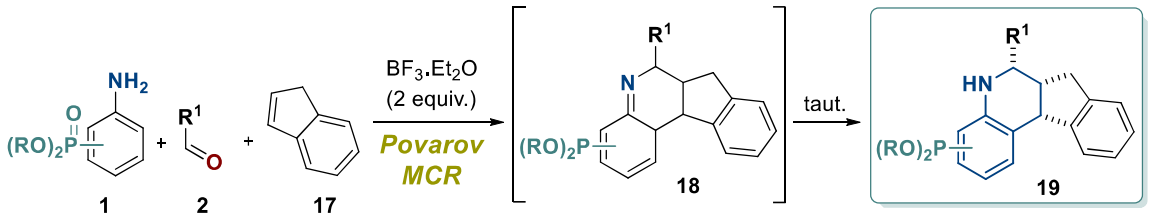

1b, R = 2-P(O)$(OEt)_2$
1c, R = 2-P(O)$(O^iPr)_2$
1d, R = 4-P(O)$(OEt)_2$

Scheme 20. ***Povarov MCR*** *synthetic route for the preparation of dialkyl tetrahydro-5H-indeno[2,1-c]quinolinylphosphonates* ***19****.*

The structure of the tetrahydro-*5H*-indenoquinoline **19d** was determined by NMR-spectroscopy and HRMS. Thus, the characteristic signals corresponding to the aliphatic protons of the tetrahydro-*5H*-indenoquinoline scaffold of the compound **19d** are clearly appreciable in the ^{1}H-

NMR spectrum shown in the Figure 19. Accordingly, at 2.41 ppm, we can observe a doublet of doublets (presenting coupling constants of $^{2}J_{HH}$ = 19.7 Hz and $^{3}J_{HH}$ = 7.9 Hz) corresponding to one of the two diastereotopic protons of the methylene group located in position C7 of the tetrahydro-*5H*-indenoquinoline. The signal for the other diastereotopic proton is overlapped with the proton of position 6, detected as a multiplet at 3.14-3.26 ppm that integrates to two protons. If we move to higher chemical shifts, we can observe a doublet at 4.55 ppm with a coupling constant of $^{3}J_{HH}$ = 7.2 Hz assigned to the proton 6-H and another doublet at 4.77 ppm ($^{3}J_{HH}$ = 2.6 Hz) corresponding to the proton located in the position 11b. Finally, the proton of the amino group is detected as a wide singlet at 4.26 ppm, which disappears upon treatment of the sample with D_2O.

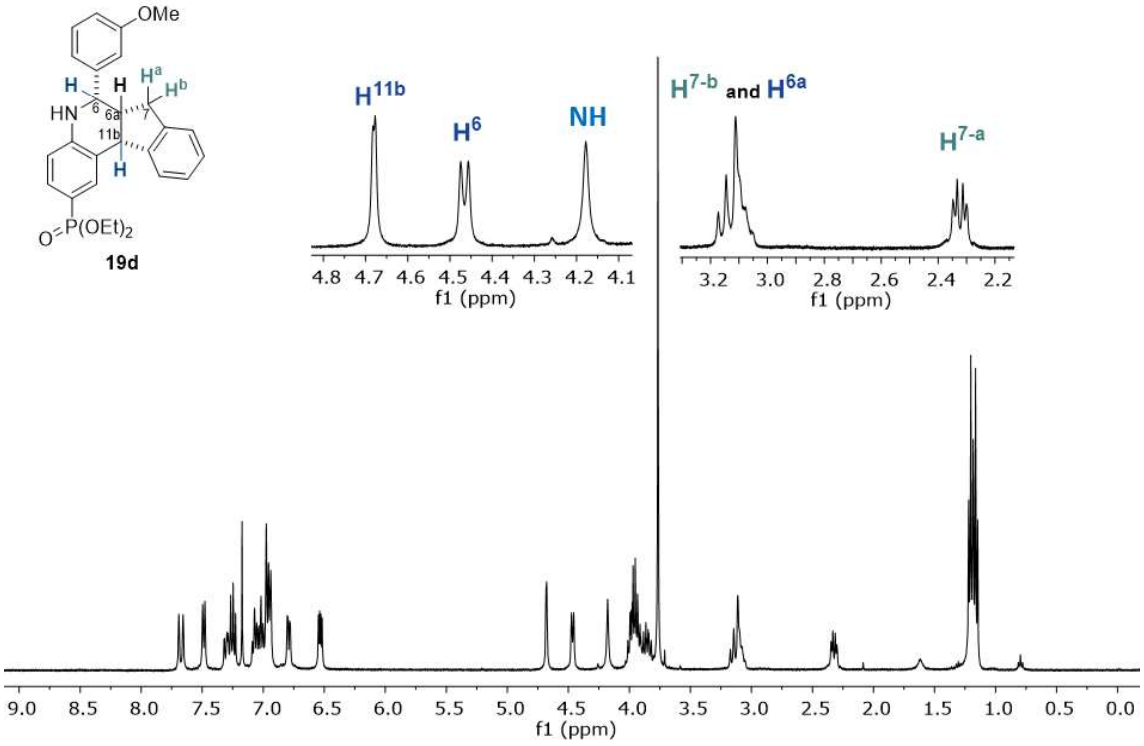

*Figure 19. ^{1}H-NMR spectrum of diethyl (6-(3-methoxyphenyl)-6,6a,7,11b-tetrahydro-5H-indeno[2,1-c]quinolin-2-yl)phosphonate **19d**.*

Likewise, ^{13}C-NMR spectrum of compound **19d** (Figure 20) shows the presence of the four aliphatic carbons of the tetrahydro-*5H*-indenoquinoline carbons: one signal at 31.4 ppm assigned to the methylenic carbon (position C7 of the tetrahydroindenoquinoline core) and three signals corresponding to the three CH (namely C-6, C-6a and C-11b) at 45.9 ppm, 47.9 ppm and 57.2 ppm, respectively. The nature of the methylenic carbon was confirmed by DEPT-135 ^{13}C-NMR (the signal appears in the reverse phase, see the blue window named as *^{13}C DEPT*). Moreover, close to these signals we can observe a singlet at 55.3 ppm assigned to the carbon of the methoxyl substituent (in red) and the signals corresponding to the 2 CH_3 (observed as two

doublets at 16.4 ppm and 16.5 ppm with a coupling constant of $^{3}J_{CP}$ = 6.7 Hz for each) and the 2 OCH_2 (observed as two doublets at 61.8 ppm with $^{2}J_{CP}$= 5.3 Hz and 61.9 ppm with $^{3}J_{CP}$ = 5.1 Hz) of the diethyl phosphonate group. Finally, we can see all the aromatic carbons of the tetrahydro-*5H*-indenoquinoline **19d** in the aromatic region (between 112.5-160.0 ppm).

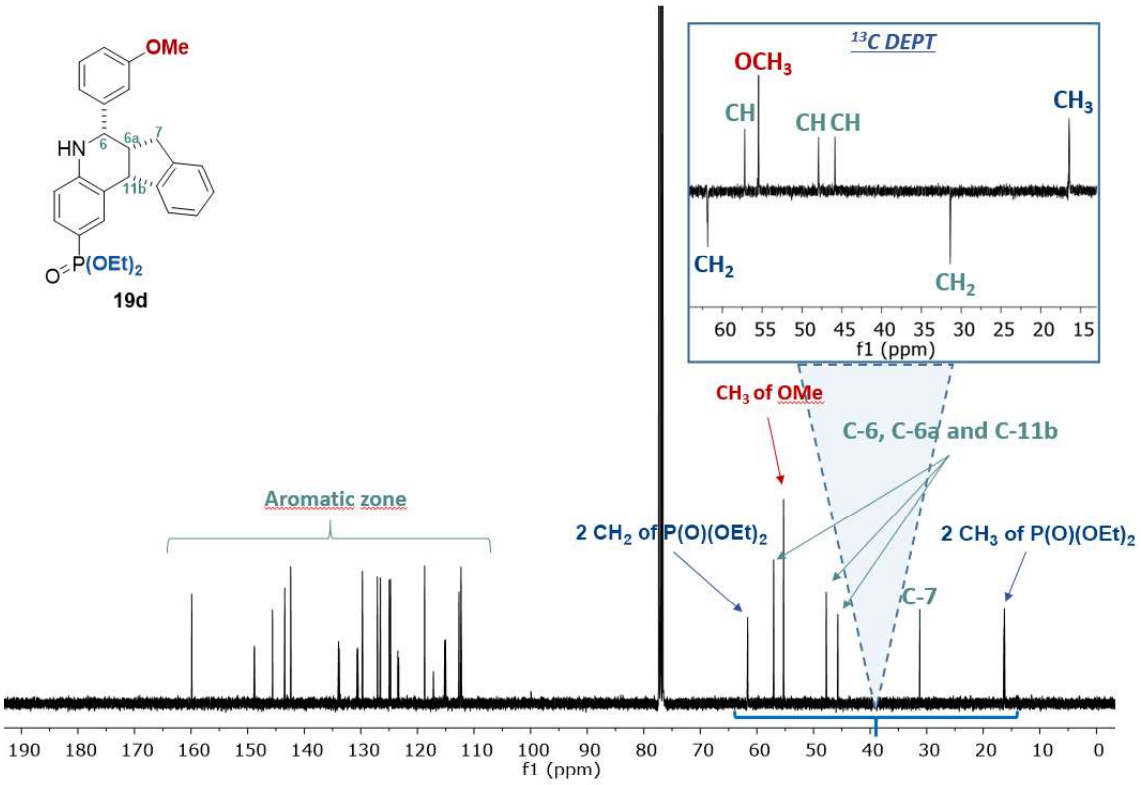

*Figure 20. ^{13}C-NMR spectrum of diethyl (6-(3-methoxyphenyl)-6,6a,7,11b-tetrahydro-5H-indeno[2,1-c]quinolin-2-yl)phosphonate **19d**.*

The scope of the reaction was then expanded to the preparation of tetrahydro-*5H*-indenoquinolinyl derivatives **19** (summarized on Table 8), which were obtained regio- and diastereoselectively[237] in moderate to high yields.

[237] Fuertes M, Selas A, Trejo A, Knudsen BR, Palacios F, Alonso C. Synthesis of hybrid phosphorated indenoquinolines and biological evaluation as topoisomerase I inhibitors and antiproliferative agents. *Bioorg Med Chem Lett*. 2021;57:128517. doi:10.1016/j.bmcl.2021.128517

Table 8. Synthesis of dialkyl tetrahydroindenoquinolinylphosphonates **19** by the Povarov MCR approach.

Entry	Compound			Reaction time (h)	Yield (%)
	Nº	R	R^1		
1	**19a/20a**	4-P(O)$(OEt)_2$	3-MeO-C_6H_4	6	62/22
2	**19b/20b**	4-P(O)$(OEt)_2$	4-MeO-C_6H_4	6	73/11
3	**19c**	4-P(O)$(OEt)_2$	4-CF_3-C_6H_4	1	48
4	**19d**	2-P(O)$(OEt)_2$	3-MeO-C_6H_4	2	65
5	**19e/20e***	2-P(O)$(OEt)_2$	4-MeO-C_6H_4	2	0/55
6	**19f**	2-P(O)$(OEt)_2$	4-CF_3-C_6H_4	1	67
7	**19g/20g***	4-P(O)$(O^iPr)_2$	4-CF_3-C_6H_4	1	0/62

**Quinolines 20 were obtained directly during purification.*

The stereochemistry of the reaction was demonstrated by 1D-NOESY-NMR spectroscopy as illustrated in the Figure 21. It was found a positive NOESY effect in the selective saturation of the 6-H proton toward the 6a-H proton (3.10 %). Furthermore, the selective saturation of the 6a-H proton presented a positive NOESY effect (2.81%) on the 11b-H proton. These results indicate a relative *cis*-configuration between the protons in positions 2, 3 and 4 of the 1,2,3,4-tetrahydroindeno[2,1-*c*]quinoline moiety, and consequently we conclude that the [4+2] Povarov reaction between arylaldimines and indene occurs *via* an *endo* transition state.

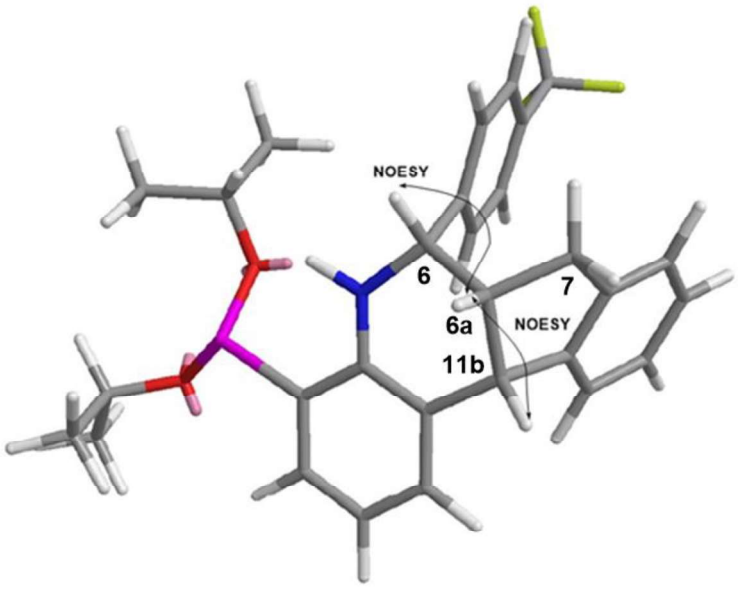

*Figure 21. Relative configuration of diisopropyl (6-(4-(trifluoromethyl)phenyl)-7H-indeno[2,1-c]quinolin-4-yl)phosphonate **20e** assigned by 1D-NOESY experiments.*

During the purification process, tetrahydro-*5H*-indenoquinolines **19a** and **19b** were spontaneously dehydrogenated and a fraction of the corresponding indenoquinoline **20** was obtained (Table 8, entries 1 and 2). Moreover, in the case of compounds **19e** and **19g**, we obtained directly the fully aromatic indenoquinolines **20e** and **20g**. For instance, when following the current Povarov MCR protocol for the preparation of the compound **19g**, upon the purification step we only obtained the corresponding fully aromatic *7H*-indenoquinoline **20g** (R = 4-P(O)(O^iPr)$_2$; R^1 = 4-CF_3-C_6H_4; Entry 7, Table 8).

In the Figure 22 we can appreciate the ^{1}H-NMR spectrum of the *7H*-indenoquinolinyl derivative **20g**, and it can be noted that the characteristic signals corresponding to the aliphatic protons of the tetrahydro-*5H*-indenoquinoline ring disappeared, while the signals of the fully aromatic *7H*-indenoquinoline core appeared in the aromatic region. Moreover, in the aliphatic area we can only observe the two diastereotopic protons of the methylene (position C-7) as a singlet at 4.25 ppm and the protons assigned to the diisopropyl phosphonate functionality: the four CH_3 groups visualized as two doublets at 1.17 ppm ($^2J_{HH}$ = 6.2 Hz) for two methyl groups and 1.38 ppm ($^2J_{HH}$ = 6.2 Hz) for the other two methyl groups; and the CH groups observed as a multiplet at 2.03 ppm that integrates for two protons.

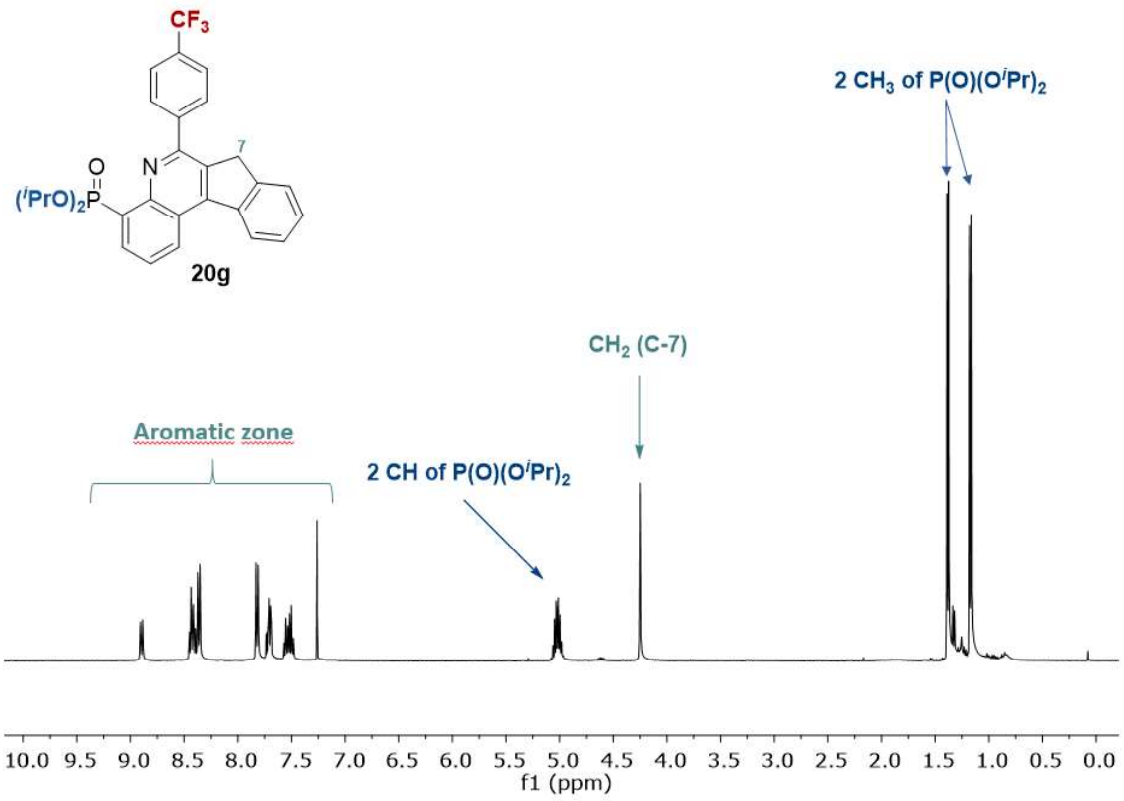

*Figure 22. ^{1}H-NMR spectrum of diisopropyl (6-(4-(trifluoromethyl)phenyl)-7H-indeno[2,1-c]quinolin-4-yl)phosphonate **20g**.*

In like manner, in the ^{13}C-NMR spectrum of the *7H*-indenoquinolinyl derivative **20g** (Figure 23) we can also observe the absence of the aliphatic protons, except for the methylene group located in the position 7 of the indenoquinoline core, which visualized as a signal in the upfield with a chemical shift of 37.7 ppm (it appears in the reverse phase in the DEPT-135 ^{13}C-NMR experiment). Furthermore, at 23.8 ppm appears a doublet with a coupling constant of $^{3}J_{CP}$ = 4.2 Hz assigned to the CH_3 of one of the isopropyl groups and at 24.3 ppm appears another doublet ($^{3}J_{CP}$ = 3.1 Hz) assigned to the two methyl groups of the other isopropyl. Finally, the two CH of the isopropyls are visualized as a doublet at 70.7 ppm with a coupling constant of $^{2}J_{CP}$= 5.5 Hz.

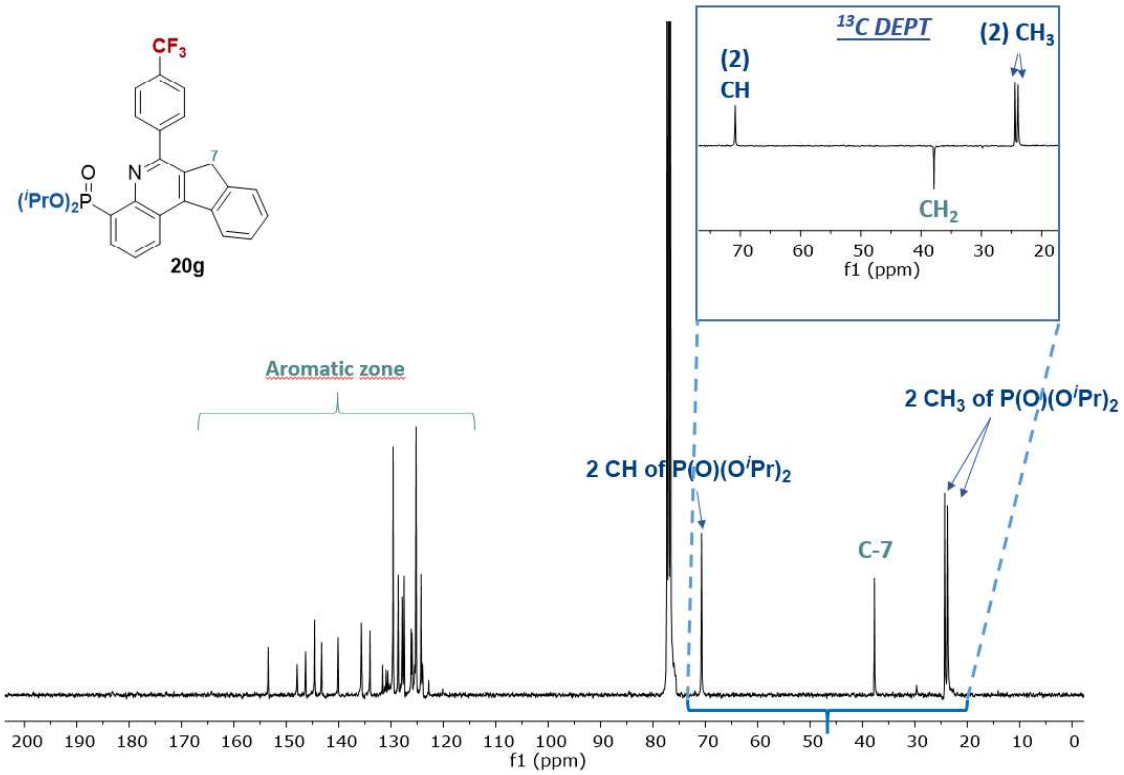

Figure 23. ^{13}C-NMR spectrum of diisopropyl (6-(4-(trifluoromethyl)phenyl)-7H-indeno[2,1-c]quinolin-4-yl)phosphonate ***20g.***

According to the results listed in the Table 8, it can be noted that overall the three-component Povarov reaction allowed the preparation of tetrahydro-*5H*-indenoquinolines **19** with various substituents in a single operation and in good yields (62-73%). In the case of the tetrahydro-*5H*-indenoquinolinyl **19b** (R = 4-P(O)(OEt)$_2$; R^1 = 4-MeO-C$_6$H$_4$; Table 8, entry 2), a 73% of yield was obtained. However, in some cases, during the purification by column chromatography of tetrahydro-*5H*-indenoquinolines **19**, small fractions of the corresponding dehydrogenated aromatic quinolines were isolated. Such is the case for compounds **19a** (R = 4-P(O)(OEt)$_2$; R^1 = 3-MeO-C$_6$H$_4$; entry 1) and **19b** (R = 4-P(O)(OEt)$_2$; R^1 = 4-MeO-C$_6$H$_4$; entry 2), where the corresponding *7H*-indenoquinolinyl derivative **20a** and **20b** were isolated respectively (yields =

22% and 11%). Furthermore, the tetrahydro-*5H*-indenoquinolinyl derivatives **19e** (R = 2-P(O)(OEt)$_2$; R^1 = 4-MeO-C$_6$H$_4$; entry 5) and **19g** (R = 4-P(O)(O^{i}Pr)$_2$; R^1 = 4-CF$_3$-C$_6$H$_4$; entry 7) resulted not to be stable under purification conditions and the corresponding aromatic *7H*-indenoquinoline derivatives **20e** and **20g** were isolated.

I-5.2. Synthesis of dialkyl *7H*-indeno[2,1-*c*]quinolinylphosphonates and dialkyl 7-oxo-*7H*-indeno[2,1-*c*]quinolinylphosphonates

The dehydrogenation of tetrahydro-*5H*-indenoquinolines **19** (Scheme 21) was studied following two protocols. On the one hand, we explored the previously mentioned DDQ oxidation protocol (2 equiv. of DDQ in chloroform at 60°C for 2h).

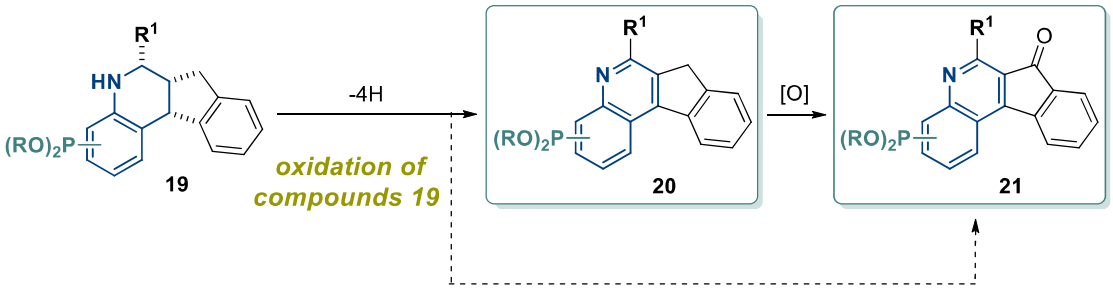

*Scheme 21. Oxidation of compounds **19** to yield the dialkyl 7H-indeno[2,1-c]quinolinylphosphonates **20** and dialkyl 7-oxo-7H-indeno[2,1-c]quinolinylphosphonates **21**.*

We started studying the dehydrogenation of diethyl (6-(4-(trifluoromethyl)phenyl)-6,6a,7,11b-tetrahydro-*5H*-indeno[2,1-*c*]quinolin-2-yl)phosphonate **19f** with 2 equivalents of DDQ in refluxing chloroform for 2h. NMR-structure elucidation experiments revealed that the corresponding diethyl (7-oxo-6-(4-(trifluoromethyl)phenyl)-*7H*-indeno[2,1-*c*]quinolin-2-yl)phosphonate **21f** was obtained upon purification by column chromatography and crystallization (Table 9, entry 6). In the Figure 24, the ^{13}C-NMR spectra of tetrahydro-*5H*-indenoquinoline **19f** and the corresponding *7H*-indenoquinolinone **21f** are compared, where it can be appreciated the disappearance of all the aliphatic carbons of the tetrahydro-5H-indenoquinoline core and the appearance of the newly formed aromatic carbons. Moreover, in the comparative of the ^{13}C-NMR spectra we can observe that diethyl (7-oxo-6-(4-(trifluoromethyl)phenyl)-*7H*-indeno[2,1-*c*]quinolin-2-yl)phosphonate **21f** lacks the methylenic carbon at C-7 position (observed as a singlet at 31.2 ppm in the tetrahydro-*5H*-indenoquinolinyl derivative **19f**, Figure 24), presenting a signal in the furthest downfield at 191.7 ppm instead, which means that the CH$_2$ at position C7 has been oxidized to the corresponding carbonyl functionality.

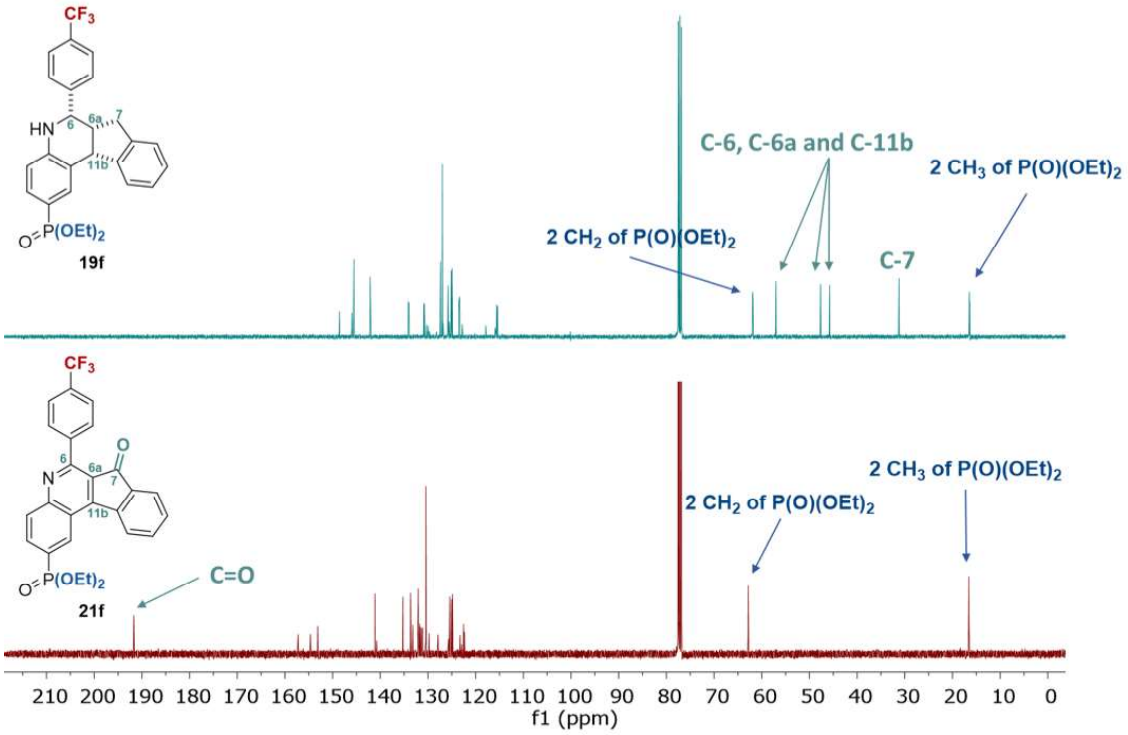

*Figure 24. Comparison between the ^{13}C-NMR spectrums of diethyl (6-(4-(trifluoromethyl)phenyl)-6,6a,7,11b-tetrahydro-5H-indeno[2,1-c]quinolin-2-yl)phosphonate **19f** and diethyl (7-oxo-6-(4-(trifluoromethyl)phenyl)-7H-indeno[2,1-c]quinolin-2-yl)phosphonate **21f.***

Furthermore, with the purpose of investigate the methylene carbonylation, we proceeded to investigate the oxidation conditions of tetrahydro-*5H*-indenoquinolinyl derivatives **19**. In this regard, manganese (III) acetate (3 equivalents) was evaluated as a mild oxidant agent, employing acetic acid as a solvent and stirring the reaction mixtures at reflux temperature. The reactions were monitored by ^{31}P/^{1}H-NMR and TLC. We tried this procedure to aromatize the tetrahydro-*5H*-indenoquinolinyl derivatives **19a** and **19c** and we obtained the corresponding 7H-indenoquinolinones **21a** (R= 4-P(O)(OEt)$_2$; R^1 = 3-MeO-C$_6$H$_4$; Table 8, entry 1) and **21c** (R = 4-P(O)(OEt)$_2$; R ^{1}= 4-MeO-C$_6$H$_4$; entry 2) in low yields (33% and 28%, respectively).

Afterwards, we applied these two oxidation protocols (DDQ and Mn III acetate) as described in the Scheme 21, and both methods lead to the formation of compounds **20** and **21** (yields are collected in the Table 9).

Table 9. Synthesis of dialkyl *7H*-indenoquinolinylphosphonates **20** and dialkyl 7-oxo-7*H*-indenoquinolin-7one-ylphosphonates **21.**

Entry	Compound			Oxidant	T (ºC)	Reaction time (h)	Yield (%)
	Nº	R	R^1				
1	**21a**	4-P(O)$(OEt)_2$	3-MeO-C_6H_4	$Mn(OAc)_3$	118	36	33
2	**21b**	4-P(O)$(OEt)_2$	4-MeO-C_6H_4	DDQ	60	2	14
3	**20c**	4-P(O)$(OEt)_2$	4-CF_3-C_6H_4	DDQ	60	2	26
4	**21c**	4-P(O)$(OEt)_2$	4-CF_3-C_6H_4	$Mn(OAc)_3$	118	36	28
5	**21d**	2-P(O)$(OEt)_2$	3-MeO-C_6H_4	DDQ	60	2	38
6	**21f**	2-P(O)$(OEt)_2$	4-CF_3-C_6H_4	DDQ	60	2	32

In view of the results collected in Table 9, we can conclude that the dehydrogenation/oxidation of tetrahydro-*5H*-indenoquinoline derivatives **19** with DDQ and $Mn(OAc)_3$ led to the formation of compounds *7H*-indeno[2,1-*c*]quinolines **20** and/or 7*H*-indeno[2,1-*c*]quinolin-7-ones **21**.

The DDQ dehydrogenation protocol led to the obtainment of the *7H*-indenoquinoline **20c** (R = 4-P(O)$(OEt)_2$; R1 = 4-CF_3-C_6H_4; Entry 3) with a low yield (26%). On the contrary, following the same reaction conditions, the DDQ protocol led to *7H*-indenoquinolinones **21b**, **21d** and **21f** in low yields (14-38%).

The dehydrogenation of tetrahydro-*5H*-indeno[2,1-*c*]quinoline derivatives **19** following the $Mn(OAc)_3$ in protocol, on the whole led to the dehydrogenation of the four aliphatic hydrogens but also to the oxidation of the methylenic carbon (position 7 of the indenoquinoline core) into a carbonyl group, obtaining directly the fully aromatic *7H*-indeno[2,1-*c*]quinolin-7-ones **21a** (R = 4-P(O)$(OEt)_2$; R^1 = 3-MeO-C_6H_4; Table 9, entry 1) and **21c** (R = 4-P(O)$(OEt)_2$; R^1 = 4-CF_3-C_6H_4; entry 4) in low yields (33% and 28% respectively).

Summary of the synthetic routes employed for the preparation of dialkyl indeno[2,1-c]quinolinylphosphonates 18, 19 and 20

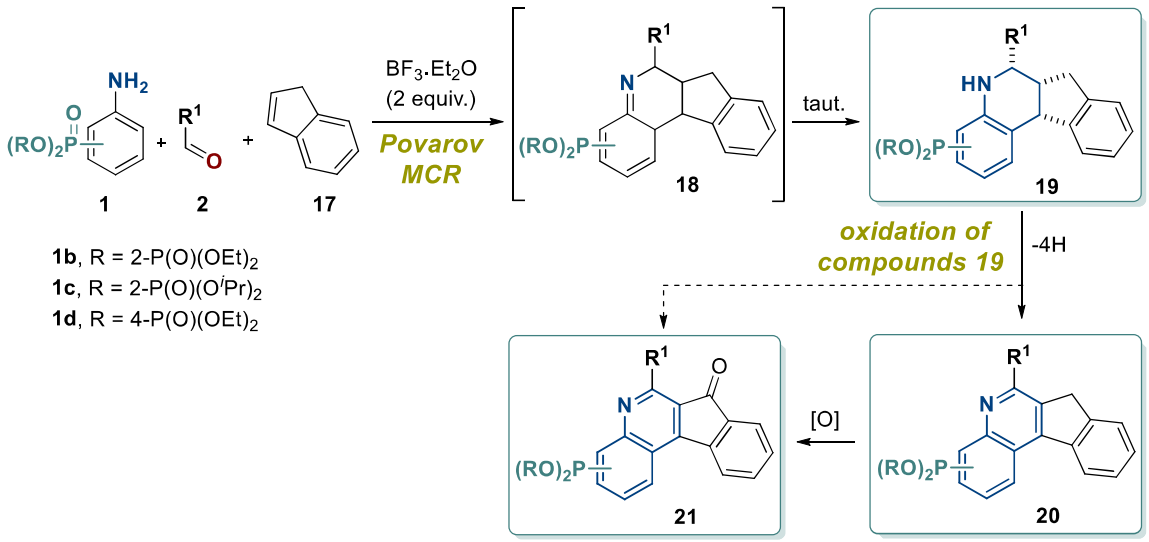

*Scheme 22. Synthetic routes for the preparation of dialkyl tetrahydro-5H-indeno[2,1-c]quinolinylphosphonates **19**, dialkyl 7H-indeno[2,1-c]quinolinylphosphonates **20** and dialkyl 7-oxo-7H-indeno[2,1-c]quinolinylphosphonates **21**.*

In conclusion, we found the Povarov MCR a convenient synthetic method for the preparation of dialkyl tetrahydro-5*H*-indeno[2,1-*c*]quinolinylphosphonates **19** (Scheme 22). Terahydroindenoquinolines **19** may be dehydrogenated to obtain the corresponding 7*H*-indeno[2,1-*c*]quinolines **20**, although considering that the methylenic carbon (position 7 of the indenoquinoline scaffold) could be subjected to oxidation and lead to 7*H*-indeno[2,1-*c*]quinolinones **21**. Accordingly, the oxidation of the methylenic carbon allowed us to incorporate a new diversity point in the indeno[2,1-*c*]quinoline core. However, it has to be mentioned that future investigations should be made to improve the current oxidation protocols.

Chapter II. Study of the *in vitro* TOP1 inhibitory activity of the newly synthesized quinoline derivatives

II-1. Introduction: *in vitro* drug screening of TOP1 inhibitors

Human topoisomerase 1B (hTOP1) is a potential and well stablished target of anti-cancer drugs[26]. In this sense, *in vitro* drug screening assays for the identification of novel hTOP1B inhibitors and further studies of their mode of action represent the first step for the biological evaluation of novel TOP1 inhibitors. The most employed state-of-the-art assays for the screening of TOP1 targeting small compounds are featured below, as well as a novel, quantitative and highly sensitive methodology for the real-time assessment of the TOP1 activity *in vitro*.

II-1.1. DNA Relaxation assay

DNA relaxation assay is the standard and most common *in vitro* assay for large drug screenings of novel sets of compounds as candidates for TOP1 inhibitors, and is based on the separation of the different topological forms of DNA by agarose gel electrophoresis. TOP1 is able to relax supercoiled circular plasmid DNA substrates (double stranded bacterial circular DNA) by introducing transient nicks (cleavage step) in one of the strands, allowing a controlled rotation of the non-cleaved strand through the nick. These nicks are rapidly sealed during the religation step, obtaining relaxed forms of the plasmid. In the DNA relaxation assay, negatively supercoiled DNA plasmids are incubated with purified TOP1 and the reaction is stopped with 0.5% of SDS (sodium dodecyl sulphate), generating a variation in the linking number (Lk) of DNA by action of the enzyme.

Topoisomers are DNA substrates with identical composition but different Lk and are further differentiated by electrophoresis in 1% agarose gel. Supercoiled DNA (*Sc*) remains compact and presents a faster electrophoretic mobility, thereby reaching the lowest part of the gel (Figure 25, below). On the contrary, relaxed forms (*Relax*) have an extended shape and consequently exhibit a slower migration. Accordingly, relaxed forms remain above, occupying a wider space as long as TOP1 action results in various relaxed topoisomers with different Lk (Figure 25, above). If the electrophoresis runs at low voltage during long times (*e.g.* 20-30 V during 12-20 h), these relaxed topoisomers could be clearly observed as shown in the example depicted in the Figure 25.

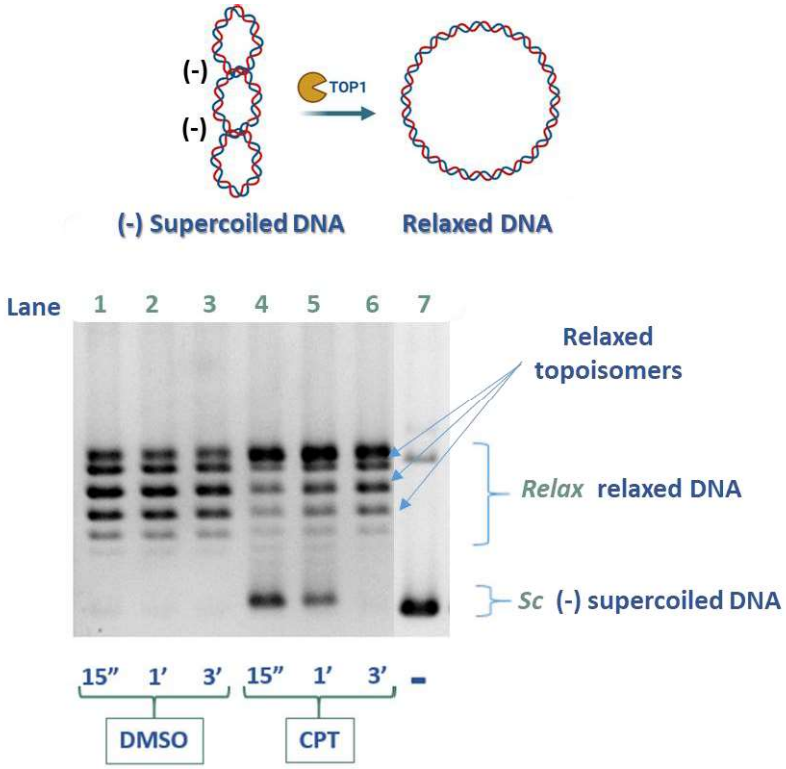

Figure 25. DNA relaxation assay, kinetic experiment with DMSO (inert solvent) and CPT (TOP1 inhibitor).

After electrophoresis completion, for the further visualization of the results, the DNA has to be stained by soaking the gel in a dissolution containing a nucleic-acid dye (mainly DNA intercalators as EtBr, SYBR safe or GelRed). Then, the gels are ready to be photographed in an UV-transilluminator. The TOP1 activity is analysed by measuring the conversion ratio of supercoiled plasmid into the relaxed form, and this assessment can be applied in order to study the inhibitor effect of drugs/candidates. If a TOP1 inhibitor agent is introduced in the reaction media, the inhibitor interferes the action of the enzyme obtaining less relaxed plasmid and a larger fraction of supercoiled form[238], as shown in the Figure 25 (the reversible TOP1 inhibitor CPT impedes the relaxation activity of the enzyme at 15'' and 1' in lanes 4 and 5 observed as the accumulation of *Sc* DNA, while at 3' in lane 6 there is no inhibition of the enzyme).

DNA relaxation assays could be performed in a time-course style (kinetic experiments) or in an end-point experiment manner. Kinetic experiments permit the study of the inhibitory activity during a selected time interval (applicable to evaluate the reversibility of the inhibition over the time)[94], while end-point experiments are indicated to reveal the optimum concentration of the

[238] Nitiss JL, Kiianitsa K, Sun Y, Nitiss KC, Maizels N. Topoisomerase Assays. *Curr Protoc*. 2021;1(10):e250. doi:10.1002/cpz1.250

drug to be used for the inhibition of TOP1[239]. In particular, in the Figure 25 is depicted an example of a kinetic experiment of the DNA relaxation assay.

II-1.2. Nicking assay

The nicking assay is mainly the same experiment as the DNA relaxation assay, but the DNA samples are loaded into an agarose gel containing ethidium bromide (EtBr). EtBr is a DNA intercalator and unwinding agent, which introduces positive supercoils into intact DNA plasmid[238]. As explained in the section II-1.1. of this chapter (*vide supra*), when performing the DNA relaxation assay experiment, during incubation in the presence of TOP1 the negatively supercoiled plasmid is relaxed by the enzyme action, obtaining the corresponding relaxed form (*Relax*). In the absence of TOP1, the negatively supercoiled form (*Sc*) is maintained (*e.g.* in a negative control, Figure 25, lane 7). However, during incubation of plasmid DNA with TOP1, some compounds are able to stabilize TOP1CC and generate a nicked plasmid (*Nick*), as illustrated in the Figure 26. The nicking assay allows the differentiation of these three forms of plasmid DNA (*Nick, Sc* and *relax*).

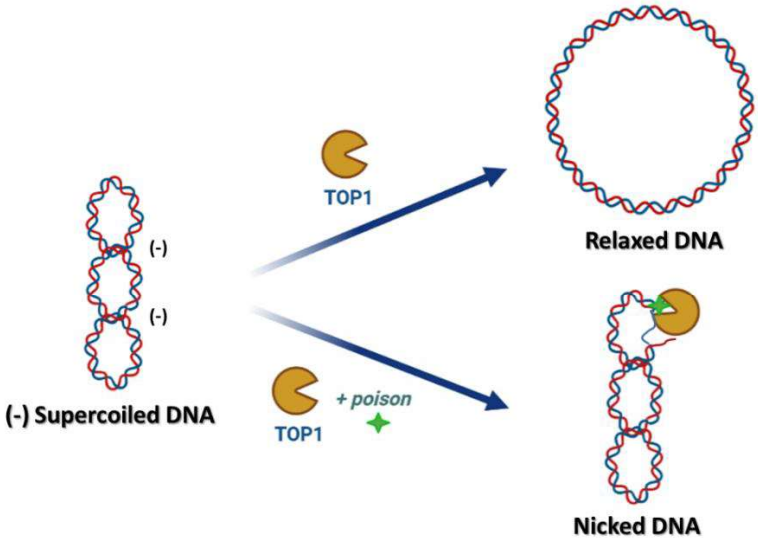

Figure 26. Supercoiled, relaxed and nicked forms of plasmid DNA after incubation with TOP1.

In the so-called nicking assay, a 1% agarose gel prestained with EtBr (0.5-1 µg/mL) is used to distinguish nicked plasmid from intact plasmid (relaxed and supercoiled)[97]. During the electrophoresis, the DNA samples are progressively being intercalated by EtBr, leading to an untwisting of the double helix of the DNA. At this point, it has to be mentioned that extended

[239] Tejería A, Pérez-Pertejo Y, Reguera RM, *et al.* Antileishmanial activity of new hybrid tetrahydroquinoline and quinoline derivatives with phosphorus substituents. *Eur J Med Chem*. 2019;162:18-31. doi:10.1016/j.ejmech.2018.10.065

relaxed form (*Relax*) is able to incorporate more EtBr than the condensed supercoiled forms (*Sc*). Hence, *Relax* form migrates slightly faster than the *Sc* form, reaching the bottom of the gel as depicted in the Figure 27.

Conversely, the writhe of nicked DNA is not affected by EtBr intercalation as long as the resulted positive supercoils will be able to escape via a nick in the double helix. In consequence, EtBr practically has no effect in the electrophoretic mobility of the nicked (*Nick*) plasmid and migrates slower than the *Sc* and *Rel* forms (as shown in the Figure 27, from slower to faster *Nick* < *Sc* < *Relax*)[240].

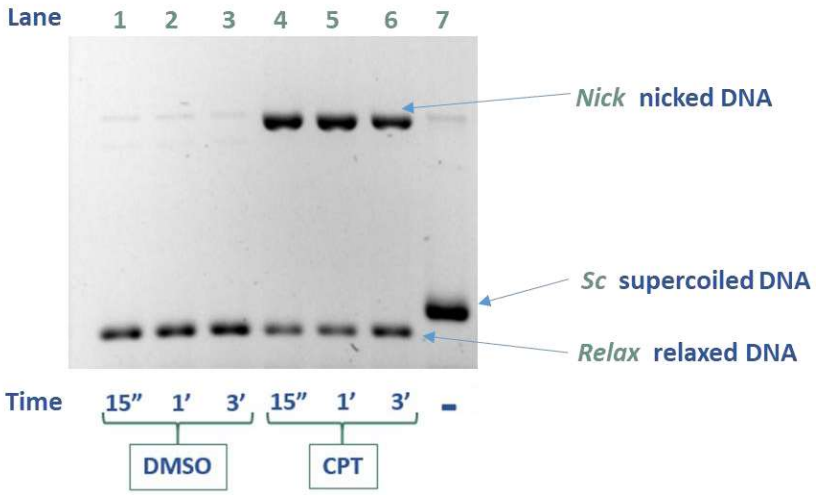

Figure 27. Nicking assay with DMSO (inert solvent) and CPT (TOP1 inhibitor).

The nick in the DNA can be caused when a compound stabilizes the TOP1CC, and therefore by the nicking assay could be determined if there is TOP1-dependant nicked plasmid (the stronger the stabilization of cleavage complexes, the stronger the *nick* band in the assay). For this reason, performing relaxation experiments in combination with nicking assays represents an improved approach to study the activity of TOP1 inhibitors, especially helpful to distinguish between TOP1 *poisons* or suppressors during the screening of the compounds.

II-1.3. DNA cleavage experiments based on synthetic dsDNA (double stranded DNA) substrates specific for TOP1

TOP1 has no sequence specificity for binding and cleaving to dsDNA substrates, even though in 1985 Westergaald *et al.* firstly identified a high affinity TOP1 binding sequence in Tetrahymena R-chromatin with the following consensus sequence: 5'-[G or A]ACTT↓AG[G or A]-3' (cleavage

[240] Bailly C. DNA relaxation and cleavage assays to study topoisomerase I inhibitors. *Methods Enzymol*. 2001;340:610-623. doi:10.1016/s0076-6879(01)40445-9

point is highlighted with an arrow)[241]. In the same way, in 1987 Pommier and collaborators revealed another TOP1 high preferred cleaving sequence in simian virus 40 (SV40), in the presence and absence of CPT[242]. This fact suggested that CPT traps TOP1CCs at high preferred sites recognized by the enzyme.

Regarding this, in the early 1990´s, the first minimum DNA duplex sequence required for TOP1 reaction *in vitro* was stablished by Westergaard and co-workers (depicted in the Figure 28)[243], based on the aforementioned high affinity sequence. Furthermore, this discovery led to the development of the first synthetic dsDNAs to study the catalytic cycle of TOP1 in detail, including both cleavage and religation steps[244].

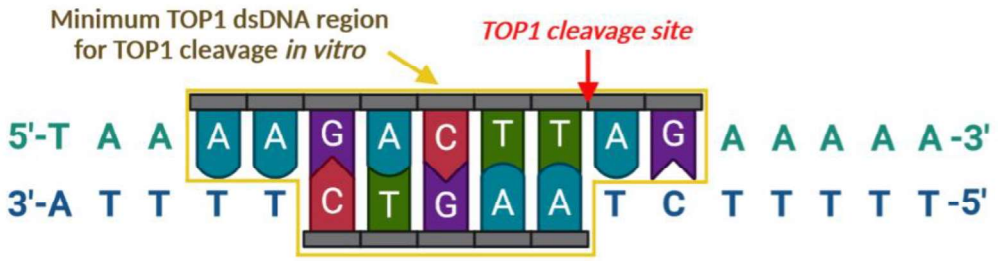

Figure 28. First minimum DNA duplex sequence necessary for TOP1 (highlighted in yellow), disclosed by Westergaard et al. in 1985.

dsDNA substrates specifically designed with high affinity TOP1 binding sequence are of particular interest in order to confirm the stabilization of TOP1CC by a drug (in particular, to distinguish *poison*-like or suppressor-like mode of actions) and to uncouple the effect of drugs on cleavage and religation steps in the catalytic cycle of TOP1[240]. In this sense, synthetic oligonucleotides (and less commonly restriction fractions obtained from plasmid DNA) with one or few TOP1 cleavage sites are widely used to assess directly cleavage and ligation reactions. These duplex DNA substrates consist of a scissile strand (the strand that TOP1 cleaves and ligates) and an annealed complementary non-scissile strand, forming a double stranded piece

[241] Bonven BJ, Gocke E, Westergaard O. A high affinity topoisomerase I binding sequence is clustered at DNAase I hypersensitive sites in Tetrahymena R-chromatin. *Cell*. 1985;*41*:541–55. doi:10.1016/s0092-8674(85)80027-1

[242] Jaxel C, Kohn KW, Pommier Y. Topoisomerase I interaction with SV40 DNA in the presence and absence of camptothecin. *Nucleic Acids Res*. 1988;*16*(23):11157-11170. doi:10.1093/nar/16.23.11157

[243] Svejstrup JQ, Christiansen K, Andersen AH, Lund K, Westergaard O. Minimal DNA duplex requirements for topoisomerase I-mediated cleavage in vitro. *J Biol Chem*. 1990;265(21):12529-12535. doi:10.1016/s0021-9258(19)38377-2

[244] Christiansen K, Svejstrup AB, Andersen AH, Westergaard O. Eukaryotic topoisomerase I-mediated cleavage requires bipartite DNA interaction. Cleavage of DNA substrates containing strand interruptions implicates a role for topoisomerase I in illegitimate recombination. *J Biol Chem*. 1993;268(13):9690-9701. doi:10.1016/s0021-9258(18)98404-8

of DNA (an example is shown in the Figure 29). The scissile strand is radiolabelled or fluorophore-labelled in order to differentiate the cleaved and uncleaved oligonucleotides by sequencing in a denaturing electrophoresis gel (*e.g.* 10-20% urea-polyacrylamide, in order to disanneal and separate the oligonucleotides of the DNA duplex). The readout of the results is subsequently achieved by visualizing the gels in a scanner, measuring the radioactivity/fluorescence of the labelled DNA samples[245].

Among DNA cleavage experiments based on synthetic dsDNA to identify stabilization of TOP1CCs in vitro, we can differentiate two major group of assays: **a)** DNA cleavage-religation equilibrium assays, and **b)** cleavage and religation assays (a straightforward approach to measure the rate of cleavage and religation separately).

[245] Castelli S, Coletta A, D'Annessa I, Fiorani P, Tesauro C, Desideri A. Interaction between natural compounds and human topoisomerase I. *Biol Chem*. 2012;393(11):1327-1340. doi:10.1515/hsz-2012-0240

II-1.3.1. DNA cleavage-religation equilibrium assay

Cleavage-religation equilibrium assays are based on DNA duplexes where TOP1 acts and the equilibrium between cleavage and religation steps is analyzed. As represented in the Figure 29, TOP1 cleaves the scissile strand and the released fragment is thereafter religated by the enzyme, which leaves the DNA intact. The cycle is repeated as long as TOP1 remains active, cleaving and religating the scissile strand continuously. At this point it should be noticed that the equilibrium is displaced towards ligation in order to finish the cycle. However, this displacement against religation can be intensified by simply increasing the NaCl concentration in the reaction media (usually from 150 mM up to 500 mM)[240,246]. Hence, after stopping the enzymatic reactions (with 0.2% SDS w/v, heat inactivation etc.) the scissile strand would remain intact (uncleaved), but when TOP1CCs are trapped by a ligand (*e.g.* a TOP1 inhibitor), the liberated fragment cannot be resealed by TOP1 and consequently the cleaved strand would be shorter than the uncleaved one. As these 2 forms (cleaved and uncleaved) possess different size, there are thoroughly differentiable by a native sequencing gel as indicated before[244].

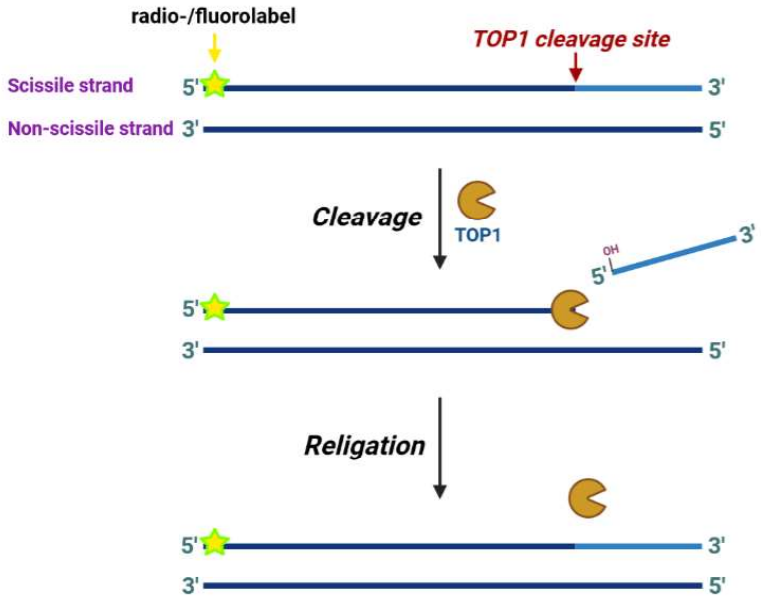

Figure 29. Schematic representation of a dsDNA equilibrium substrate to investigate stabilization of TOP1CCs in vitro.

For example, in the Figure 30, a cleavage-religation equilibrium experiment for the compounds EM1, EM2 and EM3 (panel A) is shown. Enzymatic reactions with TOP1 were performed in the presence of increasing concentrations of the drugs, using DMSO (lane 1) and CPT (lanes 2-4) as

[246] Yang Z, Champoux JJ. Reconstitution of enzymatic activity by the association of the cap and catalytic domains of human topoisomerase I. *J Biol Chem*. 2002;277(34):30815-30823. doi:10.1074/jbc.M205302200

negative and positive controls respectively. TOP1 (44 nM) was incubated during 10 minutes at 37ºC with the Cy3-labelled DNA duplex substrate of 32 base pairs (5'-Cy3-ATTTGACCTCGAGAATTATACGAAGTTA-TTAC-3'/5'-GTAATAACTTCGTATAATTCTCGAGGTCAAAT-3', 200nM) in the presence of DMSO, CPT and compounds EM1, EM2 and EM3. The reactions were stopped by adding SDS to a final concentration of 0.2% w/v, trypsin digested, EtOH precipitated and sequenced in a denaturing 20% (urea) polyacrylamide gel. Samples were visualized in a fluorescence image-scanner, obtaining the result depicted in the Figure 30 (panel B). Attending to the Figure 30, it can be observed that the presence of CPT in the reaction medium at 50 and 100 µM (lanes 2 and 3) resulted in the appearance of the cleaved strand with lower molecular weight marked by an asterisk, corresponding to the stabilization of TOP1CC induced by CPT. At 200 µM, CPT precipitated in the reaction media due to its poor solubility in aqueous solution and consequently, the accumulation of cleavage product was not observed (lane 4). Conversely, compounds EM1, EM2 and EM3 resulted to be much more soluble than CPT and it was possible to study their effect in higher concentrations. Accordingly, the compounds EM1 (lanes 5-7) and EM3 (lanes 11-13) lead to the accumulation of major cleavage products (marked by the asterisk) in a concentration dependant manner, demonstrating a *poison*-like mode of action.

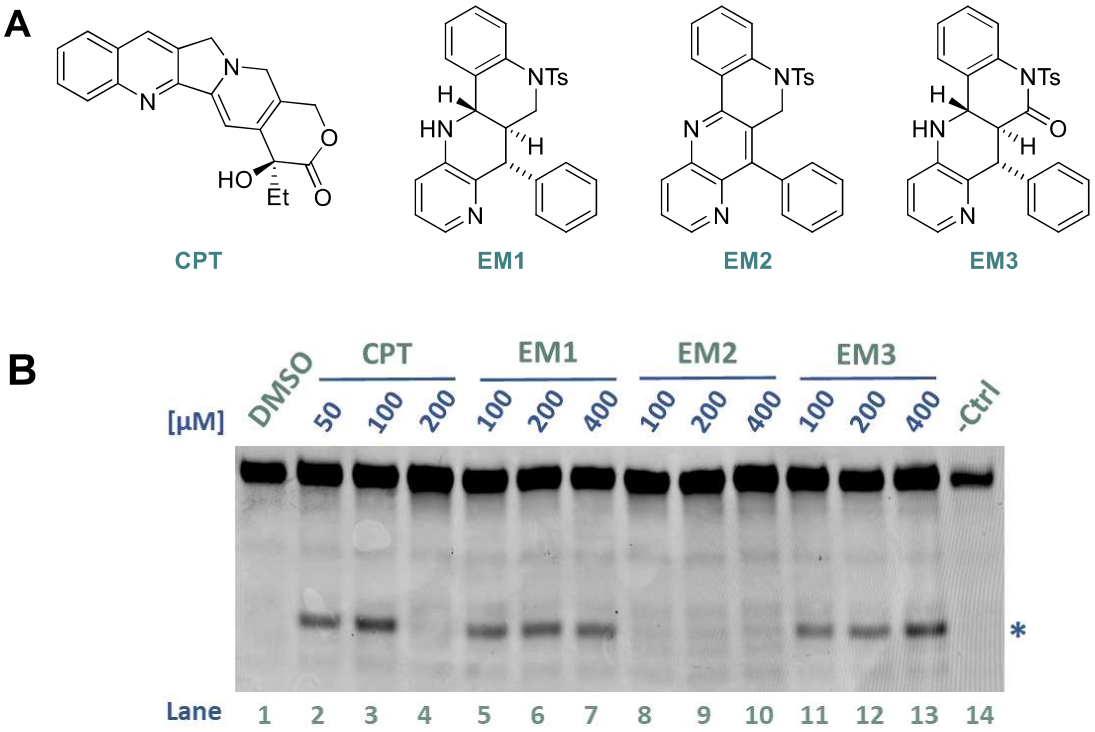

Figure 30. Cleavage-religation equilibrium assay for compounds EM1, EM2 and EM3 in increasing concentrations, using DMSO and CPT as negative and positive controls.

Even though the equilibrium assay reveals if a drug is stabilizing TOP1CCs (or not), this method does not distinguish which step is affected (stimulation of the cleavage or inhibition of the religation). For a straightforward approach to measure the rate of cleavage and ligation separately, both cleavage and ligation assays could be used.

II-1.3.2. Cleavage and religation assays

With the clear intention of studying the cleavage and religation steps separately, specific "*suicide substrates*" may be used. As illustrated in the example of Figure 31, the scissile strand of suicide substrates has a very short chain of nucleotides after the TOP1 preferred cleavage sequence, which is cleaved but cannot be religated by the enzyme. In this manner, when TOP1 cleaves the scissile strand, the released chain oligonucleotide is too short to be resealed and the TOP1 remains covalently bounded to the 3'-end of the labelled scissile strand (TOP1 literally "suicides" into the substrate). The intact scissile strand and the cleaved scissile strand could be differentiated by denaturing native gel[240] as represented in the Figure 31. Performing the reaction of TOP1 with *suicide substrates* in presence of a drug allows to disclose if the drug is affecting the cleavage step (stimulating or inhibiting).

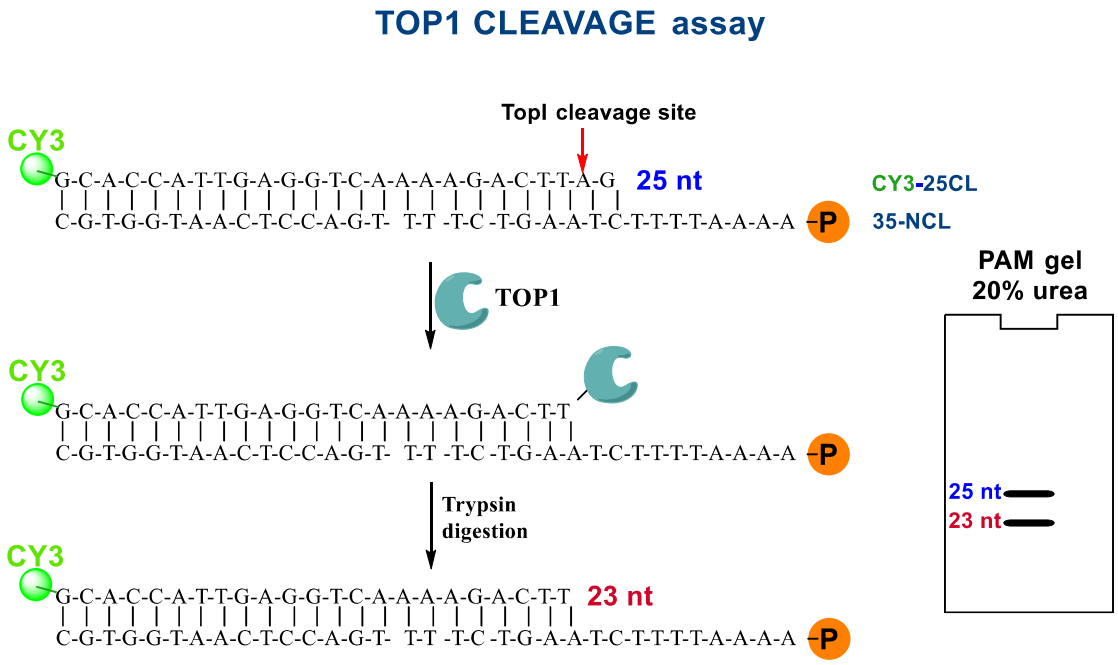

Figure 31. Scheme of the cleavage assay, with the corresponding graphic illustration of the result analysed by sequencing in a PAM 20% denaturing gel.

Likewise, the same suicide substrate could be used in order to evaluate the effect of a drug in the religation step as described in the Figure 32. In this case, first a TOP1 mediated cleavage is performed and then, instead of stopping the reactions after the cleavage, a complementary

acceptor sequence (a small oligonucleotide complementary to the non-scissile strand, with a free OH group in the 5'-end, as shown in the Figure 32 in pink) is added to the reaction mixture and TOP1 religates the acceptor[244]. Accordingly, when the religation step is specifically evaluated in this manner, the 3 possible forms of the fluoro-/radio-marked scissile strand (uncleaved, cleaved and cleaved strand with the acceptor incorporated) could be distinguished by denaturing polyacrylamide gel[238]. In this way, by simply including a drug (TOP1 inhibitor) into the reaction media, it may be studied how the religation step is affected.

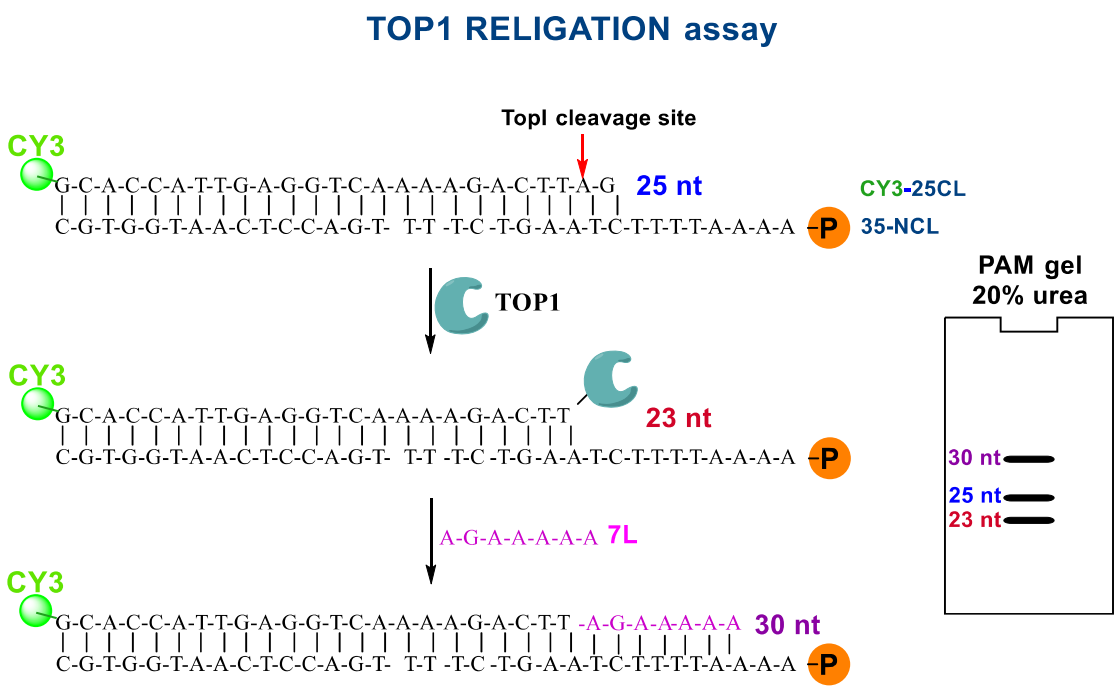

Figure 32. Scheme of the religation assay, with the corresponding graphic ilustration of the result analysed by sequencing in a PAM 20% denaturing gel.

A selective inhibitory effect in the religation step and the consequent trapping of TOP1CCs are associated with the mode of action of *poisons* (as CPT, topotecan and SN-38), attractive TOP1 inhibitors from the pharmacological point of view.

II-1.4. The REEAD assay: a DNA-based nanosensor system for the measurement of TOP1 activity

All the previous mentioned gel-based experiments require specialized personnel and furthermore, screenings of big libraries of compounds usually result categorically time consuming. In particular, assays involving sequencing of TOP1-specific DNA duplexes need to be carried out in laboratories experienced in molecular biology techniques.

In order to circumvent all the aforementioned drawbacks, the investigation of rapid, reliable, quantitative, sensitive and easy-to-use assays for the drug screening of TOP1 inhibitors is an

active field of research in molecular biology. On this regard, in 2008 Knudsen, Stougaard and collaborators developed a new assay for the real-time measurement of the TOP1 activity called Rolling-circle Enhanced Enzyme Activity Detection (REEAD) assay[247]. The REEAD assay is based on the cleavage-ligation activity of TOP1 to convert a specifically designed double stranded DNA substrate (**I** and **II**, Scheme 23) into a closed DNA circle. The circularized DNA is hybridized to a glass surface functionalized with a primer to support (**III**) and start Rolling Circle Amplification (RCA) in presence of a DNA polymerase (this setup is called REEAD-on-slide). Each rolling circle product (RCP) **IV** leads to an individual signal that could be visualized in a fluorescence microscope upon hybridization of fluorescent probes to the RCA products[248] (see the whole process in the Scheme 23), or alternatively fluorophore-labelled dNTPs could be incorporated during RCA.

Each signal (seen as a dot in the fluorescence microscope) is in fact a rolling-circle product (RCP) and represents an individual TOP1 catalytic event, allowing a quantitative single-molecule detection of the TOP1 activity. When the reactions are made in the presence of a drug that inhibits TOP1, the inhibitory activity of the drug can be quantitatively assessed by comparing the reactions either in absence or in presence of the inhibitor. Hence, the REEAD assay has revealed as an accurate, sensitive and quantitative drug screening method for the discovery of novel potential TOP1 inhibitors.

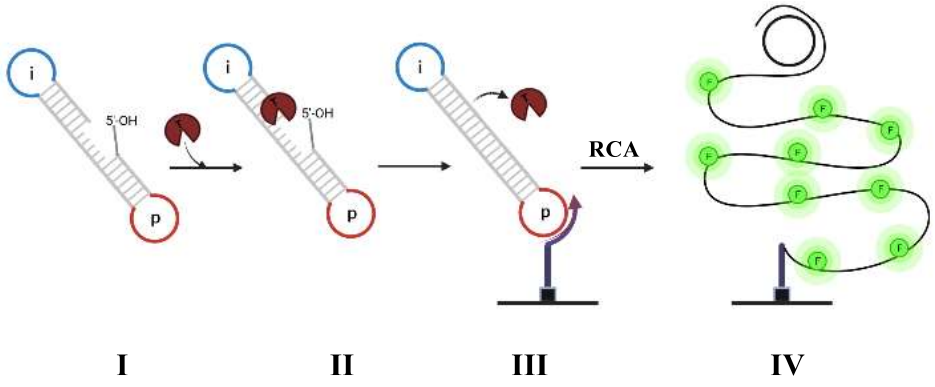

Scheme 23. General scheme for the REEAD assay (REEAD-on-slide).

In summary, the regular REEAD assay represents a powerful and reliable tool to evaluate TOP1 activity in quantitative terms. Herein we show the REEAD assay as a sensitive approach for drug screenings of TOP1 inhibitors and the further elucidation of the mode of action during the

[247] Stougaard M, Lohmann JS, Mancino A, *et al.* Single-molecule detection of human topoisomerase I cleavage-ligation activity. *ACS Nano*. 2009;3(1):223-233. doi:10.1021/nn800509b
[248] Keller JG, Stougaard M, Knudsen BR. Enzymatic activity in single cells. *Methods Enzymol*. 2019;628:43-57. doi:10.1016/bs.mie.2019.07.003

catalytic cycle of the enzyme[249]. However, the scope of the REEAD assay includes its applicability for measuring TOP1 activity in single human cells[248], human biopsy samples derived from cancer patients and human cancer cell lanes that allowed to predict the sensibility of those malignant cell lanes towards the TOP1 inhibitory effect of CPT[250]. Moreover, the REEAD assay was successfully employed to measure TOP1 from *Plasmodium falciparum* (pfTopo1) in order to detect the presence of the pathogen in blood samples from malarial patients[251].

[249] Petersen KV, Selas A, Hymøller KM, *et al.* Simple and Fast DNA Based Sensor System for Screening of Small-Molecule Compounds Targeting Eukaryotic Topoisomerase 1. *Pharmaceutics*. 2021;13(8):1255. doi:10.3390/pharmaceutics13081255

[250] Tesauro C, Keller JG, Gromova I, *et al.* Different Camptothecin Sensitivities in Subpopulations of Colon Cancer Cells Correlate with Expression of Different Phospho-Isoforms of Topoisomerase I with Different Activities. *Cancers (Basel)*. 2020;12(5):1240. doi:10.3390/cancers12051240

[251] Hede MS, Okorie PN, Fruekilde SK, *et al.* Refined method for droplet microfluidics-enabled detection of plasmodium falciparum encoded topoisomerase I in blood from malaria patients. *Micromachines*. 2015;6(10). doi:10.3390/mi6101432

II-2. *In vitro* evaluation of the hTOP1B inhibitory activity of the newly synthesized compounds

In the first chapter is presented the synthesis of novel quinoline derivatives bearing a diphenyl phosphine oxide (compounds **6**, **7**) or dialkylphosphonate (compounds **13**, **15**, **16**), along with indenoquinoline derivatives containing a dialkylphosphonate functionality (compounds **19**, **20**, **21**). In the present chapter, we show the *in vitro* assessment of human TOP1B inhibitory activity of the newly prepared families of compounds. The biological results are going to be classified by families in order to discuss their results separately, as shown in the Figure 33.

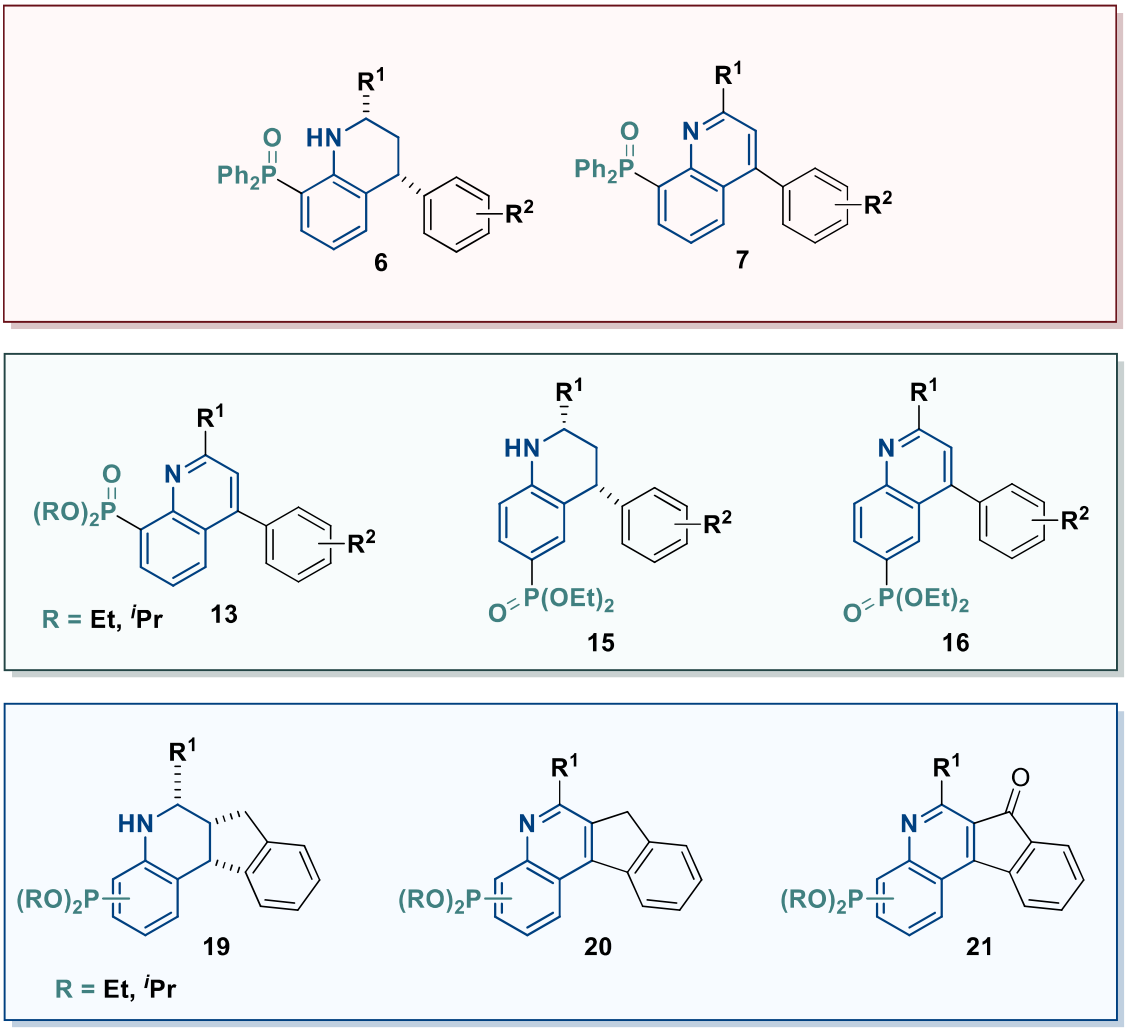

Figure 33. Families of phosphorated quinoline and indenoquinoline derivatives evaluated as potential TOP1 inhibitors.

II-2.1. *In vitro* drug screening of 1,2,3,4-tetrahydroquinolin-8-yl phosphine oxides and quinolin-8-yl phosphine oxides as TOP1 inhibitors

We started our biological studies with 1,2,3,4-tetrahydroquinolin-8-yl phosphine oxides **6** and quinolin-8-yl phosphine oxides **7** (Figure 34). The main objective of the present screening is to identify the compounds that inhibit TOP1 and investigate if the potential TOP1 inhibitors possess the ability to stabilize TOP1CC or not.

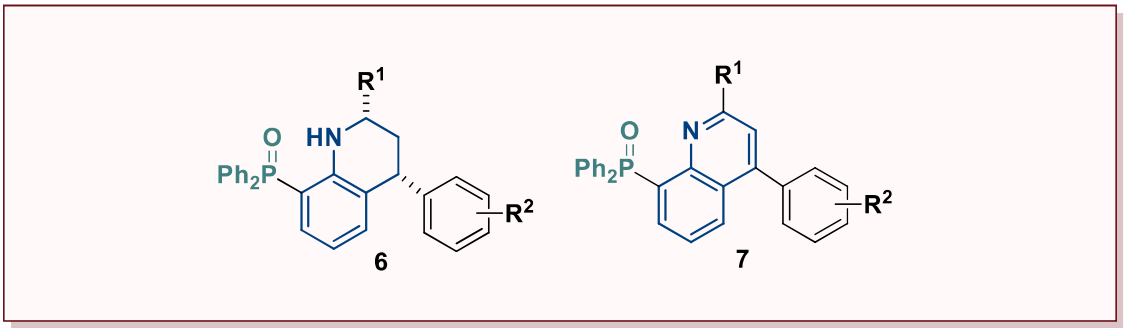

*Figure 34. General structures of 1,2,3,4-tetrahydroquinolin-8-yl phosphine oxides **6** and quinolin-8-yl phospine oxides **7**.*

II-2.1.1. Evaluation of TOP1 inhibitory activity by DNA relaxation assay

In order to perform the drug screening of the novel synthesized compounds, we outlined a study of the relaxation kinetics of human DNA TOP1B in the presence and absence of the compounds subject of research. Kinetic experiments allow us to study the reversibility of the inhibitory activity over the time. For this purpose, we incubated a negatively supercoiled plasmid DNA (pUC18) with TOP1 at 37°C and we selected 3 time points to stop the aliquots of the enzymatic reaction with SDS 0.2% w/v at 15 sec, 1 min and 3 min. This time frame allow us to observe the reversibility of CPT (as shown in the Figure 35), which exhibits a strong TOP1 inhibitory effect at short reaction times (15 sec, see lane 4 Figure 35), but starts decreasing (lane 5 at 1 min), and after 3 min there is no inhibition observed (lane 6, note that all the DNA is relaxed). In the absence of CPT (in the reaction media there is only DMSO 0.5% v/v, the solvent employed for CPT and all the tested compounds), the TOP1 activity is strong enough to relax all the plasmid DNA by 15 sec (lane 1), and remains fully active until the end of the experiment (lanes 2 and 3). Finally, the experiment includes a negative control without CPT in order to ensure that the plasmid DNA used in the experiment is negatively supercoiled (lane 7). Kinetics of DNA relaxation assay provide us the opportunity to compare the inhibitory activity of a drug candidate over the time with the well-known effect of CPT. We will not receive any information beyond 3 min, but we may predict the reversibility according to the tendency of the inhibition (it can increase, decrease or maintain constant).

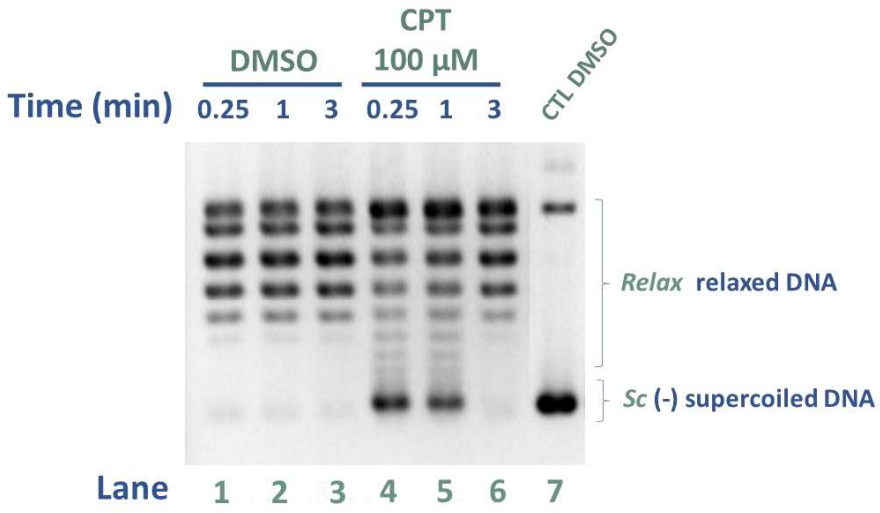

Figure 35. DNA relaxation assay to evaluate the TOP1 activity in vitro, a kinetic experiment thereof.

A second considerable feature to keep in mind when performing kinetic experiments is to establish a permanent concentration of the studied drug candidates. During the optimization of the experiment conditions, we considered appropriate to compare the newly prepared compounds at 160 µM against CPT at 100 µM. We found 100 µM as the optimal concentration of CPT, as it can precipitate at higher concentrations due to its insolubility in aqueous media. In the Figure 36, we can observe the TOP1 inhibitory effect of CPT after 30 sec of incubation with TOP1 and pUC18 plasmid DNA (lane 2). CPT inhibits strongly the TOP1 relaxation activity at 100 µM, observed as the accumulation of supercoiled (*Sc*) DNA in lane 2, whereas in the absence of CPT (lane 1) the DNA is fully relaxed (*Relax*). The reduction of the inhibitory effect of CPT results directly proportional to the decrease of CPT concentration (see lanes 2-8, from 100 µM to 5 µM of CPT).

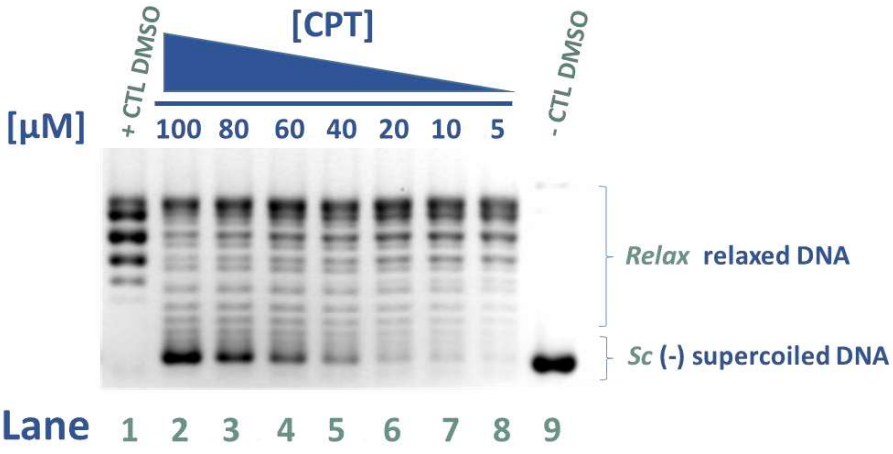

Figure 36. Dose-dependent DNA relaxation assay with CPT. The TOP1 reactions were stopped with SDS 0.2% after 30 sec of incubation at 37 °C.

We studied the TOP1 inhibitory activity of the drug candidates at 160 µM as they are much more hydrosoluble in comparison with CPT, and this fact allows to increase the concentration and hence avoid false negative results from potential TOP1 inhibitors with a lower potency. Even though the improved solubility of the novel compounds, we had to establish a fixed concentration and we set the limit at 160 µM. The main objective of the present screening is to identify those compounds with the ability to inhibit TOP1 and accordingly, we consider that a pharmacologically relevant biological effect may show any inhibition of the TOP1 at 160 µM.

1,2,3,4-tetrahydroquinolin-8-yl phosphine oxides 6

First of all we proceeded to evaluate the TOP1 inhibitory activity of 1,2,3,4-tetrahydroquinolin-8-yl phosphine oxides **7** in order to identify potential TOP1 inhibitors out of the tested library of compounds. We started with the evaluation of compounds **6e, 6i** and **6f**, following the previous mentioned conditions, and the result of the experiment is shown in the Figure 37. In all cases, negative and positive controls were included in the assay. In first place, we show the relaxation activity in the absence of any compound, only the solvent used for the preparation of further compound dissolutions was added to the reaction media (DMSO, at a final concentration of 0.5% v/v). This will be our positive control that determines the TOP1 activity in the relaxation assay, and is referred as *DMSO* (lanes 1-3) in the Figure 37. Note that the TOP1 activity is strong enough to fully relax the DNA plasmid by 15 sec (lane 1), and the activity is maintained during the studied time-interval (lanes 2-3, 1 and 3 min respectively).

In second place, we include a positive control that determines the TOP1 inhibitory activity of CPT at 100 µM, a well studied *poison*-like TOP1 inhibitor. This control is referred as *CPT* (lanes 4-6, Figure 37) and the potential inhibition of the tested compound will be compared with these lanes. CPT acts by strongly inhibiting TOP1 in an reversible manner, visualized as a considerable accumulation of *Sc* DNA at short reaction times (lanes 4 and 5, 15 sec and 1 min respectively), which is not maintained over the time and consequently after 3 minutes of incubation the plasmid DNA is completely relaxed.

In third place, a negative control in the absence of TOP1 is included in order to confirm that the plasmid DNA is in well condition and negatively supercoiled, as shown in lane 18 referred as *CTL DMSO* (Figure 37).

Then, after DMSO and CPT, the inhibitory effect of compounds **6e** (lanes 7-9), **6i** (lanes 10-12) and **6f** (lanes 13-15) was evaluated in like manner at 160 µM. The compound **6e** (R^1 = 2-pyridyl; R^2 = H) was found to inhibit TOP1 at all the selected time points but the inhibition activity displays

a decreasing tendency. At 15 sec and 1 min, the compound **6e** inhibits the TOP1 relaxation activity in a similar way as CPT does (lanes 7 and 8 respectively), while at 3 min still inhibiting the TOP1 activity but in a weaker manner. Conversely, the compound **6i** (R^1 = 3,4-F_2-C_6H_3; R^2 = 4-F) exhibits a weak inhibition of TOP1 activity at 15 sec and 1 min (lanes 10 and 11), which disappears by 3 min (lane 12). Finally, the compound **6f** (R^1 = C_6H_5; R^2 = 4-Me) exhibits a modest TOP1 inhibitory activity comparing to CPT at the tree selected time points (lanes 13-15), which appears to decrease over the time (the accumulation of *Sc* DNA is descending, 15 sec > 1 min > 3 min).

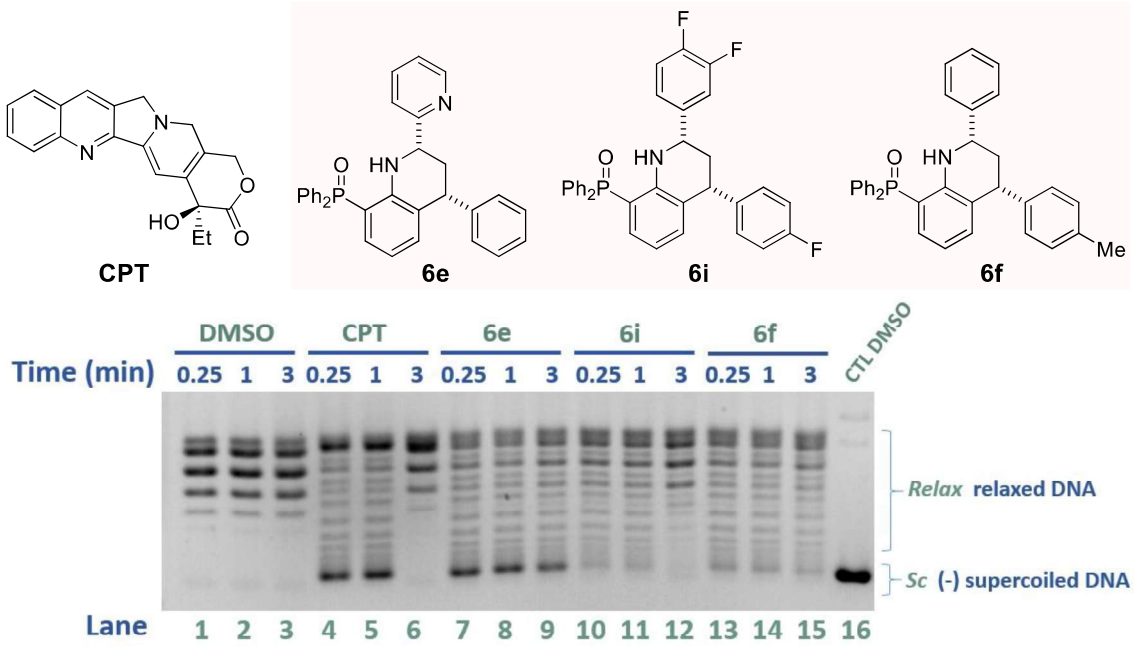

*Figure 37. DNA relaxation assay to study the TOP1 inhibitory activity of compounds **6e**, **6i** and **6f**.*

The results of the TOP1 inhibitory effect of compounds **6e**, **6i** and **6f** at 160 µM are included in the Table 10 (entries 5, 9 and 6 respectively), and expressed semiquantitatively compared to the maximum activity of CPT at 100 µM. Likewise, we continued the screening of 1,2,3,4-tetrahydroquinolin-8-yl phosphine oxides **6** and the results are collected in the Table 10 as well.

Table 10**. TOP1 inhibitory activity of 1,2,3,4-tetrahydroquinolin-8-yl phosphine oxides **6

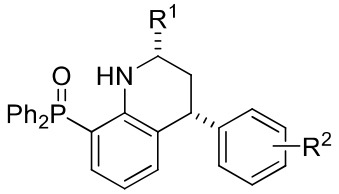

6

Entry	Compound			% Inhibition[a]		
	Nº	R^1	R^2	15 sec	1 min	3 min
1	**6a**	2-MeO-C_6H_4	H	+	+	+
2	**6b**	4-$(EtO)_2P(O)O$- C_6H_4	H	-	-	-
3	**6c**	1-naphthyl	H	+++	+++	+++
4	**6d**	2-naphthyl	H	+	+	++
5	**6e**	2-pyridyl	H	++	++	+
6	**6f**	C_6H_5	4-Me	+	+	+
7	**6g**	4-F-C_6H_4	4-Me	+	+	-
8	**6h**	4-F-C_6H_4	4-F	+	+	-
9	**6i**	3,4-F_2-C_6H_3	4-F	+	+	-

[a]The activity of the compounds inhibiting hTOP1B relaxation at 160 μM was expressed semiquantitatively by comparison with the maximum inhibitory activity observed for CPT at 100 μM as follows: -, no activity; +, weaker activity than CPT; ++ similar activity to CPT; +++ stronger activity than CPT.

The compound **6a** (R^1 = 2-MeO-C_6H_4; R^2 = H; Table 10, entry 1) presented a mild inhibitory activity but maintained over the time. On the contrary, the compound **6c** (R^1 = 1-naphthyl; R^2 = H; entry 3) exhibits an intense TOP1 inhibitory activity, stronger than CPT and constant over the time, whereas compound **6d** (R^1 = 1-naphthyl; R^2 = H; entry 4) showed a moderate TOP1 inhibitory effect at short reaction times (15 sec and 1 min) but a remarkable inhibition at 3 min. Curiously, the compounds **6c** and **6d** with naphthyl substituents were found to powerfully inhibit TOP1 activity at a longer reaction times (3 min), suggesting that big aromatic substituents in the position 2 of the tetrahydroquinoline scaffold may contribute to this biological effect.

Quinolin-8-yl phospine oxides 7

Once we studied the biological activity of tetrahydroquinolines **6** against TOP1, we performed the same experiments with the dehydrogenated quinolin-8-yl phospine oxides **7**. As expounded before, the TOP1 inhibitory activity of quinolines **7** was studied at 160 μM and we compared the results with the inhibitory effect of CPT at 100 μM. The quinolin-8-yl phospine oxides **7h** (lanes 7-9), **7i** (lanes 10-12) and **7a** (lanes 13-15) were evaluated in a DNA relaxation assay as shown in the Figure 38. The compound **7h** (R^1 = 4-F-C_6H_4; R^2 = 4-F) showed a weak inhibitory activity at short reaction times (15 sec and 1 min, lanes 7 and 8 respectively). Likewise, the compound **7i**

(R^1 = 3,4-F_2-C_6H_3; R^2 = 4-F) showed a similar behaviour, while **7a** (R^1 = 2-MeO-C_6H_4; R^2 = H) was found to strongly inhibit TOP1 relaxation activity at 15 sec and 1 min (lanes 13 and 14), even stronger than CPT at the same time points (lanes 4 and 5), and moreover maintains a weak inhibitory activity at 3 min (lane 15).

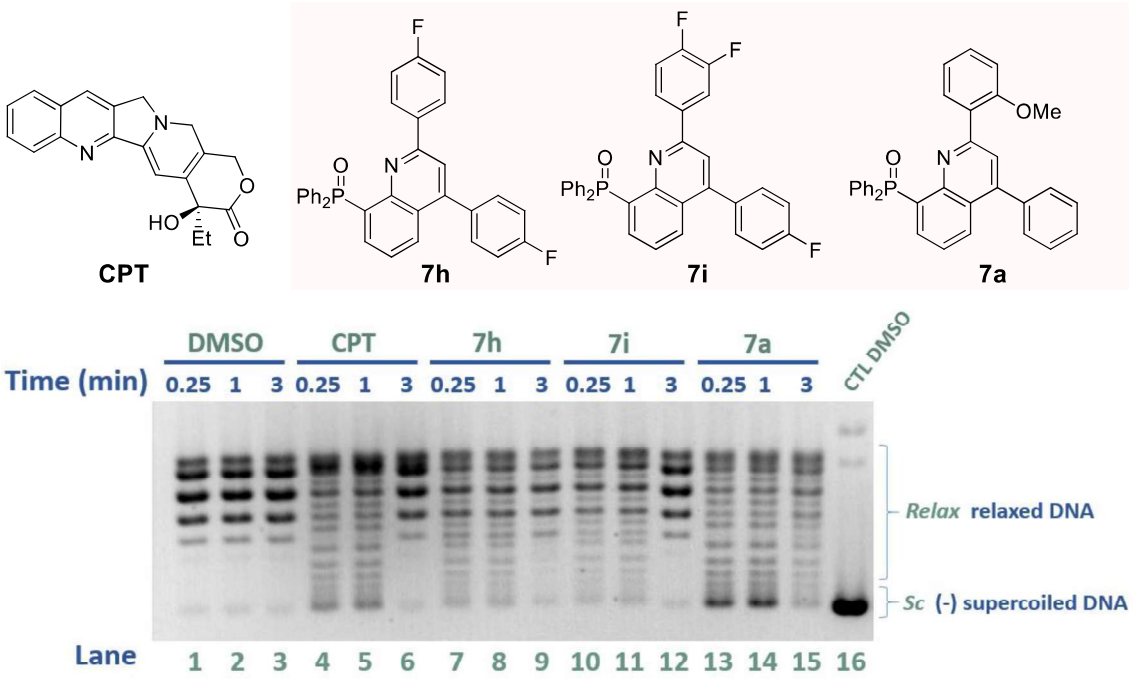

*Figure 38. DNA relaxation assay to study the TOP1 inhibitory activity of compounds **7h**, **7i** and **7a**.*

The results of compounds **7h**, **7i** and **7a** are collected in the Table 11 (entries 7, 8 and 1 specifically). We continued the drug screening with the rest of quinolin-8-yl phospine oxides **7**, and the results are exposed in the Table 11 as well.

Table 11**. TOP1 inhibitory activity of quinolin-8-yl phosphine oxides **7.

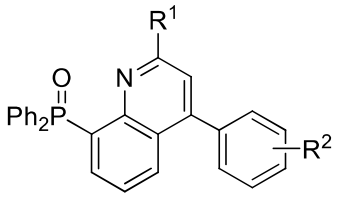

7

Entry	Compound			% Inhibition[a]		
	Nº	R^1	R^2	15 sec	1 min	3 min
1	**7a**	2-MeO-C_6H_4	H	+++	+++	+
2	**7b**	4-$(EtO)_2P(O)O$- C_6H_4	H	-	-	-
3	**7c**	1-naphthyl	H	++	++	++
4	**7d**	2-naphthyl	H	+	++	+
5	**7f**	C_6H_5	4-Me	+	+	-
6	**7g**	4-F-C_6H_4	4-Me	+	-	-
7	**7h**	4-F-C_6H_4	4-F	+	+	-
8	**7i**	3,4-F_2-C_6H_3	4-F	++	++	-
9	**7j**	C_6H_5	4-F	+	+	-
10	**7k**	4-F-C_6H_4	H	+	+	+

[a]The activity of the compounds inhibiting hTOP1B relaxation at 160 μM was expressed semiquantitatively by comparison with the maximum inhibitory activity observed for CPT at 100 μM as follows: -, no activity; +, weaker activity than CPT; ++ similar activity to CPT; +++ stronger activity than CPT.

The quinoline derivative **7c** (R^1 = 1-naphthyl; R^2 = H; Table 11, entry 3) has been reported to intensely inhibit TOP1 during all the selected time-frame, with a similar activity as the maximum activity reported for CPT at 100 μM. Likewise, the compound **7d** (R^1 = 2-naphthyl; R^2 = H; entry 4) showed a mild inhibition of TOP1 at 15 sec and 3 min but a stronger inhibition at 1 min. Accordingly, the compound **7i** (R^1 = 3,4-F_2-C_6H_3; R^2 = 4-F; entry 8) presented a similar inhibitory activity to the reference CPT, showing a strong inhibition of TOP1 relaxation activity at 15 sec and 1 min, which resulted to be reversible as long as there is no inhibitory activity at 3 min.

In summary, once concluded the biological screening of newly synthesized 1,2,3,4-tetrahydroquinolin-8-yl phosphine oxides **6** and quinolin-8-yl phosphine oxides **7,** it should be highlighted that the tetrahydroquinoline **6e** (R^1 = 2-pyridyl; R^2 = H) and quinoline **7a** (R^1 = 2-MeO-C_6H_4; R^2 = H) presented remarkable inhibitory activities, which are comparable or higher to the effect of CPT at 100 μM. Moreover, it seems that out of the phosphine oxide-containing quinoline derivatives, the naphthyl-substituted compounds (both tetrahydroquinolines **6a**, **6b**; and dehydrogenated quinolines **7a**, **7b**) present a different TOP1 inhibition behaviour. It certainly appears to be a beneficial substitution pattern in this family of compounds, as these compounds with naphthyl substituents in the position 2 of the (tetrahydro)quinoline scaffold reported a marked inhibition of TOP1, but they also appear to strongly inhibit the enzyme during a longer period of time.

II-2.1.2. Mechanistic studies of the TOP1 inhibitory activity by nicking assays

Once we identified those compounds with the ability to inhibit TOP1, we wanted to go one step forward and investigate whether they stabilize TOP1CC or not. In this regard, we outlined nicking assays in order to study if the tested compounds induce the formation of TOP1-dependant nicked plasmid DNA, what would be a clear evidence of stabilization of TOP1CC. As explained before, the nicking assay is basically the same experiment of the DNA relaxation assay, but the DNA samples are loaded in an agarose gel containing 0.5 µg/mL of EtBr, which allows us to differentiate the nicked DNA from intact DNA. As expounded before, EtBr induces positive supercoils into the intact DNA and it shows a faster mobility during the electrophoresis, while nicked plasmid runs slower, and this fact allows to differentiate between these forms of the plasmid DNA. With this aim, we basically performed the same enzymatic reactions as we did in the DNA relaxation assay but we removed the first time point of the kinetic study (15 sec) in order to give time enough to the enzyme to operate. Furthermore, we increased the amount of the enzyme to ensure a strong TOP1 activity. In short, we incubated the negatively supercoiled plasmid DNA (pUC18) with TOP1 at 37^{o}C and we stop aliquots of the enzymatic reaction with SDS 0.2% w/v at 1 min and 3 min, in absence and presence of the compound(s) subject of study. An example of these experiments is shown in the Figure 39.

1,2,3,4-tetrahydroquinolin-8-yl phosphine oxides 6

We started the mechanistic studies with tetrahydroquinolines **6**. First of all, we studied the ability of compounds **6a**, **6e**, **6c** and **6d**, using the solvent alone (*DMSO*) as a negative control (no formation of nicked DNA) and CPT at 100 µM as a positive control (formation of nicked DNA).

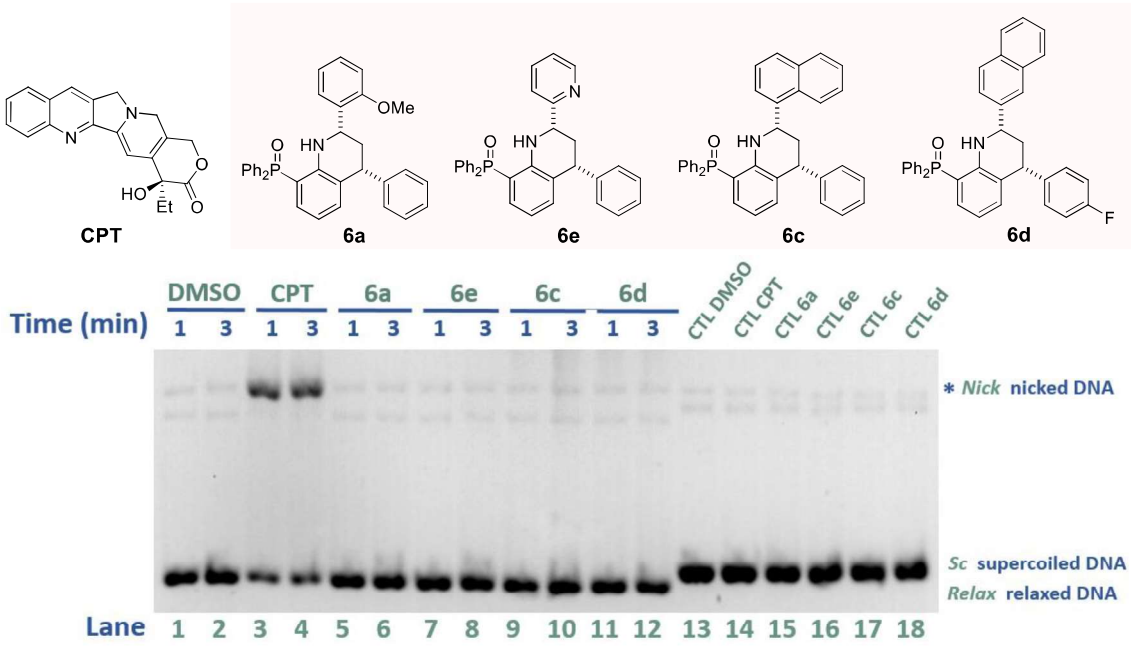

*Figure 39. Nicking assay of compounds **6a**, **6e**, **6c** and **6d**.*

In lanes 1 and 2 of the Figure 39, the enzymatic reaction was performed in the absence of any compound at 1 min and 3 min respectively, only with the solvent DMSO. It can be noted how after TOP1 action and EtBr intercalation during electrophoresis, the intact plasmid runs as relaxed DNA (*Relax*). Likewise, when the enzymatic reaction is performed in the presence of 100 µM of CPT at 1 min and 3 min (lanes 3 and 4), the TOP1 induces the stabilization of TOP1CCs and consequently introduces nicks in the DNA. The nicked plasmid DNA is capable to escape to the effect of EtBr as it presents a nick in the double helix structure and one of the chains is free to rotate over the present nick, resulting in a slower mobility in the electrophoresis. In this regard, after incubation of pUC18 with TOP1 in the presence of 100 µM of CPT, we can observe an accumulation of nicked plasmid (marked with an asterisk in the Figure 39) at 1 min and 3 min (lanes 3 and 4). It is noteworthy to mention that in the DNA relaxation assay we did not observe TOP1 inhibitory activity of CPT at 3 min, but in the nicking assay there is a clear accumulation of nicked plasmid after 3 min of incubation.

We performed the same enzymatic reactions in the presence of 160 µM of compounds **6a** (R^1 = 2-MeO-C_6H_4; R^2 = H), **6e** (R^1 = 2-pyridyl; R^2 = H), **6c** (R^1 = 1-naphthyl; R^2 = H) and **6d** (R^1 = 2-naphthyl; R^2 = H). In all cases (lanes 5-12, Figure 39), the novel tetrahydroquinoline derivatives did not induce any detectable accumulation of nicked DNA after 1 min and 3 min of incubation with TOP1.

Afterwards, we studied the remaining tetrahydroquinolines **6** (**6b**, **6f**, **6g, 6h** and **6i**) using the same nicking assay and again, and none of these compounds was found to induce the formation of nicked plasmid. Therefore, we can conclude that the tested drug behave as TOP1 suppressors.

Quinolin-8-yl phospine oxides 7

Continuing with the screening of the compounds by the nicking assay, we moved to investigate whether the quinolin-8-yl phospine oxides **7** generate TOP1-dependant nicked plasmid DNA. At this point we conceived that the quinoline derivatives **7** may be better candidates to stabilize TOP1CCs as fully aromatic scaffolds have shown to favour positive π stacking interactions with DNA base-pairs in those cleavage complexes, which are responsible of the interfacial inhibition mechanism of TOP1 *poisons* as CPT[230].

We evaluated the quinolines **7a** (R^1 = 2-MeO-C_6H_4; R^2 = H), **7c** (R^1 = 1-naphthyl; R^2 = H), **7d** (R^1 = 2-naphthyl; R^2 = H) and **7i** (R^1 = 3,4-F_2-C_6H_3; R^2 = 4-F) in the nicking assay as shown in the Figure 40, and the studied compounds did not show any ability to generate detectable nicked DNA (lanes 5-12). We extended the study to the other quinolin-8-yl phospine oxides **7** (**7b**, **7e**, **7f**, **7g**, **7h**, **7j**, **7k**) obtaining the same negative result, concluding that the quinolines **7** do not introduce nicks in the DNA. Consequently, we can conclude that these compounds do not act as *poison*-like TOP1-inhibitors, they behave as TOP1 suppressors instead.

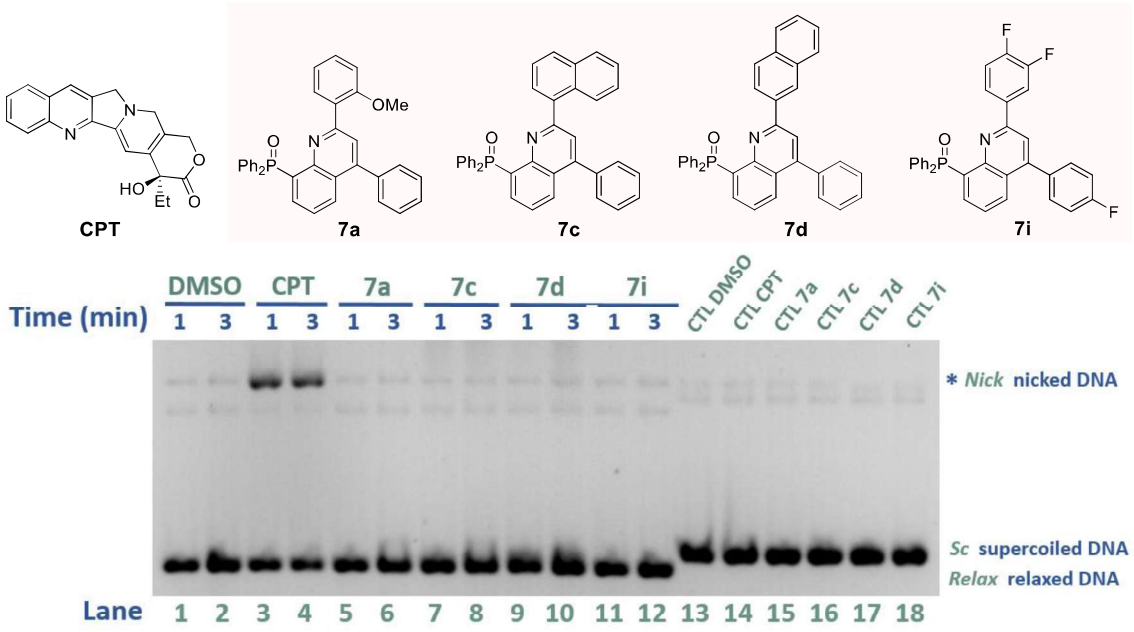

*Figure 40. Nicking assay of compounds **7a**, **7c**, **7d** and **7i.***

In conclusion, we reported that phosphine oxide containing tetrahidroquinolines **6** and quinolines **7** were not able to introduce detectable TOP1-dependant nicks in the plasmid DNA, suggesting that the studied compounds do not present the ability to generate accumulation of cleavage complexes and therefore, we dismissed a *poison*-like mode of action for the tested compounds. This fact clearly suggests that those compounds that inhibit the TOP1 act as TOP1 suppressors.

II-2.2. *In vitro* drug screening of dialkyl quinolinylphosphonates and dialkyl (indeno[2,1-*c*]quinolinyl)phosphonates as TOP1 inhibitors

In the present section we expose the *in vitro* drug screening of dialkyl quinolinyl phosphonate derivatives **13**, **15** and **16** (collected in the Figure 41, panel **A,** in green) and dialkyl (indeno[2,1-*c*]quinolinyl) phosphonate derivatives **19**, **20** and **21** (collected in the panel **B**, in blue). We investigated the TOP1 inhibitory activity and the inhibition mechanism of the drug candidates.

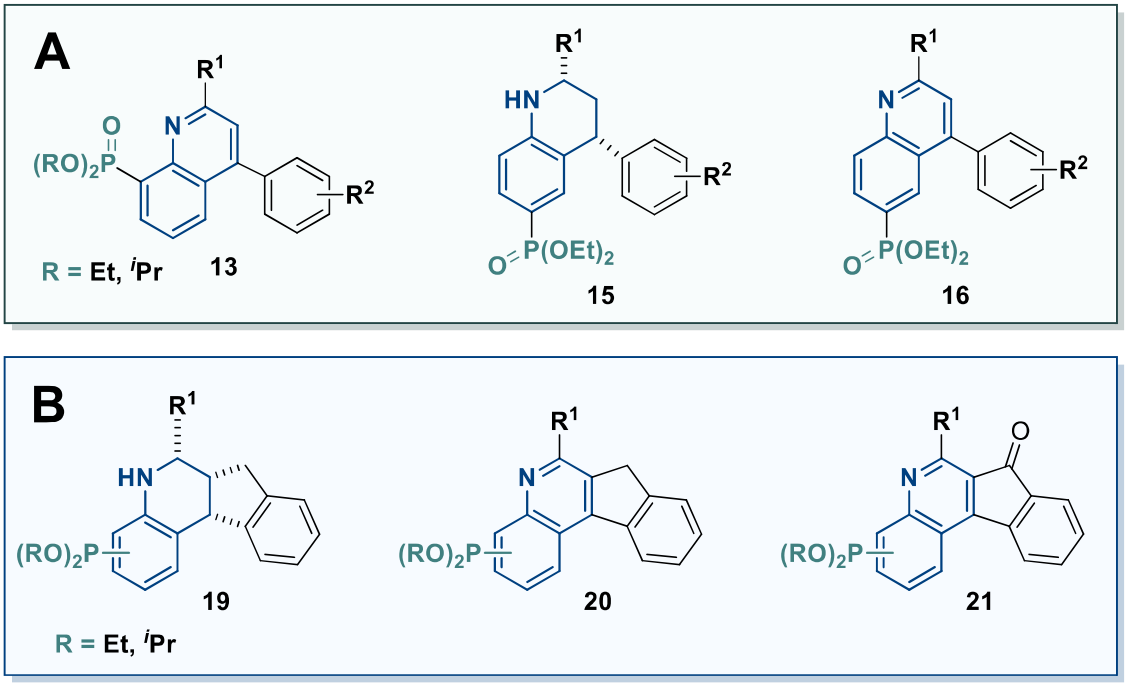

*Figure 41. **A)** General structures of dialkyl quinolin-8-yl phosphonates **13** and diethyl 1,2,3,4-tetrahydroquiolin-6-yl phosphonates **15**, diethyl quinolin-6-yl phospjonates **16** (in green); **B)** tetrahydro-5H-indeno[2,1-c]quinolinyl dialkylphosphonates **19**, dialkyl 7H-indeno[2,1-c]quinolinylphosphonates **20** and dialkyl 7-oxo-7H-indeno[2,1-c]quinolinylphosphonates **21** (in blue).*

II-2.2.1. Evaluation of TOP1 inhibitory activity by DNA relaxation assay

Dialkyl quinolin-8-ylphosphonates 13

We started the biological screening of the novel phosphonate-containing quinoline derivatives with the evaluation of the TOP1 inhibitory activity of dialkyl quinolin-8-ylphosphonates **13** by the DNA relaxation assay, in the same manner as expounded before (section II-2.1. of this chapter, *vide supra*).

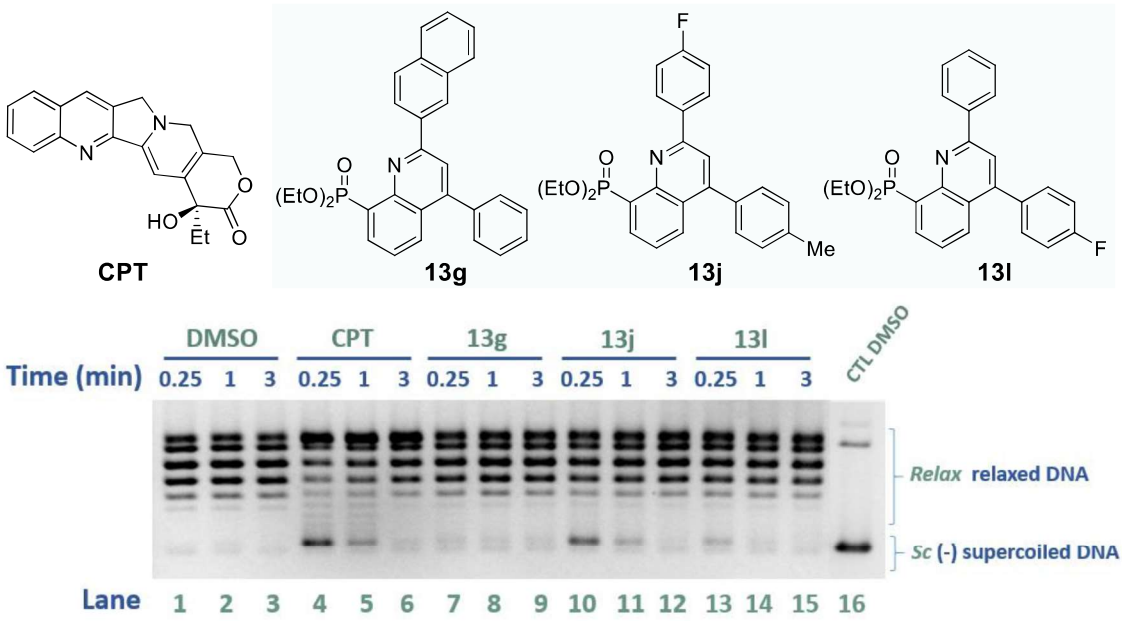

*Figure 42. DNA relaxation assay to study the TOP1 inhibitory activity of compounds **13g**, **13j** and **13l**.*

We firstly investigated the compounds **13g**, **13j** and **13l** at 160 µM, in comparison with CPT at 100 µM, and the result of the experiment is shown in the Figure 42. The compound **13j** (R^1 = 3,4-F_2-C_6H_3; R^2 = 4-Me) was found to intensely inhibit the TOP1 relaxation activity at 15 sec (lane 10, Figure 42), activity that is observed to decrease by 1 min (lane 11) and to completely expire after 3 min of incubation (lane 12). Regarding the compound **13l** (R^1 = C_6H_5; R^2 = 4-F), it exhibited a slight inhibition at 15 sec (lane 13), which declines by 1 min (lane 14), to completely disappear by 3 min (lane 15). On the contrary, the quinoline derivative **13g** (R^1 = 2-naphthyl; R^2 = H) did not show any TOP1 inhibitory activity during the tested time-interval.

We continued the assessment of TOP1 inhibitory activity of the rest of dialkyl quinolin-8-ylphosphonates **13** (**13a**-**13o**), which are collected in the Table 12.

Table 12**. TOP1 inhibitory activity of dialkyl quinolin-8-ylphosphonates **13.

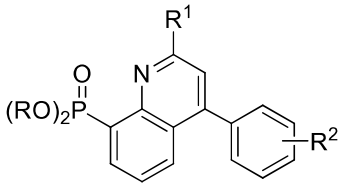

13

Entry	Compound				% Inhibition[a]		
	Nº	R	R^1	R^2	15 sec	1 min	3 min
1	**13a**	Et	C_6H_5	H	+	+	+
2	**13b**	Et	2-MeO-C_6H_4	H	+	+	-
3	**13c**	Et	3-MeO-C_6H_4	H	-	-	-
4	**13d**	Et	4-MeO-C_6H_4	H	-	-	-
5	**13e**	Et	4-$(EtO)_2P(O)O$-C_6H_4	H	+	+	-
6	**13f**	Et	1-naphthyl	H	+	+	+
7	**13g**	Et	2-naphthyl	H	+	+	-
8	**13h**	Et	3,4-F_2-C_6H_3	H	+	-	-
9	**13i**	Et	C_6H_5	4-Me	+	+	-
10	**13j**	Et	4-F-C_6H_4	4-Me	++	+	-
11	**13k**	Et	3,4-F_2-C_6H_3	4-Me	++	+	+
12	**13l**	Et	C_6H_5	4-F	+	+	-
13	**13m**	Et	4-F-C_6H_4	4-F	+	+	-
14	**13n**	Et	3,4-F_2-C_6H_3	4-F	+	+	+
15	**13o**	^{i}Pr	4-F-C_6H_4	H	+	-	-
16	**13p**	^{i}Pr	3,4-F_2-C_6H_3	H	+	+	-
17	**13q**	^{i}Pr	4-F-C_6H_4	4-Me	-	-	-
18	**13r**	^{i}Pr	3,4-F_2-C_6H_3	4-Me	+	-	-
19	**13s**	^{i}Pr	4-F-C_6H_4	4-F	+	+	+
20	**13t**	^{i}Pr	3,4-F_2-C_6H_3	4-F	+	+	+

[a]The activity of the compounds inhibiting hTOP1B relaxation at 160 μM was expressed semiquantitatively by comparison with the maximum inhibitory activity observed for CPT at 100 μM as follows: -, no activity; +, weaker activity than CPT; ++ similar activity to CPT; +++ stronger activity than CPT.

Overall, most of the compounds **13** presented a modest TOP1 inhibitory activity, specially at short reaction times (15 min at 1 min) and in any case higher than the reference compound CPT. The compounds with the ability to inhibit TOP1 mostly demonstrated a clear reversibility of the inhibitory effect over the time. It is noteworthy the marked inhibitory activity of compounds **13j** (R^1 = 4-F-C_6H_4; R^2 = 4-Me; Table 12, entry 10) and **13k** (R^1 = 3,4-F_2-C_6H_3; R^2 = 4-Me; entry 11), while surprisingly naphthyl substituted compounds **13f** (R^1 = 1-naphthyl; R^2 = H; entry 6) and **13g** (R^1 = 2-naphthyl; R^2 = H; entry 7) did not show a strong TOP1 inhibitory activity as was the case of diphenyl phosphine oxide-substituted derivatives **6** and **7**.

Moreover, in view of the results we can conclude that the phosphonates substituted with ethyl substituents (**13a-n**) presented in general better inhibitory effect than the isopropyl substituted analogues (**13o-t**).

Diethyl 1,2,3,4-tetrahydroquinolin-6-ylphosphonates 15

Once we finished the evaluation of quinolines **13**, we proceeded to assess the TOP1 inhibitory activity of 1,2,3,4-tetrahydroquiolines **15** with a diethyl phosphonate functionality in the position 6. We performed a DNA relaxation assay for the compounds **15b**, **15d** and **15f** at 160 µM, as shown in the Figure 43.

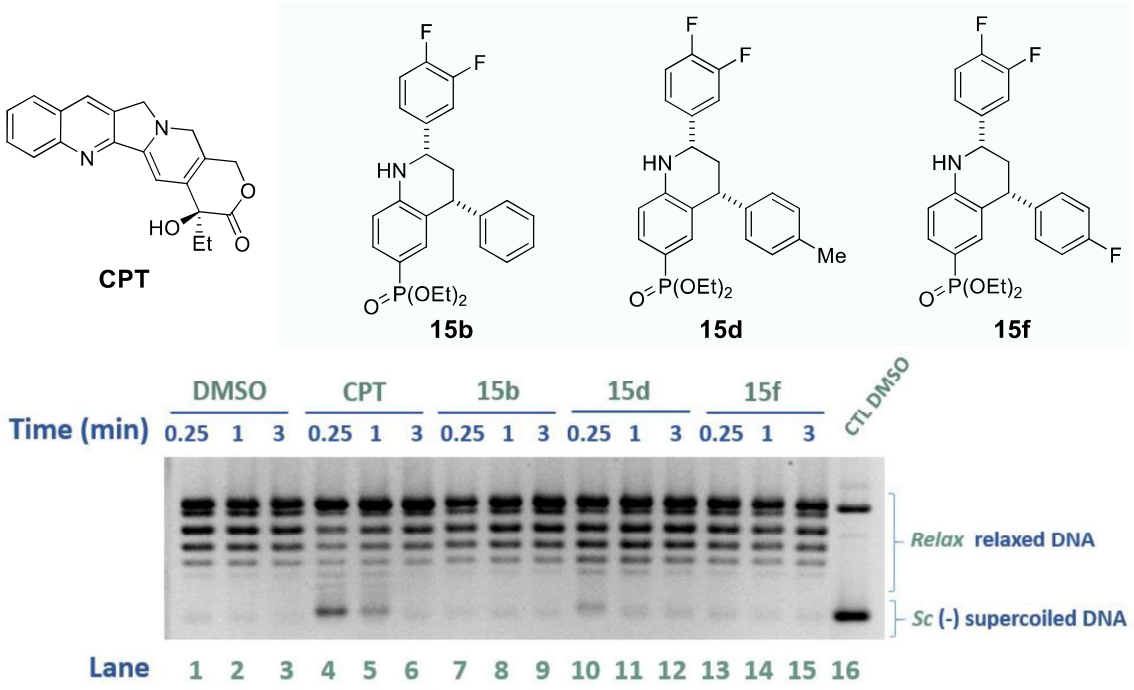

*Figure 43. DNA relaxation assay to study the TOP1 inhibitory activity of compounds **15b**, **15d** and **15f**.*

The compound **15d** (R^1 = 3,4-F_2-C_6H_3; R^2 = 4-Me) presented a moderate inhibition of TOP1 relaxation activity at 15 sec (Figure 43, lane 10) which disappears by 1 and 3 min (lanes 11 and 12 respectively). Contrarily, the compounds **15b** (R^1 = 3,4-F_2-C_6H_3; R^2 = H) and **15f** (R^1 = 3,4-F_2-C_6H_3; R^2 = 4-F) did not show any inhibitory effect in the TOP1 action.

We performed the same DNA relaxation assays with the other compounds **15** and the complete list of their inhibitory activities are collected in the Table 13. We can note that diethyl 1,2,3,4-tetrahydroquionlin-6-yl phosphonates **15** do not present TOP1 inhibitory effect under the studied conditions, only the derivative **15d** (R^1 = 3,4-F_2-C_6H_3; R^2 = 4-Me; Table 13, entry 4) exhibited a minor effect at 15 sec of incubation.

Table 13**. TOP1 inhibitory activity of diethyl 1,2,3,4-tetrahydroquinolin-6-ylphosphonates **15.

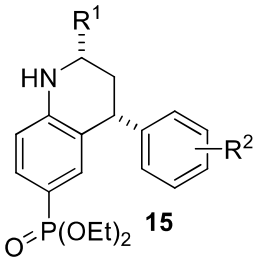

Entry	Compound			% Inhibition[a]		
	Nº	R^1	R^2	15 sec	1 min	3 min
1	**15a**	4-F-C_6H_4	H	-	-	-
2	**15b**	3,4-F_2-C_6H_3	H	-	-	-
3	**15c**	4-F-C_6H_4	4-Me	-	-	-
4	**15d**	3,4-F_2-C_6H_3	4-Me	+	-	-
5	**15e**	4-F-C_6H_4	4-F	-	-	-
6	**15f**	3,4-F_2-C_6H_3	4-F	-	-	-

[a]The activity of the compounds inhibiting hTOP1B relaxation at 160 µM was expressed semiquantitatively by comparison with the maximum inhibitory activity observed for CPT at 100 µM as follows: -, no activity; +, weaker activity than CPT; ++ similar activity to CPT; +++ stronger activity than CPT.

Diethyl quinolin-6-ylphosphonates 16

We continued our screening by evaluating the fully aromatic diethyl quinolin-6-ylphosphonates **15**, as presented in the Figure 44. We tested the derivatives **16e**, **16a** and **16b** in the DNA relaxation assay, where only compound **16e** (R^1 = 4-F-C_6H_4; R^2 = 4-F) was found to show a mild inhibition of the TOP1 relaxation effect at 15 sec and 1 min (Figure 44, lanes 7 and 8 respectively).

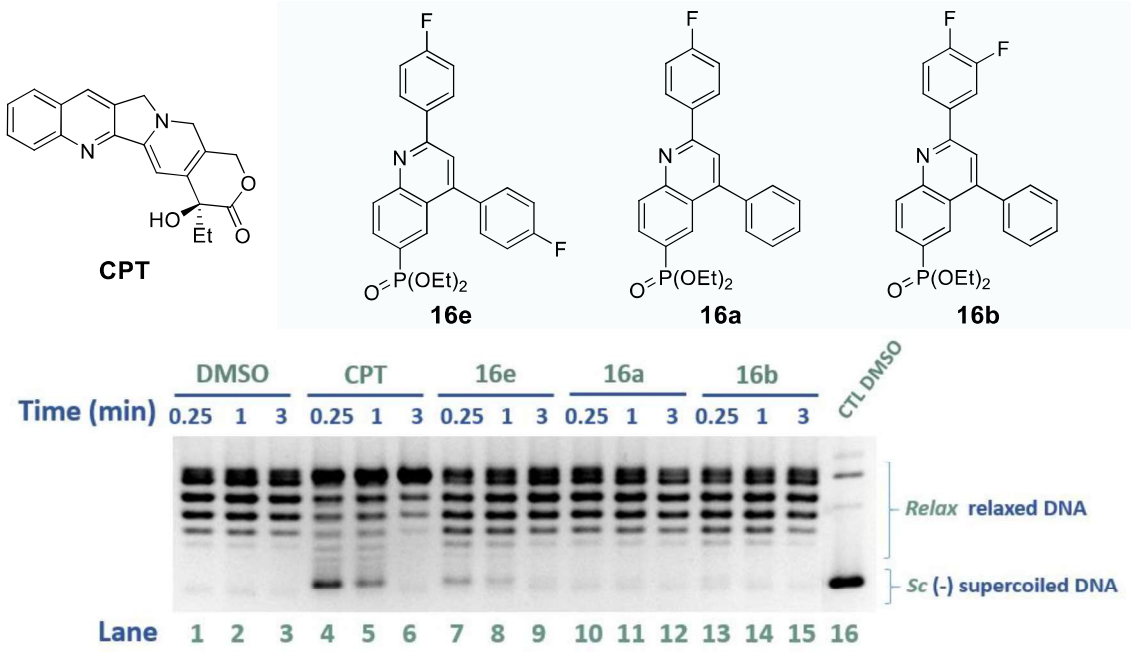

*Figure 44. DNA relaxation assay to study the TOP1 inhibitory activity of compounds **16e**, **16a** and **16b**.*

Afterwards, we extended the screening to the other quinoline derivatives **16** by the DNA relaxation assay and the results are presented in the Table 14.

Table 14**. TOP1 inhibitory activity of diethyl 1,2,3,4-tetrahydroquinolin-6-ylphosphonates **16

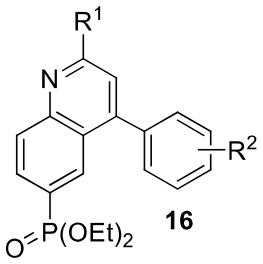

16

Entry	Compound			% Inhibition[a]		
	Nº	R^1	R^2	15 s	1 min	3 min
1	**16a**	4-F-C_6H_4	H	-	-	-
2	**16b**	3,4-F_2-C_6H_3	H	-	-	-
3	**16c**	4-F-C_6H_4	4-Me	+	+	+
4	**16d**	3,4-F_2-C_6H_3	4-Me	-	-	-
5	**16e**	4-F-C_6H_4	4-F	+	+	-
6	**16f**	3,4-F_2-C_6H_3	4-F	+	+	+

[a]The activity of the compounds inhibiting hTOP1B relaxation at 160 µM was expressed semiquantitatively by comparison with the maximum inhibitory activity observed for CPT at 100 µM as follows: -, no activity; +, weaker activity than CPT; ++ similar activity to CPT; +++ stronger activity than CPT.

Apart from the previously mentioned compound **16e**, only derivatives **16c** (R^1 = 4-F-C_6H_4; R^2 = 4-F) and **16f** (R^1 = 4-F-C_6H_4; R^2 = 4-F) presented a slight TOP1 inhibitory activity during all the tested times (Table 4, entries 3 and 6 respectively). In summary, the collected results suggest that the change of the position of the diethyl phosphonate from position 8 (compounds **13**) to position 6 (compounds **15** and **16**) of the (tetrahydro)quinoline scaffold affects negatively to the TOP1 inhibitory effect observed in the DNA relaxation assays.

Dialkyl tetrahydro-5H-indeno[2,1-c]quinolinylphosphonates 19, dialkyl 7H-indeno[2,1-c]quinolinylphosphonates 20 and dialkyl 7-oxo-7H-indeno[2,1-c]quinolinylphosphonates 21

Finally, we conclude the evaluation of TOP1 inhibitory activity investigating the tetrahydro-*5H*-indenoquinoline derivatives **19** and indenoquinoline derivatives **20** and **21** in DNA relaxation assays in the same experiment conditions, as illustrated in the Figure 4 (panel **B**, in blue).

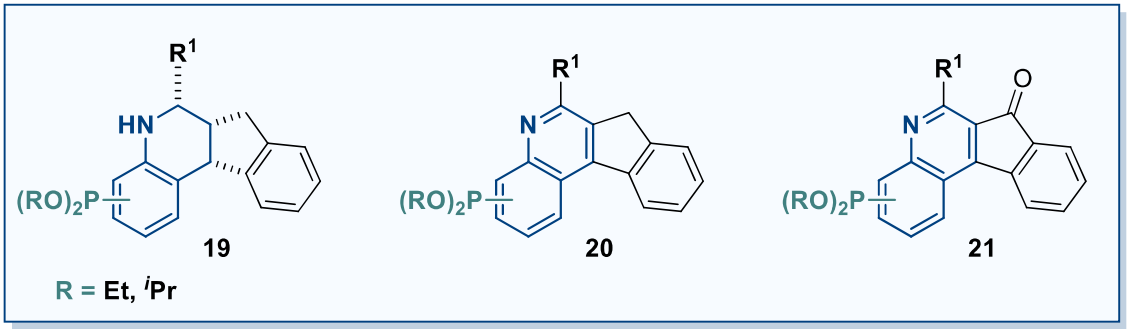

*Figure 45. General structures of dialkyl tetrahydro-5H-indeno[2,1-c]quinolinylphosphonates **19**, dialkyl 7H-indeno[2,1-c]quinolinylphosphonates **20** and dialkyl 7-oxo-7H-indeno[2,1-c]quinolinylphosphonates **21**.*

The DNA relaxation assay for compounds **20a**, **19a** and **21c** is presented in the Figure 46, where tetrahydro-*5H*-indenoquinoline derivative **19a** (R^1 = 3-MeO-C_6H_4) exhibited a strong TOP1 inhibitory activity at 15 sec and 1 min (Figure 46, lanes 10 and 11 respectively) comparable with the activity of CPT (lanes 4 and 5), while at 3 min (lane 9) only a moderate inhibition was reported. A similar inhibition behaviour is observed for the indenoquinoline derivative **20a** (R^1 = 3-MeO-C_6H_4), which presents the same substitution pattern but a fully-aromatic heterocyclic scaffold (lanes 7-9). Finally, the carbonyl-containing indenoquinoline derivative **21c** (R^1 = 3-MeO-C_6H_4) did not show any inhibition of the TOP1 relaxation effect (lanes 13-15).

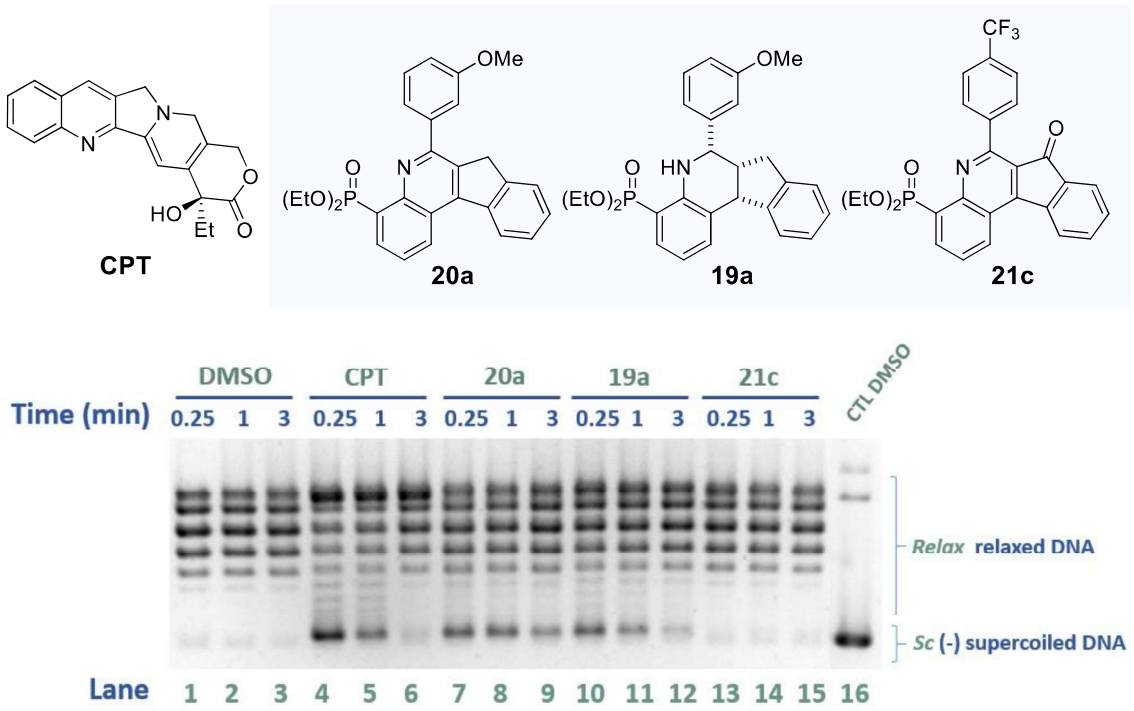

*Figure 46. DNA relaxation assay to study the TOP1 inhibitory activity of compounds **20a**, **19a** and **22c**.*

We performed the same relaxation experiment in order to investigate the rest of compounds (derivatives **19**, **20** and **21**), and the results are collected in the tables 15, 16 and 17 respectively, grouped by the main indenoquinoline core.

Table 15**. TOP1 inhibitory activity of dialkyl tetrahydro-5H-indeno[2,1-c]quinolinyl phosphonates **19.

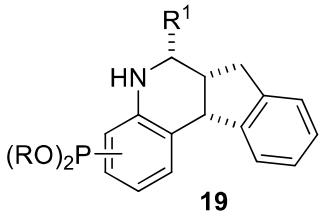

Entry	Compound			% Inhibition[a]		
	Nº	R	R^1	15 s	1 min	3 min
1	**19a**	4-P(O)(OEt)$_2$	3-MeO-C$_6$H$_4$	++	++	+
2	**19b**	4-P(O)(OEt)$_2$	4-MeO-C$_6$H$_4$	+	-	-
3	**19c**	4-P(O)(OEt)$_2$	4-CF$_3$-C$_6$H$_4$	+	+	-
4	**19d**	2-P(O)(OEt)$_2$	3-MeO-C$_6$H$_4$	-	-	-
5	**19f**	2-P(O)(OEt)$_2$	4-CF$_3$-C$_6$H$_4$	+	-	-

[a]The activity of the compounds inhibiting hTOP1B relaxation was expressed quantitatively by comparison with the maximum inhibitory activity observed for CPT as follows: -, no activity; +, weaker activity than CPT; ++ similar activity to CPT; +++ stronger activity than CPT.

Out of the tetrahydro-*5H*-indenoquinoline **19,** only the compound **19a** (R^1 = 3-MeO-C_6H_4; Table 15, entry 1) was found to strongly inhibit TOP1. Compounds **19b**, **19c** and **19f** presented a minor inhibitory activity at short reaction times, while **19d** did not show any interaction in the TOP1 effect.

Table 16*. TOP1 inhibitory activity of dialkyl 7H-indeno[2,1-c]quinolinylphosphonates* ***20.***

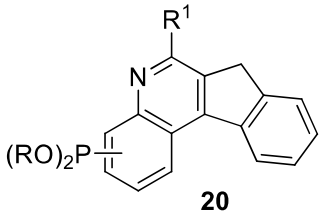

20

Entry	Compound			% Inhibition[a]		
	Nº	R	R^1	15 sec	1 min	3 min
1	**20a**	4-P(O)$(OEt)_2$	3-MeO-C_6H_4	++	++	+
2	**20c**	4-P(O)$(OEt)_2$	4-CF_3-C_6H_4	-	-	-
3	**20e**	2-P(O)$(OEt)_2$	4-MeO-C_6H_4	+	+	-
4	**20g**	4-P(O)$(O^iPr)_2$	4-CF_3-C_6H_4	-	-	-

[a]The activity of the compounds inhibiting hTOP1B relaxation was expressed quantitatively by comparison with the maximum inhibitory activity observed for CPT as follows: -, no activity; +, weaker activity than CPT; ++ similar activity to CPT; +++ stronger activity than CPT.

Then, dialkyl 7*H*-indeno[2,1-*c*]quinolinyl phosphonates **20** were tested. Besides **20a** (R^1 = 3-MeO-C_6H_4; Table 16, entry 1), which showed a marked TOP1 inhibitory effect, only the indenoquinoline **20e** (R^1 = 4-MeO-C_6H_4; entry 3) reported a modest inhibition activity at 15 sec and 1 min of the enzymatic reaction.

Table 16**. TOP1 inhibitory activity of dialkyl 7-oxo-7H-indeno[2,1-c]quinolinylphosphonates **21

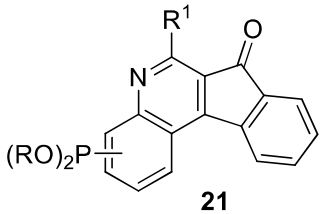

21

Entry	Compound			% Inhibition[a]		
	Nº	R	R^1	15 sec	1 min	3 min
1	**21a**	4-P(O)(OEt)$_2$	3-MeO-C_6H_4	+	+	-
2	**21b**	4-P(O)(OEt)$_2$	4-MeO-C_6H_4	-	-	-
3	**21c**	4-P(O)(OEt)$_2$	4-CF_3-C_6H_4	-	-	-
4	**21d**	2-P(O)(OEt)$_2$	3-MeO-C_6H_4	-	-	-
5	**21f**	2-P(O)(OEt)$_2$	4-CF_3-C_6H_4	-	-	-

[a]The activity of the compounds inhibiting hTOP1B relaxation was expressed quantitatively by comparison with the maximum inhibitory activity observed for CPT as follows: -, no activity; +, weaker activity than CPT; ++ similar activity to CPT; +++ stronger activity than CPT.

Regarding 7-oxo-indenoquinolines **21**, only the derivative **21a** (R = 4-P(O)(OEt)$_2$; R^1 = 3-MeO-C_6H_4; Table 17, entry 1) was found to inhibit TOP1 at 15 sec and 1 min, in a weaker manner than CPT. It certainly looks like the insertion of a carbonyl group in the position 7 of the indeno[2,1-*c*]quinoline derives in a loss of the inhibitory effect

On balance, indenoquinoline derivatives demonstrated a weak inhibitory effect of TOP1 in DNA relaxation assays. Only the tetrahydro-*5H*-indenoquinoline derivative **19a** and the *7H*-indenoquinoline derivative **20a** resulted to strongly inhibit the enzyme, both bearing a diethyl phosphonate in position 4 and a 3-MeO-C_6H_4 substituent in position 6 of the (tetrahydro)indenoquinoline framework. It seems like the methoxy substituents have a positive effect in the inhibitory activity. Finally, we observed that those derivatives which were found to inhibit TOP1 may inhibit the enzyme in a reversible way, as the inhibitory effect decreases or disappears over the time.

II-2.2.2. Mechanistic studies of the TOP1 inhibitory activity

Once we compiled the result from the TOP1 inhibitory activity, we consider to investigate the mechanism of the inhibitory effect. According to this, we studied the ability of the compounds **13**, **15**, **16**, **19**, **20** and **21** to stabilize TOP1CCs, which would be related with a *poison*-like mode of action.

Nicking assay

We carried out mechanistic studies of dialkyl quinolin-8-yl phosphonates **13** by evaluating the biological activity of the compounds **13f**, **13g**, **13e**, **13a**, **13l**, **13n**, **13i**, **13m**, **13j** and **13k** in nicking assays, as we expounded before (the result is presented in the Figure 47). The ability to introduce TOP1-dependant nicks was assessed using a negative control (*DMSO*) (Figure 47, lanes 1 and 2) and 100 µM CPT as positive control. As depicted in the Figure 47, after incubation with TOP1, CPT induces the formation of nicked DNA after 1 and 3 min of enzymatic reaction (lanes 3 and 4 respectively). On the contrary, the tested derivatives **13** were not able to introduce detectable nicks in the same conditions (lanes 5-24).

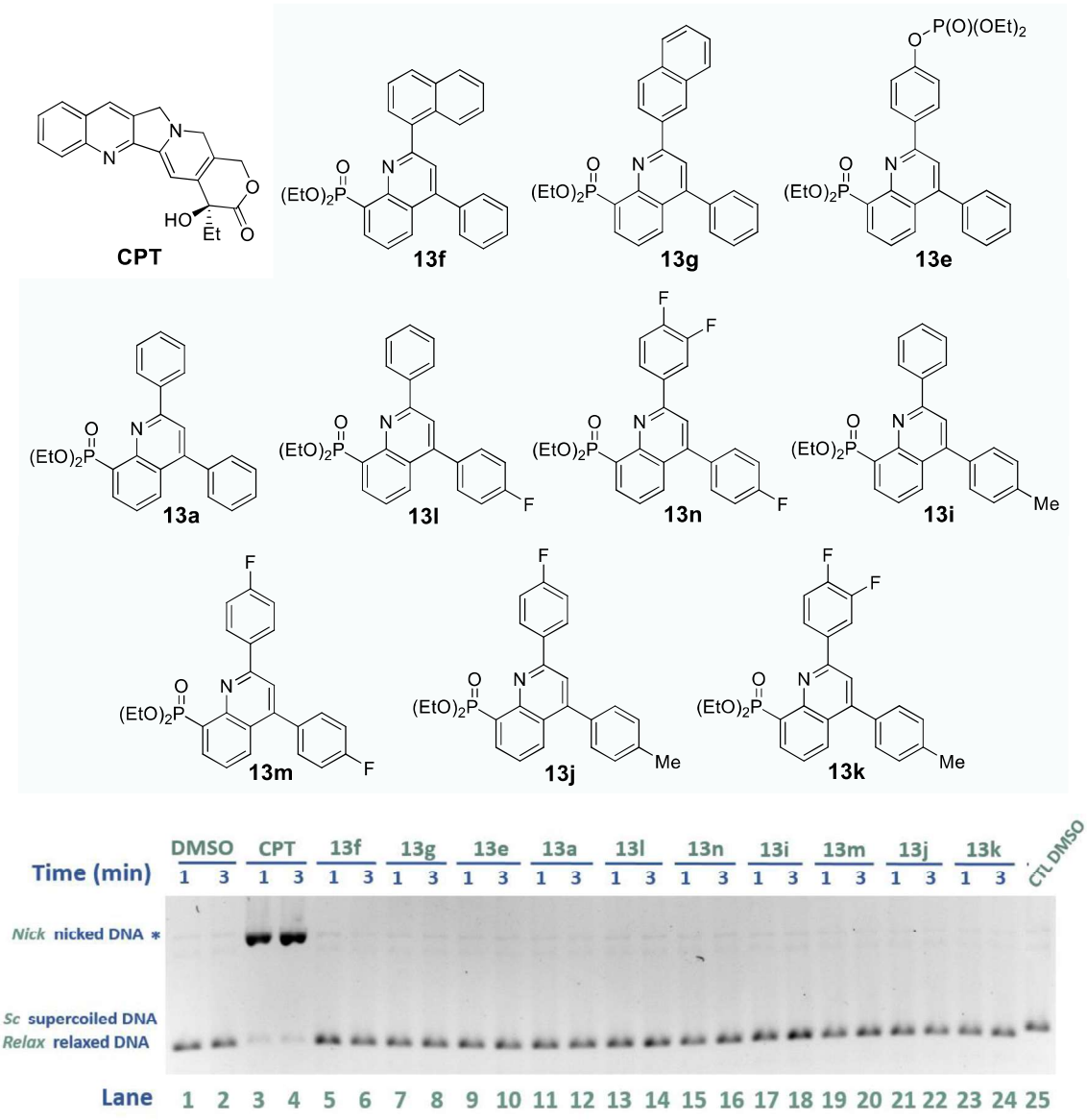

*Figure 47. Nicking assay of compounds **13f**, **13g**, **13e**, **13a**, **13l**, **13n**, **13i**, **13m**, **13j** and **13k**.*

We extended the screening to the other derivatives **13**, **15** and **16** in the nicking assay and we observed the same result, which lead us to conclude that the inhibitory activity of compounds **13**, **15** and **16** is not related with the stabilization of TOP1CCs.

Then, we proceeded to investigate the tetrahydro-*5H*-indenoquinoline derivatives **19**, **20** and **21** in nicking assays. We started the screening of the compounds **19b**, **19a**, **20a**, **21a**, **19c**, **19f**, **19d** and **19c** at 160 µM as shown in the Figure 48. Once again, the tested compounds did not show capacity to generate nicks in the DNA (Figure 48, lanes 5-20).

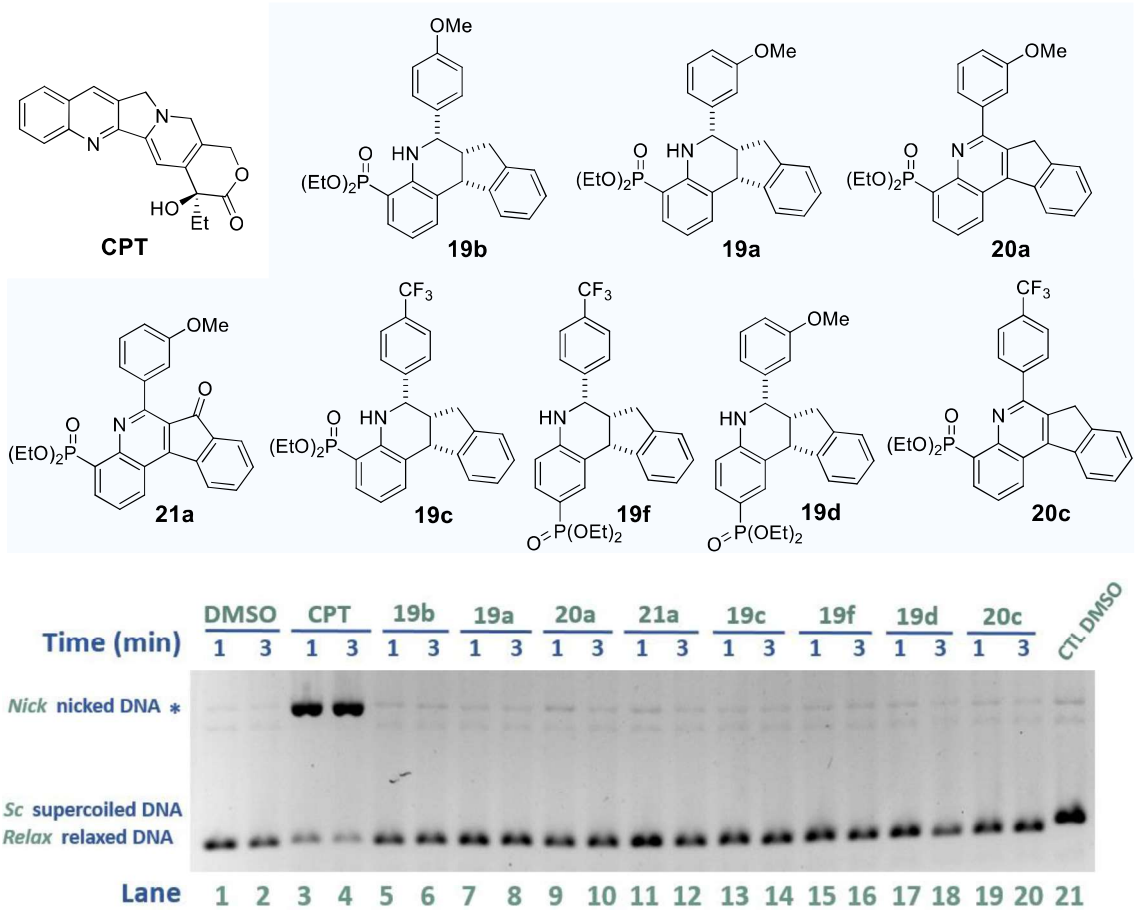

*Figure 48. Nicking assay of compounds **19b**, **19a**, **20a**, **21a**, **19c**, **19f**, **19d** and **20c**.*

We assessed the screening of the rest of derivatives **19**, **20** and **19** with the same nicking assays, and none of them was found to introduce nicks in the plasmid DNA.

In summary, the (tetrahydro)indenoquinoline derivatives **19**, **20** and **21** did not show evidence of a poison-like mode of action, suggesting that their TOP1 inhibitory effect is not related with the trapping of TOP1 cleavage complexes. In consequence, we can conclude that those (tetrahydro)indenoquinoline derivatives **19**, **20** and **21** with the ability to inhibit TOP1 may act as TOP1 supressors.

Equilibrium experiment

Once we had finished the nicking assays of all the newly synthesized compounds, the collected data suggests that the TOP1 inhibitory activity is not related with the stabilization of TOP1CCs, which would imply that the compounds **13**, **15**, **16**, **17**, **18** and **19** are not acting as TOP1 poisons. Accordingly, in order to confirm this hypothesis, we performed a specific assay to specifically measure the ability of the drugs to stabilize the TOP1CCs with three compounds, the previously explained cleavage-religation equilibrium assay (1.3.1. DNA cleavage-religation equilibrium assay, *vide supra*).

In the Figure 49 we show a cleavage-religation equilibrium experiment with the compounds **16f**, **13s** and **19a** (all of them reported an inhibitory effect in DNA relaxation assays). In the present experiment, 200nM of the Cy3-labeled equilibrium dsDNA substrate (5'-Cy3-ATTTGACCTCGAGAATTATACGAAGTTA-TTAC-3'/5'-GTAATAACTTCGTATAATTCTCGAGGTCAAAT-3') was incubated with TOP1 at 37ºC in the presence of increasing concentration of the tested compounds (100, 200 and 400 μM). We included one negative control (only with DMSO as the solvent used in the experiment, see lane 13, Figure X) and CPT as positive control (at 50, 75 and 100 μM; in lanes 10, 11 and 12 respectively). After 10 min, the enzymatic reactions were stopped by adding SDS to a final concentration of 0.2% w/v, trypsin digested and the samples were loaded in a denaturing 20% polyacrylamide gel after EtOH precipitation. The gel was subsequently visualized in a fluorescence scanner, obtaining the image sown in the Figure 49.

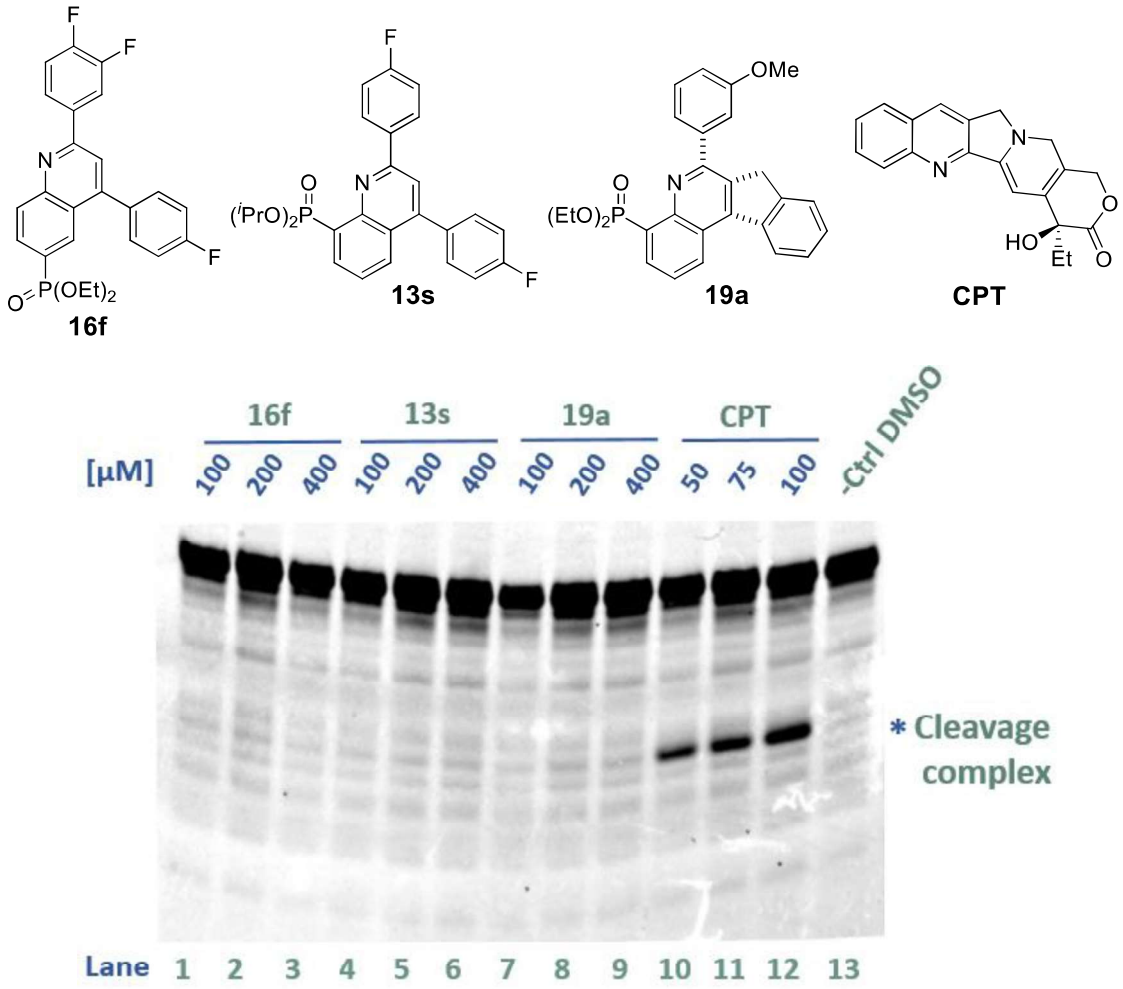

*Figure 49. Cleavage-religation equilibrium assay for compounds **16f**, **13s** and **19a** in increasing concentrations.*

In the absence of any drug candidate (DMSO, lane 13) all the DNA (32 base-pair sequence) is located above. On the contrary, in the presence of CPT we can observe the appearance of a DNA product with lower molecular weight corresponding to the formation of TOP1CCs (lanes 10-12), marked with an asterisk. The accumulation of DNA cleavage complexes induced by CPT resulted to be concentration dependent, as we can see how the band corresponding to TOP1CCs results more intense when increasing the concentration of camptothecin.

In the presence of the compounds **16f**, **13s** and **19a** the appearance of detectable accumulation of TOP1CCs is not observed in concentrations up to 400 μM, which evidences that undoubtedly the tested compounds are not acting as TOP1 poisons. This finding is consistent with the results obtained in the nicking assays and therefore we can confirm that the mechanism of the TOP1 inhibition of these phosphonate containing (indeno)quinoline derivatives (**13**, **15**, **16**, **19**, **20** and **21**) is not related with the trapping of TOP1CCs. Based in the results obtained in these *in vitro* experiments, we can conclude that the newly synthesized compounds may act as TOP1 suppressors.

II-3. Development of the REEAD assay as a novel quantitative method for the *in vitro* evaluation of the hTOP1B inhibitory activity in drug screening

As we just showed in the screening of the phosphorated quinoline derivatives as TOP1 inhibitors, the classic experiments to investigate the TOP1 inhibitory activity (namely DNA relaxation assay, nicking assay, equilibrium assay or cleavage/religation assay) require to study separately the inhibitory activity and the mechanism of inhibition. Moreover, they result time-consuming and demands specific training in molecular biology techniques. The equipment employed for polyacrylamide denaturing gels is not always easy-to-get and the obtained results are far away from being quantitative. When performing the evaluation of the inhibitory activity, we had to face this inherent drawbacks, and we got semiquantitative results that allow us to determine the TOP1 inhibitory effect of the newly prepared compounds in comparison with a reference compound (CPT) and discard a *poison*-like mode of action, but we are still conscious about the limitations of these assays. In this regard, we participated in the development of a novel assay for the quantitative and precise measurement of TOP1 activity applied as a drug-screening method for small compounds targeting human topoisomerase IB: the REEAD assay.

As introduced before (section II-1.4. of this chapter, *vide supra*), we contributed in the development of the REEAD assay as a fast, reliable and high-throughput drug-screening method to quantitatively measure the TOP1 activity with enhanced sensitivity compared with the state-of-the-art gel-based assays.

II-3.1. The REEAD-on-a-slide approach

The REEAD assay consists on the measurement of the TOP1 activity by counting the Rolling Circle Products (RCP) generated from a specific circle DNA substrate selectively closed by TOP1 catalysis. In the REEAD assay a "*dumbbell-shaped*" single stranded DNA substrate is employed, which has a partly double stranded (ds) stem region and two loops. As illustrated in the Figure 50, the ds stem region is not closed, and contains a high affinity cleaving-site for TOP1 (see the amplified area), which cleaves the last 3 nucleobases at the 3' end of the DNA substrate and consequently the released nucleotide fragment diffuses away. Note that the released fragment is too short to be religated again by the enzyme, but the substrate is designed to contain the same nucleotide-sequence that matches with the complementary strand (drawn in green in the amplified area, Figure 50), so TOP1 religates this three nucleotide sequence (in green) sealing the nick in the ds stem region and then dissociates from the DNA substrate. As a result of the TOP1 catalytic cycle, the non-closed dumbbell substrate is converted into a circle DNA.

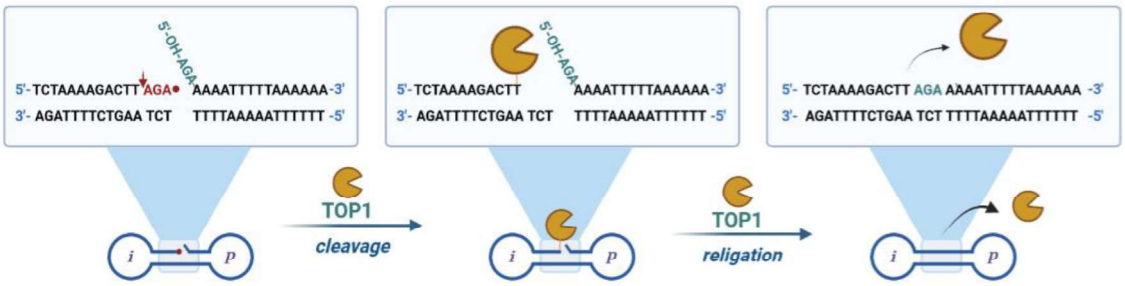

Figure 50. The dumbbell substrate employed in the REEAD assay and the formation of a closed-circular dsDNA by the action of TOP1.

The present TOP1 mediated circularization step can be carried out in two ways: **a)** the circularization can be made ***in solution*** and then hybridize the TOP1 reaction products to a glass surface functionalized with specific primers to support the subsequent RCA, or **b)** ***on-a-slide***, alternatively the REEAD DNA substrates can be hybridized first to the primers and then perform the TOP1 circularization reaction *in situ*. Herein we are going to focus on the REEAD-on-a-slide variant, as it resulted more suitable to test the TOP1 inhibitory activity of potential inhibitors.

The DNA substrates are hybridized to a glass surface-attached primers, and therefore the glass slides have to be prepared in advance. As depicted in the Figure 51, suitable pieces of activated high density (HD) slides coated with NHS (*N*-hydroxysuccinimide) are glued onto regular microscope slides (Figure 51, step **1**) and hydrophobic squares of 25 mm2 are drawn with an immunostaining pen (**2**). Then, the primer is coupled in the drawn squares, where the 5'-amino side of the primer reacts with the NHS group and binds to the glass surface. In the REEAD-on-a-slide approach, the REEAD DNA substrates are hybridized to these anchored primers and the experiment is performed in the drawn squares (**3**).

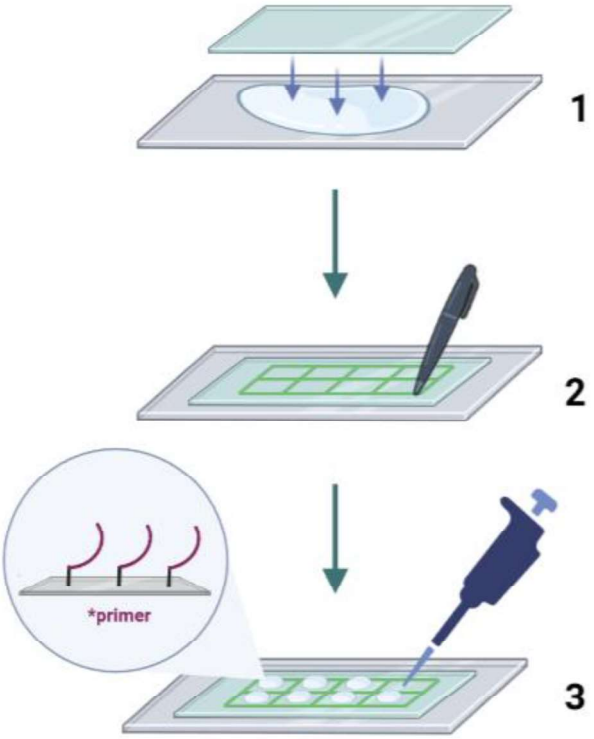

Figure 51. Preparation of the glass slide for the REEAD assay.

In the Figure 52, the general scheme of the REEAD-on-a-slide approach is represented. In first place, the REEAD DNA substrates **1** (Figure 52) are hybridized to a 5'-amino primer anchored to a glass surface **2** by the ***p*** loop (primer-matching loop). Then, the hybridized DNA substrates are reacted with TOP1, which closes the DNA substrate by cleavage-religation catalytic activity to obtain closed DNA circles **3**. The primer supports and initiates the RCA reaction upon addition of a DNA polymerase (**4**), and RCA leads to ~10^3 tandem repetitions of the DNA circle. The obtained RCPs are visualized in the fluorescence microscope upon hybridization of specific fluorescent probes that match with the ***i*** loop (identification loop), as depicted in the illustration **5** (Figure 52). Alternatively, fluorolabelled dNTPs can be used during RCA, a strategy that allows to save the last hybridization step, but in the present chapter we are going to focus on the hybridization of fluorescent probes after the RCA step.

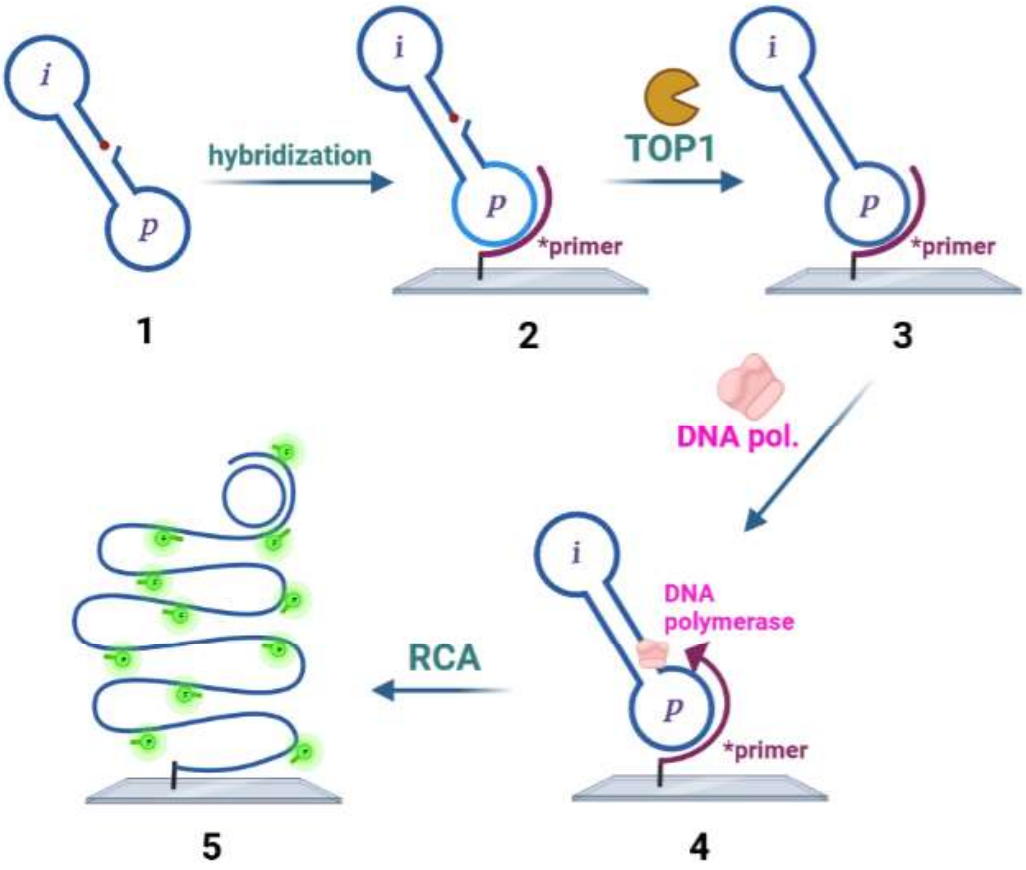

Figure 52. Schematic representation of the REEAD-on-a-slide approach to measure TOP1 activity.

In the REEAD assay, each circularized DNA substrate represents an individual TOP1 catalytic event that is going to be further amplified by Rolling Circle Amplification (RCA). On the contrary, the non-circularized DNA substrates cannot be amplified by RCA (the amplification is stopped at the strand breakage) and only the circularized ones will be detected under the fluorescence microscope in the very last step of the experiment. At this point is relevant to mention that once is closed, the REEAD DNA substrate cannot be re-cleaved again by the enzyme, so each closed DNA substrate derives in a unique RCP that represents a single TOP1 catalytic event (a complete catalytic cycle: binding, cleavage, religation and unbinding). The amount of TOP1 catalytic events visualized as RCPs in the microscope is directly proportional to the TOP1 activity and can be measured precisely with a high sensitivity. When the reactions are performed in the presence of a potential TOP1 inhibitor, the inhibitory effect can be directly quantified by comparing the reactions performed in absence or presence of the compound. In this respect, we optimized the reaction conditions and developed a REEAD-on-a-slide setup to measure TOP1 activity introducing potential TOP1 inhibitors in the reaction media, as shown in the Figure 53.

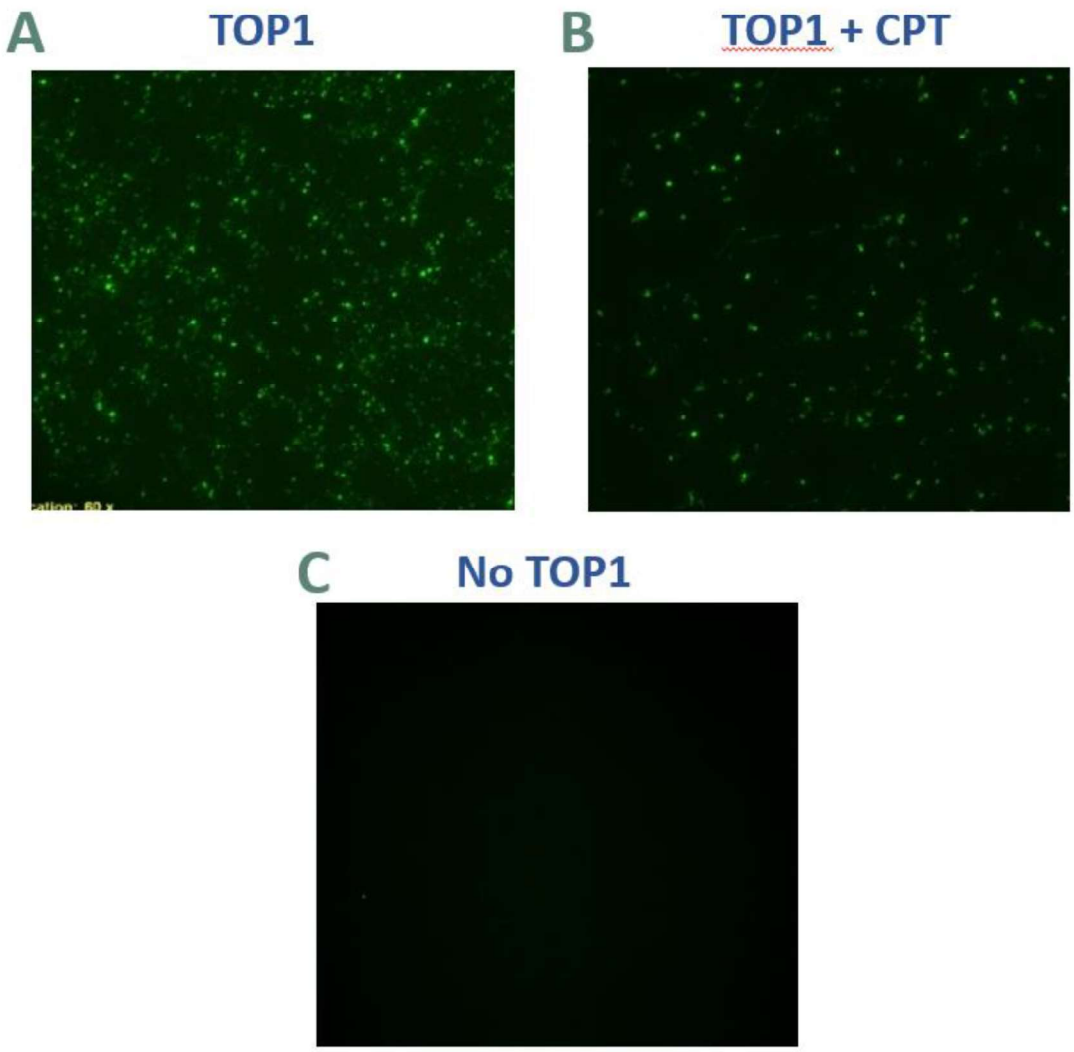

Figure 53. RCPs visualized in the fluorescence microscope after incubation of TOP1 with the dumbell-shaped substrate: A) in the absence of any inhibitor, B) in the presence of 100 µM of CPT and C) in the absence of TOP1 (negative control).

TOP1 reactions were carried out by incubating the enzyme (200 fmol) with the REEAD DNA substrate (1 pmol) hybridized to a primer-coupled HD glass slides for 10 min at 37ºC. The reaction was stopped by adding SDS to a final concentration of 0.3% w/v. The DNA circles were amplified by RCA during 1 h (37ºC, 1 Unit/µL of Phi29 DNA polymerase, 250 µM dNTPs) and the RCPs were hybridized with the REEAD fluorescent probe (FAM-labelled florescent probe, 0.17 µM) in order to be visualized under the fluorescent microscope using a 63X objective. In the panel **A** (Figure 53) is shown a picture containing an area of the slide hybridized with a TOP1 reaction in the absence of any inhibitor. Visually we can observe the high amount of fluorescent dots corresponding to a relatively high TOP1 activity. In the panel **B** we show the image of the same enzymatic reaction but in the presence of 100 µM of CPT, and the amount of visualized RCPs decreases considerably, as a result of the inhibitory effect of the drug. Finally, in the panel **C** a negative control in the absence of TOP1 is shown, where we observe a lack of signals.

In basis of these results, we moved one step forward and we performed the same experiment with DMSO (as a control of the intrinsic TOP1 activity under the stablished experiment conditions), 100 μM of CPT (as a control of the TOP1 activity in the presence of a reference TOP1 inhibitor) and the compounds **16f** and **20a** at 160 μM, maintaining the concentrations used in the DNA relaxation assay. It is noteworthy to mention that CPT is a well-studied TOP1 poison which strongly inhibits the TOP1 activity, while the recently described compounds **16f** and **20a** act as TOP1 supressors. The quinoline derivative **16f** presented a moderate TOP1 inhibitory activity in DNA relaxation assay, while the *7H*-indenoquinoline **20a** presented a stronger inhibition, comparable to CPT. We evaluated the inhibitory activity of DMSO (with no inhibitors), CPT, **16f** and **20a** after incubation of TOP1 (200 fmol) with the DNA substrate hybridized to the coupled primer in the slide (1 pmol of REEAD DNA substrate was used for the hybridization step) as previously expounded. We stopped the enzymatic reactions with 0.3% SDS and we amplified the DNA circles by RCA for 1h. The RCPs were visualized in the fluorescent microscope upon hybridization of 0.17 μM of the REEAD-FAM probe. We took 15 images of each square (each enzymatic reaction) with a 63X objective to have a representative result of the analysed square, and the TOP1 activity was measured by counting the fluorescent dots (RCPs) employing the FIJI software. The experiments were performed in triplicate, and the results of the RCP-counting for compounds **16f** and **20a** are shown in the Figure 54.

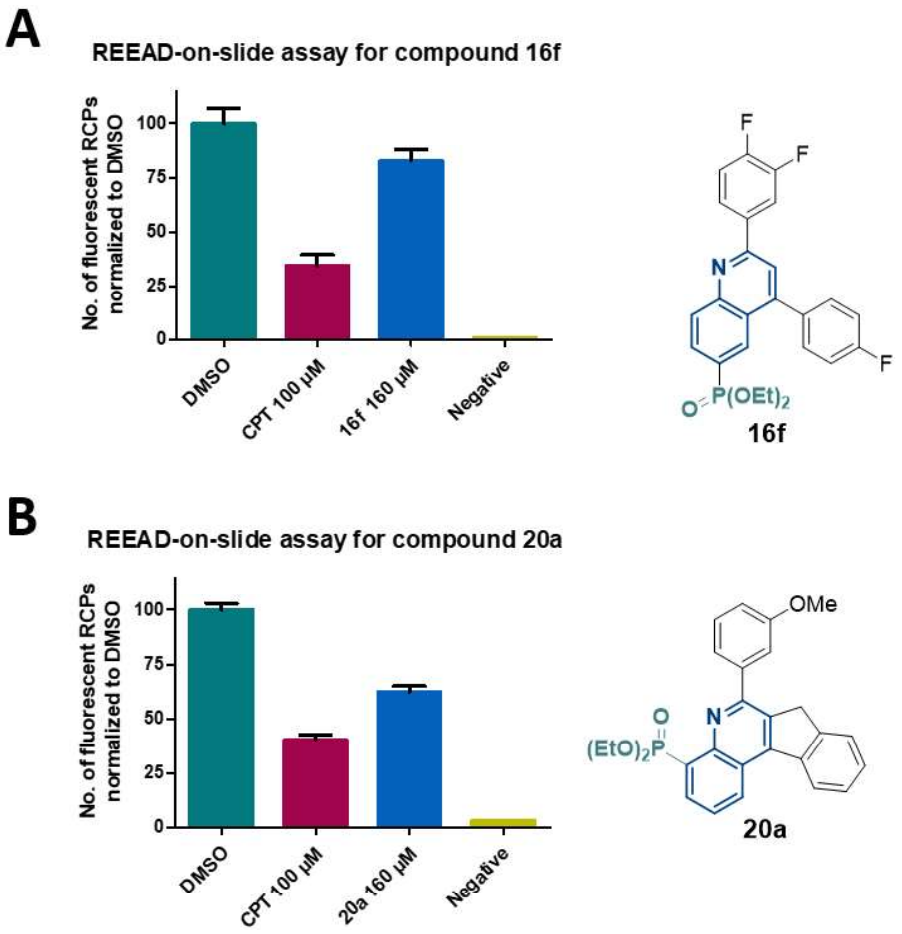

*Figure 54. REEAD-on-a-slide approach to quantitative evaluate the TOP1 inhibitory activity of compounds **16f** and **20a**.*

The amount of visualized RCPs are normalized to the RCPs obtained in the absence of any inhibitor (*DMSO*) and plotted in a graph, which allows to compare quantitative values corresponding to TOP1 activity. The basal TOP1 activity in the current experiment conditions is shown in green (*DMSO*, Figure 54, graphs **A** and **B**). We can observe how the TOP1 activity is drastically affected by CPT at 100 µM in both cases (graphs **A** and **B**, in red colour), which reported a decrease of ~65-70% of the TOP1 activity. On the contrary, compound **16f** (blue bar in graph **A**) slightly decreased the TOP1 catalytic activity (18%) and compound **20a** (blue bar in graph **B**) presented a more intense inhibitory effect (41%). These inhibitory effects are in concordance with the inhibitory results obtained in the DNA relaxation assays, and permitted a precise measurement in quantitative terms.

In summary, the REEAD assay allowed us to complete the *in vitro* biological screening of the TOP1 inhibitory activity of these compounds. We firstly identify by DNA relaxation assays that compound **16f** presents a moderate inhibition of TOP1 at 160 µM, while the compound **20a** presented a strong inhibition of the enzyme at short reaction times (15 sec, 1 min) in the same concentration. Both compounds maintained a mild inhibitory activity by 3 min, but the tendency

over the time suggests a reversibility of the TOP1 inhibitory effect. We determined that compounds **16f** and **20e** are not introducing TOP1-dependant nicks in the DNA, which would imply that these compounds do not inhibit the enzyme by stabilizing TOP1CCs (in case of **16f**, we further confirmed this fact by a direct method to study the trapping of TOP1CCs, see the equilibrium assay shown in the section II-2.2.2 *vide supra*). Based on the obtained evidences we concluded that both derivatives **16f** and **20a** act as TOP1 suppressors. Now, by the REEAD-on-a-slide assay we obtained a quantitative result to present the inhibition rate of the TOP1 activity by compounds **16f** and **20a** (and by the way, CPT)**.** This promising fact proves the suitability the REEAD assay to obtain reliable and highly sensitive screenings of the TOP1 inhibitory activity, and furthermore suggests the use of the REEAD assay as an emerging screening method to identify novel molecules as TOP1 inhibitors in the near future.

II-3.2. The Cleavage/Ligation REEAD assay (C/L REEAD)

Once we achieved to measure of the TOP1 inhibitory effect *in vitro* by potential TOP1 inhibitors, we moved to apply the REEAD assay to further investigate which steps of the TOP1 catalysis are affected by the inhibitor (mainly binding/cleavage and religation steps). For this purpose, we analysed how TOP1 activity is affected in the Cleavage/Ligation REEAD assay (C/L REEAD assay hereinafter), which is based upon the same principle of the regular REEAD assay (a TOP1-mediated circularization of a dumbbell DNA substrate, followed by RCA and visualization of the RCPs in the fluorescence microscope upon hybridization of fluorescent probes) but the structure of the DNA substrate varies considerably.

In the Figure 55 we show the structure of the DNA dumbbell-shaped substrate that is used in the C/L REEAD assay. As it can be observed, the DNA substrate is divided into two parts, the cleavage half-dumbbell **1A** (drawn in blue, Figure 55) and the ligator half-dumbbell **1B** (drawn in green, Figure 55). Note that the cleavage half-dumbbell A is phosphorylated at the 5' end, so when the two half substrates (A+B) are linked by TOP1 action (cleavage + religation), the resulted DNA substrate **2** is not completely closed. TOP1 is not able to ligate the 5'-phosphorylated end of the strand, and for this purpose a T4 DNA ligase is added. The T4 DNA ligase ligates the 5'-P end and closes the DNA substrate, giving place to a closed DNA circle **3**, which once is attached to a primer anchored to a glass surface, it can by amplified by RCA and the RCPs can be visualized under the fluorescence microscope after hybridization of the fluorolabeled DNA probes **4**. It has to be mentioned that the T4 DNA ligase is not able to ligate the 5'-OH end of the ligator half-dumbbell substrate, so the first ligation step is fully dependent of the TOP1 catalytic activity,

while the second ligation step (the one with the phosphorylated 5'-end) depends exclusively on the T4 DNA ligase activity.

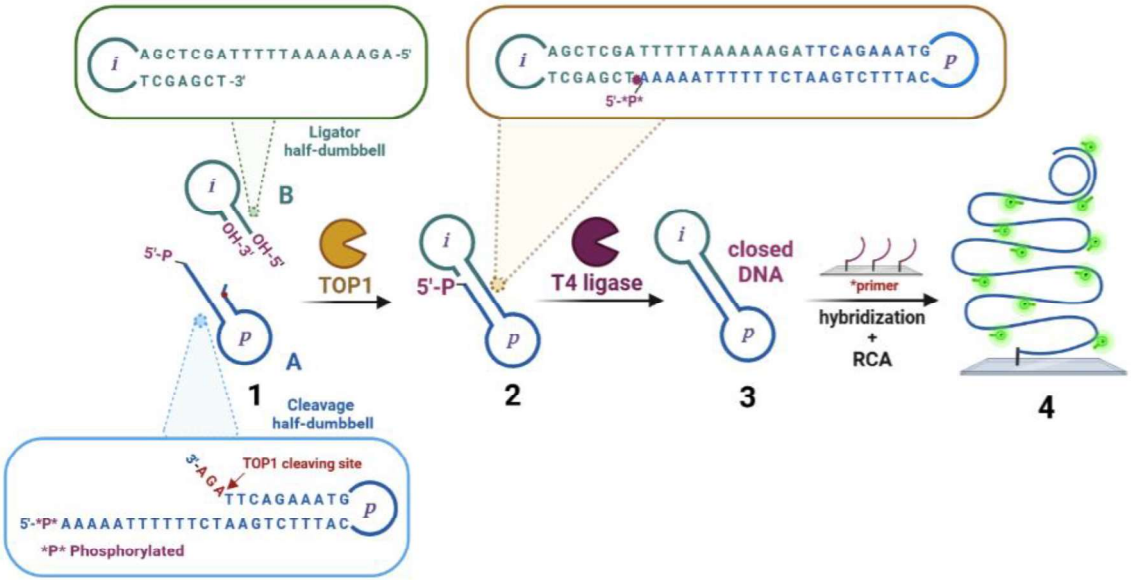

Figure 55. Scheme of the DNA substrate used in the C/L REEAD assay.

Once we have introduced the operating of the C/L REEAD assay, in the Figure 56 we show how this approach allows to separately study the cleavage and religation steps of TOP1 catalysis. First of all it has to be clarified that we performed the C/L REEAD assay ***on-a-slide*** and accordingly we started from the hybridization of the cleavage half-dumbbell DNA substrate **A** (coloured in blue) to a primer anchored to a glass surface **1** (Figure 56).

Cleavage/Ligation REEAD-on-a-slide: the **cleavage half-dumbbell** substrate (**1**, Figure 56) contains a high affinity TOP1 cleaving site three nucleotides ahead from the 3' end, so when TOP1 is added, a TOP1 cleavage reaction occurs. The released three-nucleotide fragment is too short to be religated again, so it is diffused away while the enzyme remains covalently bounded to the DNA substrate (as shown in illustration **2**). Then, the **ligator half-dumbbell** DNA substrate is added, which has a free OH-group in the 5' end, and consequently ligates to the cleaved half-dumbell substrate **2** by the religation reaction of TOP1, leading to the dumbbell substrate **3**. The substrate form **3** has a gap between the 3'-OH and the 5'-phosphate that is subsequently sealed by the addition of T4 DNA ligase. In this way, after the combination of TOP1 (cleavage reaction **A** and religation reaction **B**) and T4 DNA ligase (reaction **C**) ligation processes, the two parts of the dumbbell DNA substrate are converted into a circular closed DNA **4**, which is able to be amplified by RCA and the RCPs could be visualized and quantified as expounded before.

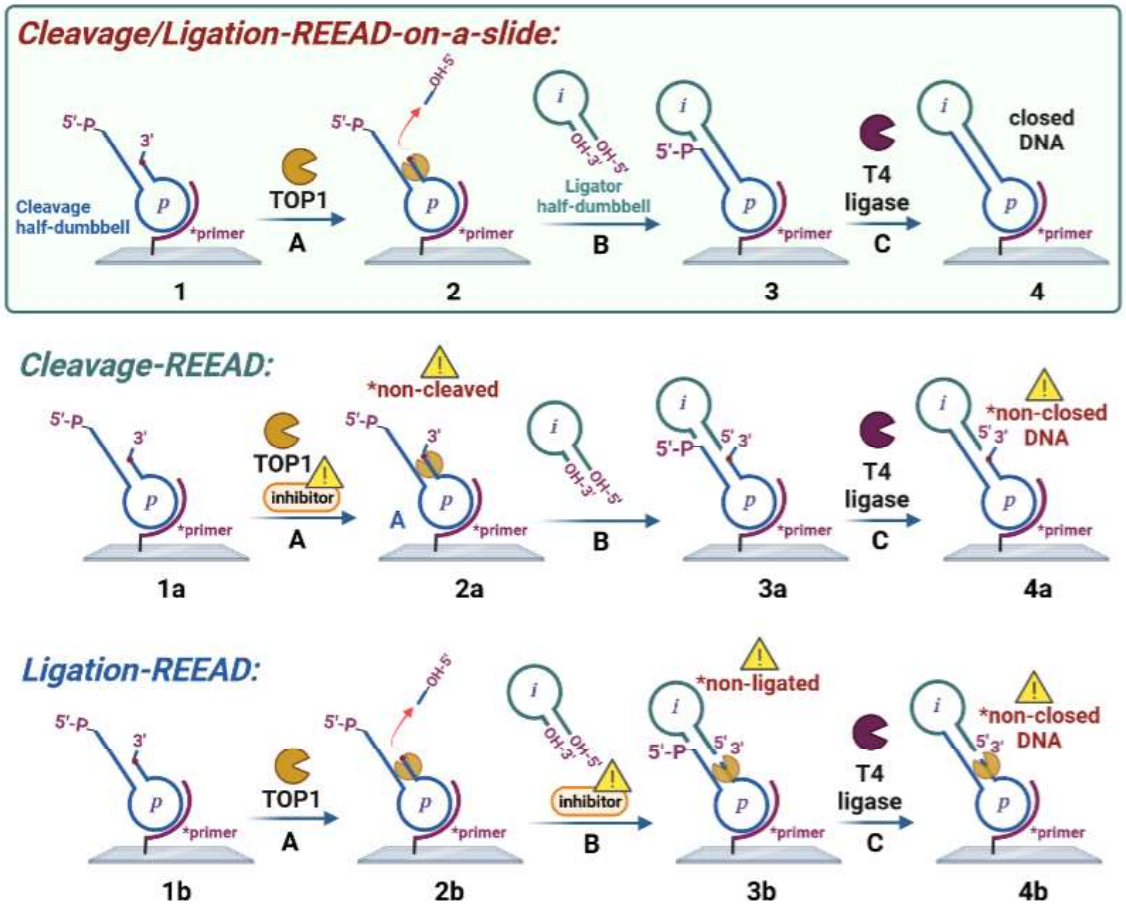

Figure 56. General scheme of the DNA circularization process in the C/L REEAD assay (framed) and the derived procedures Cleavage-REEAD and Ligation-REEAD. The circularization reaction of the DNA substrate is divided into 3 steps as follows, step A: TOP1-mediated cleavage; Step B: TOP1-mediated religation; Step C: T4 DNA ligase mediated ligation.

***Cleavage REEAD**:* following the present C/L REEAD approach, it could be selectively studied how the TOP1 cleavage step is affected by a potential TOP1 inhibitor. For this purpose, in the step **A** (Figure 56), the potential TOP1 inhibitor is added along with TOP1 to the reaction media. If the cleavage step of TOP1 catalysis is inhibited, the enzyme does not cleave and release the three-nucleotide chain in the 3'-end of the **cleavage half-dumbell** (see the structure **2a**), and consequently, when the **ligator half-dumbbell** DNA substrate is added it cannot be ligated by the TOP1. The T4 ligase may ligate the 5'-P end of the DNA substrate (**4a**), but it would still opened due to the inhibition of the cleavage step of the TOP1 catalysis. It has to be mentioned that this approach does not permit to distinguish between the affection of binding and cleavage steps in the TOP1 catalytic cycle, so the binding/cleavage activity is studied at the same time.

Ligation REEAD: in like manner, the religation step could be separately investigated using the ligation-REEAD assay. In this case, the potential TOP1 inhibitor has to be added after the cleavage step, just when the **ligator half-dumbell** is introduced in the reaction media (step **B**, Figure 56). In case of an inhibitory effect in the religation step of the TOP1 catalysis (as for

example, poison-like TOP1 inhibitors, including CPT), the TOP1 cannot ligate the 5'-OH and 3'-OH ends of the DNA substrate (see the structure **3b**), and even though the T4 ligase may ligate the 5'-P and 3'-OH ends, the DNA substrate would not be closed (**4b**).

Optimization of the C/L REEAD assay

We proceeded to optimize the C/L REEAD assay in order to evaluate separately the effect of potential small compounds on the cleavage and religation steps of TOP1 catalysis. We started by analysing how the NaCl concentration affects to the C/L. It is well known that TOP1 acts at physiological NaCl concentration (~150 mM NaCl), but this requirement affects exclusively to the cleavage step, while the religation step can be performed at higher NaCl concentrations (150-500 mM). For this purpose, we compared the TOP1 activity measured by the regular REEAD-on-a-slide approach against the TOP1 activity measured with the C/L REEAD setup at different NaCl concentrations. Accordingly, we outlined a NaCl titration from 150 to 500 mM for both setups. In the case of C/L REEAD approach, the NaCl concentration (150-500 mM) was adjusted only during the religation step of TOP1 (Figure 56, step **B**), while the TOP1 cleavage (A, Figure 56) and the T4-mediated ligation (Figure 56, step **C**) reactions were conducted at 150 mM.

For the REEAD-on-a-slide assay, we performed the same experiment as we explained before, we only changed the NaCl concentration (150-500 mM) and the incubation time of the REEAD DNA substrate with the TOP1 (60 min).

For the C/L REEAD experiment, we hybridized 1 pmol of **cleavage half-dumbell** DNA substrate to 25 mm^2 squares (per sample) of a HD glass slide coupled with the primer. Then, we added 200 fmol of TOP1 in the corresponding reaction media and the reactions were incubated 30 min at 37^{o}C. Then, the NaCl concentrations were adjusted (150-500 mM) and 200 pmol of the **ligator half-dumbell** DNA substrate was added. The reactions were incubated at 37^{o}C for 60 min. The slides were washed in a buffer containing 0.3% of SDS to stop the reactions (see the detailed protocols in the experimental section). After the religation step, the NaCl concentration of all samples was readjusted to 150 mM again and they were incubated with 10 Unit/µL of T4 DNA ligase and 1mM of ATP for 60 min at 37^{o}C. Next, RCA reaction was carried out by incubating the samples with Phi29 DNA polymerase 1 Unit/µL, dNTPs 250 µM for 60 min at 37^{o}C, and finally FAM-labelled DNA detection probes were hybridized by incubating them (0.17 µM) for 30 min at 37^{o}C. The RCPs were visualized in a fluorescent microscope with a 63X objective and we took an average of 15 pictures per sample in order to carry out a representative counting of each square. The results of the counting are shown in the Figure 57.

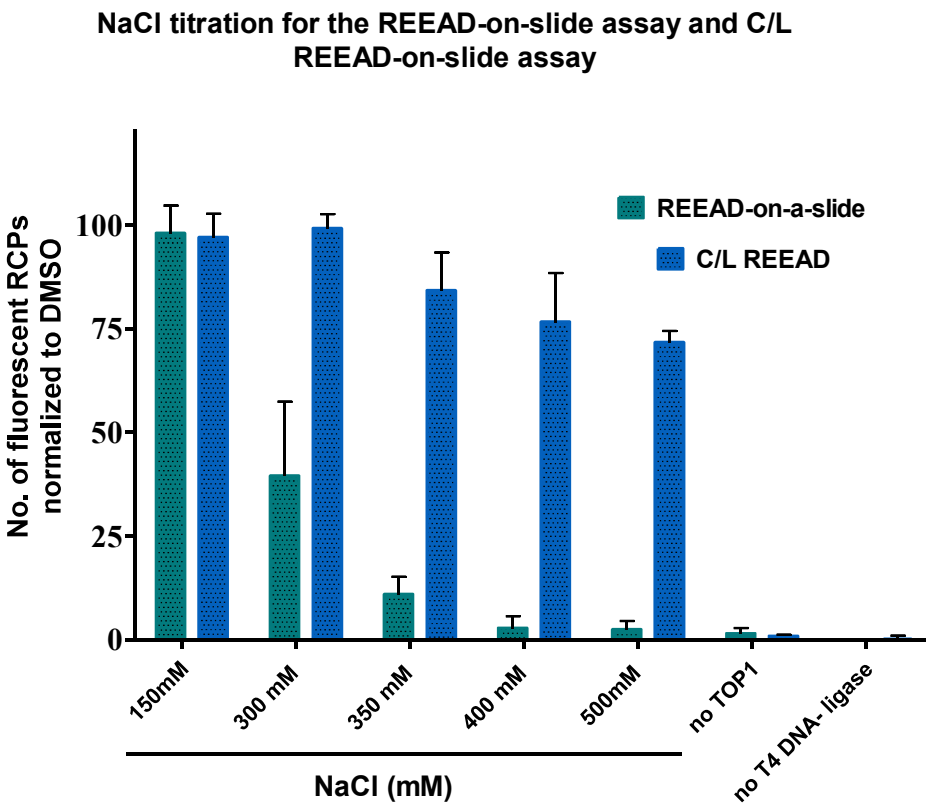

Figure 57. NaCl titration for the REEAD-on-a-slide assay and C/L REEAD assay, respectively. Note that the NaCl concentrations in the C/L REEAD assay (150-500 mM) were adjusted exclusively in the religation step.

As it can be noted in the Figure 57, the TOP1 activity expressed as the amount of RCPs visualized in the fluorescent microscope (normalzed to 150 mM NaCl on each experiment) was found to drastically decrease in the case of REEAD-on-a-slide setup, while in the C/L REEAD assay, the TOP1 activity was maintained up to 300 mM of NaCl in the religation step, and then starts to slightly decrease, reaching to a 80% of the basal activity at 500 mM. This results are in accordance with the NaCl requirements of cleavage step (150 mM) and the possibility to perform the religation stage at higher NaCl concentrations, and empirically demonstrates that the TOP1 cleavage reaction can be completelly inhibited just by adding 400 mM of NaCl (or more) but not the religation step. Based on these results, we decided to perform the religation step of the C/L REEAD assay (step **B**, Figure 56) with 400 mM of NaCl in order to avoid undesired cleavage reactions during the selective study of religation step.

Selective study of the TOP1 cleavage and religation activity in the presence of CPT and compound 6e by the C/L REEAD assay

In the previous experiment, we stablished the optimal conditions for the C/L REEAD assay and we further demonstrated that a NaCl concentration of 400 mM prevents the TOP1 cleavage step, allowing us to selectively study both steps separately. Once we stablished the experiment setup,

we proceeded to evaluate CPT and compound **6e**. CPT is an interfacial inhibitor of TOP1, which acts by trapping TOP1CCs and therefore inhibiting the religation step of TOP1. On the contrary, the compound **6e** was found to strongly inhibit TOP1 but it was found not to be TOP1 poison, so it is considered a TOP1 suppressor. We also included a positive control with DMSO (0.5% v/v), the solvent used to solve the drug candidates. We performed the experiment in triplicate, using the same condition expounded before (additionally, all the details are collected in the experimental section). We adjusted the NaCl concentration to 150 mM in the TOP1 cleavage and T4 ligase ligation steps (steps **A** and **C** respectively, Figure 56), and we performed the religation steps with 400 mM of NaCl.

We tested the compounds CPT and **6e** at 50 µM. For the **cleavage-REEAD**, we added the drug candidates in the step **A** along with TOP1, as depicted in the Figure 56 (see *inhibitor*, in the step **A**), while in the ligation-REEAD procedure the tested compounds CPT and **6e** were introduced in the step **B** along with the ligator half-dumbbell DNA substrate (see *inhibitor*, in the step **B**). The results are shown in the Figure 58.

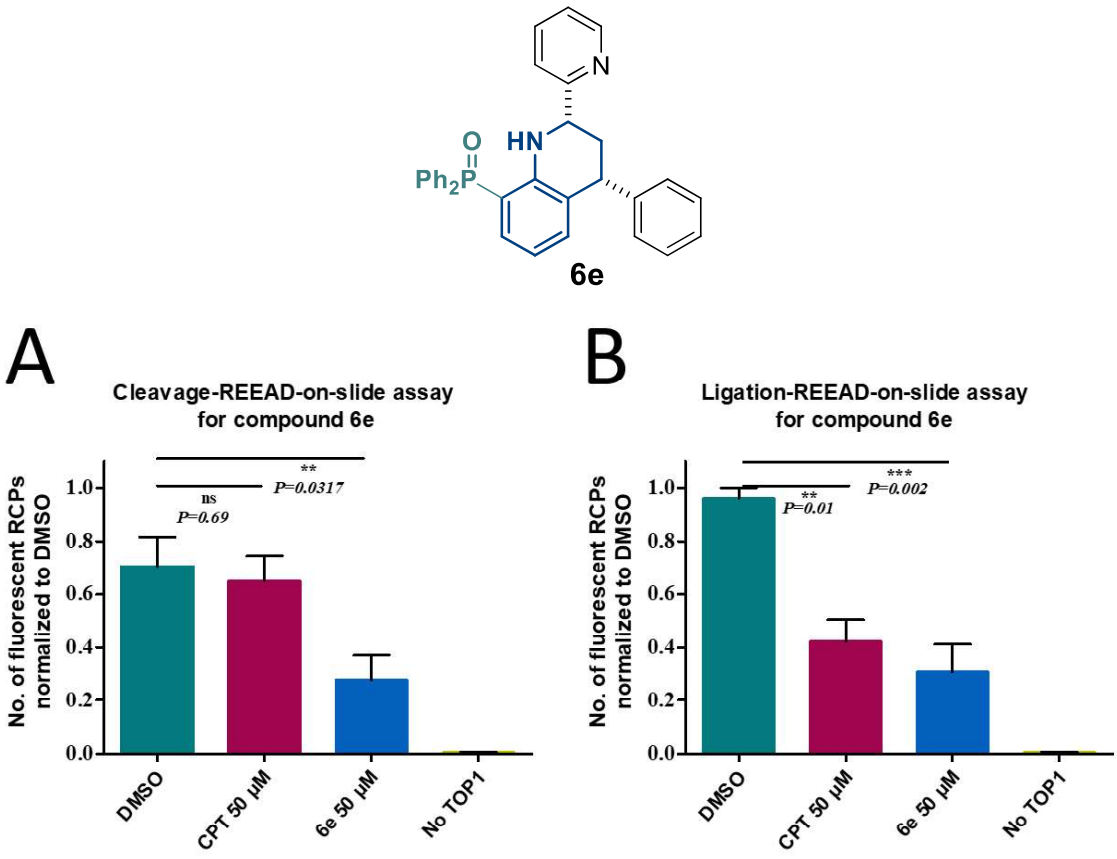

*Figure 58. Cleavage-REEAD (A) and Ligation-REEAD (B) experiments for CPT and compound **6e** at 50 µM.*

As it can be noted in the graph **A** (Figure 58), the CPT did not show any clear inhibitory activity in the binding/cleavage step(s) of TOP1 (a slight decrease of 6% of the activity is reported, which is inside the standard deviation), while the compound **6e** was found to reduce a 43% the basal binding/cleavage activity of TOP1. Conversely, the graph **B** (Figure 58) reflects a significant inhibitory effect of both CPT and **6e** in the religation step of TOP1. Surprisingly, we observed that the compound **6e** was found to inhibit the religation step in a slightly higher rate than CPT does (62% vs. 56% respectively), even though the compound **6e** resulted to inhibit both steps while CPT inhibits selectively the religation step of the TOP1 catalytic cycle (a common TOP1 inhibition pattern of *poison*-like drugs). In basis of these results, we concluded that the TOP1 suppressor **6e** seems to inhibit indiscriminately binding/cleavage and religation steps of TOP1 activity.

Likewise, we studied the TOP1 inhibitory activity of CPT and compound **6e** with the REEAD-on-a-slide approach in order to compare with the results obtained in the C/L REEAD assay. For this purpose, we followed the previously described REEAD-on-a-slide protocol and we evaluated the TOP1 activity rate in the presence of DMSO (as a control for the basal TOP1 activity), CPT at 50 µM and **6e** at 50 µM as well. The result is shown in the Figure 59 and the TOP1 inhibitory activity obtained in the DNA relaxation assay of CPT at 100 µM and compound **6e** at 160 µM is also shown (note: this is the same gel expounded in the section 2.1. of this chapter, *vide supra*).

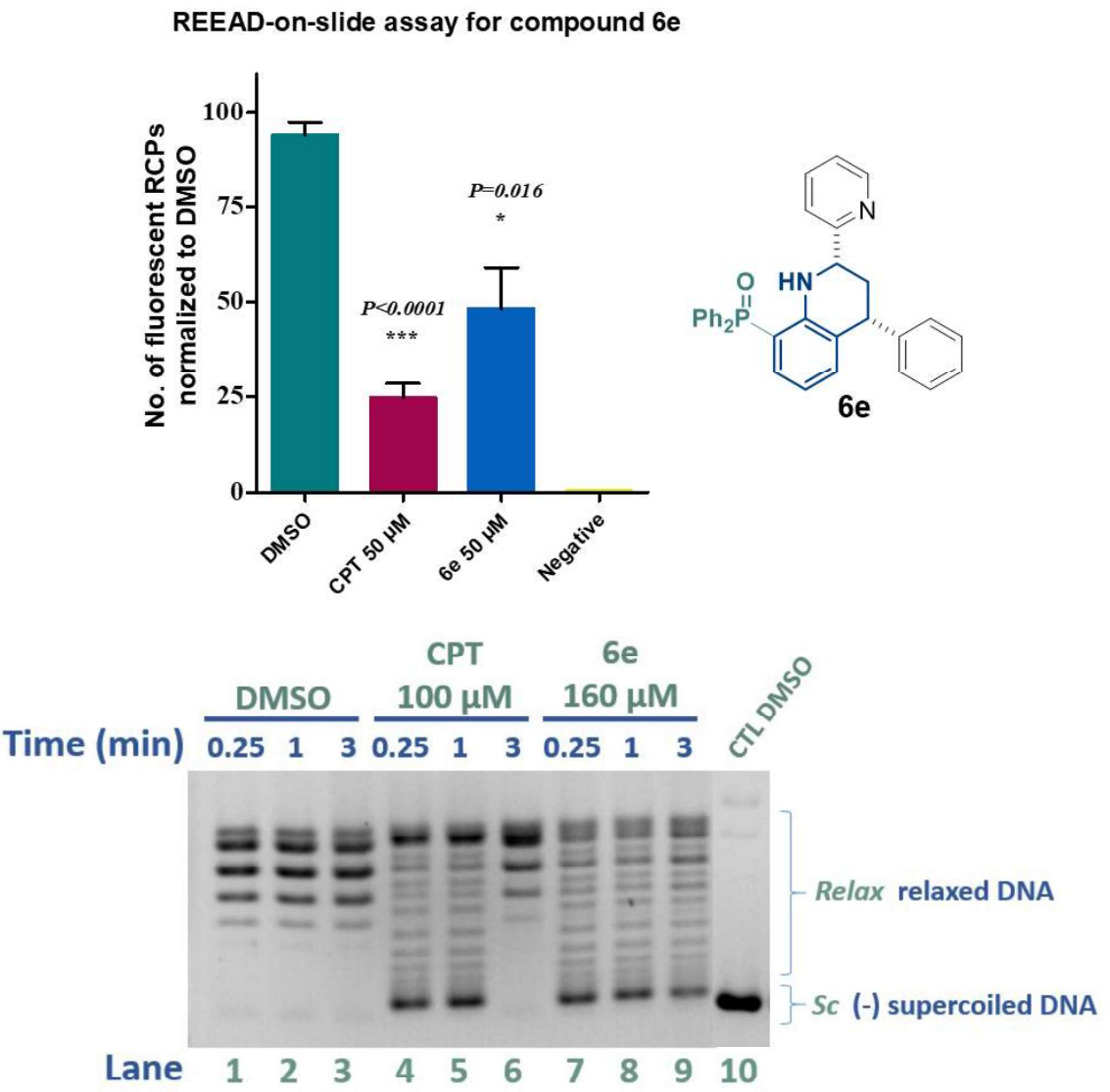

*Figure 59. REEAD-on-a-slide assay for CPT and 7e (50 µM both) and DNA relaxation assay at 100 µM (CPT) and 160 µM (**6e**).*

The compound **6e** presented an inhibition of the TOP1 activity rate of 52% in the REEAD-on-a-slide assay, while the CPT displayed an inhibition of 75% in the same conditions. These results are in concordance with the DNA relaxation assay depicted below. However, in the C/L REEAD assay, the compound **6e** showed a strong inhibitory effect both in the binding/cleavage and the religation steps of TOP1 catalysis, resulting to affect both steps in a higher manner than CPT does. As expected, CPT was found to inhibit selectively the religation step of TOP1 (a distinctive feature of TOP1 *poisons*) and surprisingly results in a stronger inhibition of the total TOP1 activity than **6e**, which separately affects in a higher rate both binding/cleavage and religation steps. The obtained results suggest that the selective inhibition of the religation stage of TOP1 catalysis may have a greater weight in the global inhibition of TOP1 activity *in vitro*.

Chapter III. Study of the *in vitro* antiproliferative activity of the newly synthesized quinoline derivatives

III-1. Introduction: Human TOP1B inhibitors in cancer chemotherapy

III-1.1. TOP1B inhibitors as cancer chemotherapeutic drugs in multitarget and drug combination therapies

Multitarget drugs involving a TOP1 inhibitory activity accompanied by a synergic pharmacological effect are subject of study in early stages of drug discovery. Representative examples of this multitarget strategy are dual TOP1 and TOP2 inhibitors, which have shown additive effects in their co-application[252]. Among the most relevant **dual TOP1/TOP2 inhibitors** are noteworthy to highlight the acridine derivatives[253], benzopyridinoindole[254] and indenoquinoline[107]. Moreover, a multitarget strategy with **dual TOP1/TDP inhibitors** has been successfully investigated (*e.g.* the development of indenoisoquinoline and oxynitidine derivatives)[255]. In this regard, the DNA damage generated by TOP1/TOP2 inhibitors could be straightforward generated through topoisomerase-selective DNA repairing systems, in particular by tyrosyl-DNA phosphodiesterases I and II (TDP1 and TDP2)[256].

On the other hand, drug combination approaches have been studied in order to improve the anticancer efficacy of TOP1 inhibitors in chemotherapeutic therapies. So far, the *poison*-like TOP1 inhibition mechanism has been found a pharmacologically relevant strategy for the treatment of cancer. As expounded before, TOP1 poisons stabilize TOP1CCs with SSBs that collide with replication forks and transcription complexes producing DNA damage. If the damage is not repaired, it leads to an irreversible DNA damage and the subsequent activation of apoptotic pathways that induce cell death[4]. Hence, the cellular response to TOP1-promoted DNA damage results essential to prevent the cell death and, accordingly, the identification of involved DNA-damage response (DDR) pathways and cell cycle checkpoint proteins has given rise to the discovery of novel therapeutic targets that may affect to the anticancer effect of TOP1

[252] Skok Ž, Zidar N, Kikelj D, Ilaš J. Dual Inhibitors of Human DNA Topoisomerase II and Other Cancer-Related Targets. *J Med Chem*. 2020;63(3):884-904. doi:10.1021/acs.jmedchem.9b00726

[253] Finlay GJ, Riou JF, Baguley BC. From amsacrine to DACA (N-[2-(dimethylamino)ethyl]acridine-4-carboxamide): selectivity for topoisomerases I and II among acridine derivatives. *Eur J Cancer*. 1996;32A(4):708-714. doi:10.1016/0959-8049(95)00604-4

[254] Poddevin B, Riou JF, Lavelle F, Pommier Y. Dual topoisomerase I and II inhibition by intoplicine (RP-60475), a new antitumor agent in early clinical trials. *Mol Pharmacol*. 1993;44(4):767-774.

[255] Baglini E, Salerno S, Barresi E, *et al.* Multiple Topoisomerase I (TopoI), Topoisomerase II (TopoII) and Tyrosyl-DNA Phosphodiesterase (TDP) inhibitors in the development of anticancer drugs. *Eur J Pharm Sci*. 2021;156:105594. doi:10.1016/j.ejps.2020.105594

[256] Zakharenko A, Dyrkheeva N, Lavrik O. Dual DNA topoisomerase 1 and tyrosyl-DNA phosphodiesterase 1 inhibition for improved anticancer activity. *Med Res Rev*. 2019;39(4):1427-1441. doi:10.1002/med.21587

inhibitors[257]. In this regard, some drug combinations involving TOP1 inhibitors accompanied by DDR/checkpoint protein inhibitors have demonstrated a synergic anticancer effect.

PARP-1 inhibitors

PARP [Poly(ADP-ribose) polymerase] is an enzyme class specialized in the restoration of DNA damage by catalyzing the transference of an ADP-ribosyl moiety to proteins (including to itself and histones), triggering the recruitment of other DNA repairing proteins (*e.g.* TDP-1) and initiating the resealing of DNA strand breaks[258]. In particular, PARP-1 is an enzyme associated with the specific repair of SSBs, which can be caused by a naturally occurring mistake during DNA metabolism or by the action of DNA damaging agents, including cancer chemotherapeutic drugs[259]. PARP-1 inhibitors have been previously reported to synergize with other DNA damaging chemotherapeutic drugs such as DNA alkylating agents (*e.g.* cisplatin)[260]. Focusing on poison-like TOP1 inhibitors, the association with PARP inhibitors has been found to prevent the repair of TOP1CC-promoted DNA breaks and therefore, to considerably increase the antiproliferative effect caused by the trapping of TOP1CCs and subsequent collision with the replication fork[259].

ATR and CHK-1 inhibitors

ATR (ataxia-telangiectasia-mutated-and-Rad3-related) and it major downstream effector CHK-1 (checkpoint kinase 1) are cell cycle checkpoint proteins that block the entry of cells into mitosis when the replication of DNA is incomplete or defective, which is the principal mode of action of cancer chemotherapeutic drugs[257]. In regard to TOP1 inhibitors, ATR/CHK-1 activity decrease the DNA damage induced by TOP1 poisons by disabling DNA replication and temporarily blocking the replication fork elongation, which limits the collisions between the replication forks and TOP1CCs (necessary for the cytotoxic effect caused by DNA damage), allowing the repair of SSBs

[257] Qiu Z, Oleinick NL, Zhang J. ATR/CHK1 inhibitors and cancer therapy. *Radiother Oncol*. 2018;126(3):450-464. doi:10.1016/j.radonc.2017.09.043

[258] Chowdhuri SP, Das BB. Top1-PARP1 association and beyond: from DNA topology to break repair. *NAR Cancer*. 2021;3(1):zcab003. Published 2021 Feb 1. doi:10.1093/narcan/zcab003

[259] Ray Chaudhuri A, Nussenzweig A. The multifaceted roles of PARP1 in DNA repair and chromatin remodelling. *Nat Rev Mol Cell Biol*. 2017;18(10):610-621. doi:10.1038/nrm.2017.53

[260] Murai J, Pommier Y. PARP trapping beyond homologous recombination and platinum sensitivity in cancers. *Annu Rev Cancer Biol*. 2019;3(1):131-150. doi: 10.1146/annurev-cancerbio-030518-055914

and broken replication forks[4]. ATR[261] and CHK-1[262] inhibitors have been found to sensibilize cells to increase the pharmacological effect of *poison*-like TOP1 inhibitors *in vitro* and *in vivo*, demonstrating a synergic anticancer effect.

III-1.2. Enhanced drug-delivery systems to improve the pharmacological properties of TOP1B inhibitors

Passive carriers

The use of TOP1 inhibitors in combination with passive carrier approaches to facilitate the drug administration is an active area of research. Among them, liposomes/nanoliposomes, nanoparticles and PEGylated (polyethylene glycol) conjugates incorporating TOP1 inhibitors as a payload provide a physical support to favour the pharmacokinetic profile of the drug and furthermore, nano-scale formulations permit a preferential accumulation of the drug in the tumor area[4].

Liposomal formulation provide to CPT and CPT derivatives enhanced permeability, increases their retention in the tumor burden and enables a sustained release. Moreover, liposomal CPTs present an improved chemical stability, resulting protected to degradation. Among CPTs, irinotecan was found to present the highest increase on it efficacy-rate in small-cell lung cancer preclinical model[263] and later on, the nanoliposomal formulation of irinotecan (NaI, Onyvide®) was developed as an alternative to the traditional chemotherapeutic drug alone presenting enhanced intratumoral accumulation and enlarged drug exposure times[68].

Furthermore, PEGylation of small molecules such as SN38 (the parental drug of irinotecan prodrug) was revealed tom improve the biodistribution *in vivo*[264]. The conjugation of PEG/PEG-polyglutamate/PEG-cyclodextrin[265] with SN-38 was found to enhance the water solubility,

[261] Jossé R, Martin SE, Guha R, *et al.* ATR inhibitors VE-821 and VX-970 sensitize cancer cells to topoisomerase i inhibitors by disabling DNA replication initiation and fork elongation responses. *Cancer Res*. 2014;74(23):6968-6979. doi:10.1158/0008-5472.CAN-13-3369

[262] Aris SM, Pommier Y. Potentiation of the novel topoisomerase I inhibitor indenoisoquinoline LMP-400 by the cell checkpoint and Chk1-Chk2 inhibitor AZD7762 [published correction appears in Cancer Res. 2012 Apr 15;72(8):2153-4] [published correction appears in Cancer Res. 2014 Aug 1;74(15):4208]. *Cancer Res*. 2012;72(4):979-989. doi:10.1158/0008-5472.CAN-11-2579

[263] Leonard SC, Lee H, Gaddy DF, *et al.* Extended topoisomerase 1 inhibition through liposomal irinotecan results in improved efficacy over topotecan and irinotecan in models of small-cell lung cancer. *Anticancer Drugs*. 2017;28(10):1086-1096. doi:10.1097/CAD.0000000000000545

[264] Zhao H, Rubio B, Sapra P, *et al.* Novel prodrugs of SN38 using multiarm poly(ethylene glycol) linkers. *Bioconjug Chem*. 2008;19(4):849-859. doi:10.1021/bc700333s

[265] a) Vangara KK, Ali HI, Lu D, Liu JL, Kolluru S, Palakurthi S. SN-38-cyclodextrin complexation and its influence on the solubility, stability, and in vitro anticancer activity against ovarian cancer. *AAPS PharmSciTech*. 2014;15(2):472-482. doi:10.1208/s12249-013-0068-5. b) Fontaine SD, Santi AD, Reid R,

enlarge the circulation time and protect the lactone ring from hydrolysis, resulting in an overall better bioavailability of the drug.

Likewise, the employment of drug-loaded nanoparticles (NPs) as physical passive nanocarriers gave rise to an improved approach for the administration of TOP1 inhibitors with a controlled release and selective accumulation of the chemotherapeutic drug in the tumor tissue environment. Out of NPs loaded with CPTs, polymeric NPs suppose the most common co-delivery platform for being totally biocompatible, present safe toxicity profiles and remain long times in blood circulation[266]. Such is the case for encapsulated irinotecan loaded into prominin-1-specific binding peptide conjugated to apoferritin NPs[267] and CPT loaded into cyclodextrin NPs[268], which reported enhanced drug-delivery that led to improved anticancer *effect in vitro* and *in vivo*. Additionally, topotecan-loaded PLGA [poly(lactic-co-glycolic acid)] NPs are under preclinical development for the oral administration of topotecan, presenting an efficient delivery to the lymphoid system (a primary metastasis site)[269]. On the other hand, mesoporous silica NPs filled with topotecan have been evaluated in combination with metformine-loaded mesoporous silica NPs (used as a coadjuvant), reporting a controlled drug-delivery and synergistic antiproliferative and apoptotic effect *in vivo* and *in vitro*[270].

Active carriers: ADCs, antibody-targeted chemotherapy

Since the discovery of immunological cancer biomarkers, the use of antibody-drug conjugates (ADCs) has emerged as a selective and personalized cancer chemotherapy approach. ADCs are conjugates of a chemotherapeutic drug and a monoclonal antibody that selectively targets

Smith PC, Ashley GW, Santi DV. PLX038: a PEGylated prodrug of SN-38 independent of UGT1A1 activity. *Cancer Chemother Pharmacol*. 2020;85(1):225-229. doi:10.1007/s00280-019-03987-z. c) Salmanpour M, Saeed-Vaghefi M, Abolmaali SS, Tamaddon AM. Sterically Stabilized Polyionic Complex Nanogels of Chitosan Lysate and PEG-b-Polyglutamic Acid Copolymer for the Delivery of Irinotecan Active Metabolite (SN-38). *Curr Drug Deliv*. 2021;18(6):741-752. doi:10.2174/1567201817999201103195846

[266] Dehshahri A, Ashrafizadeh M, Ghasemipour Afshar E, *et al.* Topoisomerase inhibitors: Pharmacology and emerging nanoscale delivery systems. *Pharmacol Res*. 2020;151:104551. doi:10.1016/j.phrs.2019.104551

[267] Chen JL, Tsai Y, Tsai M, *et al.* Prominin-1-specific binding peptide-modified apoferritin nanoparticle carrying irinotecan as a novel radiosensitizer for colorectal cancer stem-like cells. *Part Part Syst Charact*. 2017;34(5):1600424. doi:10.1002/ppsc.201600424

[268] Chen YF, Wang YH, Lei CS, Changou CA, Davis ME, Yen Y. Host immune response to anti-cancer camptothecin conjugated cyclodextrin-based polymers. *J Biomed Sci*. 2019;26(1):85. Published 2019 Oct 23. doi:10.1186/s12929-019-0583-0

[269] Jeong SH, Jang JH, Lee YB. Oral delivery of topotecan in polymeric nanoparticles: Lymphatic distribution and pharmacokinetics. *J Control Release*. 2021;335:86-102. doi:10.1016/j.jconrel.2021.05.017

[270] Banala VT, Sharma S, Barnwal P, *et al.* Synchronized Ratiometric Codelivery of Metformin and Topotecan through Engineered Nanocarrier Facilitates In Vivo Synergistic Precision Levels at Tumor Site. *Adv Healthc Mater*. 2018;7(19):e1800300. doi:10.1002/adhm.201800300

specific antigens present in cancer cells. The drug is used as a payload and the antibody plays the role of an active carrier. According to a recent bibliographical review covering this research area, currently there are 9 ADCs clinically approved for the treatment of solid tumors[271], even though they have to deal with a narrow therapeutic window that compromises the clinical outcome, and consequently individual dose-optimization processes have to be made in order to maintain the antitumor activity without serious adverse effects. Among ADCs containing a TOP1 inhibitor as a payload, trastuzumab-deruxtecan and sacituzumab-govitecan conjugates have been successfully explored as an alternative to classic chemotherapy with TOP1 inhibitors[272], as shown in the following section (III-1.3. *vide infra*).

III-1.3. Current status of TOP1B inhibitors used in clinics

Chemotherapeutic treatment of cancer implies the use of cytotoxic drugs to eradicate or decrease the tumor burden. Cancer chemotherapy is mainly administered in combination with an adjuvant therapy (surgery, radiotherapy, immunotherapy, gene therapy)[2]. These multimodality therapies are oriented to combat cancer using a customized treatment for each patient in order to fit to each individual case (*e.g.* type, stage, malignancy of the cancer).

Focusing in the cancer chemotherapy with TOP1 inhibitors, they are currently used as second line treatment for solid tumors via *i.v.* administration. The aforementioned development of CPT derivatives (CPTs) with improved pharmacodynamic profile (section 3.2.1. *vide supra*) led to the unique class of TOP1 inhibitors used in clinics. Two of these chemically stable and water soluble CPTs, **topotecan** and **irinotecan**, were approved by the FDA in 1996 to be used in the treatment of solid tumors[58], even though irinotecan was previously approved for clinical use in Japan in 1994. Likewise, in 2003 **belotecan** was approved in South Korea for ovarian and small-cell lung cancer and exhibited an efficacy toward relapsed small-cell lung cancer comparable to topotecan with a slightly better safety profile in a recent randomized phase II study, revealing as a potential second-line alternative when first line treatment fails in advanced stages of the disease[273].

---

[271] Baah S, Laws M, Rahman KM. Antibody-Drug Conjugates-A Tutorial Review. *Molecules*. 2021;26(10):2943. Published 2021 May 15. doi:10.3390/molecules26102943

[272] Adams E, Wildiers H, Neven P, Punie K. Sacituzumab govitecan and trastuzumab deruxtecan: two new antibody-drug conjugates in the breast cancer treatment landscape. *ESMO Open*. 2021;6(4):100204. doi:10.1016/j.esmoop.2021.100204

[273] Kang JH, Lee KH, Kim DW, *et al.* A randomised phase 2b study comparing the efficacy and safety of belotecan vs. topotecan as monotherapy for sensitive-relapsed small-cell lung cancer. *Br J Cancer*. 2021;124(4):713-720. doi:10.1038/s41416-020-01055-5

Topotecan is a wide spectrum CPT derivative mainly used as a second-line chemotherapeutic agent in ovarian cancer and small-cell lung cancer by intravenous administration, with a brief plasma half-life of 2-3 hours[274]. The use of topotecan is limited due to potentially serious toxicity including neutropenia and diarrhea[275].

Irinotecan is a prodrug converted to the active drug SN-38 by carboxylesterases in the liver, which is mainly used in the treatment of colon cancer and non-small cell lung cancer administered by intravenous infusion and intravenous bolus infusion[4]. The personalized medical treatment with irinotecan is still challenging due to the interidividual variability in phamacogenetics and the previous menctioned chemical instability. The heterogeneity of the drug exposure could lead to lack of efficacy or severe toxicities, which mainly involve myelosuppresion, diarrhea and vomits[276]. In this regard, pharmaceutical compositions for the oral administration of irinotecan have been successfully developed as Oncoral®, a coated tabled formulation of irinotecan for dairy administration, which reported a promising tolerance and drug exposure in phase I studies for the treatment of gastric cancer[277]. Moreover, drug conjugates of CPTs and hydrogels are under investigation as orally amdinistrated CPTs releasing systems[278].

Besides TOP1 inhibitors used in traditional chemotherapy, some emerging approaches for drug delivery have reached approval for the clinical use. On the one hand, **nanoliposomal formulation of irinotecan** (**NaI, Onyvide®**) was approved by FDA in 2015 for advanced pancreatic cancer (in combination with fluorouracil and leucovorin) by intravenous injection when first line chemotherapy fails[66]. On the other hand, the previous menctioned ADCs containing a TOP1 inhibitor payload trastuzumab-deruxtecan and sacituzumab-govitecan have received the clinical approval. **Trastuzumab-deruxtecan** (**ENHERTU®**, developed by Daiichi Sankyo in collaboration with AstraZeneca) was authorized by the FDA on 2019 for the treatment

[274] Jelovac D, Armstrong DK. Recent progress in the diagnosis and treatment of ovarian cancer. *CA Cancer J Clin*. 2011;61(3):183-203. doi:10.3322/caac.20113

[275] von Pawel J, Schiller JH, Shepherd FA, *et al.* Topotecan versus cyclophosphamide, doxorubicin, and vincristine for the treatment of recurrent small-cell lung cancer. *J Clin Oncol*. 1999;17(2):658-667. doi:10.1200/JCO.1999.17.2.658

[276] Vanhoefer U, Harstrick A, Achterrath W, Cao S, Seeber S, Rustum YM. Irinotecan in the treatment of colorectal cancer: clinical overview. *J Clin Oncol*. 2001;19(5):1501-1518. doi:10.1200/JCO.2001.19.5.1501

[277] Kümler I, Sørensen PG, Palshof J, *et al.* Oral administration of irinotecan in patients with solid tumors: an open-label, phase I, dose escalating study evaluating safety, tolerability and pharmacokinetics. *Cancer Chemother Pharmacol*. 2019;83(1):169-178. doi:10.1007/s00280-018-3720-7

[278] a) Lu YJ, Lan YH, Chuang CC, *et al.* Injectable Thermo-Sensitive Chitosan Hydrogel Containing CPT-11-Loaded EGFR-Targeted Graphene Oxide and SLP2 shRNA for Localized Drug/Gene Delivery in Glioblastoma Therapy. *Int J Mol Sci*. 2020;21(19):7111. Published 2020 Sep 26. doi:10.3390/ijms21197111. b) Wang G, Zhou Z, Zhao Z, *et al.* Enzyme-Triggered Transcytosis of Dendrimer-Drug Conjugate for Deep Penetration into Pancreatic Tumors. *ACS Nano*. 2020;14(4):4890-4904. doi:10.1021/acsnano.0c00974

of adult patients with HER2 positive breast cancer who have received 2 or more first line treatments[279], while **sacituzumab-govitecan** (**Trodelvy™**, developed by Inmunomedics) was approved on 2020 by the FDA for adult patients with metastatic triple-negative breast cancer who have received at least 2 first line therapies[280]. The timeline collecting the clinical approvals of TOP1 inhibitors is illustrated in the Figure 60. Furthermore, In a recent phase III multicenter and multi-ethnic randomized clinical trial published in 2022, trastuzumab-deruxtecan was found to detain the disease progression and effectively increase the disease control in patients with HER2 positive metastatic breast cancer previously treated with trastuzumab and taxane[281].

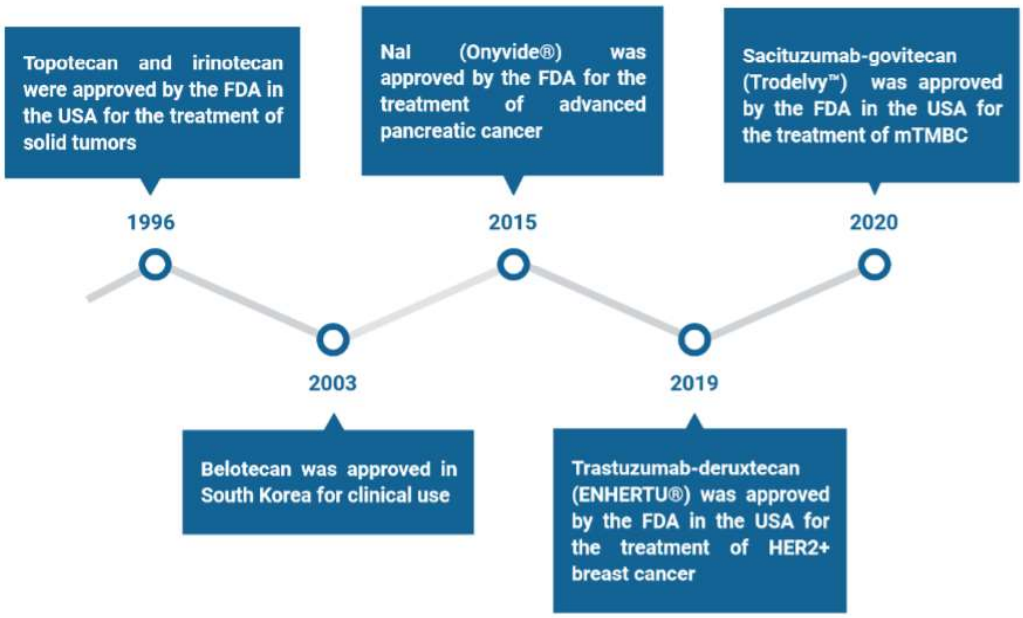

Figure 60. Chronology of the TOP1 inhibitors approved for clinical use in cancer chemotherapy.

[279] Keam SJ. Trastuzumab Deruxtecan: First Approval. *Drugs*. 2020;80(5):501-508. doi:10.1007/s40265-020-01281-4

[280] Syed YY. Sacituzumab Govitecan: First Approval. *Drugs*. 2020;80(10):1019-1025. doi:10.1007/s40265-020-01337-5

[281] Cortés J, Kim SB, Chung WP, *et al.* Trastuzumab Deruxtecan versus Trastuzumab Emtansine for Breast Cancer. *N Engl J Med*. 2022;386(12):1143-1154. doi:10.1056/NEJMoa2115022

III-2. Introduction: *in vitro* antiproliferative activity of TOP1 inhibitors

As previously mentioned, hTOP1 is a broadly explored biomolecular target in cancer research owing to a detrimental effect on cellular survival *via* inhibition of TOP1 in cancer cells. In this regard, once we performed the *in vitro* drug screening for the inhibition of TOP1 of the newly prepared phosphorated quinoline derivatives, we moved to evaluate their antiproliferative activity against human cancer cell lines. In the current chapter we show the *in vitro* assessment of the citotoxicity of the newly synthesized diphenyl phosphine oxide containing (tetrahydro)quinoline derivatives (compounds **6** and **7,** Figure 61), dialkylphosphonate substituted (tetrahydro)quinoline derivatives (compounds **13**, **15** and **16**) and dialkylphosphonate substituted (tetrahydro)indenoquinoline derivatives (compounds **19**, **20** and **21**).

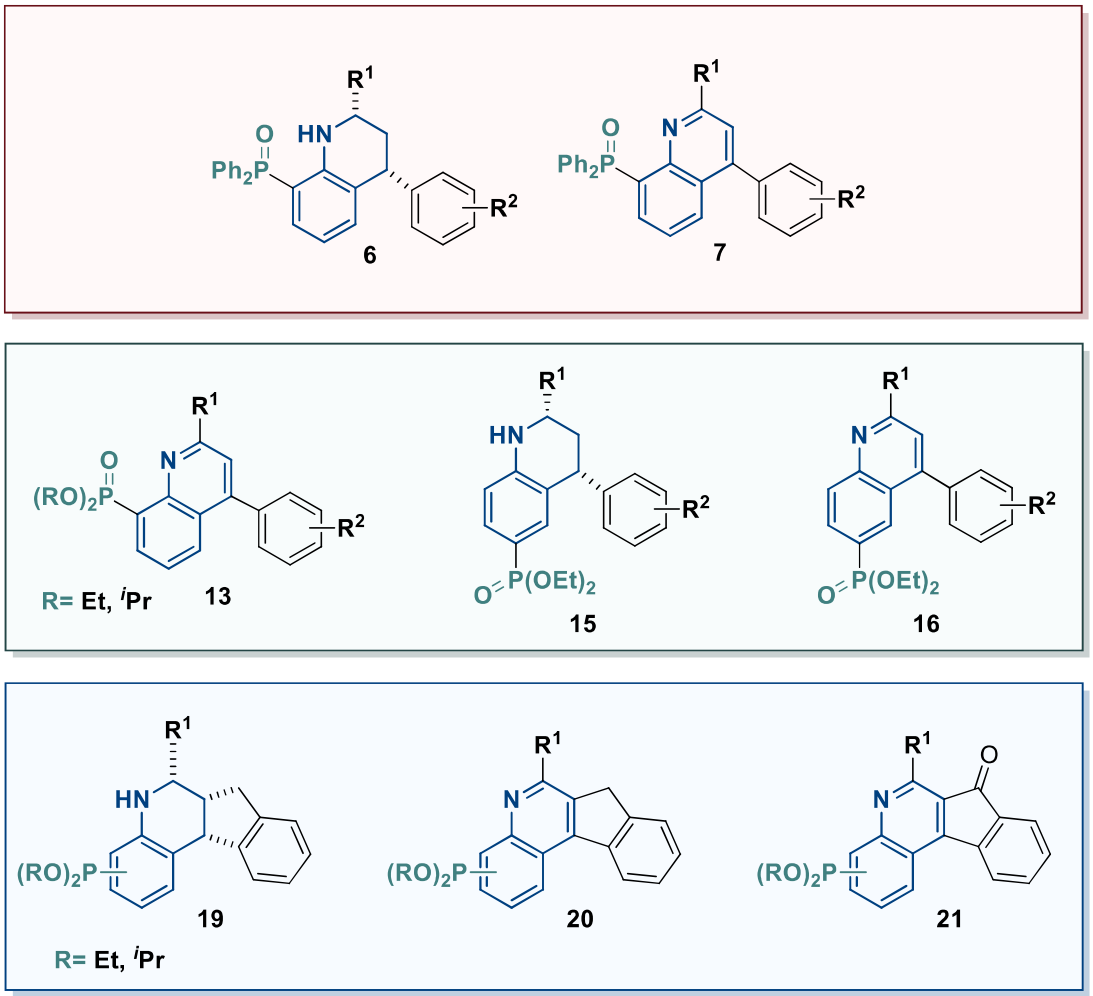

Figure 61. Families of phosphorated quinoline and indenoquinoline derivatives evaluated as potential antiproliferative agents.

The results of the antiproliferative activity was investigated by using cell viability assays against human cell lines and the corresponding results are going to be exposed categorized by families (as shown in the Figure 61) in order to facilitate the discussion of the results.

Cell viability assays provide a readout of cell viability (*i.e.* the number of healthy or viable cells in a sample) through the quantitative measurement of a particular biomarker. We studied the cell viability in the presence of different concentrations of the drug candidates in order to investigate how the cell growth is affected by the tested compounds. These experiments are also known as cytotoxicity experiments as the studied parameter is the inhibition of the cell growth by the effect of a drug candidate.

III-2.1. Metabolic cell viability assays

Metabolic cell viability assays are based on the use of a biomarker as an indicator of metabolically active healthy cells. Metabolic cell viability assays can be further classified according to the detection method employed to measure the biomarker (mainly colorimetry, fluorescence or luminescence)[282].

In colorimetric assays, the indicator acquires a colour due to the metabolic activity of viable cells, and the result is obtained by the measurement of the coloured biomarker in a spectrophotometer (generally a microplate reader). This is the case for tetrazolium reduction-based assays, such as MTT, MTS, XTT, WST-1 and WST-8 reagents[283,284].

Regarding fluorometric assays, the biomarker is transformed into a fluorescent product in respond to metabolic activity of healthy cells and it can be subsequently measured by not only a fluorescence microplate reader, but also with a fluorescence microscope, a fluorometer or even a flow-cytometer. The main fluorometric assays are resazurin reduction-based assays (AlamarBlue assay and PrestoBlue assay, which are based on the dehydrogenase activity of metabolically active cells), the carboxyfluorescein-based assay (CFDA-AM assay, which is an

[282] Riss TL, Moravec RA, Niles AL, *et al.* Cell Viability Assays. In: Markossian S, Grossman A, Brimacombe K, *et al.*, eds. *Assay Guidance Manual*. Bethesda (MD): Eli Lilly & Company and the National Center for Advancing Translational Sciences; May 1, 2013 [Updated Jul 1, 2016]

[283] Präbst K, Engelhardt H, Ringgeler S, Hübner H. Basic Colorimetric Proliferation Assays: MTT, WST, and Resazurin. *Methods Mol Biol*. 2017;1601:1-17. doi:10.1007/978-1-4939-6960-9_1

[284] Adan A, Kiraz Y, Baran Y. Cell Proliferation and Cytotoxicity Assays. *Curr Pharm Biotechnol*. 2016;17(14):1213-1221. doi:10.2174/1389201017666160808160513

indicator of plasma membrane integrity) or the aminofluorocoumarin based assay (GF-AFC assay, which is a marker for the protease viability)[285].

On the other hand, luminometric assays are measured in luminometric microplate readers after conversion of an indicator into a luminescent product in the presence of viable cells. This is the case for ATP-based viability assays such as the luciferase assay[285], which can also be performed in a real-time detection version[286].

At this point, it has to be highlighted that we studied the *in vitro* antiproliferative activity of the novel phosphorated quinoline derivatives in human cancer cell lines using primarily the CCK-8 colorimetric assay and, in some particular cases, the PrestoBlue fluorometric assay.

III-2.1.1. The CCK-8 assay

The CCK-8 (Cell Counting Kit 8) is a sensitive colorimetric assay composed of an aqueous solution containing the water soluble formazan salt WST-8 [2-(2-methoxy-4-nitrophenyl)-3-(4-nitrophenyl)-5-(2,4-disulfophenyl)-2H-tetrazolium, monosodium salt] and the electron carrier 1-methoxy PMS (1-methoxy-5-methylphenazinium methyl sulfate). The CCK-8 solution results quite stable and is reported to result considerably less harmful toward the analysed cells than other tetrazolium salts (such as the broadly used MTT, which has to be dissolved during the assay and induces a certain cytotoxic effect)[283].

As depicted in the Figure 62, CCK-8 is added directly to the cell media and the WST-8 (slightly yellow) is reduced by dehydrogenase activity of metabolically active (viable) cells, which produces a water-soluble and orange-coloured formazan dye (WST-8 Formazan) upon bioreduction by cellular dehydrogenase activity in the presence of an electron carrier (*i.e.* the 1-methoxy PMS)[285].

[285] Aslantürk ÖS. In Vitro Cytotoxicity and Cell Viability Assays: Principles, Advantages, and Disadvantages. In: Larramendy LR, Soloneski S, *Genotoxicity - A Predictable Risk to Our Actual World*. InTech; 2018. doi:10.5772/intechopen.71923

[286] Duellman SJ, Zhou W, Meisenheimer P, *et al.* Bioluminescent, Nonlytic, Real-Time Cell Viability Assay and Use in Inhibitor Screening. *Assay Drug Dev Technol*. 2015;13(8):456-465. doi:10.1089/adt.2015.669

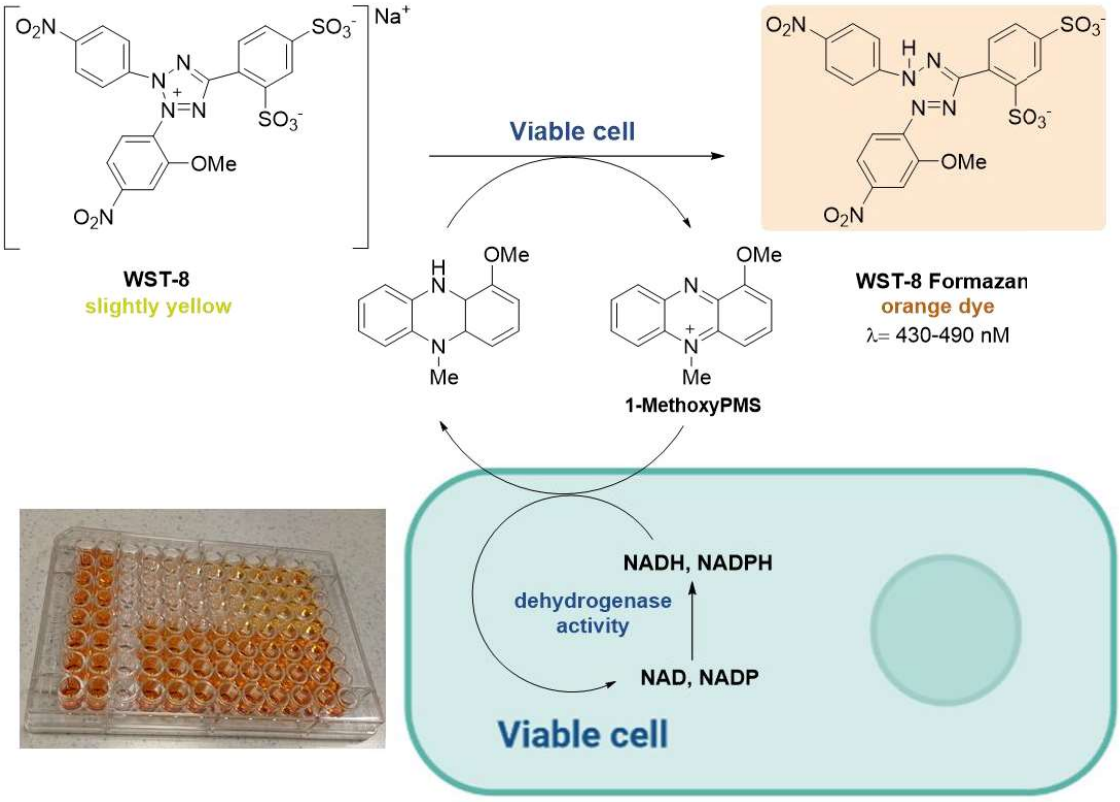

Figure 62. Conversion of WST-8 (slightly yellow) into WST-8 Formazan (orange dye) in the CCK-8 viability assay.

The amount of the WST-8 generated by the dehydrogenase activity of viable cells is directly proportional to the number of those viable cells and is subsequently measured by spectrophotometry in a microtiter plate at λ = 430-490 nm. The CCK-8 solution is directly added to the cell medium and after an incubation period of 1-4 h (under standard human cell culture conditions: 37°C, 5% CO_2 and 90% relative humidity) before measurement in the colorimetric microplate reader, and the obtained absorbance values are equivalent of the cell viability of the sample.

III-2.1.2. The PrestoBlue assay

As the previously described WST-8, PrestoBlue is a non-toxic reagent for the quick and sensitive determination of cell viability. The PrestBlue assay is based on a resazurin solution, which is notably stable and can be directly added to the cell medium. Resazurin (blue) is *in situ* converted into the pink and highly fluorescent resofurin (pink) under the reducing activity of viable cells, as illustrated in the Figure 63. Thus, the cell viability is straightforward determined by measuring the fluorescence of the samples after 10-20 min of incubation with PrestoBlue in the

corresponding cell media (*e.g.* the experiment could be easily carried out in a 12/24/96/384-well plate and measured by a fluorescent microplate reader)[287].

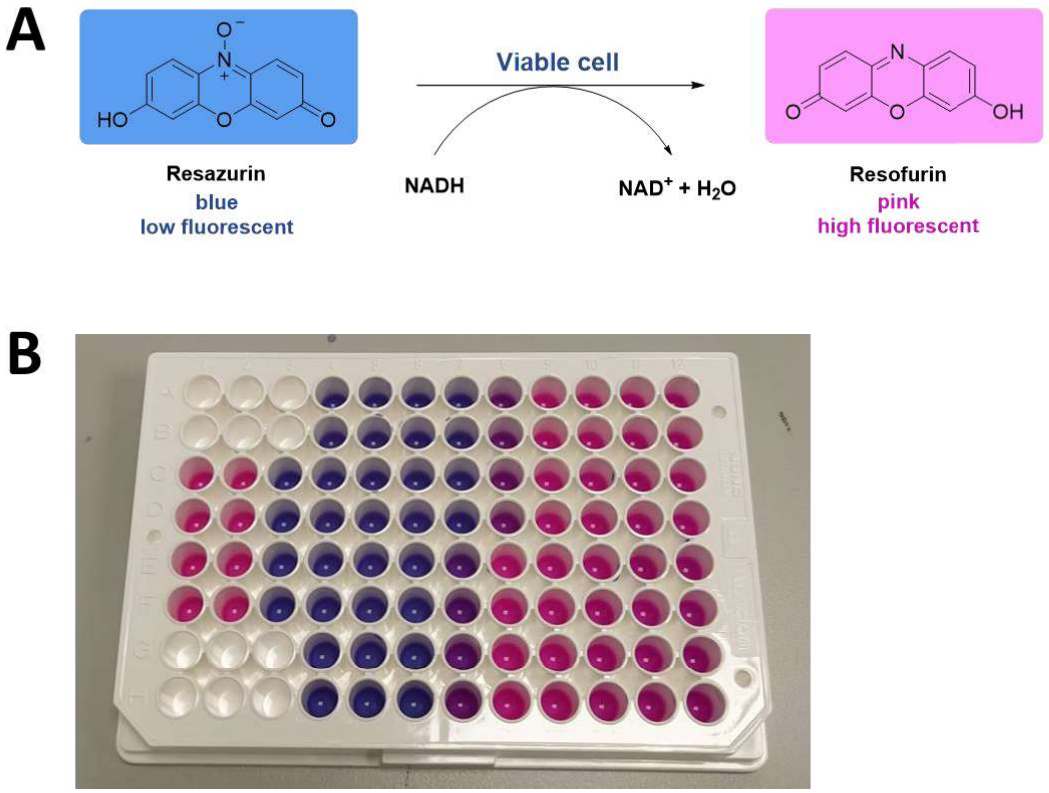

Figure 63. A) Conversion of resazurin (blue) into the highly fluorescent resofurin (pink) in the PrestoBlue viability assay. B) Visual appearance of a 96-well microplate plate after a PrestoBlue assay.

[287] Xu M, McCanna DJ, Sivak JG. Use of the viability reagent PrestoBlue in comparison with alamarBlue and MTT to assess the viability of human corneal epithelial cells. *J Pharmacol Toxicol Methods*. 2015;71:1-7. doi:10.1016/j.vascn.2014.11.003

III-3. *In vitro* evaluation of the antiproliferative activity in human cell lines

The *in vitro* cytotoxic effect of the tested compounds was assessed by using the CCK-8 cell viability assay. To put the CCK-8 viability assay into context, a schematic overview of the experiment is depicted in the Figure 64.

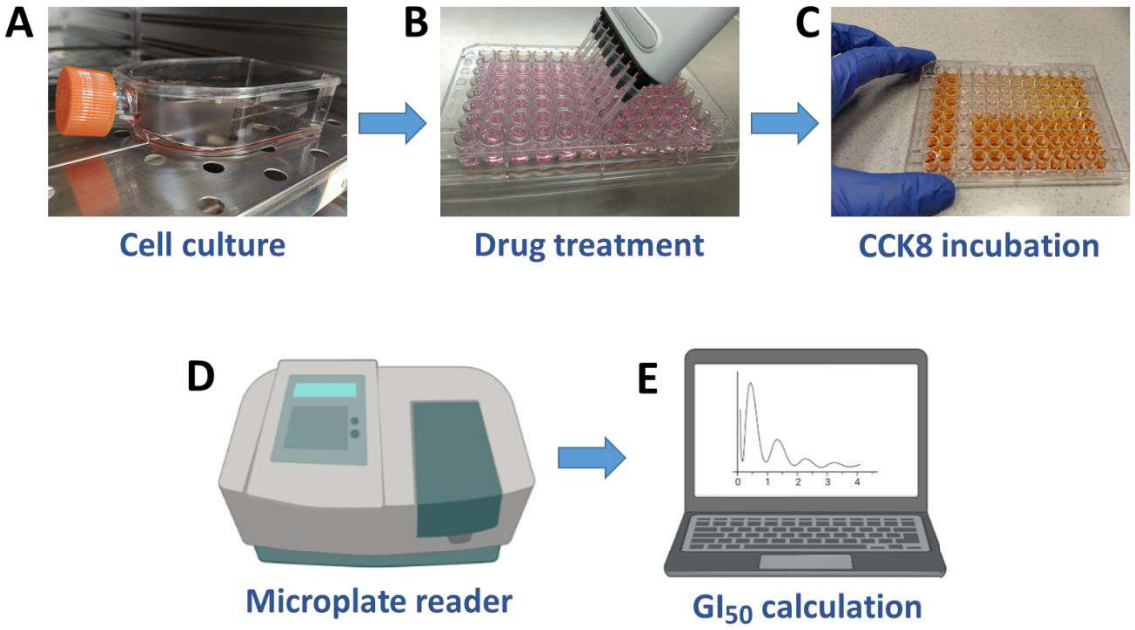

Figure 64. Schematic overview of the cell viability evaluation with the CCK-8 assay.

First of all, as illustrated in the picture A (Figure 64), adherent cells were cultivated in cell culture flasks with their corresponding medium (the details of the protocols are provided in the experimental section) and incubated under standard mammalian cell-culture conditions (37°C, 5% CO_2 and 90% relative humidity). The cell medium was replaced with fresh medium every 3 days and the cell cultures were split when cells were close to the end of their exponential growth (~70-75% of confluent). In order to perform the viability experiments, cells were harvested at 70-75% confluency and subsequently plated into 96-well microplates ($3 \cdot 10^3$ cells in 100 µL of medium per well) and incubated under standard mammalian cell-culture conditions for 24 h. Then, as shown in the picture B (Figure 64), the cells were treated by replacing the old cell medium of each well (100 µL) with fresh cell medium (100 µL) containing selected concentrations of the compound subject to study dissolved in 0.5% v/v (final concentration) of DMSO. For the negative controls, only 0.5% v/v DMSO was used. After drug treatment, the microplates were incubated for 48 h at 37°C and afterwards the CCK-8 solution was added to each well (10 µL/well). The microplates incubated for 2 extra hours at 37°C, 5% CO_2 and 90% relative humidity, leading to the formation of WST-8 formazan (seen as an orange dye, as shown

in the picture C, Figure 64), whose absorbance was measured by a microplate reader at 450 nm (picture D).

The raw data corresponding to the obtained absorbance values was processed using GraphPad Prism software (version 5.01), considering the DMSO-treated cells (negative control) as 100% viable cells (thus, by normalizing each value to the average absorbance of the DMSO-treated cells). Accordingly, GI_{50} values were calculated (*i.e.* the concentration for 50% of maximal inhibition of cell growth) from quadruplicate experiments and the results are shown as the mean ± the SD (standard deviation) of the mean.

Cell lines

Cell viability assays were performed in A-549 (human lung adenocarcinoma, Figure 65, panel **A**) and SK-OV-3 (human ovarian adenocarcinoma, panel **B**) as human cancer cell lines and HEK-293 (human embryonic kidney cell line, panel **C**), which is a non-cancerous cell line but presents some characteristics that differentiate them from canonical non-cancer cell line models. Furthermore, in order to evaluate the antiproliferative activity of the tested compounds towards a non-cancerous cell line, we included the MRC-5 (human lung fibroblasts) non-cancerous cell line (panel **D**) into the screening. All the cell lines employed in this first screening are adherent cell lines that grow as monolayer and their morphology is shown in the pictures collected in the Figure 65 (epithelial for A-549, SK-OV-3 and HEK-293; fibroblastic in case of MRC-5).

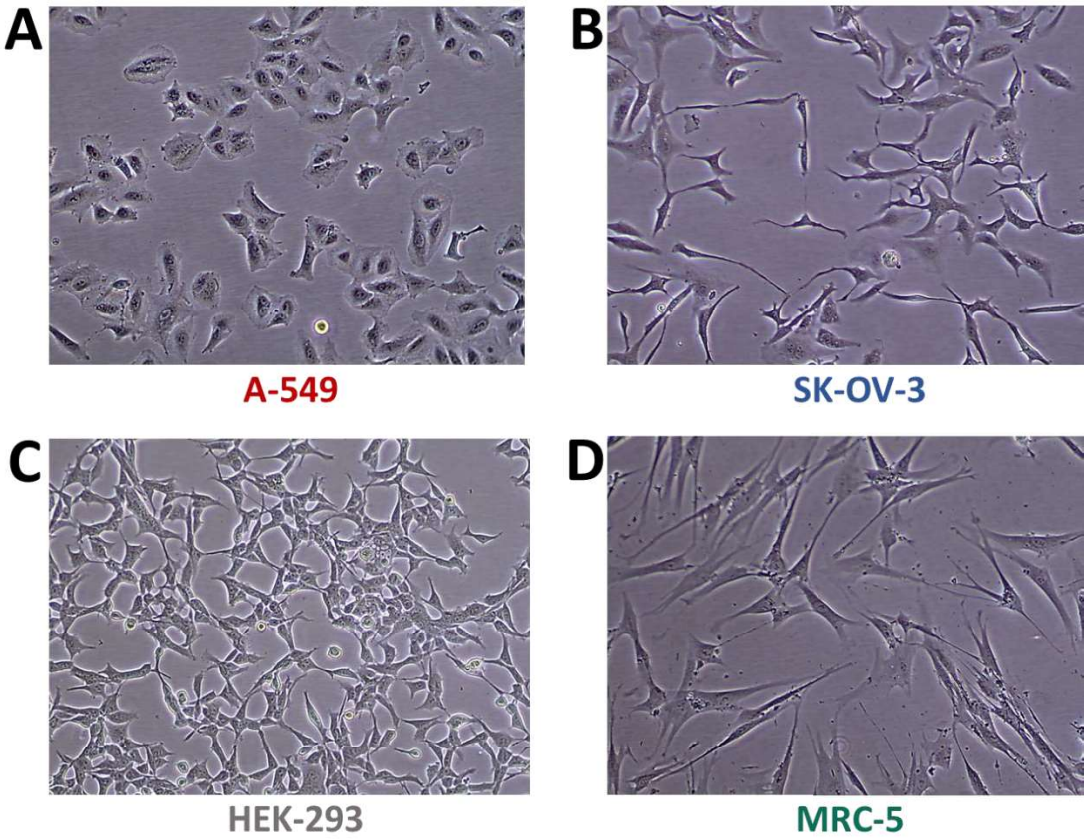

Figure 65. Microscope images (10X objective) showing the morphology of the cell lines used in the first antiproliferative screening of the newly synthesized compounds

Antiproliferative activity of CPT

Before starting to test the newly synthesized compounds, we proceeded to evaluate the antiproliferative activity of CPT (the reference TOP1 inhibitor and a strong antiproliferative agent) against A-549, SK-OV-3, HEK-293 and MRC-5 human cell lines. For this purpose, the previously expounded CCK-8 cell viability assay was performed and the GI_{50} values of CPT in the four cell lines were determined. The graph with the dose response curves corresponding to the cell viability rate (in %) versus the concentration/logarithmic concentration of CPT in the micromolar range towards A-549, SK-OV-3, HEK-293 and MRC-5 cell lines is shown in the Figure 66 (graph **A** cell viability vs. concentration; graph **B** cell viability vs. logarithmic concentration), along with the GI_{50} values obtained for each cell line (table **C**).

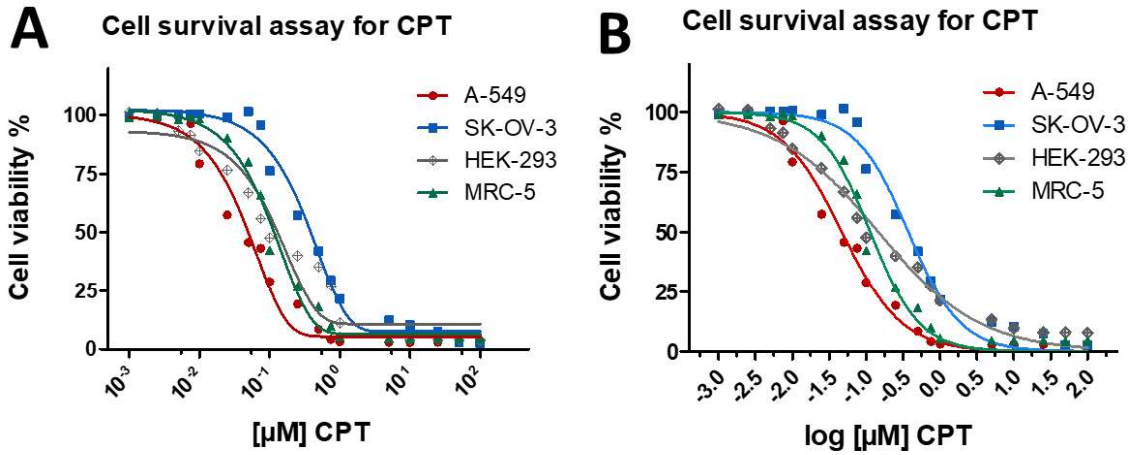

C

Compound	GI_{50} ± SD (µM)			
	A-549 (lung)	SK-OV-3 (ovarian)	HEK-293 (kidney)	MRC-5 (lung)
CPT	$(47.14 \pm 3.39).10^{-3}$	0.37 ± 0.01	0.15 ± 0.02	0.11 ± 0.02

Figure 66. Analysis of the cytotoxic effect of CPT in A-549, SK-OV-3, HEK-293 *and MRC-5 human cell lines **A**) Dose response curve of CPT corresponding to the cell viability measured by CCK-8 assays versus the concentration of CPT. **B**) Dose response curve of CPT corresponding to the cell viability measured by CCK-8 assays versus the logarithmic concentration of CPT. **C**) GI_{50} values calculated from the data represented in the graphs **A** and **B**.*

As it can be observed, in our hands the CPT was reported to show a GI_{50} of 47.14 ± 3.39 nM toward A-549 cell line, 0.37 ± 0.02 µM in SK-OV-3, 0.15 ± 0.02 µM in HEK-293 and 0.11 ± 0.02 µM towards MRC-5 cell line.

As expected, CPT resulted to be a potent antiproliferative agent, obtaining GI_{50} values between the nanomolar (in the A-549 cell line) and the low-micromolar range (MRC-5 < HEK-293 < SK-OV-3). CPT resulted specially effective in reducing the cell proliferation of the A-549 lung cancer cell line. However, CPT was revealed to show cytotoxicity towards the non-cancerous human cancer cell line MRC-5, with a GI_{50} value of 0.11 ± 0.02 µM. Therefore, CPT was revealed as a strong antiproliferative agent in all the cell lines, including in non-cancerous MRC-5 cells, resulting about three fold times more cytotoxic toward MRC-5 in comparison to the ovarian cancer cell line SK-OV-3.

III-3.1. *In vitro* evaluation of the antiproliferative activity in human cancer cell lines of 1,2,3,4-tetrahydroquinolin-8-yl phosphine oxides 6 and quinolin-8-yl phospine oxides 7

Once analysed the cytotoxicity of CPT, we proceeded to study the antiproliferative activity of 1,2,3,4-tetrahydroquinolin-8-yl phosphine oxides **6** and quinolin-8-yl phospine oxides **7** (Figure 67) by performing CCK-8 cell survival assays in A-549 , SK-OV-3, MRC-5 and HEK-293 cell lines.

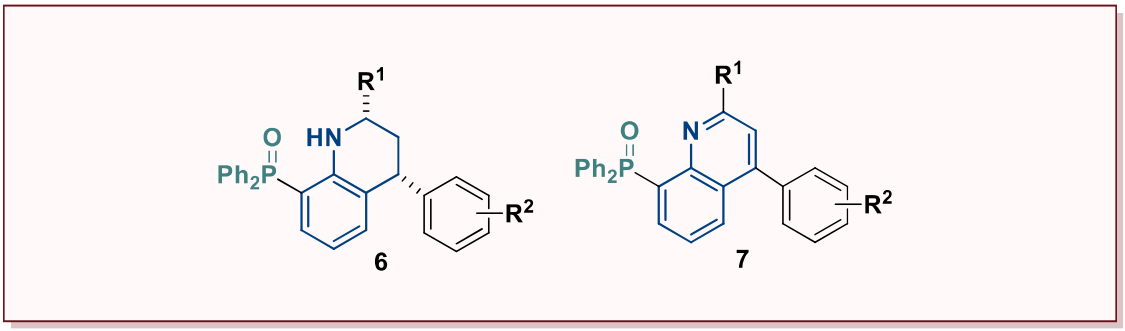

*Figure 67. General structures of 1,2,3,4-tetrahydroquinolin-8-yl phosphine oxides **6** and quinolin-8-yl phospine oxides **7**.*

We firstly investigated the antiproliferative activity of (2-(2-methoxyphenyl)-4-phenylquinolin-8-yl)diphenylphosphine oxide **7a** by using the CCK-8 cell viability assay. We plated the cells into 96-well plates ($3 \cdot 10^3$ cells in 100 µL of medium per well) and incubated the plates at 37°C, 5% CO_2 and 90% relative humidity for 24 h. Then, the drug treatment was carried out by replacing the old cell medium (100 µL/well) with fresh cell medium (100 µL) containing selected concentrations of the compound subject to study (50, 30, 20, 10, 5, 2.5 and 1 µM) dissolved in a final concentration of 0.5% v/v DMSO. In order to maintain the same sample-treatment during the experiment, DMSO (at 0.5% v/v final concentration) was added to the negative control. Another negative control without DMSO is included just to detect a possible cytotoxic effect of the solvent during the experiment conditions. Each drug concentration and control is tested four times in order to get four experiments per compound. After the drug treatment, 96-well plates were incubated for 48 h under the previous mentioned cell culture conditions and subsequently 10 µL of CCK-8 solution were added to each sample (well). The microplates were incubated again under standard cell culture conditions for 2 hours, and the absorbance was measured in a microplate reader using a filter at λ = 450 nm. The obtained data were processed with GraphPad Prism software and the absorbance values were normalized to the average absorbance of the DMSO-treated control cells. Graphs showing the dose-response curves belonging to the cell viability versus the concentration/logarithmic concentration of **7a** against A-549, SK-OV-3, HEK-293 and MRC-5 cell lines are included in the Figure 68 (graph **A**, cell viability rate in % vs. concentration; graph **B**, cell viability rate in % vs. logarithmic concentration) along with a column-bars graph comparing the cell viability rate of **7a** in the the four cell lines at the tested concentrations (graph **C**).

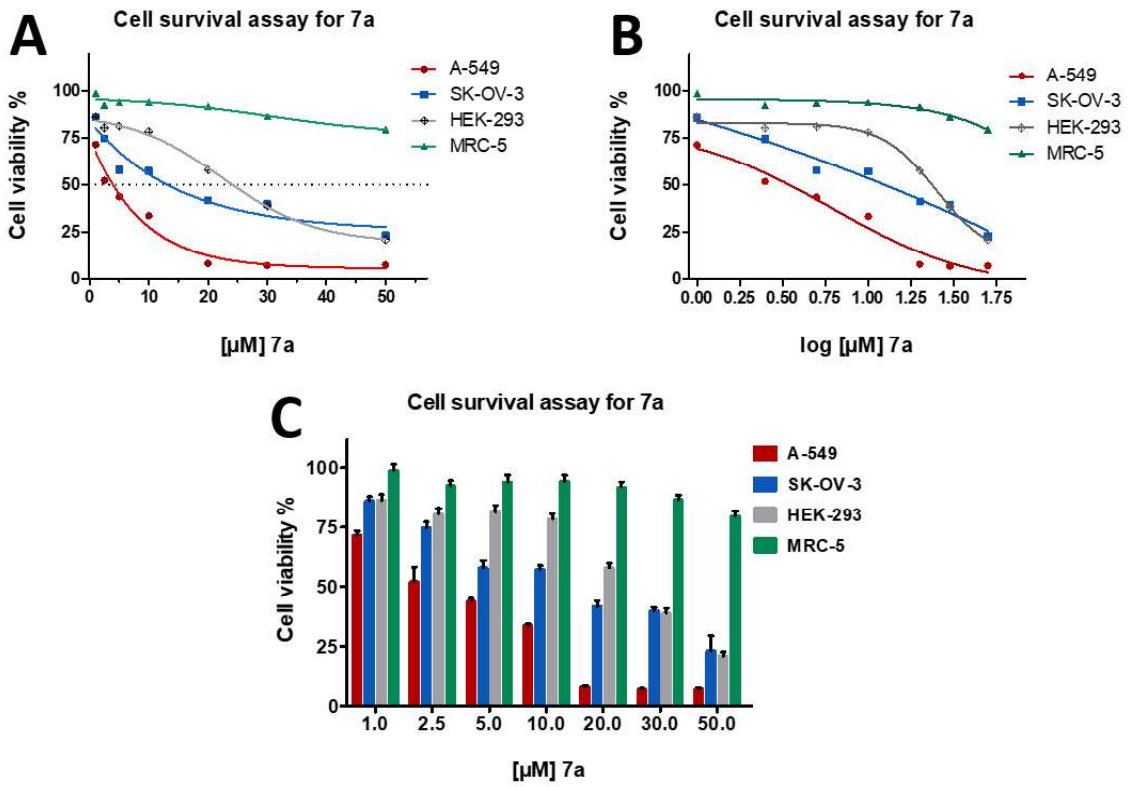

*Figure 68. Analysis of the cytotoxic effect of the quinolin-8-yl phosphine oxide **7a** in A-549, SK-OV-3, HEK-293 and MRC-5 human cell lines **A**) Dose response curve corresponding to the cell viability versus the concentration of compound **7a**. **B**) Dose response curve of CPT corresponding to the cell viability versus the logarithmic concentration of **7a**. **C**) Column-bars graph comparing the cell viability rate of **7a** between the four cell lines at the tested concentrations.*

Based on these cell viability dose-response curves, the GI_{50} is calculated using the same GraphPad Prism software. CCK-8 viability assay is performed in quadruplicate, so the result of **7a** is shown as the mean of GI_{50} ± SD of those four experiments. The compound **7a** is found to be a promising antiproliferative agent with the ability to induce cytotoxicity (in the micromolar range) in human cancer cell lines, while resulted not to be cytotoxic in MRC-5 lung fibroblast-like non-cancerous cell line, with a GI_{50} value superior to 50 µM. The compound **7a** reported GI_{50} ± SD values of 3.11 ± 0.65 µM in A-549 lung cancer cell line, 13.06 ± 1.80 µM in SK-OV-3 ovarian cancer cell line, 24.13 ± 1.76 µM in HEK-293.

The cytotoxicity of tetrahydroquinolin-8-yl phosphine oxides **6** and quinolin-8-yl phosphine oxides **7** was evaluated following the same protocol and the GI_{50} values are collected in the Table 17.

Table 17. Antiproliferative activity of tetrahydroquinolin-8-yl phosphine oxides **6** and quinolin-8-yl phosphine oxides **7** in A-549, SK-OV-3, HEK-293 and MRC-5 human cell lines.

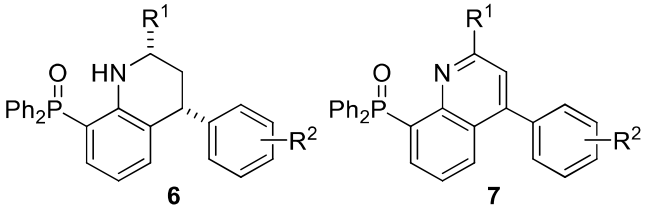

Entry	Compound			GI_{50} ± SD (μM)[a]			
				A-549	SK-OV-3	HEK-293	MRC-5
	Nº	R^1	R^2	(lung)	(ovarian)	(kidney)	(lung)
1	**CPT**	-	-	$(47.14 \pm 3.39)\cdot10^{-3}$	0.37 ± 0.01	0.15 ± 0.02	0.11 ± 0.02
2	**6a**	2-MeO-C_6H_4	H	1.40 ± 0.13	>50	16.26 ± 1.11	>50
3	**6b**	4-$(EtO)_2P(O)O$- C_6H_4	H	5.06 ± 0.28	17.41 ± 1.55	6.03 ± 1.58	>50
4	**6c**	1-naphthyl	H	3.57 ± 0.31	>50	>50	>50
5	**6d**	2-naphthyl	H	>50	26.68 ± 3.21	>50	>50
6	**6e**	2-pyridyl	H	2.26 ± 0.21	14.83 ± 2.56	19.07 ± 3.56	>50
7	**6f**	C_6H_5	4-Me	1.20 ± 0.12	>50	28.00 ± 2.26	>50
8	**6g**	4-F-C_6H_4	4-Me	1.32 ± 0.15	>50	38.34 ± 3.54	>50
9	**6h**	4-F-C_6H_4	4-F	1.35 ± 0.53	17.79 ± 5.45	23.88 ± 4.05	>50
10	**6i**	3,4-F_2-C_6H_3	4-F	1.32 ± 0.21	>50	18.01 ± 3.37	>50
11	**7a**	2-MeO-C_6H_4	H	3.11 ± 0.65	13.06 ± 1.80	24.13 ± 1.76	>50
12	**7b**	4-$(EtO)_2P(O)O$- C_6H_4	H	1.80 ± 0.41	8.36 ± 0.38	7.62 ± 0.38	>50
13	**7c**	1-naphthyl	H	1.68 ± 0.39	14.48 ± 1.55	10.47 ± 0.47	>50
14	**7d**	2-naphthyl	H	6.32 ± 1.09	>50	>50	>50
15	**7f**	C_6H_5	4-Me	7.65 ± 0.90	17.38 ± 1.58	8.97 ± 0.54	>50
16	**7g**	4-F-C_6H_4	4-Me	2.64 ± 0.43	10.51 ± 2.20	10.88 ± 0.78	>50
17	**7h**	4-F-C_6H_4	4-F	3.82 ± 0.42	6.77 ± 0.85	12.46 ± 0.87	>50
18	**7i**	3,4-F_2-C_6H_4	4-F	2.22 ± 0.34	26.26 ± 8.09	35.63 ± 7.95	>50
19	**7j**	C_6H_5	4-F	2.59 ± 0.77	16.52 ± 2.07	12.43 ± 1.11	>50
20	**7k**	4-F-C_6H_4	H	3.80 ± 1.21	17.17 ± 2.98	8.16 ± 1.99	>50

[a]The cytotoxicity GI_{50} values collected in the present table were calculated by cell viability assays and are defined as the concentrations corresponding to a 50% cell growth inhibition. The GI_{50} results are shown as the mean ± the standard deviation from independent cell viability assay experiments performed in quadruplicate.

According to the results presented in the Table 17, in general, 1,2,3,4-tetrahydroquinolin-8-yl phospine oxides **6** (entries 2-10) and quinolin-8-yl phospine oxides **7** (entries 11-20) were found to be specifically cytotoxic toward A-549 lung adenocarcinoma cell line in the single-digit micromolar range. Hence, the GI_{50} values of compounds **6** and **7** toward A-549 ranged from 1.20 ± 0.12 [corresponding to **6f** (R^1 = C_6H_5; R^2 = 4-Me; entry 7)] to 7.65 ± 0.90 μM [related to **7f** (R^1 = C_6H_5; R^2 = 4-Me; entry 15)], except for the particular case of **6d** (R^1 = 1-naphthyl; R^2 = H; entry 5) that presented a GI_{50} value superior to 50 μM. Regarding SK-OV-3 ovarian adenocarcinoma cells, the majority of the compounds **6** and **7** exhibited an appreciable cytotoxic response presenting GI_{50} values between 6.77-26.68 μM. Lastly, derivatives **6** and **7** generally showed GI_{50} values in the range 9.03-38.34 μM toward HEK-293 embryonic cell line.

Overall, the studied phosphine-oxide substituted quinoline derivatives **6** and **7** presented a notable cytotoxic response in the micromolar range toward human cancer cell lines A-549 and SK-OV-3, whereas all the compounds exhibited a reduced antiproliferative effect in MRC-5 non-cancer lung fibroblasts with GI_{50} values over 50 µM. The compounds **6** and **7** demonstrated an exclusive antiproliferative effect toward the two tested cancer cell lines, highlighting the derivatives **6e** (R^1 = 2-pyridyl; R^2 = H; Table 20, entry 6) with GI_{50} values of 2.26 ± 0.21 µM in A-549 cells and 14.83 ± 2.56 µM in SK-OV-3 cells; **7b** (R^1 = 4-$(EtO)_2P(O)O$-C_6H_4; R^2 = H; entry 12) with GI_{50} values of 1.80 ± 0.41 µM in A-549 cells and 8.36 ± 0.38 µM in SK-OV-3 cell line; and **7h** (R^1 = 4-F-C_6H_4; R^2 = 4-F; entry 17) with GI_{50} values of 3.82 ± 0.42 µM in A-549 cells and 6.77 ± 0.85 µM in SK-OV-3 cell line.

III-3.2. *In vitro* evaluation of the antiproliferative activity in human cancer cell lines of dialkyl quinolinylphosphonates and dialkyl (indeno[2,1-*c*]quinolinyl)phosphonates

In the present section we expose the evaluation of the *in vitro* antiproliferative activity of dialkyl quinolinylphosphonates (families **13**, **15** and **16**; Figure 69**,** panel **A**, in green) and dialkyl(indeno[2,1-*c]*quinolinyl)phosphonates (families **19**, **20** and **21**; Figure 69, panel **B**, in blue). The screening was assessed by the previously expounded CCK-8 cell viability assay in A-549, SK-OV-3, MRC-5 and HEK-293 cell lines.

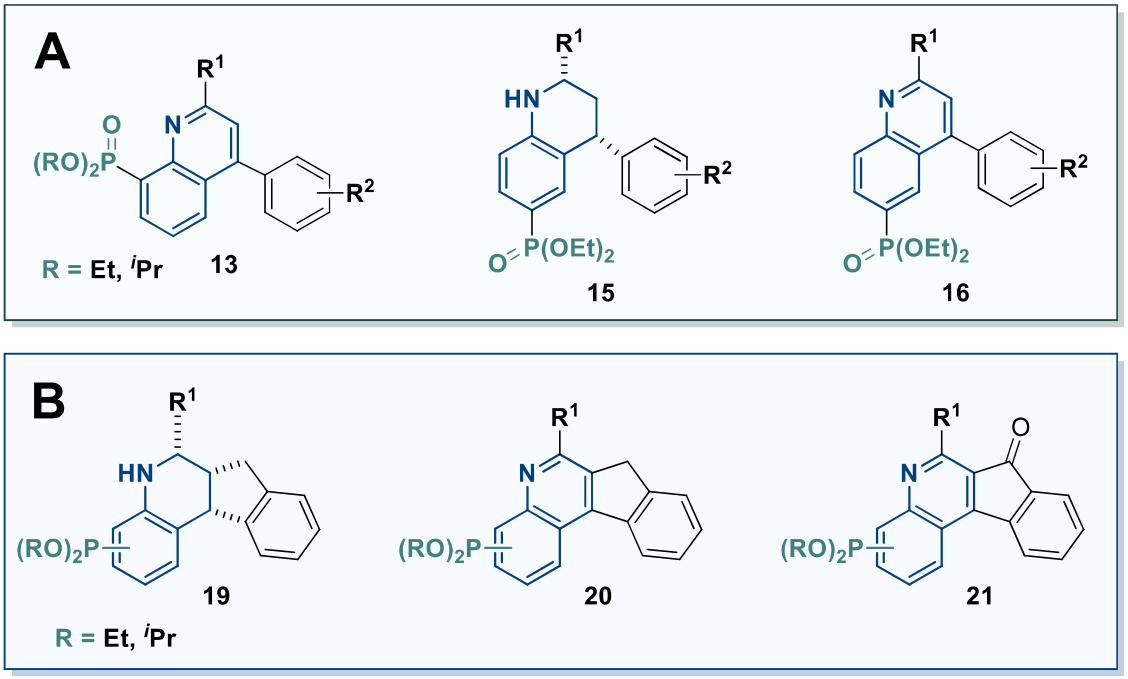

Figure 69. ***A)*** *General structures of dialkyl quinolin-8-ylphosphonates* ***13****, diethyl 1,2,3,4-tetrahydroquiolin-6-ylphosphonates* ***15*** *and diethyl quinolin-6-ylphospjonates* ***16*** *(in green);* ***B)*** *dialkyl tetrahydro-5H-indeno[2,1-c]quinolinylphosphonates* ***19****, dialkyl 7H-indeno[2,1-c]quinolinylphosphonates* ***20*** *and dialkyl 7-oxo-7H-indeno[2,1-c]quinoliny phosphonates* ***21*** *(in blue).*

Dialkyl quinolin-8-ylphosphonates 13

We started the cytotoxicity studies by the evaluation of the antiproliferative activity of dialkyl quinolin-8-yl phosphonates **13**, following the CCK-8 protocol used for the screening of families **6** and **7** (explained in the section 2.1., *vide supra*). The dose-response curves corresponding to the antiproliferative activity of the compound **13t** is shown as an example in the Figure 70.

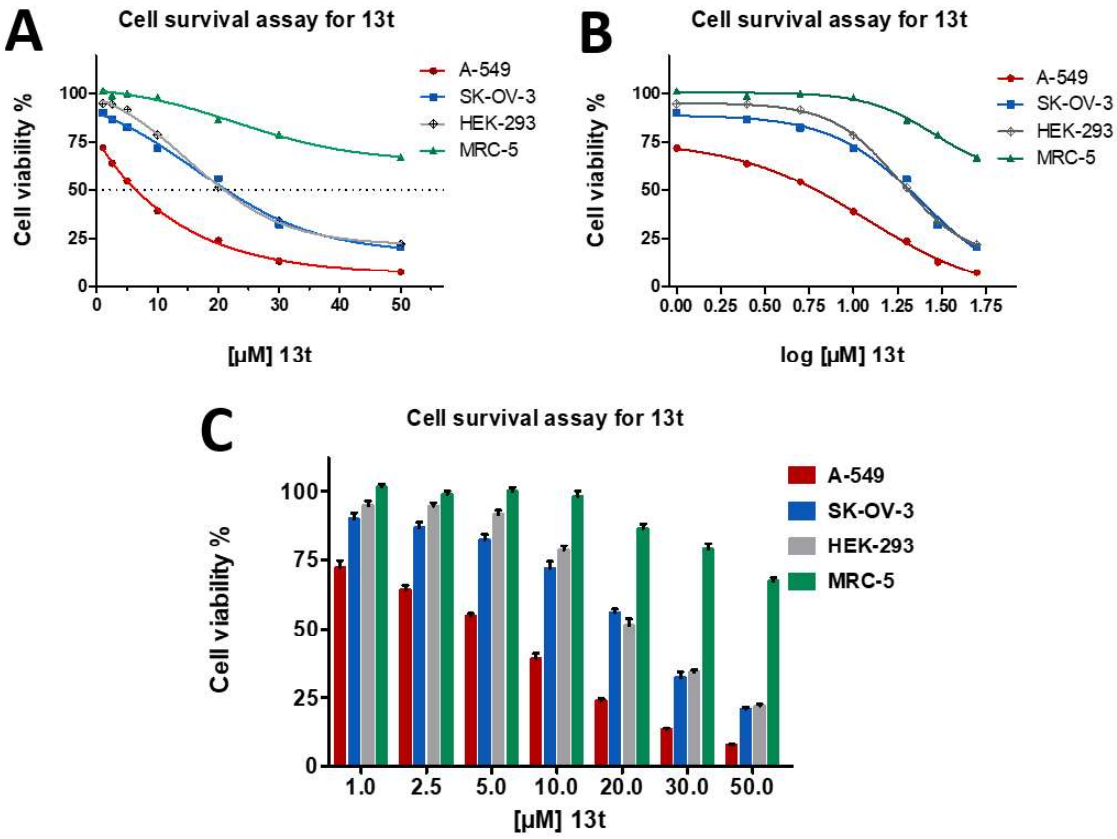

*Figure 70. Analysis of the cytotoxic effect of the dialkyl quinolin-8-ylphosphonate **13t** in A-549, SK-OV-3, HEK-293 and MRC-5 human cell lines **A**) Dose response curve corresponding to the cell viability versus the concentration of compound **13t**. **B**) Dose response curve of CPT corresponding to the cell viability versus the logarithmic concentration of **13t**. **C**) Column-bars graph comparing the cell viability rate of **13t** between the four cell lines at the tested concentrations.*

The GI_{50} values were calculated based on the cell viability data shown in the Figure 70 by using the GraphPad Prism software. For instance, the compound **13t** reported GI_{50} ± SD values of 6.79 ± 3.87 µM in A-549 cells (lung adenocarcinoma), 22.12 ± 4.47 µM in SK-OV-3 cells (ovarian adenocarcinoma), 21.04 ± 4.05 µM in HEK-293 cells and >50 µM in MRC-5 (non-malignant lung fibroblast-like non-cancerous cell line). The rest of dialkyl quinolin-8-yl phosphonates **13** were evaluated in like manner and the results are collected in the Table 18.

Table 18. Antiproliferative activity of dialkyl quinolin-8-ylphosphonates **13** in A-549, SK-OV-3, HEK-293 and MRC-5 human cell lines.

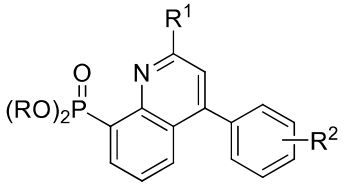

13

Entry	Compound				GI_{50} ± SD (μM)[a]			
					A-549	SK-OV-3	HEK-293	MRC-5
	Nº	R	R^1	R^2	(lung)	(ovarian)	(kidney)	(lung)
1	**CPT**	-	-	-	$(47.14 \pm 3.39)\cdot10^{-3}$	0.37 ± 0.01	0.15 ± 0.02	0.11 ± 0.02
2	**13a**	Et	C_6H_5	H	2.26 ± 0.59	9.30 ± 0.76	27.29 ± 2.22	>50
3	**13b**	Et	2-MeO-C_6H_4	H	17.26 ± 4.07	19.38 ± 1.56	>50	>50
4	**13c**	Et	3-MeO-C_6H_4	H	3.20 ± 0.35	9.08 ± 0.27	>50	>50
5	**13d**	Et	4-MeO-C_6H_4	H	12.59 ± 1.34	25.04 ± 3.61	38.29 ± 8.89	>50
6	**13e**	Et	4-$(EtO)_2P(O)O$-C_6H_4	H	26.15 ± 4.01	7.04 ± 0.21	10.84 ± 0.98	35.11 ± 5.58
7	**13f**	Et	1-naphthyl	H	2.66 ± 0.16	4.54 ± 0.52	35.67 ± 3.13	>50
8	**13g**	Et	2-naphthyl	H	3.18 ± 0.27	1.33 ± 0.76	48.14 ± 6.39	>50
9	**13h**	Et	3,4-F_2-C_6H_4	H	1.47 ± 0.12	30.80 ± 2.82	7.77 ± 0.22	>50
10	**13i**	Et	C_6H_5	4-Me	1.49 ± 0.10	9.68 ± 0.75	27.17 ± 3.45	32.03 ± 13.51
11	**13j**	Et	4-F-C_6H_4	4-Me	1.61 ± 0.17	10.24 ± 0.39	>50	>50
12	**13k**	Et	3,4-F_2-C_6H_4	4-Me	2.72 ± 0.37	10.59 ± 1.13	22.66 ± 1.36	>50
13	**13l**	Et	C_6H_5	4-F	2.27 ± 0.33	9.29 ± 1.79	24.43 ± 3.46	>50
14	**13m**	Et	4-F-C_6H_4	4-F	3.07 ± 0.22	9.79 ± 0.59	15.66 ± 1.74	>50
15	**13n**	Et	3,4-F_2-C_6H_4	4-F	4.64 ± 0.30	37.59 ± 9.10	>50	>50
16	**13o**	^{i}Pr	4-F-C_6H_4	H	5.01 ± 2.70	18.73 ± 1.98	10.12 ± 1.26	>50
17	**13p**	^{i}Pr	3,4-F_2-C_6H_4	H	18.39 ± 1.36	12.13 ± 1.68	>50	>50
18	**13q**	^{i}Pr	4-F-C_6H_4	4-Me	6.84 ± 1.74	12.13 ± 1.68	14.38 ± 1.69	>50
19	**13r**	^{i}Pr	3,4-F_2-C_6H_4	4-Me	8.24 ± 2.42	4.67 ± 1.49	12.32 ± 0.72	>50
20	**13s**	^{i}Pr	4-F-C_6H_4	4-F	10.55 ± 1.73	19.82 ± 3.82	15.01 ± 0.99	>50
21	**13t**	^{i}Pr	3,4-F_2-C_6H_4	4-F	6.79 ± 3.87	22.12 ± 4.47	21.04 ± 4.05	>50

[a]The cytotoxicity GI_{50} values collected in the present table were calculated by cell viability assays and are defined as the concentrations corresponding to a 50% cell growth inhibition. The GI_{50} results are shown as the mean ± the standard deviation from independent cell viability assay experiments performed in quadruplicate.

The results collected in the Table 18 reveal that the screened dialkyl quinolin-8-ylphosphonates **13** (entries 2-21) demonstrated on the whole a marked antiproliferative effect against human cancer cell lines A-549 (adenocarcinomic alveolar basal epithelial cells) with GI_{50} values ranging between 1.47-26.15 μM; and SK-OV-3 (adenocarcinomic ovarian cells) with GI_{50} values between 1.33-37.59 μM, while they presented a lower cytotoxic effect toward HEK-293 embryonic cells. It is noteworthy to highlight the antiproliferative activity of compounds **13f**, **13g** and **13j**. **13f** (R^1 = 1-naphthyl; R^2 = H; Table 18, entry 7) presented GI_{50} values of 2.66 ± 0.16 μM in A-549 cell line and 4.54 ± 0.52 μM in SK-OV-3 cell line; **13g** (R^1 = 2-naphthyl; R^2 = H; entry 8) showed GI_{50} values of 3.18 ± 0.27 μM in A-549 cells and 1.33 ± 0.76 μM in SK-OV-3 cells; and finally, the compound

13j (R^1 = 4-F-C_6H_4; R^2 = 4-Me; entry 11) presented GI_{50} values of 1.61 ± 0.17 µM in A-549 cell line and 10.24 ± 0.39 µM in SK-OV-3 cell line.

On the contrary, compounds **13** demonstrated a considerably weaker cytotoxic effect in MRC-5 non-malignant cell line in the same concentration range. The narrow antiproliferative response toward MRC-5 was constant in all the tested compounds **13** (**13a-13t**), exhibiting GI_{50} values superior to 50 µM, except for compounds **13e** (R^1 = 4-$(EtO)_2P(O)O$-C_6H_4; R^2 = H; entry 6) and **13i** (R^1 = C_6H_5; R^2 = 4-Me; entry 10), which presented GI_{50} values of 35.11 ± 5.58 µM and 32.03 ± 13.51 µM respectively. Consequently, we conclude that dialkyl quinolin-8-yl phosphonates **13** demonstrated a clear trend to induce an antiproliferative effect in cancerous cell lines.

Diethyl 1,2,3,4-tetrahydroquinolin-6-ylphosphonates 15 and diethyl quinolin-6-ylphosphonates 16

Once we finished the screening of quinolines **13**, we moved to assess the *in vitro* antiproliferative activity of 1,2,3,4-tetrahydroquinolines **15** and quinolines **16** with a diethyl phosphonate functionality in the position 6. At this point, it should be noted that the structural difference of the previously evaluated derivatives **13a-n** and these derivatives **15**/**16** basically lies in the position of the diethyl phosphonate moiety, from position 8 of the quinoline moiety (**13a-n**) to the position 6 (**15**/**16**). The results of the CCK-8 viability assays of compounds **15** and **16** are collected in the Table 19.

Table 19. Antiproliferative activity of diethyl 1,2,3,4-tetrahydroquinolin-6-ylphosphonates **15** and diethyl quinolin-6-yl phosphonates **16** in A-549, SK-OV-3, HEK-293 and MRC-5 cell lines.

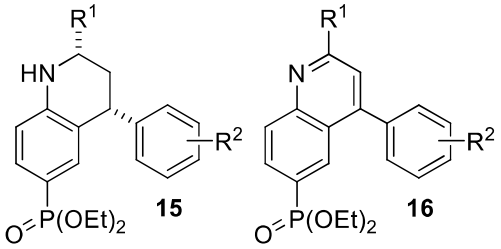

Entry	Compound			GI_{50} ± SD (μM)[a]			
				A-549	SK-OV-3	HEK-293	MRC-5
	Nº	R^1	R^2	(lung)	(ovarian)	(kidney)	(lung)
1	**CPT**	-	-	$(47.14 \pm 3.39)\cdot10^{-3}$	0.37 ± 0.01	0.15 ± 0.02	0.11 ± 0.02
2	**15a**	4-F-C_6H_4	H	1.96 ± 0.24	21.12 ± 3.84	21.71± 2.19	>50
3	**15b**	3,4-F_2-C_6H_4	H	2.21 ± 0.96	34.84 ± 6.15	18.96 ± 2.95	>50
4	**15c**	4-F-C_6H_4	4-Me	2.51 ± 0.15	14.23 ± 1.81	29.46 ± 6.28	>50
5	**15d**	3,4-F_2-C_6H_4	4-Me	5.28 ± 0.69	21.55 ± 2.07	11.99 ± 2.02	>50
6	**15e**	4-F-C_6H_4	4-F	2.50 ± 0.83	>50	47.77 ± 11.86	36.96 ± 2.93
7	**15f**	3,4-F_2-C_6H_4	4-F	9.52 ± 0.62	>50	>50	>50
8	**16a**	4-F-C_6H_4	H	2.80 ± 1.24	31.03 ± 9.96	36.86 ± 8.06	>50
9	**16b**	3,4-F_2-C_6H_4	H	6.19 ± 0.67	>50	19.18 ± 1.13	>50
10	**16c**	4-F-C_6H_4	4-Me	1.91 ± 0.33	41.61 ± 10.01	>50	>50
11	**16d**	3,4-F_2-C_6H_4	4-Me	3.05 ± 0.86	>50	>50	>50
12	**16e**	4-F-C_6H_4	4-F	27.85 ± 4.26	>50	>50	>50
13	**16f**	3,4-F_2-C_6H_4	4-F	4.33 ± 01.11	>50	25.72 ± 6.34	>50

[a]The cytotoxicity GI_{50} values collected in the present table were calculated by cell viability assays and are defined as the concentrations corresponding to a 50% cell growth inhibition. The GI_{50} results are shown as the mean ± the standard deviation from independent cell viability assay experiments performed in quadruplicate.

Overall, diethyl 1,2,3,4-tetrahydroquinolin-6-ylphosphonates **15** (entries 2-7, Table 19) presented a slightly higher antiproliferative effect than the parental fully aromatic quinoline derivatives **16** (entries 8-13). The highest cytotoxic results were observed toward A-549 cells, in most cases with GI_{50} values below 10 μM. A wider range of GI_{50} was observed for the ovarian cancer cancer cell line SK-OV-3 (14.23-34.84 μM, and some values >50 μM) and the embryonic cell line HEK-293 (11.99-47.77 μM, and some values >50 μM). Contrarily, derivatives **15**/**16** presented GI_{50} values above 50 μM in MRC-5 non-cancer cell line (except for the compound **15e**).

Out of compounds **15** and **16**, tetrahydroquinoline derivatives **15a** (R^1= 4-F-C_6H_4; R^2= H; Table 19, entry 2) and **15c** (R^1 = 4-F-C_6H_4; R^2 = 4-Me; entry 4) were found to be the most effective compounds exhibiting low GI_{50} values in the micromolar range toward A-549 and SK-OV-3 cancer cell lines. In particular, the compound **15a** (R^1 = 4-F-C_6H_4; R^2 = H; entry 2) presented GI_{50}

values of 1.96 ± 0.24 μM and 21.12 ± 3.84 μM in A549 and SK-OV-3 cells respectively, while the compound **15c** (R^1 = 4-F-C_6H_4; R^2 = 4-Me; entry 4) reported GI_{50} values of 2.51 ± 0.15 μM and 14.23 ± 1.81 μM in A549 and SK-OV-3 cells respectively.

Attending to the collected results, when the diethyl phosphonate moiety is changed from the position 8 of the quinoline core (compounds **13a-n**, Table 18, entries 2-15) to the position 6 (compounds **16**, Table 19, entries 8-13), on the whole the antiproliferative activity decreases in cancer cells (A-549 and SK-OV-3) and embryonic cells, while the behaviour in MRC-5 is maintained (>50 in all cases). For instance, the compounds **13j** (R^1 = 4-F-C_6H_4; R^2 = 4-Me; entry 11, Table 18), **13k** (R^1 = 3,4-F_2-C_6H_4; R^2 = 4-Me; Table 18, entry 12) and **13m** (R^1= 4-F-C_6H_4; R^2= 4-F, Table 18, entry 14) presented GI_{50} values between 1.61-3.04 μM in A-549, 9.79-10.59 μM in SK-OV-3, 15.66->50 μM in HEK-293 and >50 μM in MRC-5. On the contrary, the derivatives **16c** (R^1 = 4-F-C_6H_4; R^2 = 4-Me; Table 19, entry 10), **16d** (R^1 = 3,4-F_2-C_6H_4; R^2 = 4-Me, Table 19, entry 11) and **16e** (R^1 = 4-F-C_6H_4; R^2 = 4-F, Table 19, entry 12) reported GI_{50} values between 1.91-27.85 μM in A-549, 41.61- >50 μM in SK-OV-3, >50 μM in HEK-293 and >50 μM in MRC-5.

Dialkyl tetrahydro-5H-indeno[2,1-c]quinoinlylphosphonates 19, dialkyl 7H-indeno[2,1-c]quinolinylphosphonates 20 and dialkyl 7-oxo-7H-indeno[2,1-c]quinolinylphosphonates 21

Continuing our screening of phosphonate-substituted quinoline derivatives, we moved to investigate the *in vitro* cytotoxic effect of indeno(tetrahydro)quinoline derivatives **19**, **20** and **21** by following the CCK-8 cell viability protocol expounded before. The cell viability graphs obtained for the tetrahydro-*5H*-indenoquinoline derivative **19a** are collected in the Figure 71.

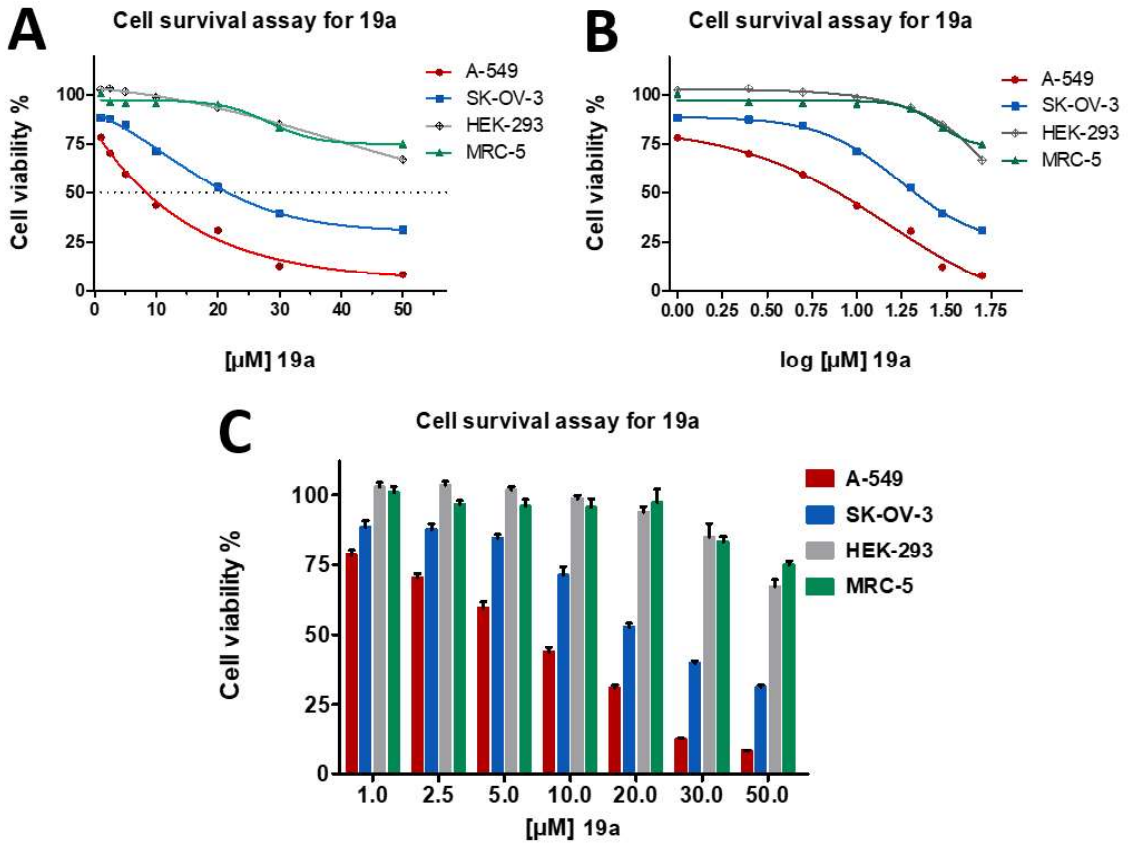

*Figure 71. Analysis of the cytotoxic effect of the dialkyl tetrahydro-5H-indeno[2,1-c]quinolinylphosphonate **19a** in A-549, SK-OV-3, HEK-293 and MRC-5 human cell lines **A**) Dose response curve corresponding to the cell viability versus the concentration of compound **19a**. **B**) Dose response curve of CPT corresponding to the cell viability versus the logarithmic concentration of **19a**. **C**) Column-bars graph comparing the cell viability rate of **19a** between the four cell lines at the tested concentrations.*

As it can be noted in the cell viability graphs (Figure 71, panels **A**, **B** and **C**), the compound **19a** showed a higher cytotoxic effect toward the cancer cell lines (A-549 and SK-OV-3) than in the embryonic cells HEK-293 and non-cancerous cells MRC-5. The GI_{50} values for the compound **19a** calculated based on the cell viability graphs (Figure 71) were 8.71 ± 0.50 µM in A-549 cells, 20.95 ± 1.88 µM in SK-OV-3 cells, >50 µM in HEK-293 and >50 µM in MRC-5 cells. All the GI_{50} values obtained for the compounds **19**, **20** and **21** are listed in the Table 20.

Table 20. Antiproliferative activity of dialkyl tetrahydro-*5H*-indeno[2,1-*c*]quinolinylphosphonates **19**, dialkyl *7H*-indeno[2,1-*c*]quinolinylphosphonates **20** and dialkyl 7-oxo-*7H*-indeno[2,1-*c*]quinolinylphosphonates **21** in A-549, SK-OV-3, HEK-293 and MRC-5 human cell lines.

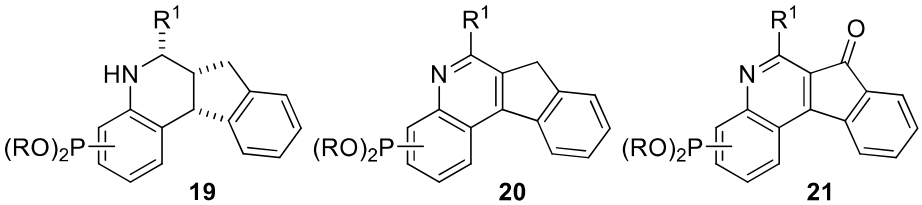

Entry	Compound			GI_{50} ± SD (μM)[a]			
				A-549 (lung)	SK-OV-3 (ovarian)	HEK-293 (kidney)	MRC-5 (lung)
	Nº	R^1	R^2				
1	**CPT**	-	-	$(47.14 \pm 3.39)\cdot10^{-3}$	0.37 ± 0.01	0.15 ± 0.02	0.11 ± 0.02
2	**19a**	4-P(O)(OEt)$_2$	3-MeO-C$_6$H$_4$	8.71 ± 0.50	20.95 ± 1.88	>50	>50
3	**19b**	4-P(O)(OEt)$_2$	4-MeO-C$_6$H$_4$	2.10 ± 0.30	12.62 ± 0.73	>50	>50
4	**19c**	4-P(O)(OEt)$_2$	4-CF$_3$-C$_6$H$_4$	3.39 ± 0.15	>50	>50	>50
5	**19d**	2-P(O)(OEt)$_2$	3-MeO-C$_6$H$_4$	2.07 ± 0.28	>50	28.60 ± 3.29	>50
6	**19f**	2-P(O)(OEt)$_2$	4-CF$_3$-C$_6$H$_4$	2.91 ± 1.09	45.53 ± 7.02	12.51 ± 1.82	>50
7	**20a**	4-P(O)(OEt)$_2$	3-MeO-C$_6$H$_4$	1.33 ± 0.22	9.79 ± 0.83	11.80 ± 0.97	>50
8	**20c**	4-P(O)(OEt)$_2$	4-CF$_3$-C$_6$H$_4$	3.14 ± 0.11	25.70 ± 3.40	>50	>50
9	**20e**	2-P(O)(OEt)$_2$	4-MeO-C$_6$H$_4$	>50	>50	>50	>50
10	**20g**	4-P(O)(O^{i}Pr)$_2$	4-CF$_3$-C$_6$H$_4$	13.50 ± 3.80	>50	31.04 ± 8.73	>50
11	**21a**	4-P(O)(OEt)$_2$	3-MeO-C$_6$H$_4$	2.58 ± 0.25	26.82 ± 3.36	39.46 ± 5.98	39.68 ± 7.37
12	**21b**	4-P(O)(OEt)$_2$	4-MeO-C$_6$H$_4$	1.51 ± 0.19	>50	>50	>50
13	**21c**	4-P(O)(OEt)$_2$	4-CF$_3$-C$_6$H$_4$	1.53 ± 0.28	4.55 ± 0.52	>50	>50
14	**21d**	2-P(O)(OEt)$_2$	3-MeO-C$_6$H$_4$	4.41 ± 1.74	>50	>50	>50
14	**21f**	2-P(O)(OEt)$_2$	4-CF$_3$-C$_6$H$_4$	>50	>50	>50	>50

[a]The cytotoxicity GI_{50} values collected in the present table were calculated by cell viability assays and are defined as the concentrations corresponding to a 50% cell growth inhibition. The GI_{50} results are shown as the mean ± the standard deviation from independent cell viability assay experiments performed in quadruplicate.

According to the results presented in the Table 20, dialkyl tetrahydro-*5H*-indeno[2,1-*c*]quinolinylphosphonates **19** (entries 2-6), dialkyl *7H*-indeno[2,1-*c*]quinolinylphosphonates **20** (entries 7-10) and dialkyl 7-oxo-*7H*-indeno[2,1-*c*]quinolinylphosphonates **21** (entries 11-14) demonstrated on the whole a notable antiproliferative effect against the tested cancerous cell lines. Regarding A-549 lung cancer cell line, a pronounced cytotoxicity is generally observed for the tested compounds **19**/**20**/**21**, where almost all the tested compounds reported GI_{50} values below 10 μM. Contrarily, in SK-OV-3 (ovarian carcinoma) and HEK-293 (kidney embryonic) cell lines lower cytotoxicities were observed , including several compounds that reported GI_{50} values over 50 μM.

It should be highlighted the cytotoxic response of *7H*-indenoquinoline derivative **20a** (R = 4-P(O)(OEt)$_2$; R^1 = 3-MeO-C$_6$H$_4$; Table 20, entry 7), which presented GI_{50} values of 1.33 ± 0.22 μM

in A-549 cells and 9.79 ± 0.83 µM in SK-OV-3 cells; and the *7H*-indenoquinolinone derivative **21c** (R = 4-P(O)(OEt)$_2$; R^1 = 4-CF$_3$-C$_6$H$_4$; entry 13), which showed GI$_{50}$ values of 1.53 ± 0.28 µM in A-549 cell line and 4.55 ± 0.52 µM in SK-OV-3 cell line.

On the other hand, indenoquinoline derivatives **19**, **20** and **21** presented GI$_{50}$ values superior to 50 µM against MRC-5 non-malignant cells in all cases except for the *7H*-indenoquinolinone **21a** (R = 4-P(O)(OEt)$_2$; R^1 = 3-MeO-C$_6$H$_4$; entry 7), which exhibited a GI$_{50}$ of 39.68 ± 7.37 µM. These results indicate that the antiproliferative activity of indenoquinoline derivatives **19**, **20** and **21** is higher in cancer cell lines rather than in non-cancer cell lines.

In summary, the screening of the *in vitro* antiproliferative activity revealed that both families namely dialkyl quinolinylphosphonates (families **13**, **15** and **16**) and dialkyl (indeno[2,1-*c*]quinolinyl)phosphonates (families **19**, **20** and **21**) presented a promising antiproliterative activity in the micromolar range toward A-549 and SK-OV-3 human cancer cell lines, while the cytotoxic effect was not maintained against the MRC-5 non-malignant cell line. This difference in the biological response suggests a selective cytotoxicity toward human cancer cells as the antiproliferative effect resulted remarkably higher in cancer cell lines in comparison with non-cancer cells. Overall, the compounds exhibited a clear antiproliferative effect toward malignant cell lines (A-549 and SKOV-3) in a range of 1-50 µM, while non-cancer cells (MRC-5) were barely affected in the same concentration interval, as the vast majority of the tested compounds presented GI$_{50}$ values higher than 50 µM against MRC-5 cell line. If we compare the antiproliferative activity of the newly synthesized compounds **13**, **15**, **16**, **19**, **20** and **21** with the CPT, we can conclude that CPT presents a substantially higher antiproliferative activity (between 47.14-370 nM) but the novel phosphonate-substituted quinoline derivatives present a sort of selective cytotoxicity toward cancer cell lines over non-cancer cell lines.

III-4. Complementary antiproliferative studies to identify the lead compounds of the phosphonate-substituted quinoline and indenoquinoline families

Once analysed the results of the first screening of antiproliferative activity of the newly synthesized compounds, we concluded that we may focus in performing complementary antiproliferative experiments in order to elucidate the possible relationship between the TOP1 inhibitory activity (through a non-*poison*-like mode of action) and their anticancer activity.

Even the newly synthesized compounds (the vast majority) induce a meaningful antiproliferative activity in human cancer cell lines, there is not a clear correlation between the TOP1 inhibitory activity and their cytotoxicity in cancer cells. Furthermore, the compounds show a clear cytotoxic effect (in the micromolar range) against at least one of the cancer cell lines. These results may suggest that some other biological targets could be involved in the reported antiproliferative response against cancer cell lines of these phosphorated quinoline derivatives. In basis of these results, we oriented the next step of our research to study the behaviour of some selected compounds in more specific human cell lines to explore the relationship between the inhibition of TOP1 and the antiproliferative activity.

First, the lead compounds of the phosphonate-substituted quinoline derivatives (families of compounds **13**, **15**, **16**, **19**, **20** and **21**) were selected based on their biological results of TOP1 inhibitory activity and antiproliferative effect in human cancer cell lines. Thus, we selected the compounds **13a**, **13f**, **13j**, **13k**, **13s**, **13t**, **16c**, **16f**, **19a** and **20a** in order to continue the study of their antiproliferative activity in close relation with the TOP1 inhibitory activity and consequently, two kinds of experiments were designed.

On the one hand, we planned to test the compounds in a cell viability assay with RPMI-8402 (T-Acute Lymphoblastic Leukaemia human cancer cell line, T-ALL) and the CPT-resistant version thereof (CPT-K5), in order to investigate whether these non-*poison*-like TOP1 inhibitors affect the viability of a CPT (*poison*-like) resistant human cancer cell line.

Furthermore, in the previous section we purposely investigated the cytotoxicity in the human cell line HEK-293 (human embryonic kidney cells) as it is a widely used adherent human cell line to transfect and cell culture[288], which allows us a sequence-specific siRNA (small interfering RNA) induced post- transcriptional silencing of the gene expressing TOP1 by targeting specific mRNA

[288] Lin YC, Boone M, Meuris L, *et al.* Genome dynamics of the human embryonic kidney 293 lineage in response to cell biology manipulations. *Nat Commun*. 2014;5:4767. Published 2014 Sep 3. doi:10.1038/ncomms5767

and lead to a down-regulation of TOP1. We planned to perform a TOP1 knockdown, with the aim of comparing the antiproliferative activity of the selected compounds in HEK-293 cells and HEK-293 cells with down-regulated TOP1 expression.

III-4.1. Study of the antiproliferative activity in RPMI-8402 and CPT-K5 human cancer cell lines

CPT-K5 is a T-ALL (T-cell-derived acute lymphoblastic leukaemia) human malignant cell line expressing a mutant TOP1 (hTOP1B) resistant to CPT and CPT derivatives, whereas RPMI-8402 is its parental CPT sensitive T-ALL human cancerous cell line. The CPT-K5 cell line was originally developed by the long-term exposure of RPMI-8402 cells to increasing sublethal doses of CPT, resulting in a highly stable and CPT resistant mutant cancer-cell line due to chromosomal and/or genomic alterations[289].

Comparison of the antiproliferative activity against CPT-resistant CPT-K5 T-ALL cell line and its parental RPMI-8402 CPT sensitive cell line represents a rational and appropriate approach to identify novel hTOP1 inhibitors with antiproliferative activity that are not affected by the resistance to CPT (and derivatives). In this regard, *suppressor*-like hTOP1 inhibitors such as the newly synthesized phosphorated quinolines may have a different behaviour as they inhibit the TOP1 through a different mechanism of action.

We found a blank in the scientific literature regarding the evaluation of antiproliferative activity of suppressor-like hTOP1 inhibitors in CPT-resistant human cancer cell lines such as CPT-K5. Nevertheless, we consider highly convenient the screening of non-*poison*-like TOP1 inhibitors in both RPMI-8402 and CPT-K5, with a focus on the development of new TOP1 inhibitors bearing a potential advantage to overcome the CPT resistance derived from mutations that induce the expression of CPT-resistant TOP1.

Taking all the previous considerations into account, we carried out the evaluation of the *in vitro* cytotoxicity of the selected compounds (**13a**, **13f**, **13j**, **13k**, **13s**, **13t**, **13c**, **13f**, **19a** and **20a**) in RPMI-8402 (CPT-sensitive T-ALL) and CPT-K5 (CPT-resistant T-ALL) cell lines by using the PrestoBlue cell viability assay.

[289] Kjeldsen E, Nielsen CJF, Roy A, *et al.* Characterization of Camptothecin-induced Genomic Changes in the Camptothecin-resistant T-ALL-derived Cell Line CPT-K5. *Cancer Genom Proteom*. 2018;15(2):91-114. doi:10.21873/cgp.20068

Antiproliferative activity of CPT

We started the screening of the cytotoxic effect in RMPI-8402 and CPT-K5 human cancer cell lines by studying the behaviour of CPT in both cell lines. In this case, we used te PrestoBlue cell viability assay in order to assess the antiproliferative activity. RPMI-8402 and CPT-K5 are not adherent cell lines, contrarily they are suspension cell lines, so some minor modifications had to be introduced in the protocol apart from the use of PrestoBlue instead of CCK-8. For instance, the cells had to be centrifuged to replace the media (also when harvesting), a much higher amount of cells had to be harvested in the 96-well plates ($2 \cdot 10^4$-$4 \cdot 10^4$ cells/well) and it was not necessary to wait 24 h after plating the cells into the microplates. Moreover, the growth rates vary considerably between these two cell lines as RMPI-8402 was found to grow significantly faster, almost two times quicker than CPT-K5. In consequence, we had to employ a different amounts of cells per well in order to have a comparable response during the same experiment conditions.

With these concerns in mind, we plated $2 \cdot 10^4$ RPMI-8402 cells (in 100 µL of medium) per well and $4 \cdot 10^4$ CPT-K5 cells (in 100 µL of medium) per well into 96-well microplates and incubated the plates at 37°C, 5% CO_2 and 90% relative humidity for 1 h. Then, the drug treatment was carried out just by directly adding the CPT dissolutions in DMSO (to achieve the desired final concentrations of CPT in the well, in a concentration range from 100 µM to 1 nM), adjusting the final concentration of DMSO to 0.5% v/v in all wells, including the negative controls. An extra negative control without DMSO was included just to detect a possible cytotoxic effect of the solvent during the experiment conditions. Each concentration and control was tested four times in order to get four experiments per compound. After the drug treatment, 96-well plates were incubated for 48 h under the previous mentioned cell culture conditions (37°C, 5% CO_2 and 90% relative humidity) and subsequently 10 µL of PrestoBlue solution were added to each well. At this point, the plates were protected from the direct light (to avoid any loss of the fluorescence signal) and incubated for 30 mins at 37°C. The emitted fluorescence was measured by a fluorescence microplate reader (540 nm excitation/590 nm emission) and the obtained fluorescence values were further processed by GraphPad Prism software upon being normalized to the average fluorescence values of the DMSO-treated control cells. The experiments were performed in quadruplicate and the graphs obtained from the dose-response curves belonging to the cell viability *versus* the concentration/logarithmic concentration of CPT are shown in the Figure 72 (graphs **A** and **B**, respectively), along with the GI_{50} values obtained for each cell line (table **C**).

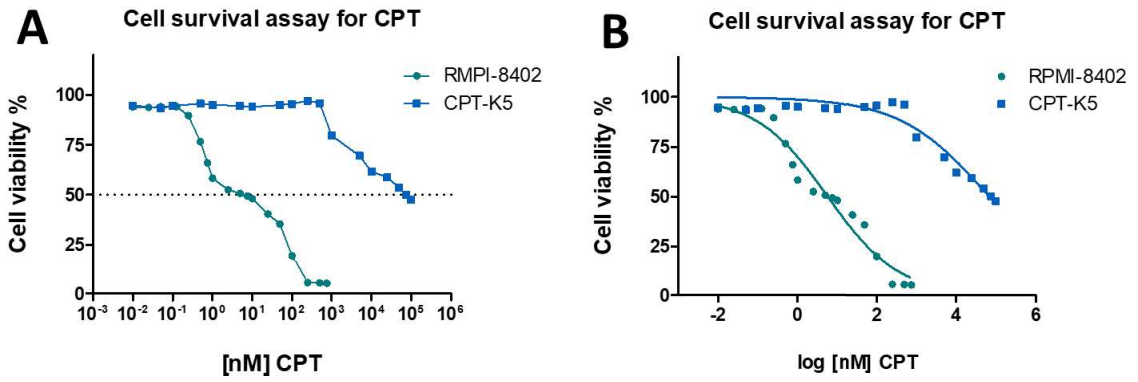

C

Compound	GI_{50} ± SD (µM)	
	RPMI-8402 (T-ALL)	CPT-K5 (CPT resistant)
CPT	$(5.74 \pm 0.16).10^{-3}$	65.67 ± 6.19

*Figure 72. Analysis of the cytotoxic effect of CPT in RPMI-8402 CPT-sensitive and CPT-K5 CPT-resistant human T-ALL cancer cell lines. **A**) Dose response curve of CPT corresponding to the cell viability measured by PrestoBlue assay versus the concentration of CPT. **B**) Dose response curve corresponding to the cell viability measured by PrestoBlue assay versus the logarithmic concentration of CPT. **C**) GI_{50} values calculated from the data represented in the graphs **A** and **B**.*

We obtained GI_{50} values of 5.74 ± 0.16 nM in RPMI-8402 cell line and 65.67 ± 6.19 µM in CPT-K5 cell line for CPT, demonstrating the strong resistance adquired by the CPT-K5 cell line. It is also noteworthy to mention that CPT showed a strong cytotoxic effect in the RPMI-8402 cell line, which resulted to be found as a highly sensitive cell line towards CPT.

Antiproliferative activity of selected compounds 13a, 13f, 13j, 13k, 13s, 13t, 16c, 16f, 19a and 20a

Once determined the cytotoxic activity of CPT, we moved on to investigate the antiproliferative activity of the previously selected compounds **13a**, **13f**, **13j**, **13k**, **13s**, **13t**, **16c**, **16f**, **19a** and **20a** in RPMI-8402 (CPT-sensitive) and CPT-K5 (CPT-resistant) T-ALL malignant cell lines. We started by evaluating the *in vitro* cytotoxicity of the tetrahydro-*5H*-indenoquinoline derivative **19a** by using the PrestoBlue cell viability assay, as previously expounded. The microplates were incubated for 48 h under standard cell culture conditions after drug treatment. After addition of the PrestoBlue reagent, the fluorescence values were measured and the obtained dose-response curves are presented in the Figure 73.

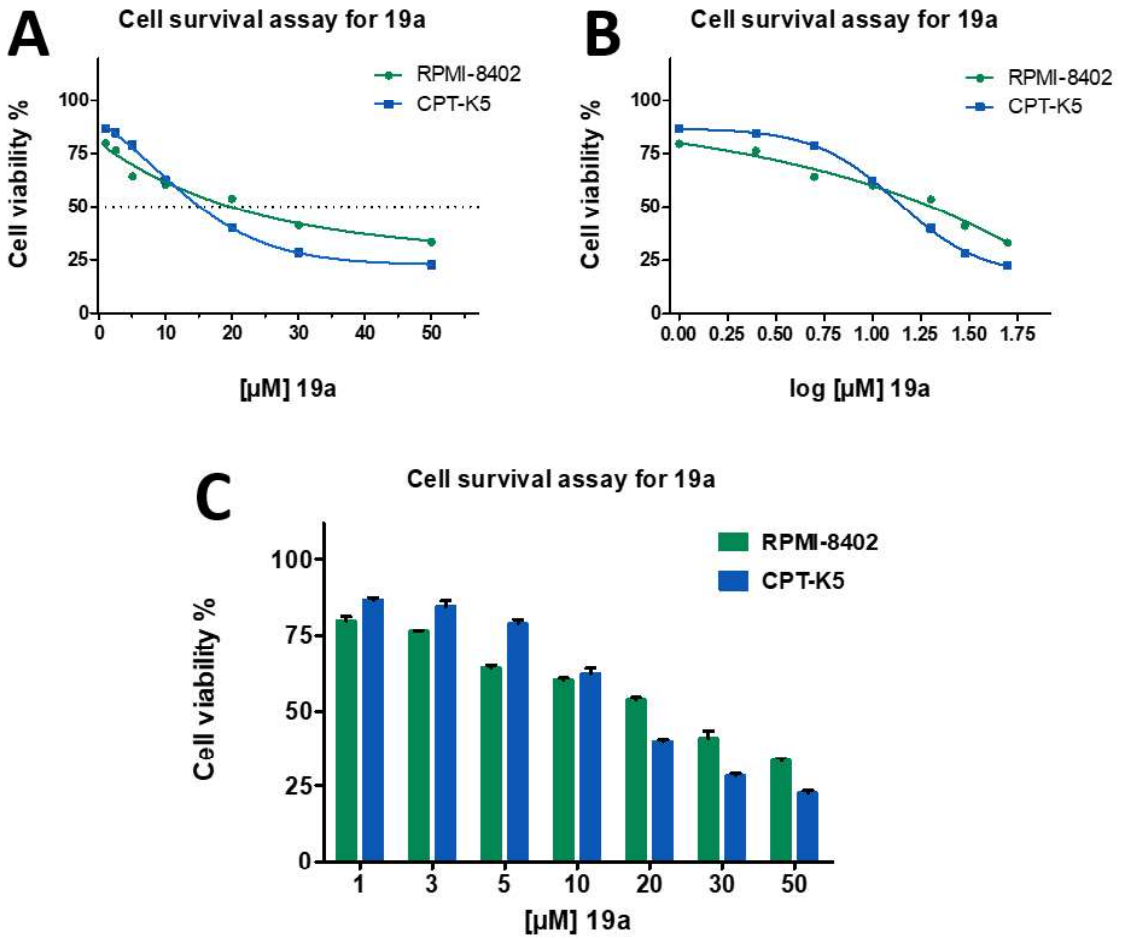

*Figure 73. Analysis of the cytotoxic effect of the compound **19a** in in RPMI-8402 and CPT-K5 T-ALL cancer cell lines **A**) Dose response curve corresponding to the cell viability versus the concentration of compound **19a**. **B**) Dose response curve corresponding to the cell viability versus the logarithmic concentration of **19a. C**) Column-bars graph comparing the cell viability rate of **19a** between the two cell lines at the tested concentrations.*

The GI_{50} values found for compound **19a** against RPMI-8402 and CPT-K5 were 20.31 ± 1.06 µM and 15.13 ± 0.72 µM respectively. These results indicate that compound **19a** possess a substantial cytotoxic effect against these T-ALL human cancer cell lines in the micromolar range, while the cytotoxicity effect of **19a** does not seem to be affected by the expression of a TOP1 resistant to CPT, what is more, the GI_{50} value of the compound **19a** is slightly lower in CPT-K5 cells than in RPMI-8402 cells.

Table 21. Antiproliferative activity of the selected compounds **13a**, **13f**, **13j**, **13k**, **13s**, **13t**, **16c**, **16f**, **19a** and **20a** in RPMI-8402 and CPT-K5 T-ALL cancer cell lines.

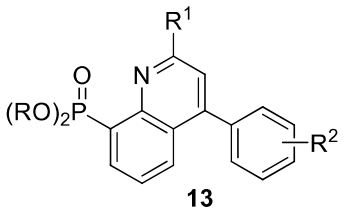

13

Entry	Compound				GI_{50} ± SD (μM)[a]	
	Nº	R	R^1	R^2	RPMI-8402 (T-ALL)	CPT-K5 (CPT resistant)
1	**CPT**	-	-	-	$(5.74 \pm 0.16)\cdot10^{-3}$	65.67 ± 6.19
2	**13a**	Et	C_6H_5	H	3.19 ± 0.21	12.27 ± 0.59
3	**13f**	Et	1-naphthyl	H	4.41 ± 0.27	11.83 ± 0.33
4	**13j**	Et	4-F-C_6H_4	4-Me	4.13 ± 0.13	21.58 ± 2.02
5	**13k**	Et	3,4-F_2-C_6H_4	4-Me	4.37 ± 0.40	31.53 ± 1.88
6	**13s**	^{i}Pr	4-F-C_6H_4	4-F	3.23 ± 0.69	19.19 ± 2.83
7	**13t**	^{i}Pr	3,4-F_2-C_6H_4	4-F	7.87 ± 0.57	16.85 ± 1.98

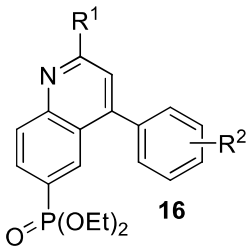

16

Entry	Compound			GI_{50} ± SD (μM)[a]	
	Nº	R^1	R^2	RPMI-8402 (T-ALL)	CPT-K5 (CPT resistant)
8	**16c**	4-F-C_6H_4	4-Me	2.19 ± 0.10	12.11 ± 0.53
9	**16f**	3.4-F_2-C_6H_4	4-F	5.18 ± 0.52	21.18 ± 1.13

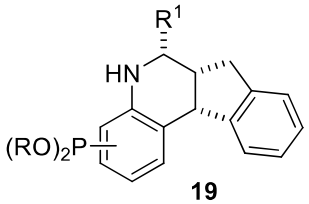

19

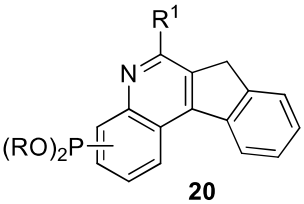

20

Entry	Compound			GI_{50} ± SD (μM)[a]	
	Nº	R^1	R^2	RPMI-8402 (T-ALL)	CPT-K5 (CPT resistant)
10	**19a**	4-P(O)(OEt)$_2$	3-MeO-C_6H_4	20.31 ± 1.06	15.13 ± 0.72
11	**20a**	4-P(O)(OEt)$_2$	3-MeO-C_6H_4	5.04 ± 0.58	12.07 ± 0.38

[a]The cytotoxicity GI_{50} values collected in the present table were calculated by cell viability assays and are defined as the concentrations corresponding to a 50% cell growth inhibition. The GI_{50} results are shown as the mean ± the standard deviation from independent cell viability assay experiments performed in quadruplicate.

Attending to the results collected in the Table 21, we can conclude that all the tested compounds (entries 2-11) showed GI_{50} values in the micromolar range (between 2.19-31.53 μM) against both RPMI-8402 and CPT-K5 cell lines.

In general, RPMI-8402 CPT-sensitive T-ALL cell line seems to be more sensitive toward the studied quinoline derivatives, since the GI_{50} values of RPMI-8402 (2.19-20.31 μM) are in all cases lower than the GI_{50} values obtained in CPT-K5 CPT-resistant cell lines (11.83-31.53 μM), except for the tetrahydro-*5H*-indenoquinoline derivative **19a** (R = 4-P(O)$(OEt)_2$; R^1 = 3-MeO-C_6H_4; Table 21, entry 10). Nevertheless, the cytotoxic activity of the tested compounds is overall maintained in both cell lines, despite the fact that CPT-K5 cells express a TOP1 resistant to CPT. In contrast to CPT, which was revealed as a highly potent antiproliferative agent in RPMI-8402 T-ALL cancer cell line (with a GI_{50} value of 5.74 nM), but loses the strong cytotoxic effect toward the parental CPT-K5 cells, due to a developed CPT resistance of the TOP1 expressed by CPT-K5 cell line.

III-4.2. Study of the antiproliferative activity in HEK-293 and HEK-293 TOP1 KD (TOP1 knockdown) human cancer cell lines

HEK-293 is not a cancer cell line, but presents some features that distinguish it from non-cancerous cell line models. HEK-293 is a human cell line derived from primary embryonic kidney cells transfected with human adenovirus type 5 DNA[290] and possess a complex karyotype. For instance, HEK-293 is described as a hypotriploid cell line, presents a modal chromosome number of 64, and induces tumour formation when injected in mice[291]. However, we consider HEK-293 a suitable cell model for our research for being a broadly used cell line for transfections in the field of cell biology as it possess a set of favourable attributes such as an easiness to grow and transfect and an efficient transfection and protein expression[292]. Hence, we outlined to test a selection of the phosphonate-substituted quinoline derivatives in HEK-293 cells and in HEK-293 cells upon knockdown of TOP1 (hTOP1B) induced by siRNA mediated gene silencing (namely HEK-293 TOP1 KD).

[290] Graham FL, Smiley J, Russell WC, Nairn R. Characteristics of a human cell line transformed by DNA from human adenovirus type 5. *J Gen Virol*. 1977;36(1):59-74. doi:10.1099/0022-1317-36-1-59

[291] Bylund L, Kytölä S, Lui WO, Larsson C, Weber G. Analysis of the cytogenetic stability of the human embryonal kidney cell line 293 by cytogenetic and STR profiling approaches. *Cytogenet Genom Res*. 2004;106(1):28-32. doi:10.1159/000078556

[292] Thomas P, Smart TG. HEK293 cell line: a vehicle for the expression of recombinant proteins. *J Pharmacol Toxicol Methods*. 2005;51(3):187-200. doi:10.1016/j.vascn.2004.08.014

siRNA mediated knockdown

To obtain the knockdown of TOP1 (*i.e.* a downregulation in the expression of the gene that encodes TOP1) in HEK-293 cells, we proceeded to induce a temporary gene silencing at the post-transcriptional level by specifically targeting the mRNA that codes TOP1 with a selective siRNA ($siRNA_{TOP1}$), just before the target mRNA is translated into TOP1 (hTOP1B)[293]. The proposed siRNA mediated gene silencing is not permanent as the genomic DNA is not modified. Consequently, the gene silencing results transient in case that the addition of $siRNA_{TOP1}$ and transfection supplements is not sustained. siRNAs are synthetic double stranded RNAi (interference RNA) molecules that enter the cells and produce a gene silencing mediated by the RISC (RNA induced silencing complex). A schematic overview of the process is depicted in the Figure 74.

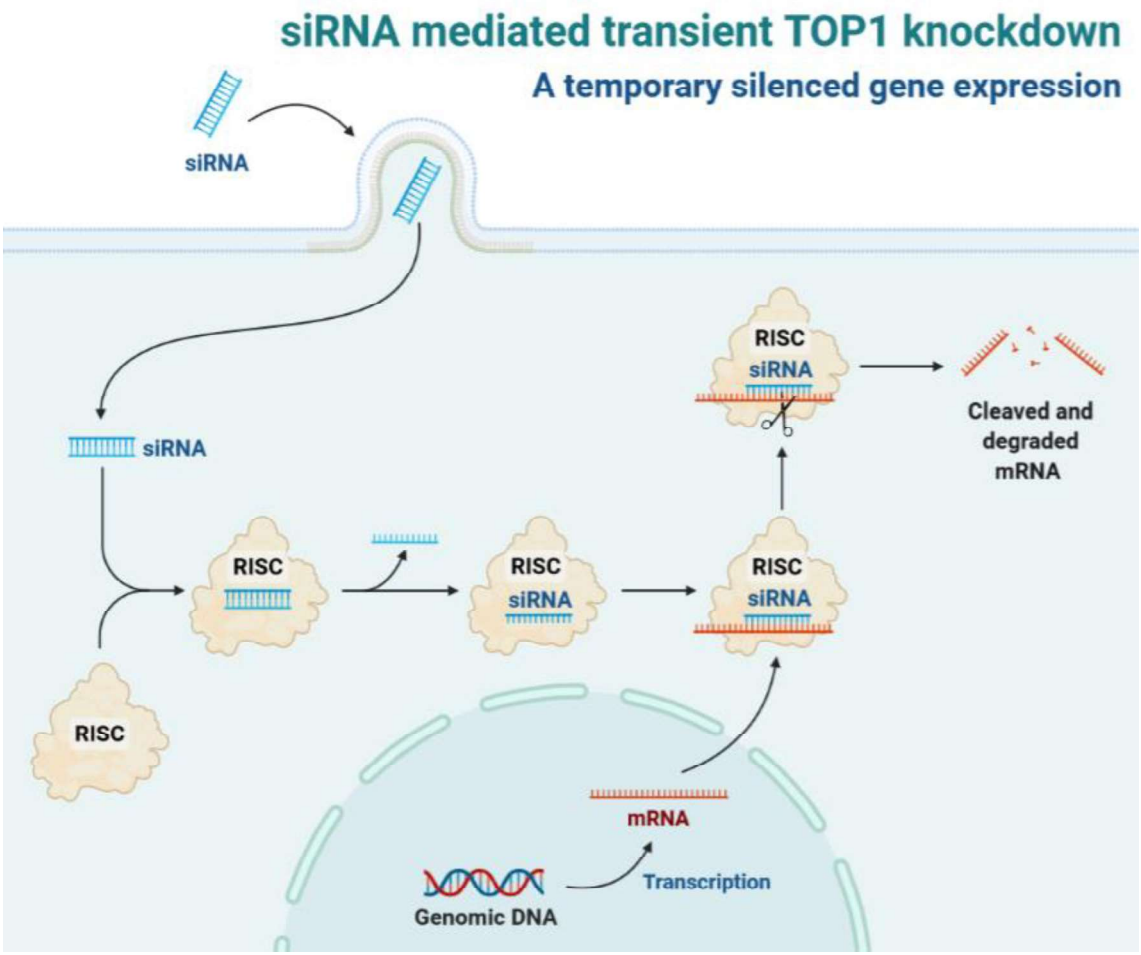

[293] Kjeldsen E, Tordrup D, Hübner GM, Knudsen BR, Andersen FF. Topoisomerase I deficiency results in chromosomal alterations in cervical cancer cells. *Anticancer Res*. 2010;30(9):3257-3265.

Figure 74. Schematic overview of a siRNA mediated knockdown, a temporary post-translational gene silencing method.

The siRNA enters into the cell and is recognized as an exogenous dsRNA. Consequently, the antiviral endoribonuclease DICER cleaves the ds siRNA and recruits other proteins to form the RISC. The RISC separates the ds siRNA into two RNA strands: a guide strand (also referred as antisense strand) and a passenger strand (also known as the sense strand). Then, the passenger strand is discarded, and the activated RISC remains holding the guide strand[294]. At this point, it has to be mentioned that the guide strand of siRNA is complementary to the target mRNA (in this case, the mRNA that is translated into a TOP1 molecule). Accordingly, when the transcribed mature mRNA leaves the nucleus, the RISC complex present in the cytoplasm locates the complementary sequence of the mRNA and associates the guide strand with it. Once the guide strand binds to its target mRNA, the mRNA is cleaved and degraded, leading to a downregulation of the protein expression[295] (TOP1 in this case).

Experimental procedure of siRNA transfection-mediated knockdown of TOP1 in HEK-293 cell line

In order to achieve the knockdown of TOP1, the HEK-293 cells were transfected with $siRNA_{TOP1}$ according to the lipofectamine transfection method. $7.5 \cdot 10^5$ HEK-293 cells were plated into a cell culture dish in complete growth medium without antibiotics and incubated under standard cell culture conditions (37°C, 5% CO_2 and 90% relative humidity). After 24 h of incubation, we proceeded to perform the transfection. 12 µL of 10 µM $siRNA_{TOP1}$ (the details of the protocols are provided in the experimental section) were mixed with 1 mL of Opti-MEM and 20 µL of lipofectamine RNAiMAX, and the mixture was incubated at room temperature for 15 min. The transfection mixture was added drop by drop to the cells while gently stirring the cell culture dish. The cells were incubated under standard cell culture conditions and after 48 h, $5 \cdot 10^6$ cells were harvested and re-suspended in complete growth medium in order to use them in the upcoming cell viability assays. Note that at this point a fraction of $1 \cdot 10^6$ cells was saved as a cell pellet and conserved at -80°C until the forthcoming western blot analysis (a checkpoint to ensure that the knockdown was developed successfully).

[294] Rana TM. Illuminating the silence: understanding the structure and function of small RNAs. *Nat Rev Mol Cell Biol*. 2007;8(1):23-36. doi:10.1038/nrm2085

[295] Back S, Manfredi JJ. Knockdown of Target Genes by siRNA In Vitro. *Methods Mol Biol*. 2021;2267:159-163. doi:10.1007/978-1-0716-1217-0_10

With the aim of ensure that the downregulation of TOP1 expression is due to a specific $siRNA_{TOP1}$ transfection, a scrambled control is used. For this purpose, we followed the same transfection protocol used for the knockdown of TOP1 except the use of scrambled siRNA instead of $siRNA_{TOP1}$. After harvesting the cells, we collected a pellet of $1 \cdot 10^6$ cells which was conserved at -80°C until western blot analysis.

Finally, we included a mock control in the absence of any siRNA. We followed the same transfection protocol used for the knockdown of TOP1 and the scramble control except for the fact that ddH_2O was added instead of any siRNA. After collecting the cells, we saved a cell pellet of $1 \cdot 10^6$ cell at -80°C until western blot analysis.

Western blot analysis of HEK-293 cells transfected with $siRNA_{TOP1}$, scrambled siRNA and mock control

The cell pellets collected after the transfection of HEK-293 cells with $siRNA_{TOP1}$, scrambled siRNA and mock control (just ddH_2O) were analysed by western blot (samples of $1 \cdot 10^6$ cells). The cell pellets were conserved at -80°C and they were defrosted on ice before cell extraction. Preparation of whole cell extracts was performed by mixing each cell pellet with 100 µM of lysis buffer. The samples containing the cells re-suspended with the lysis buffer were incubated for 15 min on ice before using them for the western blot.

Western blot analysis of HEK-293 cells transfected with $siRNA_{TOP1}$, scrambled siRNA and mock control (cell extracts) was developed by using anti-TOP1 antibody (to check the downregulation of the TOP1 expression) and anti-TBP (TATA binding protein) antibody (as a nuclear loading control that allows to ensure that nuclear proteins were successfully extracted during the cell-extraction stage). The result of the western blot analysis is shown in the Figure 75 (panel **A**, in the left side). Western blot analysis demonstrated that the TOP1 expression was downregulated only when $siRNA_{TOP1}$ was used, while scrambled siRNA did not induce any downregulation in the expression of TOP1, demonstrating that the $siRNA_{TOP1}$ mediated transfection induced a specific knockdown of TOP1.

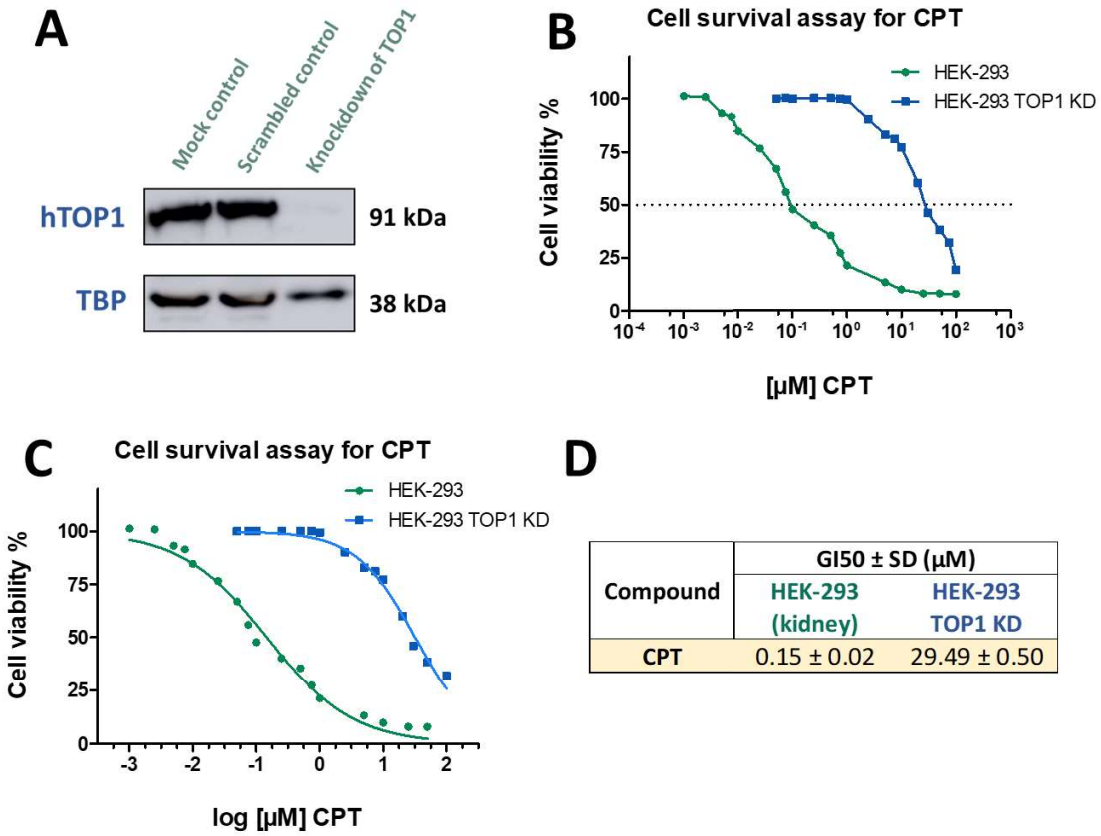

Compound	GI50 ± SD (µM)	
	HEK-293 (kidney)	HEK-293 TOP1 KD
CPT	0.15 ± 0.02	29.49 ± 0.50

Figure 75. Analysis of the cytotoxic effect of CPT in RPMI-8402, and CPT-K5 human cancer cell lines. **A**) Western blot analysis of whole cell extract from HEK-293 cells transfected with TOP1-specific-mRNA targeting siRNA (Knockdown of TOP1), scrambled non-specific siRNA (Scrambled control) or no siRNA –just ddH_2O- (Mock control). The western blot analysis was carried out using anti-hTOP1 and anti-TBP antibodies. **B**) Dose response curve of CPT corresponding to the cell viability versus the concentration of CPT. **C**) Dose response curve of CPT corresponding to the cell viability versus the logarithmic concentration of CPT. **D**) *GI_{50} values calculated from the data represented in the graphs **B** and **C**.*

Antiproliferative activity of CPT

We started the screening of the cytotoxic effect in HEK-293 and HEK-293 TOP1 KD (knockdown of TOP1) cells by exploring the cytotoxicity of CPT in both cell lines by the PrestoBlue cell viability assay. We followed the same protocol expounded in the section 4.1. of this chapter (*vide supra*), but plating $3 \cdot 10^3$ cells in 100 µL cell medium per well. PrestoBlue was added after incubation of 48 h since the drug treatment. The dose response curves obtained from these experiments are shown in the Figure 75 (graphs **B** and **C**), along with the GI_{50} values found for CPT in both HEK-293 cells and the HEK-293 cells upon TOP1 knockdown (0.15 ± 0.02 µM and 29.49 ± 0.50 µM respectively, presented in the Figure 75, table **D**). These results show that CPT reports a relatively powerful antiproliferative activity against HEK-293 cell line in the very low micromolar range, while the knockdown of TOP1 *via* $siRNA_{TOP1}$ transfection lead to a considerable reduction of the antiproliferative activity. Based on these results, we can conclude that a downregulation of TOP1 (the biological target of CPT) may induce a substantial loss in the cytotoxicity of CPT.

Antiproliferative activity of selected compounds 13a, 13f, 13j, 13k, 13s, 13t, 16c, 16f, 19a and 20a

We investigated how the selected compounds **13a**, **13f**, **13j**, **13k**, **13s**, **13t**, **16c**, **16f**, **19a** and **20a** affect to the cell proliferation of these two parented cell lines (HEK-293 and HEK-293 TOP1 KD). The cell viability assays were performed by using both CCK-8 and PrestoBlue cell viability assays as expounded before. We plated $3 \cdot 10^3$ cells in 100 µL cell medium per well and after 24 h of incubation, the cells were treated with different concentrations of the tested compounds (1-50 µM). The cells were incubated 48 h after the drug treatment, and CCK-8/PrestoBlue was added as indicated before. In the Figure 76, the dose-response curves and column bar graph corresponding to the compound **20a** are shown as an example.

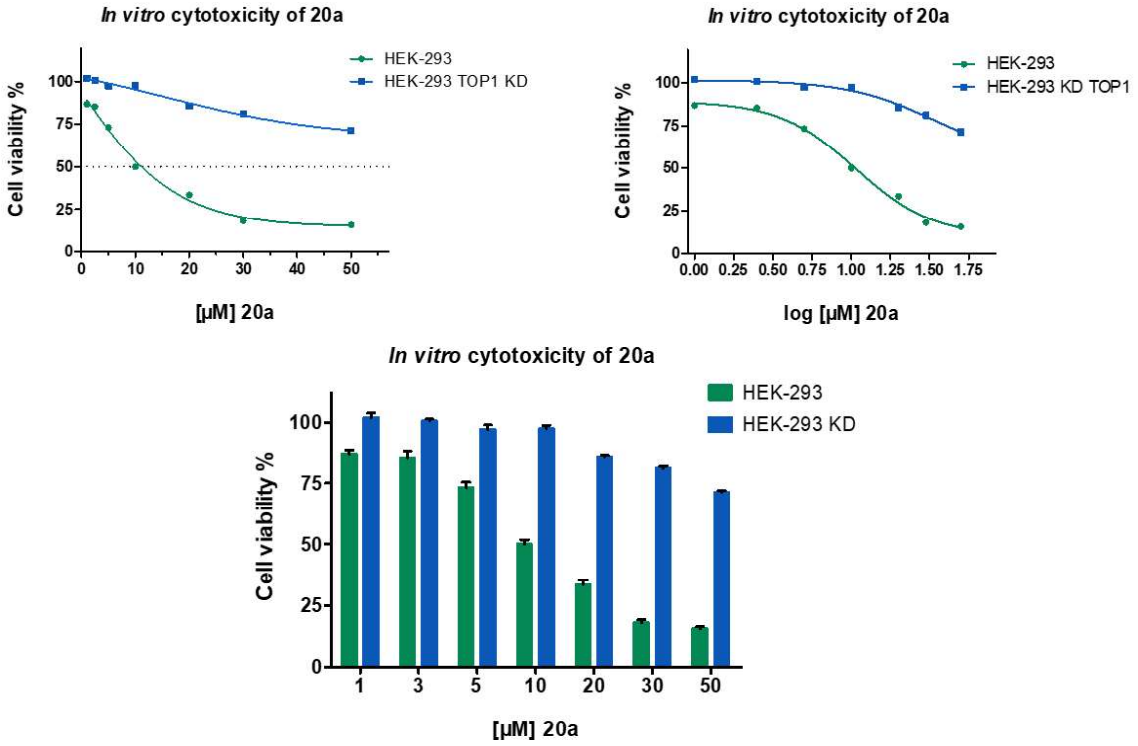

*Figure 76. Analysis of the cytotoxic effect of the compound **20a** in HEK-293 and HEK-293 TOP1 KD cell lines **A**) Dose response curve corresponding to the cell viability versus the concentration of compound **20a**. **B**) Dose response curve corresponding to the cell viability versus the logarithmic concentration of **20a**. **C**) Column-bars graph comparing the cell viability rate of **20a** between the two cell lines at the tested concentrations.*

Based on the curves shown in the Figure 76, GI_{50} values for compound **20a** were calculated. GI_{50} values of 11.15 ± 0.97 and >50 µM were found against HEK-293 and HEK-293 TOP1 KD respectively, which seems to imply a decrease in the antiproliferative activity of the compound **20a** upon downregulation of TOP1. The GI_{50} values of the compound **20a** are collected in the Table 22 along with the GI_{50} values of the other tested compounds.

Table 22. Antiproliferative activity of the selected compounds **13a**, **13f**, **13j**, **13k**, **13s**, **13t**, **16c**, **16f**, **19a** and **20a** in HEK-293 and HEK-293 TOP1 KD cell lines

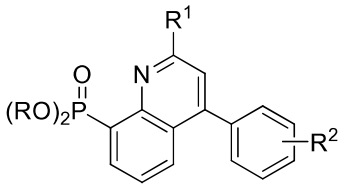

13

Entry	Compound				GI_{50} ± SD (μM)[a]	
					HEK-293	HEK-293
	Nº	R	R^1	R^2	(kidney)	TOP1 KD
1	**CPT**	-	-	-	0.15 ± 0.02	29.49 ± 0.50
2	**13a**	Et	C_6H_5	H	27.29 ± 2.22	48.12 ± 1.41
3	**13f**	Et	1-naphthyl	H	35.67 ± 3.13	32.30 ± 1.00
4	**13j**	Et	4-F-C_6H_4	4-Me	>50	>50
5	**13k**	Et	3,4-F_2-C_6H_4	4-Me	22.66 ± 1.36	>50
6	**13s**	^{i}Pr	4-F-C_6H_4	4-F	15.01 ± 0.99	>50
7	**13t**	^{i}Pr	3,4-F_2-C_6H_4	4-F	21.04 ± 4.05	>50

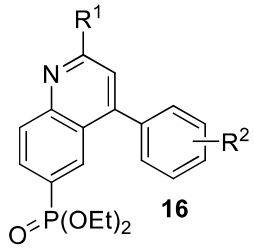

16

Entry	Compound			GI_{50} ± SD (μM)[a]	
				HEK-293	HEK-293
	Nº	R^1	R^2	(kidney)	TOP1 KD
8	**16c**	4-F-C_6H_4	4-Me	>50	12.11 ± 0.19
9	**16f**	3.4-F_2-C_6H_4	4-F	25.72 ± 6.34	36.44 ± 1.12

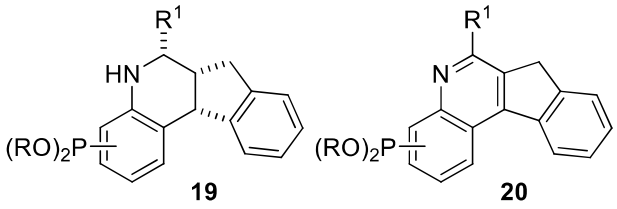

19 **20**

Entry	Compound			GI_{50} ± SD (μM)[a]	
				HEK-293	HEK-293
	Nº	R^1	R^2	(kidney)	TOP1 KD
10	**19a**	4-P(O)$(OEt)_2$	3-MeO-C_6H_4	>50	>50
11	**20a**	4-P(O)$(OEt)_2$	3-MeO-C_6H_4	11.80 ± 0.97	>50

[a]The cytotoxicity GI_{50} values collected in the present table were calculated by cell viability assays and are defined as the concentrations corresponding to a 50% cell growth inhibition. The GI_{50} results are shown as the mean ± the standard deviation from independent cell viability assay experiments performed in quadruplicate.

In first place, it has to be highlighted that CPT (poison-like TOP1 inhibitor) was found to be a much more potent antiproliferative agent toward HEK-293 (GI_{50} = 0.15 ± 0.02 μM) than the studied phosphorated quinoline derivatives (suppressor-like TOP1 inhibitors), and also presented a remarkable decrease in the cytotoxic effect upon knockdown of TOP1 (GI_{50} = 29.49 ± 0.50). In view of the results collected in the Table 22, we conclude that on balance, the antiproliferative activity of the tested compounds (entries 2-11) was reduced upon knockdown of TOP1, except for the compounds **13f** and **16c**, which reported a stronger cytotoxic effect toward HEK-293 KD TOP1 cells. The quinoline derivative **13f** (R = Et; R^1 = 1-naphthyl; R^2 = H; Table 22, entry 3) showed a GI_{50} value of 35.67 ± 3.13 μM in HEK-293 cells and 32.30 ± 1.00 μM in HEK-293 cells upon knockdown of TOP1; and the quinoline derivative **16c** (R^1 = 4-F-C_6H_4; R^2 = 4-Me; entry 8) reported GI_{50} values of >50 μM and 12.11 ± 0.19 μM in HEK-293 and HEK-293 upon TOP1 knockdown, respectively.

As said before, in most of the cases there was reported a notorious decrease of antiproliferative activity upon downregulation of TOP1. For instance, it is noteworthy the biological behaviour of compounds **13k** (R = Et; R^1 = 3,4-F_2-C_6H_4; R^2 = 4-Me; Table 22, entry 3), **13s** (R = ^{i}Pr; R^1 = 4-F-C_6H_4; R^2 = 4-F; entry 6), **13t** (R = ^{i}Pr; R^1 = 3,4-F_2-C_6H_4; R^2 = 4-F; entry 7) and **20a** (R = 4-P(O)$(OEt)_2$; R^1 = 3-MeO-C_6H_4; entry 11), reporting GI_{50} values in the range 11.80-22.66 μM in HEK-293 cells, whereas the GI_{50} values presented in HEK-293 cells upon TOP1 knockdown were over 50 μM. In particular, the compound **20a** showed the strongest antiproliferative effect against HEK-293 (GI_{50} = 11.80 ± 0.97 μM) while presented a GI_{50} value above 50 μM in HEK-293 upon knockdown of TOP1.

In conclusion, the obtained results suggest that the selected phosphonate-substituted quinoline derivatives **13a**, **13j**, **13k**, **13s**, **13t**, **16f**, **19a** and **20a**, which were previously reported as *suppressor*-like TOP1 inhibitors, demonstrated a biological response similar to the *poison*-like inhibitor CPT, presenting a stronger antiproliferative activity toward HEK-293 than in the TOP1 knockdown version thereof.

IV. *Addenda*: Study of the antileishmanial effect of phosphorated quinoline derivatives in *Leishmania infantum*: *in vitro/ex vivo* cytotoxicity in *L. infantum* parasites and *in vitro* inhibitory activity against *Leishmania* TOP1 (LTOP1)

IV-1. Introduction: leishmaniasis

Leishmaniasis is a vector-borne infectious disease caused by intracellular protozoan parasites of the genus *Leishmania*. It is transmitted by infected female *Phlebotomus* (in the Old World) and *Lutzomyia* (in the New World) sand flies (*Diptera* order, *Psychodidae* family, *Phlebotominae* subfamily) when feeding from the blood of vertebrates, and consequently, in addition to humans, other mammals are usually affected by infections with *Leishmania* parasites, being the dog the principal reservoir[296]. It has to be noted that this **addenda** will be exclusively focused on the human leishmaniasis (from now on, leishmaniasis will refer to human leishmaniasis).

The geographical distribution of leishmaniasis is closely related to the distribution of its vector and it generally occurs in the tropical and subtropical zones of America, east of Africa, the Mediterranean basin (particularly in the north of Africa) and the south-east Asia[297]. The global incidence of leishmaniasis has considerably decreased over the last decade but nowadays it is still considered a neglected tropical disease, affecting to about 12 million people globally. Leishmaniasis remains endemic in almost 100 countries and ~1 million new cases and 20.000-30.000 deaths per year are reported[298]. Nonetheless, since 2014 seven countries have reported the ~90% of the worldwide visceral leishmaniasis cases (the most severe and life threatening form of the disease): India, Brazil, Ethiopia, Sudan, South Sudan, Kenya and Somalia[296]. Leishmaniasis predominantly affects to developing countries with poor socioeconomic conditions and this fact critically hinders the prophylaxis, diagnosis and the access to the pharmacological treatment, compromising the outcome of the disease. Moreover, the detection and treatment of the leishmaniasis (specially visceral leishmaniasis) co-infection with HIV supposes a major challenge as the available drug-spectrum to treat leishmaniasis is reduced and potentially causes severe side-effects, resulting in an increase of the lethality in HIV-seropositive immunocompromised patients.

IV-1.1. Parasites from *Leishmania* species: the ethiological agent of leishmaniasis

Leishmania is a eukaryotic unicellular organism belonging to the subkingdom of Protozoa and the Kinetoplastida order. The main feature of kinetoplastids is the presence of a highly

[296] Burza S, Croft SL, Boelaert M. Leishmaniasis. *Lancet*. 2018;392(10151):951-970. doi:10.1016/S0140-6736(18)31204-2

[297] Sharma U, Singh S. Insect vectors of Leishmania: distribution, physiology and their control [retracted in: *J Vector Borne Dis*. 2012;49(1):54]. *J Vector Borne Dis*. 2008;45(4):255-272

[298] Ruiz-Postigo JA, Jain S, Mikhailov A, *et al.* Global leishmaniasis surveillance: 2019–2020, a baseline for the 2030 roadmap. *Wkly Epidemiol Rec*. 2021;35:401–420

condensed and large massed mitochondrial DNA called kinetoplast (hence the name) associated with the cell flagellum. At present, there are 53 identified species of *Leishmania* parasites from which 21 are pathogenic for humans[299]. The *Leishmania* species causing human leishmaniasis are collected in the Figure 77 (*L. infantum* and *L. donovani* species are highlighted in red for being the principal ethiological agents causing visceral leishmaniasis).

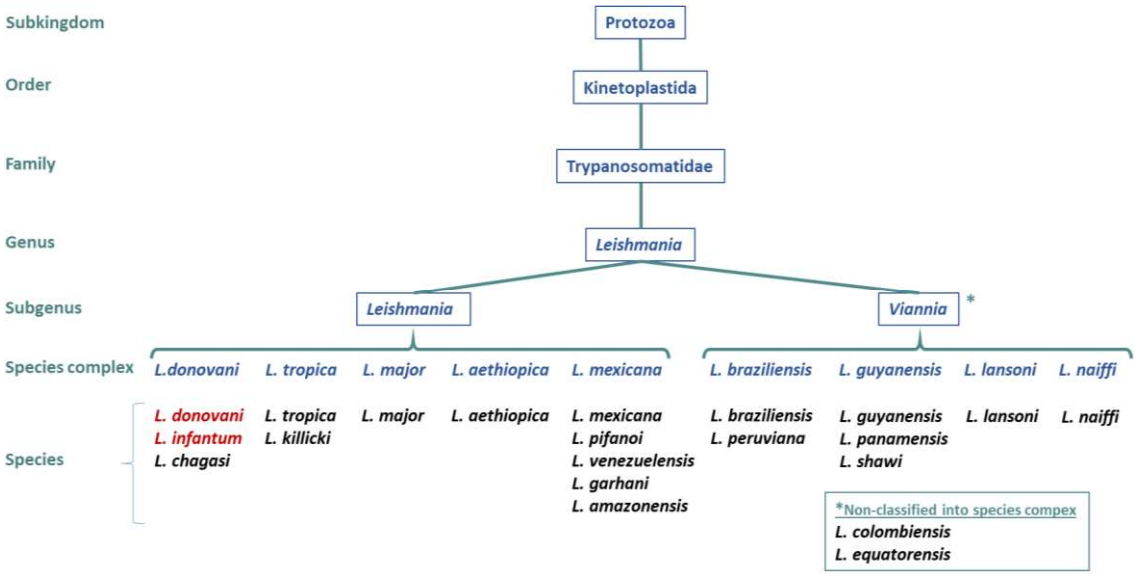

Figure 77. Taxonomical classification of Leishmania parasites causing leishmaniasis in humans.

All the members of *Leishmania* genus are parasites of vertebrates and need a phlebotomine vector to infect the host. Currently, *Leishmania* genus is divided into three subgenders, namely *Leishmania*, *Viannia* and *Sauroleishmania*, but only two of them (*Leishmania* and *Viannia* subgenders) affect to mammals[300]. Consequently, *Sauroleismania* has not been included in the Figure 78 for being selectively related to reptilians. *Leishmania* and *Viannia* subgenders differ on their location in the intestine of the phlebotomine vector (*Leishmania* species mature in the midgut and foregut, while *Viannia* species mature in the hindgut)[301].

Leishmania and *Viannia* species were initially classified based on geographical or clinical features[299], however, they were further grouped into species complexes based on isoenzyme

[299] Akhoundi M, Kuhls K, Cannet A, *et al.* A Historical Overview of the Classification, Evolution, and Dispersion of Leishmania Parasites and Sandflies. *PLoS Negl Trop Dis*. 2016;10(3):e0004349. doi:10.1371/journal.pntd.0004349

[300] Akhoundi M, Downing T, Votýpka J, *et al.* Leishmania infections: Molecular targets and diagnosis. *Mol Aspects Med*. 2017;57:1-29. doi:10.1016/j.mam.2016.11.012

[301] a) Lainson R, Ryan L, Shaw JJ. Infective stages of Leishmania in the sandfly vector and some observations on the mechanism of transmission. *Mem Inst Oswaldo Cruz*. 1987;82(3):421-424. doi:10.1590/s0074-02761987000300015. b) Bates PA. Transmission of Leishmania metacyclic promastigotes by phlebotomine sand flies. *Int J Parasitol*. 2007;37(10):1097-1106. doi:10.1016/j.ijpara.2007.04.003

analysis[302]. This fact leads to the preparation of reliable taxonomic schemes and allowed a classification based on the immunological, biochemical and genetic criteria, maintaining the name that refers to the endemic geographical location.

Forms and life-cycle of Leishmania parasites

The form and morphology of *Leishmania* parasites is determined by its life cycle, which is a complex digenetic cycle involving an alternation between a mammalian host (human in this case) and a phlebotomine sand fly vector[300]. A schematic representation of the *Leishmania* life-cycle is depicted in the Figure 78 (being the host a human).

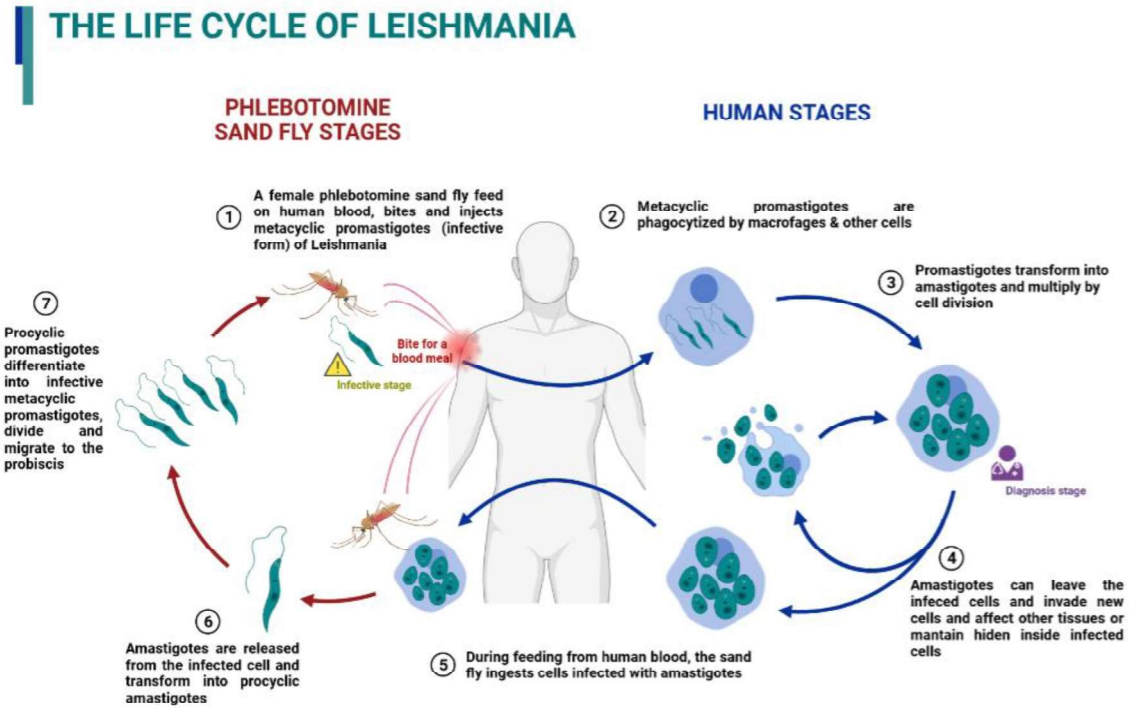

Figure 78. The life cycle of Leishmania

In the sand fly vector, the parasites are exposed to an extracellular environment and hence present a promastigote form, which is the extracellular motile form of *Leishamania* parasites bearing a long flagellum. At the very first stages, *Leishmania* parasites inhabit inside the sand fly vector in a procyclic promastigote form, which is a replicative and non-infective form with reduced motility. Then, procyclic promastigotes replicate and differentiate into metacyclic promastigotes in the intestine of the sand fly[297]. Metacyclic promastigotes are strongly motile

[302] Rioux JA, Lanotte G, Serres E, Pratlong F, Bastien P, Perieres J. Taxonomy of Leishmania. Use of isoenzymes. Suggestions for a new classification. *Ann Parasitol Hum Comp*. 1990;65(3):111-125. doi:10.1051/parasite/1990653111

and represent the infective form of *Leishmania* parasites. Accordingly, mature metacyclic promastigotes migrate to the proboscis of the sand fly and they get already prepared to infect a vertebrate host (a human, in this case)[303].

Metacyclic promastigotes are introduced into the skin of the host by the bite of a female phlebotomine sand fly when feeding from human blood (Figure 78, Stage **1**)[301b]. The *Leishmania* promastigotes are phagocytized by macrophages or other phagocytes (*e.g.* granulocytes) and are subsequently transformed into amastigotes (stage **2**). Amastigotes represent the intracellular oval and non-motile form of *Leishmania* parasites (the flagellum is very short, only visible under electron microscopy), and amastigotes multiply by simple cell-division inside the phagolysosomes of the phagocytes (stage **3**)[304]. At this point, intracellular amastigotes can be maintained hidden inside the infected cells, or they can leave the cells (usually by cell lysis) and infect other cells and tissues (stage **4**). Then, during feeding from human blood, the phlebotomine sand fly ingests the cells infected with amastigotes (stage **5**) and amastigotes are transformed into extracellular metacyclic promastigotes in the intestine of the sand fly (stage **6**)[297]. As expounded before, metacyclic promastigotes replicate and differentiate into infective procyclic promastigotes in the intestine of the sand fly and finally migrate to the proboscis (stage **7**), getting ready to restart the cycle by infecting a new host.

IV-1.2. Clinical forms of leishmaniasis

The infection with *Leishmania* parasites can range from asymptomatic to severe and accordingly, the development of the leismaniasis disease can be presented in two major forms: visceral leishmaniasis (VL) and cutaneous leishmaniasis (CL). The development into one clinical form or the other is determined by the *Leishmania* species (*e.g. L. donovani* and *L. infantum* are the principal species causing VL), the host-parasite interaction and the immune response of the host.

[303] Giraud E, Martin O, Yakob L, Rogers M. Quantifying *Leishmania* Metacyclic Promastigotes from Individual Sandfly Bites Reveals the Efficiency of Vector Transmission. *Commun Biol*. 2019;2:84. doi:10.1038/s42003-019-0323-8

[304] Handman E, Bullen DV. Interaction of Leishmania with the host macrophage. *Trends Parasitol*. 2002;18(8):332-334. doi:10.1016/s1471-4922(02)02352-8

Visceral leishmaniasis (VL or kala-azar)

VL is the most severe and life-threatening clinical form of leishmaniasis and is highly lethal without treatment (95% of mortality in untreated patients) [305]. In VL, the infected host cells full of amastigotes burst and the amastigotes are released in the bloodstream, reaching the cells of the reticuloendothelial system (*i.e.* lymph nodes, bone narrow, spleen, liver, intestine and the lungs) and invading the phagocytic cells thereof[306]. The size of the infected visceral organs is considerably increased (hence the name) and both anaemia and leukopenia appear from early stages of the disease.

Cutaneous leishmaniasis (CL)

CL is the mildest and most common clinical form of leishmaniasis, which principally causes ulcers in the skin that usually self-heal after 2-20 months, but sometimes leads to scarring and/or disfigurement of the affected tissue[307]. In CL, *Leishmania* parasites infect phagocytes located in the skin and when infected cells burst, the released amastigotes infect nearby skin-cells[308]. The outcome of CL is generally non-complicated and ulcers self-cure in the 90% of the cases (however, it causes lesions in exposed areas of the skin), but in some cases CL involves into more serious clinical manifestations as disseminated cutaneous leishmaniasis (DCL) mucocutaneous leishmaniasis (MCL) and localised cutaneous leishmaniasis (LCL) that cause deep ulcers, disfigurements and other complicated lesions in the skin[307].

IV-1.3. Treatment of leishmaniasis

IV-1.3.1. Current chemotherapy in leishmaniasis

The main strategy of chemotherapeutic drugs is based on inducing a selective damage in *Leishmania* cells and thereby causing the death of the parasite. Chemotherapy against leishmaniasis (visceral/cutaneous) comprises the use of antileishmanial drugs alone or in combinations. The choice of the pharmacological treatment cannot be always done in basis of

[305] Roatt BM, de Oliveira Cardoso JM, De Brito RCF, Coura-Vital W, de Oliveira Aguiar-Soares RD, Reis AB. Recent advances and new strategies on leishmaniasis treatment. *Appl Microbiol Biotechnol*. 2020;104(21):8965-8977. doi:10.1007/s00253-020-10856-w

[306] van Griensven J, Diro E. Visceral Leishmaniasis: Recent Advances in Diagnostics and Treatment Regimens. *Infect Dis Clin North Am*. 2019;33(1):79-99. doi:10.1016/j.idc.2018.10.005

[307] Novais FO, Amorim CF, Scott P. Host-Directed Therapies for Cutaneous Leishmaniasis. *Front Immunol*. 2021;12:660183. doi:10.3389/fimmu.2021.660183

[308] Gurel MS, Tekin B, Uzun S. Cutaneous leishmaniasis: A great imitator. *Clin Dermatol*. 2020;38(2):140-151. doi:10.1016/j.clindermatol.2019.10.008

the most effective therapeutic options, as patients are usually constrained by socioeconomic limitations. Moreover, the repeated use of the same drugs during ages has induced the appearance of drug resistance, so the pharmacotherapy guidelines vary from country to country[296]. Herein are collected the principal drugs used in leishmaniasis chemotherapy.

Sb(V) complexes

Sb(V) Pentavalent antimony complexes are a class of antileishmanial drugs that have been employed as a first-line treatment for more than 50 years. Initially, Sb(III) complexes were found to be potent antileismanial agents but their high toxicity impeded their therapeutic use. Nonetheless, Sb(III) complexes led to the preparation of highly stable Sb(V) complexes that overcome the clinical limitations of their predecessors[309]. Accordingly, pentavalent antimonials (as meglumine antimoniate **1** and sodium stibogluconate **2**, depicted in the Figure 79) are prodrugs that require an *in vivo* bioactivation by oxidizing the stable Sb(V) form to the active Sb(III) form. Despite the fact that pentavalent antimonials have been used as antileishmanial agents for almost 8 decades, their mechanism of action is not certainly clear. It seems like the mode of action of Sb(V) complexes relies in the selective intracellular accumulation of Sb(III)[310] that interferes in the cell metabolism of *Leishmania* parasites. In particular, pentavalent antimonials were found to inhibit the tripanothione reductase and related glycolytic enzymes, leading to a detrimental effect in the oxidation of fatty acids and the formation of ATP/GTP[311]. Moreover, Sb(V) antileishmanial drugs have reported an inhibitory effect toward the leishmanial TOP1, which induces the cell death of the parasite[312].

Parenteral pentavalent antimonials (meglumine antimoniate and sodium stibogluconate) are still the first-line drugs for the treatment of all forms of leishmaniasis in developing countries. Despite having largely improved the limitations of Sb(III) predecessors in terms of toxicity and safety in the pharmacokinetic (PK) profile, pentavalent antimonial-based clinical therapy usually presents local sharp pain in the injection zone and life-threatening side effects (cardiotoxicity,

[309] Fernandes FR, Ferreira WA, Campos MA, *et al.* Amphiphilic Antimony(V) Complexes for Oral Treatment of Visceral Leishmaniasis. *Antimicrob Agents Chemother*. 2013;57(9):4229-4236. doi: 10.1128/AAC.00639-13

[310] Frézard F, Monte-Neto R, Reis PG. Antimony transport mechanisms in resistant leishmania parasites. *Biophys Rev*. 2014;6(1):119-132. doi:10.1007/s12551-013-0134-y

[311] Haldar AK, Sen P, Roy S. Use of antimony in the treatment of leishmaniasis: current status and future directions. *Mol Biol Int*. 2011;2011:571242. doi:10.4061/2011/571242

[312] Chakraborty AK, Majumder HK. Mode of action of pentavalent antimonials: Specific inhibition of type I DNA topoisomerase of leishmaniadonovani. *Biochem Biophys Res Commun*. 1988;152(2):605-611. doi: https://doi.org/10.1016/S0006-291X(88)80081-0

hepatotoxicity, pancreatitis, abdominal colic, vomiting, severe diarrhea etc.)[309] that require medical monitoring of the patients.

Amphotericin B

Amphotericin B (AmB) **3** (Figure 79) is a broad-spectrum antifungal drug that acts by selectively binding to ergosterol in the photogenic cell membranes and generates changes in the cell membrane permeability[313] (including methabolic shock), leading to cell death of *Leishmania* parasites.

Once administered, AmB presents a slow elimination-rate as it is not metabolyzed in the liver, and furthermore AmB is subject of many drug-drug interactions. Nevertheless, AmB is still considered an essential antileishmanial drug and consequently alternative strategies have been investigated to improve its PK profile. In this regard, the development of a liposomal preparation of amphotericin B (LAmB) in the 1990´s provided an effective antileishmanial drug formulation with a much better safety profile[314]. Nowadays, both forms of AmB are used in clinics to treat leishmaniasis by intravenous administration, namely AmB (formulated as AmB deoxycholate) and LAmB, as LAmB is not always affordable for the patients from countries where leishmaniasis is endemic[296].

Miltefosine

Miltefosine (**4**, Figure 79) belongs to the drug class called APLs (alkylphospholipids), which are currently applied to anticancer drug discovery (namely anticancer lipids), but also present a remarkable antileishmanial activity[315]. Synthetic APLs are analogues of phospholipids that do not target DNA, they directly act at the cell membrane level instead, and in particular, miltefosine is an alkylphosphocholine that acts as an analogue of phosphatidylcholine (a major cell membrane constituent of *Leishmania* species)[316]. The mode of action for the antileishmanial effect of miltefosine is not well understood. It is known that miltefosine inhibits the synthesis of

[313] Baginski M, Czub J. Amphotericin B and its new derivatives - mode of action. *Curr Drug Metab*. 2009;10(5):459-469. doi:10.2174/138920009788898019

[314] Stone NR, Bicanic T, Salim R, Hope W. Liposomal Amphotericin B (AmBisome(®)): A Review of the Pharmacokinetics, Pharmacodynamics, Clinical Experience and Future Directions. *Drugs*. 2016;76(4):485-500. doi:10.1007/s40265-016-0538-7

[315] Ríos-Marco P, Marco C, Gálvez X, Jiménez-López JM, Carrasco MP. Alkylphospholipids: An update on molecular mechanisms and clinical relevance. *Biochim Biophys Acta Biomembr*. 2017;1859(9 Pt B):1657-1667. doi:10.1016/j.bbamem.2017.02.016

[316] Zulueta Díaz YLM, Ambroggio EE, Fanani ML. Miltefosine inhibits the membrane remodeling caused by phospholipase action by changing membrane physical properties. *Biochim Biophys Acta Biomembr*. 2020;1862(10):183407. doi:10.1016/j.bbamem.2020.183407

phosphatidylcholine, interfering with the lipid metabolism and therefore affecting the membrane remodelling[315]. Moreover, it is reported that miltefosine also induces the inhibition of the cytochrome C oxidase, altering the mitochondrial response[317]. Nonetheless, it seems that there may be some other targets involved in the antileishmanial effect of miltefosine.

At present, miltefosine is the most effective APL both in *Leishmania* amastigotes and in promastigotes. Furthermore, miltefosine has been the first oral antileishmanial agent. It was introduced in 2002, and up to now is still being the unique oral antileishmanial drug accepted by the FDA for the treatment of visceral and cutaneous leishmaniasis[296] (the rest of antileishmanial drugs are administrated intravenously by an initial load dosage and subsequent maintenance administrations).

Paromomycin

Paromomycin (**5**, Figure 79) is a wide spectrum aminoglycoside antibiotic that has revealed as an effective antimalarial agent, even though its mode of action is largely unclear. As an aminoglycoside antibiotic, paromomycin specifically binds to the 30s ribosomal subunit and therefore stabilizes the ribosomal complex, leading to a blockade in the protein translocation step. Hence, some authors claim that the antileishmanial effect may be related with the inhibition of the protein synthesis[318]. Conversely, other authors suggest that the cationic paromomycin acts by binding to anionic components of the leishmanial cell membrane (*i.e.* glycocalix and lipophosphoglycan), leading to a fatal cell membrane alteration[319]. Paromomycin is clinically used by intravenous administration in both visceral and cutaneous leishmaniasis since 2006 and, in some cases, it is topically administered to treat cutaneous leishmaniasis[296].

Pentamidine

Pentamidine (**6**, Figure 79) is an antimicrobial agent employed in the treatment of leishmaniasis. The mode of action of pentamidine relies on a selective intracellular accumulation in *Leishmania*

[317] Santa-Rita RM, Henriques-Pons A, Barbosa HS, de Castro SL. Effect of the lysophospholipid analogues edelfosine, ilmofosine and miltefosine against Leishmania amazonensis. *J Antimicrob Chemother*. 2004;54(4):704-710. doi:10.1093/jac/dkh380

[318] Davidson RN, den Boer M, Ritmeijer K. Paromomycin. *Trans R Soc Trop Med Hyg*. 2009;103(7):653-660. doi:10.1016/j.trstmh.2008.09.008

[319] Chawla B, Jhingran A, Panigrahi A, Stuart KD, Madhubala R. Paromomycin affects translation and vesicle-mediated trafficking as revealed by proteomics of paromomycin -susceptible -resistant Leishmania donovani. *PLoS One*. 2011;6(10):e26660. doi:10.1371/journal.pone.0026660

cells and proceeds by selectively binding to the kinetoplast DNA, resulting in the inhibition of the DNA synthesis[320].

Pentamidine is currently used as a second-line drug in both visceral and cutaneous leishmaniasis due to the reported elevated toxicity. In this regard, the pharmacological treatment with pentamidine could be accompanied by gastrointestinal toxicity, cardiotoxicity and the induction of irreversible insulin-dependent diabetes mellitus[321].

[320] Singh K, Garg G, Ali V. Current Therapeutics, Their Problems and Thiol Metabolism as Potential Drug Targets in Leishmaniasis. *Curr Drug Metab*. 2016;17(9):897-919. doi:10.2174/1389200217666160819161444

[321] Scholar E. Pentamidine. In: Enna SJ, Bylund DB, eds. *xPharm: The comprehensive pharmacology reference.* New York: Elsevier; 2009:1-7. https://doi.org/10.1016/B978-008055232-3.62388-8

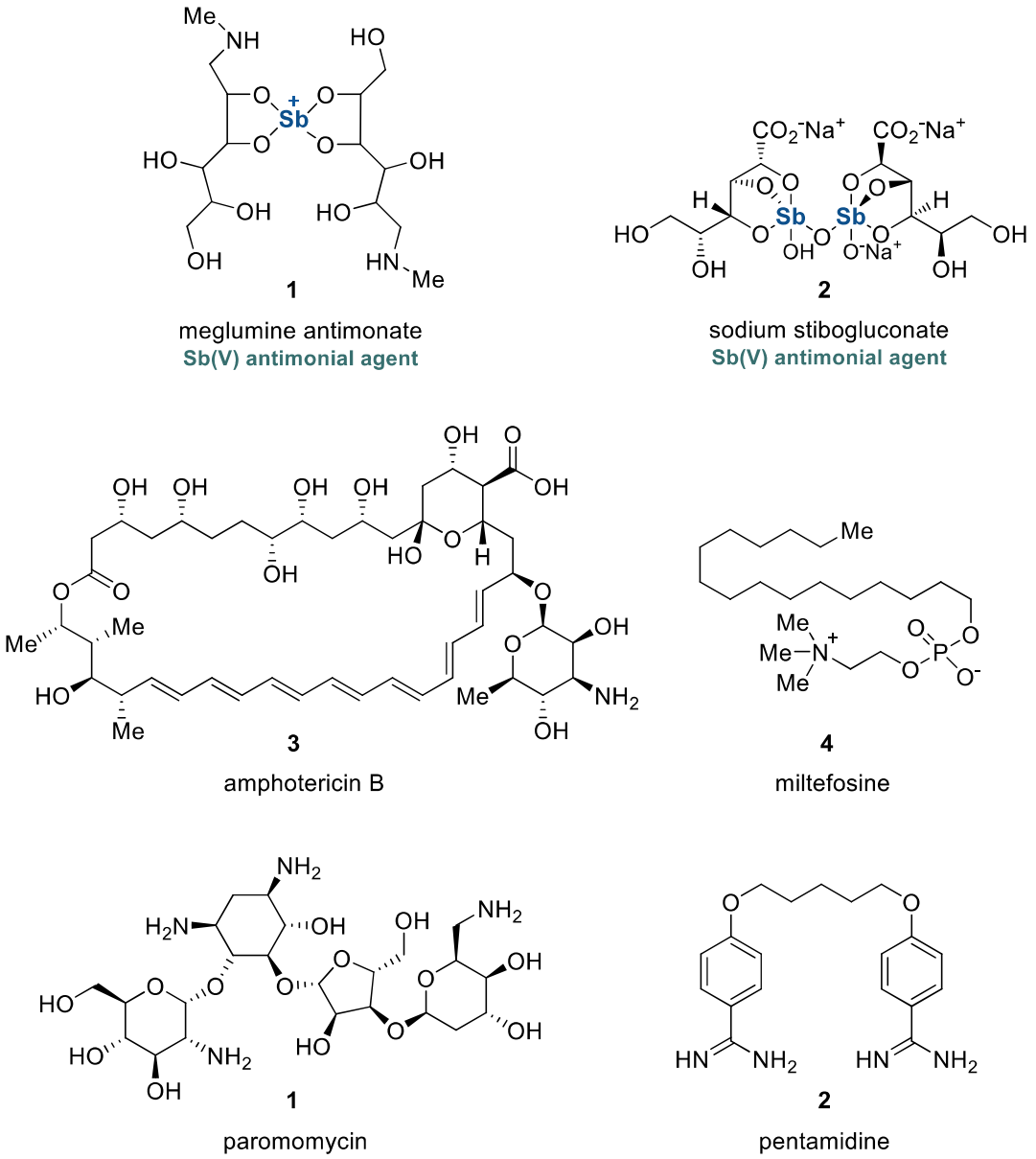

Figure 79. Structures of principal drugs currently used in chemotherapy of leishmaniasis.

IV-1.3.2. Immunotherapy for the treatment of leishmaniasis

The immune response of the host to *Leishm*ania intracelular infection results quite complex and its efficacy is determined by the species and strains of *Leishmania* parasites, the host-parasite interaction and both innate and adaptive immunities of the host.

Regarding to the immune response, it has to be considered that *Leishmania* parasites have developed systematic resistance toward the immune system of the host. Hence, macrophages, dendritic cells and neutrophils are essentially the phagocytes implicated in the cellular uptake of *Leishmania* metacyclic promastigotes in the very first stage of the infection, and consequently, *Leishmania* parasites have adapted to survive and evade the immune system once

infected the phagocytes[322]. For instance, *L. donovani* has been found to inhibit the apoptosis of macrophages upon cellular uptake by stimulating the production of GM-CSF (granulocyte-macrophage colony-stimulating factor, a cytokine that slows down the induced apoptosis of macrophages) and TNF-α (tumour necrotic factor α, an inflammatory cytokine that can block the apoptosis of macrophages)[323], whereas TNF-α presents the contrary effect (stimulating apoptosis) in polimorphonuclear granulocytes such as neutrophils[324]. On the other hand, it has to be mentioned that *Leishmania* seems to use different pathways to induce apoptosis of PAM and in the case of neutrophils, *L. major* promastigotes have been reported to inhibit the apoptosis of neutrophils by blocking the caspase 3 pathway[325].

As usually occurs with infections, when *Leishmania* parasites enters in the phagocytes of the host, dendritic cells (DCs) emerge to initiate and regulate the adaptive immune response toward the *Leishmania* infection. DCs play a key role in the modulation of the adaptive immunity in leishmaniasis and influence the ability of the host T cells to produce IFN-γ (interferon gamma)[326]. IFN-γ is an essential cytokine that promotes the production of nitric oxide (NO) and reactive oxygen species (ROS), leading to the activation of macrophages, which turn able to kill the intracellular *Leishmania* parasites[327]. For instance, the treatment with human recombinant IFN-γ has reported to induce the macrophage activation and improve the outcome of *Leishmania* alone[328] and (specially) as adjuvant of chemotherapy drugs[322].

The outcome of *Leishmania* infection depends to a large extent on the nature of the cytokines secreted by the antigen presenting cells (APCs), mainly DCs but also macrophages (Figure 80). For example, the release of IL-12 (interleukin 12) by APCs stimulates the development of $CD4^+$ Th1 (T helper cells) lymphocytes that primarily produce IFN-γ, leading to a higher rate of

[322] Okwor I, Uzonna JE. Immunotherapy as a strategy for treatment of leishmaniasis: a review of the literature. *Immunotherapy*. 2009;1(5):765-76. doi: 10.2217/imt.09.40

[323] Moore KJ, Matlashewski G. Intracellular infection by Leishmania donovani inhibits macrophage apoptosis. *J Immunol*. 1994;152(6):2930-7. PMID: 8144893

[324] Niwa M, Hara A, Kanamori Y, Hatakeyama D, Saio M, Takami T, Matsuno H, Kozawa O, Uematsu T. Nuclear factor-kappaB activates dual inhibition sites in the regulation of tumor necrosis factor-alpha-induced neutrophil apoptosis. *Eur J Pharmacol*. 2000;407(3):211-9. doi: 10.1016/s0014-2999(00)00735-4

[325] Aga E, Katschinski DM, van Zandbergen G, Laufs H, Hansen B, Müller K, Solbach W, Laskay T. Inhibition of the spontaneous apoptosis of neutrophil granulocytes by the intracellular parasite Leishmania major. *J Immunol*. 2002;169(2):898-905. doi: 10.4049/jimmunol.169.2.898.

[326] Tibúrcio R, Nunes S, Nunes I, Rosa Ampuero M, Silva IB, Lima R, Machado Tavares N, Brodskyn C. Molecular Aspects of Dendritic Cell Activation in Leishmaniasis: An Immunobiological View. *Front Immunol.* 2019;10:227. doi: 10.3389/fimmu.2019.00227

[327] Liu D, Uzonna JE. The early interaction of Leishmania with macrophages and dendritic cells and its influence on the host immune response. *Front Cell Infect Microbiol*. 2012;2:83. doi: 10.3389/fcimb.2012.00083

[328] Sundar S, Murray HW. Effect of treatment with interferon-gamma alone in visceral leishmaniasis. *J Infect Dis*. 1995;172(6):1627-9. doi: 10.1093/infdis/172.6.1627

macrophage activation and therefore, to a higher antileishmanial adaptive immune response[329]. On the contrary, the secretion of IL-4 by APCs enhances the development of $CD4^+$ Th2 cells that produce IL-4 and IL-10 (among other cytokines), leading progressively to complications in the outcome of leishmaniasis[330].

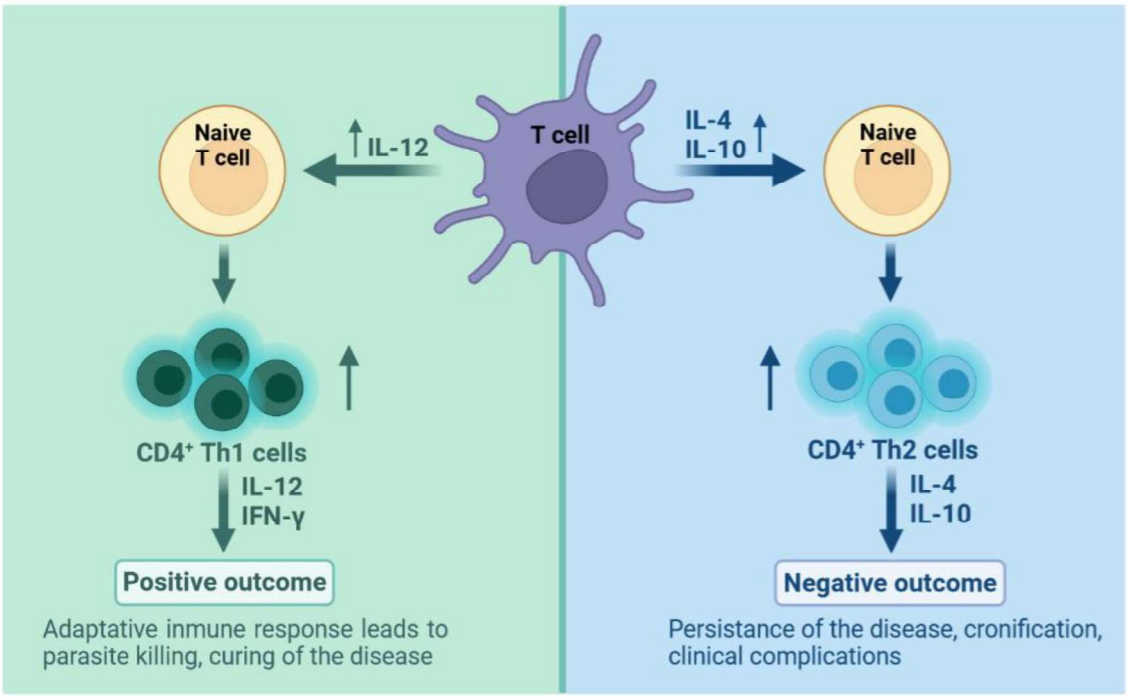

Figure 80. The effect of secreted cytokines in the outcome of leishmaniasis.

Cytokine and monoclonal antibody-based immunotherapy

We previously expounded the relevance of the released cytokines in the outcome of leishmaniasis disease. The vast majority of the information regarding the effect of cytokines in leishmaniasis are collected from studies in mice models, which means that their application in humans is still challenging. For instance, the treatment with IL-12 recombinant cytokine and anti-IL-4 monoclonal antibody in the susceptible BALB/c mice model led to the reverse of chronic disease caused by *L. major* infection, by the stimulation of the IFN-γ pathway[331]. On the other hand, the use of anti-IL-10 monoclonal antibody in human patients with cutaneous leishmaniasis

[329] Mirzaei A, Maleki M, Masoumi E, Maspi N. A historical review of the role of cytokines involved in leishmaniasis. *Cytokine*. 2021;145:155297. doi: 10.1016/j.cyto.2020.155297

[330] Mattner F, Alber G, Magram J, Kopf M. The role of IL-12 and IL-4 in Leishmania major infection. *Chem Immunol*. 1997;68:86-109. doi: 10.1159/000058696

[331] Uzonna JE, Bretscher PA. Anti-IL-4 antibody therapy causes regression of chronic lesions caused by medium-dose Leishmania major infection in BALB/c mice. *Eur. J. Immunol*. 2001;31:3175-3184. doi: 10.1002/1521-4141(200111)31:11<3175::AID-IMMU3175>3.0.CO;2-L

caused by *L. braziliensis* induced a remarkable decrease in the levels of IL-4, IL-10 and TNF-γ, cytokines associated with complications in the outcome of the disease[332].

Likewise, the combination of chemotherapeutic drugs with cytokines has been explored as an alternative to the use of cytokines alone. Cytokines present a short half-life[329] and some difficulties to adjust the dose, but exhibit a therapeutic potential and are further investigated as adjuvants of drugs currently used in clinics. Accordingly, the effect of human recombinant GM-CSF (hr-GM-CSF) used in combination with pentavalent antimonial drugs was investigated for the treatment of acute leishmaniasis caused by *L.donovani* and *L. major* in human neutropenic patients, reporting a rapid recovery of the neutropenia and a complete resolution of the infection within 3 months[333]. In like manner, hr-GM-CSF also showed a synergic effect when using in combination with liposomal amphotericin B to treat visceral leishmaniasis/HIV coinfection, leading to the restore of the immune response of the patient (leukocytopenia was reverted and a higher macrophage activation rate was observed)[334].

Vaccine-based immunotherapy

Many efforts have been focused in order to afford effective, stable and affordable vaccines to induce a long-term immunization towards *Leishmania* infections, specially to protect from VL. Nonetheless, up to now, antileishmanial vaccines have not been reached to the approval for their clinical use.

Investigations to develop vaccines against *Leishmania* were initiated by using killed or inactivated *Leishmania* parasites (the so-called first generation vaccines), alone or with adjuvants. In this regard, vaccines containing killed *Leismania* promastigotes alone[335] or in combination with BCG[336] (Bacillus Calmette–Guérin) as an adjuvant were found to improve the evolution of the disease. Moreover, the employment of pasteurized *Leishmania* promastigotes along with BCG also reported an improvement in the recovery rate of patients with severe

[332] Castellano LR, Argiro L, Dessein H, Dessein A, da Silva MV, Correia D, Rodrigues V. Potential Use of Interleukin-10 Blockade as a Therapeutic Strategy in Human Cutaneous Leishmaniasis. *J Immunol Res*. 2015;2015:152741. doi: 10.1155/2015/152741

[333] Al-Zamel F, Al-Shammary FJ, El-Shewemi S, Soliman R. Enhancement of leishmanicidal activity of human macrophages against Leishmania major and Leishmania donovani infection using recombinant human granulocyte macrophage colony stimulating factor. *Zentralbl Bakteriol*. 1996;285(1):92-105

[334] Mastroianni A. Liposomal amphotericin B and rHuGM-CSF for treatment of visceral leishmaniasis in AIDS. *Infez Med*. 2004;12(3):197-204

[335] Mayrink W, Magalhaes PA, Michalick MS, da Costa CA, Lima Ade O, Melo MN, Toledo VP, Nascimento E, Dias M, Genaro O, *et al.* Immunotherapy as a treatment of American cutaneous leishmaniasis: preliminary studies in Brazil. *Parassitologia*. 1992;34(1-3):159-65

[336] Genaro O, de Toledo VP, da Costa CA, Hermeto MV, Afonso LC, Mayrink W. Vaccine for prophylaxis and immunotherapy, Brazil. *Clin Dermatol*. 1996;14(5):503-12. doi: 10.1016/0738-081x(96)00040-5

leishmaniasis[337]. In like manner, the combination of chemotherapy (sodium stibogluconate) with a first generation vaccine (autoclaved *L. major* + BCG) elucidated an improved cure-rate in VL patients in comparison with the chemotherapeutic treatment alone[338], which suggests a beneficial effect of the vaccine in patients sensitive to chemotherapeutic drugs.

In order to solve the standardization difficulties of the first generation vaccines, a second generation was developed based on purified (or recombinant) *Leishmania* fractions/protein subunits and DCs. Among investigated *Leishmania* subunits, A2 amastigote antigen, FML (fucose-mannose ligand), L-Ag (*L. donovani* membrane antigen) and HSP-70/HSP-83 (heat shock proteins) have been reported to induce Th1 cell-based immunity that favours the outcome of leishmaniasis in animal models[339]. Furthermore, the polyprotein-based vaccine LEISH-F1 (a *L. major* derived three recombinant antigen mixture named as 111-f) formulated with MPL-SE (monophosphoryl lipid Ain stable emulsion) is reported as the first defined vaccine for leishmaniasis and reached to phase I and phase II clinical trials. LEISH-F1/MPL-SE vaccine presented a safe profile but further studies have to be made in order to prove its efficacy to prevent VL[340].

More recently, the disclosure of a third generation vaccines based on DNA (namely DNA vaccines), allowed the development of more stable and highly immunogenic vaccines. DNA vaccines are based on plasmids containing specific *Leishmania* antigens that are transfected to the cells of the host. Thereby, the host cell transcribes the transfected genes and translates the corresponding mRNA to express the encoded protein (*i.e.* the specific *Leishmania* antigens), which induces a T-cell based immune response[341]. For instance, a vaccine based on bifunctional HbR-encoding DNA (HbR: haemoglobin receptor, an essential receptor for the viability of *Leishmania* cells by acting on the haemoglobin metabolism of the parasites) that induced a

[337] Convit J, Ulrich M, Polegre MA, Avila A, Rodríguez N, Mazzedo MI, Blanco B. Therapy of Venezuelan patients with severe mucocutaneous or early lesions of diffuse cutaneous leishmaniasis with a vaccine containing pasteurized Leishmania promastigotes and bacillus Calmette-Guerin: preliminary report. *Mem Inst Oswaldo Cruz*. 2004;99(1):57-62. doi: 10.1590/s0074-02762004000100010

[338] Musa AM, Khalil EA, Mahgoub FA, Elgawi SH, Modabber F, Elkadaru AE, Aboud MH, Noazin S, Ghalib HW, El-Hassan AM; Leishmaniasis Research Group/Sudan. Immunochemotherapy of persistent post-kala-azar dermal leishmaniasis: a novel approach to treatment. *Trans R Soc Trop Med Hyg*. 2008;102(1):58-63. doi: 10.1016/j.trstmh.2007.08.006

[339] Das A, Ali N. Vaccine Development Against Leishmania donovani. *Front Immunol*. 2012;3:99. doi: 10.3389/fimmu.2012.00099

[340] Chakravarty J, Kumar S, Trivedi S, Rai VK, Singh A, Ashman JA, Laughlin EM, Coler RN, Kahn SJ, Beckmann AM, Cowgill KD, Reed SG, Sundar S, Piazza FM. A clinical trial to evaluate the safety and immunogenicity of the LEISH-F1+MPL-SE vaccine for use in the prevention of visceral leishmaniasis. *Vaccine*. 2011;29(19):3531-7. doi: 10.1016/j.vaccine.2011.02.096

[341] Kumar A, Samant M. DNA vaccine against visceral leishmaniasis: a promising approach for prevention and control. *Parasite Immunol*. 2016;38(5):273-81. doi: 10.1111/pim.12315

complete protection on BALB/c mice model against VL caused by *L. donovani*. The immune response was found to be related with the upregulation of IL-12, TNF-α and IFN-γ levels, accompanied by a decrease in the secretion of IL-4 and IL-10 cytokines[342]. In like manner, a DNA-based vaccine containing UBQ-ORFF (ubiquitin conjugation of open reading frame F) was found to develop a protective effect in BALB/c mice model against *L. donovani* induced VL *via* upregulation of IL-12 and IFN-γ levels and the concomitant downregulation of IL-4 and IL-10 cytokines[343].

Finally, it has to be mentioned that genetically modified live attenuated vaccines are also under preclinical development. Accordingly, leishmanization with LmCen$^{-/-}$ (centrin gene deleted *L. major*) strain in preclinical animal models has recently been found to induce an inflammatory immune response and provide protection against both *L. major* and *L.donovani* infections[344].

IV-1.3.3. Miscellaneous treatments of leishmaniasis

Besides chemotherapy and immunotherapy, there are some other experimental approaches to treat leishmaniasis as auxiliary therapies or under preclinical development (Figure 81). For instance, physical modalities as cryotherapy/thermotherapy and application of CO_2 laser imply a direct method to apply cold/heat in the affected skin area in CL[345], in an attempt to kill the parasites in the open wounds. Furthermore, surgery is necessary in the most severe intra-abdominal injuries and in some disfiguring local wounds[296].

Likewise, drug repurposing emerged as a rational strategy to identify new antileishmanial drug candidates from existing clinical/preclinical drugs for other purposes, which have been widely studied and usually offer a safe pharmacokinetic profile. In this regard, the azole antifungal drugs

[342] Guha R, Gupta D, Rastogi R, *et al.* Vaccination with leishmania hemoglobin receptor-encoding DNA protects against visceral leishmaniasis. *Sci Transl Med*. 2013;5(202):202ra121. doi:10.1126/scitranslmed.3006406

[343] Sharma A, Madhubala R. Ubiquitin conjugation of open reading frame F DNA vaccine leads to enhanced cell-mediated immune response and induces protection against both antimony-susceptible and -resistant strains of Leishmania donovani. *J Immunol*. 2009;183(12):7719-7731. doi:10.4049/jimmunol.0900132

[344] Karmakar S, Ismail N, Oliveira F, Oristian J, Zhang WW, Kaviraj S, Singh KP, Mondal A, Das S, Pandey K, Bhattacharya P, Volpedo G, Gannavaram S, Satoskar M, Satoskar S, Sastry RM, Oljuskin T, Sepahpour T, Meneses C, Hamano S, Das P, Matlashewski G, Singh S, Kamhawi S, Dey R, Valenzuela JG, Satoskar A, Nakhasi HL. Preclinical validation of a live attenuated dermotropic Leishmania vaccine against vector transmitted fatal visceral leishmaniasis. *Commun Biol*. 2021;4(1):929. doi: 10.1038/s42003-021-02446-x

[345] a) Wolf Nassif P, DE Mello TFP, Navasconi TR, *et al.* Safety and efficacy of current alternatives in the topical treatment of cutaneous leishmaniasis: a systematic review. *Parasitology*. 2017;144(8):995-1004. doi:10.1017/S0031182017000385. b) Valencia BM, Miller D, Witzig RS, Boggild AK, Llanos-Cuentas A. Novel low-cost thermotherapy for cutaneous leishmaniasis in Peru. *PLoS Negl Trop Dis*. 2013;7(5):e2196. doi:10.1371/journal.pntd.0002196

(fluconazole[346] and itraconazole[347]) evidenced a promising antileishmanial potential in CL patients and clarithromycin macrolide antibiotic presented a leishmanicidal effect toward *L. donovani* parasites *in vitro*[348]. Furthermore, Tamoxifen, an estrogen receptor modulator for the treatment of breast cancer, reported an *in vitro* antileishmanial effect by affecting the sphingolipid metabolism in *Leishmania* cells and presents promising results in preclinical assays with animal models and in a pilot clinical trial with human patients[349].

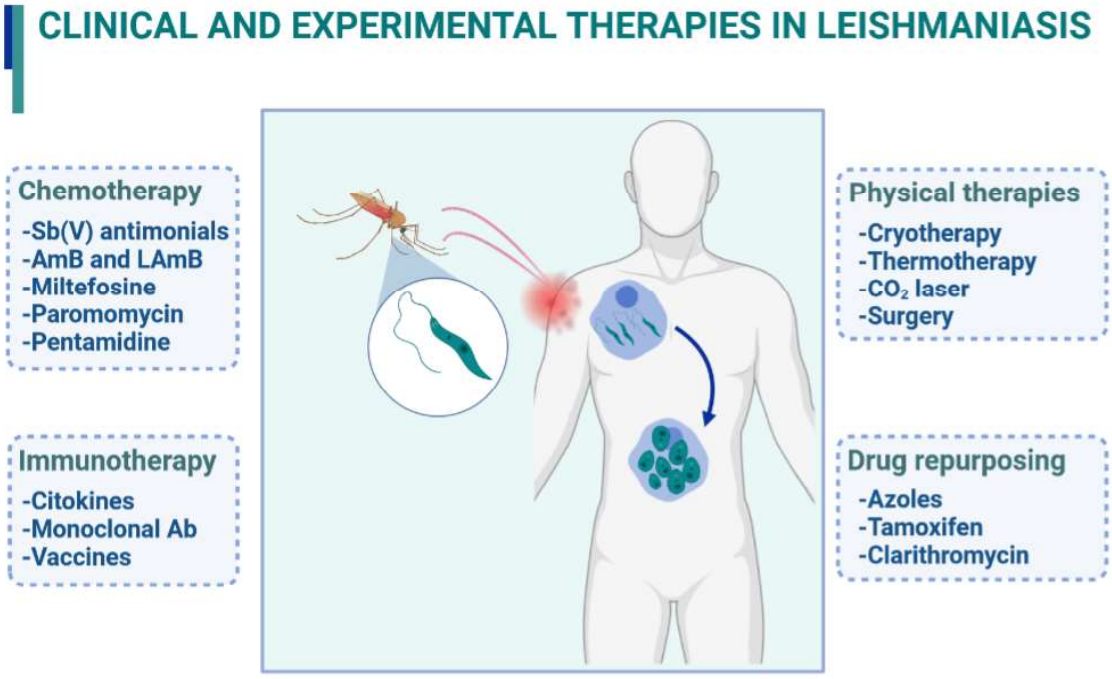

Figure 81. Summary of experimental and clinical therapies for the treatment of leishmaniasis.

IV-1.4. LTOP1B as a druggable target in antileishmanial drug discovery

TOP1B is present in all trypanosomatids and results essential for their cell viability. Trypanosomal TOP1B differs from other eukaryotic analogues on its oligomeric nature, which results a curious particularity in a highly conserved enzyme family. The genes encoding each monomer are located in different chromosomes and upon gene expression, both protomers

[346] Sousa AQ, Frutuoso MS, Moraes EA, Pearson RD, Pompeu MM. High-dose oral fluconazole therapy effective for cutaneous leishmaniasis due to Leishmania (Vianna) braziliensis. *Clin Infect Dis*. 2011;53(7):693-695. doi:10.1093/cid/cir496

[347] Calvopina M, Guevara AG, Armijos RX, Hashiguchi Y, Davidson RN, Cooper PJ. Itraconazole in the treatment of New World mucocutaneous leishmaniasis. *Int J Dermatol*. 2004;43(9):659-663. doi:10.1111/j.1365-4632.2004.02183.x

[348] Roy K, Das S, Mondal S, Roy AK, Bera T. The *in Vitro* effect of clarithromycin on amastigote of *Leishmania Donovani*. *Int J Drug Dev Res*. 2013;5(3):425–431

[349] Zewdie KA, Hailu HG, Ayza MA, Tesfaye BA. Antileishmanial Activity of Tamoxifen by Targeting Sphingolipid Metabolism: A Review. *Clin Pharmacol*. 2022;14:11-17. doi:10.2147/ CPAA.S344268

need to be assembled in order to get the active form of the enzyme[350]. Accordingly, the large subunit (composed of 636 amino acids with a molecular mass of ~73 kDa in *L. donovani*) contains the core domain, while the small subunit (composed of 262 amino acids with a molecular mass ~28 kDa in *L. donovani*) encloses the C terminal domain bearing the phylogenetically conserved SKxxY motif that harbors the catalytic Tyr residue (located in position 222 in the case of LTOP1B)[351]. The schematic representation of LTOP1B domain organization from *L. donovani* is illustrated in the Figure 82, along with the human isoform (hTOP1B).

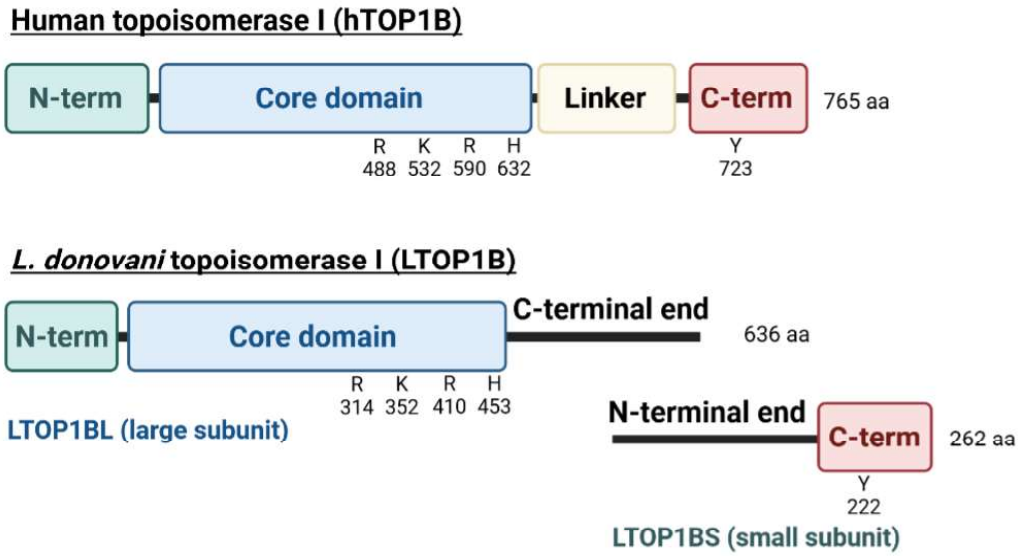

Figure 82. Schematic overview of the domain organization of human hTOP1B (monomeric) and L.donovani LTOP1B (heterodimeric, small and large subunits).

LTOP1B, as a member of eukaryotic TOP1B subfamily, relaxes both positive and negative DNA by introducing transient single-stranded breaks in dsDNA that allows strand rotation (as expounded in the introduction, *vide supra*). Thereby, LTOP1B generates transient TOP1CCs in an ATP-independent manner by covalently binding to the 3' termini of the cleaved DNA strand to permit strand passage and then, religates the scission.

Leishmanial topoisomerase IB (LTOP1B) inhibitors as drug candidates for leishmaniasis

LTOP1B shares the catalytic mechanism with the other eukaryotic TOP1B isoforms as the SKxxY motif is maintained, including the catalytic Tyr residue. Conversely, there coexist clear

[350] Balaña-Fouce R, Alvarez-Velilla R, Fernández-Prada C, García-Estrada C, Reguera RM. Trypanosomatids topoisomerase re-visited. New structural findings and role in drug discovery. *Int J Parasitol Drugs Drug Resist*. 2014;4(3):326-37. doi: 10.1016/j.ijpddr.2014.07.006

[351] Villa H, Otero Marcos AR, Reguera RM, Balaña-Fouce R, García-Estrada C, Pérez-Pertejo Y, Tekwani BL, Myler PJ, Stuart KD, Bjornsti MA, Ordóñez D. A novel active DNA topoisomerase I in Leishmania donovani. *J Biol Chem*. 2003;278(6):3521-6. doi: 10.1074/jbc.M203991200

differences in regard to the structure, function and gene-expression between LTOP1B of *Leishmania* parasites and hTOP1B of the host (human) that convert LTOP1B a druggable target in antileishmanial research. Accordingly, LTOP1B acts on both genomic DNA and kinetoplastic DNA of the *Leishmania* parasite, and hence it is located in the nucleus and in the kinetoplast[352]. On the contrary, in human there are two TOP1B encoded by different genes, a nuclear one (TOP1B) acting exclusively on genomic DNA and a mitochondrial mtTOP1B acting on mitochondrial DNA[353]. Moreover, the heterodimeric constitution of LTOP1B confers a distinctive structural feature regarding the human isoform (monomeric), in which the protomers need to be assembled in order to get a functional enzyme (see Figure 82). The reconstitution of the two subunits comprises ionic bonds and polar interactions due to the charge differences between the two subunits, derived from the presence of many polar groups in the assembling regions[354].

In this sense, these mechanistic similarities and structural/functional differences suggested the exploration of compounds that selectively target LTOP1B over hTOP1, a strategy that may confer an antileishmanial effect without affecting the host.

The natural alkaloid CPT and its synthetic analogues topotecan, SN-38 and gimatecan (Figure 83) are well known *poison*-like hTOP1B inhibitors with a strong anticancer activity and in fact, topotecan and SN-38 are clinically used in current cancer chemotherapy. In like manner, they have been investigated as LTOP1B inhibitors reporting a potent *in vitro* inhibition of *L. infantum* LTOP1B in the nanomolar range *via* trapping of TOP1CCs. Furthermore, CPT and derivatives reported a strong in vitro leishmanicidal effect toward both promastigotes and intracellular amastigotes of *L. infantum*. In particular, gimatecan presented an IC_{50} of 1 nM and a selectivity index of 175 against BALB/c mice splenocytes, resulting in a promising antileishmanial candidate that selectively targets the parasite[355].

[352] BoseDasgupta S, Ganguly A, Das BB, Roy A, Khalkho NV, Majumder HK. The large subunit of Leishmania topoisomerase I functions as the 'molecular steer' in type IB topoisomerase. *Mol Microbiol*. 2008;67(1):31-46. doi: 10.1111/j.1365-2958.2007.06002.x

[353] Zhang H, Barceló JM, Lee B, *et al.* Human mitochondrial topoisomerase I. *Proc Natl Acad Sci U S A*. 2001;98(19):10608-10613. doi:10.1073/pnas.191321998

[354] Das BB, Sen N, Dasgupta SB, Ganguly A, Majumder HK. N-terminal region of the large subunit of *leishmania donovani* bisubunit topoisomerase I is involved in DNA relaxation and interaction with the smaller subunit *. *J Biol Chem*. 2005;280(16):16335-16344. doi: 10.1074/jbc.M412417200

[355] Prada CF, Alvarez-Velilla R, Balaña-Fouce R, Prieto C, Calvo-Álvarez E, Escudero-Martínez JM, Requena JM, Ordóñez C, Desideri A, Pérez-Pertejo Y, Reguera RM. Gimatecan and other camptothecin derivatives poison Leishmania DNA-topoisomerase IB leading to a strong leishmanicidal effect. *Biochem Pharmacol*. 2013;85(10):1433-40. doi: 10.1016/j.bcp.2013.02.024

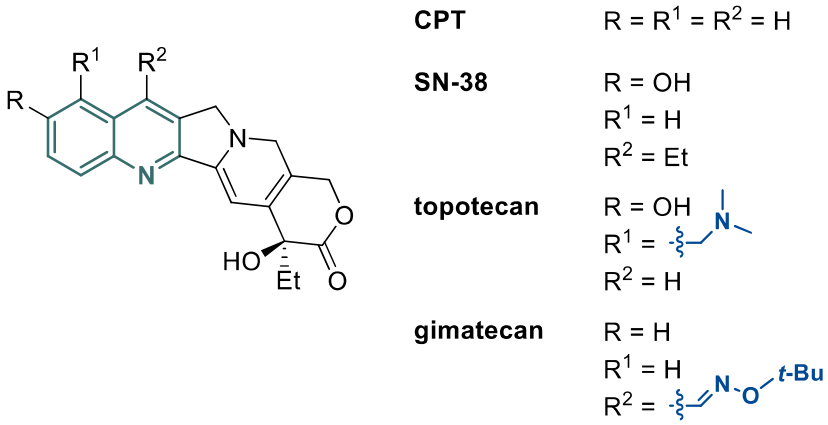

Figure 83. Structures of CPT and derivatives with antileishmanial activity.

Besides CPT, other natural compounds were found to inhibit LTOP1B. Such is the case for the naphtoquinones lapachol (extracted from *Handroanthus impetiginosus*)[356] and diospyrin (present in plants from *diospyrus* gender)[357] (Figure 84), which were found as LTOP1B poisons with *in vitro* leishmanicide activity in *L. donovani* promastigotes.

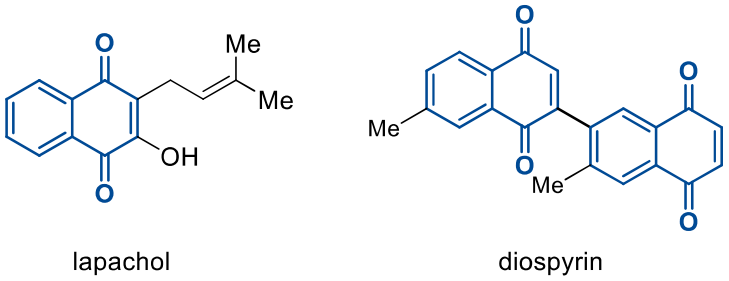

Figure 84. Natural naphtoquinones reporting LTOP1B inhibitory activity.

The synthetic indenoisoquinoline hTOP1B inhibitors indotecan (LMP400) and AM13-55 (Figure 85) were screened as antileishmanial drug candidates, reporting a higher *in vitro* leishmanicidal effect toward both *L. infantum* promastigotes and amastigotes than the reference drug paromomycin with elevated selectivity indexes[358]. In addition, indotecan and AM13-55

[356] Ramos-Milaré ÁCFH, Oyama J, Murase LS, Souza JVP, Guedes BS, Lera-Nonose DSSL, Monich MT, Brustolin AÁ, Demarchi IG, Teixeira JJV, Lonardoni MVC. The anti-Leishmania potential of bioactive compounds derived from naphthoquinones and their possible applications. A systematic review of animal studies. *Parasitol Res*. 2022;121(5):1247-1280. doi: 10.1007/s00436-022-07455-1

[357] Ray S, Hazra B, Mittra B, Das A, Majumder HK. Diospyrin, a bisnaphthoquinone: a novel inhibitor of type I DNA topoisomerase of Leishmania donovani. *Mol Pharmacol*. 1998;54(6):994-9. doi: 10.1124/mol.54.6.994

[358] Balaña-Fouce R, Prada CF, Requena JM, *et al.* Indotecan (LMP400) and AM13-55: two novel indenoisoquinolines show potential for treating visceral leishmaniasis. *Antimicrob Agents Chemother*. 2012;56(10):5264-5270. doi:10.1128/AAC.00499-12

compounds demonstrated a *poison*-like mode of action and in particular, indotecan was found to strongly induce the stabilization of leishmanial TOP1CCs.

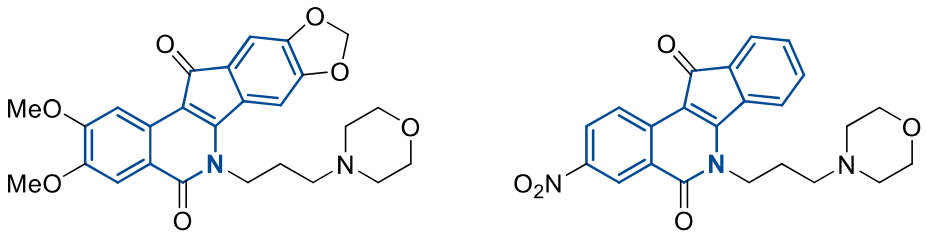

Figure 85. Indenoisoquinolines with LTOP1B inhibitory activity.

Likewise, aromathecins (**1**, Figure 86), a family of non-camptothecinic hTOP1B inhibitors broadly studied as anticancer drug candidates, were tested in *L.infantum* parasites and presented promising leismanicide activity *in vitro* in the low micromolar range (in both promastigote and amastigote forms). Surprisingly, when aromathecins were evaluated in LTOP1B assays, they demonstrated a LTOP1B inhibitory activity but not a *poison*-like mode of action, interfering in the TOP1 catalytic cycle of *L. infantum* without the trapping of TOP1CC[359]. This finding suggests a different inhibition mechanism in eukaryotic TOP1B human (monomeric) and leishmanial (heterodimeric) isoforms.

Besides aromathecins, some other families of compounds presented an antileishmanial effect in combination with LTOP1B inhibitory activity through a TOP1 suppressor-like mode of action. Such is the case for 1,5-naphthyridine[360] and fused indeno-1,5-naphtyridine[361] derivatives (**2**, Figure 86), which reported a leishmanicidal effect in the micromolar range with a remarkably selectivity toward the parasite cells a in a BALB/c murine model.

[359] Reguera RM, Álvarez-Velilla R, Domínguez-Asenjo B, *et al.* Antiparasitic effect of synthetic aromathecins on Leishmania infantum. *BMC Vet Res*. 2019;15(1):405. doi:10.1186/s12917-019-2153-9

[360] Tejería A, Pérez-Pertejo Y, Reguera RM, *et al.* Substituted 1,5-naphthyridine derivatives as novel antileishmanial agents. Synthesis and biological evaluation. *Eur J Med Chem*. 2018;152:137-147. doi:10.1016/j.ejmech.2018.04.033

[361] Tejería A, Pérez-Pertejo Y, Reguera RM, *et al.* Antileishmanial effect of new indeno-1,5-naphthyridines, selective inhibitors of Leishmania infantum type IB DNA topoisomerase. *Eur J Med Chem*. 2016;124:740-749. doi:10.1016/j.ejmech.2016.09.017

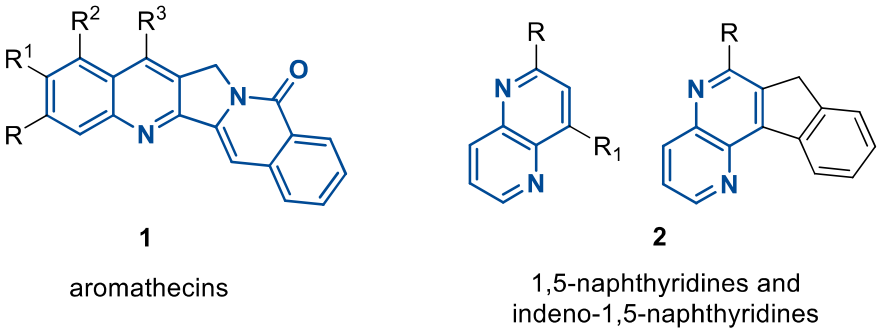

Figure 86. Aromathecins and 1,5-naphthyridine derivatives with LTOP1 inhibitory activity (suppressor-like inhibitors).

Finally, it has to be mentioned that pentavalent antimonial drugs (meglumine antimoniate and sodium stibogluconate, Figure 80 in the section 1.3.1. of this *addenda*, *vide supra*) are complexes of Sb^{V} currently used in *Leishmania* chemotherapy and reported a LTOP1B inhibition *via* stabilization of TOP1CCs that contribute to their leishmanicidal effect, even though this is not the primary mode of action[362]. Pentavalent antimonials also target tripanothione reductase and other glycolytic enzymes, affecting to the energetic and lipid-metabolism of *Leishamia* parasites.

IV-2. Study of the antileishmanial effect of phosphorated quinoline derivatives in *Leishmania infantum*

In view of the former considerations, the newly synthesized phosphorated quinoline derivatives were evaluated as antileishmanial agents. We firstly investigated the *in vitro* hTOP1B inhibitory activity (Chapter II) and the antiproliferative activity in human cells (Chapter III), where several phosphorated 2,4-quinoline derivatives and 7*H*-indeno[2,1-*c*]quinoline derivatives were found as suppressor-like inhibitors of hTOP1B with a selective cytotoxic effect toward human cancer cells. Afterwards, we decided to take one step beyond and further investigate the ability of the novel quinoline derivatives to target the leishmanial isoform of TOP1B and therefore, the antileishmanial effect of the compounds was investigated in *L. infantum* parasites. Accordingly, the *in vitro*/*ex vivo* cytotoxicity in *L.infantum* promastigotes/amastigotes and the *in vitro* inhibitory activity against LTOP1B were performed in the research group headed by the Prof. Rafael Balaña-Fouce in the department of Biomedical Sciences (University of León, Spain).

[362] Das BB, Ganguly A, Majumder HK. DNA topoisomerases of leishmania: The potential targets for anti-leishmanial therapy. In: Majumder HK, ed. *Drug targets in kinetoplastid parasites.* New York, NY: Springer New York; 2008:103-115. https://doi.org/10.1007/978-0-387-77570-8_9

IV-2.1. Antileishmanial effect of 1,2,3,4-tetrahydroquinolin-8-yl phosphine oxides and quinolin-8-yl phosphine oxides

In first place, 1,2,3,4-tetrahydroquinolin-8-yl phosphine oxides **6** (Figure 87) and quinolin-8-yl phosphine oxides **7** were investigated as antileishmanial agents.

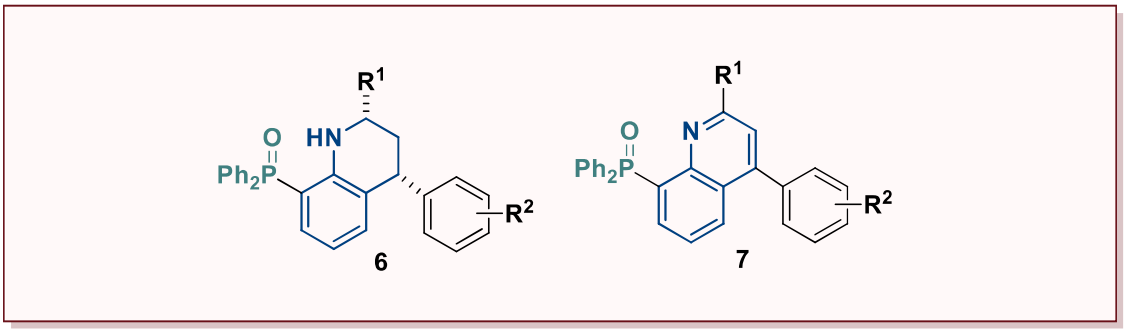

*Figure 87. General structures of 1,2,3,4-tetrahydroquinolin-8-yl phosphine oxides **7** and quinolin-8-yl phospine oxides **8.***

In vitro/ex vivo antileismanial activity in L. infantum parasites (amastigotes and promastigotes)

The effect of newly synthesized 1,2,3,4-tetrahydroquinolin-8-yl phosphine oxides **6** and quinolin-8-yl phosphine oxides **7** was assessed on *L. infantum* parasites (promastigotes and amastigotes, Figure 88).

On the one hand*, in vitro* viability assays were made in free-living promastigotes of *L. infantum*-iRFP mutant parasites. The genetically modified *L. infantum*-iRFP strain constitutively produces iRFP (infrared fluorescent protein) when cells are viable, allowing a reliable and fast readout proportional to the corresponding *Leishmania*-cell viability ($\lambda_{excitation}$ = 600 nm, $\lambda_{emission}$ = 708 nm).

On the other hand, *ex vivo* viability assays were carried out with intramacrophage amastigotes of *L. infantum* isolated from BALB/c mice. The *ex vivo* experiment was outlined in order to simulate natural *in vivo* infections and accordingly, BALB/c mice were inoculated with 10^8 *L. infantum*-iRFP metacyclic promastigotes. Five weeks after the infection, the spleens were dissected to establish a primary cell culture of splenocytes, which contains macrophages harbouring *L. infantum* intracellular amastigotes.

Furthermore, a primary cell culture of an *ex vivo* splenic explant derived from uninfected BALB/c mice was prepared under the same conditions, *i.e*. splenocytes from a non-infected murine. Cytotoxicity studies in the present *ex vivo* splenic explant culture containing free-parasite macrophages permitted the calculation of a selectivity index (SI). The SI is a parameter that

measures the effect of the tested compounds on the target parasite (intracellular *L. infantum* amastigotes) with respect to the toxicity induced in host cells (splenocytes).

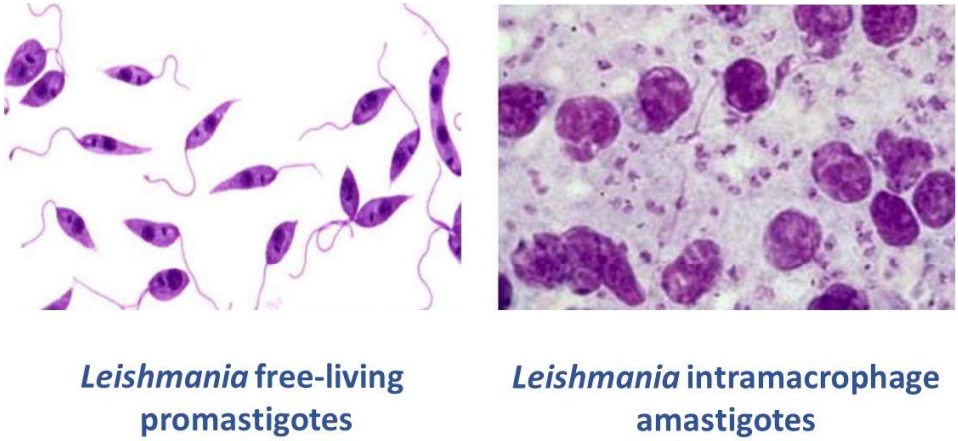

Figure 88. Promastigote (free-living) and amastigote (intracellular) forms of Leishmania.

Once established the experiment conditions, the antileishmanial effect of (tetrahydro)quinolin-8-yl phosphine oxide derivatives **6** and **7** was evaluated in *L. infantum*-iRFP promastigotes *in vitro*, *L. infantum*-iRFP intramacrophage amastigotes (in an *ex vivo* murine splenic explant culture) and murine splenocytes (in an *ex vivo* splenic explant culture). In the case of *in vitro* promastigotes and *ex vivo* amastigotes, the *Leishmania*-cell viability was measured by the detection of near-infrared radiation emitted by living parasites (λ = 708 nm) exposed to the tested drugs in different concentrations upon 72 h of incubation. The reduction of the *Leishmania*-cell viability was plotted in dose-response curves employed to calculate the EC_{50} values of the tested compounds, referred as the 50% effective concentration to kill the parasites. On the other hand, the murine splenocyte-cell viability was measured by the Alamar Blue viability assay upon 72 h of incubation with the tested drugs. The obtained results were used to plot dose-response curves and calculate the corresponding GI_{50} values.

In all cases, experiments were performed in triplicate, dose-response curves were fitted with nonlinear regression analysis and the EC_{50}/GI_{50} values were calculated by using Sigma-Plot 10.0 software. The SI was calculated as the ratio between GI_{50} value toward *ex vivo* splenocytes and EC_{50} value obtained for *ex vivo* intramacrophage amastigotes. All the results obtained for the tested compounds **6** and **7** (EC_{50} amastigotes, EC_{50} promastigotes, GI_{50} splenocytes and SI) are collected in the Table 23.

Table 23. Antileishmanial activity of 1,2,3,4-tetrahydroquinolin-8-yl phosphine oxides **6** and quinolin-8-yl phosphine oxides **7**.

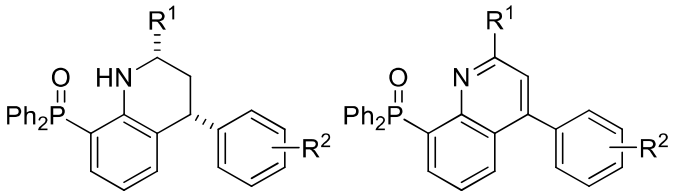

Entry	Compound			EC_{50} (µM) *L. infantum*[a]		GI_{50} (µM)[b]	SI[c]
				promastigotes	amastigotes	splenocytes	
	Nº	R^1	R^2	(*Leishmania*)	(*Leishmania*)	(murine)	
1	**AmB**	-	-	0.77 ± 0.15	0.32 ± 0.05	>20	62.50
2	**6a**	2-MeO-C_6H_4	H	9.29 ± 2.25	0.98 ± 0.73	34.23 ± 1.78	34.93
3	**6g**	4-F-C_6H_4	4-Me	7.10 ± 0.81	1.85 ± 1.09	13.82 ± 0.39	7.47
4	**6i**	3,4-F_2-C_6H_3	4-F	6.15 ± 1.24	1.46 ± 0.16	63.70 ± 1.88	43.63
5	**7d**	2-naphthyl	H	4.91 ± 0.38	4.14 ± 1.64	57.11 ± 6.60	13.79
6	**7i**	3,4-F_2-C_6H_3	4-F	2.23 ± 0.25	2.15 ± 1.23	23.95 ± 1.36	11.14
7	**7j**	C_6H_5	4-F	6.01 ± 0.80	1.39 ± 1.08	71.03 ± 2.11	51.10

[a,b] The cytotoxicity EC_{50}/GI_{50} values collected in the present table were calculated by cell viability assays and are defined as the concentrations corresponding to a 50% cell growth inhibition. The EC_{50}/ GI_{50} results are shown as the mean ± the standard deviation from independent cell viability assay experiments performed in quadruplicate. [c] The SI was calculated as the ratio between $GI_{50\ splenocytes}$/ $EC_{50\ promastigotes}$.

Overall, all of the studied (tetrahydro)quinolin-8-yl phosphine oxide derivatives **6** and **7** reported a notable antileishmanial effect toward *L.infantum* promastigotes and amastigotes in the single digit micromolar range, with EC_{50} values ranging between 2.23-9.29 µM in free living promastigotes *in vitro* and between 0.98-4.14 µM toward intramacrophage amastigotes *ex vivo*. The antileishmanial activity of the studied compounds **6**/**7** was slightly minor but comparable to the reference drug amphotericin B (Table 23, entry 1), which reported EC_{50} values of 0.77 ± 0.15 µM in free living promastigotes and 0.32 ± 0.05 µM toward intracellular amastigotes. However, AmB presented an elevated SI of 62.50 and only the compounds **6i** (R^1 = 3,4-F_2-C_6H_3; R^2 = 4-F; entry 4) and **7j** (R^1 = C_6H_5; R^2 = 4-F; entry 7) were close in terms of selective cytotoxicity toward *L. infantum* parasites. In fact, the (tetrahydro)quinolin-8-yl phosphine oxide derivatives **6i** and **7j** reported the best antileishmanial activity of the current study due to the selective antileishmanial effect.

Inhibition of L. infantum LTOP1B

Once concluded the evaluation of antileishmanial activity with compounds **6**/**7**, the *L. infantum* LTOP1B inhibitory activity of (2-(3,4-difluorophenyl)-4-(4-fluorophenyl)quinolin-8-yl)diphenylphosphine oxide **7i** was then evaluated. The quinolin-8-yl derivative **7i** was previously found as a suppressor-like hTOP1B (human isoform) inhibitor with a quite strong potency at

short reaction times (up to 1 min) in DNA relaxation assays (see Figure 38 and Table 11, entry 8; in Chapter II, *vide supra*). In view of the former results, the compound **7i** was tested in the previously expounded DNA relaxation assay with LTOP1B of *L. infantum* and human hTOP1B in order to investigate whether the inhibitory activity is maintained in the leishmanial heterodimeric isoform or not, and hence, to further compare the potential inhibitory activities in both eukaryotic TOP1B enzymes.

Accordingly, *in vitro* DNA relaxation assays were performed as previously explained with the negatively supercoiled pBluescript-SK DNA (pSK DNA) plasmid. The enzymatic reactions were incubated at 26ºC (LTOP1B)/ 37ºC (hTOP1B) in the presence of 100 µM of compound **7i** and aliquots were stopped at 2 min, 4 min, 8 min and 16 min reaction times with 1% sarkosyl (final concentration). Moreover, endpoint DNA relaxation assays were made for a fixed time period of 5 min with increasing compound concentrations (in triplicate) in order to calculate IC_{50} values for the inhibition of TOP1B[239]. IC_{50} was referred as the 50% of the effective concentration to effectively inhibit the TOP1B relaxation activity. The results obtained in the present DNA relaxation assays are collected in the Table 24.

Table 24. LTOP1B and hTOP1B inhibitory activity of quinolin-8-yl phosphine oxide derivative **7i**.

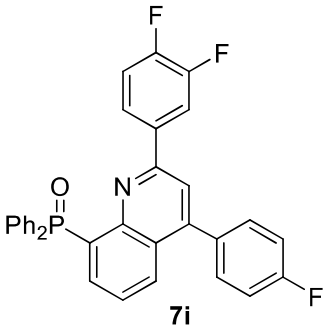

7i

Entry	Compound	% Inhibition LTOP1B [a]				IC_{50} LTOP1B (µM)	IC_{50} hTOP1B (µM)
	Nº	2 min	4 min	8 min	16 min		
1	**7i**	+++	+++	+++	-	48.11 ± 0.33	69.65 ± 1.29

[a]The activity of the compound inhibiting LTOP1B relaxation at 1O0 µM was expressed semiquantitatively by comparison with the maximum inhibitory activity observed for CPT at 100 µM as follows: -, no activity; +, weaker activity than CPT; ++ similar activity to CPT; +++ stronger activity than CPT

Attending to the Table 24, the compound **7i** was found to inhibit LTOP1B in a higher rate than CPT and the inhibitory activity was maintained up to 8 min of incubation. Moreover, the quinolyn-8-yl phosphine oxide **7i** presented IC_{50} value of 48.11 ± 0.33 µM on LTOP1B and a IC_{50} value of 69.65 ± 1.29 µM on hTOP1B. In view of the collected results, we may conclude that the

compound **7i** maintained the TOP1B inhibitory activity previously presented toward the human isoform in the *L. infantum* LTOP1B. Finally, it has to me mentioned that the IC_{50} values obtained in both eukaryotic enzymes resulted to be quite similar, even though it was a bit higher in the case of hTOP1B enzyme.

IV-2.2. Antileishmanial effect of dialkyl quinolinyl phosphonates

In the present section is shown the screening of dialkyl quinolin-8-yl phosphonates **13** and diethyl quinolin-6-yl phosphonates **16** (Figure 89) as antileishmanial drug candidates.

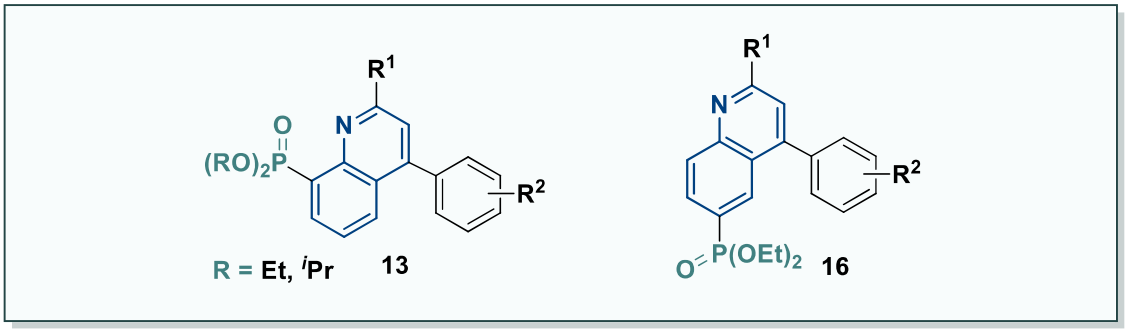

*Figure 89. General structures of dialkyl quinolin-8-yl phosphonates **12** and diethyl quinolin-6-yl phospjonates **15**.*

In vitro antileismanial activity in L. infantum parasites (amastigotes and promastigotes)

In first place, the antileishmanial effect of dialkyl quinolin-8-ylphosphonates **13** and diethyl quinolin-6-ylphosphonates **16** was evaluated against *L. infantum* promastigotes and amastigotes.

The optimized experiment conditions used in the section IV-2.1. of this *addenda* were followed (*vide supra*). Accordingly, the antileishmanial effect of dialkyl quinolinylphosphonate derivatives **13** and **16** was assessed in *L. infantum*-iRFP promastigotes *in vitro*, *L. infantum*-iRFP intramacrophage amastigotes (from an *ex vivo* murine splenic explant culture) and murine splenocytes (an *ex vivo* splenic explant culture).

The cell viability of viable *L. infantum* promastigotes and amastigotes was measured by the detection of near-infrared radiation (λ = 708 nm) upon 96 h of incubation with the tested compounds (three independent experiments per compound) in different concentrations. The obtained *Leishmania*-cell viability was plotted in dose-response curves and therefore EC_{50} values were calculated with Sigma-Plot 10.0 software.

On the other hand, the cell viability of *ex vivo* murine splenocytes was measured by using the Alamar Blue viability assay upon 96 h of incubation with the tested compounds at different

concentrations (experiments were performed in triplicate). The resulting cell viability was plotted in dose-response curves and GI_{50} values were further calculated by using Sigma-Plot 10.0 statistical package.

Finally, the SI was calculated as the relationship between EC_{50} of *ex vivo* intramacrophage amastigotes and GI_{50} of *ex vivo* splenocytes. The results involving EC_{50} in amastigotes, EC_{50} in promastigotes, GI_{50} in splenocytes and SI are collected in the Table 25.

Table 25. Antileishmanial activity of dialkyl quinolin-8-ylphosphonates **13** and diethyl quinolin-6-ylphosphonates **16**.

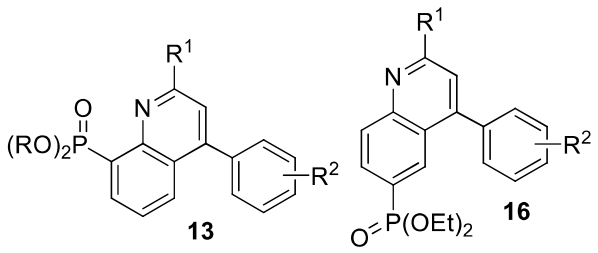

Entry	Compound				EC_{50} (µM) *L. infantum*		GI_{50} (µM)	SI
					promastigotes	amastigotes	splenocytes	
	Nº	R	R^1	R^2	(*Leishmania*)	(*Leishmania*)	(murine)	
1	**AmB**	-	-	-	0.77 ± 0.15	0.32 ± 0.05	>20	62.50
2	**13a**	Et	C_6H_5	H	0.91 ± 0.04	4.03 ± 0.30	3.61 ± 0.45	0.90
3	**13b**	Et	2-MeO-C_6H_4	H	11.37 ± 0.62	19.46 ± 2.38	30.09 ± 6.05	1.55
4	**13d**	Et	4-MeO-C_6H_4	H	9.46 ± 1.67	8.23 ± 1.70	15.90 ± 1.65	1.93
5	**13f**	Et	1-naphthyl	H	20.55 ± 2.19	19.66 ± 2.39	12.22 ± 1.49	0.62
6	**13g**	Et	2-naphthyl	H	20.38 ± 1.57	20.44 ± 5.62	51.62 ± 1.52	2.53
7	**13j**	Et	4-F-C_6H_4	4-Me	7.29 ± 0.94	9.80 ± 0.48	14.54 ± 1.56	1.48
8	**13k**	Et	3,4-F_2-C_6H_3	4-Me	2.59 ± 0.48	26.23 ± 3.65	24.07 ± 7.79	0.92
9	**13l**	Et	C_6H_5	4-F	16.05 ± 1.94	11.89 ± 5.17	33.86 ± 7.98	2.85
10	**13m**	Et	4-F-C_6H_4	4-F	8.43 ± 0.92	24.17 ± 2.37	20.26 ± 7.49	0.84
11	**13n**	Et	3,4-F_2-C_6H_3	4-F	6.35 ± 0.16	13.43 ± 5.53	20.64 ± 3.11	1.54
12	**13o**	^{i}Pr	4-F-C_6H_4	H	9.57 ± 0.40	19.47 ± 2.23	22.10 ± 4.70	1.13
13	**13p**	^{i}Pr	3,4-F_2-C_6H_3	H	11.18 ± 0.74	10.20 ± 1.34	19.79 ± 3.76	1.94
14	**13q**	^{i}Pr	4-F-C_6H_4	4-Me	5.01 ± 0.35	24.32 ± 2.53	21.23 ± 3.50	0.87
15	**13r**	^{i}Pr	3,4-F_2-C_6H_3	4-Me	7.46 ± 0.76	13.91 ± 3.65	28.33 ± 9.16	2.04
16	**13s**	^{i}Pr	4-F-C_6H_4	4-F	4.86 ± 0.50	5.52 ± 1.11	15.29 ± 1.72	2.77
17	**13t**	^{i}Pr	3,4-F_2-C_6H_3	4-F	19.26 ± 1.79	19.65 ± 1.73	18.60 ± 1.10	0.94
18	**16a**	Et	4-F-C_6H_4	H	15.22 ± 1.14	29.23 ± 14.00	28.07 ± 1.23	0.96
19	**16b**	Et	3,4-F_2-C_6H_3	H	14.72 ± 1.78	14.20 ± 2.83	26.23 ± 0.51	1.85
20	**16c**	Et	4-F-C_6H_4	4-Me	7.02 ± 0.94	17.56 ± 7.81	11.18 ± 4.42	0.64
21	**16d**	Et	3,4-F_2-C_6H_3	4-Me	21.29 ± 2.34	32.95 ± 6.55	32.33 ± 3.36	0.98
22	**16e**	Et	4-F-C_6H_4	4-F	16.73 ± 0.72	31.46 ± 2.71	44.97 ± 10.24	1.43
23	**16f**	Et	3,4-F_2-C_6H_3	4-F	7.07 ± 0.61	26.36 ± 2.33	>100	>3.79

[a,b] The cytotoxicity EC_{50}/GI_{50} values collected in the present table were calculated by cell viability assays and are defined as the concentrations corresponding to a 50% cell growth inhibition. The EC_{50}/ GI_{50} results are shown as the mean ± the standard deviation from independent cell viability assay experiments performed in quadruplicate. [c] The SI was calculated as the ratio between $GI_{50\ splenocytes}$/ $EC_{50\ promastigotes}$.

As it can be observed in the Table 25, all the tested compounds **13**/**16** were found to be active in both promastigote and amastigote forms of *L. infantum*-iRFP strain, presenting EC_{50} values ranging from 0.91 ± 0.04 µM (compound **13a**, R = Et; R^1 = C_6H_5; R^2 = H; Table 25, entry 2) to 21.29 ± 2.34 µM (compound **16d**, R= Et; R^1 = 4-F-C_6H_4; R^2 = 4-Me; entry 21) in free living promastigotes *in vitro* and from 4.03 ± 0.30 µM (compound **13a**, R = Et; R^1 = C_6H_5; R^2 = H; entry 2) to 26.36 ± 2.33 µM (compound **16a**, R = Et; R^1 = 4-F-C_6H_4; R^2 = H; entry 18) toward *ex vivo* intramacrophage

amastigotes. However, the SI was generally low (below 2.85 in all the quantifiable cases) for all the studied dialkyl quinolinyl phosphonates **13**/**16**, which indicates a high toxicity toward the host cells except for the compound **16f** (R = Et; R^1 = 3,4-F_2-C_6H_3; R^2 = 4-F; entry 23) that reported a GI_{50} value higher than 100 μM in murine splenocytes and therefore presents a much better selectivity toward the infective agent.

Inhibition of L. infantum LTOP1B

The LTOP1B inhibitory activity of dialkyl quinolinyl phosphonate derivatives **13** and **16** was evaluated by DNA relaxation assays performed with pSK DNA plasmid and L. infantum LTOP1B. Endpoint DNA relaxation assays were carried out by incubating the enzymatic reactions at 26°C in the presence of the tested compounds (100 μM) and stopping them after a reaction time of 5 min with 1% of sarkosyl (final concentration). The inhibitory activity of the tested compounds was expressed as the percentage of LTOP1B inhibition (0-100%), which was determined by measuring the band corresponding to the supercoiled pSK plasmid[363]. The obtained results are listed in the Table 26.

[363] Selas A, Fuertes M, Melcón-Fernández E, *et al.* Hybrid Quinolinyl Phosphonates as Heterocyclic Carboxylate Isosteres: Synthesis and Biological Evaluation against Topoisomerase 1B (TOP1B). *Pharmaceuticals (Basel)*. 2021;14(8):784. doi:10.3390/ph14080784

Table 26. LTOP1B inhibitory activity of dialkyl quinolin-8-ylphosphonates **13** and diethyl quinolin-6-ylphosphonates **16**.

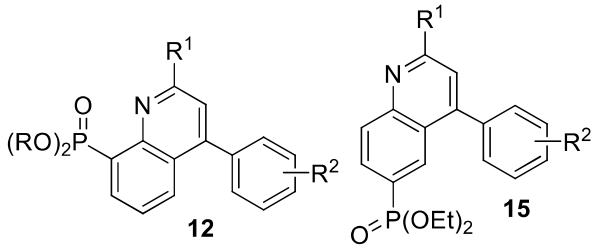

Entry	Compound				LTOP1B inhibition[a]
	Nº	R	R^1	R^2	
1	**13a**	Et	C_6H_5	H	**58.87**
2	**13b**	Et	2-MeO-C_6H_4	H	46.41
3	**13d**	Et	4-MeO-C_6H_4	H	45.45
4	**13f**	Et	1-naphthyl	H	7.50
5	**13g**	Et	2-naphthyl	H	18.36
6	**13j**	Et	4-F-C_6H_4	4-Me	41.21
7	**13k**	Et	3,4-F_2-C_6H_3	4-Me	**77.02**
8	**13l**	Et	C_6H_5	4-F	16.49
9	**13m**	Et	4-F-C_6H_4	4-F	22.44
10	**13n**	Et	3,4-F_2-C_6H_3	4-F	54.01
11	**13o**	^{i}Pr	4-F-C_6H_4	H	3.55
12	**13p**	^{i}Pr	3,4-F_2-C_6H_3	H	5.41
13	**13q**	^{i}Pr	4-F-C_6H_4	4-Me	41.62
14	**13r**	^{i}Pr	3,4-F_2-C_6H_3	4-Me	52.65
15	**13s**	^{i}Pr	4-F-C_6H_4	4-F	43.31
16	**13t**	^{i}Pr	3,4-F_2-C_6H_3	4-F	**73.27**
17	**16a**	Et	4-F-C_6H_4	H	1.94
18	**16b**	Et	3,4-F_2-C_6H_3	H	14.56
19	**16c**	Et	4-F-C_6H_4	4-Me	43.25
20	**16d**	Et	3,4-F_2-C_6H_3	4-Me	43.84
21	**16e**	Et	4-F-C_6H_4	4-F	37.86
22	**16f**	Et	3,4-F_2-C_6H_3	4-F	50.24

[a] The LTOP1B inhibitory activity is shown as the percentage of TOP1 inhibition (0-100%)

As it can be observed in Table 26, at 100 µM and a reaction time of 5 min the majority of the compounds were found to inhibit LTOP1B from *L. infantum in vitro* in overall moderate to good inhibition rates. In particular, the dialkyl quinolin-8-ylphosphonate derivatives **13k** (R = Et; R^1 = 3,4-F_2-C_6H_3; R^2 = 4-Me; Table 26, entry 7) and **13t** (R = ^{i}Pr; R^1 = 3,4-F_2-C_6H_3; R^2 = 4-F, entry 16) reported the best LTOP1B inhibitory rates (77.02% and 73.27% respectively) upon 5 min of enzymatic reaction. The compound **13k** previously presented a strong TOP1 inhibitory activity against the human hTOP1B isoform (see the Table 12 of the Chapter II, entry 11; *vide supra*) at very short enzymatic reaction times (15 sec) and a moderate inhibition at 1-3 min time frame, so it seems slightly more active toward the *L. infantum* LTOP1B isoform. On the other hand, the

quinolin-8-yl derivative **13t** had previously reported a moderate hTOP1B activity up to 3 min at 160 µM (see the Table 12, Chapter II, entry 20; *vide supra*), whereas demonstrated a stronger inhibitory effect toward the LTOP1B of *L. infantum* at 100 µM.

On balance, in light of the obtained results we may conclude that the tested dialkyl quinolinylphosphonates **13**/**16** reported overall moderate to high LTOP1B inhibition *in vitro* at 100 µM. Likewise, compounds **13**/**16** demonstrated a promising antileishmanial effect in *L. infantum* promastigotes (*in vitro*) and amastigotes (*ex vivo*) in the micromolar range, even though the selectivity toward the infective agent in the BALB/c mice model was on the whole low, resulting in elevated toxicities against the host cells. Finally, the absence of a clear relationship between the LTOP1 inhibitory activity and the EC_{50} values in *L. infantum* promastigotes/amastigotes suggests that other targets may be involved in the antileishmanial response of the compounds subject to study.

V. Conclusions

Conclusions:

I-1. The versatility of the Povarov reaction allowed us the preparation of diverse libraries of compounds based on hybrids of 2,4-disubstituted quinoline derivatives and phosphine oxide or dialkyl phosphonate moieties in positions 6 and 8 of the quinoline core. In this regard, the adaptability of the Povarov reaction by using styrenes/acetylenes as dienophiles facilitated the optimization of step-by-step/MCR one-pot methodologies to straightforwardly obtain 1,2,3,4.tetrahydroquinolines and fully aromatic and quinolines.

I-2. Futhermore, the range-expansion of the olefinic component, from styrenes to their cyclic analogue indene, allowed us to jump from a combinatorial chemistry strategy (*i.e.* exploring hybrids of phosphorated 1,2,3,4-tetrahydroquinolines/quinolines) to a diversity oriented chemistry, obtaining scaffolds of quinolines fused with indene with a higher structural complexity and a similar substitution pattern.

I-3. In summary, the applicability of the Povarov reaction to a wide range of dienophiles opened the door to a higher structural diversity in quinoline/indenoquinoline-based scaffolds, permitted the molecular hybridization between the pentavalent phosphorus-containing moieties (diphenyl phosphine oxide and dialkyl phosphonates) in the quinoline core and enabled the functionalization of the quinoline-derived frameworks with a broad variety of substituents.

II-1. The biological screening of the novel hybrid phosphorated quinoline derivatives as TOP1 inhibitors allowed to identify those ones with the ability to inhibit the enzyme at 160 µM (as reversible TOP1 inhibitors). Further mechanistic studies (nicking assays and cleavage/religation equilibrium experiment) revealed that the studied phosphorated quinolines act as *suppressor*-like TOP1 inhibitors, as they do not induce the accumulation of TOP1-dependant nicked plasmid in the nicking assay and no accumulation of TOP1CC products was observed in the cleavage/religation equilibrium experiment.

II-2. Furthermore, we participated in the development of the REEAD assay applied to the in vitro drug screening of novel TOP1 inhibitors in early stages of the drug discovery process, with the aim of discriminate among all the drug candidates those small compounds with the ability to inhibit the hTOP1B at pharmacologically relevant concentrations. We achieved to successfully study some of the novel hybrid phosphorated quinoline derivative by the REEAD assay, proving that this novel scrrening methodology provides the TOP1 activity rate in quantitative terms with a high sensitivity, which primarily implies to obtain reliable and precise inhibitory values during the biological evaluation of the tested drug candidates.

II-3. Besides the regular REEAD assay, we participated in the development of the Cleavage-Ligation variant of the REEAD assay (C/L REEAD) in order to elucidate the mechanism of action of the potential TOP1 inhibitors and in particular to disclose how the compounds may separately affect to the different catalytic steps of TOP1 catalytic cycle. The obtained results were in concordance with those obtained in the broadly used nicking assays and cleavage/religation equilibrium experiments. In consequence, we conclude that the C/L REEAD experiment permits to distinguish between poison-like or suppressor-like TOP1 inhibitors, a key information that would determine the scheduling of the subsequent biological studies with the studied compounds for a deeper research of their drug phenotype.

III-1. The evaluation of the *in vitro* antiproliferative activity of the newly prepared hybrid phosphorated quinoline derivatives by cell viability assays in A-549 (lung adenocarcinoma), SK-OV-3 (ovarian adenocarcinoma), HEK-293 (embryonic kidney cell line) and MRC-5 (lung fibroblasts) human cell lines revealed them as promising antiproliferative agents toward human cancer cell lines (A-549 and SK-OV-3) in the micromolar range (1-50 μM), while the cytotoxicity effect is not maintained in MRC-5 non-cancerous cell line. Nonetheless, if we attend to the results, the correlation between TOP1 inhibitory activity and the antiprolferative activity of the prepared phosphorated quinoline derivatives is not completely clear, suggesting that appart from TOP1, other biological targets could be implicated in the antiproliferative response of phosphorated 2,4-disubstituted quinoline derivatives (**6**, **7**, **13**, **15**, **16**) and 6-substituted indenoquinoline derivatives (**19**, **20**, **21**). In this regard, it was considered to investigate the implication of the inhibition of TOP1 in the antiproliferative response of the dialkyl phosphonate derivatives which showed the strongest TOP1 inhibitory activity (**13a**, **13f**, **13j**, **13k**, **13s**, **13t**, **16c**, **16f**, **19a** and **20a**) by complementary studies. Accordingly, the *in vitro* antiproliferative activity of these selected compounds was studied toward RPMI-8402 (T-ALL) cell line, CPT-K5 (the CPT-resistant version of RPMI-8402) cell line and HEK-293 cells upon knockdown of TOP1.

III-1. Once concluded the complementary antiproliferative studies with the selected dialkyl phosphonate derivatives **13a**, **13f**, **13j**, **13k**, **13s**, **13t**, **16c**, **16f**, **19a** and **20a**, all their biological results were collected in order to analyse the relationship between the inhibition of hTOP1 and the antiproliferative activity in human cancer cell lines. We may remark the biological response of the compounds **13k**, **13s** and **20a**, which is shown in the Figure 90 by cross matching the data collected from the *in vitro* screenings of TOP1 inhibitory activity (**Chapter II**) and antiproliferative activity (**Chapter III**). The lead compounds **13k** (compound **A**), **13s** (compound **B**) and **20a** (compound **C**) were identified from the biological screenings performed with dialkyl phosphonate-substituted quinoline derivatives (families **13**/**15**/**16**/**19**/**20**/**21**).

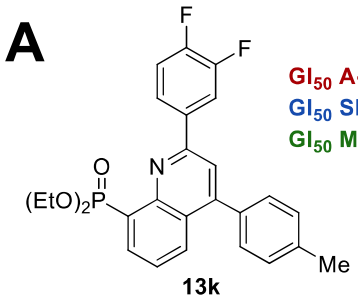

GI_{50} A-549 = 2.72 µM
GI_{50} SK-OV-3 = 10.59 µM
GI_{50} MRC-5 = >50 µM

GI_{50} RPMI-8402 = 4.37 µM vs. GI_{50} CPT-K5 = 31.53 µM
GI_{50} HEK-293 = 22.66 µM vs. GI_{50} HEK-293 TOP1 KD = >50 µM
TOP1 inhibition 15 sec/1 min/ 3 min: ++/+/+

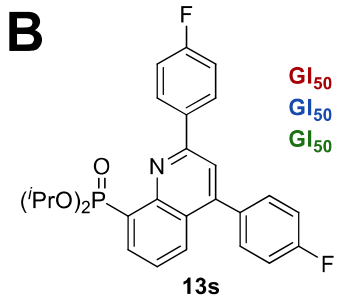

GI_{50} A-549 = 10.55 µM
GI_{50} SK-OV-3 = 19.82 µM
GI_{50} MRC-5 = >50 µM

GI_{50} RPMI-8402 = 3.23 µM vs. GI_{50} CPT-K5 = 19.19 µM
GI_{50} HEK-293 = 15.01 µM vs. GI_{50} HEK-293 TOP1 KD = >50 µM
TOP1 inhibition 15 sec/1 min/ 3 min: +/+/+

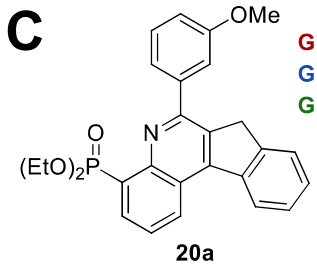

GI_{50} A-549 = 1.33 µM
GI_{50} SK-OV-3 = 9.79 µM
GI_{50} MRC-5 = >50 µM

GI_{50} RPMI-8402 = 5.04 µM vs. GI_{50} CPT-K5 = 12.07 µM
GI_{50} HEK-293 = 11.80 µM vs. GI_{50} HEK-293 TOP1 KD = >50 µM
TOP1 inhibition 15 sec/1 min/ 3 min: ++/++/+
inhibition of TOP1 activity rate (REEAD) = 41%

*Figure 90. In vitro biological response of dialkyl phosphonate-substituted quinoline derivatives **13k**, **13s** and **20a**. TOP1 inhibitory activity vs. antiproliferative activity.*

III-2. First, it can be noted that compounds **13k** and **20a** presented a strong TOP1 inhibitory activity in DNA relaxation assays (**20a** was also screened by the REEAD assay, reporting a inhibition of 41% of the TOP1 activity rate), while the compound 12 showed a moderate TOP1 inhibition.

In second place, derivatives **13k**, **13s** and **20a** were found to exhibit a notable cytotoxicity toward human cancer cell lines A-549 and SK-OV-3 (GI_{50} = 1.33-19.82 µM), while a loss of the antiproliferative effect in MRC-5 non-cancerous cancer cell line (GI_{50} = 1.33-19.82 µM). Moreover, they also presented a strong antiproliferative activity in RPMI-8402 T-ALL cancer cell line (GI_{50} = 3.23-5.04 µM), which was maintained with slightly lower antiproliferative values in the parental CPT-K5 cell line expressing a mutant TOP1 resistant to CPT (GI_{50} = 12.07-31.53 µM).

Finally, we observed that the silencing of the TOP1 expression in the embryonic HEK-293 cell line leads to the loss of the antiproliferative activity of compounds **13k, 13s and 20a** (from GI_{50} = 11.80-22.66 µM in HEK-293 cells to GI_{50} = > 50 µM in HEK-293 cells upon knockdown of TOP1). These results are in concordance with the inhibitory results obtained in DNA relaxation assays and in the REEAD assay, suggesting that TOP1 may be involved in the *in vitro* antiproliferative effect of phosphorated quinolinyl derivatives **13k, 13s and 20a**.

III-3. In view of the results, it certainly seems to be a clear correlation between the TOP1 inhibitory activity of the studied lead compounds (specially in **13k, 13s and 20a**) and the selective antiproliferative activity toward human cancer cell lines, which is unaffected (or slightly affected) by the expression of a mutant TOP1 resistant to CPT (*poison*-like TOP1 inhibitor) and drastically affected upon silencing of the TOP1 expression.

VI. Experimental section

VI-1. Chemistry

VI-1.1 General experimental information

General reaction conditions, reagents and solvents: all reactions were conducted under inert dry N_2 gas atmosphere in dried glassware.

High purity-grade solvents were used in reactions and crystallizations, which were previously freshly distilled and/or dried over molecular sieves (3-4 Å) as detailed in the literature[364]. Technical grade solvents were directly used in extractions and column chromatography purifications.

All the commercially available reagents (obtained from Sigma Aldrich, Merck, Acros and Fluorochem) were stored and manipulated by following the manufacturer´s instructions, and were directly used without further purification, unless stated otherwise.

Nuclear magnetic resonance (NMR) spectroscopy characterization: ^{1}H (300, 400 MHz), ^{13}C (at 75 MHz or 100 MHz), ^{31}P NMR (at 120 MHz or 160 MHz) and 19F NMR (282 MHz) spectra were recorded on Varian Unity Plus (300 MHz) or Bruker Avance 400 (400 MHz) spectrometers at 25^{o}C, respectively, while NOESY and HMBC experiments were performed in a Bruker Avance 400 (400 MHz) spectrometer. Unless stated otherwise, NMR experiments were carried out by using deuterated chloroform ($CDCl_3$) as a solvent. Chemical shifts for ^{1}H NMR spectra are reported in parts per million (ppm) downfield from TMS. Data for ^{13}C NMR spectra are reported in terms of chemical shift (ppm) relative to the peak of the $CDCl_3$ solvent as an internal reference (δ = 77.16 ppm) and furthermore, the corresponding peak assignments were supported by DEPT-135 NMR spectra (distortionless enhanced polarization transfer ^{13}C NMR mode). Chemical shifts for ^{31}P NMR and ^{19}F NMR are reported in ppm relative to an external reference, by the signal of a sealed capillary of an aqueous 85% phosphoric acid solution at δ = 0.0 ppm (^{31}P NMR) and the signal of $CFCl_3$ at δ = 0.0 ppm as a standard (^{19}F NMR), respectively. Both ^{13}C NMR and ^{19}F NMR were recorded in a broadband decoupled mode from hydrogen nuclei. All the coupling constants (*J*) are reported in Hz (hertz). The multiplicity of NMR signals is being given as follows: s (singlet), d (doublet), dd (doublet of doublets), ddd (doublet of doublets of doublets), q (quadruplet) and m (multiplet).

[364] Williams DB, Lawton M. Drying of organic solvents: Quantitative evaluation of the efficiency of several desiccants. *J Org Chem*. 2010;75(24):8351-8354. doi:10.1021/jo101589h

High resolution mass-spectroscopy (HRMS) characterization: HRMS experiments were performed by the SGIker (central analysis service of the UPV/EHU, University of the Basque Country) by using an Agilent LC-Q-TOF-MS 6520 spectrometer and a positive electrospray-ioizantion (ESI) method for the exact mass-elucidation of the synthesized compounds.

High-performance liquid chromatography (HPLC): All synthesized compounds were analyzed by HPLC to determine their purity. The analyses were performed on Agilent 1260 infinity HPLC system (C-18 column, Hypersil, BDS, 5 mm, 0.4 mm x 25 mm) at room temperature. All the tested compounds were dissolved in dichloromethane, and 5 mL of the sample was loaded onto the column. Ethanol and heptane were used as mobile phase, and the flow rate was set at 1.0 mL/min. The maximal absorbance at the range of λ = 190-400 nm was used as the detection wavelength. The purity of the compounds was found to be over 95% in all cases.

Melting points (MP): MP were determined with an electrothermal digital melting point apparatus Büchi MPB-540 in opened glass capillaries and are given as an interval in Celsius degrees (^{o}C) uncorrected.

Thin layer chromatography (TLC): TLC was used for the monitoring of some reactions and the further analytical characterization of purified oil-state products. Unless explicitly quoted otherwise, TLC was performed on pre-coated silica gel 60 F254 aluminium plates (Alugram, SIL G/UV254) and visualized under ultraviolet light (λ = 254 nm). In some cases, TLC plates had to be developed with potassium permanganate stain (1.5 g of $KMnO_4$, 10g of K_2CO_3 and 1.25 mL 10% NaOH in 200mL of water).

Column chromatography: flash column chromatography has been used as a purification technique by using silica gel (60 Å, 230-400 mesh ASTM) or neutral alumina (70-290 mesh ASTM) and the corresponding mixture of technical-grade solvents (which is indicated in each particular case).

VI-1.2. Synthesis of quinolinylphosphine oxide derivatives

Preparation of (2-aminophenyl)diphenylphosphine oxide 1a

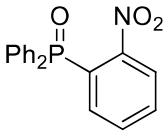

(2-nitrophenyl)diphenylphosphine oxide.

A solution of ethyl diphenylphosphinite (19.44 mL, 90 mmol, 1.2 equiv.) in 30 mL of dry *dimethylformamide* (DMF) was added drop by drop during 2.5 h to a stirred -10°C solution of 1,2-dinitrobenzene (12.61 g, 75 mmol, 1 equiv.) in 40 mL of dry acetonitrile (MeCN). Upon addition, the reaction mixture was maintained stirring at room temperature for 12h. The resultant precipitate was filtered off, washed with DMF, dried *in vacuo* and recrystalized in ethyl acetate (EtOAc) at 4°C, obtaining 20.08 g (62.10 mmol) of (2-nitrophenyl)diphenylphosphine oxide as a yellow solid (69%); mp 226-227°C (EtOAc).

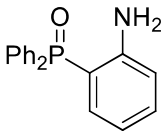

1a

(2-Aminophenyl)diphenylphosphine oxide (1a):

(2-Nitrophenyl)diphenylphosphine oxide (19.40 g, 60 mmol) was hydrogenated with a spoon of RANEY® Nickel (approx. 5 g) in 60 mL of MeOH at 80 psi at room temperature for 12 h. The reaction mixture was then filtered off through a pad of cellite and evaporated to dryness to obtain (2-aminophenyl)diphenylphosphine oxide **1a** (17.59 g, 59.97 mmol) as a white solid (99%); mp 167-168°C (methanol).

General procedure for the preparation of aldimines 4

To a solution of (2-aminophenyl)diphenylphosphine oxide 1 (2.93 g, 10 mmol, 1 equiv.) in $CHCl_3$ (25 mL) was added the corresponding aldehyde (10 mmol). The mixture was stirred at $CHCl_3$ reflux until consumption of starting materials was confirmed by ^{1}H NMR, ^{31}P NMR and/or ^{19}F NMR spectroscopy. The yielded aldimines **4** were proved unstable during distillation and/or chromatography conditions, so they were used *in situ* without further purification for the upcoming reactions.

General procedure for the preparation of 1,2,3,4-tetrahydroquinolin-8-yl phosphine oxides 6

A) Step-by step Povarov procedure (*route A*).

Styrenes **3** (12 mmol, 1.2 equiv.) and 2 equivalent of $BF_3{\cdot}Et_2O$ (1.23 mL, 10 mmol) were added to a solution of the corresponding *in situ* prepared aldimine **4** (10 mmol) in $CHCl_3$ (25 mL). The mixture was stirred and heated to $CHCl_3$ reflux until TLC, ^{31}P NMR and ^{1}H NMR spectroscopy analysis indicated the disappearance of the aldimine. The molecular sieves were removed by

filtration and the resulting solution was diluted with methylene chloride (20 ml), washed with a solution of NaOH 2M (50 ml), extracted with methylene chloride (2 x 10 mL) and dried over $MgSO_4$. Upon *in vacuo* solvent evaporation, the resultant reaction crude was further purified by silica gel flash column chromatography on silica gel using a gradient of elution of 5-70% ethyl acetate in hexane to afford 1,2,3,4-tetrahydroquinolin-8-yl phosphine oxides **6**.

B) MCR Povarov procedure (*route B*):

A mixture of (2-aminophenyl)diphenylphosphanoxide **1a** (10 mmol, 1 equiv.), freshly distilled aldehydes **2** (10 mmol, 1 equiv.), styrenes **3** (12 mmol, 1.2 equiv.) and 2 equivalents of $BF_3{\cdot}Et_2O$ (2.47 mL, 20 mmol) dissolved in $CHCl_3$ (25 mL) was stirred and heated to reflux in the presence of molecular sieves (4 Å), until TLC, ^{3}1P NMR and ^{1}H NMR spectroscopy analysis indicated the consumption of the starting materials. The molecular sieves were removed by filtration and the resulting solution was diluted with methylene chloride (15 ml), washed with a solution of NaOH 2M (50 ml), extracted with methylene chloride (2 x 10 mL) and dried over $MgSO_4$. Upon *in vacuo* solvent evaporation, the resultant reaction crude was further purified by silica gel flash column chromatography on silica gel using a gradient of elution of 5-70% ethyl acetate in hexane to afford 1,2,3,4-tetrahydroquinolin-8-yl phosphine oxides **6**.

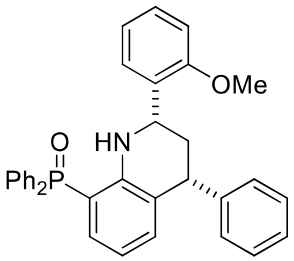

6a

(2-(2-Methoxyphenyl)-4-phenyl-1,2,3,4-tetrahydroquinolin-8-yl)diphenylphosphine oxide (**6a**).

The general procedure A was followed using *o*-anisaldehyde (1.21 mL, 10 mmol) and styrene (1.37 mL, 12 mmol). The reaction was heated to $CHCl_3$ reflux for 36 h, affording the compound **6a** (4.69 g, 91%) as a white solid.

Melting point: 233-235ºC (ethyl acetate/hexane).

^{1}H RMN (400 MHz, $CDCl_3$): δ = 1.80 (ddd, $^3J_{HH}$ = 12.3 Hz, $^3J_{HH}$ = 11.1 Hz, $^2J_{HH}$ = 12.5 Hz, 1 H, CH_2), 1.82 (s, NH), 2.36-2.41 (m, 1 H, CH_2), 3.68 (s, 3 H, OCH_3), 4.23 (dd, $^4J_{HH}$ = 4.3 Hz, $^3J_{HH}$ = 12.3 Hz, 1 H, CH), 5.11 (dd, $^4J_{HH}$ = 4.3 Hz, $^3J_{HH}$ = 12.3.1 Hz, 1 H, CH), 6.25 (ddd $^3J_{HH}$ = 7.6 Hz, $^3J_{HH}$ = 7.4 Hz, $^4J_{HP}$ = 2.9 Hz, 1 H), 6.51-6.75 (m, 5 H), 7.03-7.73 (m, 16 H) ppm.

^{13}C RMN (100 MHz, $CDCl_3$): δ = 38.0 (CH_2), 44.8 (HC), 50.0 (OCH_3), 55.4 (HC), 110.2 (HC), 110.9 (d, $^1J_{CP}$ = 105.6 Hz, C), 114.4 (d, $^3J_{CP}$ = 13.8 Hz, HC), 121.0 (HC), 125.8-133.8 (m, 19 HC and 4 C), 144.5 (C), 150.5 (d, $^2J_{CP}$ = 4.6 Hz, C), 156.5 (C) ppm.

^{31}P NMR (120 MHz, $CDCl_3$): δ = 36.3 ppm.

HRMS (EI): calculated for $C_{34}H_{30}NO_2P$ $[M]^+$ 515.2014; found 515.2022.

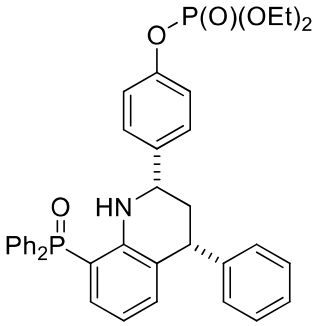

6b

4-(8-(diphenylphosphoryl)-4-phenyl-1,2,3,4-tetrahydroquinolin-2-yl)phenyl diethyl phosphate (**6b**).

The general procedure A was followed using diethyl (4-formylphenyl) phosphate (2.58 g, 10 mmol) and styrene (1.37 mL, 12 mmol). The reaction was heated to $CHCl_3$ reflux for 24 h, affording the compound **6b** (2.81 g, 44%) as a white solid.

Melting point: 66-68°C (ethyl acetate/hexane).

^{1}H RMN (300 MHz, $CDCl_3$): δ = 1.31-1.36 (m, 6 H, 2 CH_3), 1.92-1.99 (m, 1H, CH_2), 2.16-2.26 (m, 1H, CH_2), 4.17-4.22 (m, 5 H, 1 CH and 2 CH_2), 4.70 (dd, $^3J_{HH}$ = 11.2 Hz, $^3J_{HH}$ =2.9 Hz, 1H, HC), 6.33-7.78 (m, NH and 22 H) ppm.

^{13}C RMN (75 MHz, $CDCl_3$): δ = δ = 16.2 (2 CH_3), 41.0 (CH_2), 44.7 (HC), 56.2 (HC), 64.7 (2 CH_2), 111.0 (d, $^1J_{CP}$ = 106.0 Hz, C), 115.0 (d, $^3J_{CP}$ = 13.8 Hz, HC), 120.0-133.2 (m, 21 HC and 4 C), 140.6 (C), 144.1 (C), 149.8 (d, $^2J_{CP}$ = 5.9 Hz, C) ppm.

^{31}P NMR (120 MHz, $CDCl_3$): δ = -5.3, 36.3 ppm.

HRMS (EI): calculated for $C_{37}H_{37}NO_5P_2$ $[M]^+$ 637.2147; found 637.2158.

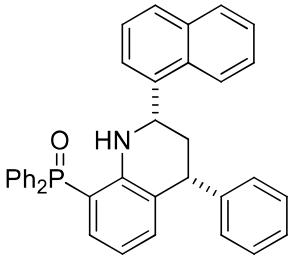

6c

(2-(Naphthalen-1-yl)-4-phenyl-1,2,3,4-tetrahydroquinolin-8-yl)diphenylphosphine oxide (**6c**).

The general procedure A was followed using 1-naphthaldehyde (1.36 mL, 10 mmol) and styrene (1.37 mL, 12 mmol). The reaction was heated to $CHCl_3$ reflux for 24 h, affording the compound **6c** (3.48 g, 65%) as a white solid.

Melting point: 267-269°C (ethyl acetate/hexane).

^{1}H RMN (300 MHz, $CDCl_3$): δ = 2.11 (ddd, $^3J_{HH}$ = 12.7 Hz, $^3J_{HH}$ = 11.3 Hz, $^2J_{HH}$ = 12.5 Hz, 1 H, CH_2), 2.48-2.55 (m, 1 H, CH_2), 4.39 (dd, $^3J_{HH}$ = 4.3 Hz, $^3J_{HH}$ = 12.7 Hz, 1 H, CH), 5.56 (dd, $^3J_{HH}$ = 2.7 Hz, $^3J_{HH}$ = 11.3 Hz, 1 H, CH), 6.40 (ddd $^3J_{HH}$ = 7.6 Hz, $^3J_{HH}$ = 7.5 Hz, $^4J_{HP}$ = 3.0 Hz, 1 H), 6.66-6.75 (m, 2 H), 7.16-7.99 (m, NH, 22 H) ppm.

^{13}C RMN (75 MHz, $CDCl_3$): δ = 39.3 (CH_2), 45.1 (HC), 52.9 (HC), 114.4 (d, $^1J_{CP}$ = 105.5 Hz, C), 114.8 (d, $^3J_{CP}$ = 13.8 Hz, HC), 120.5 (C), 125.5 (HC), 122.8 (HC), 125.4 (HC), 125.9 (HC), 126.1 (HC), 126.3 (d, $^3J_{CP}$ = 7.8 Hz, C), 126.9 (HC), 127.8 (HC), 128.5-129.0 (m, 6 HC), 130.7 (C), 131.8-133.9 (m, 11 HC and 2C), 139.3 (C), 144.3 (C), 150.3 (d, $^2J_{CP}$ = 4.6 Hz, C) ppm.

^{31}P NMR (120 MHz, $CDCl_3$): δ = 36.3 ppm.

HRMS (EI): calculated for $C_{37}H_{30}NOP$ $[M]^+$ 535.2065; found 535.2076.

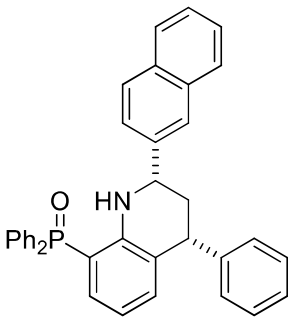

6d

(2-(Naphthalen-2-yl)-4-phenyl-1,2,3,4-tetrahydroquinolin-8-yl)diphenylphosphine oxide (**6d**).

The general procedure B was followed using 2-naphthaldehyde (1.36 g, 10 mmol) and styrene (1.37 mL, 12 mmol). The reaction was heated to $CHCl_3$ reflux for 36 h, affording the compound **6d** (3.85 g, 72%) as a white solid.

Melting point: 245-247°C (ethyl acetate/hexane).

^{1}H RMN (400 MHz, $CDCl_3$): δ = 2.12 (ddd, $^{3}J_{HH}$ = 12.6 Hz, $^{3}J_{HH}$ = 11.9 Hz, $^{2}J_{HH}$ = 12.7 Hz, 1 H, CH_2), 2.33-2.39 (m, 1 H, CH_2), 4.33 (dd, $^{3}J_{HH}$ = 4.1 Hz, $^{3}J_{HH}$ = 12.2 Hz, 1 H, CH), 4.93 (dd, $^{3}J_{HH}$ = 3.1 Hz, $^{3}J_{HH}$ = 11.5 Hz, 1 H, CH), 6.42 (ddd $^{3}J_{HH}$ = 7.6 Hz, $^{3}J_{HH}$ = 7.6 Hz, $^{4}J_{HP}$ = 2.9 Hz, 1 H), 6.67-6.75 (m, 2 H), 7.16-7.86 (m, NH, 22 H) ppm.

^{13}C RMN (100 MHz, $CDCl_3$): δ = 40.9 (CH_2), 44.9 (HC), 56.9 (HC), 111.2 (d, $^{1}J_{CP}$ = 105.5 Hz, C), 114.8 (d, $^{3}J_{CP}$ = 13.8 Hz, HC), 124.6 (HC), 124.6 (HC), 125.7 (HC), 125.9 (HC), 126.2 (d, $^{3}J_{CP}$ = 7.8 Hz, C), 126.8 (HC), 127.6 (HC), 128.0-133.5 (m, 19 HC and 3 C), 141.4 (C), 144.3 (C), 150.2 (d, $^{2}J_{CP}$ = 4.6 Hz, C) ppm.

^{31}P NMR (120 MHz, $CDCl_3$): δ = 36.4 ppm.

HRMS (EI): calculated for $C_{37}H_{30}NOP$ $[M]^+$ 535.2065; found 535.2086.

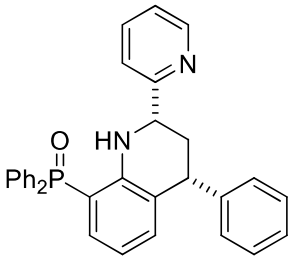

6e

(4-Phenyl-2-(pyridin-2-yl)-1,2,3,4-tetrahydroquinolin-8-yl)diphenylphosphine oxide (**6e**).

The general procedure B was followed using 2-Pyridinecarboxaldehyde (0.95 mL, 10 mmol) and styrene (1.37 mL, 12 mmol). The reaction was heated to $CHCl_3$ reflux for 12 h, affording the compound **6e** (3.36 g, 69%) as a yellow solid.

Melting point: 110-112°C (ethyl acetate/hexane).

^{1}H RMN (300 MHz, $CDCl_3$): δ = 1.97 (ddd, $^{3}J_{HH}$ = 12.5 Hz, $^{3}J_{HH}$ = 11.4 Hz, $^{2}J_{HH}$ = 12.5 Hz, 1 H, CH_2), 2.45-2.52 (m, 1 H, CH_2), 4.27 (dd, $^{3}J_{HH}$ = 4.6 Hz, $^{3}J_{HH}$ = 12.5 Hz, 1 H, CH), 4.85 (dd, $^{3}J_{HH}$ = 3.3 Hz, $^{3}J_{HH}$ = 11.3 Hz, 1 H, CH), 6.38 (ddd $^{3}J_{HH}$ = 7.6 Hz, $^{3}J_{HH}$ = 7.6 Hz, $^{4}J_{HP}$ = 3.0 Hz, 1 H), 6.63-6.74 (m, 2 H), 6.96 (d, $^{3}J_{HH}$ = 7.9 Hz, 1 H), 7.17-7.81 (m, NH, 18 H) ppm.

^{13}C RMN (75 MHz, $CDCl_3$): δ = 39.1 (CH_2), 45.6 (HC), 57.9 (HC), 111.0 (d, $^{1}J_{CP}$ = 105.6 Hz, C), 115.1 (d, $^{3}J_{CP}$ = 13.9 Hz, HC), 119.6 (C), 122.2 (HC), 126.2 (d, $^{3}J_{CP}$ = 7.9 Hz, C), 126.8 (HC), 128.2-132.1 (m, 15 HC and C), 133.3 (d, $^{1}J_{CP}$ = 104.8 Hz, C), 133.4 (2 HC), 137.2 (HC), 144.3 (C), 148.9 (HC), 149.9 (d, $^{2}J_{CP}$ = 4.5 Hz, C) ppm.

^{31}P NMR (120 MHz, $CDCl_3$): δ = 37.0 ppm.

HRMS (EI): calculated for $C_{32}H_{27}N_2OP$ $[M]^+$ 486.1861; found 486.1869.

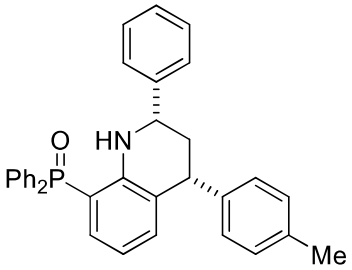

6f

(2-Phenyl-4-(p-tolyl)-1,2,3,4-tetrahydroquinolin-8-yl)diphenylphosphine oxide (**6f**).

The general procedure B was followed using benzaldehyde (1.02 mL, 10 mmol) and 1-methyl-4-vinylbenzene (1.58 mL, 12 mmol). The reaction was heated to $CHCl_3$ reflux for 48 h, affording the compound **6f** (3.05 g, 61%) as a white solid.

Melting point: 223-225°C (ethyl acetate/hexane).

^{1}H RMN (300 MHz, $CDCl_3$): δ = 1.97-2.25 (m, 2 H, CH_2), 2.33 (s, 3 H, CH_3), 4.19 (dd, $^3J_{HH}$ = 4.0 Hz, $^3J_{HH}$ = 12.4 Hz, 1 H, CH), 4.71 (dd, $^3J_{HH}$ = 3.4 Hz, $^3J_{HH}$ = 11.4 Hz, 1 H, CH), 6.35 (ddd $^3J_{HH}$ = 7.8 Hz, $^3J_{HH}$ = 7.4 Hz, $^4J_{HP}$ = 2.8 Hz, 1 H), 6.57-6.68 (m, 2 H), 6.99-7.78 (m, NH, 19 H) ppm.

^{13}C RMN (75 MHz, $CDCl_3$): δ = 22.1 (CH_3), 41.0 (CH_2), 44.4 (HC), 57.0 (HC), 111.0 (d, $^1J_{CP}$ = 108.0 Hz, C), 114.8 (d, $^3J_{CP}$ = 11.7 Hz, HC), 126.1-133.6 (m, 21 HC and 3 C), 136.4 (C), 141.2 (C), 143.9 (C), 150.0 (d, $^2J_{CP}$ = 3.6 Hz, C) ppm.

^{31}P NMR (120 MHz, $CDCl_3$): δ = 36.4 ppm.

HRMS (EI): calculated for $C_{34}H_{30}NOP$ $[M]^+$ 499.2065; found 499.2077.

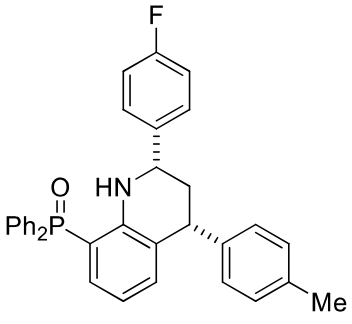

6g

2-(4-fluorophenyl)-4-(p-tolyl)-1,2,3,4-tetrahydroquinolin-8-yl)diphenylphosphine oxide (**6g**).

The general procedure B was followed using 4-fluorobenzaldehyde (1.08 mL, 10 mmol) and 1-methyl-4-vinylbenzene (1.58 mL, 12 mmol). The reaction was heated to $CHCl_3$ reflux for 36 h, affording the compound **6g** (3.67 g, 71%) as a white solid.

Melting point: 207-209°C (ethyl acetate/hexane).

^{1}H RMN (300 MHz, $CDCl_3$): δ = 1.93 (ddd, $^3J_{HH}$ = 12.7 Hz, $^3J_{HH}$ = 11.5 Hz, $^2J_{HH}$ = 12.7 Hz, 1 H, CH_2), 2.18 (ddd, $^3J_{HH}$ = 4.7 Hz, $^3J_{HH}$ = 3.4 Hz, $^2J_{HH}$ = 12.7 Hz, 1 H, CH_2), 2.34 (s, 3 H, CH_3), 4.18 (dd, $^3J_{HH}$ =

4.7 Hz, $^{3}J_{HH}$ = 12.7 Hz, 1 H, CH), 4.69 (dd, $^{3}J_{HH}$ = 3.4 Hz, $^{3}J_{HH}$ = 11.5 Hz, 1 H, CH), 6.36 (ddd $^{3}J_{HH}$ = 10.4 Hz, $^{3}J_{HH}$ = 7.6 Hz, $^{4}J_{HP}$ = 3.0 Hz, 1 H), 6.81-7.15 (m, NH and 11 H), 7.44-7.78 (m, 10 H) ppm.

^{13}C RMN (75 MHz, $CDCl_3$): δ = 22.2 (CH_3), 41.2 (CH_2), 44.3 (HC), 56.3 (HC), 111.0 (d, $^{1}J_{CP}$ = 105.0 Hz, C), 114.9 (d, $^{3}J_{CP}$ = 13.1 Hz, HC), 115.3 (d, $^{3}J_{CF}$ = 21.3 Hz, 2 HC), 126.3 (d, $^{3}J_{CP}$ = 7.5 Hz, C), 127.6-129.5 (m, 12 HC), 131.8-133.5 (m, 6 HC and 2 C), 136.5 (C), 139.8 (C), 141.1 (C), 149.0 (C), 162.0 (d, $^{1}J_{CF}$ = 243.8 Hz, C-F) ppm.

^{31}P NMR (120 MHz, $CDCl_3$): δ = 35.5 ppm.

^{19}F NMR crude reaction mixture (282 MHz, $CDCl_3$): δ = -116.3 to -116.1 ppm.

HRMS (EI): calculated for $C_{34}H_{29}FNOP$ $[M]^+$ 517.1971; found 517.1982.

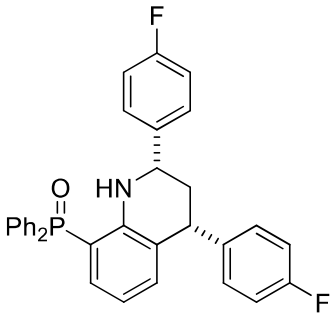

6h

2,4-Bis(4-fluorophenyl)-1,2,3,4-tetrahydroquinolin-8-yl)diphenylphosphine oxide (**6h**).

The general procedure B was followed using 4-fluorobenzaldehyde (1.08 mL, 10 mmol) and 4-fluorostyrene (1.44 mL, 12 mmol). The reaction was heated to $CHCl_3$ reflux for 24 h, affording the compound **6h** (2.30 g, 44%) as a white solid.

Melting point: 183-185°C (ethyl acetate/hexane).

^{1}H RMN (300 MHz, $CDCl_3$): δ = 1.90 (ddd, $^{3}J_{HH}$ = 12.4 Hz, $^{3}J_{HH}$ = 11.3 Hz, $^{2}J_{HH}$ = 12.7 Hz, 1 H, CH_2), 2.14-2.20 (m, 1 H, CH_2), 4.22 (dd, $^{3}J_{HH}$ = 4.3 Hz, $^{3}J_{HH}$ = 12.4 Hz, 1 H, CH), 4.70 (dd, $^{3}J_{HH}$ = 3.2 Hz, $^{3}J_{HH}$ = 11.3 Hz, 1 H, CH), 6.37 (ddd $^{3}J_{HH}$ = 7.6 Hz, $^{3}J_{HH}$ = 7.4 Hz, $^{4}J_{HP}$ = 3.0 Hz, 1 H), 6.62-7.19 (m, NH and 11 H), 7.44-7.78 (m, 9 H) ppm.

^{13}C RMN (75 MHz, $CDCl_3$): δ = 41.3 (CH_2), 44.0 (HC), 56.2 (HC), 111.3 (d, $^{1}J_{CP}$ = 105.5 Hz, C), 114.9 (d, $^{3}J_{CP}$ = 13.8 Hz, HC), 115.4 (d, $^{3}J_{CF}$ = 21.3 Hz, 2 HC), 115.6 (d, $^{3}J_{CF}$ = 21.3 Hz, 2 HC), 125.8 (d, $^{3}J_{CP}$ = 8.0 Hz, C), 127.6-133.6 (m, 16 HC and 2 C), 139.6 (d, $^{4}J_{CF}$ = 3.1 Hz, C), 139.8 (d, $^{4}J_{CF}$ = 3.2 Hz, C), 149.9 (d, $^{2}J_{CP}$ = 4.6 Hz, C), 161.8 (d, $^{1}J_{CF}$ = 245.0 Hz, C-F) ppm.

^{31}P NMR (120 MHz, $CDCl_3$): δ = 36.3 ppm.

^{19}F NMR crude reaction mixture (282 MHz, $CDCl_3$): δ = -116.5 to -116.4 and -116.0 to -115.8 (m) ppm.

HRMS (EI): calculated for $C_{33}H_{26}F_2NOP$ $[M]^+$ 521.1720; found 521.1727.

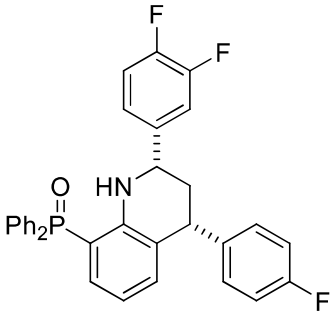

6i

2-(3,4-difluorophenyl)-4-(4-fluorophenyl)-1,2,3,4-tetrahydroquinolin-8-yl)diphenylphosphine oxide (**6i**).

The general procedure A was followed using 3,4-difluorobenzaldehyde (1.10 mL, 10 mmol) and 4-fluorostyrene (1.44 mL, 12 mmol). The reaction was heated to $CHCl_3$ reflux for 36 h, affording the compound **6i** (2.64 g, 49%) as a white solid.

Melting point: 167-169°C (ethyl acetate/hexane).

^{1}H RMN (300 MHz, $CDCl_3$): δ = 1.72 (s, 1 H, NH), 1.88 (ddd, $^3J_{HH}$ = 11.7 Hz, $^3J_{HH}$ = 11.4 Hz, $^2J_{HH}$ = 11.4 Hz, 1 H, CH_2), 2.15-2.20 (m, 1 H, CH_2), 4.21 (dd, $^3J_{HH}$ = 4.6 Hz, $^3J_{HH}$ = 11.7 Hz, 1 H, CH), 4.67 (dd, $^3J_{HH}$ = 3.4 Hz, $^3J_{HH}$ = 11.7 Hz, 1 H, CH), 6.40 (ddd $^3J_{HH}$ = 10.4 Hz, $^3J_{HH}$ = 7.5 Hz, $^4J_{HP}$ = 3.0 Hz, 1 H), 6.64-7.14 (m, 9 H), 7.46-7.77 (m, 10 H) ppm.

^{13}C RMN (75 MHz, $CDCl_3$): δ = 41.1 (CH_2), 43.9 (HC), 55.9 (HC), 111.8 (d, $^1J_{CP}$ = 103.7 Hz, C), 114.9 (d, $^2J_{CF}$ = 17.7 Hz, HC), 115.4 (d, $^3J_{CP}$ = 13.6 Hz, HC), 115.7 (d, $^3J_{CF}$ = 20.2 Hz, 2 HC), 117.3 (d, $^2J_{CF}$ = 17.7 Hz, HC), 121.1 (HC), 125.7 (C), 128.6-133.3 (m, 14 HC and 2 C), 139.6 (C), 141.0 (C), 149.4 (Dd, $^1J_{CF}$ = 246.5 Hz, $^2J_{CF}$ = 12.8 Hz, C-F), 161.8 (d, $^1J_{CF}$ = 243.4 Hz, C-F) ppm.

^{31}P NMR (120 MHz, $CDCl_3$): δ = 36.4 ppm.

^{19}F NMR crude reaction mixture (282 MHz, $CDCl_3$): δ = -116.2 to -116.1, -137.8 to -137.6 and -115.9 to -115.8 (m) ppm.

HRMS (EI): calculated for $C_{33}H_{25}F_3NOP$ $[M]^+$ 539.1626; found 539.1636.

General procedure for the preparation of quinolin-8-yl phospine oxides 7

A) *Oxidation of compounds 6 with DDQ*

DDQ (0.45 g, 2 mmol, 2 equiv.) was added to a solution of the corresponding 1,2,3,4-tetrahydroquinolin-8-yl phosphine oxide **6** (1 mmol, 1 equiv.) in chloroform (5 mL) and the reaction mixture was stirred and heated to reflux until TLC, ^{31}P NMR and ^{1}H NMR spectroscopy analysis indicated the consumption of the 1,2,3,4-tetrahydroquinolin-8-yl phosphine oxide **6** and the subsequent formation of the quinolin-8-yl phospine oxide **7** (2 h). The formed reaction brute was filtered off, dried *in vacuo* and purified by silica gel flash column chromatography (40% of ethyl acetate in hexane) and a further recrystallization in EtOAc/hexane to yield quinolin-8-yl phosphine oxides **7**.

B) One-pot Povarov reaction with acetylenes (*Route C*).

The corresponding acetylene **8** (2 mmol, 1 equiv.) and 2 equivalents of $BF_3{\cdot}Et_2O$ (0.5 mL, 4 mmol) were added to a solution of the in situ prepared aldimine **4** (2 mmol) in dry $CHCl_3$ and the mixture was stirred at reflux during 2 h. Then, the reaction was allow to reach room temperature and DDQ (0.91 g, 4 mmol, 2 equiv.) was added, to subsequently heat again to reflux for 30 minutes. The reaction mixture was then washed with an aqueous solution of NaOH 2M (25 mL) and water (25 mL), extracted with dichloromethane (2 × 25 mL), and dried over anhydrous $MgSO_4$. Upon the removal of the solvent under vacuum, the resultant crude oil was purified by silica gel flash column chromatography using a gradient elution of 10−40% ethyl acetate in hexane to afford quinolin-8-yl phospine oxides **7**.

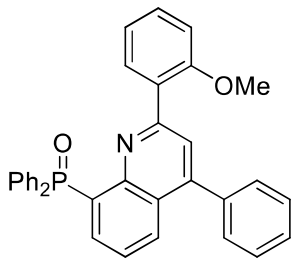

7a

(2-(2-Methoxyphenyl)-4-phenylquinolin-8-yl)diphenylphosphine oxide (**7a**).

The general procedure A (*oxidation of compounds 6 with DDQ*) was employed with **6a** (0.52 g, 1 mmol) to afford **7a** (0.38 g, 74%) as a white solid.

Melting point: 267-269°C (ethyl acetate/hexane).

^{1}H RMN (300 MHz, $CDCl_3$): δ = 3.80 (s, 3 H, OCH_3), 6.52 (dd J = 1.6 Hz, J = 7.6 Hz, 1 H), 6.69-6.75 (m, 1 H), 6.94 (d, $^{3}J_{HH}$ = 8.7 Hz, 1 H), 7.20-7.66 (m, 13 H), 7.89 (dd, $^{3}J_{HP}$ = 12.5 Hz, $^{3}J_{HH}$ = 7.0 Hz, 4 H), 7.96 (s, 1 H), 8.12 (d, $^{3}J_{HH}$ = 9.0 Hz, 1 H), 8.67 (ddd, $^{3}J_{HP}$ = 13.9 Hz, $^{3}J_{HH}$ = 7.1 Hz, $^{4}J_{HH}$ = 1.6 Hz, 1 H) ppm.

^{13}C RMN (75 MHz, $CDCl_3$): δ = 55.7 (OCH_3), 111.3 (HC), 120.9 (HC), 121.0-138.5 (m, 21 HC and 6 C), 147.7 (d, $^{2}J_{CP}$ = 5.6 Hz, C), 155.5 (C), 157.5 (C) ppm.

^{31}P NMR (120 MHz, $CDCl_3$): δ = 29.4 ppm.

HRMS (EI): calculated for $C_{34}H_{26}NO_2P$ $[M]^+$ 511.1701; found 511.1719.

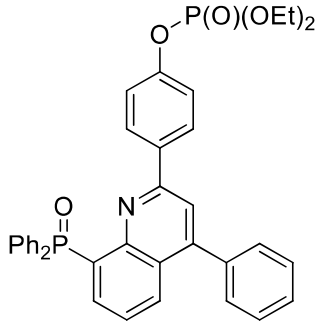

7b

4-(8-(diphenylphosphoryl)-4-phenylquinolin-2-yl)phenyl diethyl phosphate (**7b**).

The general procedure A (*oxidation of compounds 6 with DDQ*) was employed with **6b** (0.64 g, 1 mmol) to afford **7b** (0.41 g, 65%) as a white solid.

Melting point: 128-130ºC (ethyl acetate/hexane).

^{1}H RMN (400 MHz, $CDCl_3$): δ = 1.36-1.41 (m, 6 H, 2 CH_3), 4.20-4.30 (m, 4 H, 2 CH_2), 7.11-7.15 (m, 2 H), 7.36-7.65 (m, 14 H), 7.75 (s, 1 H), 7.88-7.95 (m, 4 H), 8.15 (d, $^{3}J_{HH}$ = 8.4 Hz, 1 H), 8.64 (ddd, $^{3}J_{HP}$ = 13.9 Hz, $^{3}J_{HH}$ = 7.1 Hz, $^{4}J_{HH}$ = 1.5 Hz, 1 H) ppm.

^{13}C RMN (75 MHz, $CDCl_3$): δ = δ = 16.3 (2 CH_3), 64.9 (2 CH_2), 119.1 (HC), 120. (HC), 120.1 (HC), 120.4 (C), 126.0-132.3 (m, 19 HC and 2 C), 134.2 (d, $^{1}J_{CP}$ = 108.2 Hz, 2 C), 135.5 (C), 138.0 (d, $^{3}J_{CP}$ = 5.8 Hz, HC), 148.2 (d, $^{2}J_{CP}$ = 5.7 Hz, C), 149.8 (C), 152.3 (d, $^{2}J_{CP}$ = 6.7 Hz, C), 154.8 (C) ppm.

^{31}P NMR (120 MHz, $CDCl_3$): δ = -5.4, 28.9 ppm.

HRMS (EI): calculated for $C_{37}H_{33}NO_5P_2$ $[M]^+$ 633.1834; found 633.1849.

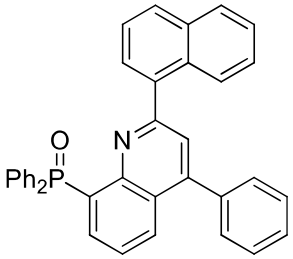

7c

(2-(Naphthalen-1-yl)-4-phenylquinolin-8-yl)diphenylphosphine oxide (**7c**).

The general procedure A (*oxidation of compounds 6 with DDQ*) was employed with **6c** (0.54 g, 1 mmol) to afford **7c** (0.38 g, 72%) as a white solid.

Melting point: 263-265°C (ethyl acetate/hexane).

^{1}H RMN (300 MHz, $CDCl_3$): δ = 6.85-6.88 (m, 1 H), 7.18-7.91 (m, 23 H), 8.23 (d, $^{3}J_{HP}$ = 8.7 Hz, 1 H), 8.80 (ddd, $^{3}J_{HP}$ = 13.7 Hz, $^{3}J_{HH}$ = 7.2 Hz, $^{4}J_{HH}$ = 1.5 Hz, 1 H) ppm.

^{13}C RMN (75 MHz, $CDCl_3$): δ = 123.9 (HC), 125.4 (HC), 125.7-133.2 (m, 23 HC and 4 C), 133.8 (C), 134.3 (d, $^{1}J_{CP}$ = 108.7 Hz, 2 C), 137.8 (d, $^{3}J_{CP}$ = 9.8 Hz, C), 138.0 (d, $^{3}J_{CP}$ = 6.7 Hz, HC), 148.3 (d, $^{2}J_{CP}$ = 6.2 Hz, C), 149.0 (C), 158.5 (C) ppm.

^{31}P NMR (120 MHz, $CDCl_3$): δ = 29.7 ppm.

HRMS (EI): calculated for $C_{37}H_{26}NOP$ $[M]^+$ 531.1752; found 531.1763.

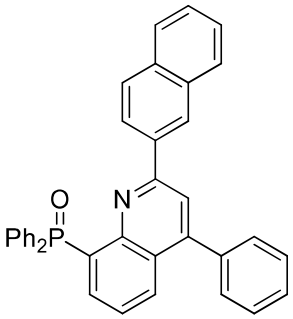

7d

(2-(Naphthalen-2-yl)-4-phenylquinolin-8-yl)diphenylphosphine oxide (**7d**).

The general procedure A (*oxidation of compounds 6 with DDQ*) was employed with **6d** (0.54 g, 1 mmol) to afford **7d** (0.53 g, 82%) as a white solid.

Melting point: 236-238°C (ethyl acetate/hexane).

^{1}H RMN (300 MHz, $CDCl_3$): δ = 7.24--7.68 (m, 18 H), 7.76 (dd, $^{3}J_{HH}$ = 8.4 Hz, $^{4}J_{HH}$ = 1.4 Hz, 1 H), 7.87-7.91 (m, 5 H), 8.07 (d, $^{3}J_{HP}$ = 8.4 Hz, 1 H), 8.60 (m, 1 H) ppm.

^{13}C RMN (75 MHz, $CDCl_3$): δ = 119.8 (HC), 125.4 (HC), 125.3-135.1 (m, 24 HC and 6 C), 136.2 (C), 138.2 (d, $^{3}J_{CP}$ = 9.0 Hz, HC), 144.8 (C), 148.4 (d, $^{2}J_{CP}$ = 5.2 Hz, C), 149.2 (C), 155.9 (C) ppm.

^{31}P NMR (120 MHz, $CDCl_3$): δ = 29.1 ppm.

HRMS (EI): calculated for $C_{37}H_{26}NOP$ $[M]^+$ 531.1752; found 531.1740.

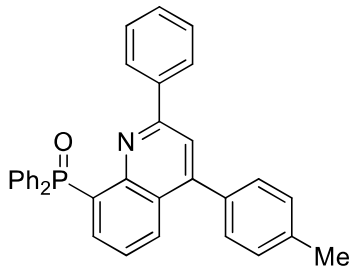

7f

(2-Phenyl-4-(p-tolyl)quinolin-8-yl)diphenylphosphine oxide (**7f**).

The general procedure A (*oxidation of compounds 6 with DDQ*) was employed with **6f** (0.50 g, 1 mmol) to afford **7f** (0.44 g, 88%) as a white solid.

The general procedure B was followed using (2-(benzylideneamino)phenyl)diphenylphosphine oxide and 1-ethynyl-4-methylbenzene (0.28 mL, 2 mmol), to afford **7f** (0.81 g, 82%) as a white solid.

Melting point: 148-150°C (ethyl acetate/hexane).

^{1}H RMN (300 MHz, $CDCl_3$): δ = 2.49 (s, 3 H, CH_3), 7.27-7.65 (m, 16 H), 7.78 (s, 1 H), 7.93 (dd, $^3J_{HP}$ = 12.3 Hz, $^3J_{HH}$ = 7.3 Hz, 4H), 8.15 (d, $^3J_{HH}$ = 8.6 Hz, 1 H), 8.64 (dd, $^3J_{HP}$ = 13.7 Hz, $^3J_{HH}$ = 6.9 Hz, 1 H) ppm.

^{13}C RMN (75 MHz, $CDCl_3$): δ = 21.5 (CH_3), 119.3 (HC), 126.0 (d, $^3J_{CP}$ = 13.2 Hz, HC), 126.2 (d, $^3J_{CP}$ = 7.3 Hz, C), 127.8-138.8 (m, 21 HC and 6 C), 148.2 (d, $^2J_{CP}$ = 6.0 Hz, C), 149.7 (C), 155.8 (C) ppm.

^{31}P NMR (120 MHz, $CDCl_3$): δ = 29.0 ppm.

HRMS (EI): calculated for $C_{34}H_{26}NOP$ $[M]^+$ 495.1752; found 495.1760.

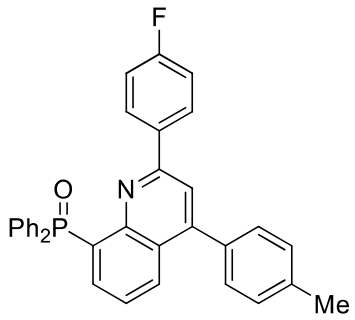

7g

2-(4-fluorophenyl)-4-(p-tolyl)quinolin-8-yl)diphenylphosphine oxide (**7g**).

The general procedure A (*oxidation of compounds 6 with DDQ*) was employed with **6g** (0.52 g, 1 mmol) to afford **7g** (0.47 g, 93%) as a white solid/the general procedure B was followed using

(2-((4-fluorobenzylidene)amino)phenyl)diphenylphosphine oxide and 1-ethynyl-4-methylbenzene (0.28 mL, 2 mmol), to afford **7g** (0.73 g, 71%) as a white solid.

Melting point: 271-273°C (ethyl acetate/hexane).

^{1}H RMN (300 MHz, $CDCl_3$): δ = 2.49 (s, 1H, CH_3), 6.91-6.97 (m, 2 H), 7.35-7.50 (m, 13 H), 7.72 (s, 1 H), 7.90 (dd, $^{3}J_{HP}$= 12.5 Hz,$^{3}J_{HH}$= 7.0 Hz, 4 H), 8.14 (d, $^{3}J_{HH}$= 8.4 Hz, 1 H), 8.54 (ddd,$^{3}J_{HP}$= 14.2 Hz,$^{3}J_{HH}$= 7.1 Hz,$^{4}J_{HH}$= 1.4 Hz, 1 H) ppm.

^{13}C RMN (75 MHz, $CDCl_3$): δ = 21.5 (CH_3), 115.7 (d, $^{2}J_{CF}$ = 21.5 Hz, 2 HC), 119.0 (HC), 126.1 (d, $^{3}J_{CP}$= 12.9 Hz, HC), 128.3-135.2 (m, 6 C, 17 HC), 138.1 (d, $^{3}J_{CP}$= 7.4 Hz, HC), 139,0 (C), 148.4 (d, $^{2}J_{CP}$= 5,7 Hz, C), 150.0 (C), 154.9 (C), 164.0 (d, $^{1}J_{CF}$= 249,8 Hz, C-F) ppm.

^{31}P NMR (120 MHz, $CDCl_3$): δ = 29.1 ppm.

^{19}F NMR crude reaction mixture (282 MHz, $CDCl_3$): δ = -112.3 to -112.1 (m) ppm.

HRMS (EI): calculated for $C_{34}H_{25}FNOP$ $[M]^+$ 513.1658; found 513.1669.

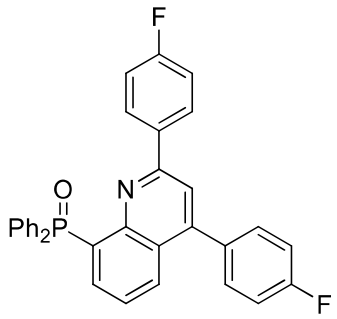

7h

2,4-Bis(4-fluorophenyl)quinolin-8-yl)diphenylphosphine oxide (**7h**).

The general procedure A (*oxidation of compounds 6 with DDQ*) was employed with **6h** (0.52 g, 1 mmol) to afford **7h** (0.50 g, 96%) as a white solid/the general procedure B was followed using (2-((4-fluorobenzylidene)amino)phenyl)diphenylphosphine oxide and 4-fluorophenylacetylene (0.24 mL, 2 mmol), to afford **7h** (0.70 g, 68%) as a white solid.

Melting point: 258-260°C (ethyl acetate/hexane).

^{1}H RMN (300 MHz, $CDCl_3$): δ = 6.93-6.99 (m, 2 H), 7.23-7.66 (m, 13 H), 7.73 (s, 1 H), 7.88-7.94 (m, 4 H), 8.07 (d, $^{3}J_{HH}$ = 8.4 Hz, 1 H), 8.55 (ddd, $^{3}J_{HP}$ = 13.9 Hz, $^{3}J_{HH}$ = 7.0 Hz, $^{4}J_{HH}$ = 1.3 Hz, 1 H) ppm.

^{13}C RMN (75 MHz, $CDCl_3$): δ = 115.6 (d, $^{2}J_{CF}$ = 22.0 Hz, 2 HC), 116.0 (d, $^{2}J_{CF}$ = 21.6 Hz, 2 HC), 119.1 (HC), 125.9 (d, $^{3}J_{CP}$ = 7.2 Hz, C), 126.2 (d, $^{3}J_{CP}$ = 12.9 Hz, HC), 128.2-132.3 (m, 15 HC), 134.0 (d, $^{4}J_{CF}$ = 3.2 Hz, C), 134.1 (d, $^{1}J_{CP}$ = 108.2 Hz, 2 C), 134.7 (d, $^{2}J_{CP}$ = 3.0 Hz, C), 138.1 (d, $^{3}J_{CP}$ = 7.2 Hz, HC), 148.2 (d, $^{2}J_{CP}$ = 5.6 Hz, C), 148.8 (2C), 154.8 (C), 163.7 (d, $^{1}J_{CF}$ = 248.9 Hz, C-F), 164.0 (d, $^{1}J_{CF}$ = 250.0 Hz, C-F) ppm.

^{31}P NMR (120 MHz, $CDCl_3$): δ = 28.8 ppm.

^{19}F NMR crude reaction mixture (282 MHz, $CDCl_3$): δ = -112.0 to -111.9 (m) and -113.1 to -113.0 (m) ppm.

HRMS (EI): calculated for $C_{33}H_{22}F_2NOP$ $[M]^+$ 517.1407; found 517.1417.

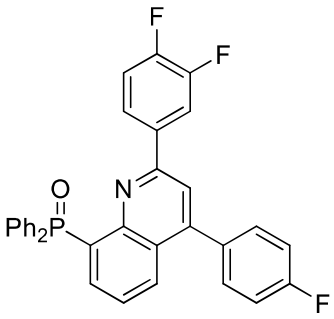

7i

2-(3,4-difluorophenyl)-4-(4-fluorophenyl)quinolin-8-yl)diphenylphosphine oxide (**7i**).

The general procedure A (*oxidation of compounds 6 with DDQ*) was employed with **6i** (0.54 g, 1 mmol) to afford **7i** (0.53 g, 99%) as a white solid.

Melting point: 273-275°C (ethyl acetate/hexane).

^{1}H RMN (400 MHz, $CDCl_3$): δ = 7.04-7.14 (m, 3 H), 7.39-7.52 (m, 10 H), 7.63 (ddd, $^4J_{HP}$ = 1.3 Hz, $^3J_{HH}$ = 7.1 Hz, $^3J_{HH}$ = 8.4 Hz, 1 H), 7.68 (s, 1 H), 7.86-7.92 (m, 4 H), 8.06 (ddd, $^3J_{HH}$ = 8.4 Hz, $^4J_{HH}$ = 1.2 Hz, $^5J_{PH}$ = 2.6 Hz, 1 H), 8.49 (ddd, $^3J_{HP}$ = 14.1 Hz, $^3J_{HH}$ = 7.1 Hz, $^4J_{HH}$ = 1.4 Hz, 1 H) ppm.

^{13}C RMN (75 MHz, $CDCl_3$): δ = 116.1 (d, $^2J_{CF}$ = 21.6 Hz, 2 HC), 116.9 (d, $^2J_{CF}$ = 18.3 Hz, HC), 117.4 (d, $^2J_{CF}$ = 18.3 Hz, HC), 118.9 (HC), 123.6 (HC), 126.2-135.7 (m, 15 HC and 6 C), 138.3 (HC), 148.3 (C), 149.1 (C), 150.6 (dd, $^1J_{CF}$ = 248.4 Hz, $^2J_{CF}$ = 12.9 Hz, C-F), 151.4 (dd, $^1J_{CF}$ = 251.3 Hz, $^2J_{CF}$ = 13.5 Hz, C-F), 153.7 (C), 163.2 (d, $^1J_{CF}$ = 248.9 Hz, C-F), ppm.

^{31}P NMR (120 MHz, $CDCl_3$): δ = 28.6 ppm.

^{19}F NMR crude reaction mixture (282 MHz, $CDCl_3$): δ = -112.8 to -112.7 (m), -136.6 to -136.4 (m), -137.6 to -137.3 (m) ppm.

HRMS (EI): calculated for $C_{33}H_{21}F_3NOP$ $[M]^+$ 535.1313; found 535.1316.

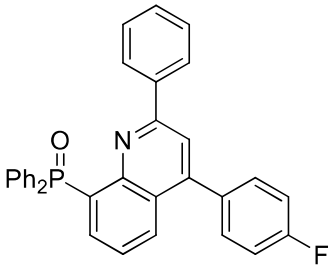

7j

(4-(4-fluorophenyl)-2-phenylquinolin-8-yl)diphenylphosphine oxide (**7j**).

The general procedure B was followed using (2-(benzylideneamino)phenyl)diphenylphosphine oxide and 4-fluorophenylacetylene (0.24 mL, 2 mmol), to afford **7j** (0.56 g, 56%) as a white solid.

Melting point: 193-195°C (ethyl acetate/hexane).

^{1}H RMN (300 MHz, $CDCl_3$): δ = 7.17-7.52 (m, 15 H), 7.64 (ddd, $^{3}J_{HH}$ = 9.3 Hz, $^{3}J_{HH}$ = 7.1 Hz, $^{4}J_{HP}$ = 1.3 Hz, 1 H), 7.76 (s, 1 H), 7.93 (dd, $^{3}J_{HH}$ = 7.1 Hz, $^{4}J_{HP}$ = 1.3 Hz, 4 H), 8.07 (dd, $^{3}J_{HH}$ = 8.4 Hz, $^{4}J_{HH}$ = 1.4 Hz, 1 H), 8.64 (ddd, $^{3}J_{HP}$ = 13.6 Hz, $^{3}J_{HH}$ = 7.2 Hz, $^{4}J_{HH}$ = 1.3 Hz, 1 H) ppm.

^{13}C RMN (75 MHz, $CDCl_3$): δ = 115.9 (d, $^{2}J_{CF}$ = 21.5 Hz, 2 HC), 119.4 (HC), 126.0 (d, $^{2}J_{CP}$ = 7.7 Hz, C), 126.2 (d, $^{2}J_{CP}$ = 12.8 Hz, HC), 127.7-134.8 (m, 18 HC and 1 C), 134.0 (d, $^{4}J_{CF}$ = 3.2 Hz, C), 134.1 (d, $^{1}J_{CP}$ = 108.4 Hz, 2 C), 134.7, 138.1 (d, $^{3}J_{CP}$ = 7.2 Hz, HC), 148.2 (d, $^{2}J_{CP}$ = 5.6 Hz, C), 148.6 (C), 155.9 (C), 163.2 (d, $^{1}J_{CF}$ = 247.8 Hz, C-F) ppm.

^{31}P NMR (120 MHz, $CDCl_3$): δ = 28.8 ppm.

^{19}F NMR crude reaction mixture (282 MHz, $CDCl_3$): δ = -113.2 to -113.0 (m) ppm.

HRMS (EI): calculated for $C_{33}H_{23}FNOP$ $[M]^+$ 499.1501; found 499.1503.

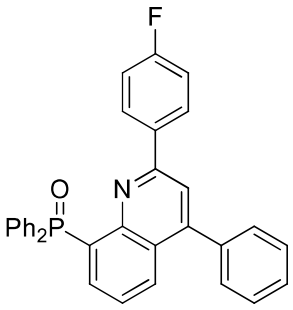

7k

(2-(4-fluorophenyl)-4-phenylquinolin-8-yl)diphenylphosphine oxide (**7k**).

The general procedure B was followed using (2-((4-fluorobenzylidene)amino)phenyl)diphenylphosphine oxide and acetylene (0.22 mL, 2 mmol), to afford **7k** (0.50 g, 50%) as a white solid.

Melting point: 224-226°C (ethyl acetate/hexane).

^{1}H RMN (300 MHz, $CDCl_3$): δ = 6.84-6.88 (m, 2H), 7.27-7.54 (m, 14 H), 7.65 (s, 1 H), 7.80-7.85 (m, 4 H), 8.02 (d, $^{3}J_{HH}$ = 8.4 Hz, 1 H), 8.46 (ddd, $^{3}J_{HP}$ = 13.8 Hz, $^{3}J_{HH}$ = 7.2 Hz, $^{4}J_{HH}$ = 2.0 Hz, 1 H) ppm.

^{13}C RMN (75 MHz, $CDCl_3$): δ = 115.4 (d, $^{2}J_{CF}$ = 22.1 Hz, 2 HC), 118.9 (HC), 125.2 (d, $^{2}J_{CP}$ = 7.6 Hz, C), 125.9 (d, $^{2}J_{CP}$ = 13.1 Hz, HC), 128.2-132.3 (m, 18 HC and 1 C), 134.1 (d, $^{1}J_{CP}$ = 108.2 Hz, 2 C), 134.7 (d, $^{4}J_{CF}$ = 2.6 Hz, C), 137.9 (C), 137.9 (d, $^{3}J_{CP}$ = 7.2 Hz, HC), 148.2 (d, $^{2}J_{CP}$ = 5.7 Hz, C), 149.8 (C), 154.8 (C), 163.8 (d, $^{1}J_{CF}$ = 249.9 Hz, C-F) ppm.

^{31}P NMR (120 MHz, $CDCl_3$): δ = 29.0 ppm.

^{19}F NMR crude reaction mixture (282 MHz, $CDCl_3$): δ = -112.2 to -112.0 ppm.

HRMS (EI): calculated for $C_{33}H_{23}FNOP$ [M]+ 499.1501; found 499.1511.

VI-1.3. Synthesis of hybrid 1,2,3,4-tetrahydroquinolinyl and quinolinyl dialkyl phosphonates

Preparation of anilines substituted with dialkyl phosphonate 1b, 1c and 1d

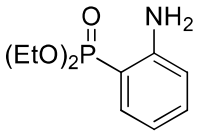

1b

Diethyl (2-aminophenyl)phosphonate 1b.

To a suspension of 2-bromoaniline (4.30 g, 25 mmol, 1 equiv.), diethyl phosphite (3.86 mL, 30 mmol, 1.2 equiv.) and freshly distilled triethlamine (5.23 mL, 37.5 mmol, 1.5 equiv.) in 30 mL of dry deoxydenated EtOH were added 5% mol of $Pd(OAc)_2$ (0.28 g) and 15% mol of triphenylphosphine (1.01 g). The reaction mixture was stirred and heated to EtOH reflux for 12h and the resulted reaction crude was purified by silica gel column chromatography (30% of ethyl acetate in hexane) and subsequently vacuum-evaporated to dryness to afford 15.28 g (59 mmol) of diethyl (2-aminophenyl)phosphonate **1b** as a yellow solid (73%); mp 58–60 ◦C (ethyl acetate/hexane).

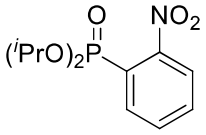

Diisopropyl (2-nitrophenyl)phosphonate.

1,2-Dinitrobenzene (12.61 g, 75 mmol, 1 equiv.) and triisopropyl phosphite (22.21 mL, 90 mmol, 1.2 equiv.) were dissolved in 70 mL of dry dimethylformamide (DMF) and the reaction mixture was maintained stirring at MeCN reflux for 12 h. The resultant reaction crude was filtered off, dried *in vacuo*, and purified by silica gel column chromatography (10% of ethyl acetate in hexane) to yield 17.88 g (62.25 mmol) of diisopropyl (2-nitrophenyl)phosphonate as a brown oil (83%); Rf = 0.39 (50:50 EtOAc/hexane).

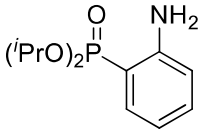

1c

Diisopropyl (2-aminophenyl)phosphonate 1c.

(Diisopropyl (2-nitrophenyl)phosphonate (19.40 g, 60 mmol) was hydrogenated with a spoon of RANEY® Nickel (approx. 5 g) in 60 mL of MeOH at 80 psi at room temperature for 12 h. The reaction mixture was then filtered off through a pad of cellite and evaporated to dryness to obtain (2-aminophenyl)diphenylphosphine oxide **1a** (17.59 g, 59.97 mmol) as a white solid (99%).

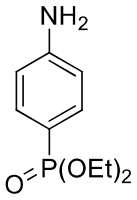

1d

Diethyl (4-aminophenyl)phosphonate 1d.

To a suspension of 4-bromoaniline (4.30 g, 25 mmol, 1 equiv.), triethylphosphite (17.15 ml, 100 mmol, 4 equiv.), TBAB (tetrabutylammonium bromide, 8.06 g, 25 mmol, 1 equiv.) and freshly distilled triethylamine (6.97 mL, 50 mmol, 2 equiv.) in 30 mL of deoxygenated distilled water, 4.4% mol of palladium(II) chloride (0.20g) were added and the reaction mixture was stirred at 100°C for 8h. The obtained reaction crude was purified by silica gel column chromatography (30% of ethyl acetate in hexane) and vacuum-evaporated to dryness, affording 4.15 g (18.11 mmol) of diethyl (4-aminophenyl)phosphonate **1d** as a white solid (72%); mp 125–127°C (ethyl acetate/hexane).

General procedure for the preparation of dialkyl quinolin-8-ylphosphonates 13

A) Step-by-step Povarov-DDQ oxidation sequential procedure

Styrenes **3** (1.2 mmol, 1.2 equiv.) and 2 equivalent of $BF_3{\cdot}Et_2O$ (0.25 mL, 2 mmol) were added to a solution of the corresponding *in situ* prepared aldimine **4** (1 mmol) in $CHCl_3$ (3 mL). The mixture was stirred and heated to $CHCl_3$ reflux until TLC, ^{31}P NMR and ^{1}H NMR spectroscopy analysis indicated the disappearance of the aldimine. Then, the reaction was allow to reach room temperature and DDQ (0.45 g, 2 mmol, 2 equiv.) was added, to subsequently heat the reaction again to reflux for 2 h. The reaction mixture was then diluted in 10 mL of dichloromethane, washed with a 2M aqueous solution of NaOH (25 mL) and water (25 mL), extracted with dichloromethane (2 × 10 mL), and dried over anhydrous $MgSO_4$. The solvent was removed under vacuum affording an oil that was purified by silica gel flash column chromatography using an elution of 20–80% ethyl acetate-hexane to afford dialkyl quinolin-8-yl phosphonates **13**.

B) MCR Povarov-DDQ oxidation sequential procedure

A mixture of dialkyl (4-aminophenyl)phosphonate **1b/1c** (1 mmol, 1 equiv.), freshly distilled aldehydes **2** (1 mmol, 1 equiv.), styrenes **3** (1.2 mmol, 1.2 equiv.) and 2 equivalents of $BF_3{\cdot}Et_2O$ (0.25 mL, 2 mmol) dissolved in $CHCl_3$ (3 mL) was stirred and heated to reflux in the presence of molecular sieves (4 Å), until TLC, ^{31}P NMR and ^{1}H NMR spectroscopy analysis indicated the consumption of the starting materials (16 h). Then, the reaction was allow to reach room temperature and DDQ (0.45 g, 2 mmol, 2 equiv.) was added, to subsequently heat the reaction again to reflux for 2 h. The reaction mixture was then diluted in 10 mL of dichloromethane, washed with a 2M aqueous solution of NaOH (25 mL) and water (25 mL), extracted with dichloromethane (2 × 10 mL), and dried over anhydrous $MgSO_4$. The solvent was removed under vacuum affording an oil that was purified by silica gel flash column chromatography using an elution of 20–80% ethyl acetate-hexane to afford dialkyl quinolin-8-yl phosphonates **13**.

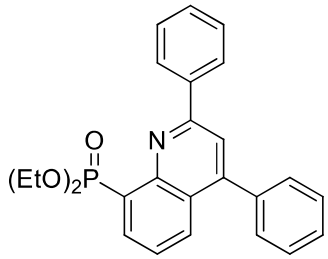

13a

Diethyl (2,4-diphenylquinolin-8-yl)phosphonate (**13a**).

The general procedure A (step-by step Povarov-DDQ oxidation sequential procedure) was followed using aminophenylphosphonate **1b** (0.23 g, 1 mmol), benzaldehyde (0.10 mL, 1 mmol), styrene (0.14 mL, 1.2 mmol) and $BF_3.Et_2O$, affording (0.31 g, 74%) of a white solid identified as **13a**.

Melting point: 118-120°C (ethyl acetate/hexane).

^{1}H RMN (300 MHz, $CDCl_3$): δ = 1.32-1.36 (m, 6 H, 2 CH_3), 4.26-4.44 (m, 4 H, 2 CH_2), 7.45-7.57 (m, 9 H), 7.92 (s, 1 H), 8.06-8.08 (d, $^3J_{HH}$ = 8.4 Hz, 1 H) 8.37-8.43 (m, 3 H) ppm.

^{13}C RMN (75 MHz, $CDCl_3$): δ = 16.7 (d, $^3J_{CP}$ = 6.6 Hz, 2 CH_3), 62.5 (d, $^2J_{CP}$ = 5.7 Hz, 2 CH_2), 119.3 (HC), 125.5 (d, $^3J_{CP}$ = 16.2 Hz, HC), 126.0 (d, $^3J_{CP}$ = 10.7 Hz, C), 128.0 (2 HC), 128.6 (d, $^1J_{CP}$ = 193.7 Hz, C), 128.7 (HC), 128.8 (2 HC), 128.9 (2 HC), 129.7 (2 HC), 129.9 (HC), 130.7 (HC), 136.9 (d, $^2J_{CP}$ = 7.4 Hz, HC), 138.2 (C), 139.0 (C), 148.8 (d, $^2J_{CP}$ = 6.7 Hz, C), 149.6 (C), 156.6 (C) ppm.

^{31}P NMR (120 MHz, $CDCl_3$): δ = 18.5 ppm.

HRMS (EI): calculated for $C_{25}H_{24}NO_3P$ $[M]^+$ 417.1494; found 417.1494.

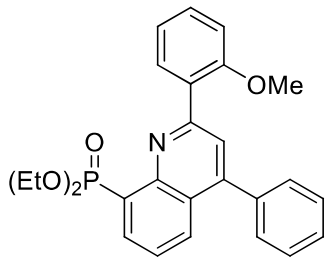

13b

Diethyl (2-(2-methoxyphenyl)-4-phenylquinolin-8-yl)phosphonate (**13b**).

The general procedure A (step-by-step Povarov-DDQ oxidation sequential procedure) was followed using aminophenylphosphonate **1b** (0.23 g, 1 mmol), *o*-anisaldehyde (0.12 mL, 1 mmol), styrene (0.14 mL, 1.2 mmol) and $BF_3.Et_2O$, affording (0.21 g, 48%) of a white solid identified as **13b**.

Melting point: 121-123°C (ethyl acetate/hexane).

^{1}H RMN (400 MHz, $CDCl_3$): δ = 1.25-1.28 (m, 6 H, 2 CH_3), 3.81 (s, 3 H, OCH_3), 4.17-4.35 (m, 4 H, 2 OCH_2), 6.95-6.97 (m, 2 H), 7.36-7.49 (m, 6 H), 7.77 (s, 1 H), 7.95-7.97 (d, $^{3}J_{HH}$ = 8.4 Hz, 1 H), 8.26-8.31 (m, 3 H) ppm.

^{13}C RMN (100 MHz, $CDCl_3$): δ = 16.5 (d, $^{3}J_{CP}$ = 6.6 Hz, 2 CH_3), 55.4 (OCH_3), 62.3 (d, $^{2}J_{CP}$ = 5.5 Hz, 2 OCH_2), 114.1 (3 HC), 118.6 (HC), 124.9 (d, $^{3}J_{CP}$ = 16.2 Hz, HC), 125.6 (d, $^{3}J_{CP}$ = 10.7 Hz, C), 128.1 (d, $^{1}J_{CP}$ = 187.9 Hz, C), 128.5 (HC), 128.6 (3 HC), 129.3 (HC), 129.5 (HC), 130.6 (HC), 131.5 (C), 136.7 (d, $^{2}J_{CP}$ = 7.5 Hz, HC), 138.2 (C), 148.7 (d, $^{2}J_{CP}$ = 6.7 Hz, C), 149.2 (C), 156.1 (C), 161.1 (C) ppm.

^{31}P NMR (120 MHz, $CDCl_3$): δ = 18.8 ppm.

HRMS (EI): calculated for $C_{26}H_{26}NO_4P$ $[M]^+$ 447.1599; found 447.1597.

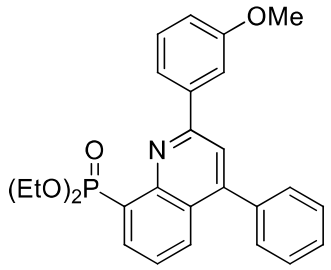

13c

Diethyl (2-(3-methoxyphenyl)-4-phenylquinolin-8-yl)phosphonate (**13c**).

The general procedure B (MCR Povarov-DDQ oxidation sequential procedure) was followed using aminophenylphosphonate **1b** (0.23 g, 1 mmol), *m*-anisaldehyde (0.12 mL, 1 mmol), styrene (0.14 mL, 1.2 mmol) and $BF_3{\cdot}Et_2O$, affording (0.42 g, 89%) of a white solid identified as **13c**.

Melting point: 127-129°C (ethyl acetate/hexane).

^{1}H RMN (300 MHz, $CDCl_3$): δ = 1.25-1.28 (m, 6 H, 2 CH_3), 3.81 (s, 3 H, OCH_3), 4.17-4.35 (m, 4 H, 2 OCH_2), 6.95-6.97 (m, 2 H), 7.36-7.49 (m, 6 H), 7.77 (s, 1 H), 7.95-7.97 (d, $^{3}J_{HH}$ = 8.4 Hz, 1 H), 8.26-8.31 (m, 3 H) ppm.

^{13}C RMN (75 MHz, $CDCl_3$): δ = 16.5 (d, $^{3}J_{CP}$ = 6.6 Hz, 2 CH_3), 55.4 (OCH_3), 62.3 (d, $^{2}J_{CP}$ = 5.5 Hz, 2 OCH_2), 114.1 (3 HC), 118.6 (HC), 124.9 (d, $^{3}J_{CP}$ = 16.2 Hz, HC), 125.6 (d, $^{3}J_{CP}$ = 10.7 Hz, C), 128.1 (d, $^{1}J_{CP}$ = 187.9 Hz, C), 128.5 (HC), 128.6 (3 HC), 129.3 (HC), 129.5 (HC), 130.6 (HC), 131.5 (C), 136.7 (d, $^{2}J_{CP}$ = 7.5 Hz, HC), 138.2 (C), 148.7 (d, $^{2}J_{CP}$ = 6.7 Hz, C), 149.2 (C), 156.1 (C), 161.1 (C) ppm.

^{31}P NMR (120 MHz, $CDCl_3$): δ = 18.8 ppm.

HRMS (EI): calculated for $C_{26}H_{26}F_3NO_4P$ $[M]^+$ 447.1599; found 447.1597.

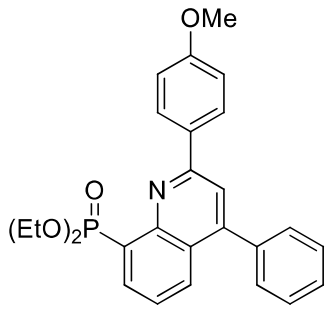

13d

Diethyl (2-(4-methoxyphenyl)-4-phenylquinolin-8-yl)phosphonate (**13d**).

The general procedure A (step-by-step Povarov-DDQ oxidation sequential procedure) was followed using aminophenylphosphonate **1b** (0.23 g, 1 mmol), *p*-anisaldehyde (0.12 mL, 1 mmol), styrene (0.14 mL, 1.2 mmol) and $BF_3{\cdot}Et_2O$, affording (0.18 g, 41%) of a white solid identified as **13d**.

Melting point: 120-122°C (ethyl acetate/hexane).

^{1}H RMN (400 MHz, $CDCl_3$): δ = 1.23-1.27 (m, 6 H, 2 CH_3), 3.86 (s, 3 H, OCH_3), 4.16-4.35 (m, 4 H, 2 OCH_2), 6.93-6.95 (m, 1 H), 7.31-7.48 (m, 7 H), 7.79-7.82 (m, 2 H), 7.98-8.00 (m, 2 H), 8.28-8.34 (m, H) ppm.

^{13}C RMN (100 MHz, $CDCl_3$): δ = 16.5 (d, $^3J_{CP}$ = 6.7 Hz, 2 CH_3), 55.4 (OCH_3), 62.3 (d, $^2J_{CP}$ = 5.7 Hz, 2 OCH_2), 112.6 (HC), 116.3 (HC), 119.2 (HC), 120.0 (HC), 125.4 (d, $^3J_{CP}$ = 16.3 Hz, HC), 125.9 (d, $^2J_{CP}$ = 10.7 Hz, C), 128.5 (d, $^1J_{CP}$ = 188.5 Hz, C), 128.6 (HC), 128.7 (2 HC), 129.5 (2 HC), 129.6 (HC), 130.6 (HC), 136.9 (d, $^2J_{CP}$ = 7.5 Hz, HC), 138.0 (C), 140.3 (C), 148.5 (d, $^2J_{CP}$ = 6.8 Hz, C), 149.4 (C), 156.1 (C), 160.1 (C) ppm.

^{31}P NMR (120 MHz, $CDCl_3$): δ = 18.7 ppm.

HRMS (EI): calculated for $C_{26}H_{26}NO_4P$ $[M]^+$ 447.1599; found 447.1597.

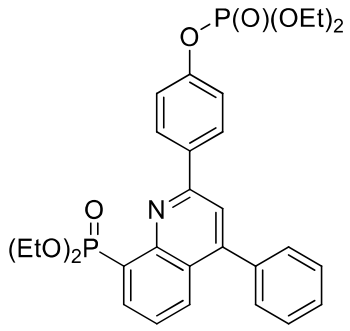

13e

Diethyl (2-(4-methoxyphenyl)-4-phenylquinolin-8-yl)phosphonate (**13e**).

The general procedure A (step-by-step Povarov-DDQ oxidation sequential procedure) was followed using aminophenylphosphonate **1b** (0.23 g, 1 mmol), diethyl (4-formylphenyl) phosphate (0.26 mL, 1 mmol), styrene (0.14 mL, 1.2 mmol) and $BF_3.Et_2O$, affording (0.36 g, 64%) of a brown oil identified as **13e**.

Rf: 0.22 (20:80 ethyl acetate/hexane).

^{1}H RMN (300 MHz, $CDCl_3$): δ = 1.31-1.39 (m, 12 H, 4 CH_3), 4.20-4.40 (m, 8 H, 4 CH_2), 7.26-7.53 (m, 8 H), 7.86 (s, 1 H), 8.04-8.07 (m, 1 H), 8.33-8.40 (m, 3 H) ppm

^{13}C RMN (75 MHz, $CDCl_3$): δ = 16.2 (d, $^3J_{CP}$ = 6.5 Hz, 2 CH_3), 16.6 (d, $^3J_{CP}$ = 6.4 Hz, 2 CH_3), 62.5 (d, $^2J_{CP}$ = 5.6 Hz, 2 CH_2), 64.9 (d, $^2J_{CP}$ = 5.9 Hz, 2 CH_2), 118.9 (HC), 125.4-138.0 (m, 4 C and 12 HC), 148.7 ppm (d, $^2J_{CP}$ = 6.7 Hz, C), 149.7 (m, C), 152.3 (m, C), 155.5 (C) ppm.

^{31}P NMR (120 MHz, $CDCl_3$): δ = 18.5, -5.4 ppm.

HRMS (EI): calculated for $C_{29}H_{33}NO_7P_2$ $[M]^+$ 569,1732; found 569,1732.

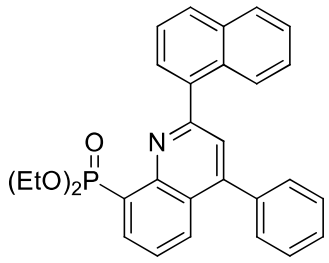

13f

Diethyl (2-(naphthalen-1-yl)-4-phenylquinolin-8-yl)phosphonate (**13f**).

The general procedure B (MCR Povarov-DDQ oxidation sequential procedure) was followed using aminophenylphosphonate **1b** (0.23 g, 1 mmol), 1-napthaldehyde (0.13 mL, 1 mmol), styrene (0.14 mL, 1.2 mmol) and $BF_3.Et_2O$, affording (0.28 g, 60%) of a yellow solid identified as **13f**.

Melting point: 140-142°C (ethyl acetate/hexane).

^{1}H RMN (400 MHz, $CDCl_3$): δ = 1.16-1.20 (m, 6 H, 2 CH_3), 4.19-4.30 (m, 4 H, 2 CH_2), 7.51-7.62 (m, 9 H), 7.77 (s, 1 H), 7.86-7.97 (m, 3 H), 8.15-8.17 (d, $^{3}J_{HH}$ = 8.4 Hz, 1 H), 8.39-8.44 (m, 1 H), 8.58-8.60 (d, $^{3}J_{HH}$ = 8.3 Hz, 1 H) ppm.

^{13}C RMN (100 MHz, $CDCl_3$): δ = 16.5 (d, $^{3}J_{CP}$ = 6.1 Hz, 2 CH_3), 62.9 (d, $^{2}J_{CP}$ = 5.3 Hz, 2 CH_2), 124.0 (HC), 125.4 (HC), 125.7 (C), 125.8 (HC), 125.9 (HC), 126.2 (HC), 126.5 (HC), 126.9 (HC), 128.4 (HC), 128.8 (HC), 128.9 (2 HC), 129.5 (d, $^{1}J_{CP}$ = 191.1 Hz, C), 129.6 (HC), 129.8 (2 HC), 130.6 (HC), 131.1 (C), 134.0 (C), 136.5 ppm (d, $^{2}J_{CP}$ = 6.6 Hz, HC), 137.9 (C), 138.1 (C), 148.7 ppm (d, $^{2}J_{CP}$ = 5.8 Hz, C), 149.2 (C), 159.0 (C) ppm.

^{31}P NMR (120 MHz, $CDCl_3$): δ = 17.2 ppm.

HRMS (EI): calculated for $C_{29}H_{26}NO_3P$ $[M]^+$ 467.1650; found 467.1651.

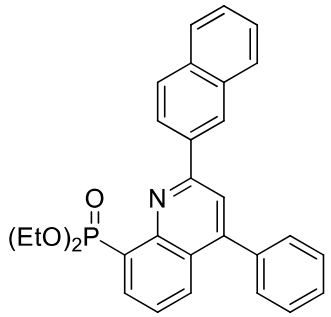

13g

Diethyl (2-(naphthalen-2-yl)-4-phenylquinolin-8-yl)phosphonate (**13g**).

The general procedure B (MCR Povarov-DDQ oxidation sequential procedure) was followed using aminophenylphosphonate **1b** (0.23 g, 1 mmol), 2-napthaldehyde (0.16 g, 1 mmol), styrene (0.14 mL, 1.2 mmol) and $BF_3{\cdot}Et_2O$, affording (0.39 g, 83%) of a yellow solid identified as **13g**.

Melting point: 135-137°C (ethyl acetate/hexane).

^{1}H RMN (300 MHz, $CDCl_3$): δ = 1.34-1.39 (m, 6 H, 2 CH_3), 4.30-4.48 (m, 4 H, 2 CH_2), 7.53-7.58 (m, 8 H), 7.90-8.11 (m, 5 H), 8.38-8.46 (m, 1 H), 8.65-8.75 (m, 2 H) ppm.

^{13}C RMN (75 MHz, $CDCl_3$): δ = 16.7 (d, $^{3}J_{CP}$ = 6.5 Hz, 2 CH_3), 62.6 (d, $^{2}J_{CP}$ = 5.3 Hz, 2 CH_2), 119.5 (HC), 125.5 (HC), 125.6 (HC), 125.7 (HC), 126.1 (d, $^{3}J_{CP}$ = 10.6 Hz, C), 126.5 (HC), 127.1 (HC), 127.4 (HC), 127.6 (HC), 128.6 (HC), 128.7 (d, $^{1}J_{CP}$ = 187.5 Hz, C), 128.8 (HC), 128.9 (2 HC), 129.0 (HC), 129.7 (2 HC), 130.7 (HC), 133.5 (C), 134.3 (C), 136.5 (C), 137.0 (d, $^{2}J_{CP}$ = 7.3 Hz, HC), 138.2 (C), 148.9 (d, $^{2}J_{CP}$ = 6.3 Hz C), 149.7 (C), 156.5 (C) ppm.

^{31}P NMR (120 MHz, $CDCl_3$): δ = 18.6 ppm.

HRMS (EI): calculated for $C_{29}H_{26}NO_3P$ $[M]^+$ 467.1650; found 467.1649.

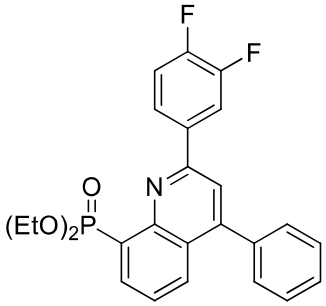

13h

Diethyl (2-(3,4-difluorophenyl)-4-phenylquinolin-8-yl)phosphonate (**13h**).

The general procedure B (MCR Povarov-DDQ oxidation sequential procedure) was followed using aminophenylphosphonate **1b** (0.23 g, 1 mmol), 3,4-difluorobenzaldehyde (0.11 g, 1 mmol), styrene (0.14 mL, 1.2 mmol) and $BF_3.Et_2O$, affording (0.34 g, 76%) of a white solid identified as **13h**.

Melting point: 153-155ºC (ethyl acetate/hexane).

^{1}H RMN (400 MHz, $CDCl_3$): δ = 1.25-1.29 (m, 6 H, 2 CH_3), 4.19-4.30 (m, 4 H, 2 CH_2), 7.18-7.20 (m, 1 H), 7.42-7.44 (m, 6 H), 7.74 (s, 1 H), 7.97-8.01 (m, 2 H), 8.18-8.33 (m, 2 H) ppm.

^{13}C RMN (100 MHz, $CDCl_3$): δ = 16.6 (d, $^3J_{CP}$ = 6.5 Hz, 2 CH_3), 62.4 (d, $^2J_{CP}$ = 5.8 Hz, 2 CH_2), 116.9 (d, $^2J_{CF}$ = 18.6 Hz, HC), 117.5 (d, $^2J_{CF}$ = 17.5 Hz, HC),118.5 (HC), 123.8 (dd, $^3J_{CF}$ = 6.6 Hz, $^4J_{C\text{-}F}$ = 3.3 Hz, HC), 125.8 (d, $^3J_{CP}$ = 16.2 Hz, HC), 126.0 (d, $^3J_{CP}$ = 10.6 Hz, C), 128.5 (d, $^1J_{CP}$ = 188.6 Hz, C), 129.5 (2 HC), 136.1.3 (dd, $^3J_{CF}$ = 5.7 Hz, $^4J_{CF}$ = 3.6 Hz, C), 137.2 (d, $^2J_{CP}$ = 7.6 Hz, HC), 137.8 (C), 148.5 (d, $^2J_{CP}$ = 6.6 Hz, C), 150.2 (C), 150.9 (dd, $^1J_{CF}$ = 248.6 Hz, $^2J_{CF}$ = 12.2 Hz, C), 151.7 (dd, $^1J_{CF}$ = 250.5 Hz, $^2J_{CF}$ = 12.3 Hz, C), 154.1 (C) ppm.

^{31}P NMR (120 MHz, $CDCl_3$): δ = 18.4 ppm.

^{19}F NMR crude reaction mixture (282 MHz, $CDCl_3$): δ = -136.6 to -136.5 (m) and -137.5 to -137.4 (m) ppm.

HRMS (EI): calculated for $C_{25}H_{22}F_2NO_3P$ $[M]^+$ 453.1305; found 453.1321.

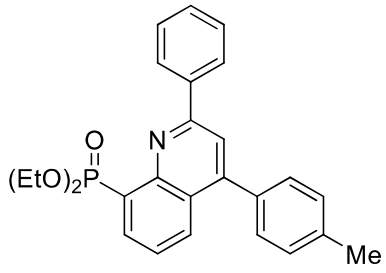

13i

Diethyl (2-(4-methoxyphenyl)-4-phenylquinolin-8-yl)phosphonate (**13i**).

The general procedure A (step-by-step Povarov-DDQ oxidation sequential procedure) was followed using aminophenylphosphonate **1b** (0.23 g, 1 mmol), benzaldehyde (0.10 mL, 1 mmol), 4-methylstyrene (0.16 mL, 1.2 mmol) and $BF_3.Et_2O$, affording (0.24 g, 54%) of a white solid identified as **13i**.

Melting point: 125-127°C (ethyl acetate/hexane).

^{1}H RMN (300 MHz, $CDCl_3$): δ = 1.31-1.36 (m, 6 H, 2 CH_3), 2.48 (s, 3 H, CH_3), 4.27-4.43 (m, 4 H, 2 CH_2), 7.26-7.35 (m, 10 H), 7.91 (s, 1 H), 8.09-8.02 (m, 1 H), 8.35-8.42 (m, 3 H) ppm.

^{13}C RMN (75 MHz, $CDCl_3$): δ = 16.6 (d, $^3J_{CP}$ = 6.5 Hz, 2 CH_3), 21.4 (CH_3), 62.5 (d, $^2J_{CP}$ = 5.8 Hz, 2 CH_2), 119.2 (HC), 125.4 (d, $^3J_{CP}$ = 16.1 Hz, HC), 126.1 (d, $^2J_{CP}$ = 10.7 Hz, C), 128.0 (2HC), 128.8 (2HC), 127.3-130.8 (m, 1 C and 7 HC), 135.2 (C), 136.9 (d, $^3J_{CP}$ = 10.7 Hz, C), 138.7 (C), 138,9 (C), 148.7 (m, C), 149.8 (C), 156.5 (C) ppm.

^{31}P NMR (120 MHz, $CDCl_3$): δ = 17.6 ppm.

HRMS (EI): calculated for $C_{26}H_{26}NO_3P$ $[M]^+$ 431,1650; found 431,1651.

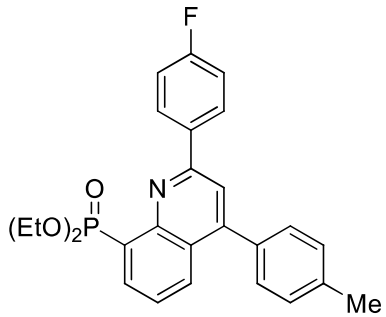

13j

Diethyl (2-(4-fluorophenyl)-4-(p-tolyl)quinolin-8-yl)phosphonate (**13j**).

The general procedure A (step-by-step Povarov-DDQ oxidation sequential procedure) was followed using aminophenylphosphonate **1b** (0.23 g, 1 mmol), 4-fluorobenzaldehyde (0.11 mL, 1 mmol), 4-methylstyrene (0.16 mL, 1.2 mmol) and $BF_3.Et_2O$, affording (0.23 g, 52%) of a white solid identified as **13j**.

Melting point: 139-141°C (ethyl acetate/hexane).

^{1}H RMN (300 MHz, $CDCl_3$): δ = 1.32-1.36 (m, 6 H, 2 CH_3), 2.48 (s, 3 H, CH_3), 4.22-4.44 (m, 4 H, 2 CH_2), 7.17-7.23 (m, 2 H), 7.35-7.43 (m, 4 H), 7.47-7.53 (m, 1 H), 7.86 (s, 1 H), 8.08-8.11 (m, 1 H), 8.32-8.40 (m, 3 H) ppm.

^{13}C RMN (75 MHz, $CDCl_3$): δ = 16.6 (d, $^{3}J_{CP}$ = 6.5 Hz, 2 CH_3), 21.5 (CH_3), 62.5 (m, 2 CH_2), 115.9 (d, $^{2}J_{CF}$ = 21.7 Hz, 2 HC), 118.9 (HC), 125.5 (d, $^{3}J_{CP}$ = 18.0 Hz, HC), 126.0 (d, $^{3}J_{CP}$ = 10.7 Hz, C), 128.2 (d, $^{1}J_{CP}$ = 166.3 Hz, C), 129.6 (3 HC), 129.8 (HC), 129.9 (HC), 130.9 (2 HC), 135.1 (2 C), 136.9 (HC), 138.9 (C), 148.7 (C), 150.1 (d, $^{2}J_{CP}$ = 17.2 Hz, C), 155.4 (C), 164.2 (d, $^{1}J_{CF}$ = 249.8 Hz, C-F) ppm.

^{31}P NMR (120 MHz, $CDCl_3$): δ = 18.6 ppm.

^{19}F NMR crude reaction mixture (282 MHz, $CDCl_3$): δ = -112.1 to -111.9 (m) ppm.

HRMS (EI): calculated for $C_{26}H_{25}FNO_3P$ $[M]^+$ 449.1556; found 449.1562.

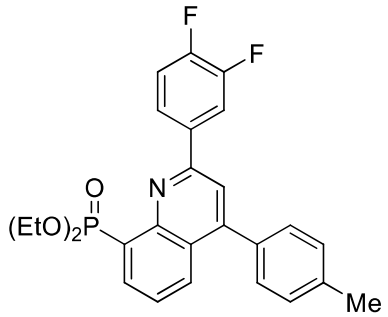

13k

Diethyl (2-(3,4-difluorophenyl)-4-(p-tolyl)quinolin-8-yl)phosphonate (**13k**).

The general procedure A (step-by-step Povarov-DDQ oxidation sequential procedure) was followed using aminophenylphosphonate **1b** (0.23 g, 1 mmol), 3,4-difluorobenzaldehyde (0.11 g, 1 mmol), 4-methylstyrene (0.16 mL, 1.2 mmol) and $BF_3.Et_2O$, affording (0.32 g, 47%) of a white solid identified as **13k**.

Melting point: 133-135°C (ethyl acetate/hexane).

^{1}H RMN (300 MHz, $CDCl_3$): δ = 1.34-1.39 (m, 6 H, 2 CH_3), 2.49 (s, 1 H, CH_3), 4.21-4.43 (m, 4 H, 2 CH_2), 7.28-7.31 (m, 1 H), 7.36-7.43 (m, 4 H), 7.49-7.56 (m, 1 H), 7.82 (s, 1 H), 8.07-8.12 (m, 2 H), 8.26-8.43 (m, 2 H) ppm.

^{13}C RMN (75 MHz, $CDCl_3$): δ = 16.7 (d, $^{3}J_{CP}$ = 6.5Hz, 2 CH_3), 21.5 (CH_3), 62.4 (d, $^{2}J_{CP}$ = 5.8 Hz, 2 CH_2), 117.0 (d, $^{2}J_{CF}$ = 18.9 Hz, HC), 117.6 (d, $^{2}J_{CF}$ = 17.4 Hz, HC),118.6 (HC), 123.9 (dd, $^{3}J_{CF}$ = 6.5 Hz, $^{4}J_{C-F}$ = 3.3 Hz, HC), 125.8 (d, $^{3}J_{CP}$ = 16.2 Hz, HC), 126.2 (d, $^{3}J_{CP}$ = 10.6 Hz, C), 128.5 (d, $^{1}J_{CP}$ = 188.5 Hz, C), 129.5 (2 HC), 129.6 (2 HC), 130.9 (C), 135.0 (C), 136.3 (C), 137.2 (d, $^{2}J_{CP}$ = 7.6 Hz, HC), 139.0 (C), 148.7 (d, $^{2}J_{CP}$ = 6.6 Hz, C), 150.2 (C), 150.8 (dd, $^{1}J_{CF}$ = 247.4 Hz, $^{2}J_{CF}$ = 12.1 Hz, C), 151.7 (dd, $^{1}J_{CF}$ = 250.7 Hz, $^{2}J_{CF}$ = 12.3 Hz, C), 153.5 (C) ppm.

^{31}P NMR (120 MHz, $CDCl_3$): δ = 18.5 ppm.

^{19}F NMR crude reaction mixture (282 MHz, $CDCl_3$): δ = -136.7 to -136.6 (m) and -137.6 to -137.4 (m) ppm.

HRMS (EI): calculated for $C_{26}H_{24}F_2NO_3P$ $[M]^+$ 467.1465; found 467.1465.

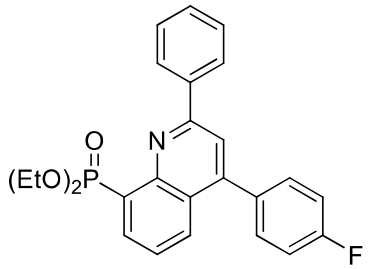

13l

Diethyl (4-(4-fluorophenyl)-2-phenylquinolin-8-yl))phosphonate (**13l**).

The general procedure A (step-by-step Povarov-DDQ oxidation sequential procedure) was followed using aminophenylphosphonate **1b** (0.23 g, 1 mmol), benzaldehyde (0.11 mL, 1 mmol), 4-fluorostyrene (0.14 mL, 1.2 mmol) and $BF_3{\cdot}Et_2O$, affording (0.26 g, 60%) of a white solid identified as **13l**.

Melting point: 172-174°C (ethyl acetate/hexane).

^{1}H RMN (300 MHz, $CDCl_3$): δ = 1.32-1.37 (m, 6 H, 2 CH_3), 4.27-4.44 (m, 4 H, 2 CH_2), 7.26-7.29 (m, 2 H), 7.48- 7.56 (m, 6 H), 7.89 (s, 1 H), 8.01(d, $^3J_{HP}$ = 8.4 Hz, 1 H), 8.37-8.44 (m, 3 H) ppm.

^{13}C RMN (75 MHz, $CDCl_3$): δ = 16.6 (d, $^3J_{CP}$ = 6.6 Hz, 2 CH_3), 62.5 (d, $^2J_{CP}$ = 5.8 Hz, 2 CH_2), 115.9 (d, $^2J_{CF}$ = 21.6 Hz, 2 HC), 119.3 (HC), 125.6 (d, $^3J_{CP}$ = 16.2 Hz, HC), 126.0 (d, $^3J_{CP}$ = 10.7 Hz, C), 128.0 (2 HC), 128.5 (d, $^1J_{CP}$ = 188.5 Hz, C), 128.9 (2 HC), 130.0 (HC), 130.4 (HC), 131.3 (HC), 131.4 (HC), 134.1 (C), 136.9 (d, $^2J_{CP}$ = 7.4 Hz, HC), 138.8 (C), 148.5 (C), 148.7 (d, $^2J_{CP}$ = 6.8 Hz, C), 156.6 (C), 163.1 (d, $^1J_{CF}$ = 248.6 Hz, C-F) ppm.

^{31}P NMR (120 MHz, $CDCl_3$): δ = 18.4 ppm.

^{19}F NMR crude reaction mixture (282 MHz, $CDCl_3$): δ = -113.4 to -113.2 (m) ppm.

HRMS (EI): calculated for $C_{25}H_{23}FNO_3P$ $[M]^+$ 435.1400; found 435.1402.

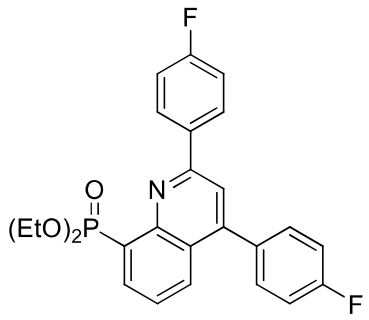

13m

Diethyl (2,4-bis(4-fluorophenyl)quinolin-8-yl)phosphonate (**13m**).

The general procedure A (step-by-step Povarov-DDQ oxidation sequential procedure) was followed using aminophenylphosphonate **1b** (0.23 g, 1 mmol), 4-fluorobenzaldehyde (0.11 mL, 1 mmol), 4-fluorostyrene (0.14 mL, 1.2 mmol) and $BF_3{\cdot}Et_2O$, affording (0.29 g, 68%) of a white solid identified as **13m**.

Melting point: 121-123°C (ethyl acetate/hexane).

^{1}H RMN (300 MHz, $CDCl_3$): δ = 1.32-1.36 (m, 6 H, 2 CH_3), 4.25-4.42 (m, 4 H, 2 CH_2), 7.18-7.28 (m, 4 H), 7.47-7.55 (m, 3 H), 7.83 (s, 1 H), 8.02 (d, $^3J_{HP}$ = 8.4 Hz, 1 H), 8.33-8.41 (m, 3 H) ppm.

^{13}C RMN (75 MHz, $CDCl_3$): δ = 16.6 (d, $^3J_{CP}$ = 6.4 Hz, 2 CH_3), 62.5 (d, $^2J_{CP}$ = 5.5 Hz, 2 CH_2), 115.8 (d, $^2J_{CF}$ = 21.6 Hz, 2 HC), 116.1 (d, $^2J_{CF}$ = 21.6 Hz, HC), 118.9 (HC), 125.7 (d, $^3J_{CP}$ = 15.8 Hz, HC), 125.9 (C), 128.7 (d, $^1J_{CP}$ = 188.8 Hz, C), 129.9 (d, $^3J_{CF}$ = 8.3 Hz, 2 HC), 130.4 (HC), 131.4 (d, $^3J_{CF}$ = 8.2 Hz, 2 HC), 134.0 (C), 135.0 (C), 137.0 (d, $^2J_{CP}$ = 7.4 Hz, HC), 148.7 (C), 155.5 (C), 163.2 (d, $^1J_{CF}$ = 248.6 Hz, C-F), 164.2 (d, $^1J_{CF}$ = 249.8 Hz, C-F) ppm.

^{31}P NMR (120 MHz, $CDCl_3$): δ = 18.3 ppm.

^{19}F NMR crude reaction mixture (282 MHz, $CDCl_3$): δ = -112.0 to -111.8 (m) and -113.0 to -113.1 (m) ppm.

HRMS (EI): calculated for $C_{25}H_{22}F_2NO_3P$ $[M]^+$ 453.1305; found 453.1307.

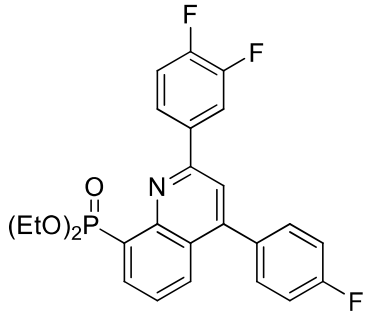

13n

Diethyl (2-(3,4-difluorophenyl)-4-(4-fluorophenyl)quinolin-8-yl)phosphonate (**13n**).

The general procedure A (step-by-step Povarov-DDQ oxidation sequential procedure) was followed using aminophenylphosphonate **1b** (0.23 g, 1 mmol), 3,4-difluorobenzaldehyde (0.11 mL, 1 mmol), 4-fluorostyrene (0.14 mL, 1.2 mmol) and $BF_3.Et_2O$, affording (0.20 g, 43%) of a white solid identified as **13n**.

Melting point: 159-161ºC (ethyl acetate/hexane).

^{1}H RMN (300 MHz, $CDCl_3$): δ = 1.33-1.38 (m, 6 H, 2 CH_3), 4.21-4.44 (m, 4 H, 2 CH_2), 7.23-7.58 (m, 6 H), 7.81 (s, 1 H), 8.01-8.11 (m, 2 H), 8.25-8.44 (m, 2 H) ppm.

^{13}C RMN (75 MHz, $CDCl_3$): 16.7 (d, $^3J_{CP}$ = 6.5 Hz, 2 CH_3), 62.5 (d, $^2J_{CP}$ = 5.8 Hz, 2 CH_2), 116.1 (d, $^2J_{CF}$ = 21.7 Hz, 2 HC), 117.0 (d, $^2J_{CF}$ = 18.7 Hz, HC), 117.7 (d, $^2J_{CF}$ = 17.4 Hz, HC),118.7 (HC), 120.5 (C), 124.0 (HC), 126.0 (d, $^3J_{CP}$ = 16.0 Hz, HC), 128.7 (d, $^1J_{CP}$ = 188.8 Hz, C), 130.5 (HC), 131.3 (HC), 131.4 (HC), 133.9 (C), 136.0 (C), 137.4 (HC), 148.6 (d, $^2J_{CP}$ = 6.4 Hz, C), 149.1 (C), 151.0 (dd, $^2J_{CF}$ = 12.5 Hz, $^1J_{CF}$ = 239.2 Hz, C), 151.8 (dd, $^2J_{CF}$ = 12.5 Hz, $^1J_{CF}$ = 247.6 Hz, C), 154.2 (C), 163.2 (d, $^1J_{CF}$ = 249.0 Hz, C-F) ppm.

^{31}P NMR (120 MHz, $CDCl_3$): δ = 18.3 ppm.

^{19}F NMR crude reaction mixture (282 MHz, $CDCl_3$): δ = -112.9 to -112.8 (m), -136.4 to -136.3 (m) and -137.4 to -137.2 (m) ppm.

HRMS (EI): calculated for $C_{25}H_{21}F_3NO_3P$ $[M]^+$ 471.1211; found 471.1217.

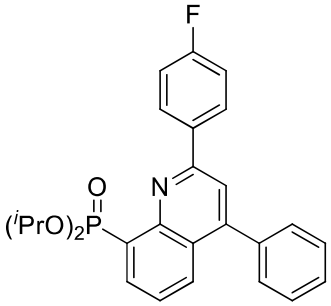

13o

Diisopropyl (2-(4-fluorophenyl)-4-phenylquinolin-8-yl)phosphonate (**13o**).

The general procedure B (MCR Povarov-DDQ oxidation sequential procedure) was followed using aminophenylphosphonate **1c** (0.26 g, 1 mmol), 4-fluorobenzaldehyde (0.11 mL, 1 mmol), styrene (0.14 mL, 1.2 mmol) and $BF_3.Et_2O$, affording (0.16 g, 34%) of a white solid identified as **13o**.

Melting point: 107-109ºC (ethyl acetate/hexane).

^{1}H RMN (400 MHz, $CDCl_3$): δ = 1.15 (d, $^3J_{HH}$ = 6.2 Hz, 2 CH_3), 1.33 (d, $^3J_{HH}$ = 6.2 Hz, 2 CH_3), 4.90-4.98 (m, 2 H, 2 CH), 7.10-7.14 (m, 2 H), 7.39-7.50 (m, 6 H), 7.77 (s, 1 H), 7.96-7.98 (m, 1 H), 8.27-8.33 (m, 3 H) ppm.

^{13}C RMN (100 MHz, $CDCl_3$): δ = 23.9 (d, $^3J_{CP}$ = 5.1 Hz, 2 CH_3), 24.3 (d, $^3J_{CP}$ = 3.8 Hz, 2 CH_3), 70.7 (d, $^2J_{CP}$ = 6.0 Hz, 2 CH), 115.6 (d, $^2J_{CF}$ = 21.6 Hz, 2 HC), 118.6 (HC), 125.3 (d, $^3J_{CP}$ = 16.2 Hz, HC), 125.7 (d, $^3J_{CP}$ = 10.8 Hz, C), 128.6 (HC), 128.7 (2 HC), 129.4 (d, $^1J_{CP}$ = 189.7 Hz, C), 129.5 (2 HC), 129.7 (d, $^3J_{CF}$ = 8.4 Hz, 2 HC), 130.4 (HC), 135.1 (C), 136.8 (d, $^2J_{CP}$ = 7.5 Hz, HC), 138.0 (C), 148.5 (d, $^2J_{CP}$ = 6.7 Hz, C), 149.5 (C), 155.1 (C), 164.0 (d, $^1J_{CF}$ = 249.6 Hz, C-F) ppm.

^{31}P NMR (120 MHz, $CDCl_3$): δ = 16.3 ppm.

^{19}F NMR crude reaction mixture (282 MHz, $CDCl_3$): δ = -112.3 to -112.1 (m) ppm.

HRMS (EI): calculated for $C_{27}H_{27}FNO_3P$ $[M]^+$ 463.1713; found 463.1720.

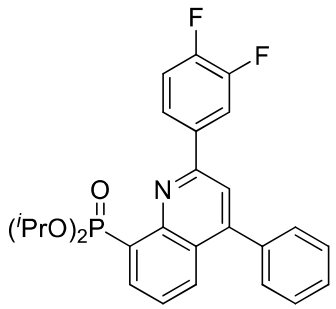

13p

Diisopropyl (2-(3,4-difluorophenyl)-4-phenylquinolin-8-yl)phosphonate (**13p**).

The general procedure B (MCR Povarov-DDQ oxidation sequential procedure) was followed using aminophenylphosphonate **1c** (0.26 g, 1 mmol), 3,4-difluorobenzaldehyde (0.11 mL, 1 mmol), styrene (0.14 mL, 1.2 mmol) and $BF_3{\cdot}Et_2O$, affording (0.18 g, 38%) of a white solid identified as **13p**.

Melting point: 127-129ºC (ethyl acetate/hexane).

^{1}H RMN (400 MHz, $CDCl_3$): δ = 1.15 (d, $^3J_{HH}$ = 6.2 Hz, 2 CH_3), 1.35 (d, $^3J_{HH}$ = 6.2 Hz, 2 CH_3), 4.88-4.96 (m, 2 H, 2 CH), 7.17-7.23 (m, 1 H), 7.40-7.49 (m, 6 H), 7.74 (s, 1 H), 7.95-7.98 (m, 1 H), 8.00-8.03 (m, H), 8.23-8.28 (m, H), 8.30-8.37 (m, H) ppm.

^{13}C RMN (100 MHz, $CDCl_3$): δ = 23.9 (d, $^3J_{CP}$ = 5.0 Hz, 2 CH_3), 24.3 (d, $^3J_{CP}$ = 4.0 Hz, 2 CH_3), 70.7 (d, $^2J_{CP}$ = 6.0 Hz, 2 CH), 116.8 (d, $^2J_{CF}$ = 18.7 Hz, HC), 117.3 (d, $^2J_{CF}$ = 17.5 Hz, HC), 118.2 (HC), 123.6 (dd, $^3J_{CF}$ = 6.6 Hz, $^4J_{CF}$ = 3.5 Hz, HC), 125.6 (d, $^3J_{CP}$ = 16.3 Hz, HC), 125.9 (d, $^3J_{CP}$ = 10.6 Hz, C), 128.7 (2 HC), 129.5 (2 HC), 129.5 (d, $^1J_{CP}$ = 189.3 Hz, C), 130.4 (HC), 130.6 (HC), 136.1 (dd, $^3J_{CF}$ = 6.7 Hz, $^4J_{CF}$ = 3.6 Hz, C), 137.1 (d, $^3J_{CF}$ = 7.7 Hz, HC), 137.8 (C), 148.4 (d, $^2J_{CP}$ = 6.4 Hz, C), 149.8 (C), 150.8 (dd, $^2J_{CF}$ = 12.7 Hz, $^1J_{CF}$ = 247.7 Hz, C), 151.6 (dd, $^2J_{CF}$ = 12.7 Hz, $^1J_{CF}$ = 251.7 Hz, C), 153.7 (C) ppm.

^{31}P NMR (120 MHz, $CDCl_3$): δ = 16.2 ppm.

^{19}F NMR crude reaction mixture (282 MHz, $CDCl_3$): δ = -136.7 to -136.6 (m) and -137.8 to 137.6 (m) ppm.

HRMS (EI): calculated for $C_{27}H_{26}F_2NO_3P$ $[M]^+$ 481.1618; found 481.1625.

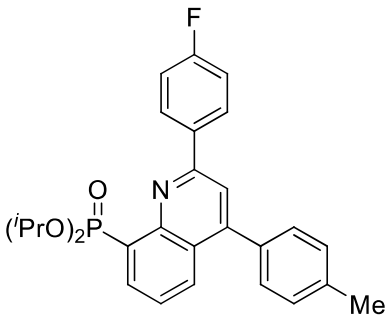

13q

Diisopropyl (2-(4-fluorophenyl)-4-(p-tolyl)quinolin-8-yl)phosphonate (**13q**).

The general procedure B (MCR Povarov-DDQ oxidation sequential procedure) was followed using aminophenylphosphonate **1c** (0.26 g, 1 mmol), 4-fluorobenzaldehyde (0.11 mL, 1 mmol), 4-methylstyrene (0.16 mL, 1.2 mmol) and $BF_3.Et_2O$, affording (0.28 g, 58%) of a white solid identified as **13q**.

Melting point: 121-123°C (ethyl acetate/hexane).

^{1}H RMN (400 MHz, $CDCl_3$): δ = 1.14 (d, $^3J_{HH}$ = 6.1 Hz, 2 CH_3), 1.33 (d, $^3J_{HH}$ = 6.2 Hz, 2 CH_3), 2.40 (CH_3), 4.89-4.97 (m, 2 H, 2 CH), 7.09-7.13 (m, 2 H), 7.27-7.34 (m, 4 H), 7.37-7.42 (m, 1 H), 7.75 (s, 1 H), 7.98-8.00 (m, 1 H), 8.26-8.32 (m, 3 H) ppm.

^{13}C RMN (100 MHz, $CDCl_3$): δ = 21.3 (CH_3), 23.9 (d, $^3J_{CP}$ = 5.1 Hz, 2 CH_3), 24.3 (d, $^3J_{CP}$ = 3.8 Hz, 2 CH_3), 70.6 (d, $^2J_{CP}$ = 6.0 Hz, 2 CH), 115.5 (d, $^2J_{CF}$ = 21.6 Hz, 2 HC), 118.5 (HC), 125.2 (d, $^3J_{CP}$ = 16.2 Hz, HC), 125.8 (d, $^3J_{CP}$ = 10.7 Hz, C), 129.4 (2 HC), 129.4 (2 HC), 129.7 (d, $^3J_{CF}$ = 7.4 Hz, 2 HC), 130.0 (d, $^1J_{CP}$ = 189.3 Hz, C), 130.5 (d, $^4J_{CP}$ = 5.0 Hz, HC), 135.1 (d, $^4J_{CP}$ = 4.7 Hz, C), 135.1 (C), 136.7 (d, $^2J_{CP}$ = 7.5 Hz, HC), 138.6 (C), 148.6 (d, $^2J_{CP}$ = 6.6 Hz, C), 149.6 (C), 155.1 (C), 164.0 (d, $^1J_{CF}$ = 249.5 Hz, C) ppm.

^{31}P NMR (120 MHz, $CDCl_3$): δ = 16.4 ppm.

^{19}F NMR crude reaction mixture (282 MHz, $CDCl_3$): δ = -112.4 to -112.2 (m) ppm.

HRMS (EI): calculated for $C_{28}H_{29}FNO_3P$ $[M]^+$ 477.1869; found 477.1876.

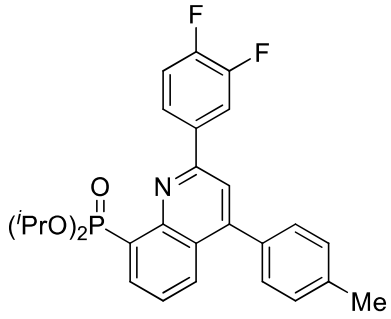

13r

Diisopropyl (2-(3,4-difluorophenyl)-4-(p-tolyl)quinolin-8-yl)phosphonate (**13r**).

The general procedure B (MCR Povarov-DDQ oxidation sequential procedure) was followed using aminophenylphosphonate **1c** (0.26 g, 1 mmol), 3,4-difluorobenzaldehyde (0.11 mL, 1 mmol), 4-methylstyrene (0.16 mL, 1.2 mmol) and $BF_3.Et_2O$, affording (0.19 g, 39%) of a white solid identified as **13r**.

Melting point: 140-142°C (ethyl acetate/hexane).

^{1}H RMN (400 MHz, $CDCl_3$): δ = 1.15 (d, $^3J_{HH}$ = 6.2 Hz, 2 CH_3), 1.34 (d, $^3J_{HH}$ = 6.2 Hz, 2 CH_3), 2.39 (CH_3), 4.88-4.96 (m, 2 H, 2 CH), 7.16-7.23 (m, 1 H), 7.26-7.33 (m, 4 H), 7.40-7.44 (m, 1 H), 7.72 (s, 1 H), 7.99-8.02 (m, 2 H), 8.23-8.36 (m, 2 H) ppm.

^{13}C RMN (100 MHz, $CDCl_3$): δ = 21.2 (CH_3), 23.9 (d, $^3J_{CP}$ = 5.0 Hz, 2 CH_3), 24.3 (d, $^3J_{CP}$ = 4.8 Hz, 2 CH_3), 70.7 (d, $^2J_{CP}$ = 5.9 Hz, 2 CH), 116.8 (d, $^2J_{CF}$ = 18.7 Hz, HC), 117.3 (d, $^2J_{CF}$ = 17.5 Hz, HC), 118.2 (HC), 123.6 (dd, $^3J_{CF}$ = 6.6 Hz, $^4J_{CF}$ = 3.4 Hz, HC), 125.5 (d, $^3J_{CP}$ = 16.2 Hz, HC), 126.0 (d, $^3J_{CP}$ = 10.4 Hz, C), 129.4 (2 HC), 129.4 (2 HC), 129.5 (d, $^1J_{CP}$ = 188.1 Hz, C), 130.5 (HC), 134.9 (HC), 136.2 (dd, $^3J_{CF}$ = 5.8 Hz, $^4J_{CF}$ = 3.6 Hz, C), 137.1 (d, $^3J_{CF}$ = 7.7 Hz, HC), 138.7 (C), 148.4 (d, $^2J_{CP}$ = 6.4 Hz, C), 149.9 (C), 150.8 (dd, $^2J_{CF}$ = 12.6 Hz, $^1J_{CF}$ = 247.6 Hz, C), 151.6 (dd, $^2J_{CF}$ = 12.7 Hz, $^1J_{CF}$ = 251.3 Hz, C), 153.7 (C) ppm.

^{31}P NMR (120 MHz, $CDCl_3$): δ = 16.3 ppm.

^{19}F NMR crude reaction mixture (282 MHz, $CDCl_3$): δ = -136.9 to -136.7 (m) and -137.9 to 137.7 (m) ppm.

HRMS (EI): calculated for $C_{28}H_{28}F_2NO_3P$ $[M]^+$ 435.1400; found 435.1415.

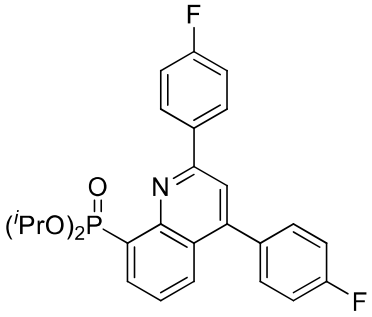

13s

Diisopropyl (2,4-bis(4-fluorophenyl)quinolin-8-yl)phosphonate (**13s**).

The general procedure B (MCR Povarov-DDQ oxidation sequential procedure) was followed using aminophenylphosphonate **1c** (0.26 g, 1 mmol), 4-fluorobenzaldehyde (0.11 mL, 1 mmol), 4-fluorostyrene (0.14 mL, 1.2 mmol) and $BF_3{\cdot}Et_2O$, affording (0.30 g, 68%) of a white solid identified as **13s**.

Melting point: 113-115ºC (ethyl acetate/hexane).

^{1}H RMN (400 MHz, $CDCl_3$): δ = 1.15 (d, $^3J_{HH}$ = 6.2 Hz, 2 CH_3), 1.35 (d, $^3J_{HH}$ = 6.1 Hz, 2 CH_3), 4.90-4.99 (m, 2 H, 2 CH), 7.11-7.20 (m, 4 H), 7.40-7.46 (m, 3 H), 7.75 (s, 1 H), 7.91-7.93 (m, 1 H), 8.29-8.35 (m, 3 H) ppm.

^{13}C RMN (100 MHz, $CDCl_3$): δ = 23.9 (d, $^3J_{CP}$ = 5.1 Hz, 2 CH_3), 24.3 (d, $^3J_{CP}$ = 3.8 Hz, 2 CH_3), 70.7 (d, $^2J_{CP}$ = 6.0 Hz, 2 CH), 115.6 (d, $^2J_{CF}$ = 21.5 Hz, 2 HC), 115.8 (d, $^2J_{CF}$ = 21.6 Hz, 2 HC), 118.6 (HC), 125.5 (d, $^3J_{CP}$ = 16.1 Hz, HC), 125.7 (d, $^3J_{CP}$ = 10.6 Hz, C), 129.6 (d, $^1J_{CP}$ = 189.7 Hz, C), 131.2 (d, $^3J_{CF}$ = 8.1 Hz, 2 HC), 134.0 (C), 134.9 (C), 136.8 (d, $^2J_{CP}$ = 7.4 Hz, HC), 148.4 (C), 148.5 (d, $^2J_{CP}$ = 6.8 Hz, C), 150.1 (C), 163.0 (d, $^1J_{CF}$ = 248.3 Hz, C-F), 164.0 (d, $^1J_{CF}$ = 249.7 Hz, C-F) ppm.

^{31}P NMR (120 MHz, $CDCl_3$): δ = 16.1 ppm.

^{19}F NMR crude reaction mixture (282 MHz, $CDCl_3$): δ = -112.2 to -112.0 (m) and -113.4 to -113.2 (m) ppm.

HRMS (EI): calculated for $C_{27}H_{26}F_2NO_3P$ $[M]^+$ 481.1618; found 481.1632.

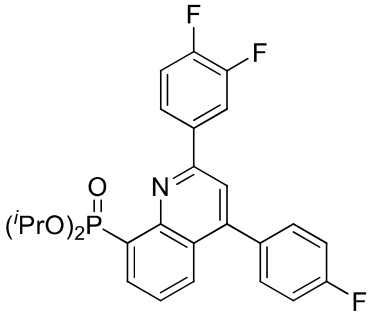

13t

Diisopropyl (2-(3,4-difluorophenyl)-4-(4-fluorophenyl)quinolin-8-yl)phosphonate (**13t**).

The general procedure B (MCR Povarov-DDQ oxidation sequential procedure) was followed using aminophenylphosphonate **1c** (0.26 g, 1 mmol), 3,4-difluorobenzaldehyde (0.11 mL, 1 mmol), 4-fluorostyrene (0.44 mL, 1.2 mmol) and $BF_3{\cdot}Et_2O$, affording (0.19 g, 88%) of a white solid identified as **13t**.

Melting point: 144-146ºC (ethyl acetate/hexane).

^{1}H RMN (400 MHz, $CDCl_3$): δ = 1.06 (d, $^3J_{HH}$ = 6.2 Hz, 2 CH_3), 1.25 (d, $^3J_{HH}$ = 6.2 Hz, 2 CH_3), 4.79-4.87 (m, 2 H, 2 CH), 7.17-7.23 (m, 1 H), 7.40-7.49 (m, 6 H), 7.74 (s, 1 H), 7.95-7.98 (m, 1 H), 8.00-8.03 (m, H), 8.23-8.28 (m, H), 8.30-8.37 (m, H) ppm.

^{13}C RMN (100 MHz, $CDCl_3$): δ = 23.8 (d, $^3J_{CP}$ = 5.0 Hz, 2 CH_3), 24.1 (d, $^3J_{CP}$ = 3.9 Hz, 2 CH_3), 70.7 (d, $^2J_{CP}$ = 6.0 Hz, 2 CH), 115.7 (d, $^3J_{CF}$ = 20.6 Hz, 2 HC), 116.8 (d, $^2J_{CF}$ = 18.7 Hz, HC), 117.2 (d, $^2J_{CF}$ = 17.5 Hz, HC), 118.2 (HC), 123.6 (dd, $^3J_{CF}$ = 6.5 Hz, $^4J_{CF}$ = 3.3 Hz, HC), 125.7 (d, $^3J_{CP}$ = 17.6 Hz, HC), 125.7 (C), 129.4 (d, $^1J_{CP}$ = 189.5 Hz, C), 129.9 (HC), 131.1 (HC), 131.2 (2 HC), 133.6 (C), 135.8 (dd, $^3J_{CF}$ = 5.7 Hz, $^4J_{CF}$ = 3.5 Hz, C), 136.9 (d, $^3J_{CF}$ = 7.6 Hz, HC), 148.3 (d, $^2J_{CP}$ = 6.5 Hz, C), 148.6 (C), 150.6 (dd, $^2J_{CF}$ = 12.6 Hz, $^1J_{CF}$ = 247.8 Hz, C), 151.5 (dd, $^2J_{CF}$ = 12.7 Hz, $^1J_{CF}$ = 251.6 Hz, C), 153.6 (C), 162.9 (d, $^1J_{CF}$ = 248.9 Hz, C-F) ppm.

^{31}P NMR (120 MHz, $CDCl_3$): δ = 15.9 ppm.

^{19}F NMR crude reaction mixture (282 MHz, $CDCl_3$): δ = -113.0 to -112.8 (m), -136.8 to -136.5 (m) and -137.8 to 137.6 (m) ppm.

HRMS (EI): calculated for $C_{27}H_{25}F_3NO_3P$ $[M]^+$ 499.1524; found 499.1534.

General procedure for the preparation of diethyl 1,2,3,4-tetrahydroquinolin-6-ylphosphonates 15

MCR Povarov procedure

A mixture of diethyl (4-aminophenyl)phosphonate **1d** (1 mmol, 1 equiv.), freshly distilled aldehydes **2** (1 mmol, 1 equiv.), styrenes **3** (1.2 mmol, 1.2 equiv.) and 2 equivalents of $BF_3{\cdot}Et_2O$ (0.25 mL, 2 mmol) dissolved in $CHCl_3$ (3 mL) was stirred and heated to reflux in the presence of molecular sieves (4 Å), until TLC, ^{3}1P NMR and ^{1}H NMR spectroscopy analysis indicated the consumption of the starting materials. The molecular sieves were removed by filtration and the resulting solution was diluted with methylene chloride (15 ml), washed with a solution of NaOH 2M (25 ml), extracted with methylene chloride (2 x 10 mL) and dried over $MgSO_4$. Upon *in vacuo* solvent evaporation, the resultant reaction crude was further purified by flash column chromatography on silica gel using a gradient of elution of 5-70% ethyl acetate in hexane, to afford 1,2,3,4-tetrahydroquinolin-6-yl phosphonates **15**.

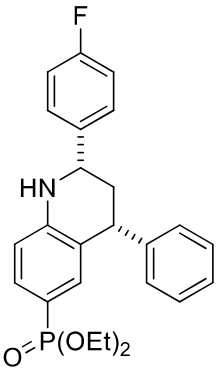

15a

Diethyl (2-(4-fluorophenyl)-4-phenyl-1,2,3,4-tetrahydroquinolin-6-yl)phosphonate (**15a**).

The general procedure (MCR Povarov) was followed using aminophenylphosphonate **1d** (0.26 g, 1 mmol), 4-fluorobenzaldehyde (0.11 mL, 1 mmol), styrene (0.14 mL, 1.2 mmol) and $BF_3{\cdot}Et_2O$, affording (0.36 g, 81%) of a white solid identified as **15a**.

Melting point: 146-148°C (ethyl acetate/hexane).

^{1}H RMN (400 MHz, $CDCl_3$): δ = 1.13-1.24 (m, 6 H, 2 CH_3), 1.75 (ddd, $^3J_{HH}$ = 12.3 Hz, $^3J_{HH}$ = 11.3 Hz, $^2J_{HH}$ = 11.4 Hz, 1 H, CH_2), 2.25-2.30 (m, 1 H, CH_2), 3.83-4.02 (m, 4 H, 2 CH_2), 4.26 (dd, $^3J_{HH}$ = 5.0 Hz, $^3J_{HH}$ = 12.8 Hz, 1 H, CH), 4.42 (s, NH), 4.64 (dd, $^3J_{HH}$ = 2.8 Hz, $^3J_{HH}$ = 11.3 Hz, 1 H, CH), 6.58-6.61 (m, 7.01-7.07 (m, 3 H), 7.20-7.32 (m, 5 H), 7.38-7.49 (m, 3 H) ppm.

^{13}C RMN (100 MHz, $CDCl_3$): δ = 16.4 (d, $^3J_{CP}$ = 6.7 Hz, 2 CH_3), 41.8 (CH_2), 44.6 (HC), 56.5 (HC), 61.8 (d, $^2J_{CP}$ = 5.4 Hz, 2 CH_2), 113.8(d, $^3J_{CP}$ = 16.1 Hz, HC), 114.8 (d, $^1J_{CP}$ = 196.9 Hz, C), 115.8 (d, $^2J_{CF}$ =

21.5 Hz, 2 HC), 124.4 (d, $^{3}J_{CP}$ = 15.5 Hz, C), 127.0 (HC), 128.2 (HC), 128.3 (2 HC), 128.6 (2 HC), 128.9 (2 HC), 131.8 (d, $^{2}J_{CP}$ = 11.3 Hz, HC), 133.6 (d, $^{2}J_{CP}$ = 12.0 Hz, HC), 138.9 (d, $^{4}J_{CF}$ = 3.1 Hz, C), 144.2 (C), 148.8 (d, $^{4}J_{CP}$ = 3.0 Hz, C), 162.5 (d, $^{1}J_{CF}$ = 246.3 Hz, C-F) ppm.

^{31}P NMR (120 MHz, $CDCl_3$): δ = 22.3 ppm.

^{19}F NMR crude reaction mixture (282 MHz, $CDCl_3$): δ = -114.7 to -114.5 (m) ppm.

HRMS (EI): calculated for $C_{25}H_{27}FNO_3P$ $[M]^+$ 439,1713; found 439,1725.

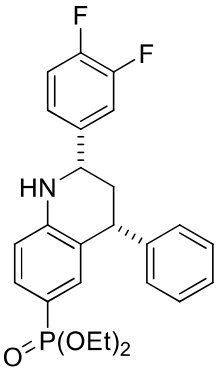

15b

Diethyl (2-(3,4-difluorophenyl)-4-phenyl-1,2,3,4-tetrahydroquinolin-6-yl)phosphonate (**15b**).

The general procedure (MCR Povarov) was followed using aminophenylphosphonate **1d** (0.26 g, 1 mmol), 3,4-difluorobenzaldehyde (0.11 mL, 1 mmol), styrene (0.14 mL, 1.2 mmol) and $BF_3.Et_2O$, affording (0.44 g, 97%) of a white solid identified as **15b**.

Melting point: 164-166°C (ethyl acetate/hexane).

^{1}H RMN (400 MHz, $CDCl_3$): δ = 1.19-1.29 (m, 6 H, 2 CH_3), 2.17 (ddd, $^{3}J_{HH}$ = 12.5 Hz, $^{3}J_{HH}$ = 11.6 Hz, $^{2}J_{HH}$ = 11.5 Hz, 1 H, CH_2), 2.31-2.36 (m, 1 H, CH_2), 3.89-4.07 (m, 4 H, 2 CH_2), 4.28 (dd, $^{3}J_{HH}$ = 5.3 Hz, $^{3}J_{HH}$ = 12.5 Hz, 1 H, CH), 4.52 (s, NH), 4.67 (dd, $^{3}J_{HH}$ = 2.5 Hz, $^{3}J_{HH}$ = 11.1 Hz, 1 H, CH), 6.65-6.68 (m, 7.07-7.10 (m, 1 H), 7.18-7.37 (m, 8 H), 7.49-7.54 (m, 1 H) ppm.

^{13}C RMN (100 MHz, $CDCl_3$): δ = 16.3 (d, $^{3}J_{CP}$ = 6.8 Hz, 2 CH_3), 41.8 (CH_2), 44.4 (HC), 56.3 (HC), 61.8 (d, $^{2}J_{CP}$ = 5.1 Hz, 2 CH_2), 114.0 (d, $^{2}J_{CF}$ = 16.2 Hz, HC), 115.6 (d, $^{2}J_{CF}$ = 17.6 Hz, HC), 117.6 (d, $^{2}J_{CF}$ = 17.3 Hz, HC), 122.6 (dd, $^{3}J_{CF}$ = 6.2 Hz, $^{4}J_{CF}$ = 3.6 Hz, HC), 124.3 (d, $^{3}J_{CP}$ = 15.6 Hz, C), 127.1 (HC), 128.6 (2 HC), 128.9 (2 HC), 131.8 (d, $^{3}J_{CP}$ = 11.2 Hz, HC), 133.6 (d, $^{2}J_{CP}$ = 11.8 Hz, HC), 140.3 (dd, $^{3}J_{CF}$ = 5.0 Hz, $^{4}J_{CF}$ = 3.7 Hz, C), 144.0 (2 C), 148.5 (d, $^{4}J_{CP}$ = 3.1 Hz, C), 149.9 (dd, $^{2}J_{CF}$ = 12.6 Hz, $^{1}J_{CF}$ = 248.6 Hz, C), 150.7 (dd, $^{2}J_{CF}$ = 12.7 Hz, $^{1}J_{CF}$ = 248.9 Hz, C) ppm.

^{31}P NMR (120 MHz, $CDCl_3$): δ = 22.1 ppm.

^{19}F NMR crude reaction mixture (282 MHz, $CDCl_3$): δ = = -137.5 to -137.2 (m) and -139.1 to 139.3 (m) ppm.

HRMS (EI): calculated for $C_{25}H_{26}F_2NO_3P$ $[M]^+$ 457,1618; found 457,1630.

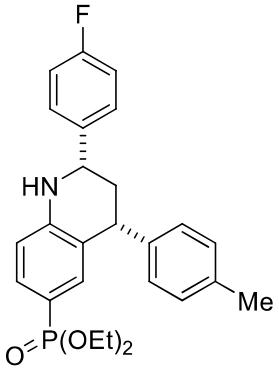

15c

Diisopropyl (2-(4-fluorophenyl)-4-(p-tolyl) -1,2,3,4-tetrahydroquinolin-8-yl)phosphonate (**15c**).

The general procedure (MCR Povarov) was followed using aminophenylphosphonate **1d** (0.26 g, 1 mmol), 4-fluorobenzaldehyde (0.11 mL, 1 mmol), 4-methylstyrene (0.16 mL, 1.2 mmol) and $BF_3{\cdot}Et_2O$, affording (0.29 g, 65%) of a white solid identified as **15c**.

Melting point: 160-162°C (ethyl acetate/hexane).

^{1}H RMN (400 MHz, $CDCl_3$): δ = 1.13-1.40 (m, 6 H, 2 CH_3), 2.13 (ddd, $^3J_{HH}$ = 12.3 Hz, $^3J_{HH}$ = 11.6 Hz, $^2J_{HH}$ = 11.7 Hz, 1 H, CH_2), 2.21-2.27 (m, 1 H, CH_2), 2.32 (s, 1 H, CH_3), 3.83-4.01 (m, 4 H, 2 CH_2), 4.21 (dd, $^3J_{HH}$ = 5.2 Hz, $^3J_{HH}$ = 12.2 Hz, 1 H, CH), 4.49 (s, NH), 4.49 (dd, $^3J_{HH}$ = 2.8 Hz, $^3J_{HH}$ = 11.2 Hz, 1 H, CH), 6.56-6.601 (m, 7.01-7.12 (m, 6 H), 7.37-7.46 (m 3 H) ppm.

^{13}C RMN (100 MHz, $CDCl_3$): δ = 16.3 (d, $^3J_{CP}$ = 6.8 Hz, 2 CH_3), 21.1 (CH_3), 41.8 (CH_2), 44.2 (HC), 56.5 (HC), 62.2 (d, $^2J_{CP}$ = 4.8 Hz, 2 CH_2), 113.7 (d, $^2J_{CF}$ = 16.2 Hz, HC), 114.5 (d, $^1J_{CP}$ = 196.4 Hz, C), 115.7 (d, $^2J_{CF}$ = 21.4 Hz, 2 HC), 124.5 (d, $^3J_{CP}$ = 15.4 Hz, C), 128.2 (HC), 128.3 (HC), 128.4 (2 HC), 129.5 (3 HC), 131.7 (d, $^2J_{CP}$ = 11.2 Hz, HC), 133.6 (d, $^2J_{CP}$ = 12.0 Hz, HC), 136.5 (C), 139.0 (d, $^4J_{CP}$ = 3.2 Hz, C), 141.1 (C), 148.8 (d, $^4J_{CP}$ = 3.0 Hz, C), 162.4 (d, $^1J_{CF}$ = 246.1 Hz, C-F) ppm.

^{31}P NMR (120 MHz, $CDCl_3$): δ = 22.4 ppm.

^{19}F NMR crude reaction mixture (282 MHz, $CDCl_3$): δ = -114.7 to -114.6 (m) ppm.

HRMS (EI): calculated for $C_{26}H_{25}FNO_3P$ $[M]^+$ 453,1869; found 453,1879.

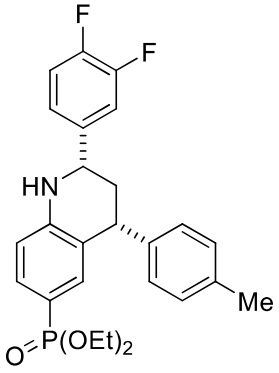

15d

Diethyl (2-(3,4-difluorophenyl)-4-(p-tolyl)-1,2,3,4-tetrahydroquinolin-6-yl)phosphonate (**15d**).

The general procedure (MCR Povarov) was followed using aminophenylphosphonate **1d** (0.26 g, 1 mmol), 3,4-difluorobenzaldehyde (0.11 mL, 1 mmol), 4-methylstyrene (0.16 mL, 1.2 mmol) and $BF_3.Et_2O$, affording (0.37 g, 79%) of a white solid identified as **15d**.

Melting point: 156-158°C (ethyl acetate/hexane).

^{1}H RMN (400 MHz, $CDCl_3$): δ = 1.14-1.24 (m, 6 H, 2 CH_3), 2.10 (ddd, $^3J_{HH}$ = 12.8 Hz, $^3J_{HH}$ = 11.4 Hz, $^2J_{HH}$ = 11.5 Hz, 1 H, CH_2), 2.22-2.27 (m, 1 H, CH_2), 2.32 (s, 3 H, CH_3), 3.83-4.02 (m, 4 H, 2 CH_2), 4.20 (dd, $^3J_{HH}$ = 5.1 Hz, $^3J_{HH}$ = 12.4 Hz, 1 H, CH), 4.49 (s, NH), 4.61 (dd, $^3J_{HH}$ = 2.7 Hz, $^3J_{HH}$ = 11.2 Hz, 1 H, CH), 6.59-6.62 (m, 1 H), 7.02-7.15 (m, 7 H), 7.23-7.29 (m, 1 H), 7.41-7.47 (m, 1 H) ppm.

^{13}C RMN (100 MHz, $CDCl_3$): δ = 16.3 (d, $^3J_{CP}$ = 6.8 Hz, 2 CH_3), 21.2 (CH_3), 41.8 (CH_2), 44.1 (HC), 56.3 (HC), 61.7 (d, $^2J_{CP}$ = 5.1 Hz, 2 CH_2), 113.9 (d, $^2J_{CF}$ = 16.1 Hz, HC), 115.1 (d, $^1J_{CP}$ = 220.4 Hz, C), 115.5 (d, $^2J_{CF}$ = 17.7 Hz, HC), 117.6 (d, $^3J_{CP}$ = 17.3 Hz, HC), 122.6 (dd, $^3J_{CF}$ = 6.2 Hz, $^4J_{CF}$ = 3.5 Hz, HC), 124.5 (d, $^3J_{CP}$ = 15.5 Hz, C), 128.4 (2 HC), 129.6 (2 HC), 131.0 (d, $^2J_{CP}$ = 11.2 Hz, HC), 133.6 (d, $^2J_{CP}$ = 11.9 Hz, HC), 136.6 (C), 140.4 (dd, $^4J_{CF}$ = 3.6 Hz, $^3J_{CF}$ = 5.0 Hz, C), 140.8 (C), 148.5 (d, $^4J_{CP}$ = 3.0 Hz, C), 149.9 (dd, $^2J_{CF}$ = 12.7 Hz, $^1J_{CF}$ = 248.4 Hz, C), 150.7 (dd, $^2J_{CF}$ = 12.8 Hz, $^1J_{CF}$ = 248.8 Hz, C) ppm.

^{31}P NMR (120 MHz, $CDCl_3$): δ = 22.2 ppm.

^{19}F NMR crude reaction mixture (282 MHz, $CDCl_3$): δ = -137.3 to -137.2 (m) and -139.2 to 139.0 (m) ppm.

HRMS (EI): calculated for $C_{26}H_{28}F_2NO_3P$ $[M]^+$ 471,1775; found 471,1786.

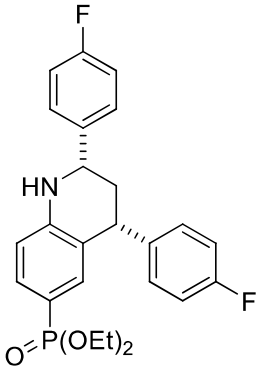

15e

Diethyl (2,4-bis(4-fluorophenyl)-1,2,3,4-tetrahydroquinolin-6-yl)phosphonate (**15e**).

The general procedure (MCR Povarov) was followed using aminophenylphosphonate **1d** (0.26 g, 1 mmol), 4-fluorobenzaldehyde (0.11 mL, 1 mmol), 4-fluorostyrene (0.14 mL, 1.2 mmol) and $BF_3.Et_2O$, affording (0.39 g, 86%) of a white solid identified as **15e**.

Melting point: 185-187°C (ethyl acetate/hexane).

^{1}H RMN (400 MHz, $CDCl_3$): δ = 1.16-1.25 (m, 6 H, 2 CH_3), 2.10 (ddd, $^3J_{HH}$ = 12.5 Hz, $^3J_{HH}$ = 11.2 Hz, $^2J_{HH}$ = 11.5 Hz, 1 H, CH_2), 2.23-2.28 (m, 1 H, CH_2), 3.86-4.04 (m, 4 H, 2 CH_2), 4.26 (dd, $^3J_{HH}$ = 5.2 Hz, $^3J_{HH}$ = 12.3 Hz, 1 H, CH), 4.41 (s, NH), 4.64 (dd, $^3J_{HH}$ = 2.9 Hz, $^3J_{HH}$ = 11.2 Hz, 1 H, CH), 6.57-6.60 (m, 6.98-7.07 (m, 5 H), 7.16-7.20 (m, 2 H), 7.37-7.48 (m, 3 H) ppm.

^{13}C RMN (100 MHz, $CDCl_3$): δ = 16.4 (d, $^3J_{CP}$ = 6.7 Hz, 2 CH_3), 41.9 (CH_2), 43.9 (HC), 56.5 (HC), 61.8 (d, $^2J_{CP}$ = 5.2 Hz, 2 CH_2), 113.9 (d, $^2J_{CF}$ = 16.1 Hz, HC), 115.1 (d, $^1J_{CP}$ = 197.2 Hz, C), 115.6-115.9 (m, 4 HC), 124.1 (d, $^3J_{CF}$ = 16.0 Hz, C), 128.2-130.1 (m, 4 HC), 131.8 (d, $^2J_{CP}$ = 11.1 Hz, HC), 133.5 (d, $^2J_{CP}$ = 11.8 Hz, HC), 138.8 (d, $^4J_{CF}$ = 3.1 Hz, C), 139.9 (d, $^4J_{CF}$ = 3.2 Hz, C), 148.7 (d, $^4J_{CP}$ = 3.1 Hz, C), 162.2 (d, $^1J_{CF}$ = 245.0 Hz, C-F), 162.5 (d, $^1J_{CF}$ = 246.4 Hz, C-F) ppm.

^{31}P NMR (120 MHz, $CDCl_3$): δ = 22.1 ppm.

^{19}F NMR crude reaction mixture (282 MHz, $CDCl_3$): δ = -114.5 to -114.4 (m) and -116.5 to -116.4 (m) ppm.

HRMS (EI): calculated for $C_{25}H_{26}F_2NO_3P$ $[M]^+$ 457,1618; found 457,1626.

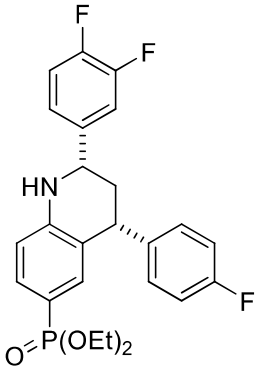

15f

Diethyl (2-(3,4-difluorophenyl)-4-(4-fluorophenyl)-1,2,3,4-tetrahydroquinolin-6-yl)phosphonate (**15f**).

The general procedure (MCR Povarov) was followed using aminophenylphosphonate **1d** (0.26 g, 1 mmol), 3,4-difluorobenzaldehyde (0.11 mL, 1 mmol), 4-fluorostyrene (0.44 mL, 1.2 mmol) and $BF_3{\cdot}Et_2O$, affording (0.31 g, 65%) of a white solid identified as **15f**.

Melting point: 178-180°C (ethyl acetate/hexane).

^{1}H RMN (400 MHz, $CDCl_3$): δ = 1.15-1.24 (m, 6 H, 2 CH_3), 2.06 (ddd, $^3J_{HH}$ = 12.6 Hz, $^3J_{HH}$ = 11.4 Hz, $^2J_{HH}$ = 11.7 Hz, 1 H, CH_2), 2.22-2.27 (m, 1 H, CH_2), 3.84-4.00 (m, 4 H, 2 CH_2), 4.24 (dd, $^3J_{HH}$ = 5.1 Hz, $^3J_{HH}$ = 12.2 Hz, 1 H, CH), 4.58 (s, NH), 4.61 (dd, $^3J_{HH}$ = 2.7 Hz, $^3J_{HH}$ = 11.3 Hz, 1 H, CH), 6.60-6.63 (m, 1 H), 6.96-7.01 (m, 3 H), 7.11-7.28 (m, 5 H), 7.40-7.46 (m, 1 H) ppm.

^{13}C RMN (100 MHz, $CDCl_3$): δ = 16.3 (d, $^3J_{CP}$ = 6.7 Hz, 2 CH_3), 41.9 (CH_2), 43.7 (HC), 56.1 (HC), 61.8 (d, $^2J_{CP}$ = 5.2 Hz, 2 CH_2), 114.1 (d, $^2J_{CF}$ = 16.1 Hz, HC), 115.3 (d, $^1J_{CP}$ = 197.1 Hz, C), 115.4-115.6 (m, 5 HC), 117.6 (d, $^3J_{CF}$ = 17.2 Hz, HC), 122.6 (dd, $^3J_{CF}$ = 6.3 Hz, $^4J_{CF}$ = 3.6 Hz, HC), 124.0 (d, $^3J_{CP}$ = 15.7 Hz, C), 130.0-136.5 (m, 4 HC), 139.7 (d, $^4J_{CF}$ = 3.3 Hz, C), 140.1 (dd, $^4J_{CF}$ = 3.7 Hz, $^3J_{CF}$ = 4.9 Hz, C), 148.5 (d, $^4J_{CP}$ = 3.0 Hz, C), 150.0 (dd, $^2J_{CF}$ = 12.8 Hz, $^1J_{CF}$ = 248.6 Hz, C), 150.6 (dd, $^2J_{CF}$ = 12.8 Hz, $^1J_{CF}$ = 248.9 Hz, C) 161.9 (d, $^1J_{CF}$ = 245.1 Hz, C-F) ppm.

^{31}P NMR (120 MHz, $CDCl_3$): δ = 22.0 ppm.

^{19}F NMR crude reaction mixture (282 MHz, $CDCl_3$): δ = -116.4 to -116.2 (m), -137.3 to -137.1 (m) and -139.0 to 138.9 (m) ppm.

HRMS (EI): calculated for $C_{25}H_{25}F_3NO_3P$ $[M]^+$ 475,1524; found 475,1534.

General procedure for the preparation of diethyl quinolin-6-yl phosphonates 16

Oxidation of compounds 16 with DDQ

DDQ (0.45 g, 2 mmol, 2 equiv.) was added to a solution of the corresponding 1,2,3,4-tetrahydroquinolin-6-yl phosphonate **15** (1 mmol, 1 equiv.) in chloroform (5 mL) and the reaction mixture was stirred and heated to reflux until TLC, ^{31}P NMR and ^{1}H NMR spectroscopy

analysis indicated the consumption of the 1,2,3,4-tetrahydroquinolin-6-yl phosphonate **15** and the subsequent formation of the diethyl quinolin-6-yl phosphonate **16** (2 h). The formed reaction brute was filtered off, dried *in vacuo* and purified by silica gel flash column chromatography (40% of ethyl acetate in hexane) and a further recrystallization in EtOAc/hexane to yield quinolin-6-yl phosphonates **16**.

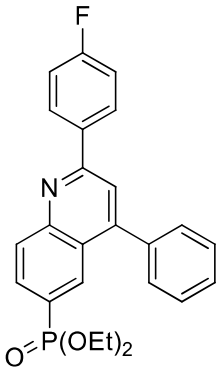

16a

Diethyl (2-(4-fluorophenyl)-4-phenylquinolin-6-yl)phosphonate (**16a**).

The general procedure (*oxidation of compounds 15 with DDQ*) was employed with **15a** (0.44 g, 1 mmol) to afford **16a** (0.40 g, 91%) as a white solid.

Melting point: 137-139°C (ethyl acetate/hexane).

^{1}H RMN (400 MHz, $CDCl_3$): δ = 1.29-1.33 (m, 6 H, 2 CH_3), 4.06-4.19 (m, 4 H, 2 CH_2), 7.19-7.26 (m, 2 H), 7.53-7.60 (m, 5 H), 7.84 (s, 1 H), 8.00-8.05 (m, 1 H), 8.20-8.24 (m, 2 H), 8.26-8.29 (m, 1 H), 8.45-8.49 (m, 1 H) ppm.

^{13}C RMN (100 MHz, $CDCl_3$): δ = 16.3 (d, $^{3}J_{CP}$ = 6.5 Hz, 2 CH_3), 62.3 (d, $^{2}J_{CP}$ = 5.5 Hz, 2 CH_2), 115.9 (d, $^{2}J_{CF}$ = 21.7 Hz, 2 HC), 119.8 (HC), 124.9 (d, $^{3}J_{CP}$ = 17.3 Hz, C), 126.2 (d, $^{1}J_{CP}$ = 189.7 Hz, C), 128.9 (2 HC), 128.9 (HC), 129.5 (2 HC), 129.6 (d, $^{3}J_{CF}$ = 8.5 Hz, 2 HC), 130.4 (d, $^{2}J_{CP}$ = 3.8 Hz, HC), 130.6 (HC), 131.6 (d, $^{2}J_{CP}$ = 11.9 Hz, HC), 135.2 (C), 137.4 (C), 150.2 (d, $^{4}J_{CP}$ = 3.0 Hz, C), 150.3 (C), 157.6 (C), 164.1 (d, $^{1}J_{CF}$ = 250.2 Hz, C-F) ppm.

^{31}P NMR (120 MHz, $CDCl_3$): δ = 19.3 ppm.

^{19}F NMR crude reaction mixture (282 MHz, $CDCl_3$): δ = -111.9 to -111.7 (m) ppm.

HRMS (EI): calculated for $C_{25}H_{23}FNO_3P$ $[M]^+$ 435.1400; found 435.1415.

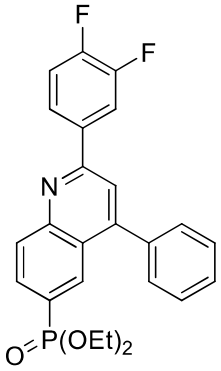

16b

Diethyl (2-(3,4-difluorophenyl)-4-phenylquinolin-6-yl)phosphonate (**16b**).

The general procedure (*oxidation of compounds 15 with DDQ*) was employed with **15b** (0.46 g, 1 mmol) to afford **16b** (0.40 g, 89%) as a white solid.

Melting point: 134-136°C (ethyl acetate/hexane).

^{1}H RMN (400 MHz, $CDCl_3$): δ = 1.28-1.33 (m, 6 H, 2 CH_3), 4.03-4.21 (m, 4 H, 2 CH_2), 7.29-7.32 (m, 1 H), 7.50-7.59 (m, 5 H), 7.80 (s, 1 H), 7.90-7.93 (m, 1 H), 7.99-8.14 (m, 2 H), 8.24-8.28 (m, 1 H), 8.44-8.50 (m, 1 H) ppm.

^{13}C RMN (100 MHz, $CDCl_3$): δ = 16.2 (d, $^{3}J_{CP}$ = 6.5 Hz, 2 CH_3), 62.3 (d, $^{2}J_{CP}$ = 5.5 Hz, 2 CH_2), 116.7 (d, $^{2}J_{CF}$ = 18.5 Hz, HC), 117.6 (d, $^{2}J_{CF}$ = 17.6 Hz, HC), 119.4 (HC), 123.7 (dd, $^{3}J_{CF}$ = 6.7 Hz, $^{4}J_{CF}$ = 3.5 Hz, HC), 125.1 (d, $^{3}J_{CP}$ = 17.3 Hz, C), 126.7 (d, $^{1}J_{CP}$ = 189.5 Hz, C), 128.9 (2 HC), 129.0 (HC), 129.4 (2 HC), 130.6 (d, $^{2}J_{CP}$ = 24.5 Hz, C), 130.6 (HC), 131.6 (d, $^{2}J_{CP}$ = 11.7 Hz, HC), 136.0 (dd, $^{3}J_{CF}$ = 5.7 Hz, $^{4}J_{CF}$ = 3.7 Hz, C), 137.2 (C), 150.1 (d, $^{4}J_{CP}$ = 3.0 Hz, C), 150.6 (C), 150.7 (dd, $^{2}J_{CF}$ = 12.7 Hz, $^{1}J_{CF}$ = 248.4 Hz, C), 151.6 (dd, $^{2}J_{CF}$ = 12.7 Hz, $^{1}J_{CF}$ = 251.9 Hz, C), 156.2 (C) ppm.

^{31}P NMR (120 MHz, $CDCl_3$): δ = 19.1 ppm.

^{19}F NMR crude reaction mixture (282 MHz, $CDCl_3$): δ = -136.3 to -136.1 (m) and -137.3 to 137.1 (m) ppm.

HRMS (EI): calculated for $C_2H_{22}F_2NO_3P$ $[M]^+$ 453.1305; found 453.1317.

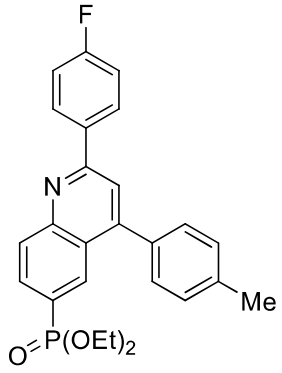

16c

Diisopropyl (2-(4-fluorophenyl)-4-(p-tolyl)quinolin-8-yl)phosphonate (**16c**).

The general procedure (*oxidation of compounds 15 with DDQ*) was employed with **15c** (0.45 g, 1 mmol) to afford **16c** (0.44 g, 98%) as a white solid.

Melting point: 153-155°C (ethyl acetate/hexane).

^{1}H RMN (400 MHz, $CDCl_3$): δ = 1.21-1.25 (m, 6 H, 2 CH_3), 2.40 (s, CH_3), 3.96-4.12 (m, 4 H, 2 CH_2), 7.11-7.16 (m, 2 H), 7.28-7.30 (m, 2 H), 7.35-7.37 (m, 2 H), 7.75 (s, 1 H), 7.90-7.95 (m, 1 H), 8.11-8.15 (m, 2 H), 8.16-8.19 (m, 1 H), 8.40-8.44 (m, 1 H) ppm.

^{13}C RMN (100 MHz, $CDCl_3$): δ = 16.3 (d, $^{3}J_{CP}$ = 6.5 Hz, 2 CH_3), 21.3 (CH_3), 62.2 (d, $^{2}J_{CP}$ = 5.4 Hz, 2 CH_2), 115.8 (d, $^{2}J_{CF}$ = 21.6 Hz, 2 HC), 119.71 (HC), 125.0 (d, $^{3}J_{CP}$ = 17.3 Hz, C), 126.1 (d, $^{1}J_{CP}$ = 189.3 Hz, C), 129.3 (2 HC), 129.6 (3 HC), 129.7 (d, $^{3}J_{CF}$ = 8.5 Hz, 2 HC), 130.4 (d, $^{2}J_{CP}$ = 12.8 Hz, HC), 131.9 (d, $^{2}J_{CP}$ = 12.0 Hz, HC), 134.5 (C), 135.2 (C), 138.9 (C), 150.2 (C), 150.4 (C), 157.7 (C), 164.0 (d, $^{1}J_{CF}$ = 249.9 Hz, C-F) ppm.

^{31}P NMR (120 MHz, $CDCl_3$): δ = 19.4 ppm.

^{19}F NMR crude reaction mixture (282 MHz, $CDCl_3$): δ = -112.0 to -111.9 (m) ppm.

HRMS (EI): calculated for $C_{26}H_{25}FNO_3P$ $[M]^+$ 449.1556; found 449.1573.

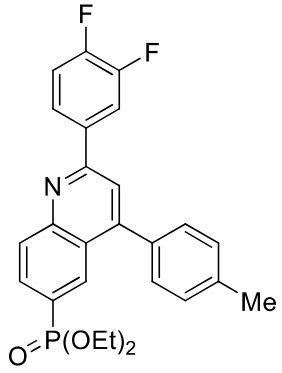

16d

Diethyl (2-(3,4-difluorophenyl)-4-(p-tolyl)quinolin-6-yl)phosphonate (**16d**).

The general procedure (*oxidation of compounds 15 with DDQ*) was employed with **15d** (0.47 g, 1 mmol) to afford **16d** (0.46 g, 84%) as a white solid.

Melting point: 158-160°C (ethyl acetate/hexane).

^{1}H RMN (400 MHz, $CDCl_3$): δ = 1.21-1.25 (m, 6 H, 2 CH_3), 2.40 (s, CH_3), 3.96-4.13 (m, 4 H, 2 CH_2), 7.19-7.25 (m, 1 H), 7.28-7.30 (m, 2 H), 7.34-7.36 (m, 2 H), 7.72 (s, 1 H), 7.83-7.87 (m, 1 H), 7.91-7.96 (m, 1 H), 8.01-8.07 (m, 1 H), 8.16-8.19 (m, 1 H), 8.40-8.44 (m, 1 H) ppm.

^{13}C RMN (100 MHz, $CDCl_3$): δ = 16.3 (d, $^{3}J_{CP}$ = 6.5 Hz, 2 CH_3), 21.3 (CH_3), 62.3 (d, $^{2}J_{CP}$ = 5.4 Hz, 2 CH_2), 116.8 (d, $^{2}J_{CF}$ = 19.3 Hz, HC), 117.6 (d, $^{2}J_{CF}$ = 17.6 Hz, HC), 119.4 (HC), 123.7 (dd, $^{4}J_{CF}$ = 3.5 Hz, $^{3}J_{CF}$ = 6.6 Hz, HC), 125.2 (d, $^{3}J_{CP}$ = 17.4 Hz, C), 126.5 (d, $^{1}J_{CP}$ = 189.4 Hz, C), 129.3 (2 HC), 129.6 (2 HC), 130.5 (d, $^{2}J_{CP}$ = 11.7 Hz, HC), 130.6 (d, $^{3}J_{CP}$ = 7.4 Hz, HC), 131.9 (d, $^{2}J_{CP}$ = 11.9 Hz, HC), 134.3 (C), 136.2 (dd, $^{4}J_{CF}$ = 3.6 Hz, $^{3}J_{CF}$ = 6.7 Hz, C), 139.1 (C), 150.1 (d, $^{4}J_{CP}$ = 3.0 Hz, C), 150.7 (dd, $^{2}J_{CF}$ = 13.8 Hz, $^{1}J_{CF}$ = 248.1 Hz, C), 150.7 (C), 151.6 (dd, $^{2}J_{CF}$ = 12.7 Hz, $^{1}J_{CF}$ = 250.4 Hz, C), 156.3 (C) ppm.

^{31}P NMR (120 MHz, $CDCl_3$): δ = 19.2 ppm.

^{19}F NMR crude reaction mixture (282 MHz, $CDCl_3$): δ = -134.5 to -134.3 (m) and -137.4 to 137.1 (m) ppm.

HRMS (EI): calculated for $C_{26}H_{24}F_2NO_3P$ $[M]^+$ 467.1462; found 467.1472.

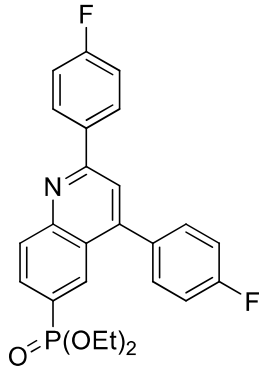

16e

Diethyl (2,4-bis(4-fluorophenyl)quinolin-6-yl)phosphonate (**16e**).

The general procedure (*oxidation of compounds 15 with DDQ*) was employed with **15e** (0.46 g, 1 mmol) to afford **16e** (0.35 g, 78%) as a white solid.

Melting point: 161-163°C (ethyl acetate/hexane).

^{1}H RMN (400 MHz, $CDCl_3$): δ = 1.21-1.25 (m, 6 H, 2 CH_3), 3.97-4.13 (m, 4 H, 2 CH_2), 7.12-7.21 (m, 4 H), 7.43-7.47 (m, 2 H), 7.73 (s, 1 H), 7.91-7.96 (m, 1 H), 8.12-8.15 (m, 2 H), 8.18-8.21 (m, 1 H), 8.32-8.36 (m, 1 H) ppm.

^{13}C RMN (100 MHz, $CDCl_3$): δ = 16.3 (d, $^{3}J_{CP}$ = 6.5 Hz, 2 CH_3), 62.3 (d, $^{2}J_{CP}$ = 5.5 Hz, 2 CH_2), 115.9 (d, $^{2}J_{CF}$ = 21.7 Hz, 2 HC), 116.1 (d, $^{2}J_{CF}$ = 21.5 Hz, HC), 119.8 (HC), 124.8 (d, $^{3}J_{CP}$ = 17.3 Hz, C), 126.5 (d, $^{1}J_{CP}$ = 189.7 Hz, C), 129.6 (d, $^{3}J_{CF}$ = 8.5 Hz, 2 HC), 130.5 (d, $^{2}J_{CP}$ = 2.5 Hz, HC), 130.6 (d, $^{2}J_{CP}$ = 1.8 Hz, HC), 131.2 (d, $^{3}J_{CF}$ = 8.3 Hz, 2 HC), 131.4 (d, $^{3}J_{CP}$ = 11.9 Hz, HC), 133.4 (C), 135.0 (C), 149.2 (C), 150.2 (C), 157.7 (C), 163.2 (d, $^{1}J_{CF}$ = 249.1 Hz, C-F), 164.1 (d, $^{1}J_{CF}$ = 250.2 Hz, C-F) ppm.

^{31}P NMR (120 MHz, $CDCl_3$): δ = 19.1 ppm.

^{19}F NMR crude reaction mixture (282 MHz, $CDCl_3$): δ = -114.6 to -114.4 (m) and -116.5 to -116.3 (m) ppm.

HRMS (EI): calculated for $C_{25}H_{22}F_2NO_3P$ $[M]^+$ 453.1305; found 453.1317.

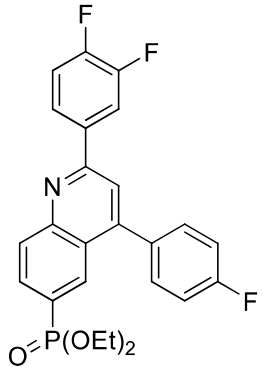

16f

Diethyl (2-(3,4-difluorophenyl)-4-(4-fluorophenyl)quinolin-8-yl)phosphonate (**16f**).

The general procedure (*oxidation of compounds 15 with DDQ*) was employed with **15a** (0.48 g, 1 mmol) to afford **16a** (0.33 g, 71%) as a white solid.

Melting point: 130-132°C (ethyl acetate/hexane).

^{1}H RMN (400 MHz, $CDCl_3$): δ = 1.22-1.25 (m, 6 H, 2 CH_3), 3.97-4.14 (m, 4 H, 2 CH_2), 7.17-7.27 (m, 3 H), 7.42-7.47 (m, 2 H), 7.71 (s, 1 H), 7.84-7.88 (m, 1 H), 7.92-7.98 (m, 1 H), 8.02-8.07 (m, 1 H), 8.17-8.21 (m, 1 H), 8.32-8.37 (m, 1 H) ppm.

^{13}C RMN (100 MHz, $CDCl_3$): δ = 16.3 (d, $^{3}J_{CP}$ = 6.4 Hz, 2 CH_3), 62.3 (d, $^{2}J_{CP}$ = 5.1 Hz, 2 CH_2), 116.1 (d, $^{2}J_{CF}$ = 21.7 Hz, 2 HC), 116.8 (d, $^{2}J_{CF}$ = 19.3 Hz, HC), 117.6 (d, $^{2}J_{CF}$ = 17.4 Hz, HC), 119.5 (HC), 123.7 (dd, $^{4}J_{CF}$ = 3.5 Hz, $^{3}J_{CF}$ = 8.7 Hz, C), 125.0 (d, $^{3}J_{CP}$ = 17.2 Hz, HC), 126.9 (d, $^{1}J_{CP}$ = 189.8 Hz, C), 130.5 (d, $^{3}J_{CF}$ = 24.0 Hz, HC), 130.7 (HC), 131.2 (d, $^{3}J_{CF}$ = 8.3 Hz, 2 HC), 131.4 (d, $^{3}J_{CP}$ = 11.8 Hz, HC), 133.2 (C), 136.0 (C), 149.5 (C), 150.1 (d, $^{4}J_{CP}$ = 3.0 Hz, C), 150.7 (dd, $^{2}J_{CF}$ = 12.7 Hz, $^{1}J_{CF}$ = 248.6 Hz, C), 151.8 (dd, $^{2}J_{CF}$ = 12.4 Hz, $^{1}J_{CF}$ = 252.0 Hz, C), 156.3 (C), 163.2 (d, $^{1}J_{CF}$ = 249.3 Hz, C-F) ppm.

^{31}P NMR (120 MHz, $CDCl_3$): δ = 19.0 ppm.

^{19}F NMR crude reaction mixture (282 MHz, $CDCl_3$): δ = -112.7 to -112.5 (m), -136.2 to -136.0 (m) and -137.2 to 137.0 (m) ppm.

HRMS (EI): calculated for $C_{25}H_{24}F_3NO_3P$ $[M]^+$ 471.1211; found 471.1224.

VI-1.4.. Synthesis of of hybrid dialkyl indeno[2,1-*c*]quinolinylphosphonates

General procedure for the preparation of dialkyl tetrahydroindenoquinolinylphosphonates 19

MCR Povarov procedure

A mixture of dialkyl (4-aminophenyl)phosphonate **1b/1c/1d** (1 mmol, 1 equiv.), freshly distilled aldehydes **2** (1 mmol, 1 equiv.), indene **17** (1.2 mmol, 1.2 equiv.) and 2 equivalents of $BF_3{\cdot}Et_2O$ (0.25 mL, 2 mmol) dissolved in $CHCl_3$ (3 mL) was stirred and heated to reflux in the presence of molecular sieves (4 Å), until TLC, ^{31}P NMR and ^{1}H NMR spectroscopy analysis indicated the consumption of the starting materials (1-6 h). The formed reaction brute was filtered off, dried *in vacuo* and purified by silica gel flash column chromatography (using an elution of 20–80% ethyl acetate-hexane) to yield dialkyl tetrahydroindenoquinolinyl phosphonates **19** (in some cases, a mix of products **19** and **20** was obtained).

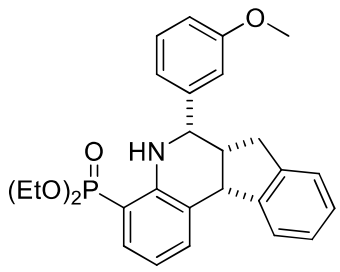

19a

Diethyl 6-(3-methoxyphenyl)-6,6a,7,11b-tetrahydro-5H-indeno[2,1-c]quinolin-4-yl)phosphonate (**19a**).

The general procedure (MCR Povarov) was followed using diethyl (2-aminophenyl)phosphonate **1b (1 mmol,** 0.23 g), 3-methoxybenzaldehyde (0.12 mL, 1 mmol), indene (0.14 mL, 1.2 mmol) and $BF_3{\cdot}Et_2O$. The reaction mixture was heated to reflux for 6 h to yield 0.29 g (62%) of a white solid identified as **19a**.

Melting point: 178-180°C (ethyl acetate/hexane).

^{1}H RMN (400 MHz, $CDCl_3$): δ = 1.32-1.36 (m, 6 H, 2 CH_3), 2.37-2.48 (m, 1 H), 3.20-3.27 (m, 2 H), 3.86 (s, 3 H, OCH_3), 4.07-4.24 (m, 5 H), 4.56-4.58 (m, 1 H), 4.83 (s, 1 H) 6.68-6.74 (m, 1 H), 6.88-6.91 (m, 1 H), 7.07-7.56 (m, 7 H), 7.52-7.56 (m, 2 H) ppm

^{13}C RMN (100 MHz, $CDCl_3$): δ = 16.6 (d, $^{3}J_{CP}$ = 6.4 Hz, 2 CH_3), 31.6 (CH_2), 46.3 (HC), 47.8 (HC), 55.4 (OCH_3), 55.5 (HC), 62.3 (d, $^{2}J_{CP}$ = 4.9 Hz, 2 OCH_2), 109.0 (d, $^{1}J_{CP}$ = 181.7 Hz, C), 112.4 (HC), 112.7 (HC), 117.0 (d, $^{3}J_{CP}$ = 15.0 Hz, HC), 118.8 (HC), 124.2 (d, $^{2}J_{CP}$ = 12.0 Hz, C), 125.2 (HC), 125.3 (HC), 126.6 (HC), 127.4 (HC), 130.0 (HC), 131.8 (d, $^{3}J_{CP}$ = 6.8 Hz, HC), 135.7 (d, $^{3}J_{CP}$ = 1.8 Hz, HC), 143.2 (C), 144.1 (C), 146.5 (C), 149.6 (d, $^{3}J_{CP}$ = 9.3 Hz, C), 160.2 (C) ppm.

^{31}P NMR (120 MHz, $CDCl_3$): δ = 22.6 ppm.

HRMS (EI): calculated for $C_{27}H_{30}NO_4P$ $[M]^+$ 463.1935; found 463.1942.

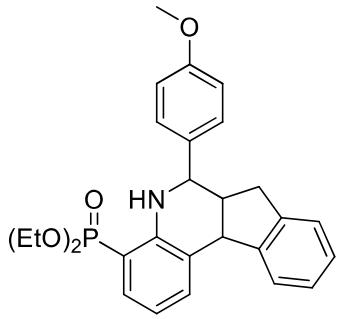

19b

Diethyl (6-(4-methoxyphenyl)-6,6a,7,11b-tetrahydro-5H-indeno[2,1-c]quinolin-4-yl)phosphonate (**19b**).

The general procedure (MCR Povarov) was followed using diethyl (2-aminophenyl)phosphonate **1b (1 mmol,** 0.23 g), 4-methoxybenzaldehyde (0.12 mL, 1 mmol), indene (0.14 mL, 1.2 mmol) and $BF_3{\cdot}Et_2O$. The reaction mixture was heated to reflux for 6 h to yield 0.34 g 73%) of a white solid identified as **19b**.

Melting point: 183-185°C (ethyl acetate/hexane).

^{1}H RMN (400 MHz, $CDCl_3$): δ = 1.32-1.36 (m, 6 H, 2 CH_3), 2.37-2.48 (m, 1 H), 3.20-3.27 (m, 2 H), 3.86 (s, 3 H, OCH_3), 4.07-4.24 (m, 5 H), 4.56-4.58 (m, 1 H), 4.83 (s, 1 H) 6.68-6.74 (m, 1 H), 6.88-6.91 (m, 1 H), 7.07-7.56 (m, 7 H), 7.52-7.56 (m, 2 H) ppm;

^{13}C RMN (100 MHz, $CDCl_3$): δ = 16.6 (d, $^3J_{CP}$ = 6.4 Hz, 2 CH_3), 31.6 (CH_2), 46.3 (HC), 47.8 (HC), 55.4 (OCH_3), 55.5 (HC), 62.3 (d, $^2J_{CP}$ = 4.9 Hz, 2 OCH_2), 109.0 (d, $^1J_{CP}$ = 181.7 Hz, C), 112.4 (HC), 112.7 (HC), 117.0 (d, $^3J_{CP}$ = 15.0 Hz, HC), 118.8 (HC), 124.2 (d, $^2J_{CP}$ = 12.0 Hz, C), 125.2 (HC), 125.3 (HC), 126.6 (HC), 127.4 (HC), 130.0 (HC), 131.8 (d, $^3J_{CP}$ = 6.8 Hz, HC), 135.7 (d, $^3J_{CP}$ = 1.8 Hz, HC), 143.2 (C), 144.1 (C), 146.5 (C), 149.6 (d, $^3J_{CP}$ = 9.3 Hz, C), 160.2 (C) ppm.

^{31}P NMR (120 MHz, $CDCl_3$): δ = 22.6 ppm.

HRMS (EI): calculated for $C_{27}H_{30}NO_4P$ $[M]^+$ 463.1935; found 463.1910.

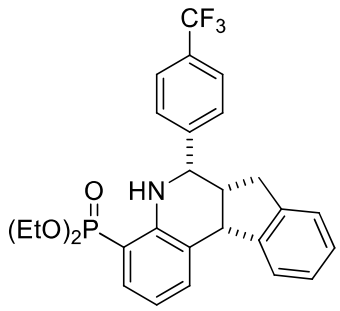

19c

Diethyl (6-(4-fluorophenyl)-6,6a,7,11b-tetrahydro-5H-indeno[2,1-c]quinolin-4-yl)phosphonate (**19c**).

The general procedure (MCR Povarov) was followed using diethyl (2-aminophenyl)phosphonate **1b (1 mmol,** 0.23 g), 4-trifluoromethylbenzaldehyde (0.16 mL, 1 mmol), indene (0.14 mL, 1.2 mmol) and $BF_3{\cdot}Et_2O$. The reaction mixture was heated to reflux for 6 h to yield 0.24 g 48%) of a white solid identified as **19b**.

Melting point: 157-159°C (ethyl acetate/hexane).

^{1}H RMN (400 MHz, $CDCl_3$): δ = 1.29-1.36 (m, 6 H, 2 CH_3), 2.28-2.37 (m, 1 H), 3.11-3.21 (m, 2 H), 4.01-4.18 (m, 4 H, 2 OCH_2), 4.56-4.58 (m, 1 H), 4.86-4.87 (m, 1 H), 6.66-6.71 (m, 1 H), 7.04-7.34 (m, NH and 4 H), 7.48-7.52 (m, 2 H), 7.60-7.67 (m, 4 H) ppm.

^{13}C RMN (100 MHz, $CDCl_3$): δ = 16.4 (s, $^3J_{CP}$ = 6.7 Hz, CH_3), 31.3 (CH_2), 46.1 (HC), 47.0 (HC), 56.2 (CH), 62.3 (s, $^2J_{CP}$ = 5.1 Hz, 2 OCH_2), 108.9 (d, $^1J_{CP}$ = 181.7 Hz, C), 123.9 (d, $^3J_{CP}$ = 12.1 Hz, C), 124.3 (d, $^1J_{CF}$ = 272.9 Hz, CF_3), 125.1-127.4 (m, 8 HC), 131.6 (d, $^2J_{CP}$ = 6.7 Hz, HC), 134.5 (d, $^4J_{CF}$ = 2.6 Hz, HC), 142.7 (C), 146.1 (C), 146.3 (d, $^3J_{CP}$ = 1.3 Hz, C), 149.3 (d, $^3J_{CP}$ = 9.5 Hz, C) ppm.

^{31}P NMR (120 MHz, $CDCl_3$): δ = 22.4 ppm.

^{19}F NMR crude reaction mixture (282 MHz, $CDCl_3$): δ = -62.8. to -62.7 (m) ppm

HRMS (EI): calculated for $C_{27}H_{27}F_3NO_3P$ $[M]^+$ 501,1681; found 501,1685.

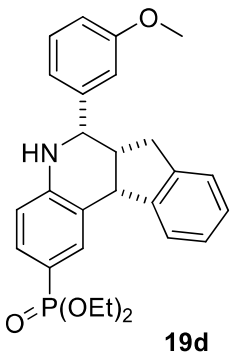

19d

Diethyl (6-(4-fluorophenyl)-6,6a,7,11b-tetrahydro-5H-indeno[2,1-c]quinolin-2-yl)phosphonate (**19d**).

The general procedure (MCR Povarov) was followed using diethyl (4-aminophenyl)phosphonate **1d (1 mmol,** 0.23 g), 3-methoxybenzaldehyde (0.12 mL, 1 mmol), indene (0.14 mL, 1.2 mmol) and $BF_3.Et_2O$. The reaction mixture was heated to reflux for 6 h to yield 0.30 g 65%) of a white solid identified as **19d**.

Melting point: 157-159°C (ethyl acetate/hexane).

^{1}H RMN (400 MHz, $CDCl_3$): δ 1.15-1.22 (m, 6 H, 2 CH_3), 2.30-2.34 (m, 1 H), 3.11-3.17 (m, 2 H), 3.77 (s, 3 H, OCH_3), 3.83-3.99 (m, 4 H, 2 OCH_2), 4.18 (s, 1 H, NH), 4.46-4.48 (m, 1 H), 4.67-4.69 (m, 1 H), 6.52-6.55 (m, 1 H), 6.78-6.80 (m, 1 H), 6.98-7.09 (m, 5 H), 7.23-7.32 (m, 2 H), 7.47-7.50 (m, 1 H), 7.65-7.69 (m, 1 H) ppm.

^{13}C RMN (100 MHz, $CDCl_3$): δ = 16.4 (d, $^3J_{CP}$ = 6.7 Hz, CH_3), 16.5 (d, $^3J_{CP}$ = 6.7 Hz, CH_3), 31.4 (CH_2), 45.9 (HC), 47.9 (HC), 55.5 (OCH_3), 57.2 (HC), 61.8 (s, $^2J_{CP}$ = 5.3 Hz, OCH_2), 61.9 (s, $^2J_{CP}$ = 5.1 Hz, OCH_2), 112.5 (HC), 112.8 (HC), 115.3 (d, $^3J_{CP}$ = 16.0 Hz, HC), 116.4 (d, $^1J_{CP}$ = 196.0 Hz, C), 118.9 (HC), 123.6 (d, $^3J_{CP}$ = 15.5 Hz, C), 124.9 (HC), 125.2 (HC), 124.9 (HC), 125.2 (HC), 126.7 (HC), 127.2 (HC), 129.9 (HC), 130.8 (d, $^2J_{CP}$ = 10.8 Hz, HC), 134.1 (d, $^2J_{CP}$ = 11.7 Hz, HC), 142.6 (C), 143.6 (C), 145.8 (C), 149.0 (d, $^3J_{CP}$ = 3.0 Hz, C), 160.0 (C) ppm.

^{31}P NMR (120 MHz, $CDCl_3$): δ = 22.0 ppm.

HRMS (EI): calculated for $C_{27}H_{30}NO_4P$ $[M]^+$ 463.1912; found 463.1911.

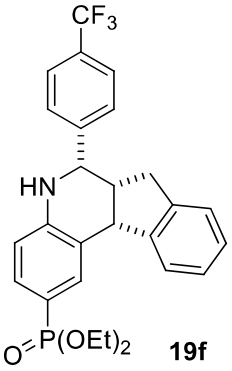

19f

Diethyl (6-(4-trifluoromethylphenyl)-6,6a,7,11b-tetrahydro-5H-indeno[2,1-c]quinolin-2-yl)phosphonate (**19f**).

The general procedure (MCR Povarov) was followed using diethyl (4-aminophenyl)phosphonate **1d (1 mmol,** 0.23 g), 4-trifluoromethylbenzaldehyde (0.16 mL, 1 mmol), indene (0.14 mL, 1.2 mmol) and $BF_3.Et_2O$. The reaction mixture was heated to reflux for 6 h to yield 0.34 g 67%) of a white solid identified as **19d**.

Melting point: 225-227°C (ethyl acetate/hexane).

^{1}H RMN (400 MHz, $CDCl_3$): δ = 1.15-1.22 (m, 6 H, 2 CH_3), 2.22-2.29 (m, 1 H), 3.07-3.16 (m, 2 H), 3.82-4.00 (m, 4 H, 2 OCH_2), 4.25 (s, 1 H, NH), 4.47-4.49 (m, 1 H), 4.75-4.78 (m, 1 H), 6.56-6.59 (m, 1 H), 6.94-6.97 (m, 1 H), 7.00-7.10 (m, 2 H), 7.28-7.33 (m, 1 H), 7.48-7.60 (m, 5 H), 7.67-7.70 (m, 1 H) ppm.

^{13}C RMN (100 MHz, $CDCl_3$): δ = 16.4 (s, $^3J_{CP}$ = 6.7 Hz, CH_3), 16.5 (s, $^3J_{CP}$ = 7.0 Hz, CH_3), 31.2 (CH_2), 45.7 (HC), 47.6 (HC), 57.0 (CH), 61.8 (s, $^2J_{CP}$ = 5.3 Hz, 2 OCH_2), 115.5 (d, $^3J_{CP}$ = 15.9 Hz, HC), 116.9 (d, $^1J_{CP}$ = 197.6 Hz, C), 123.4 (d, $^3J_{CP}$ = 15.5 Hz, C), 124.2 (d, $^1J_{CF}$ = 272.1 Hz, CF_3), 124.9 (HC), 125.1 (HC), 125.5-130.3 (m, 1 C and 6 HC), 130.8 (d, $^2J_{CP}$ = 10.8 Hz, HC), 134.0 (d, $^2J_{CP}$ = 11.6 Hz, HC), 142.1 (C), 145.5 (C), 146.0 (d, $^3J_{CP}$ = 1.3 Hz, C), 148.6 (d, $^3J_{CP}$ = 3.0 Hz, C) ppm.

^{31}P NMR (120 MHz, $CDCl_3$): δ = 21.70 ppm.

^{19}F NMR crude reaction mixture (282 MHz, $CDCl_3$): δ = -62.9. to -62.7 (m) ppm.

HRMS (EI): calculated for $C_{27}H_{27}F_3NO_3P$ $[M]^+$ 501.1681; found 501.1698.

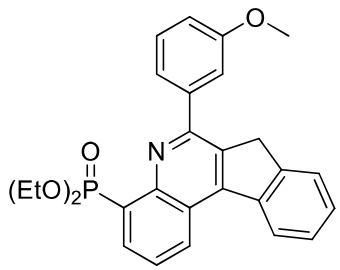

20a

Diethyl (6-(2-methoxyphenyl)-7H-indeno[2,1-c]quinolin-4-yl)phosphonate (**20a**).

The general procedure (MCR Povarov) was followed using diethyl (2-aminophenyl)phosphonate **1b (1 mmol,** 0.23 g), 3-methoxybenzaldehyde (0.12 mL, 1 mmol), indene (0.14 mL, 1.2 mmol) and $BF_3{\cdot}Et_2O$. The reaction mixture was heated to reflux for 6 h to yield 0.10 g (22%) of a white solid identified as **20a**.

Melting point: 143-145°C (ethyl acetate/hexane).

^{1}H RMN (400 MHz, $CDCl_3$): δ = 1.27-1.32 (m, 6 H, 2 CH_3), 3.97 (s, 3 H, OCH_3), 4.28-4.42 (m, 6 H), 7.04-7.08 (m, 1 H), 7.45-7.88 (m, 7 H), 8.37-8.47 (m, 2 H), 8.92-8.95 (m, 1 H) ppm.

^{13}C RMN (100 MHz, $CDCl_3$): δ = 16.6 (d, $^3J_{CP}$ = 6.5 Hz, 2 CH_3), 38.1 (CH_2), 55.6 (OCH_3), 62.6 (d, $^2J_{CP}$ = 5.9 Hz, 2 OCH_2), 114.8 (HC), 115.2 (HC), 121.7 (HC), 123.9 (d, $^3J_{CP}$ = 10.7 Hz, HC), 124.1 (HC), 125.4 (HC), 125.7 (d, $^2J_{CP}$ = 16.2 Hz, HC), 127.4 (HC), 128.1 (d, $^4J_{CP}$ = 3.1 Hz, HC), 128.5 (HC), 129.3 (HC), 129.6 (d, $^1J_{CP}$ = 189.5 Hz, C), 134.4 (C), 135.5 (d, $^3J_{CP}$ = 7.1 Hz, HC), 140.2 (C), 141.2 (C), 144.2 (C), 145.9 (d, $^4J_{CP}$ = 2.0 Hz, C), 148.0 (d, $^3J_{CP}$ = 6.7 Hz, C),155.0 (d, $^4J_{CP}$ = 1.2 Hz,C), 159.7 (C) ppm.

^{31}P NMR (120 MHz, $CDCl_3$): δ = 18.40 ppm.

HRMS (EI): calculated for $C_{27}H_{30}NO_4P$ $[M]^+$ 459.1599; found 459.1603.

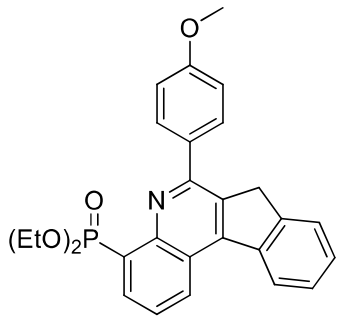

20b

Diethyl (6-(4-methoxyphenyl)-5H-indeno[2,1-c]quinolin-4-yl)phosphonate (**20b**).

The general procedure (MCR Povarov) was followed using diethyl (2-aminophenyl)phosphonate **1b (1 mmol,** 0.23 g), 4-methoxybenzaldehyde (0.12 mL, 1 mmol), indene (0.14 mL, 1.2 mmol)

and $BF_3{\cdot}Et_2O$. The reaction mixture was heated to reflux for 6 h to yield 0.05 g 11%) of a white solid identified as **20b**.

Melting point: 183-185°C (ethyl acetate/hexane).

^{1}H RMN (400 MHz, $CDCl_3$): δ = 1.27-1.30 (m, 6 H, 2 CH_3), 3.96 (s, 3 H, OCH_3), 4.25-4.39 (m, 6 H), 7.04-7.07 (m, 1 H), 7.45-7.87 (m, 6 H), 8.37-8.47 (m, 2 H), 8.92-8.95 (m, 1 H) ppm.

^{13}C RMN (100 MHz, $CDCl_3$): δ = 16.6 (d, $^3J_{CP}$ = 6.0 Hz, 2 CH_3), 38.2 (CH_2), 55.7 (OCH_3), 62.7 (d, $^2J_{CP}$ = 4.9 Hz, 2 OCH_2), 114.9 (HC), 115.9 (HC), 121.8 (HC), 124.1 (d, $^3J_{CP}$ = 10.6 Hz, HC), 124.4 (HC), 125.4 (HC), 125.8 (d, $^2J_{CP}$ = 16.1 Hz, HC), 127.6 (HC), 128.2 (HC), 128.6 (HC), 129.4 (HC), 129.8 (d, $^1J_{CP}$ = 189.8 Hz, C), 134.6 (C), 135.6 (d, $^3J_{CP}$ = 6.3 Hz, HC), 140.8 (C), 141.4 (C), 145.2 (C), 146.1 (C), 148.2 (d, $^3J_{CP}$ = 6.0 Hz, C),155.2 (C), 159.8 (C) ppm.

^{31}P NMR (120 MHz, $CDCl_3$): δ = 18.40 ppm.

HRMS (EI): calculated for $C_{27}H_{26}NO_4P$ $[M]^+$ 459.1599; found 459.1594.

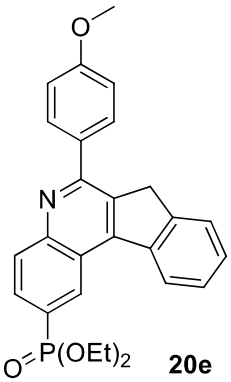

20e

Diethyl (6-(2,4-difluorophenyl)-5H-indeno[2,1-c]quinolin-2-yl)phosphonate (**20e**).

The general procedure (MCR Povarov) was followed using diethyl (4-aminophenyl)phosphonate **1d (1 mmol,** 0.23 g), 4-methoxybenzaldehyde (0.12 mL, 1 mmol), indene (0.14 mL, 1.2 mmol) and $BF_3{\cdot}Et_2O$. The reaction mixture was heated to reflux for 6 h to yield 0.25 g 55%) of a white solid identified as **20e**.

Melting point: 138-140°C (ethyl acetate/hexane).

^{1}H RMN (400 MHz, $CDCl_3$): δ = 1.28-1.32 (m, 6 H, 2 CH_3), 3.82 (s, 3 H, OCH_3), 4.06-4.21 (m, 6 H), 7.40-7.51 (m, 2 H), 7.59-7.61 (m, 1 H), 7.86-7.95 (m, 3 H), 8.23-8.27 (m, 1 H), 8.47-8.49 (m, 1 H), 9.23-9.27 (m, 1H) ppm.

^{13}C RMN (100 MHz, $CDCl_3$): δ = 16.6 (d, $^3J_{CP}$ = 6.5 Hz, 2 CH_3), 36.1 (CH_2), 55.6 (OCH_3), 62.5 (d, $^2J_{CP}$ = 5.3 Hz, 2 OCH_2), 114.2 (2 HC), 123.1 (d, $^2J_{CP}$ = 17.7 Hz, C), 124.9 (HC), 125.2 (HC), 125.9 (d, $^1J_{CP}$ = 189.1 Hz, C), 129.5 (d, $^2J_{CP}$ = 9.5 Hz, HC), 129.9 (d, $^3J_{CP}$ = 11.5 Hz, HC), 130.5 (2 HC), 131.1 (d, $^3J_{CP}$ = 14.3 Hz, HC), 132.6 (C), 135.2 (d, $^4J_{CP}$ = 1.1 Hz, C), 140.2 (C), 145.1 (C), 146.6 (C), 149.9 (d, $^2J_{CP}$ = 3.1 Hz, C), 157.9 (C), 160.7 (C) ppm.

^{31}P NMR (120 MHz, $CDCl_3$): δ = 19.8 ppm.

HRMS (EI): calculated for $C_{27}H_{26}NO_4P$ $[M]^+$ 459.1599; found 459.1606.

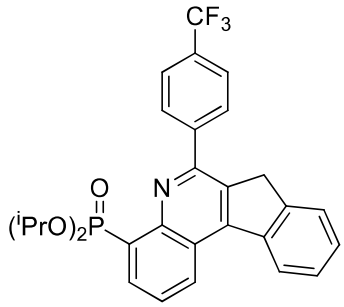

20g

Diisopropyl (6-(4-trifluoromethylphenyl)-5H-indeno[2,1-c]quinolin-4-yl)phosphonate (**20g**).

The general procedure (MCR Povarov) was followed using diisopropyl (4-aminophenyl)phosphonate **1c (1 mmol,** 0.26 g), 4-trifluoromethylbenzaldehyde (0.16 mL, 1 mmol), indene (0.14 mL, 1.2 mmol) and $BF_3{\cdot}Et_2O$. The reaction mixture was heated to reflux for 6 h to yield 0.33 g 62%) of a white solid identified as **20g**.

Melting point: 164-166°C (ethyl acetate/hexane).

^{1}H RMN (400 MHz, $CDCl_3$): δ = 1.17 (m, 6 H, 2 CH_3), 1.38 (d, $^3J_{HH}$= 6.2 Hz, 6 H, 2 CH_3) 4.25 (s, 2 H, CH_2), 4.98-5.06 (m, 2 H, 2 OCH), 7.48-7.57 (m, 2 H), 7.69-7.74 (m, 2 H), 7.81-7.83 (m, 2 H), 8.35-8.37 (m, 2 H), 8.39-8.45 (m, 2 H), 8.89-8.91 (m, 1 H) ppm.

^{13}C RMN (100 MHz, $CDCl_3$): δ = 23.8 (d, $^3J_{CP}$ = 4.4 Hz, 2 CH_3), 24.3 (d, $^3J_{CP}$ = 2.9 Hz, 2 CH_3), 38.1 (CH_2), 70.7 (d, $^2J_{CP}$ = 5.5 Hz, 2 CH), 124.0 (d, $^3J_{CP}$ = 11.4 Hz, C), 124.2 (d, $^1J_{CF}$ = 272.5 Hz, CF_3), 124.3 (HC), 125.2 (s, 3 HC), 126.1 (d, $^2J_{CP}$ = 16.1 Hz, HC), 127.5 (HC), 127.8 (HC), 128.6 (HC), 129.6 (s, 2 HC), 129.7-131.6 (m, 2 C), 134.0 (C), 135.7 (d, $^3J_{CP}$ = 6.4 Hz, HC), 140.1 (C), 143.3 (C), 144.6 (C), 146.3 (C), 147.9 (d, $^3J_{CP}$ = 6.6 Hz, C), 153.4 (C) ppm.

^{31}P NMR (120 MHz, $CDCl_3$): δ = 15.82 ppm.

^{19}F NMR crude reaction mixture (282 MHz, $CDCl_3$): δ = -62.8. to -62.7 (m) ppm.

HRMS (EI): calculated for $C_{29}H_{27}F_3NO_3P$ $[M]^+$ 525.1681; found 525.1678.

General procedures for the preparation of dialkyl 7H-indeno[2,1-*c*]quinolinyl phosphonates 20 and dialkyl 7-oxo-7H-indeno[2,1-*c*]quinolinyl phosphonates 21

A) Oxidation of compounds 19 with DDQ

DDQ (0.45 g, 2 mmol, 2 equiv.) was added to a solution of the corresponding dialkyl tetrahydroindenoquinolinyl phosphonate **19** (1 mmol) in chloroform (5 mL) and the reaction mixture was stirred and heated to reflux until TLC, ^{31}P NMR and ^{1}H NMR spectroscopy analysis indicated the consumption of the starting material or until no further evolution was observed (2 h). The formed reaction brute was filtered off, dried *in vacuo* and purified by silica gel flash column chromatography (40% of ethyl acetate in hexane) and a further recrystallization in EtOAc/hexane to yield the corresponding 7H-indeno[2,1-c]quinolinyl phosphonate **20** or dialkyl 7-oxo-7H-indeno[2,1-c]quinolinyl phosphonate **21**.

B) Oxidation of compounds 19 with $Mn(OAc)_3$

$Mn(OAc)_3$ (2.15 g, 4 mmol, 4 equiv.) was added to a solution of the corresponding dialkyl tetrahydroindenoquinolinyl phosphonate **19** (1 mmol) in acetic acid (15 mL) and the reaction mixture was stirred and heated to reflux until TLC, ^{31}P NMR and ^{1}H NMR spectroscopy analysis indicated the consumption of the starting material or until the reaction does not progress any longer (36 h). The formed reaction brute was extracted with 25 mL of dichloromethane and 25 mL of water and then quenched with a aqueous saturated solution of $NaHCO_3$ (2x 20 mL). The resultant crude oil was dried over $MgSO_4$ and purified by silica gel flash column chromatography (25% of ethyl acetate in hexane) and a further recrystallization in EtOAc/hexane to yield the corresponding 7H-indeno[2,1-c]quinolinyl phosphonate **20** or dialkyl 7-oxo-7H-indeno[2,1-c]quinolinyl phosphonate **21**.

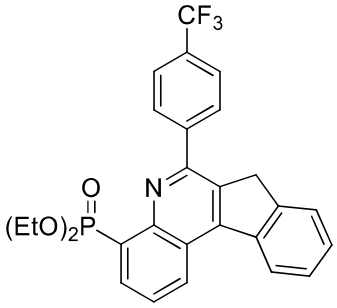

20c

Diethyl (6-(4-trifluoromethylphenyl)- 5H-indeno[2,1-c]quinolin-4-yl)phosphonate (**20c**).

The general procedure A (*oxidation of compounds 19 with DDQ*) was followed using the diethyl tetrahydro-5*H*-indeno[2,1-c]quinolin-4-yl phosphonate **19c** (0.48 g, 1 mmol) to afford 0.05 g (11%) of a yellow solid identified as **20c**.

Melting point: 164-166°C (ethyl acetate/hexane).

^{1}H RMN (400 MHz, $CDCl_3$): δ 1.18-1.20 (m, 6H, 2CH3), 2.22 (dd, 2*J*HH = 12.5 Hz, 3*J*HH = 7.8 Hz, 1H, CH2), 3.00-3.07 (m, 2H, CH2 y HC-CH2), 3.91-4.09 (m, 4H, 2OCH2), 4.16 (s, 1H, NH), 4.46 (d, 3*J*HH = 6.6 Hz, 1H, CH), 4.77 (s, 1H, CH), 6.56- 6.61 (m, 1H), 6.94-7.09 (m, 3H), 7.19-7.27 (m, 1H), 7.39-7.58 (m, 6H) ppm.

^{13}C RMN (100 MHz, $CDCl_3$): δ = 16.1 (CH3), 16.2 (CH3), 31.1 (CH2), 45.9 (d, 4*J*CP = 2.4 Hz, HC-C), 47.2 (HC-CH2), 56.0 (HC-N), 62.0 (OCH2), 62.1 (OCH2), 108.8 (d, 1*J*CP = 182.1 Hz, C), 117.0 (d, 3*J*CP = 14.9 Hz, HC), 123.8 (d, 3*J*CP = 12.1 Hz, C), 124.5 (q, 1*J*CF = 272.1 Hz, CF3), 124.8 (2HC), 125.55 (d, 4*J*CP = 3.6 Hz, HC), 126.4 (HC), 126.5 (2HC), 127.1 (HC), 129.5 (q, 2*J*CF = 32.4 Hz, C-CF3), 129.6 (HC), 131.43 (d, 2*J*CP = 6.6 Hz, HC), 134.3 (HC), 142.5 (C), 145.8 (C), 146.4 (C), 149.0 (d, 2*J*CP = 9.5 Hz, C) ppm.

^{31}P NMR (120 MHz, $CDCl_3$): δ = 22.40 ppm.

^{19}F NMR (282 MHz, $CDCl_3$): δ = -62.8 ppm.

HRMS (EI): calculated for $C_{27}H_{23}F_3NO_3P$ $[M]^+$ 497,1368; found 497,1374.

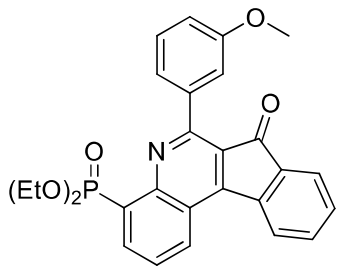

21a

Diethyl 6-(3-methoxyphenyl)-7-oxo-5H-indeno[2,1-c]quinolin-4-yl)phosphonate (**21a**).

The general procedure B (*oxidation of compounds 19 with $Mn(OAc)_3$*) was followed using the diethyl tetrahydro-5*H*-indeno[2,1-c]quinolin-4-yl phosphonate **19a** (0.47 g, 1 mmol) to afford 0.16 g (33%) of a yellow solid identified as **21a**.

Melting point: 158-160°C (ethyl acetate/hexane).

^{1}H RMN (400 MHz, $CDCl_3$): δ = 1.22-1.26 (m, 6 H, 2 CH_3), 3.91 (s, 3 H, OCH_3), 4.22-4.39 (m, 4 H, 2 OCH_2), 7.04-7.07 (m, 2 H), 7.39-7.47 (m, 2 H), 7.56-7.69 (m, 5 H), 8.08-8.10 (m, 1 H), 8.42-8.48 (m, 1 H), 8.65-8.67 (m, 1 H) ppm.

^{13}C RMN (100 MHz, $CDCl_3$): δ = 16.5 (d, $^3J_{CP}$ = 6.5 Hz, 2 CH_3), 55.5 (OCH_3), 62.9 (d, $^2J_{CP}$ = 5.9 Hz, 2 OCH_2), 115.5 (HC), 116.2 (HC), 122.7 (C), 123.0 (d, $^3J_{CP}$ = 10.5 Hz, HC), 123.2 (HC), 124.5 (HC), 124.6 (HC), 127.0 (d, $^2J_{CP}$ = 15.7 Hz, HC), 128.6 (HC), 129.0 (d, $^4J_{CP}$ = 2.5 Hz, HC), 130.7 (d, $^1J_{CP}$ = 190.1 Hz, C), 131.4 (HC), 133.6 (C), 134.7 (HC), 138.4 (C), 139.1 (d, $^3J_{CP}$ = 6.8 Hz, HC), 141.4 (C), 151.6 (d, $^3J_{CP}$ = 6.6 Hz, C), 153.6 (d, $^4J_{CP}$ = 1.4 Hz,C), 156.3 (C), 159.1 (C), 191.8 (CO) ppm.

^{31}P NMR (120 MHz, $CDCl_3$): δ = 16.5 ppm.

HRMS (EI): calculated for $C_{27}H_{24}NO_5P$ $[M]^+$ 473,1392; found 473,1398.

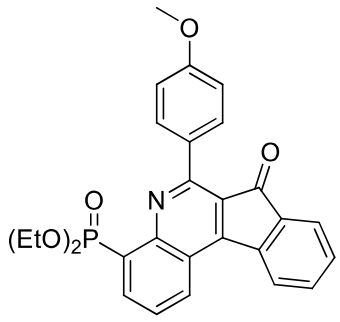

21b

Diethyl (6-(4-methoxyphenyl)-7-oxo-5H-indeno[2,1-c]quinolin-4-yl)phosphonate (**21b**).

The general procedure A (*oxidation of compounds 19 with DDQ*) was followed using the diethyl tetrahydro-5*H*-indeno[2,1-c]quinolin-4-yl phosphonate **19b** (0.47 g, 1 mmol) to afford 0.07 g (14%) of a yellow solid identified as **21b**.

Melting point: 155-157°C (ethyl acetate/hexane).

^{1}H RMN (400 MHz, $CDCl_3$): δ = 1.24-1.27 (m, 6 H, 2 CH_3), 3.91 (s, 3 H, OCH_3), 4.21-4.38 (m, 4 H, 2 OCH_2), 7.02-7.04 (m, 2 H), 7.47-7.51 (m, 1 H), 7.60-7.68 (m, 2 H), 7.72-7.74 (m, 1 H), 8.05-8.8 (m, 2 H), 8.12-8.14 (m, 1 H), 8.42-8.47 (m, 1 H), 8.67-8.69 (m, 1 H) ppm.

^{13}C RMN (100 MHz, $CDCl_3$): δ = 16.4 (d, $^{3}J_{CP}$ = 6.5 Hz, 2 CH_3), 55.3 (OCH_3), 62.7 (d, $^{2}J_{CP}$ = 5.9 Hz, 2 OCH_2), 112.9 (2 HC), 122.3 (C), 125.1 (d, $^{3}J_{CP}$ = 10.6 Hz, C), 124.4 (HC), 124.5 (HC), 126.5 (d, $^{2}J_{CP}$ = 16.7 Hz, HC), 129.0 (d, $^{3}J_{CP}$ = 2.9 Hz, HC), 129.6 (C), 130.2 (d, $^{1}J_{CP}$ = 190.8 Hz, C), 131.2 (HC), 132.2 (s, 2 HC), 133.5 (C), 134.6 (HC), 138.9 (d, $^{3}J_{CP}$ = 7.0 Hz, HC), 141.4 (C), 151.7 (d, $^{3}J_{CP}$ = 6.8 Hz, C), 153.6 (d, $^{4}J_{CP}$ = 1.7 Hz, C), 156.1 (C), 161.0 (C), 192.1 (CO) ppm.

^{31}P NMR (120 MHz, $CDCl_3$): δ = 16.7 ppm.

HRMS (EI): calculated for $C_{27}H_{24}NO_5P$ $[M]^+$ 473.1392; found 473.1397.

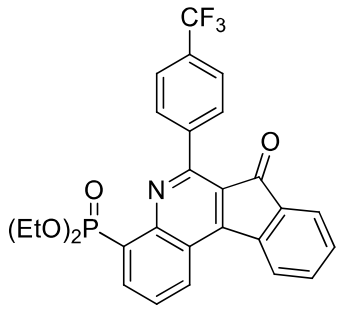

21c

Diethyl (6-(4-trifluoromethylphenyl)-7-oxo-5H-indeno[2,1-c]quinolin-4-yl)phosphonate (**21c**).

The general procedure B (*oxidation of compounds 19 with $Mn(OAc)_3$*) was followed using the diethyl tetrahydro-5*H*-indeno[2,1-c]quinolin-4-yl phosphonate **19c** (0.48 g, 1 mmol) to afford 0.14 g (28%) of a yellow solid identified as **20c**.

Melting point: 155-157°C (ethyl acetate/hexane).

^{1}H RMN (400 MHz, $CDCl_3$): δ = 1.23-1.27 (m, 6H, 2 CH_3), 4.23-4.32 (m, 4 H, 2 OCH_2), 7.52-7.78 (m, 4 H), 8.15-8.19 (m, 3 H), 8.47-8.53 (m, 1 H), 8.73-8.76 (m, 1 H) ppm

^{13}C RMN (100 MHz, $CDCl_3$): δ = 16.5 (d, $^{3}J_{CP}$ = 4.5 Hz, 2 CH_3), 62.9 (d, $^{2}J_{CP}$ = 6.0 Hz, 2 OCH_2), 122.9 (C), 123.3 (d, $^{3}J_{CP}$ = 10.6 Hz, C), 125.1 (d, $^{1}J_{CF}$ = 272.5 Hz, CF_3), 124.6-124.9 (m, 4 CH), 127.6 (d, $^{2}J_{CP}$ = 15.6 Hz, HC), 129.1 (d, $^{3}J_{CP}$ = 3.1 Hz, HC), 130.9 (d, $^{1}J_{CP}$ = 190.4 Hz, C), 131.0 (2 HC), 131.8 (HC), 133.6 (C), 135.0 (HC), 139.3 (d, $^{3}J_{CP}$ = 6.6 Hz, HC), 140.6 (d, $^{4}J_{CF}$ = 1.4 Hz, C), 141.6 (d, $^{4}J_{CF}$ = 1.0 Hz, C), 151.8 (d, $^{3}J_{CP}$ = 6.6 Hz, C), 153.8 (d, $^{4}J_{CP}$ = 1.9 Hz, C), 155.1 (C), 191.9 (CO) ppm.

^{31}P NMR (120 MHz, $CDCl_3$): δ = 16.2 ppm.

^{19}F NMR (282 MHz, $CDCl_3$): δ = -62.7 to -62.6 (m) ppm.

HRMS (EI): calculated for $C_{27}H_{21}F_3NO_4P$ $[M]^+$ 511,1160; found 511,1165.

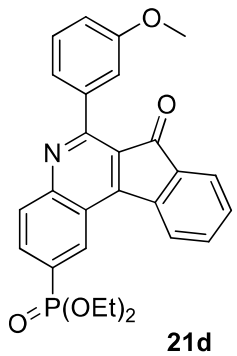

21d

Diethyl (6-(3-methoxyphenyl)-7-oxo-5H-indeno[2,1-c]quinolin-2-yl)phosphonate (**21d**).

The general procedure A (*oxidation of compounds 19 with DDQ*) was followed using the diethyl tetrahydro-5*H*-indeno[2,1-c]quinolin-4-yl phosphonate **19d** (0.47 g, 1 mmol) to afford 0.18 g (38%) of a yellow solid identified as **21d**.

Melting point: 128-140°C (ethyl acetate/hexane).

^{1}H RMN (400 MHz, $CDCl_3$): δ = 1.39 (m, 6 H, 2 CH_3), 3.90 (s, 3 H, OCH_3), 4.14-4.32 (m, 4 H, 2 OCH_2), 7.07-7.10 (m, 1 H), 7.40-7.47 (m, 3 H), 7.51-7.55 (m, 1 H), 7.65-7.69 (m, 1 H), 7.74-7.76 (m, 1 H), 8.06-8.11 (m, 1 H), 8.25-8.31 (m, 2 H), 9.17 (dd, $^{3}J_{HH}$= 15.7 Hz, $^{4}J_{HH}$= 1.2 Hz 1 H) ppm.

^{13}C RMN (100 MHz, $CDCl_3$): δ = 16.6 (d, $^{3}J_{CP}$ = 6.3 Hz, 2 CH_3), 55.6 (OCH_3), 62.8 (d, $^{2}J_{CP}$ = 5.4 Hz, 2 OCH_2), 115.2 (HC), 116.0 (HC), 122.6 (HC), 123.3 (d, $^{2}J_{CP}$ = 17.9 Hz, C), 123.4 (d, $^{4}J_{CP}$ = 1,2 Hz, C), 124.7 (HC), 125.3 (HC), 128.2 (d, $^{1}J_{CP}$ = 189.6 Hz, C), 129.1 (HC), 131.2 (d, $^{3}J_{CP}$ = 11.5 Hz, HC), 131.6 (d, $^{3}J_{CP}$ = 14.2 Hz, HC), 131.8 (HC), 132.9 (d, $^{2}J_{CP}$ = 9.1 Hz, HC), 133.8 (C), 135.0 (HC), 138.6 (C), 141.2 (C), 153.1 (d, $^{2}J_{CP}$ = 3.1 Hz, C), 154.5 (d, $^{4}J_{CP}$ = 0.8 Hz, C), 158.7 (d, $^{4}J_{CP}$ = 0.8 Hz, C), 159.4 (C), 191.7 (CO) ppm.

^{31}P NMR (120 MHz, $CDCl_3$): δ = 18.20 ppm.

HRMS (EI): calculated for $C_{27}H_{24}NO_5P$ $[M]^+$ 473.1392; found 473.1402.

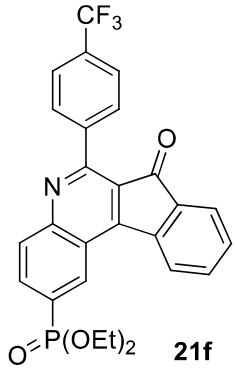

21f

The general procedure A (*oxidation of compounds 19 with DDQ*) was followed using the diethyl tetrahydro-5*H*-indeno[2,1-c]quinolin-4-yl phosphonate **19f** (0.48 g, 1 mmol) to afford 0.16 g (32%) of a yellow solid identified as **21f**.

Melting point: 211-213ºC (ethyl acetate/hexane).

^{1}H RMN (400 MHz, $CDCl_3$): δ = = 1.38-1.42 (m, 6 H, 2 CH_3), 4.15-4.33 (m, 4 H, 2 OCH_2), 7.53-7.57 (m, 1 H), 7.67-7.71 (m, 1 H), 7.75-7.80 (m, 3 H), 7.96-7.99 (m, 1 H), 8.09-8.14 (m, 1 H), 8.25-8.31 (m, 1 H) ppm.

^{13}C RMN (100 MHz, $CDCl_3$): δ = 16.4 (d, $^{3}J_{CP}$ = 6.3 Hz, 2 CH_3), 62.6 (d, $^{2}J_{CP}$ = 5.5 Hz, 2 OCH_2), 122.5 (d, $^{2}J_{CP}$ = 17.8 Hz, C), 123.2 (d, $^{4}J_{CP}$ = 1,1 Hz, C), 124.3 (d, $^{1}J_{CF}$ = 272.1 Hz, CF_3), 124.9 (HC), 125.0-125.1 (m, 2 CH), 125.4 (HC), 125.6 (C), 128.8 (d, $^{1}J_{CP}$ = 189.0 Hz, C), 130.4 (2 HC), 131.2 (d, $^{3}J_{CP}$ = 11.5 Hz, HC), 131.7 (d, $^{3}J_{CP}$ = 13.7 Hz, HC), 132.0 (HC), 133.2 (d, $^{2}J_{CP}$ = 8.9 Hz, HC), 133.7 (C), 135.3 (HC), 140.8 (d, $^{3}J_{CP}$ = 1.3 Hz, C), 141.1 (C), 153.1 (d, $^{3}J_{CP}$ = 3.0 Hz, C), 154.7 (C), 157.2 (C), 191.7 (CO) ppm.

^{31}P NMR (120 MHz, $CDCl_3$): δ = 17.9 ppm.

^{19}F NMR (282 MHz, $CDCl_3$): δ = -63.3 to -63.0 (m) ppm.

HRMS (EI): calculated for $C_{27}H_{21}F_3NO_4P$ $[M]^+$ 511.1160; found 511.1173.

VI-2. TOP1 assays

VI-2.1. Materials and enzyme

Reagents and solvents were used as purchased without further purification. CPT was purchased from Sigma-Aldrich. All stock solutions of the investigated compounds were freshly prepared by dissolving the powdered materials in an appropriate amount of DMSO. The final concentration of DMSO never exceeded 5% (v/v) in the enzymatic reactions. These conditions were maintained in the controls as 5% DMSO was no seen to affect hTOP1B activity.

Recombinant human TOP1B (hTOP1B): the pUC18 plasmid and the recombinant hTOP1B were a kind gift from Dr. B.R. Knudsen (Department of Molecular Biology and Genetics, Aarhus University, Aarhus, Denmark).

The yeast *Saccharomyces cerevisiae TopI null strain RS190* was used for the expression of recombinant human topoisomerase IB (hTOP1B). The plasmid *pHT143* was employed for the expression of recombinant hTOP1B under the control of an inducible GAL promoter as described in the literature[365]. The plasmids *pHT143* were transformed into the yeast *S. cerevisiae* strain *RS190*. The proteins were expressed and purified by ion-exchange affinity chromatography essentially as described in the literature[366]. The protein concentrations were estimated from Coomassie blue-stained SDS/polyacrylamide gels by comparison to serial dilutions of bovine serum albumin (BSA).

VI-2.2. DNA relaxation assay

hTOP1B activity was assayed using a DNA relaxation assay by incubating 110 ng/µL of hTOP1B with 0.5 µg of negatively supercoiled pUC18 in 20 µL of reaction buffer (10 mM Tris–HCl, 5 mM $MgCl_2$, 5 mM $CaCl_2$, 50 µg/mL, 150 mM NaCl, pH 7.5). The pUC18 plasmid was stored in TE buffer (10 mM tris-HCl, 1 mM EDTA) to prevent nuclease activity from external contamination. The effect of the investigated compounds on topoisomerase activity was measured by adding the compounds at different time points as indicated in the text (Chapter II). The reactions were performed at 37°C and stopped at indicated time points by the addition of 0.2% SDS after indicated time intervals. The samples were protease digested by adding 2 µL of proteinase K (10

[365] Lisby M, Krogh BO, Boege F, Westergaard O, Knudsen BR. Camptothecins inhibit the utilization of hydrogen peroxide in the ligation step of topoisomerase I catalysis. Biochemistry. 1998;37(30):10815-10827. doi:10.1021/bi980757r

[366] Knudsen BR, Straub T, Boege F. Separation and functional analysis of eukaryotic DNA topoisomerases by chromatography and electrophoresis. J Chromatogr B Biomed Appl. 1996;684(1-2):307-321. doi:10.1016/0378-4347(96)00152-1

mg/mL) and subsequently electrophoresed in a freshly prepared 1× TBE buffer (50 mM Tris base, 45 mM boric acid, 1 mM EDTA) horizontal 1% agarose gel at 26V for 16 h. The

gel was then stained with a GelRed® 1x solution (Biotium, CA, USA) for 0,5-2h, destained with water and photographed in an UV transilluminator. The results were analysed by using the Image J software to process the images of the gels.

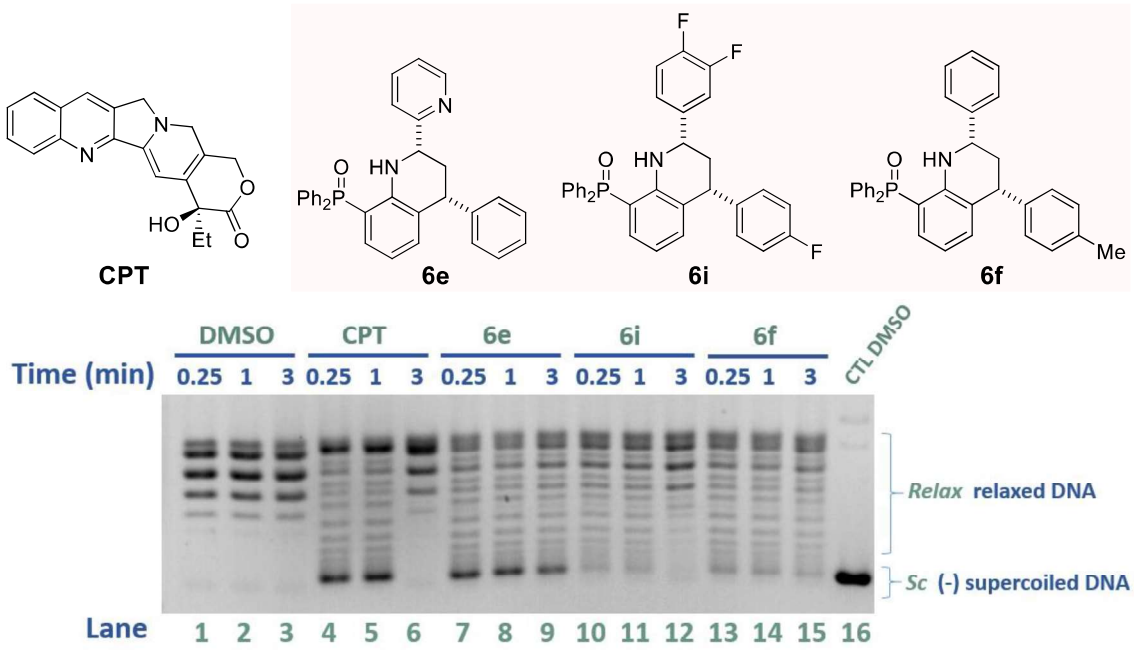
CPT
6e
6i
6f
DMSO
CPT
6e
6i
6f
CTL DMSO
Time (min)
0.25 1 3 0.25 1 3 0.25 1 3 0.25 1 3 0.25 1 3
Relax relaxed DNA
Sc (-) supercoiled DNA
Lane
1 2 3 4 5 6 7 8 9 10 11 12 13 14 15 16

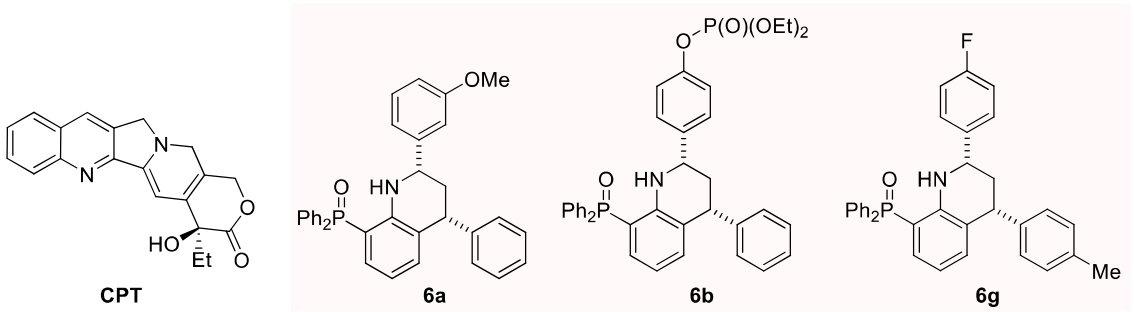
CPT
6a
6b
6g
DMSO
CPT
6a
6b
6g
CTL DMSO
CTL CPT
CTL 6a
CTL 6b
CTL 6g
Time (min)
0.25 1 3 0.25 1 3 0.25 1 3 0.25 1 3 0.25 1 3
Lane
1 2 3 4 5 6 7 8 9 10 11 12 13 14 15 16 17 18 19 20

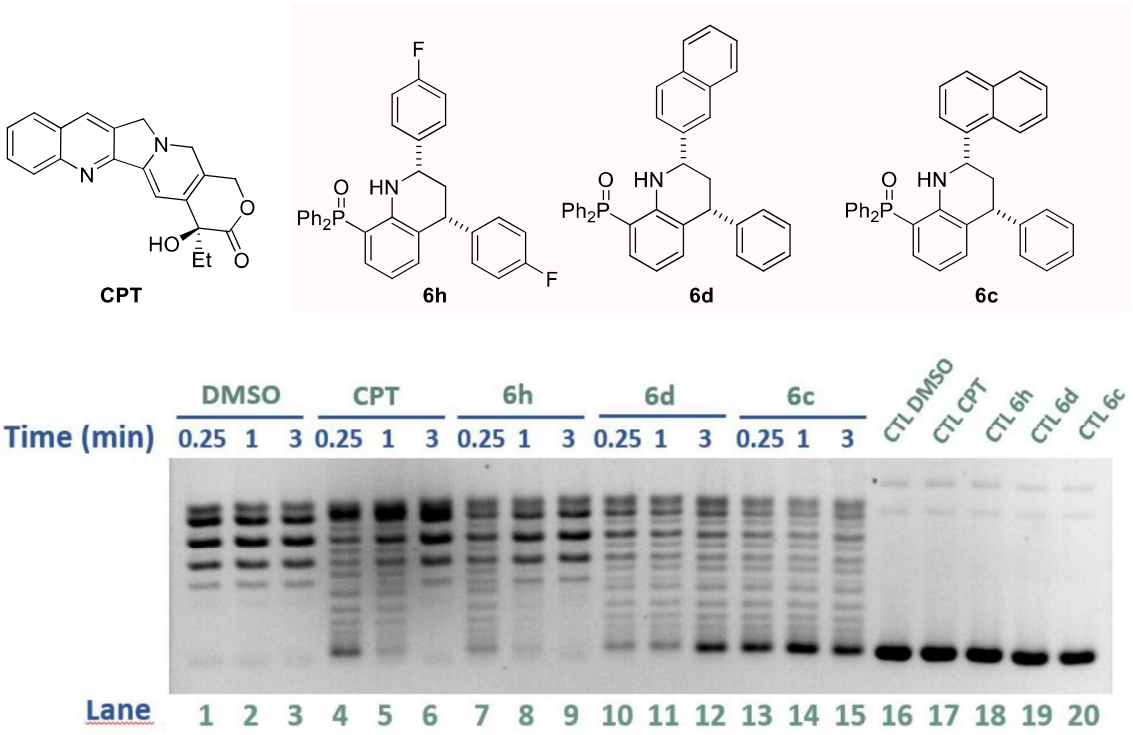
CPT
6h
6d
6c
DMSO
CPT
6h
6d
6c
CTL DMSO
CTL CPT
CTL 6h
CTL 6d
CTL 6c
Time (min)
0.25 1 3 0.25 1 3 0.25 1 3 0.25 1 3 0.25 1 3
Lane
1 2 3 4 5 6 7 8 9 10 11 12 13 14 15 16 17 18 19 20

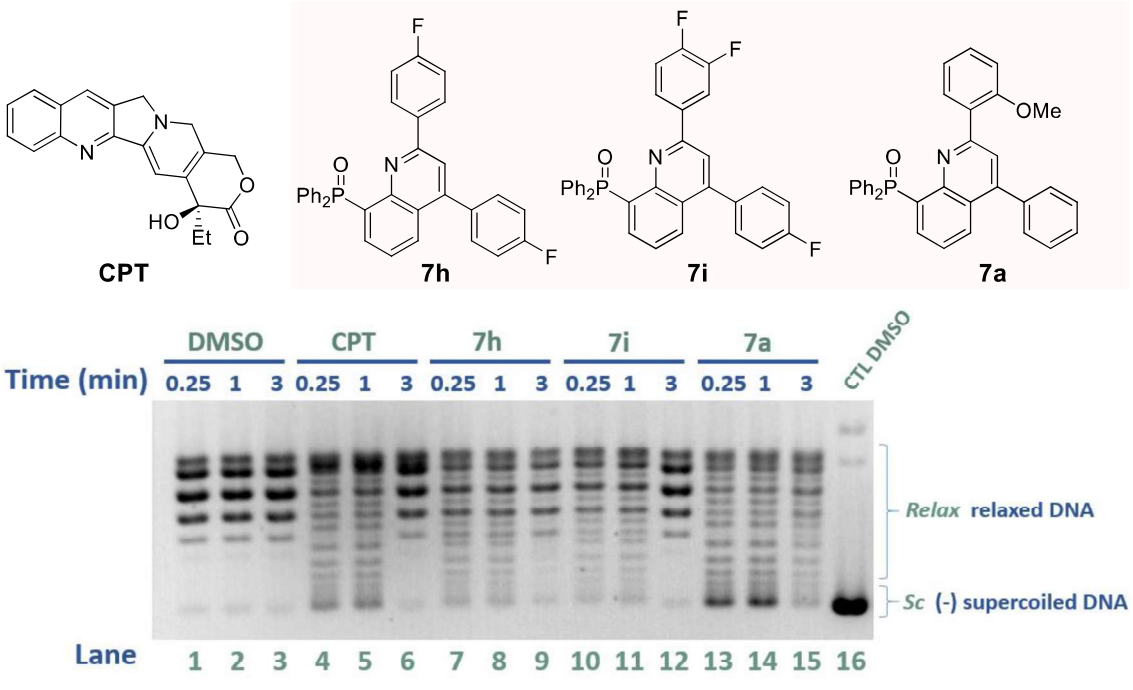
CPT
7h
7i
7a
DMSO
CPT
7h
7i
7a
CTL DMSO
Time (min)
0.25 1 3 0.25 1 3 0.25 1 3 0.25 1 3 0.25 1 3
Relax relaxed DNA
Sc (-) supercoiled DNA
Lane
1 2 3 4 5 6 7 8 9 10 11 12 13 14 15 16

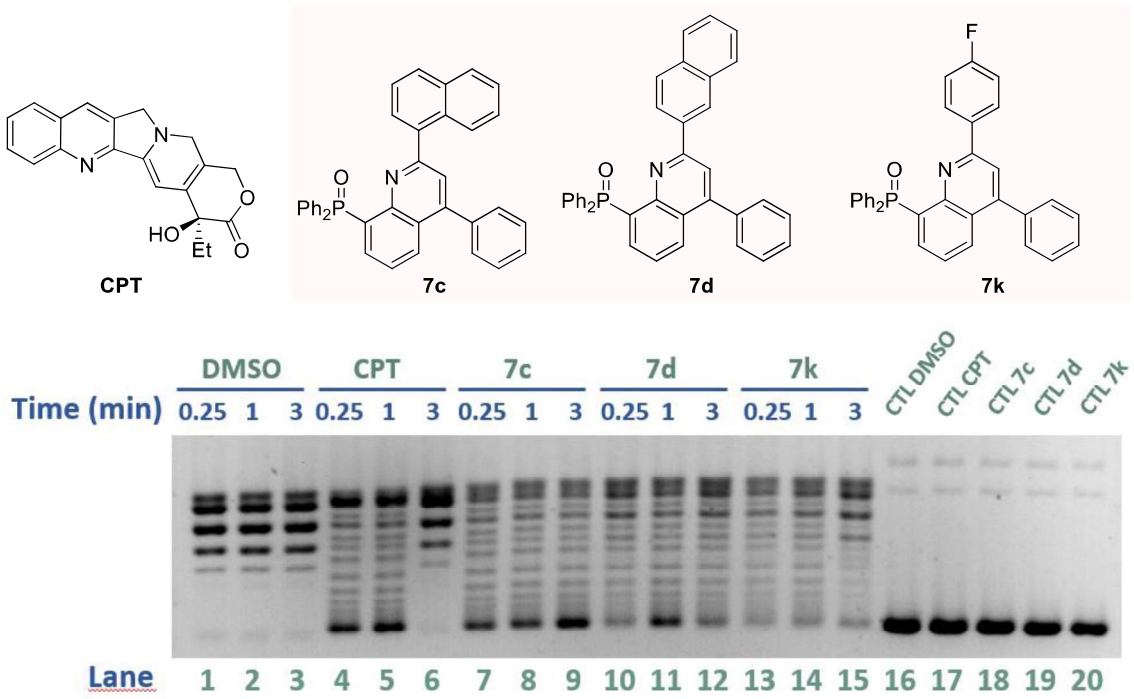
CPT
7c
7d
7k
DMSO
CPT
7c
7d
7k
CTL DMSO
CTL CPT
CTL 7c
CTL 7d
CTL 7k
Time (min)
0.25 1 3 0.25 1 3 0.25 1 3 0.25 1 3 0.25 1 3
Lane
1 2 3 4 5 6 7 8 9 10 11 12 13 14 15 16 17 18 19 20

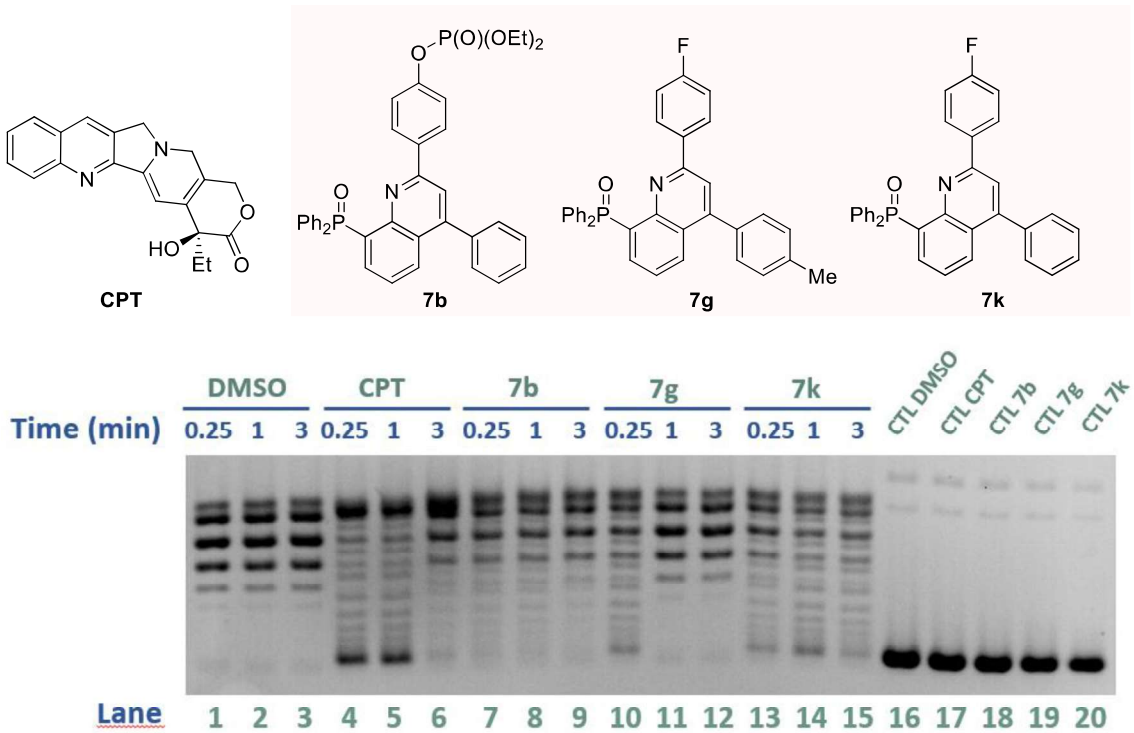
CPT
7b
7g
7k
DMSO
CPT
7b
7g
7k
CTL DMSO
CTL CPT
CTL 7b
CTL 7g
CTL 7k
Time (min)
0.25 1 3 0.25 1 3 0.25 1 3 0.25 1 3 0.25 1 3
Lane
1 2 3 4 5 6 7 8 9 10 11 12 13 14 15 16 17 18 19 20

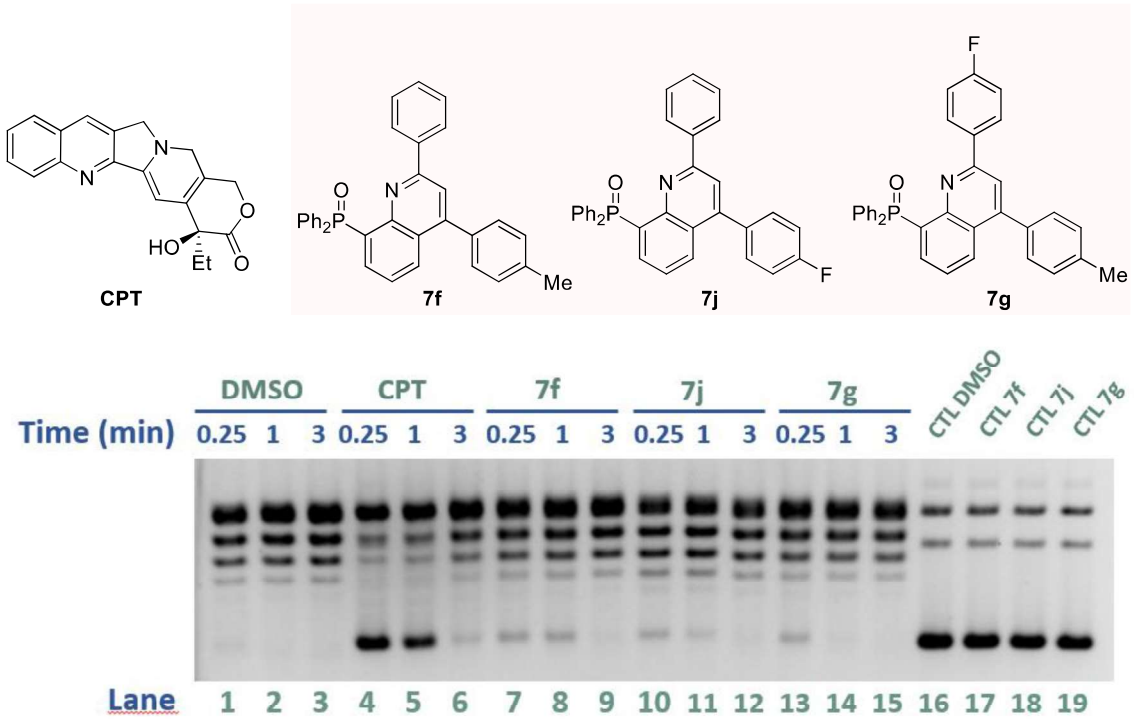
CPT
7f
7j
7g
DMSO
CPT
7f
7j
7g
CTL DMSO
CTL 7f
CTL 7j
CTL 7g
Time (min)
0.25 1 3 0.25 1 3 0.25 1 3 0.25 1 3 0.25 1 3
Lane
1 2 3 4 5 6 7 8 9 10 11 12 13 14 15 16 17 18 19

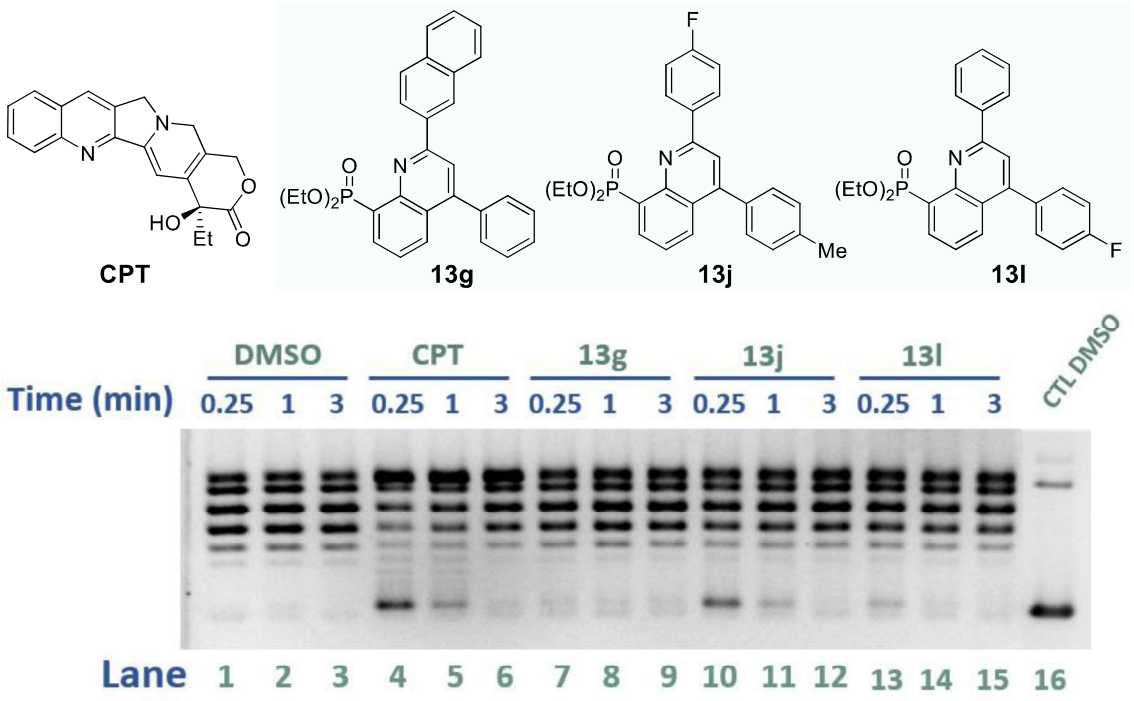
CPT
13g
13j
13l
DMSO
CPT
13g
13j
13l
CTL DMSO
Time (min)
0.25 1 3 0.25 1 3 0.25 1 3 0.25 1 3 0.25 1 3
Lane
1 2 3 4 5 6 7 8 9 10 11 12 13 14 15 16

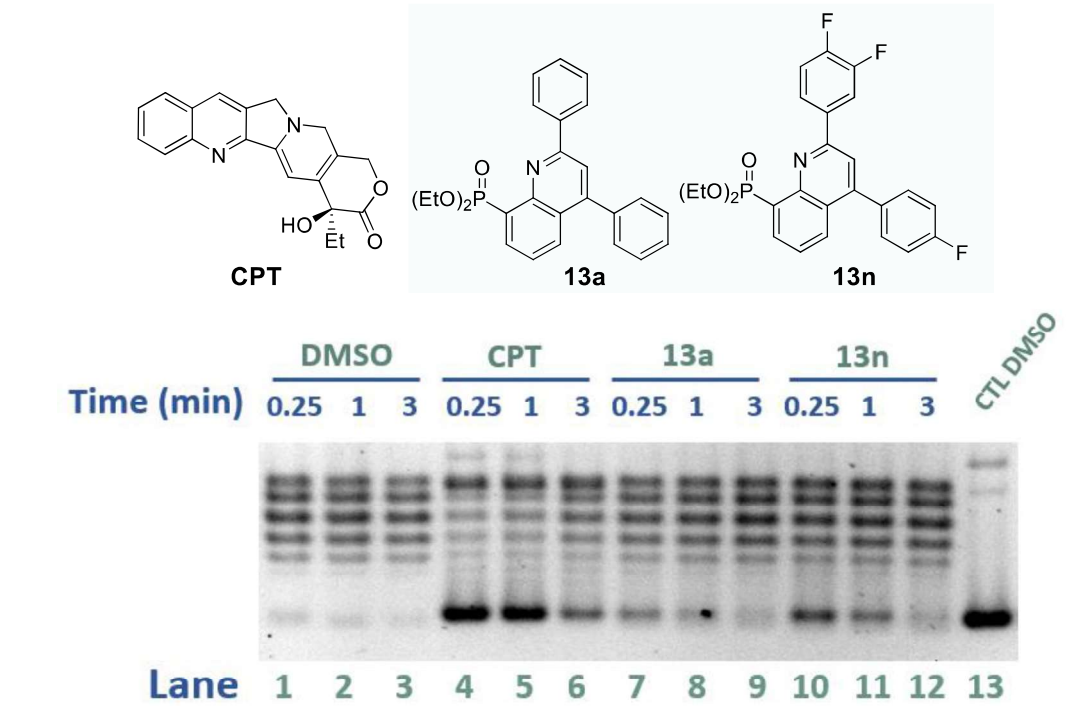
CPT
13a
13n
DMSO
CPT
13a
13n
CTL DMSO
Time (min)
0.25 1 3 0.25 1 3 0.25 1 3 0.25 1 3
Lane 1 2 3 4 5 6 7 8 9 10 11 12 13

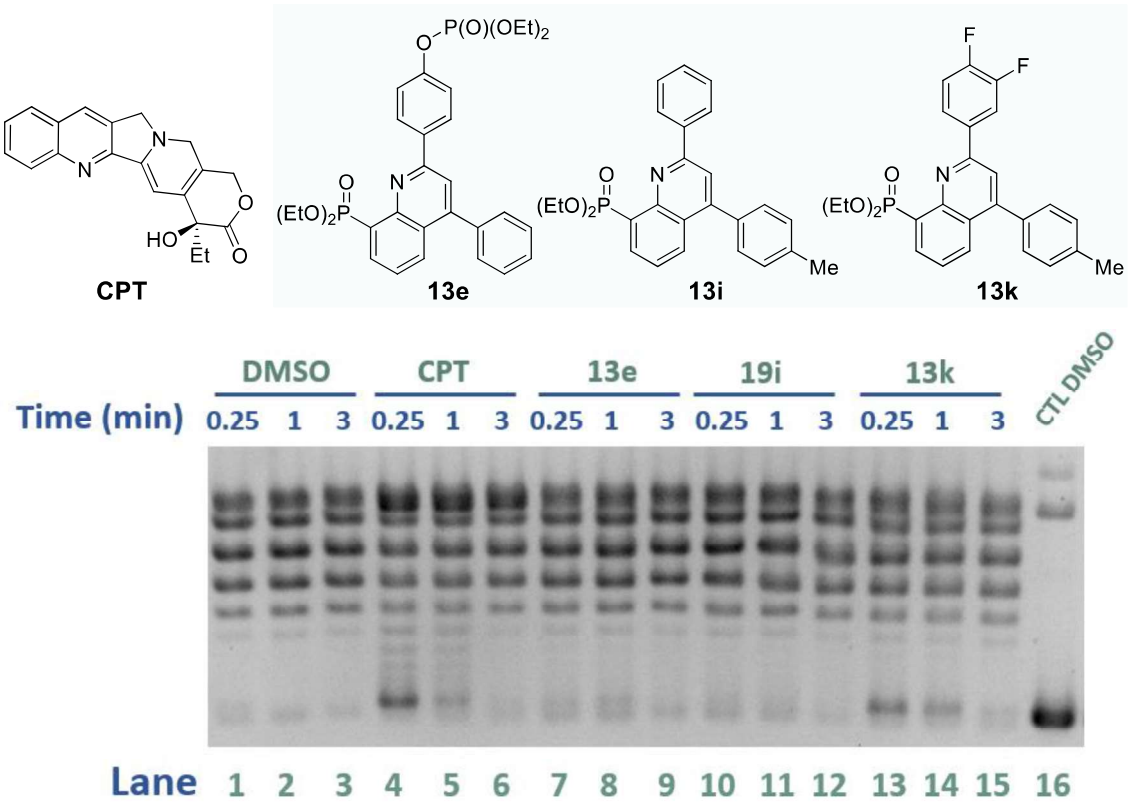
CPT
13e
13i
13k
DMSO
CPT
13e
19i
13k
CTL DMSO
Time (min)
0.25 1 3 0.25 1 3 0.25 1 3 0.25 1 3 0.25 1 3
Lane 1 2 3 4 5 6 7 8 9 10 11 12 13 14 15 16

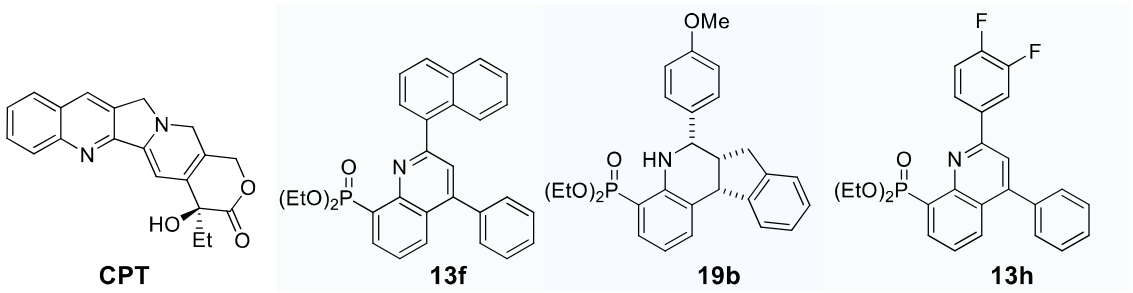
CPT
13f
19b
13h

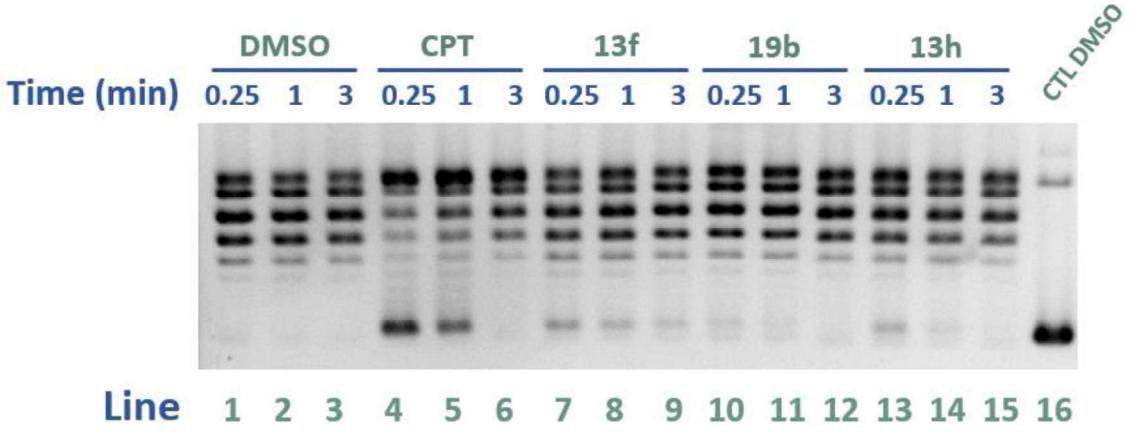
DMSO
CPT
13f
19b
13h
CTL DMSO
Time (min)
0.25 1 3 0.25 1 3 0.25 1 3 0.25 1 3 0.25 1 3
Line
1 2 3 4 5 6 7 8 9 10 11 12 13 14 15 16

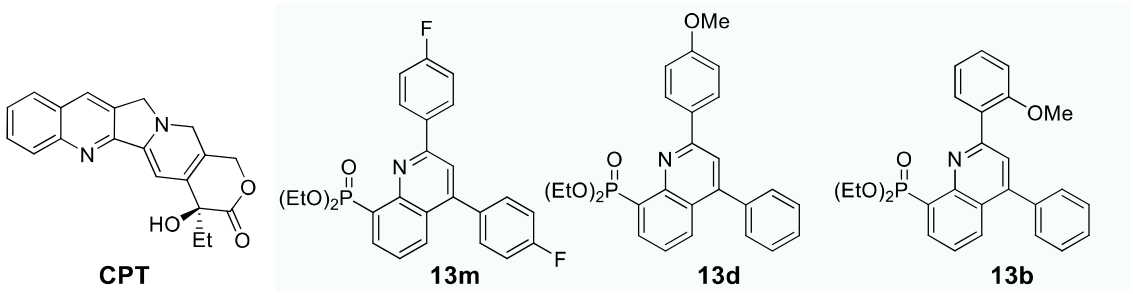
CPT
13m
13d
13b

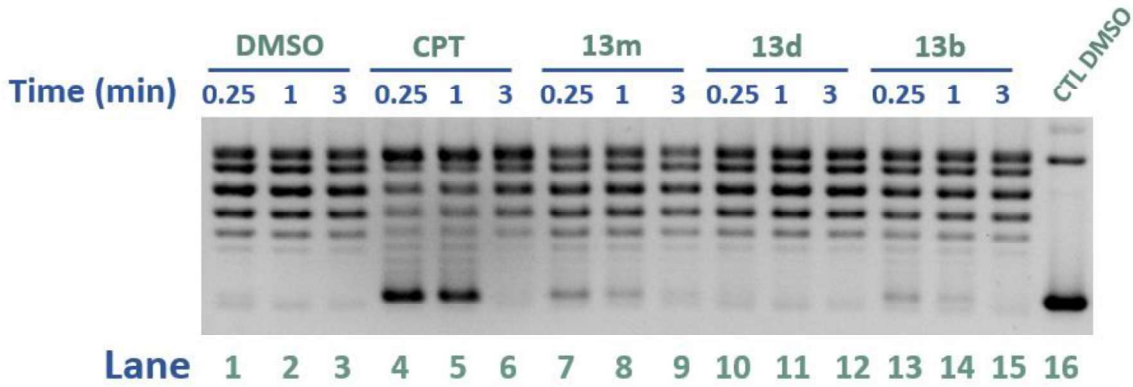
DMSO
CPT
13m
13d
13b
CTL DMSO
Time (min)
0.25 1 3 0.25 1 3 0.25 1 3 0.25 1 3 0.25 1 3
Lane
1 2 3 4 5 6 7 8 9 10 11 12 13 14 15 16

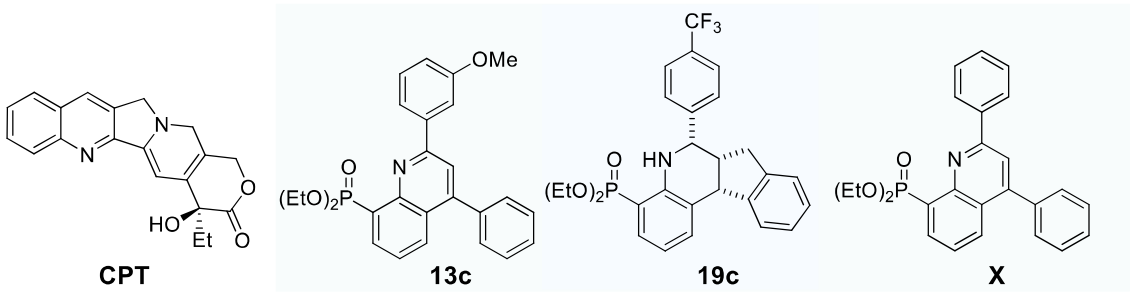
CPT
13c
19c
X

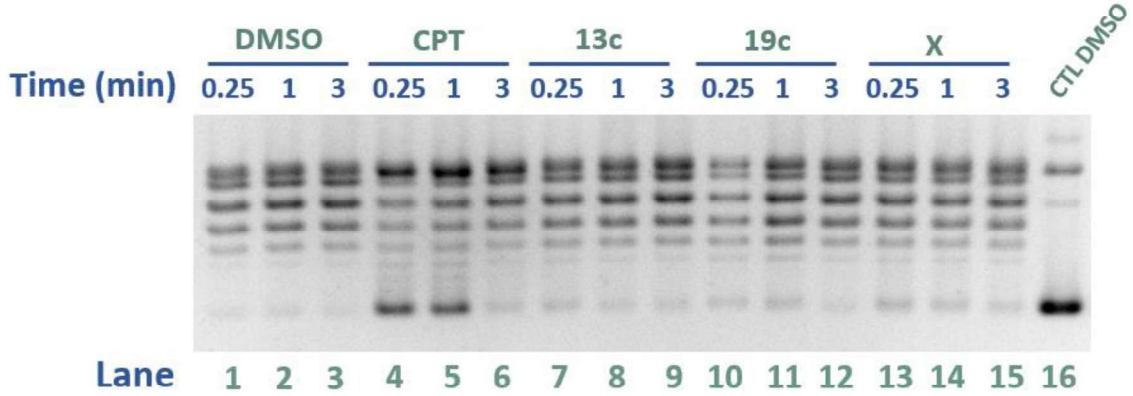
DMSO
CPT
13c
19c
X
CTL DMSO
Time (min)
0.25 1 3 0.25 1 3 0.25 1 3 0.25 1 3 0.25 1 3
Lane
1 2 3 4 5 6 7 8 9 10 11 12 13 14 15 16

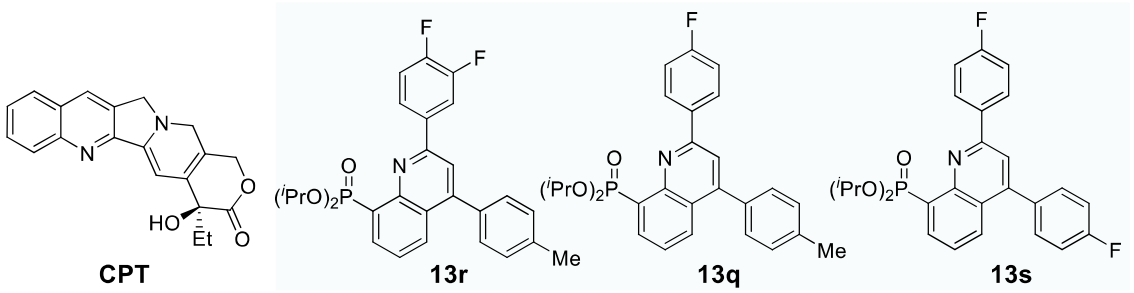
CPT
13r
13q
13s

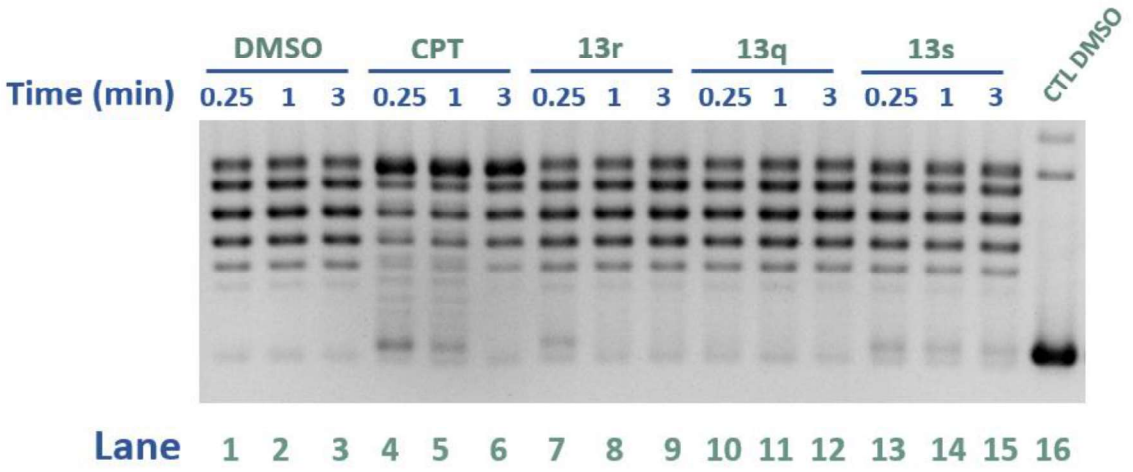
DMSO
CPT
13r
13q
13s
CTL DMSO
Time (min)
0.25 1 3 0.25 1 3 0.25 1 3 0.25 1 3 0.25 1 3
Lane
1 2 3 4 5 6 7 8 9 10 11 12 13 14 15 16

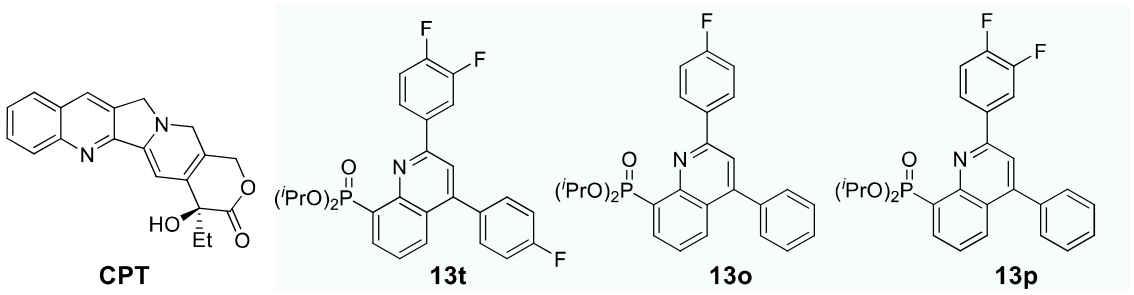
CPT
13t
13o
13p

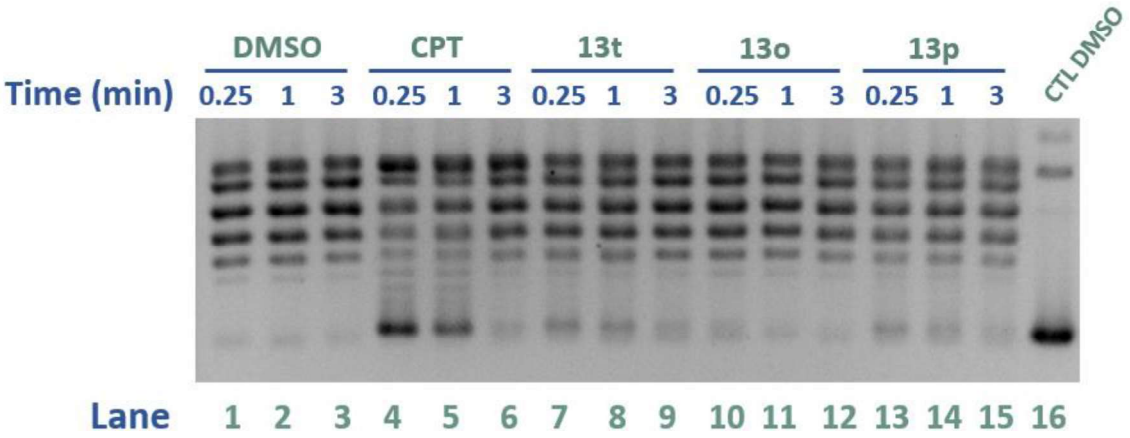
DMSO
CPT
13t
13o
13p
CTL DMSO
Time (min)
0.25 1 3 0.25 1 3 0.25 1 3 0.25 1 3 0.25 1 3
Lane
1 2 3 4 5 6 7 8 9 10 11 12 13 14 15 16

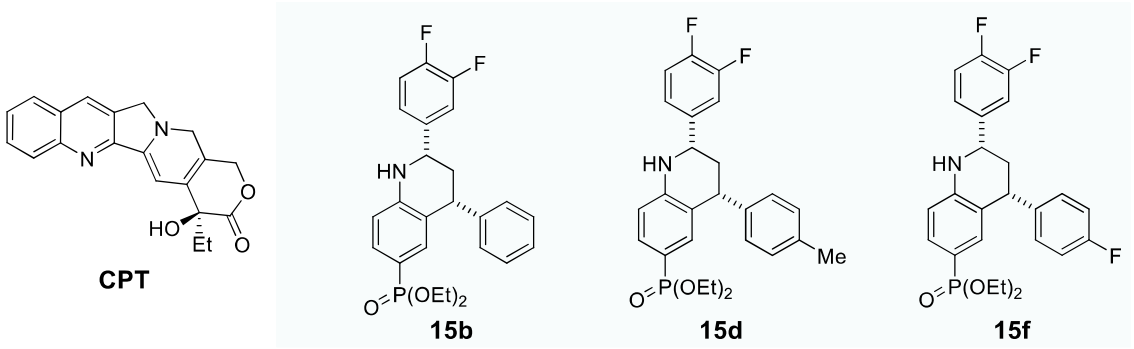
CPT
15b
15d
15f

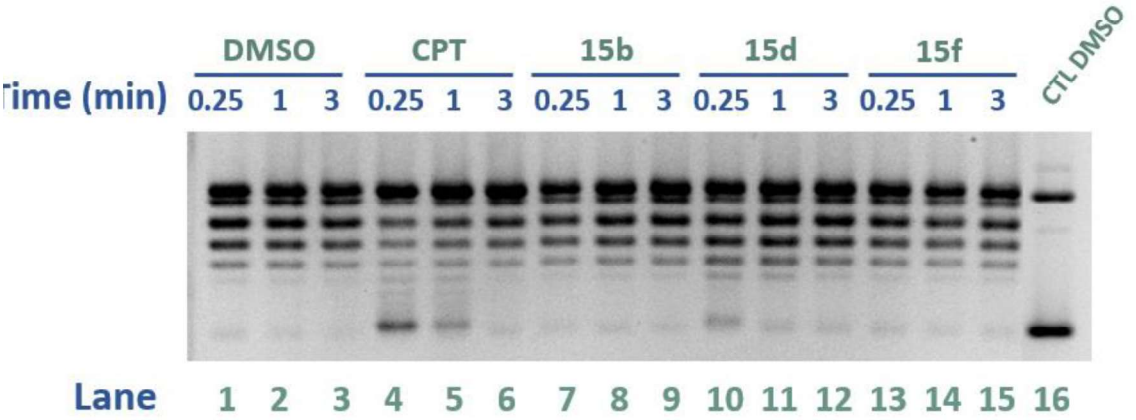
DMSO
CPT
15b
15d
15f
CTL DMSO
Time (min)
0.25 1 3 0.25 1 3 0.25 1 3 0.25 1 3 0.25 1 3
Lane
1 2 3 4 5 6 7 8 9 10 11 12 13 14 15 16

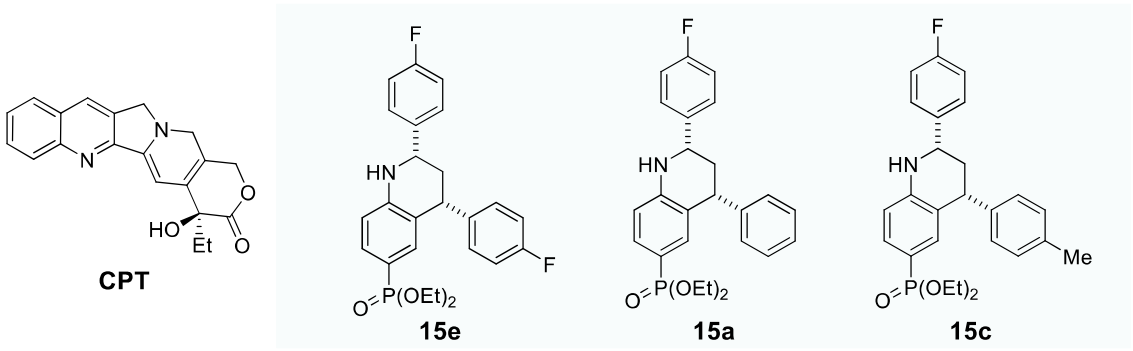
CPT
15e
15a
15c

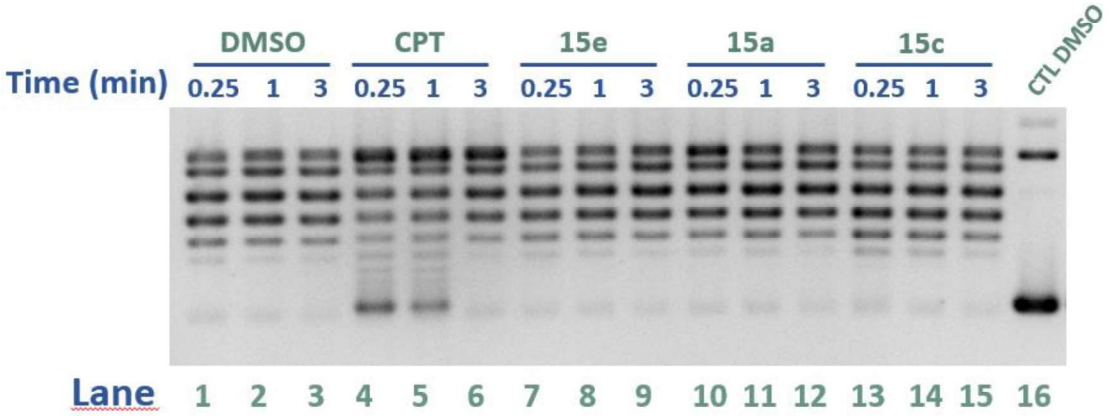
DMSO
CPT
15e
15a
15c
CTL DMSO
Time (min)
0.25 1 3 0.25 1 3 0.25 1 3 0.25 1 3 0.25 1 3
Lane
1 2 3 4 5 6 7 8 9 10 11 12 13 14 15 16

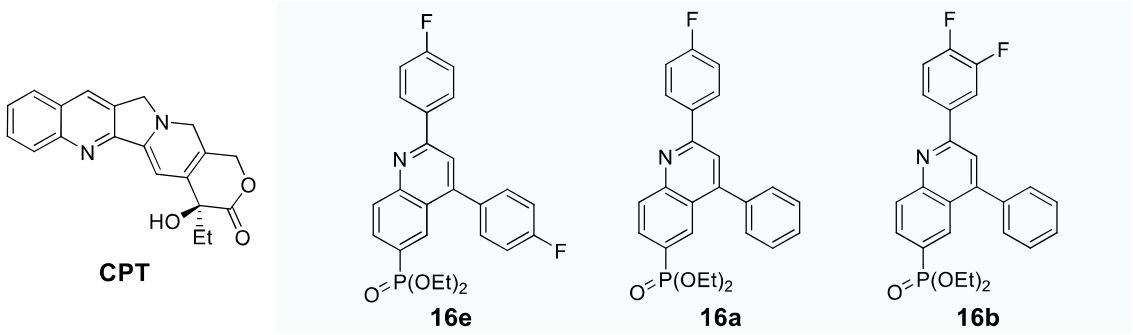
CPT
16e
16a
16b

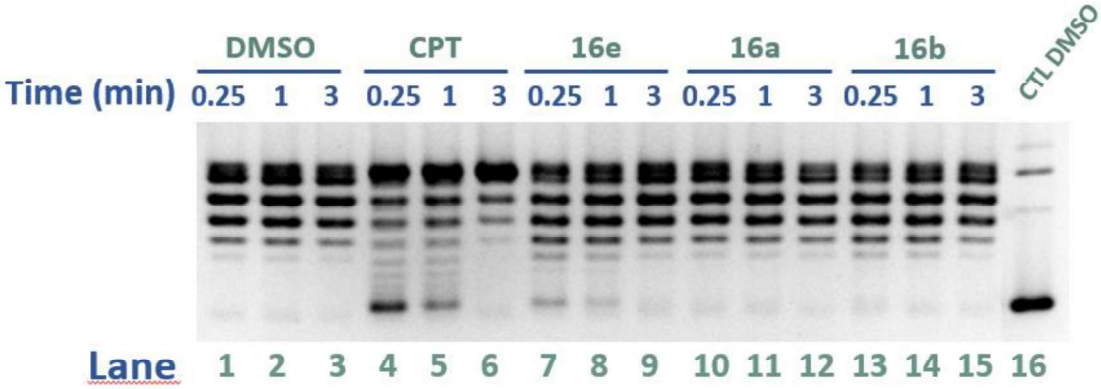
DMSO
CPT
16e
16a
16b
CTL DMSO
Time (min)
0.25 1 3 0.25 1 3 0.25 1 3 0.25 1 3 0.25 1 3
Lane
1 2 3 4 5 6 7 8 9 10 11 12 13 14 15 16

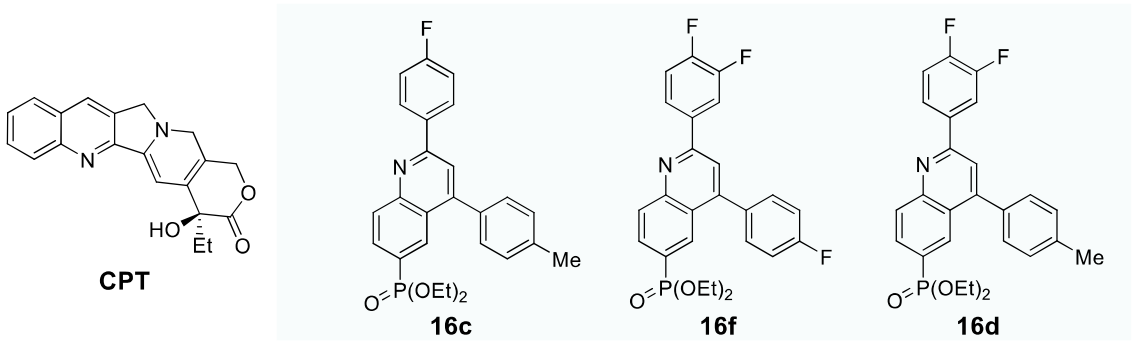
CPT
16c
16f
16d

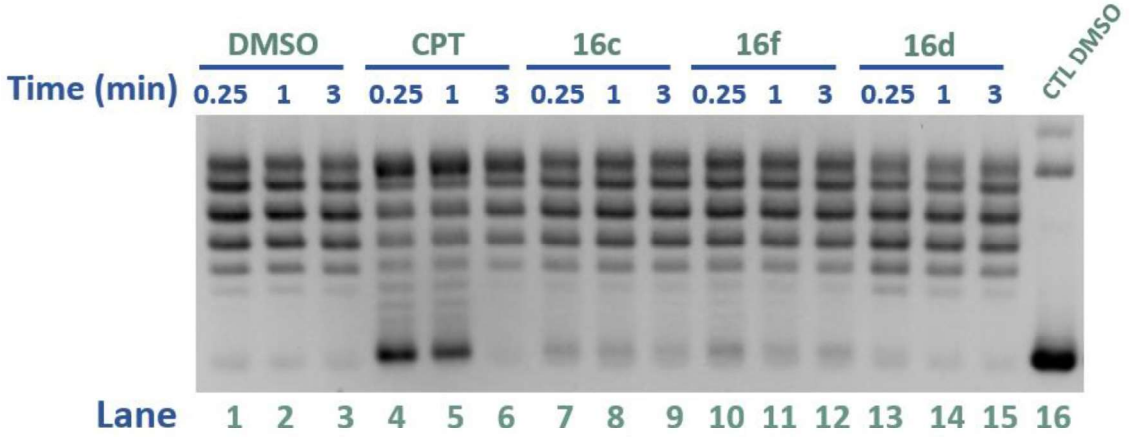
DMSO
CPT
16c
16f
16d
CTL DMSO
Time (min)
0.25 1 3 0.25 1 3 0.25 1 3 0.25 1 3 0.25 1 3
Lane
1 2 3 4 5 6 7 8 9 10 11 12 13 14 15 16

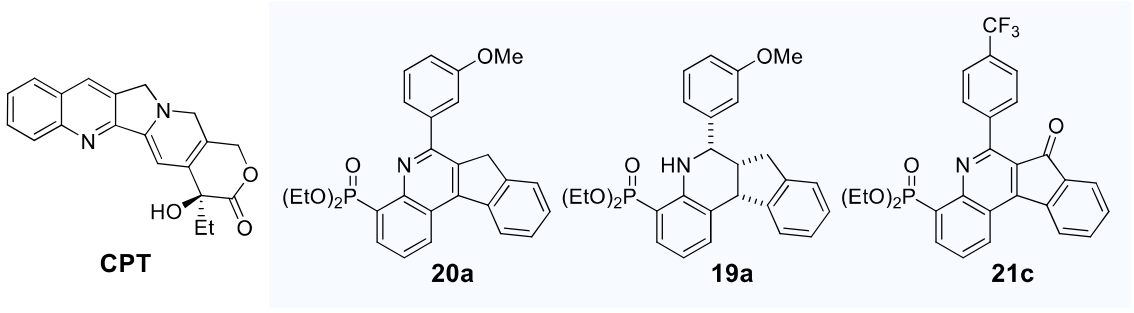
CPT
20a
19a
21c

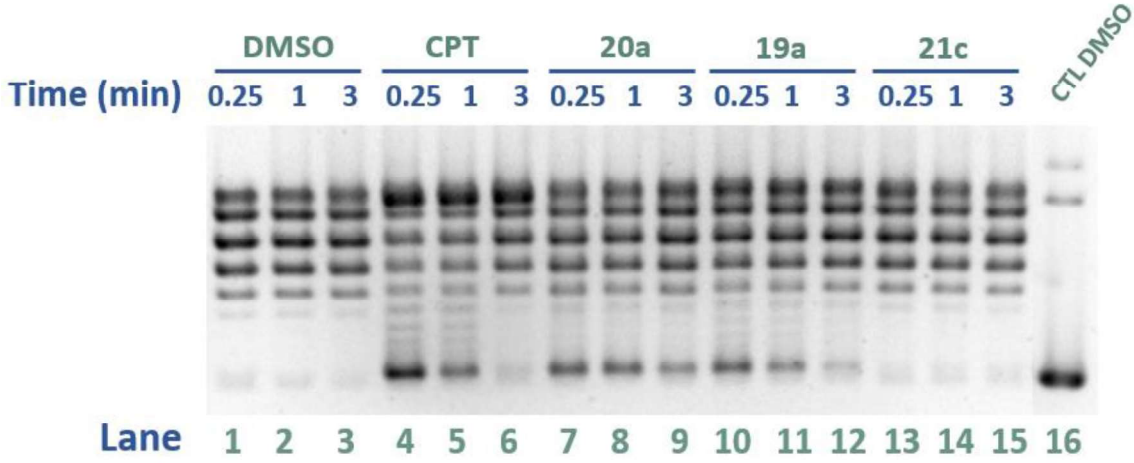
DMSO
CPT
20a
19a
21c
CTL DMSO
Time (min)
0.25 1 3 0.25 1 3 0.25 1 3 0.25 1 3 0.25 1 3
Lane
1 2 3 4 5 6 7 8 9 10 11 12 13 14 15 16

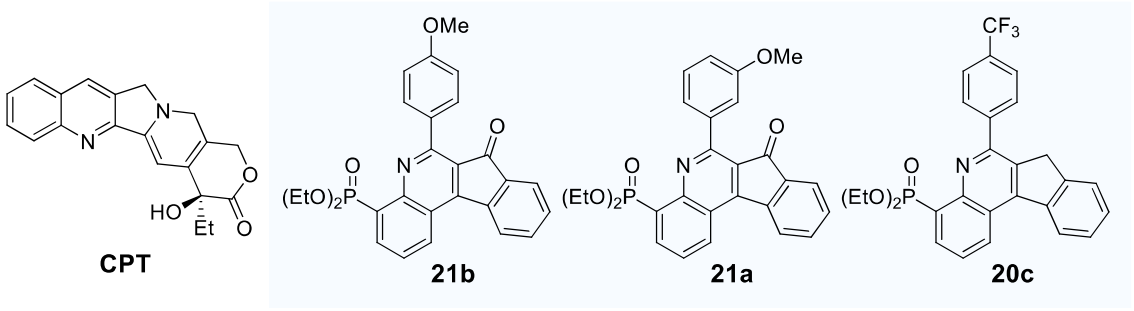
CPT
21b
21a
20c

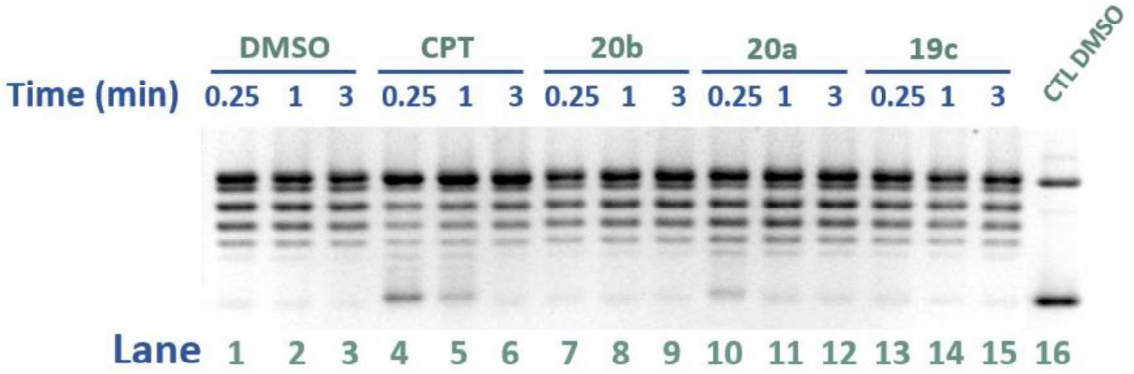
DMSO
CPT
20b
20a
19c
CTL DMSO
Time (min) 0.25 1 3 0.25 1 3 0.25 1 3 0.25 1 3 0.25 1 3
Lane 1 2 3 4 5 6 7 8 9 10 11 12 13 14 15 16

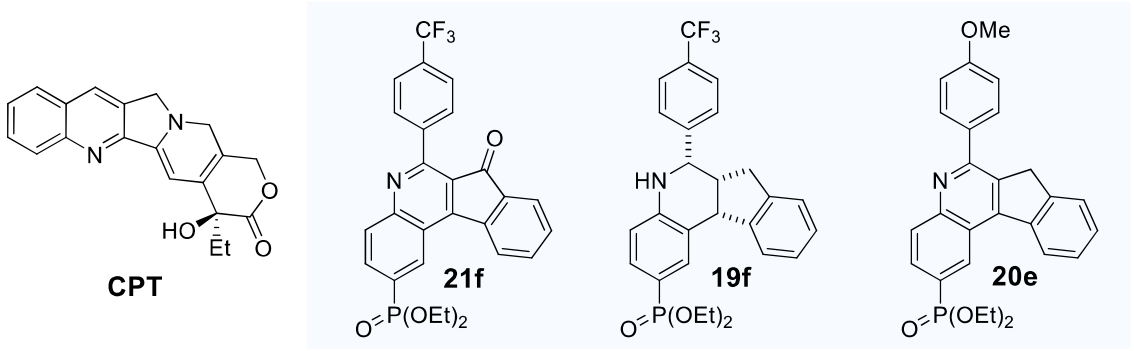
CPT
21f
19f
20e

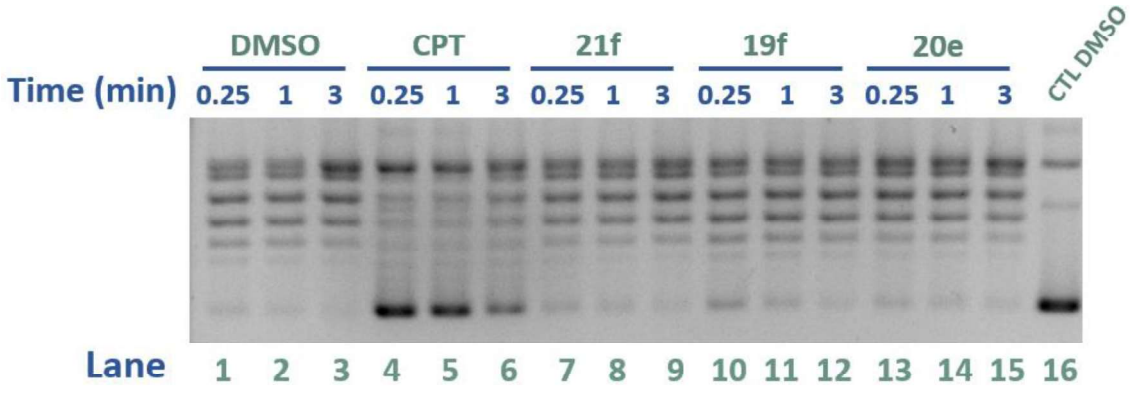
DMSO
CPT
21f
19f
20e
CTL DMSO
Time (min) 0.25 1 3 0.25 1 3 0.25 1 3 0.25 1 3 0.25 1 3
Lane 1 2 3 4 5 6 7 8 9 10 11 12 13 14 15 16

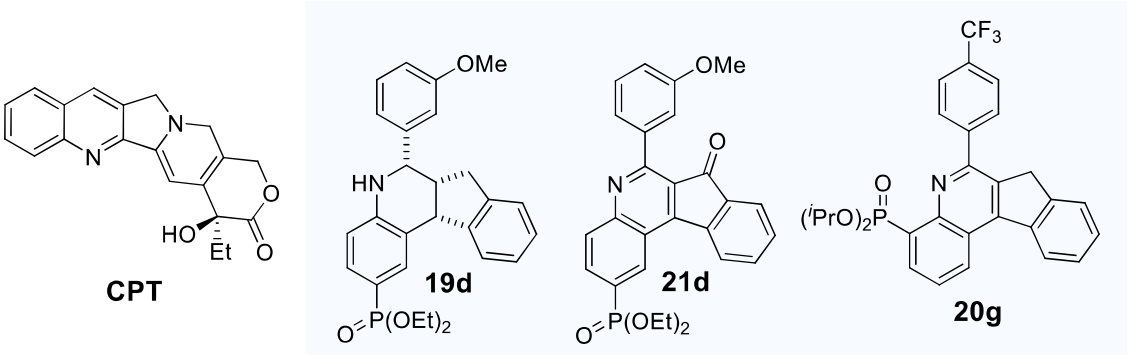
CPT
19d
21d
20g

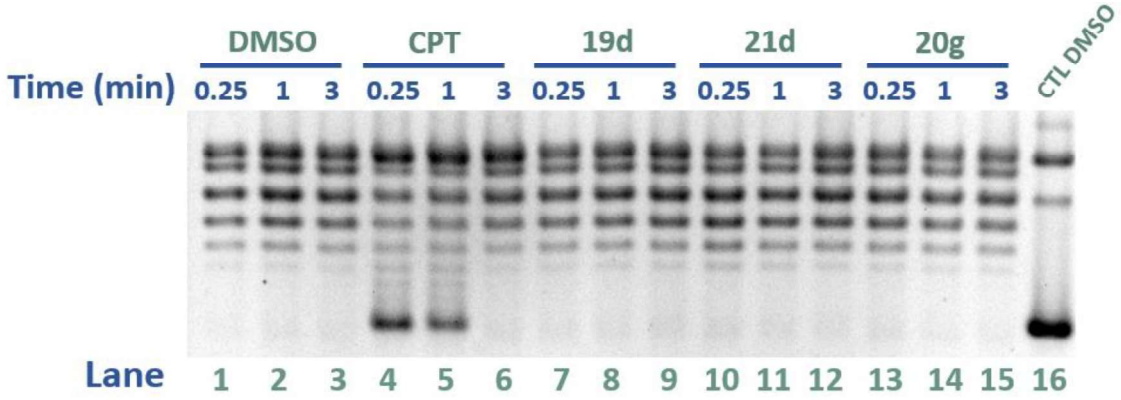
DMSO
CPT
19d
21d
20g
CTL DMSO
Time (min)
0.25 1 3 0.25 1 3 0.25 1 3 0.25 1 3 0.25 1 3
Lane
1 2 3 4 5 6 7 8 9 10 11 12 13 14 15 16

VI-2.3. Nicking assay

The ability of investigated compounds to induce hTOP1B-dependant nicks into the pUC18 negatively supercoiled plasmid was evaluated by the so-called nicking assay. The nicking assay was carried out by performing a DNA relaxation assay, incubating 330 ng/µL of hTOP1B with 0.5 µg of negatively supercoiled pUC18 in 20 µL of reaction buffer (10 mM Tris–HCl, 5 mM $MgCl_2$, 5 mM $CaCl_2$, 50 µg/mL, 150 mM NaCl, pH 7.5). The pUC18 plasmid was stored in TE buffer (10 mM tris-HCl, 1 mM EDTA) to prevent nuclease activity from external contamination. The effect of the investigated compounds on topoisomerase activity was measured by adding the compounds at different time points as indicated in the text (Chapter II). The reactions were performed at 37°C and stopped at indicated time points by the addition of 0.2% SDS after indicated time intervals. The samples were electrophoresed in a freshly prepared 1× TBE buffer (50 mM Tris base, 45 mM boric acid, 1 mM EDTA) horizontal 1% agarose gel containing 0.5 µg/mL of EtBr at 26V for 16 h. The gel was then directly photographed in an UV transilluminator. The results were analysed by using the Image J software to process the images of the gels.

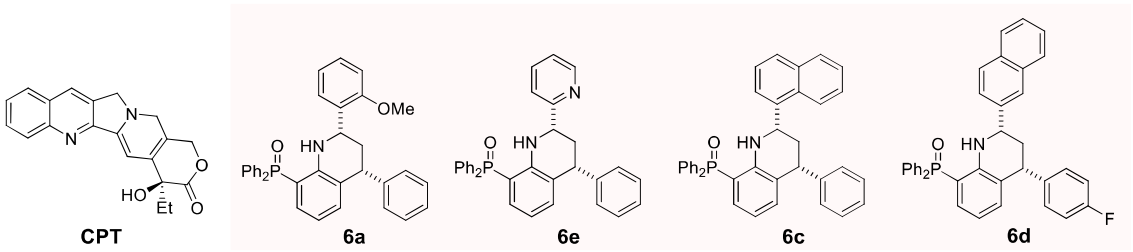

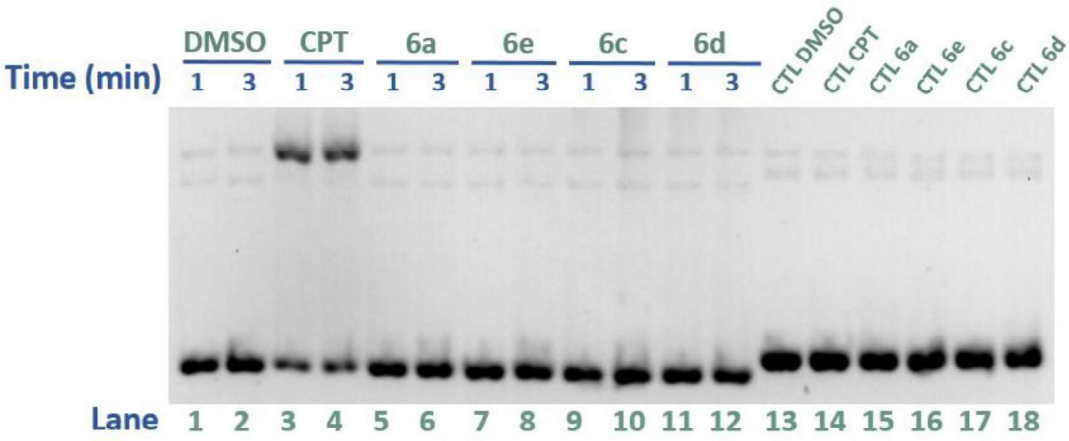

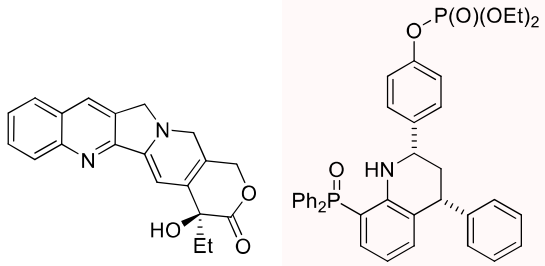

CPT

6b

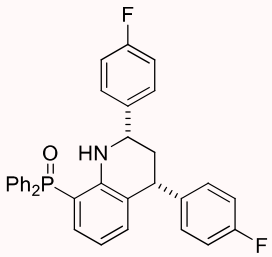

6h

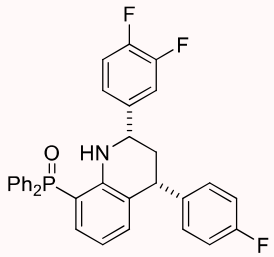

6i

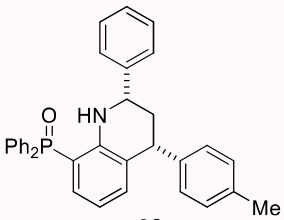

6f

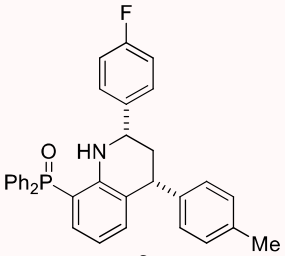

6g

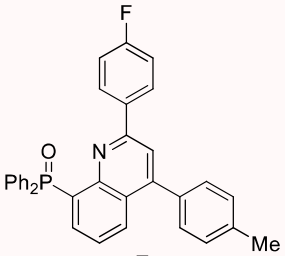

7g

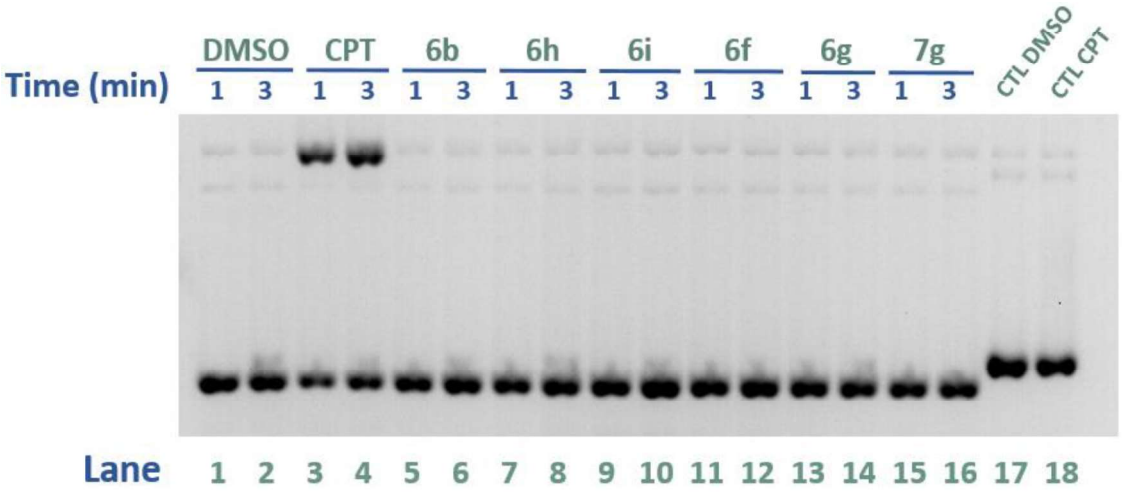

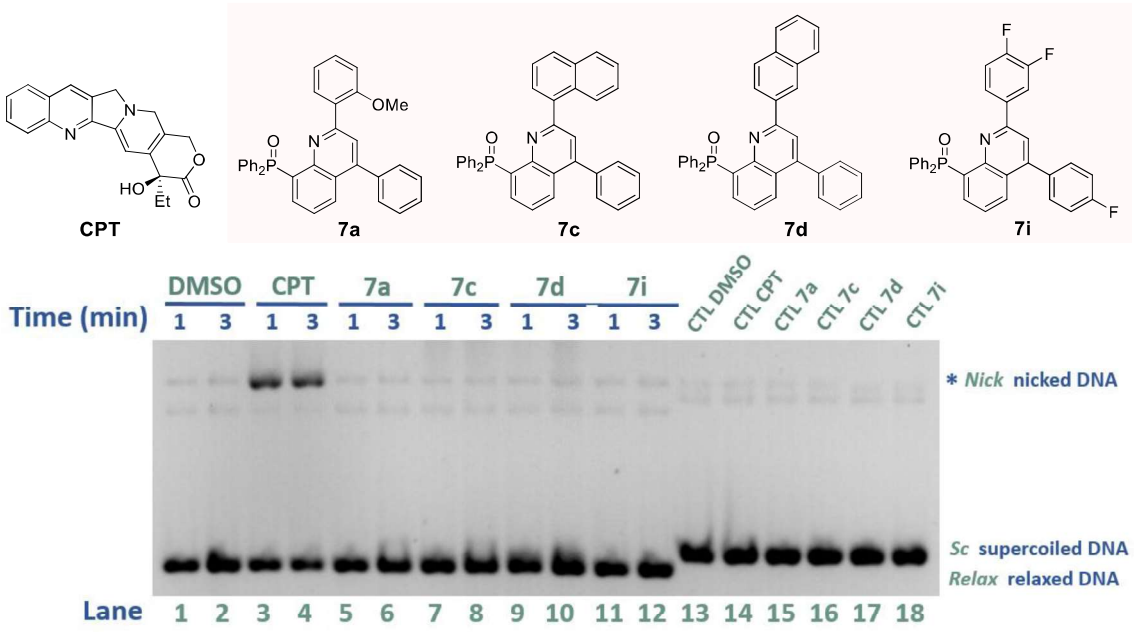
CPT
7a
7c
7d
7i
DMSO
CPT
7a
7c
7d
7i
CTL DMSO
CTL CPT
CTL 7a
CTL 7c
CTL 7d
CTL 7i
Time (min)
1 3 1 3 1 3 1 3 1 3 1 3
* Nick nicked DNA
Sc supercoiled DNA
Relax relaxed DNA
Lane
1 2 3 4 5 6 7 8 9 10 11 12 13 14 15 16 17 18

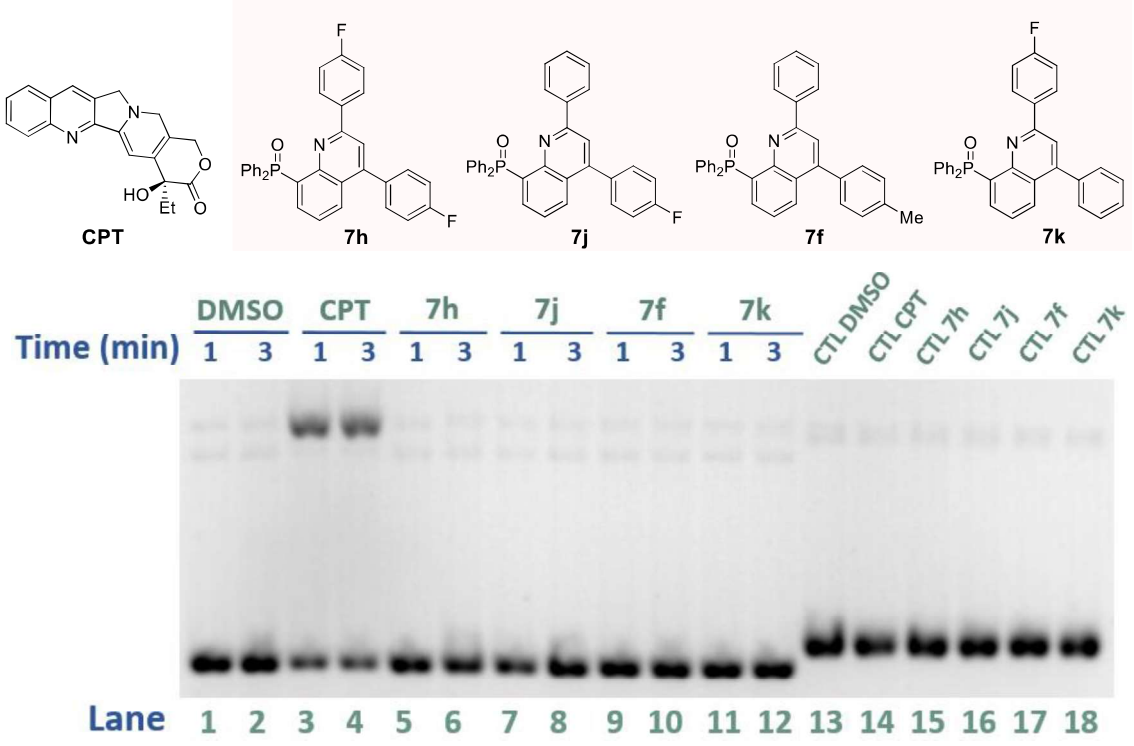
CPT
7h
7j
7f
7k
DMSO
CPT
7h
7j
7f
7k
CTL DMSO
CTL CPT
CTL 7h
CTL 7j
CTL 7f
CTL 7k
Time (min)
1 3 1 3 1 3 1 3 1 3 1 3
Lane
1 2 3 4 5 6 7 8 9 10 11 12 13 14 15 16 17 18

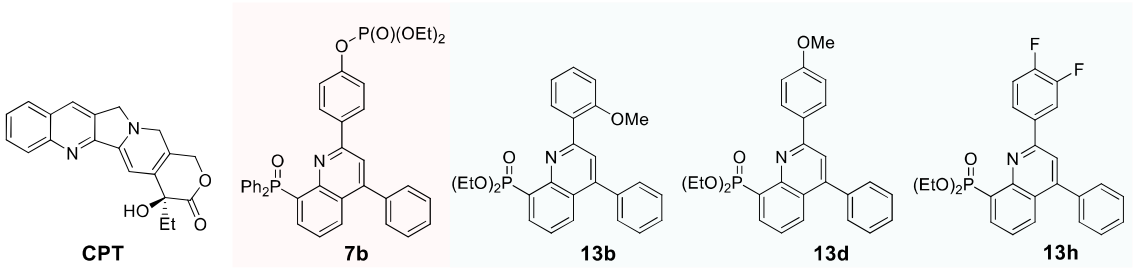
CPT
7b
13b
13d
13h

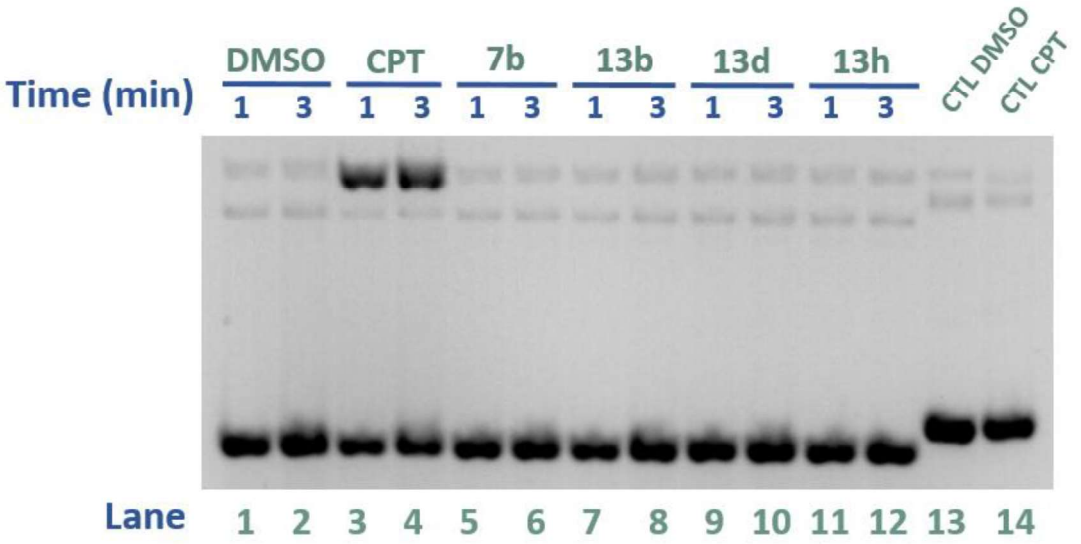
Time (min)
DMSO
CPT
7b
13b
13d
13h
CTL DMSO
CTL CPT
1 3 1 3 1 3 1 3 1 3 1 3
Lane
1 2 3 4 5 6 7 8 9 10 11 12 13 14

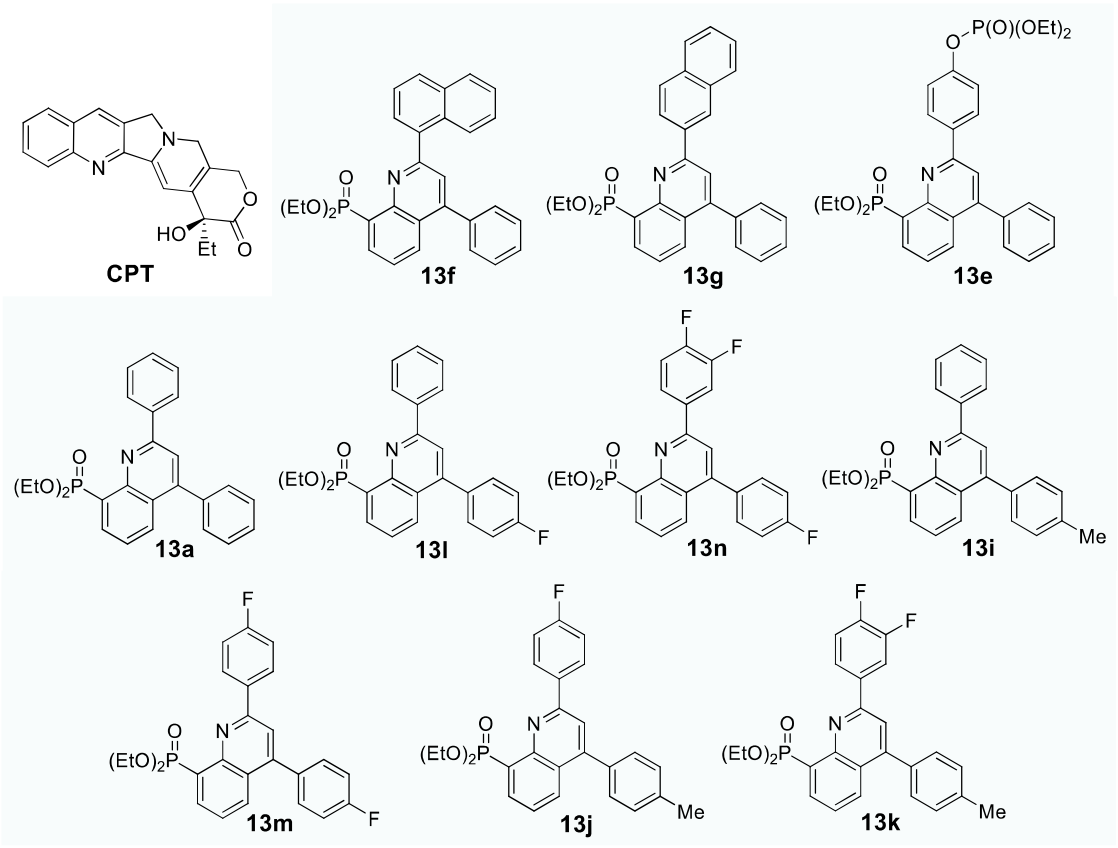
CPT
13f
13g
13e
13a
13l
13n
13i
13m
13j
13k

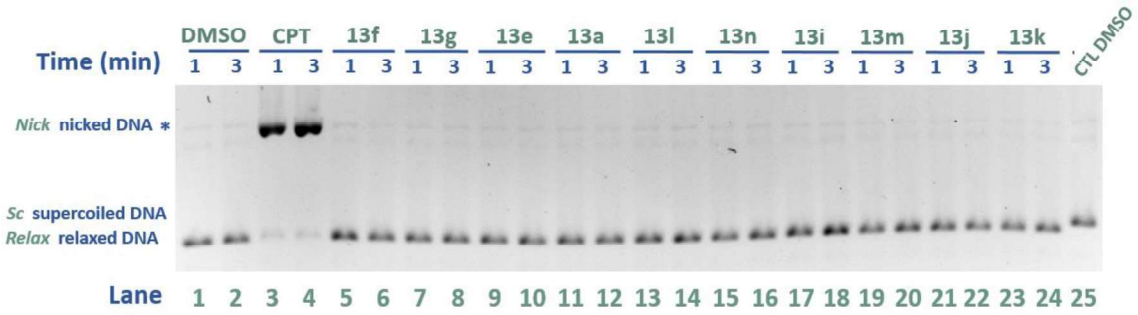
Time (min)
DMSO
CPT
13f
13g
13e
13a
13l
13n
13i
13m
13j
13k
CTL DMSO
Nick nicked DNA *
Sc supercoiled DNA
Relax relaxed DNA
Lane 1 2 3 4 5 6 7 8 9 10 11 12 13 14 15 16 17 18 19 20 21 22 23 24 25

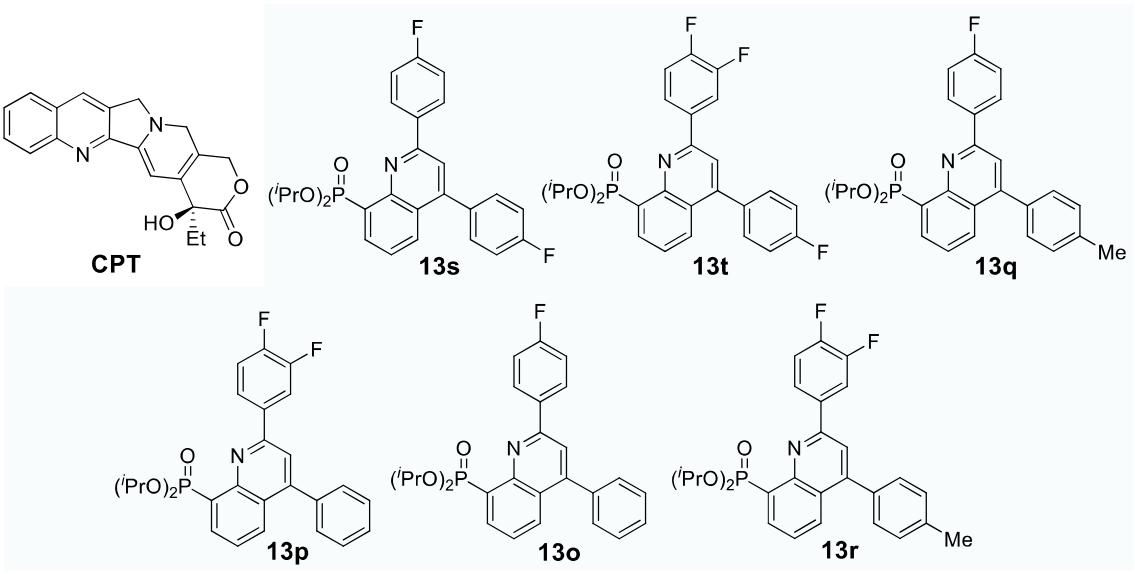
CPT
13s
13t
13q
13p
13o
13r

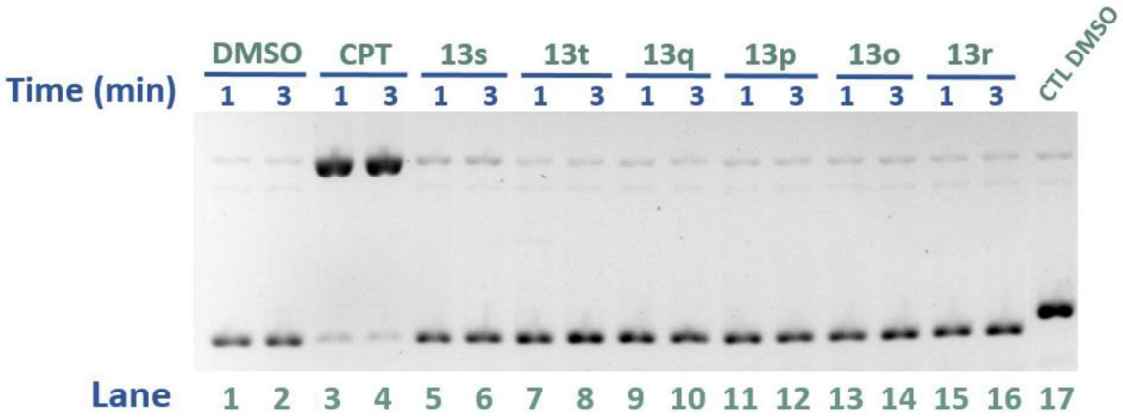
Time (min)
DMSO
CPT
13s
13t
13q
13p
13o
13r
CTL DMSO
1 3 1 3 1 3 1 3 1 3 1 3 1 3 1 3
Lane
1 2 3 4 5 6 7 8 9 10 11 12 13 14 15 16 17

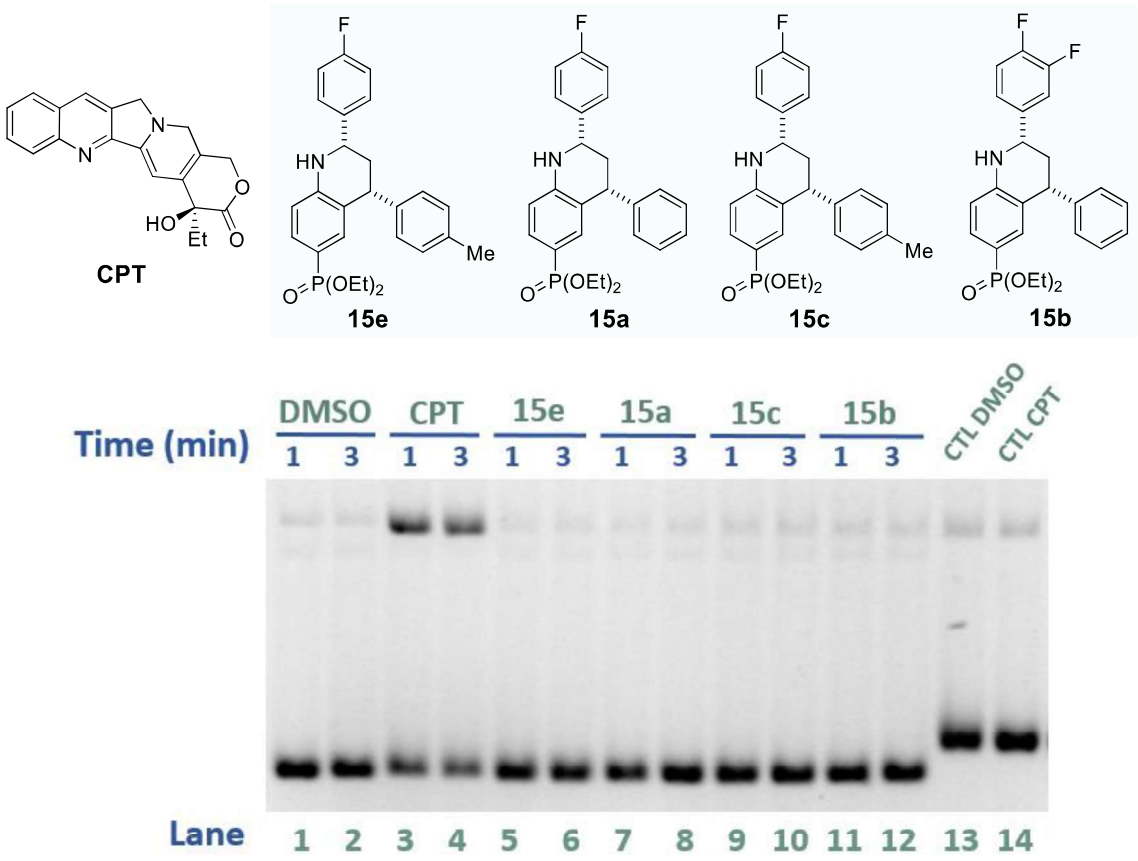
CPT
15e
15a
15c
15b
Time (min)
DMSO
CPT
15e
15a
15c
15b
CTL DMSO
CTL CPT
1 3 1 3 1 3 1 3 1 3 1 3
Lane
1 2 3 4 5 6 7 8 9 10 11 12 13 14

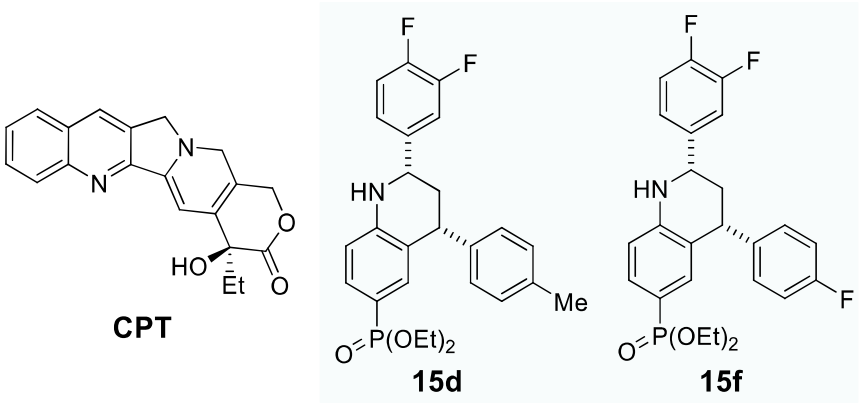
F
F
HN
Me
O
P(OEt)2
F
F
HN
F
O
P(OEt)2
N
N
O
HO
Et
O

CPT **15d** **15f**

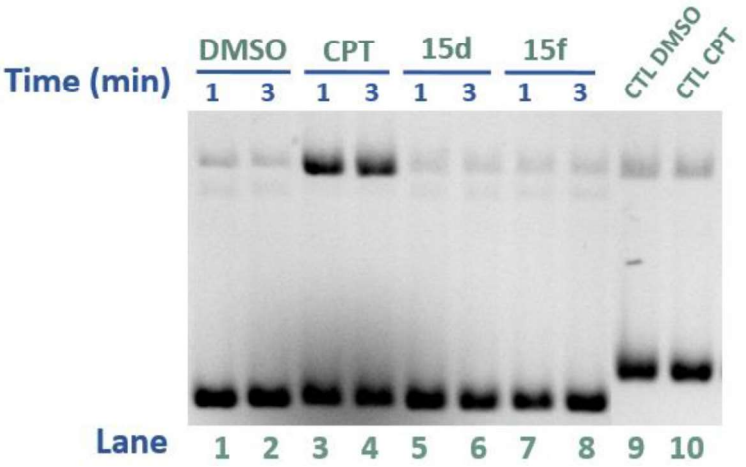
Time (min)
DMSO
CPT
15d
15f
CTL DMSO
CTL CPT
1 3 1 3 1 3 1 3
Lane
1 2 3 4 5 6 7 8 9 10

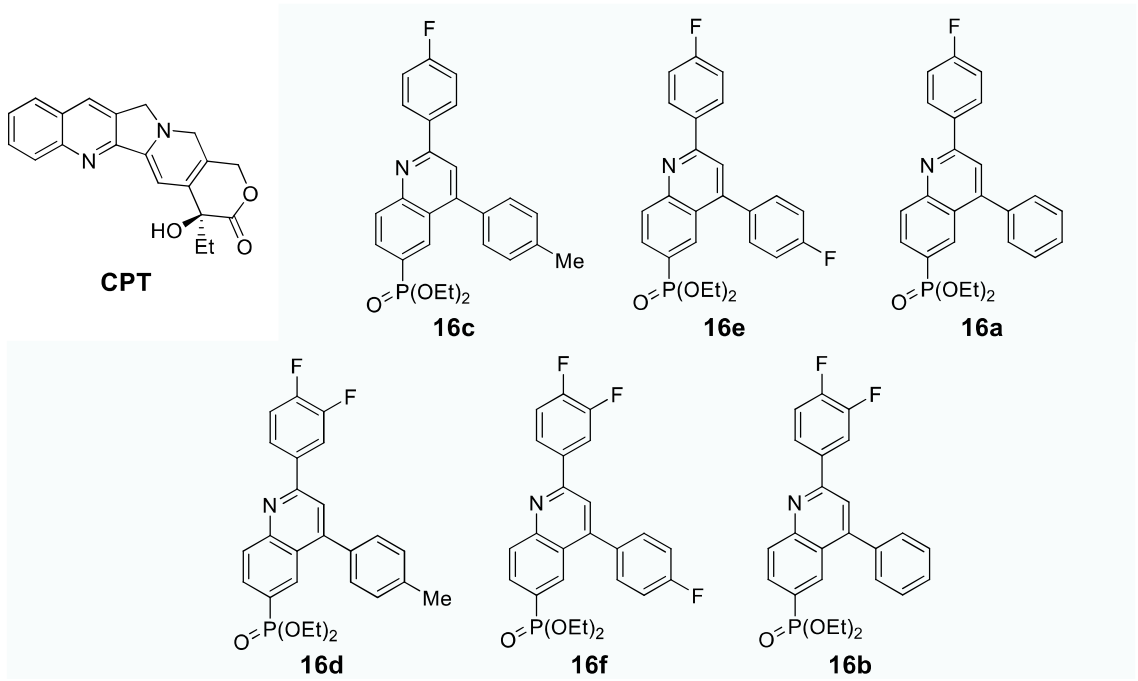
CPT
16c
16e
16a
16d
16f
16b

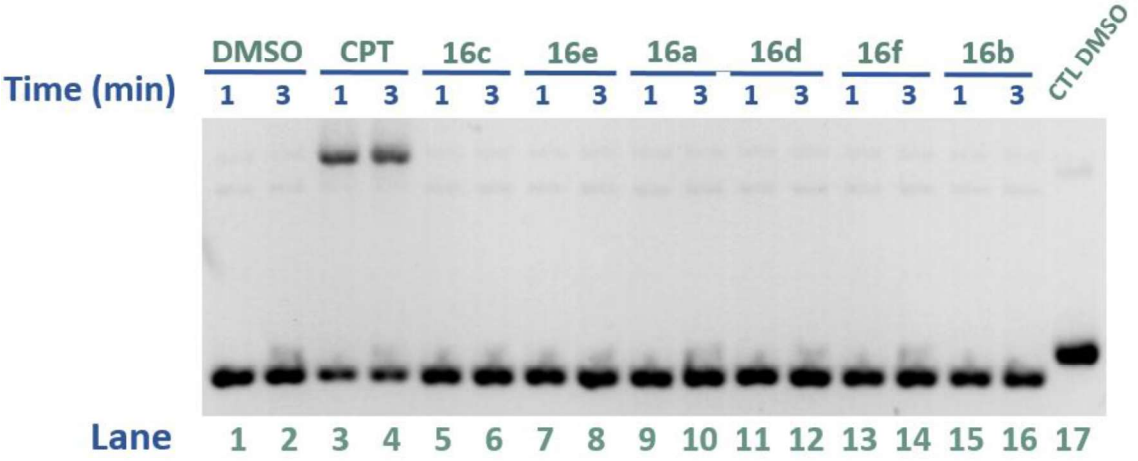
Time (min)
DMSO
CPT
16c
16e
16a
16d
16f
16b
CTL DMSO
1 3 1 3 1 3 1 3 1 3 1 3 1 3 1 3
Lane
1 2 3 4 5 6 7 8 9 10 11 12 13 14 15 16 17

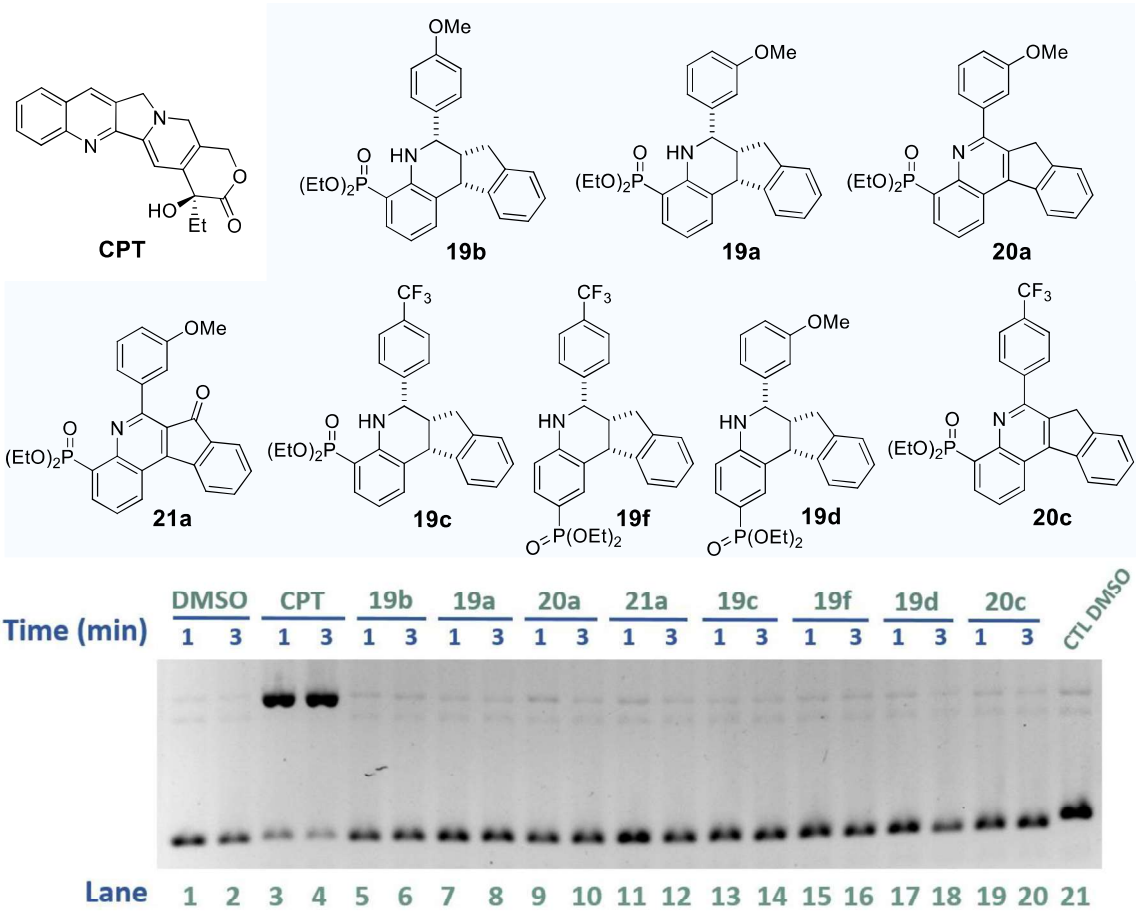
CPT
19b
19a
20a
21a
19c
19f
19d
20c
Time (min)
DMSO
CPT
19b
19a
20a
21a
19c
19f
19d
20c
CTL DMSO
1 3 1 3 1 3 1 3 1 3 1 3 1 3 1 3 1 3 1 3
Lane
1 2 3 4 5 6 7 8 9 10 11 12 13 14 15 16 17 18 19 20 21

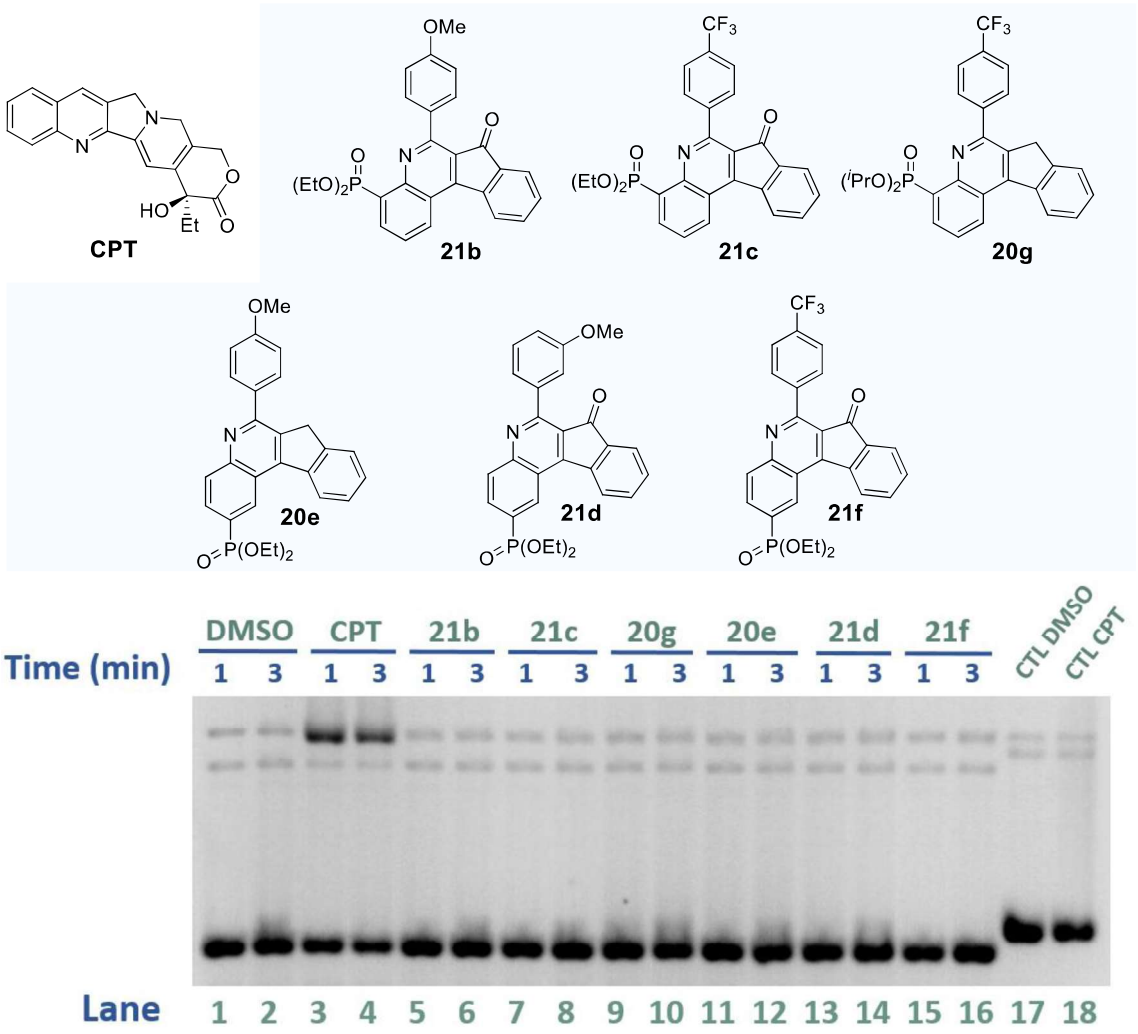
CPT
21b
21c
20g
20e
21d
21f
Time (min)
DMSO
CPT
21b
21c
20g
20e
21d
21f
CTL DMSO
CTL CPT
1 3 1 3 1 3 1 3 1 3 1 3 1 3 1 3
Lane
1 2 3 4 5 6 7 8 9 10 11 12 13 14 15 16 17 18

VI-2.4. Cleavage-religation equilibrium assay

The cleavage-religation equilibrium was investigated by incubating 200 nM of Cy3-labelled DNA substrate (5'-Cy3-ATTTGACCTCGAGAATTATACGAAGTTATTAC-3'/5'-GTAATAACTTCGTATAATTC-TCGAGGTCAAAT-3') with 44 nM of hTOP1B in the presence of 5% v/v DMSO (as negative control), CPT or either compounds **16f**, **13s** or **19a** (as indicated in Chapter II, Figure 49) in a reaction buffer containing 10 mM Tris–HCl, 5 mM $MgCl_2$, 5 mM $CaCl_2$, 50 µg/mL, 150 mM NaCl, (pH 7.5) for 10 min at 37°C. The reactions were stopped by the addition of SDS to a final concentration of 0.2%, EtOH precipitated and trypsinized following standard protocols as described in the literature[95]. The reaction products were analyzed in a 20% denaturing polyacrylamide gel and the product visualized by a Typhoon Scannner FLA 9500.

VI-2.5. REEAD assay

Reagents: all chemicals were purchased from Sigma Aldrich. Phi29 reaction buffer and dNTP were from Thermo Fisher Scientific. The recombinant enzymes Phi29 polimerase and T4 DNA ligase were kindly provided by Dr B.R. Knudsen (Department of Molecular Biology and Genetics, Aarhus University, Aarhus, Denmark). DNA oligonucleotides were purchased from Microsynth Seqlab (Germany).

VI-2.5.1. REEAD-on-slide assay

DNA oligonucleotides for the REEAD-on-a-slide assay:

- 5'-amine REEAD primer: 5'-amine-CCAACCAACCAACCAAATAAG CGATCTTCACAGT- 3'.

- REEAD dumbbell substrate: 5'-AGAAAAATTTTTAAAAAAACTGTGAAGATCGCTTATTT TT TTAAA AATTTTTCTAAGTCTTTTAGATCCCTCAATGCTGCTGCTGTACTACGATCTAAAAGACTTAGA-3'-amine.

- REEAD probe: 5'-FAM- CCTCAATGCTGCTGCTGTACTAC-3'.

The REEAD-on-a-slide procedure: The reactions were carried out onto primer-coupled high density (HD) glass slides (#DHD1-0023 Surmodics, Eden Prairie, MN, USA). Then, 25 mm^2 squared hydrophobic areas were drawn on the glass surface using a fluorescent mini pap pen (#008877 Thermo Fischer, Denmark). The 5'-amine REEAD primer was coupled to the squares of the slides according to the Surmodics manufacturer descriptions. A total of 1 pmol of the REEAD substrate was hybridized to the primer-coupled squares of the slide for 60 min at 37°C. In total, 200 fmol of TOP1 was incubated with the REEAD dumbbell substrate, coupled to the squares of the slide, in 3 µL standard TOP1 reaction buffer containing 10 mM Tris-HCl, 5 mM $CaCl_2$, 5 mM $MgCl_2$, and

150 mM (pH 7.5) or higher concentrations of NaCl as indicated, for 30 min at 37 °C. The circularization reactions were terminated by addition of 0.3% SDS. The slides were washed for one minute at room temperature in wash buffer 1 (0.1 M Tris-HCl, 150 mM NaCl, and 0.3% SDS, pH 7.5) followed by one minute at room temperature in wash buffer 2 (0.1 M Tris-HCl, 150 mM NaCl, and 0.05% Tween-20, pH 7.5). Finally, the slides were dehydrated in 99.9% ethanol for one minute and air-dried. The RCA was performed for 60 min at 37 ◦C in 1× phi29 buffer (50 mM Tris-HCl, 10 mM $MgCl_2$, 10 mM $(NH_4)_2SO_4$, 4 mM DTT pH 7.5) supplemented with 0.2 µg/µL BSA, 250 µM dNTP, and 1 Unit/µL Phi29 DNA polymerase, according to commercial vendor guidelines. The RCA reaction was stopped by washing the slide for 10 min in wash buffer 1, followed by one minute in wash buffer 2 and one minute in 99.9% ethanol and the slide was then air-dried. The Rolling Circle Products (RCPs) were detected by hybridization of 0.17 µM of REEAD fluorescent probe in a buffer containing 20% formamide, 2× SSC (300 mM NaCl, 30 mM sodium citrate) and 5% glycerol for 30 min at 37 °C. The slides were washed for one minute in wash buffer 1 followed by one minute in wash buffer 2, dehydrated with 99.9% ethanol, mounted with Vectashield (#H-100 Vector laboratories, Burlingame, CA, USA), and visualized in a Olympus IX73/Olympus IX71 fluorescent microscope. Fifteen pictures for every square of the slide were taken using a 63x/60x objective and the TOP1 activity was quantified counting the fluorescent dots using the Image J software

VI-2.5.2. (C/L) REEAD assay

DNA oligonucleotides for the (C/L) REEAD assay:

-5'-amine REEAD (C/L) primer: 5'-amine-CCAACCAACCAACCAAGGAGCCAAACATGTGCATTGAGG-3'.

-Cleavage half-dumbbell: 5'-phospho-AAAAATTTTTTCTAAGTCTTTTACCCTCAATGCACATGTTTG GCTCCGTAAAAGACTTAGA-3'-amine.

-Ligator half-dumbbell: 5'-AGAAAAAATTTTTAGCTCGAACTGTGAAGATCGCTTATTCGAGCT-3'.

- REEAD (C/L) probe: 5'-FAM-ACTGTGAAGATCGCTTAT-3'

(C/L) REEAD procedure: The reactions were carried out onto primer-coupled HD glass slides as described for the REEAD-on-a-slide. The 5'-amine REEAD (C/L) primer was coupled to the squares of the slides according to the Surmodics manufacturer descriptions. In total, 1 pmol of cleavage-half-dumbbell substrate was hybridized to the primer-coupled slides. To measure the effect of the studied compounds on the binding/cleavage step of TOP1 catalytic cycle, 200 fmol

of purified TOP1 was added to the cleavage half-dumbbell-coupled squares of the slide in 3 µL of a standard TOP1 reaction buffer containing 10 mM Tris-HCl, 5 mM $CaCl_2$, 5 mM $MgCl_2$, 100 mM NaCl (pH 7.5) for 30 min at 37°C and in the presence of 5% DMSO, or 50 µM CPT or 50 µM of the studied compounds. Note, the substrate was added in an approximate five-time surplus compared to enzyme. Since, the enzyme was consumed in this dead-end reaction this ensured sufficient surplus of substrate in the duration of the experiment for the potential inhibitory effect of the added compounds to be measured. The slides were then washed twice for three minutes with a buffer containing 10 mM Tris-HCL (pH 7.5) and 1 mM EDTA to remove all traces of DMSO, CPT or the studied compound. Subsequently, 3 µL standard TOP1 reaction buffer with 200 pmol ligator-half dumbbell and 500 mM NaCl was added to the squares of the slide and incubated for 60 min at 37°C. The slides were then washed for one minute in wash buffer 1, one minute in wash buffer 2 and one minute in 99.9% ethanol as described in the REEAD-on slide. The circularization reactions were completed by the addition of 10 Unit/µL of T4 DNA-ligase in a buffer containing 50 mM Tris-HCl, 10 mM $MgCl_2$, 1mM ATP (pH 7.5) for 60 min at 25°C. The slides were washed in wash buffers 1 and 2 and dehydrated. RCA was performed as described in the REEAD-on-a-slide procedure and the RCPs were detected by hybridization to 0.17 µM of REEAD (C/L) probe in a buffer containing 20% formamide, 2× SSC (300 mM NaCl, 30 mM Sodium citrate) and 5% glycerol for 30 min at 37°C. RCPs were visualized and quantified as described in the REEAD-on-a-slide the literature[247]. For the measurement of the inhibition of the ligation step of the TOP1 catalytic cycle, cleavage was performed as described above, but in the absence of any added inhibitor. Subsequently, 3 µL of standard TOP1 buffer with 200 pmol ligator-half dumbbell and 500 mM NaCl was added to the squares of the slide in the presence of 5% DMSO, 50 µM CPT or 50 µM of the investigated compounds and incubated for 10 min at 37°C. The circularization and rolling circle amplification were completed as described for the measurement of the inhibition of the REEAD-on-a-slide.

VI-3. Cell viability assays

VI-3.1. Cell culture

A-549 (CCL-185™), SK-OV-3 (HTB-77™) and MRC-5 (CCL-171™) human cell lines were purchased from the American Type Culture Collection (ATCC). HEK-293 human cell line was obtained from Cell Lines Service (CLS). RPMI-8402 and CPT-K5 human suspension cell lines were kindly gifted by Dr. B.R. Knudsen (Department of Molecular Biology and Genetics, Aarhus University, Aarhus, Denmark).

Cells were cultured according to manufacturer´s guidelines in their respectives cell-culture media supplemented with 10% v/v heat-inactivated fetal bovine serum and 1x Normocin™ (InvivoGen) antimicrobial agent (*except when doing the siRNA transfection with HEK-293 cells, which were cultured without any antimicrobial agent). RPMI-8402 and CPT-K5 cell lines were cultured with 100 units/mL penicillin and 100 mg/mL streptomycin (Sigma Aldrich) instead of Normocin™. Herein are exposed the respective cell-culture media:

-A-549 cells ere cultured in F12-K medium (Gibco).

-SK-OV-3 cells were cultured in Mc Coy 5 a modified medium (Gibco).

-MRC-5 cells were cultured in EMEM medium (Gibco).

-HEK-293 and HEK 293 KD cells were cultured in DMEM medium (Gibco).

-RPMI-8402 and CPT-K5 cells were cultured in RPMI 1640 medium (Gibco).

The cell cultures were plated into 25/75/150 cm^2 culture flasks for growth in a humidified incubator under standard mammalian cell-culture conditions (37^oC, 5% CO_2, 90% relative humidity).

Monolayer adherent cell lines (A-549, SK-OV-3, HEK-293, HEK-293 KD and MRC-5) were grown attached to a solid support (the bottom of the culture flask) and the media was replaced every 3 days and/or were split to maintain ~70-75% of cell-confluence. The cells were harvested by trypsin treatment for 1 min at 37^oC (0.25% trypsin-EDTA solution, Sigma Aldrich) upon two consecutive washes with PBS (phosphate buffered saline).

Suspension cell lines (RPMI-8402 and CPT-K5) were grown as single cells. 0.5-0.7·10^6 cells/mL were seeded and a concentration of 0.3-1.5·10^6 cell/mL was maintained splitting by dilution or by replacement of the media (by centrifugation at 100 × g for 5 min to resuspend the resultant pellet into fresh media) when the colour indicator turned into yellow (every 4-5 days).

VI-3.2. CCK-8 cell viability assays

For the cell viability assay with adherent human cell lines (A-549, SK-OV-3, HEK-293 and MRC-5), first 3000 cells/100 µL culture media were seeded into 96-well plates and the cells were incubated under standard mammalian cell-culture conditions (37°C, 5% CO_2, 90% relative humidity). After 24 h, the old culture media was replaced by fresh medium containing DMSO 0.5% or dilutions of fresh medium with different concentrations of the investigated compounds in 0.5% DMSO (see the cell viability graphs for each concentration-range) and were incubated for 48 h under standard mammalian cell-culture conditions (37°C, 5% CO_2, 90% relative humidity). Upon 48 h after the drug treatment, 10 µL of CCK-8 cell viability reagent was added to each well and the plates were further incubated for 2 h before measuring the absorbance in an automatic ELISA plate reader system (Multiskan™ FC Photometer, Thermo Fischer) at 450 nm wavelength. The absorbance values were processed and plotted using GraphPad Prism 5.01 software to obtain the cell viability graphs and the GI_{50} values (given as the mean ± the SD of the mean from quadruplicate experiments).

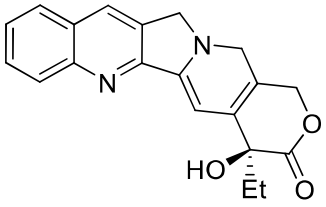

CPT

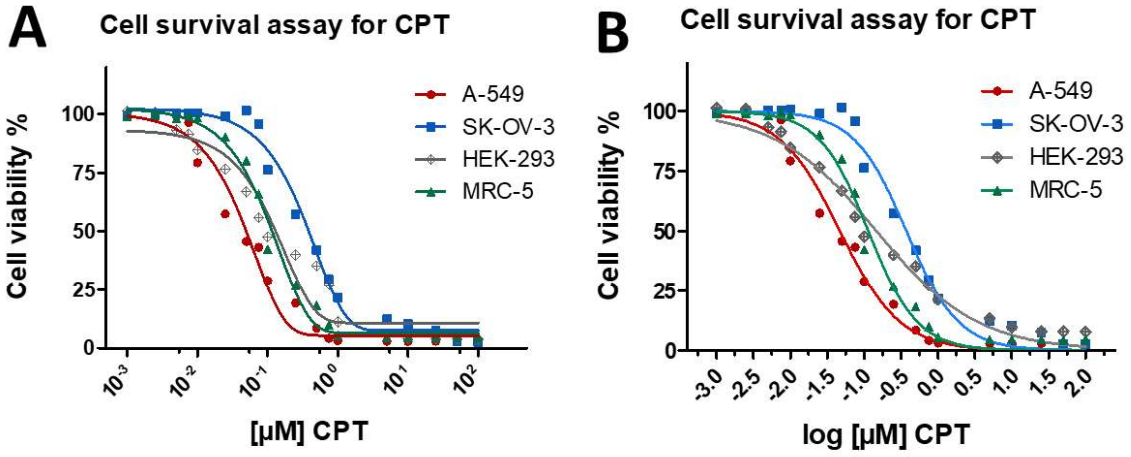

A-549 GI_{50}: 47.14 ± 3.39 nM

SK-OV-3 GI_{50}: 0.37 ± 0.01 µM

HEK-293 GI_{50}: 0.15 ± 0.02 µM

MRC-5 GI_{50}: 0.11 ± 0.02 µM

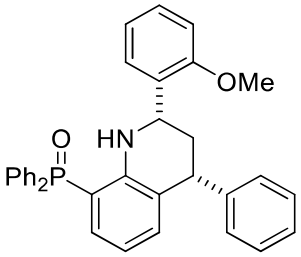

6a

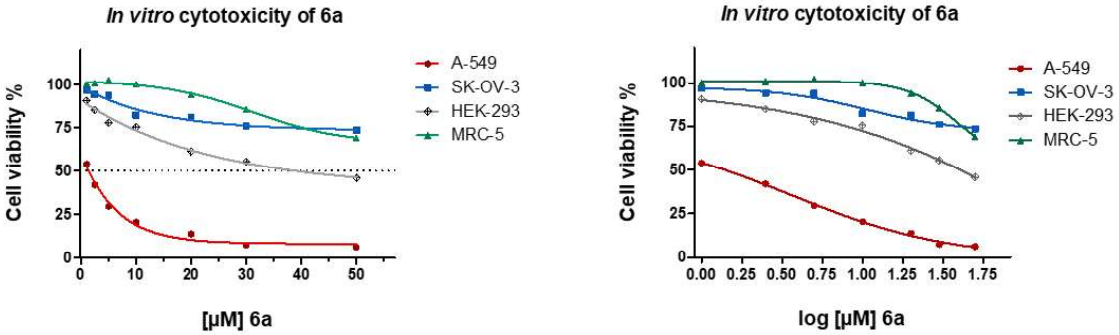

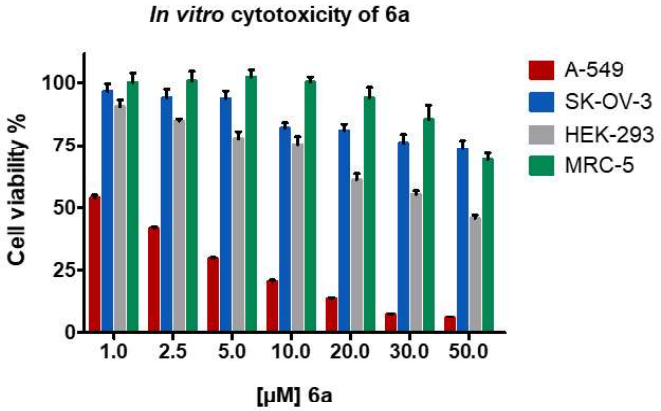

A-549 GI_{50}: 1.40 ± 0.13 μM

SK-OV-3 GI_{50}: > 50 μM

HEK-293 GI_{50}: 16.26 ± 1.11 μM

MRC-5 GI_{50}: > 50 μM

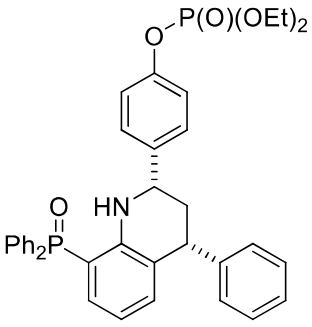

6b

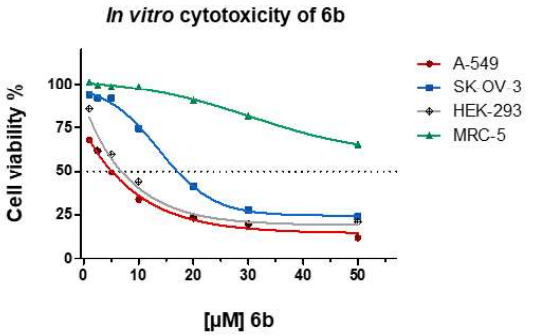

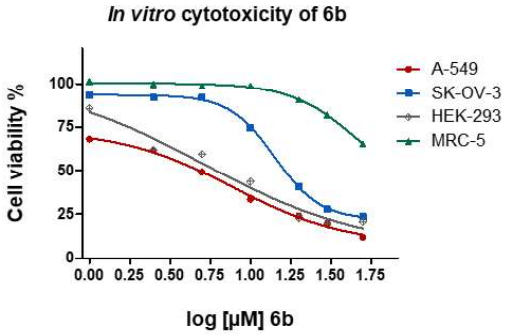

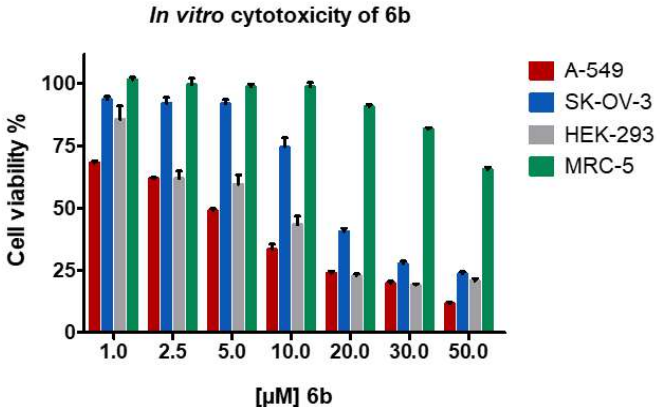

A-549 GI_{50}: 5.06 ± 0.28 µM

SK-OV-3 GI_{50}: 17.41 ± 1.55 µM

HEK-293 GI_{50}: 6.03 ± 1.58 µM

MRC-5 GI_{50}: > 50 µM

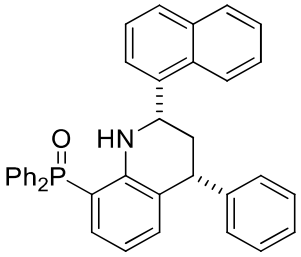

6c

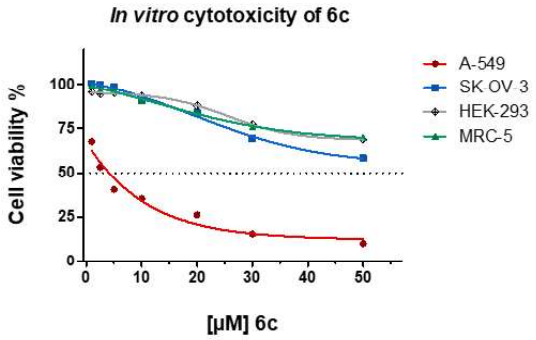

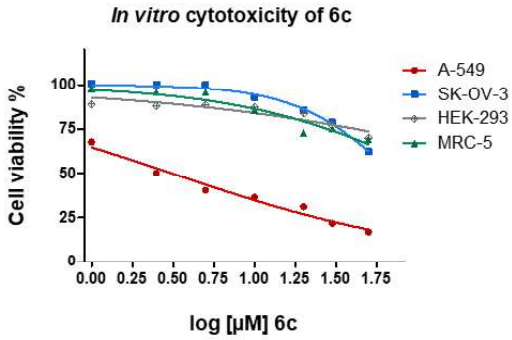

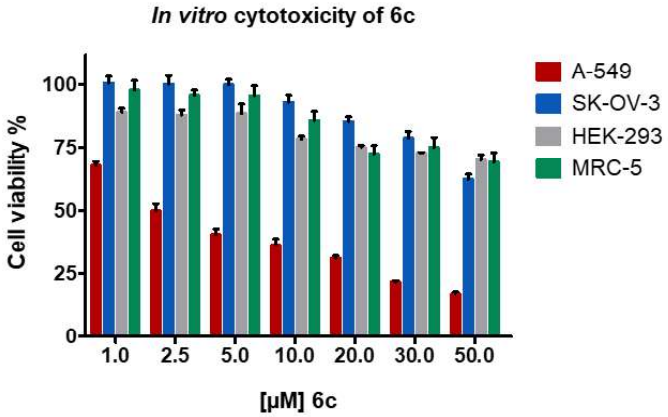

A-549 GI_{50}: 3.57 ± 0.31 µM

SK-OV-3 GI_{50}: > 50 µM

HEK-293 GI_{50}: > 50 µM

MRC-5 GI_{50}: > 50 µM

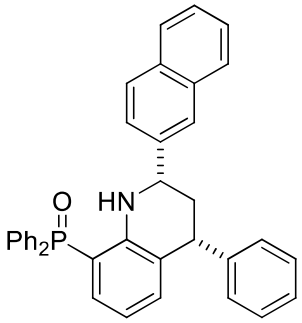

6d

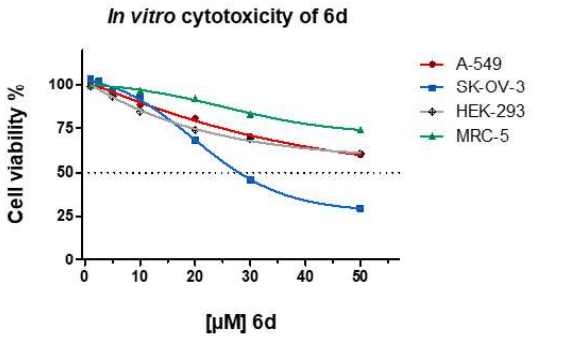

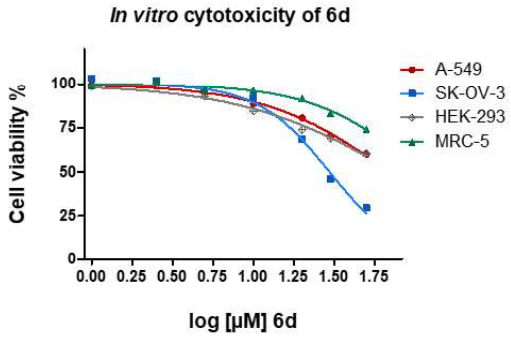

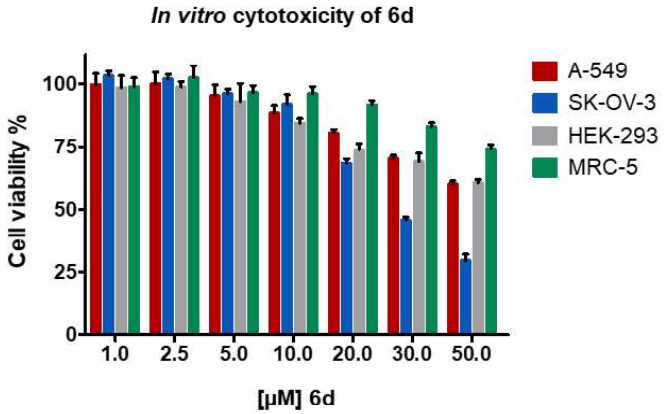

A-549 GI_{50}: > 50 µM

SK-OV-3 GI_{50}: 26.68 ± 3.21 µM

HEK-293 GI_{50}: > 50 µM

MRC-5 GI_{50}: > 50 µM

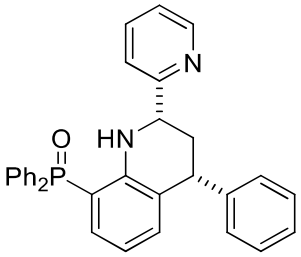

6e

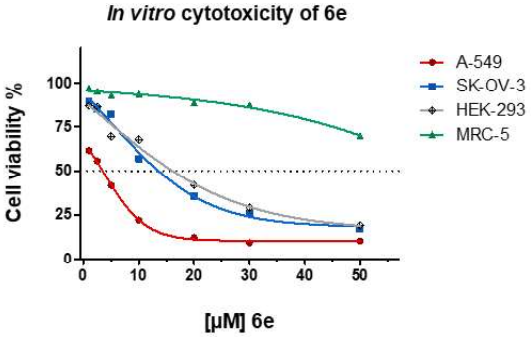

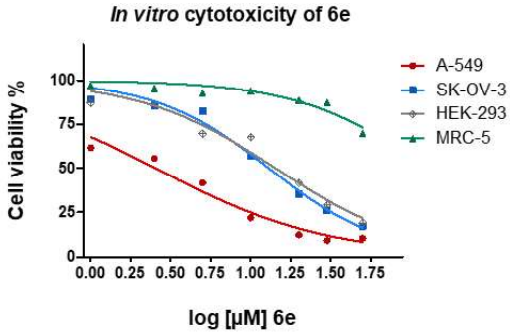

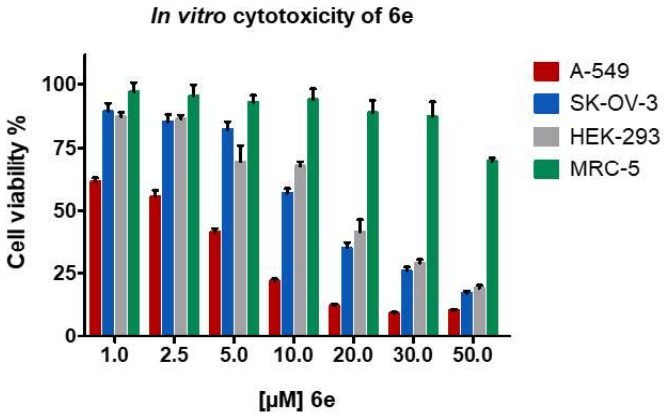

A-549 GI_{50}: 2.26 ± 0.21 µM

SK-OV-3 GI_{50}: 14.83 ± 2.56 µM

HEK-293 GI_{50}: 19.07 ± 3.56 µM

MRC-5 GI_{50}: > 50 µM

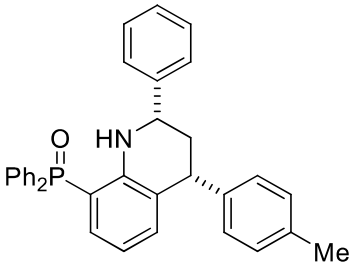

6f

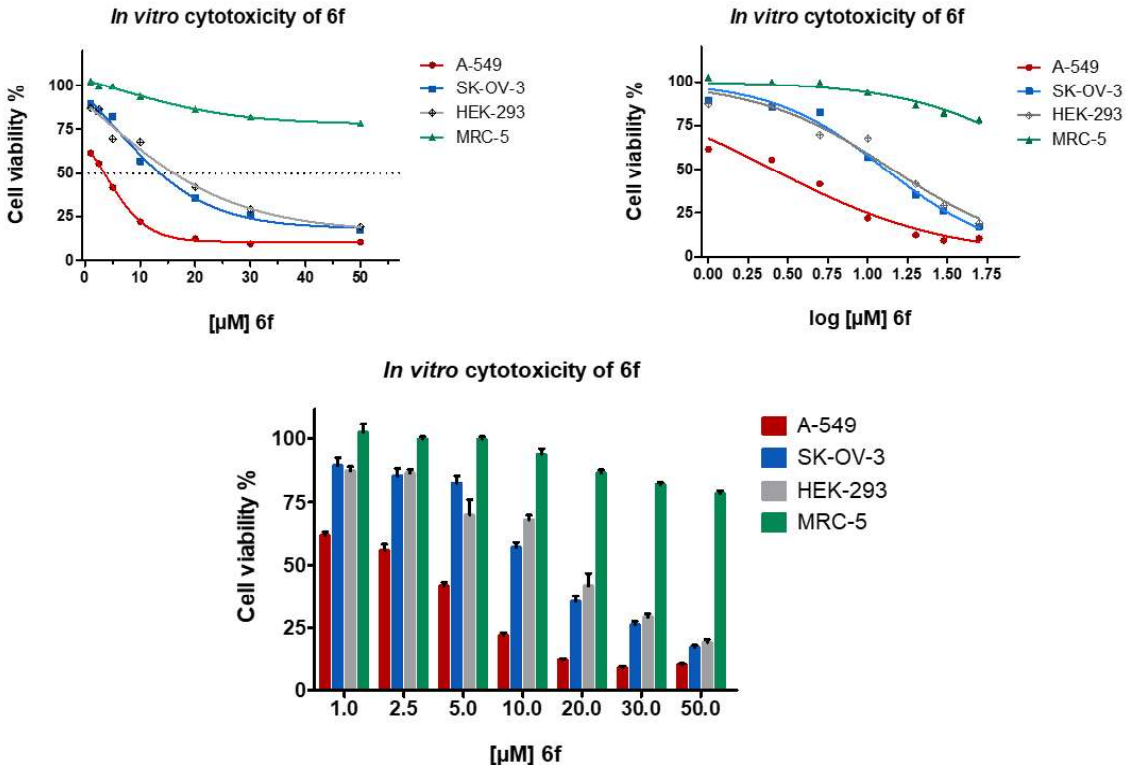

A-549 GI_{50}: 1.20 ± 0.12 µM

SK-OV-3 GI_{50}: > 50 µM

HEK-293 GI_{50}: 28.00 ± 2.26 µM

MRC-5 GI_{50}: > 50 µM

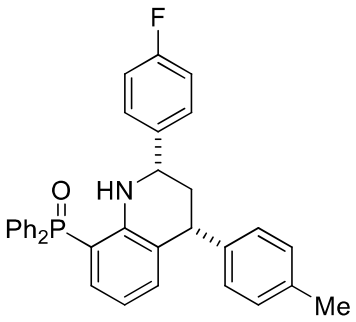

6g

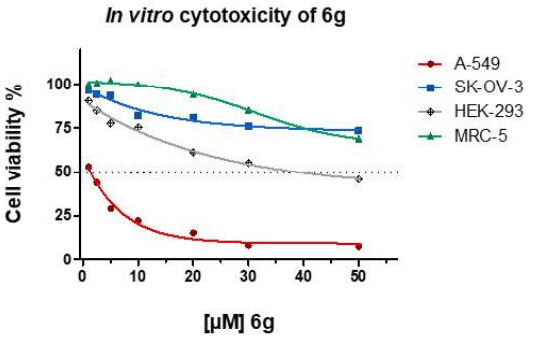

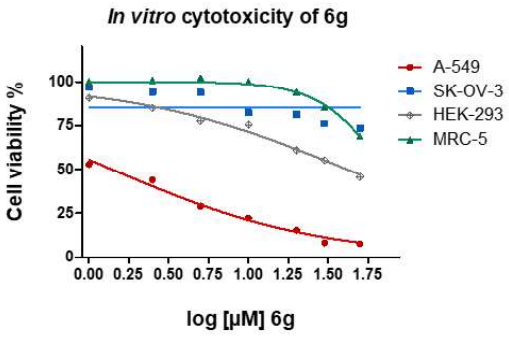

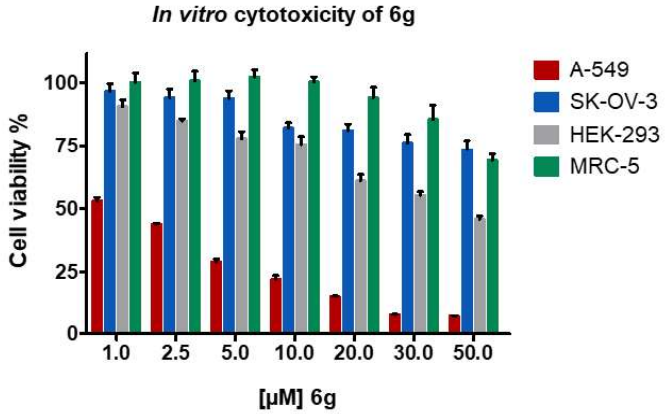

A-549 GI_{50}: 1.32 ± 0.15 µM

SK-OV-3 GI_{50}: > 50 µM

HEK-293 GI_{50}: 38.34 ± 3.54 µM

MRC-5 GI_{50}: > 50 µM

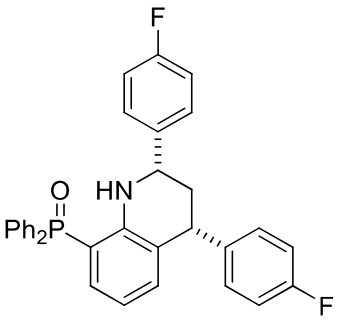

6h

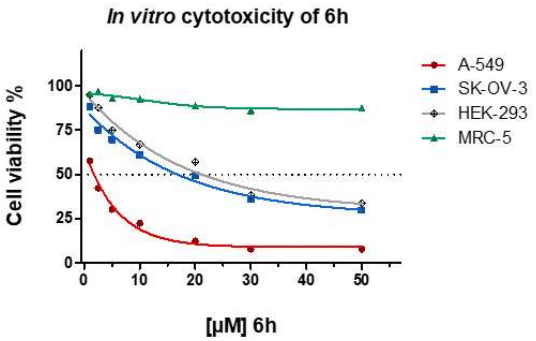

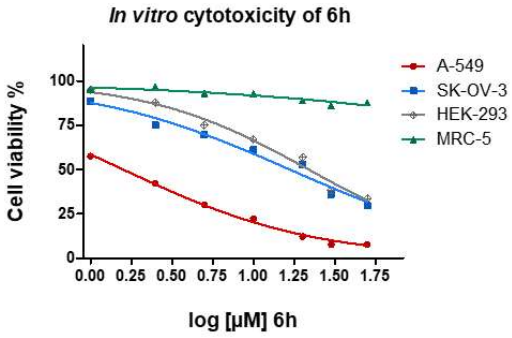

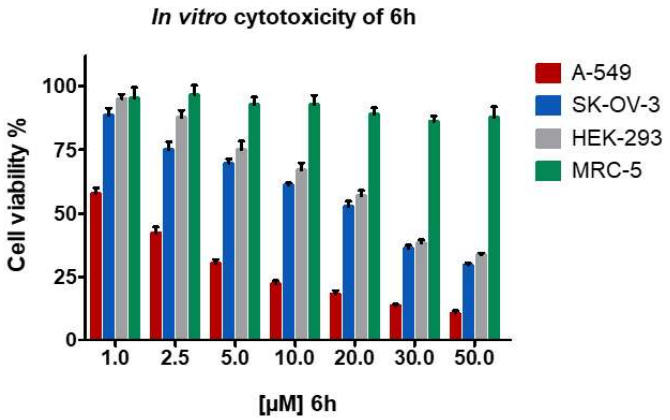

A-549 GI_{50}: 1.35 ± 0.53 µM

SK-OV-3 GI_{50}: 17.79 ± 5.45 µM

HEK-293 GI_{50}: 23.88 ± 4.05 µM

MRC-5 GI_{50}: > 50 µM

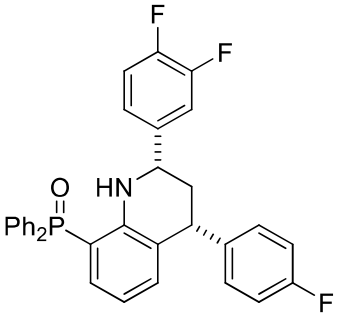

6i

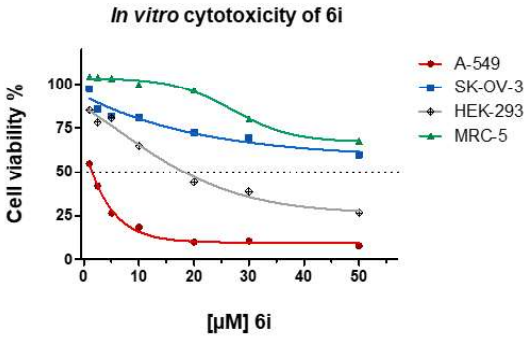

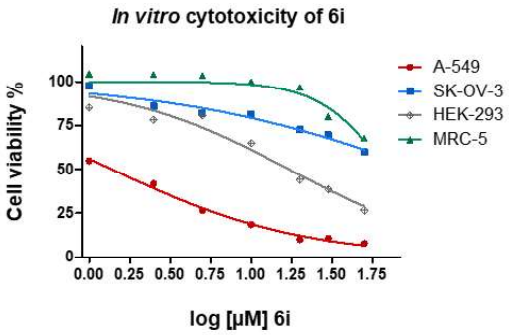

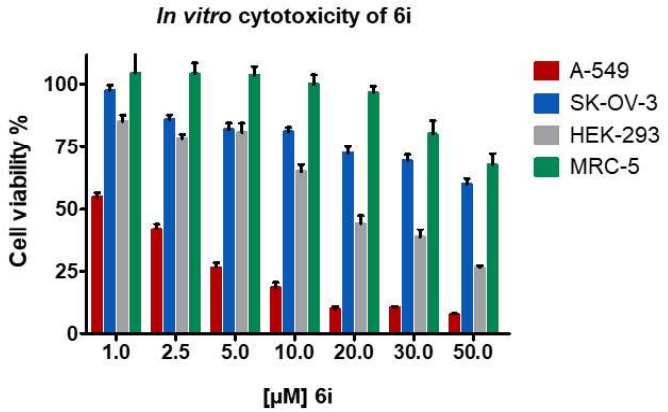

A-549 GI_{50}: 1.32 ± 0.21 µM

SK-OV-3 GI_{50}: > 50 µM

HEK-293 GI_{50}: 18.01 ± 3.37 µM

MRC-5 GI_{50}: > 50 µM

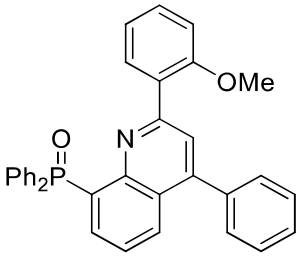

7a

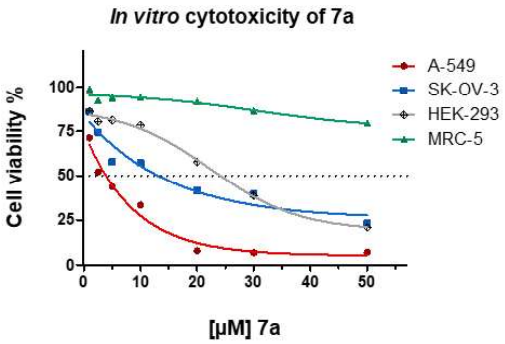

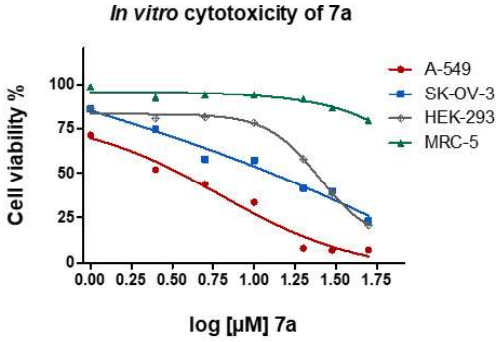

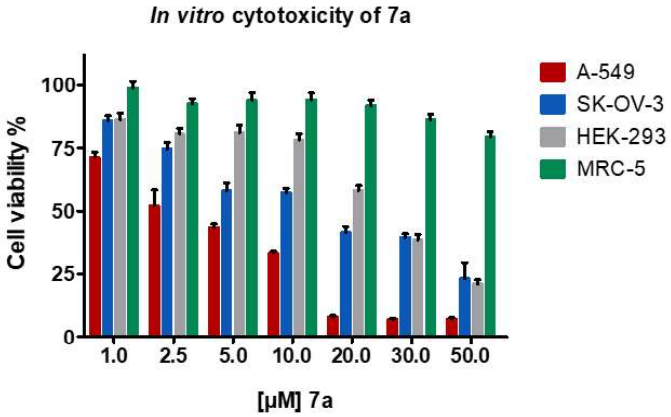

A-549 GI_{50}: 3.11 ± 0.65 µM

SK-OV-3 GI_{50}: 13.06 ± 1.80 µM

HEK-293 GI_{50}: 24.13 ± 1.76 µM

MRC-5 GI_{50}: > 50 µM

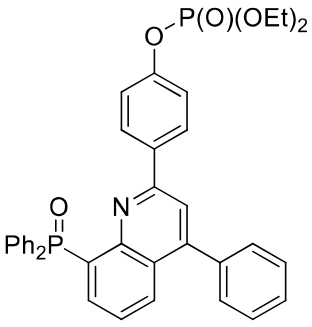

7b

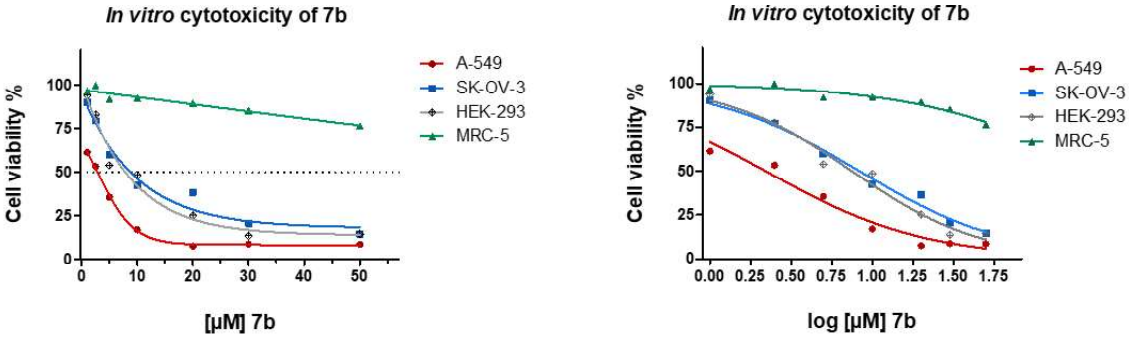

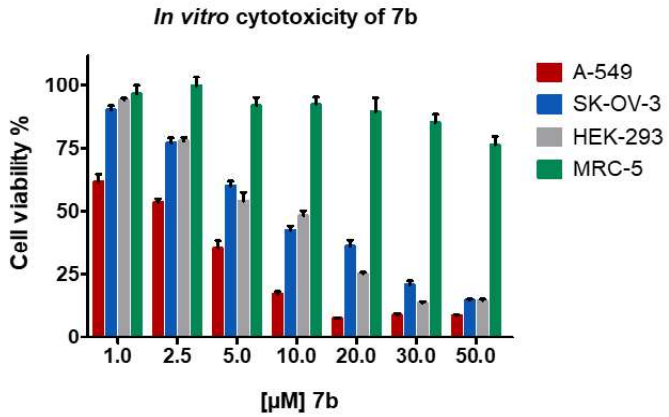

A-549 GI_{50}: 1.80 ± 0.41 µM

SK-OV-3 GI_{50}: 8.36 ± 0.38 µM

HEK-293 GI_{50}: 7.62 ± 0.38 µM

MRC-5 GI_{50}: > 50 µM

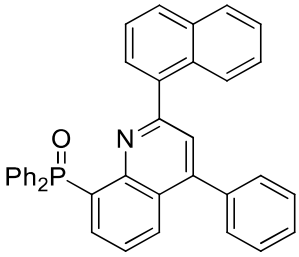

7c

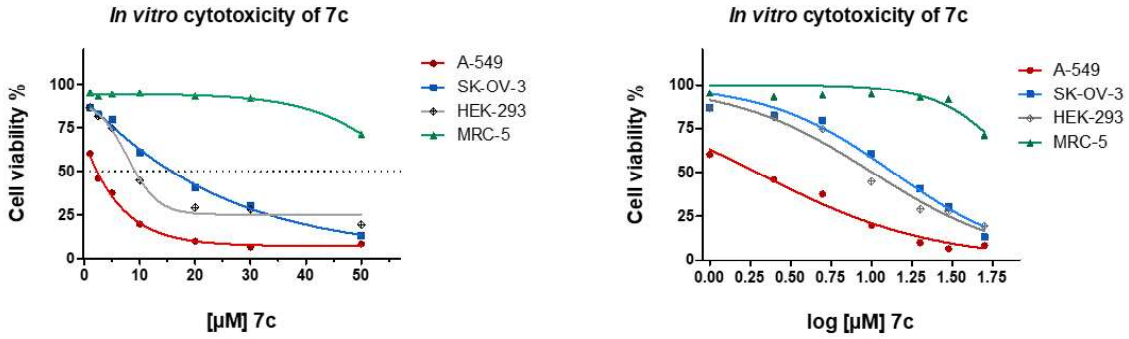

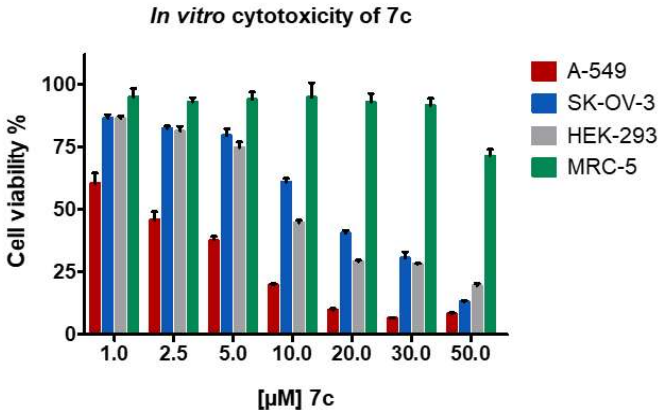

A-549 GI_{50}: 1.68 ± 0.39 μM

SK-OV-3 GI_{50}: 14.48 ± 1.55 μM

HEK-293 GI_{50}: 10.47 ± 0.47 μM

MRC-5 GI_{50}: > 50 μM

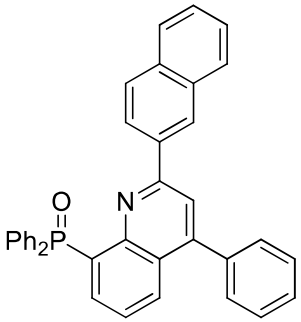

7d

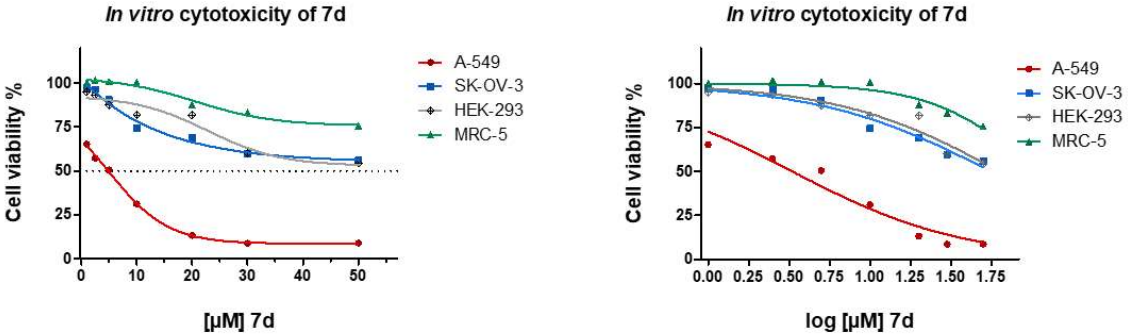

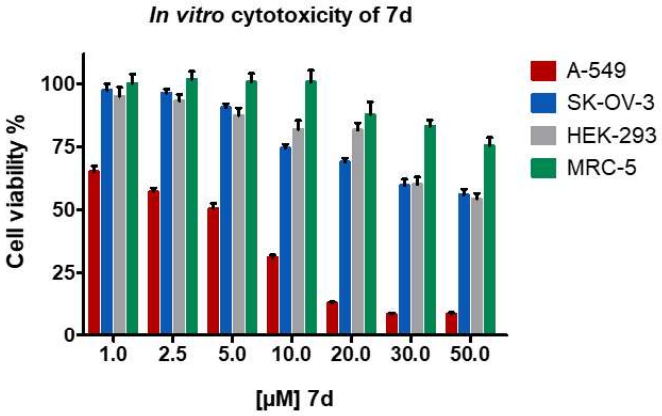

A-549 GI_{50}: 6.32 ± 1.09 µM

SK-OV-3 GI_{50}: > 50 µM

HEK-293 GI_{50}: > 50 µM

MRC-5 GI_{50}: > 50 µM

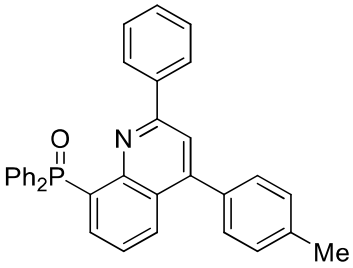

7f

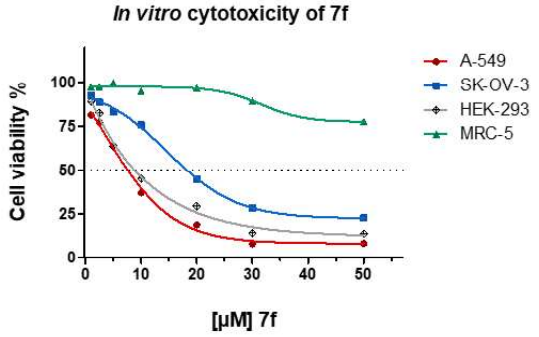

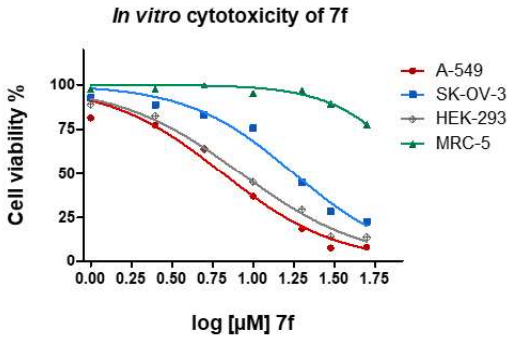

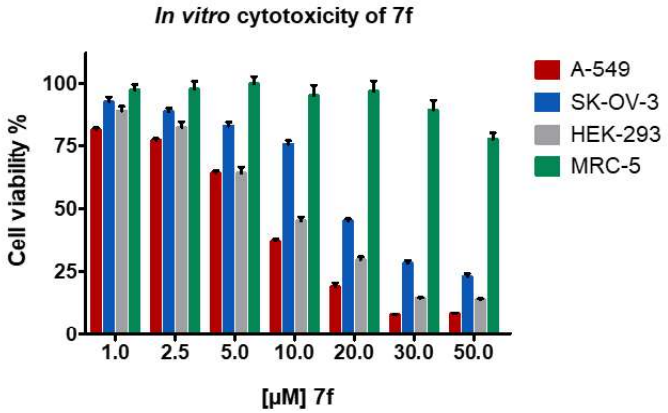

A-549 GI_{50}: 7.65 ± 0.90 µM

SK-OV-3 GI_{50}: 17.38 ± 1.58 µM

HEK-293 GI_{50}: 8.97 ± 0.54 µM

MRC-5 GI_{50}: > 50 µM

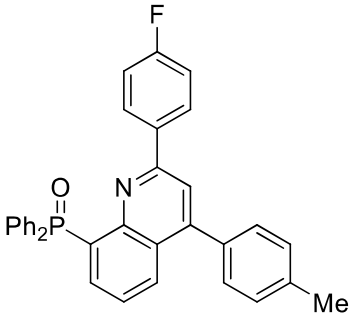

7g

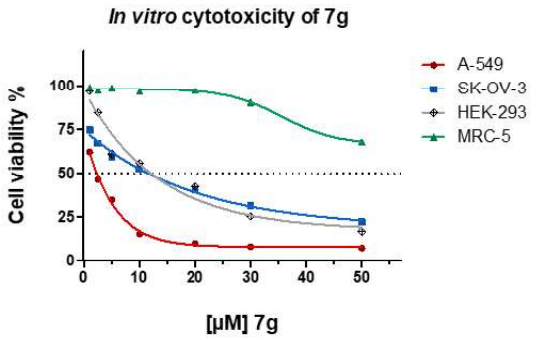

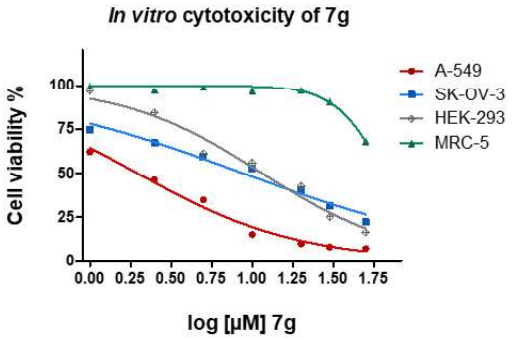

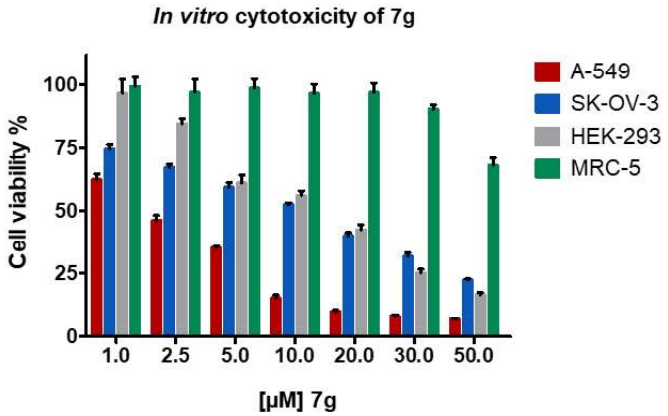

A-549 GI_{50}: 2.64 ± 0.43 μM

SK-OV-3 GI_{50}: 10.51 ± 2.20 μM

HEK-293 GI_{50}: 10.88 ± 0.78 μM

MRC-5 GI_{50}: > 50 μM

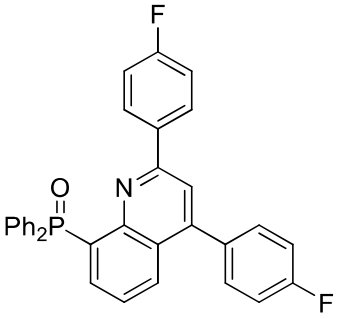

7h

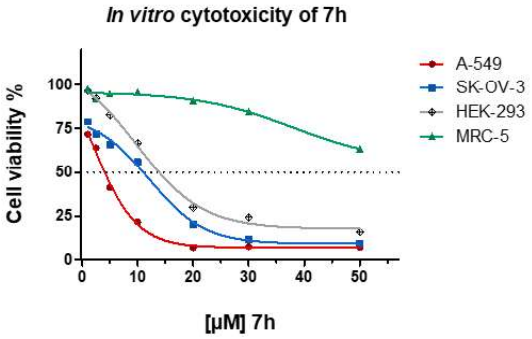

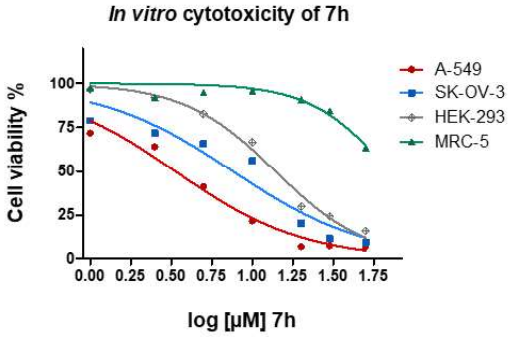

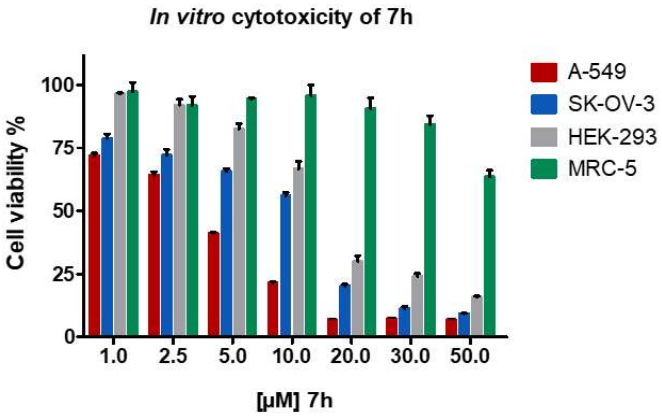

A-549 GI_{50}: 3.82 ± 0.42 µM

SK-OV-3 GI_{50}: 6.77 ± 0.85 µM

HEK-293 GI_{50}: 12.46 ± 0.87 µM

MRC-5 GI_{50}: > 50 µM

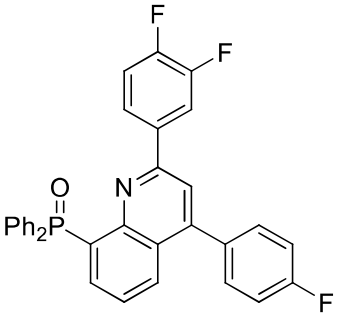

7i

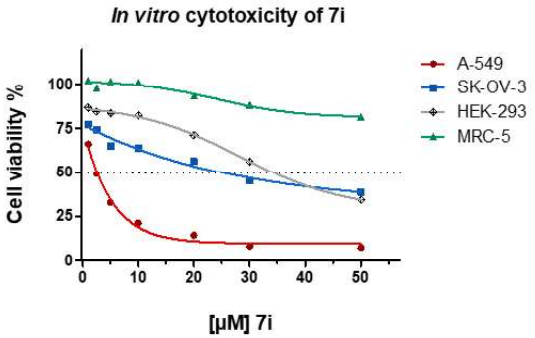

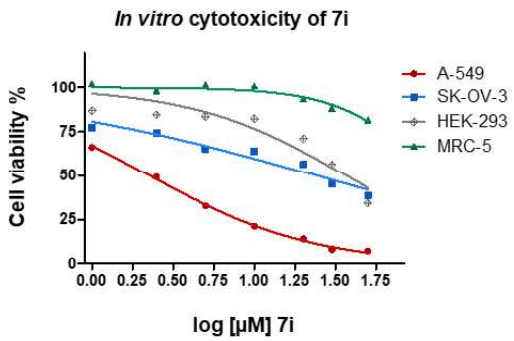

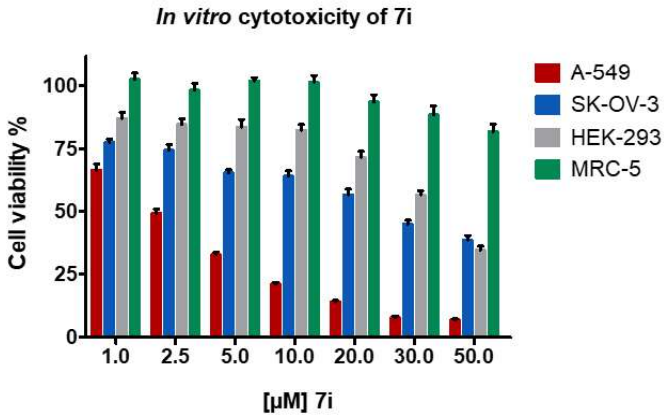

A-549 GI_{50}: 2.22 ± 0.34μM

SK-OV-3 GI_{50}: 26.26 ± 8.09 μM

HEK-293 GI_{50}: 35.63 ± 7.95 μM

MRC-5 GI_{50}: > 50 μM

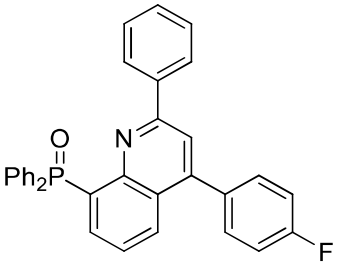

7j

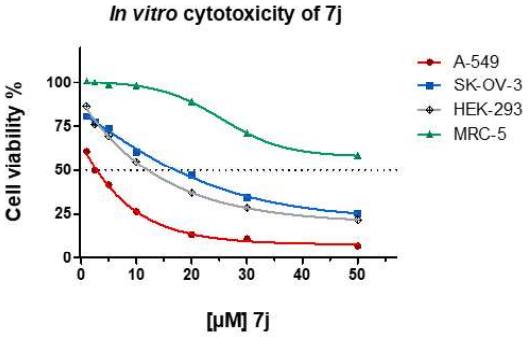

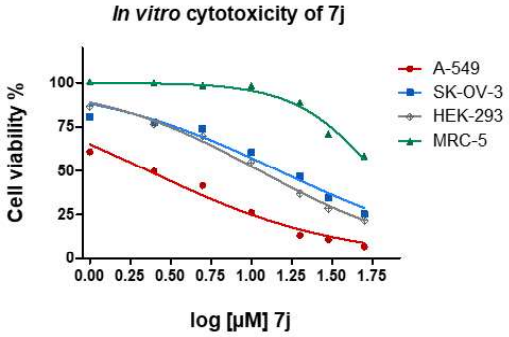

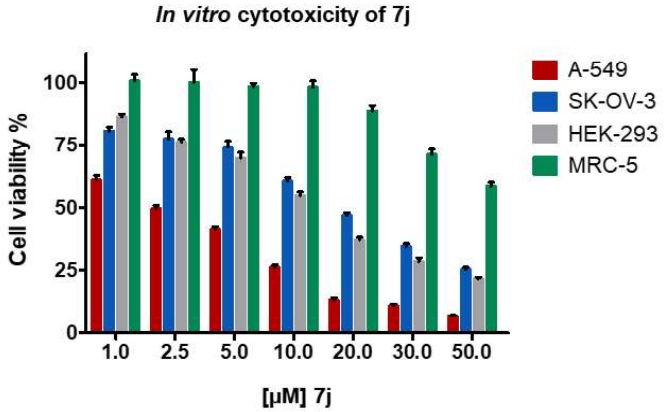

A-549 GI_{50}: 2.59 ± 0.77 µM

SK-OV-3 GI_{50}: 16.52 ± 2.07 µM

HEK-293 GI_{50}: 12.43 ± 1.11 µM

MRC-5 GI_{50}: > 50 µM

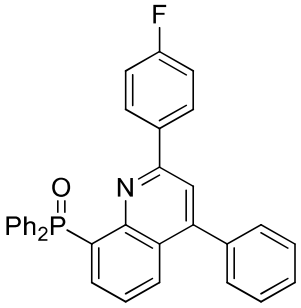

7k

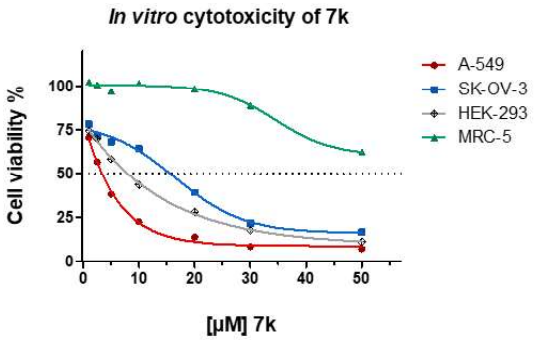

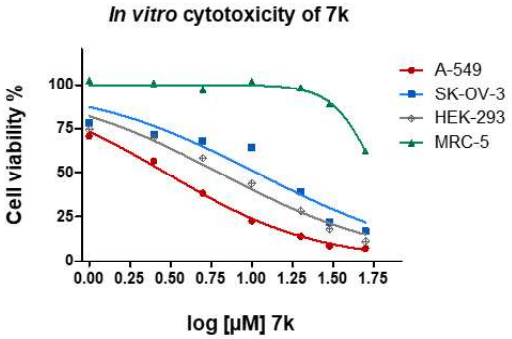

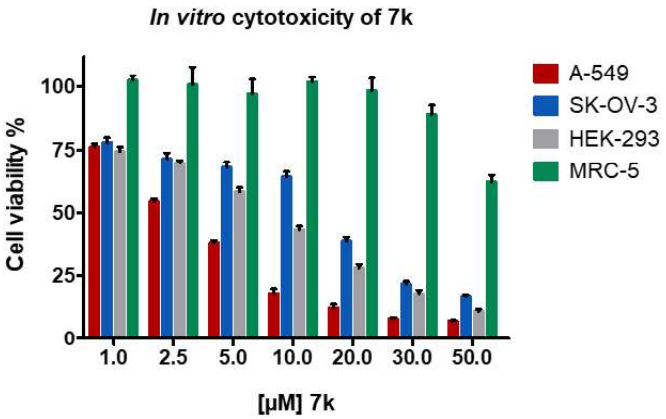

A-549 GI_{50}: 3.80 ± 1.21 µM

SK-OV-3 GI_{50}: 17.17 ± 2.98 µM

HEK-293 GI_{50}: 8.16 ± 1.99 µM

MRC-5 GI_{50}: > 50 µM

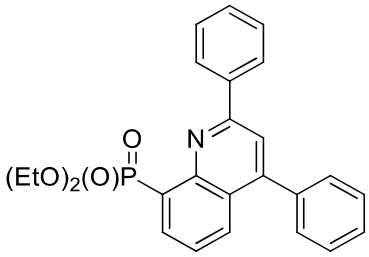

13a

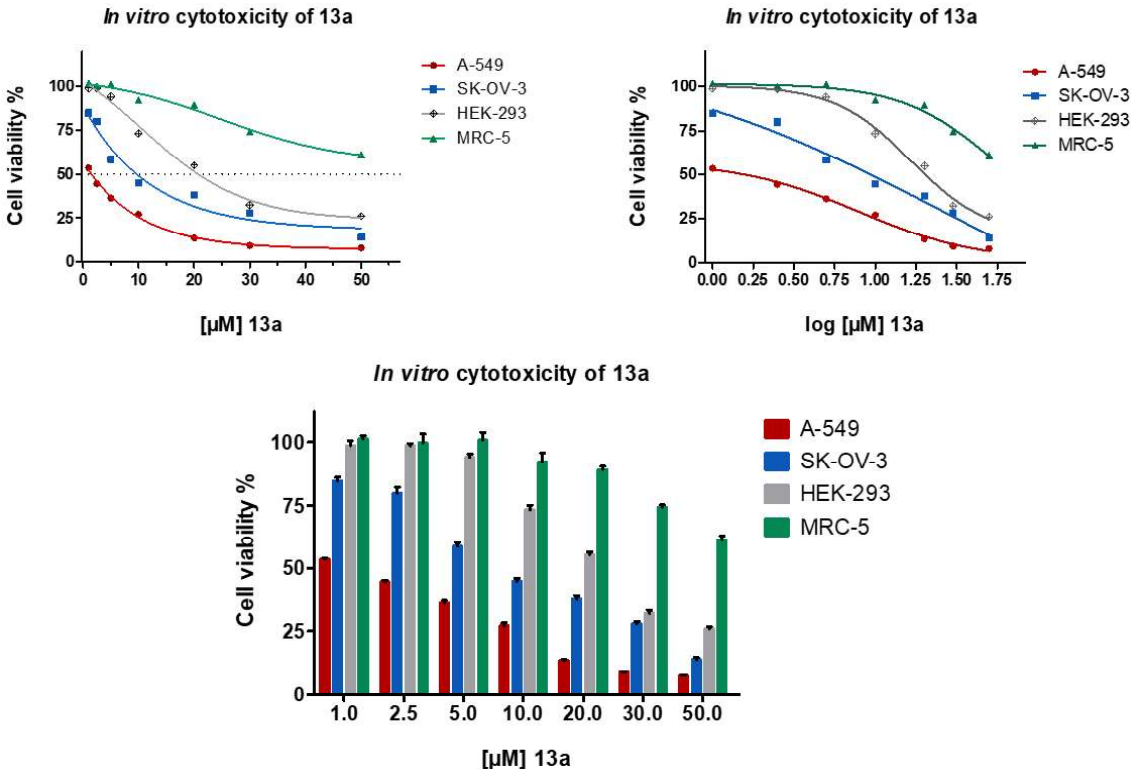

A-549 GI_{50}: 2.26 ± 0.59 µM

SK-OV-3 GI_{50}: 9.30 ± 0.76 µM

HEK-293 GI_{50}: 27.29 ± 2.22 µM

MRC-5 GI_{50}: > 50 µM

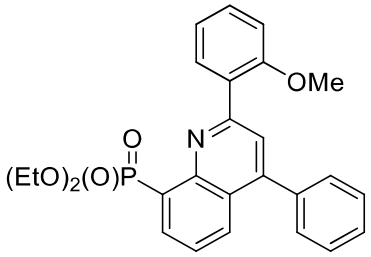

13b

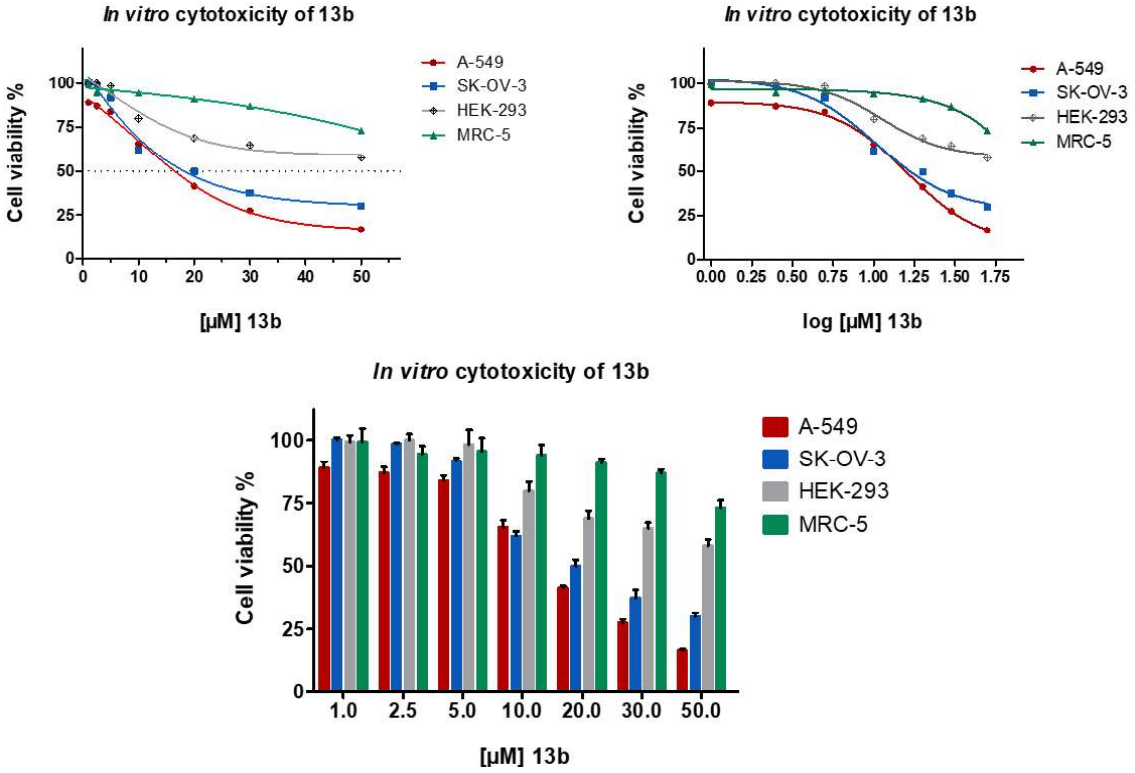

A-549 GI_{50}: 17.26 ± 4.07 µM

SK-OV-3 GI_{50}: 19.38 ± 4.07 µM

HEK-293 GI_{50}: > 50 µM

MRC-5 GI_{50}: > 50 µM

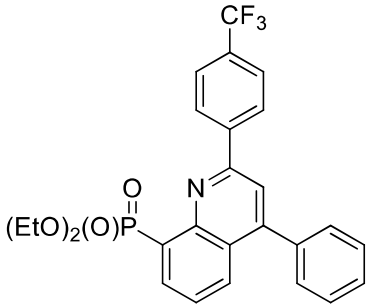

13c

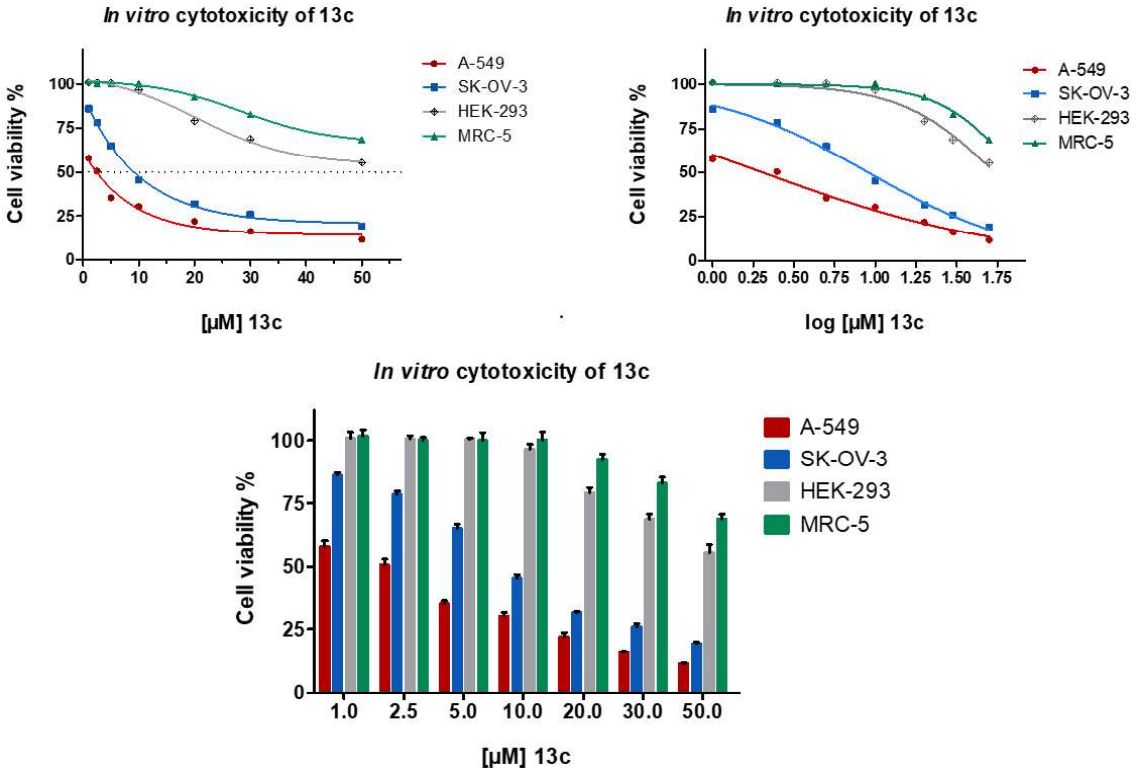

A-549 GI_{50}: 3.20 ± 0.35 μM

SK-OV-3 GI_{50}: 9.08 ± 0.27 μM

HEK-293 GI_{50}: > 50 μM

MRC-5 GI_{50}: > 50 μM

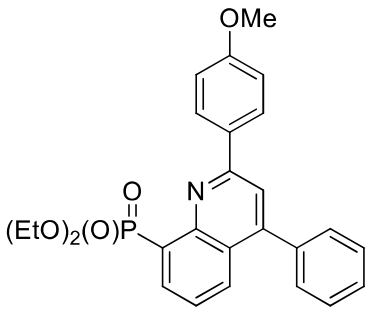

13d

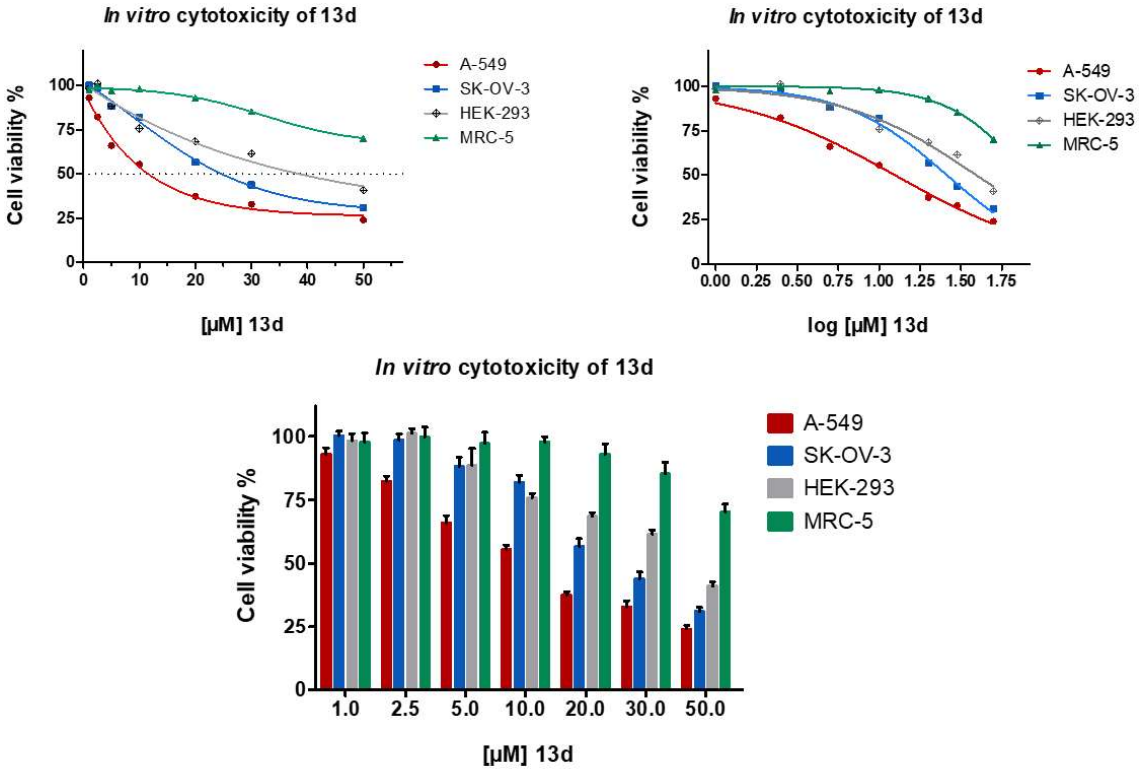

A-549 GI_{50}: 12.59 ± 1.34 µM

SK-OV-3 GI_{50}: 25.04 ± 3.61 µM

HEK-293 GI_{50}: 38.29 ± 8.89 µM

MRC-5 GI_{50}: > 50 µM

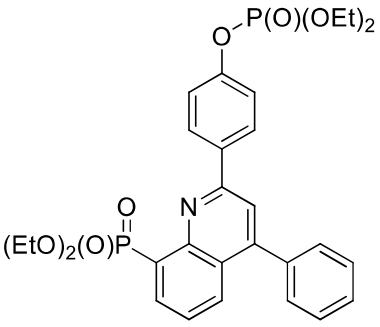

13e

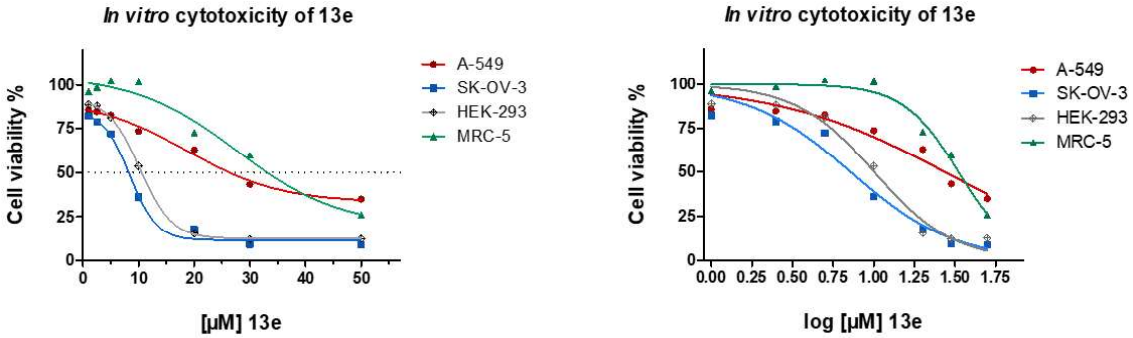

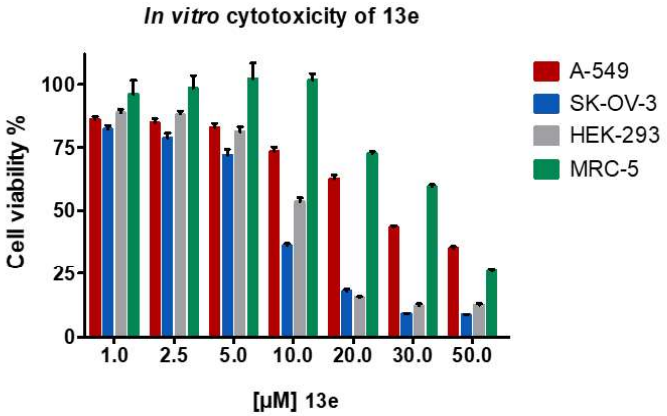

A-549 GI_{50}: 26.15 ± 4.01 µM

SK-OV-3 GI_{50}: 7.04 ± 0.21 µM

HEK-293 GI_{50}: 10.84 ± 0.98 µM

MRC-5 GI_{50}: 35.11 ± 5.58 µM

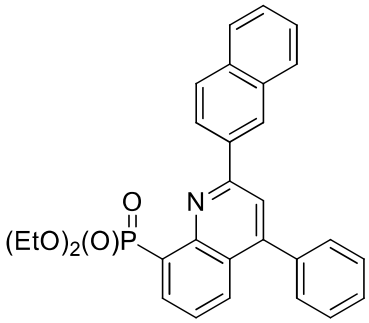

13g

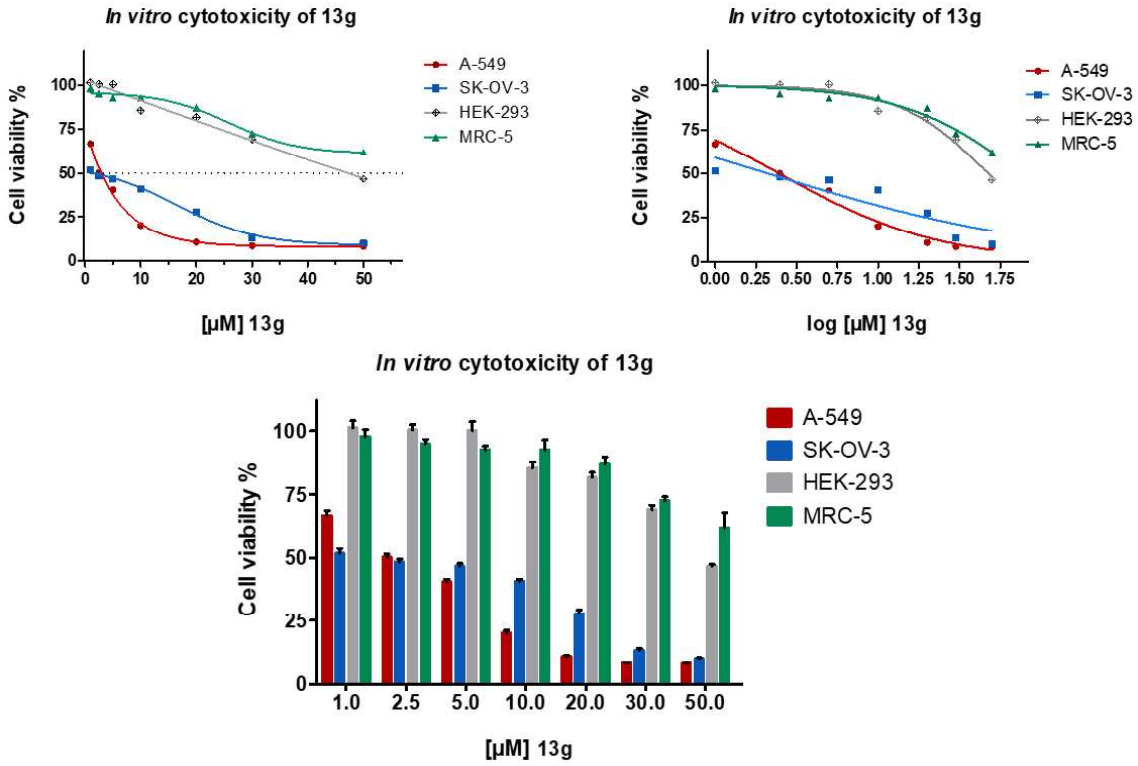

A-549 GI_{50}: 3.18 ± 0.27 μM

SK-OV-3 GI_{50}: 1.33 ± 0.76 μM

HEK-293 GI_{50}: 48.14 ± 6.39 μM

MRC-5 GI_{50}: > 50 μM

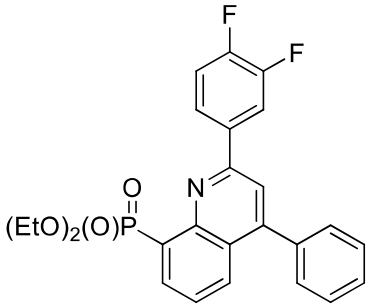

13h

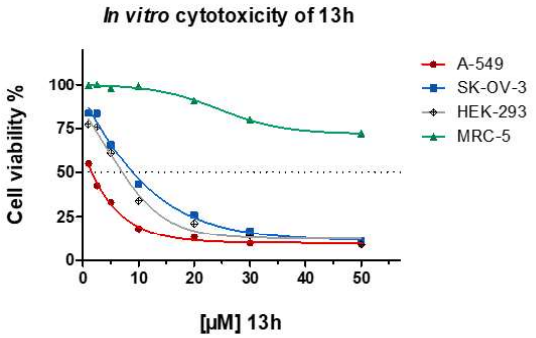

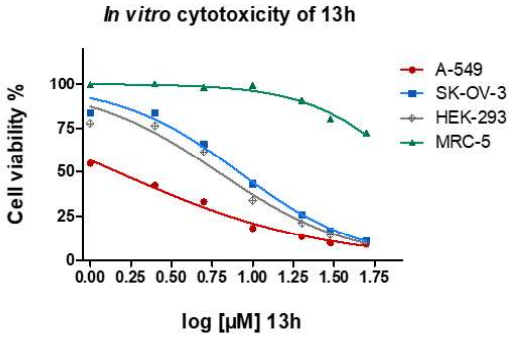

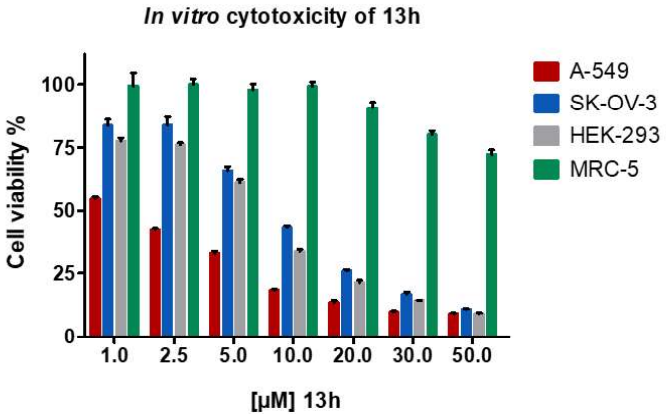

A-549 GI_{50}: 1.47 ± 0.12 µM

SK-OV-3 GI_{50}: 30.80 ± 2.82 µM

HEK-293 GI_{50}: 7.77 ± 0.22 µM

MRC-5 GI_{50}: > 50 µM

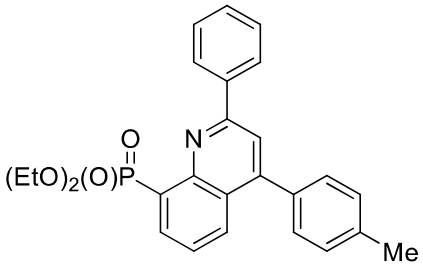

13i

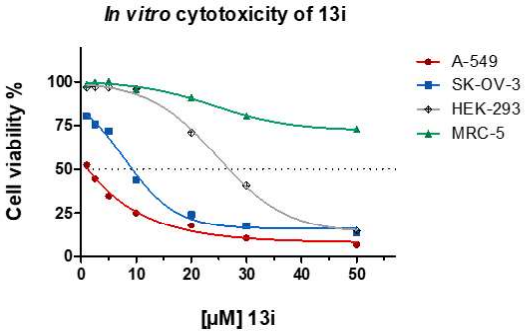

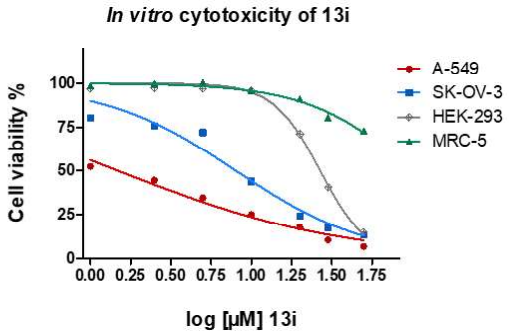

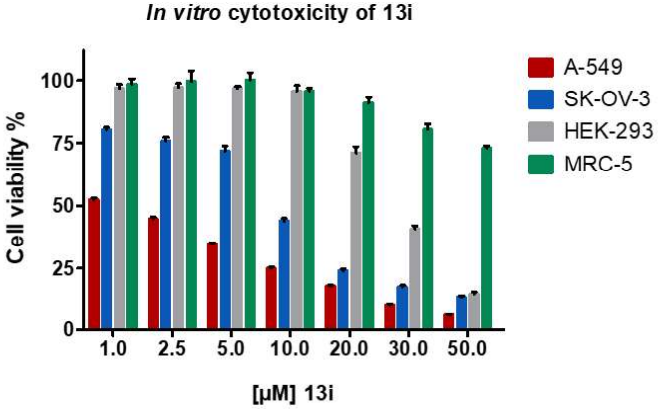

A-549 GI_{50}: 1.49 ± 0.10 µM

SK-OV-3 GI_{50}: 9.68 ± 0.75 µM

HEK-293 GI_{50}: 27.17 ± 3.45 µM

MRC-5 GI_{50}: 32.03 ± 13.51 µM

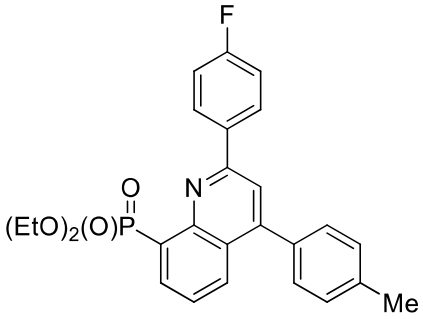

13j

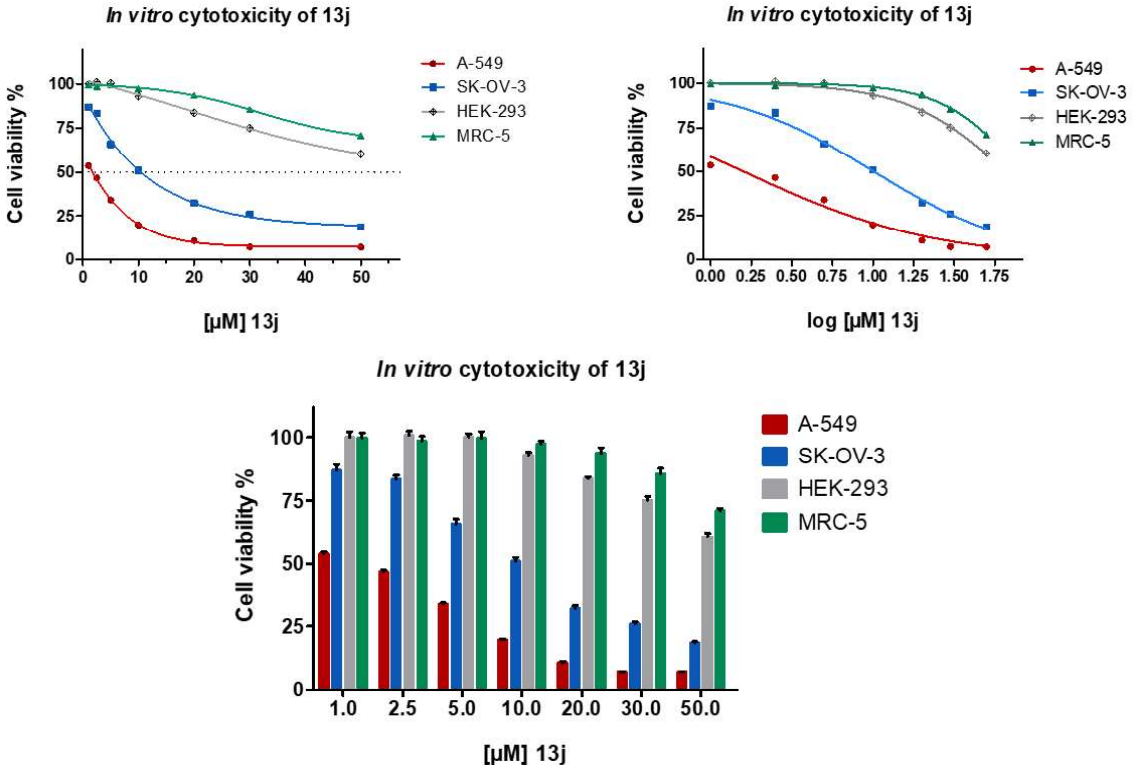

A-549 GI_{50}: 1.61 ± 0.17 µM

SK-OV-3 GI_{50}: 10.24 ± 0.39 µM

HEK-293 GI_{50}: > 50 µM

MRC-5 GI_{50}: > 50 µM

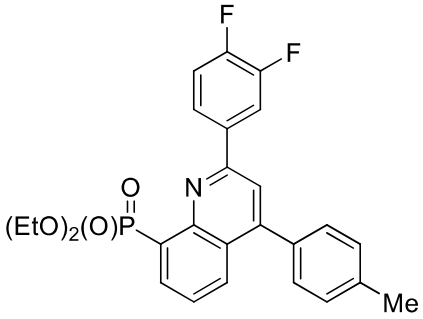

13k

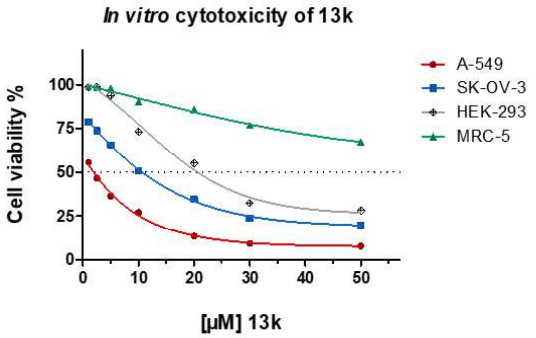

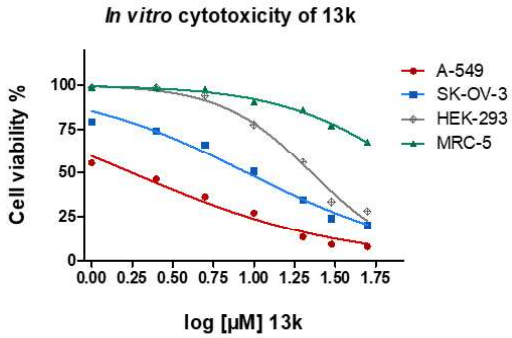

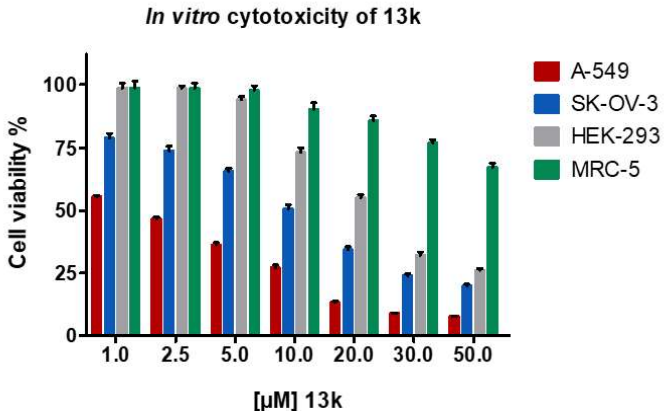

A-549 GI_{50}: 2.72 ± 0.37 μM

SK-OV-3 GI_{50}: 10.59 ± 1.13 μM

HEK-293 GI_{50}: 22.66 ± 1.36 μM

MRC-5 GI_{50}: > 50 μM

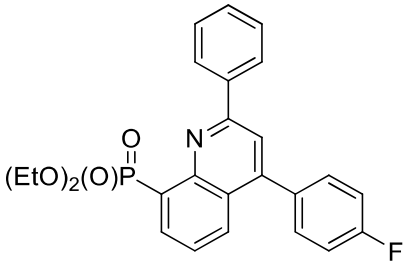

13l

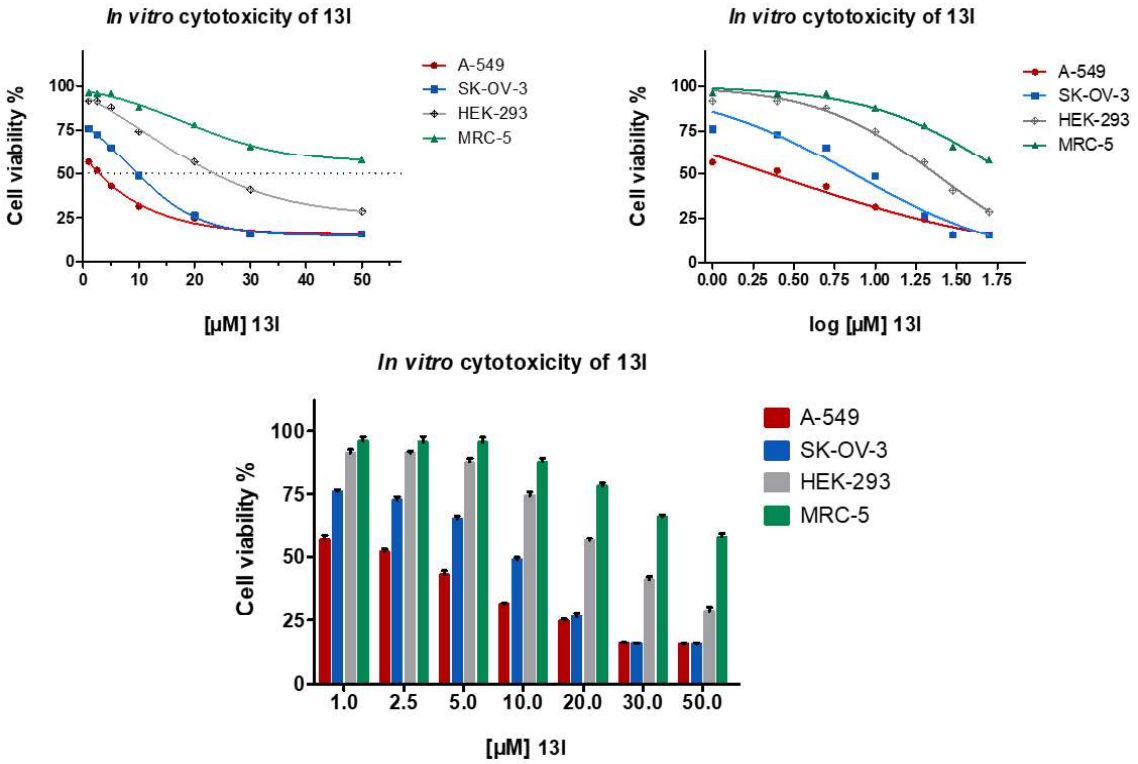

A-549 GI_{50}: 2.27 ± 0.33 µM

SK-OV-3 GI_{50}: 9.29 ± 1.79 µM

HEK-293 GI_{50}: 24.43 ± 3.46 µM

MRC-5 GI_{50}: > 50 µM

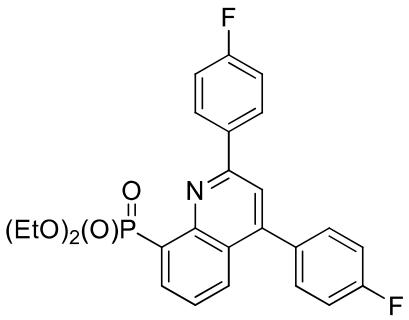

13m

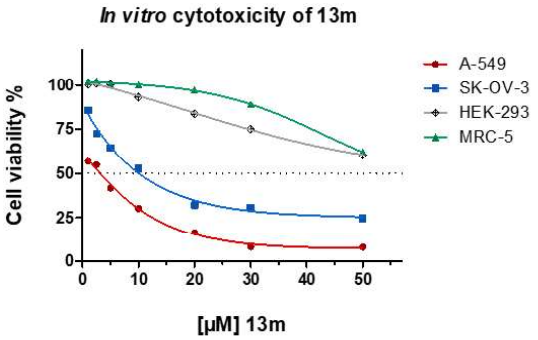

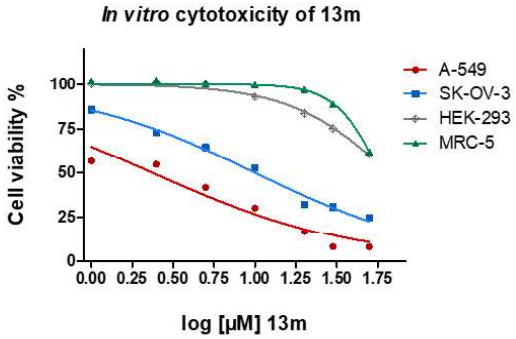

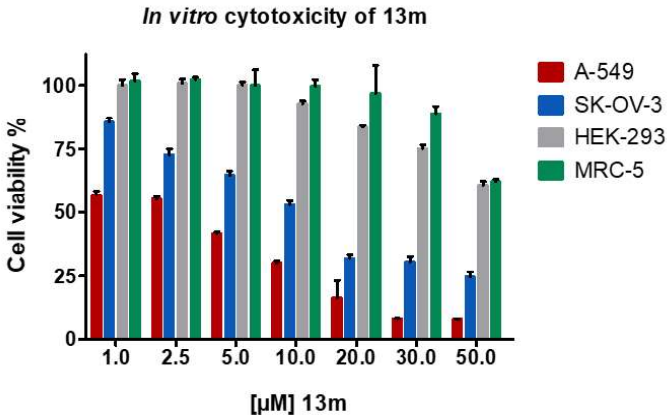

A-549 GI_{50}: 3.07 ± 0.22 μM

SK-OV-3 GI_{50}: 9.79 ± 0.59 μM

HEK-293 GI_{50}: 15.66 ± 1.74 μM

MRC-5 GI_{50}: > 50 μM

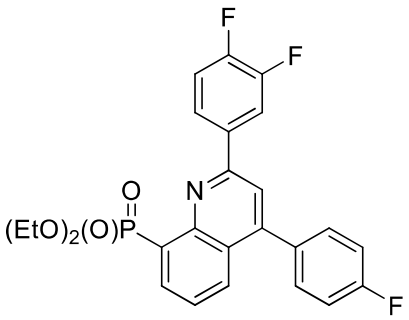

13n

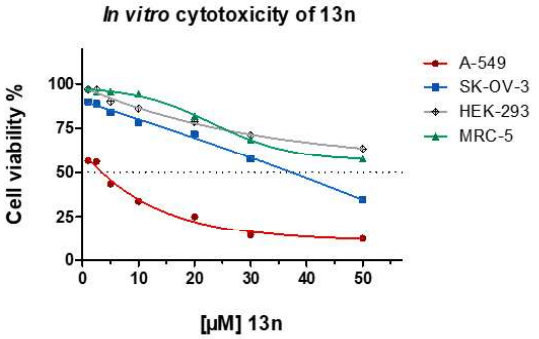

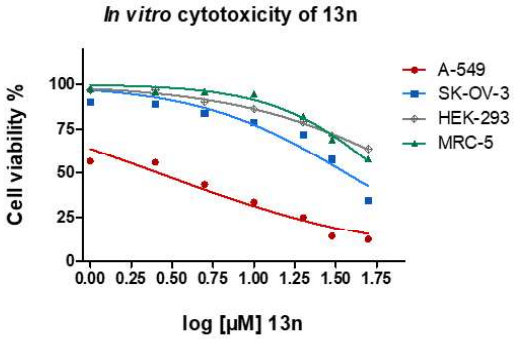

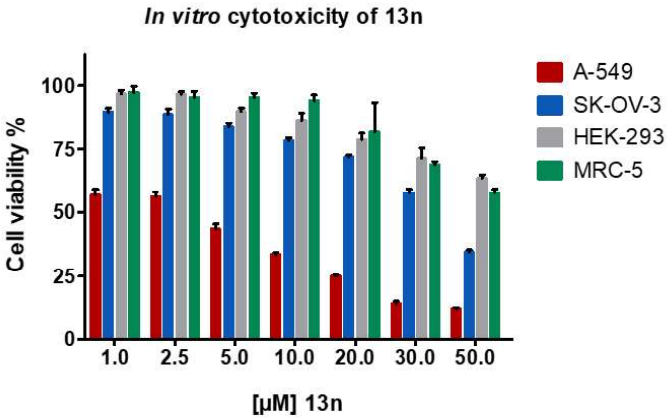

A-549 GI_{50}: 4.64 ± 0.30 μM

SK-OV-3 GI_{50}: 37.59 ± 9.10 μM

HEK-293 GI_{50}: > 50 μM

MRC-5 GI_{50}: > 50 μM

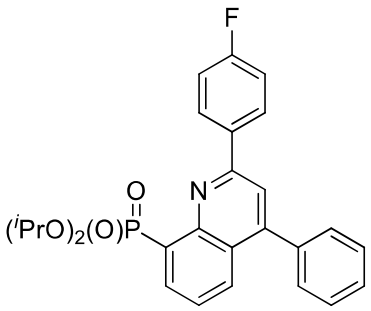

13o

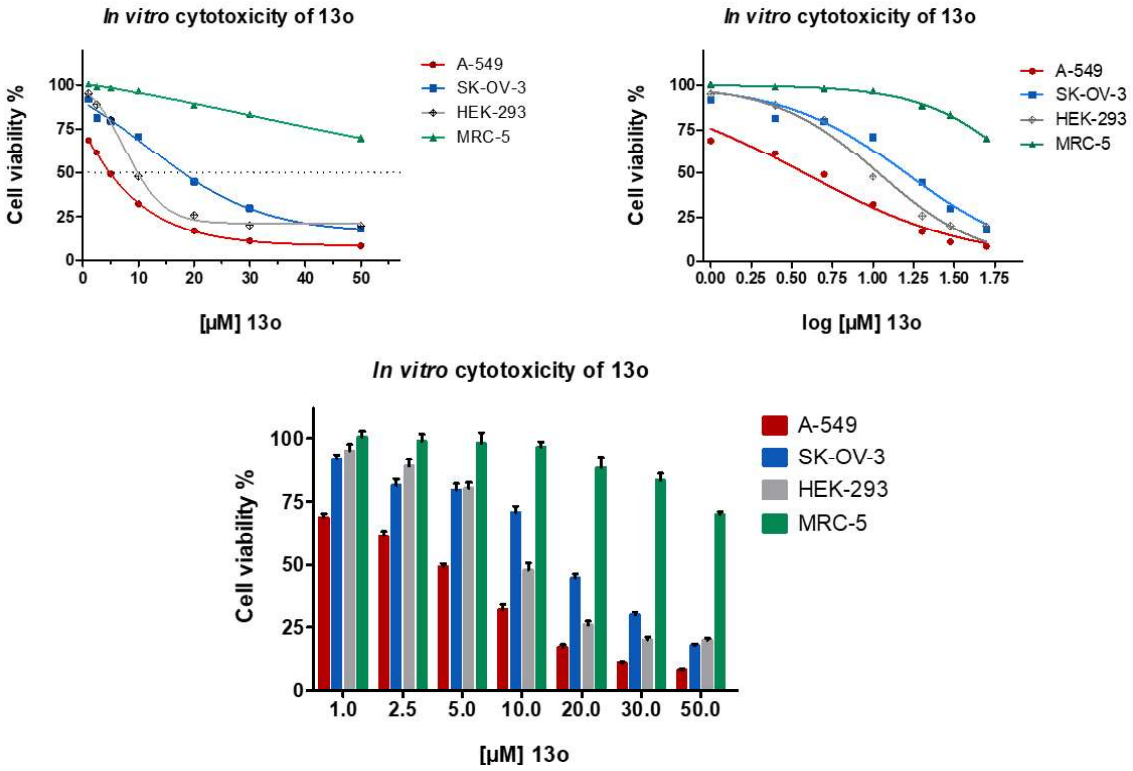

A-549 GI_{50}: 5.01 ± 2.70 μM

SK-OV-3 GI_{50}: 18.73 ± 1.98 μM

HEK-293 GI_{50}: 10.12 ± 1.26 μM

MRC-5 GI_{50}: > 50 μM

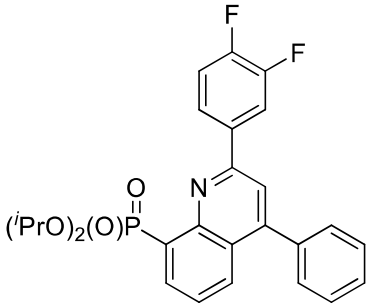

13p

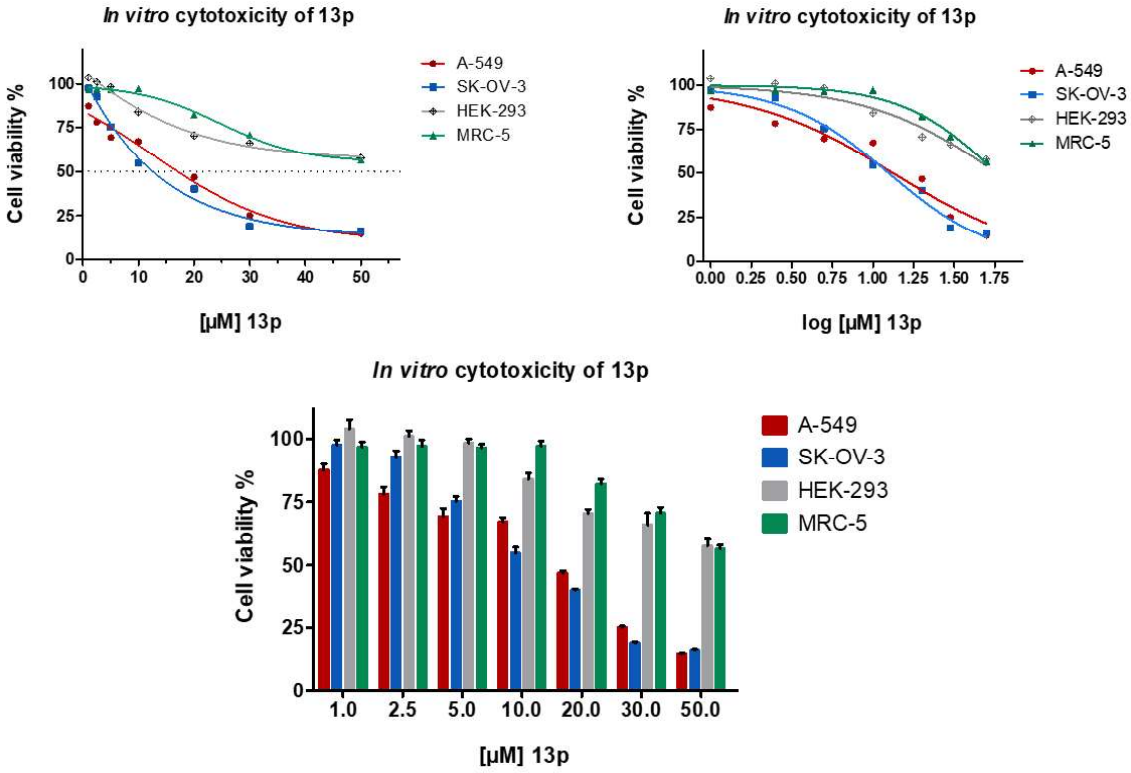

A-549 GI_{50}: 18.39 ± 1.36 µM

SK-OV-3 GI_{50}: 12.13 ± 1.68 µM

HEK-293 GI_{50}: > 50 µM

MRC-5 GI_{50}: > 50 µM

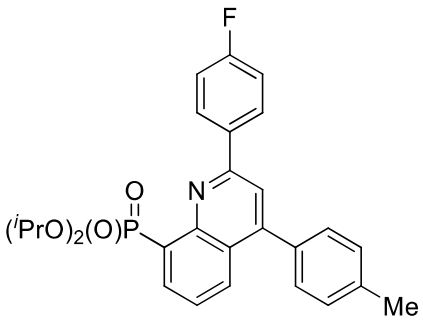

13q

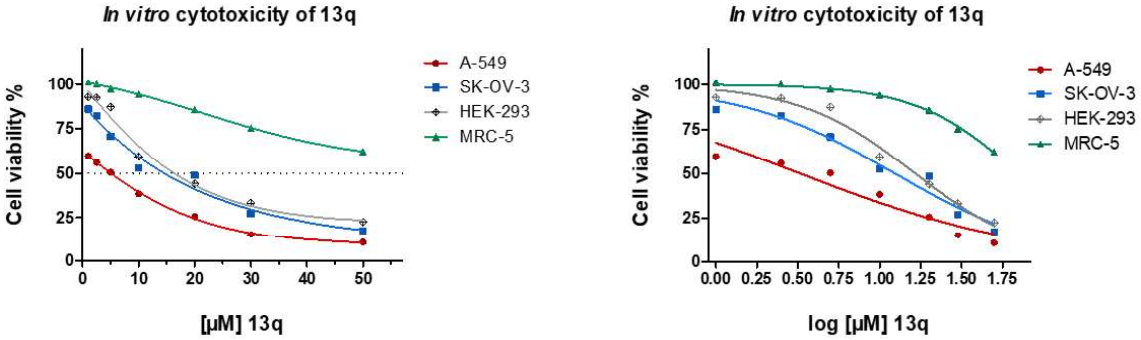

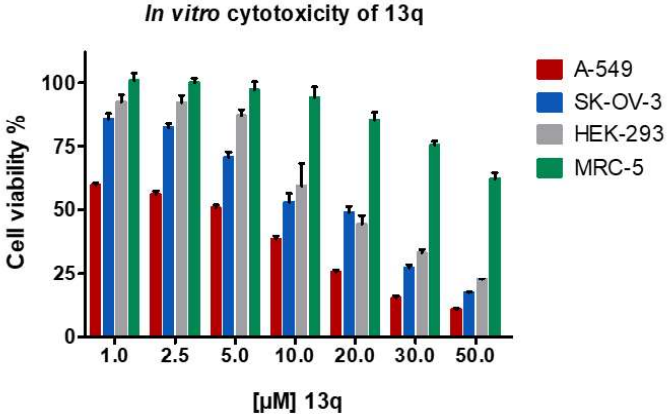

A-549 GI_{50}: 6.84 ± 1.74 μM

SK-OV-3 GI_{50}: 12.13 ± 1.68 μM

HEK-293 GI_{50}: 14.38 ± 1.69 μM

MRC-5 GI_{50}: > 50 μM

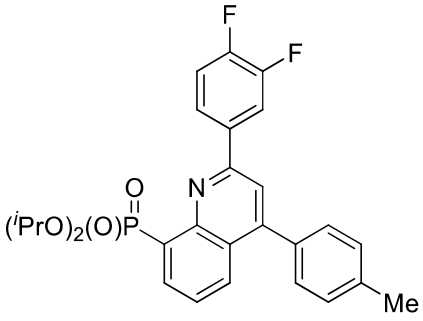

13r

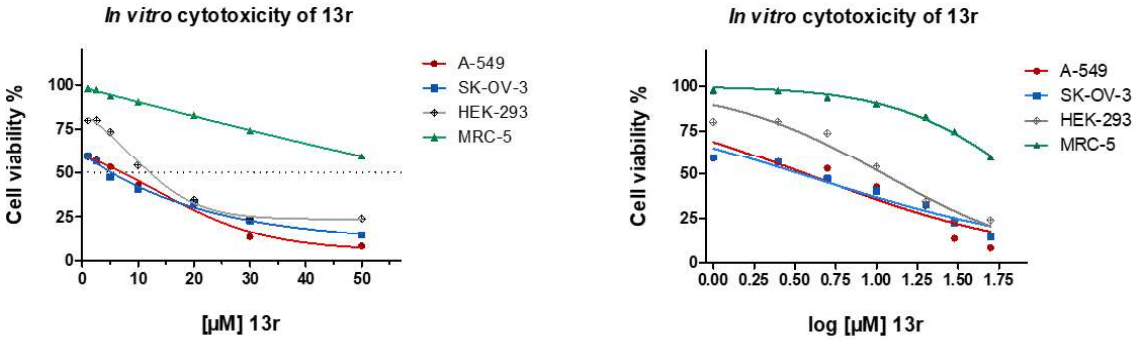

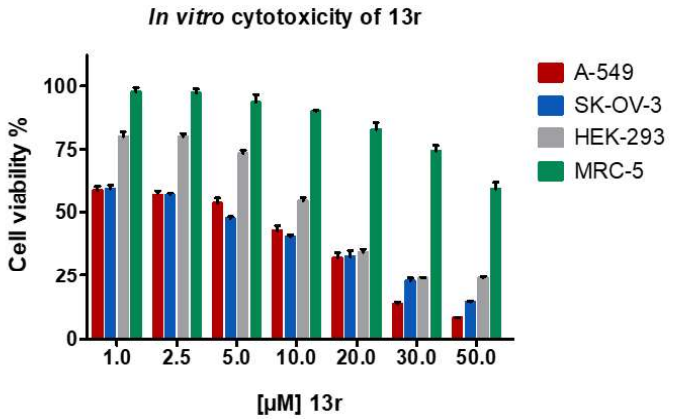

A-549 GI_{50}: 8.24 ± 2.42 μM

SK-OV-3 GI_{50}: 4.67 ± 1.49 μM

HEK-293 GI_{50}: 12.32 ± 0.72 μM

MRC-5 GI_{50}: > 50 μM

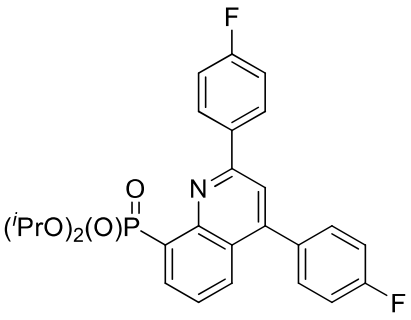

13s

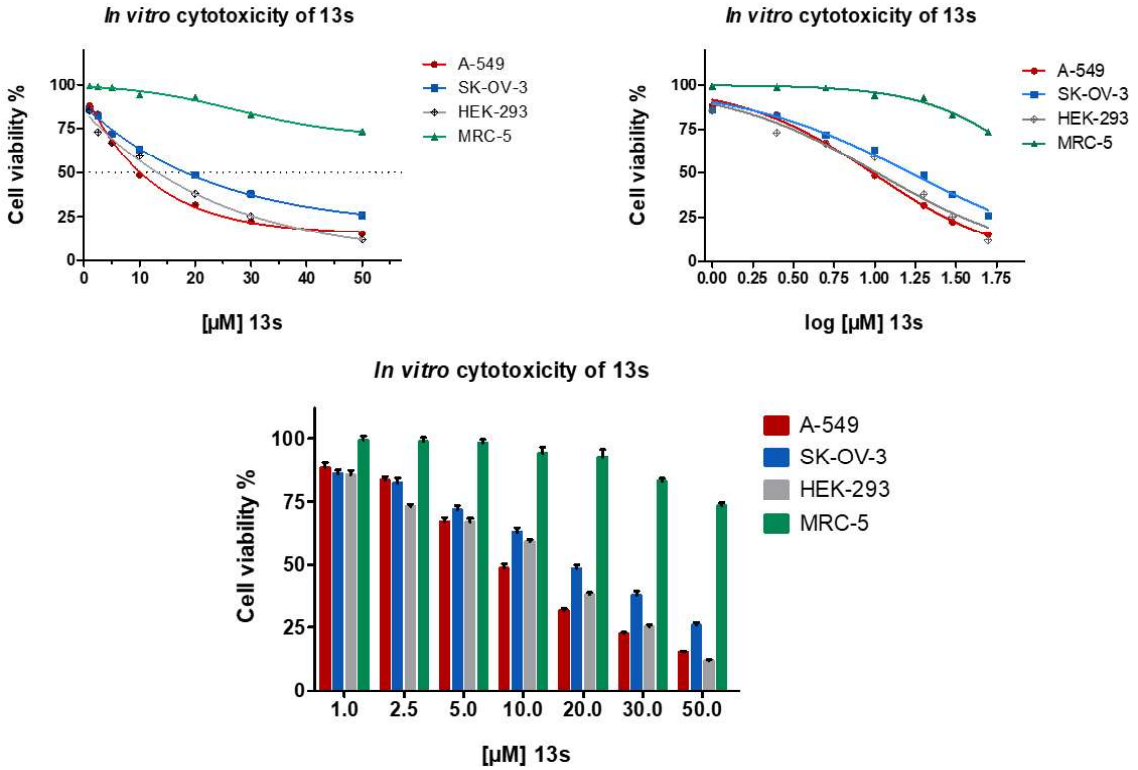

A-549 GI_{50}: 10.55 ± 1.73 μM

SK-OV-3 GI_{50}: 19.82 ± 3.82 μM

HEK-293 GI_{50}: 15.01 ± 0.99 μM

MRC-5 GI_{50}: > 50 μM

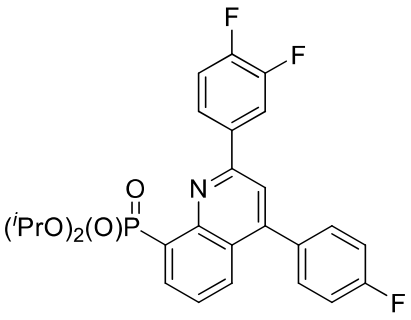

13t

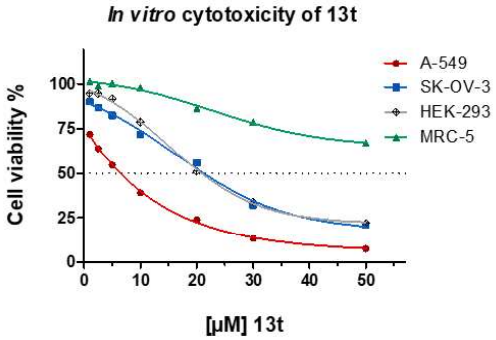

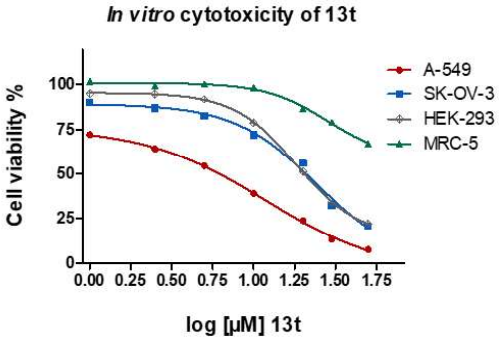

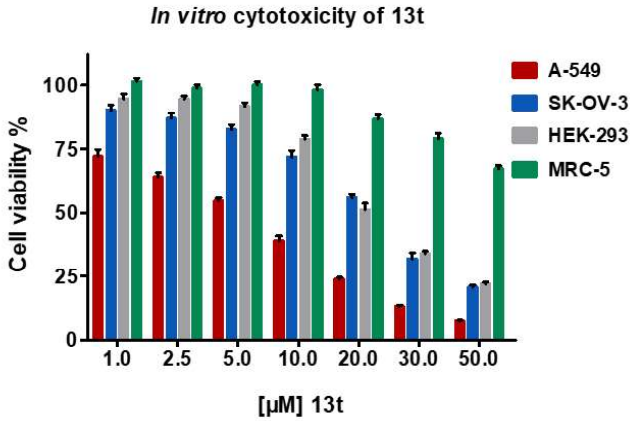

A-549 GI_{50}: 6.79 ± 3.87 μM

SK-OV-3 GI_{50}: 22.12 ± 4.47 μM

HEK-293 GI_{50}: 21.04 ± 4.05 μM

MRC-5 GI_{50}: > 50 μM

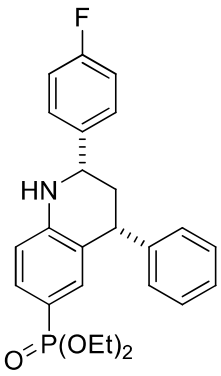

15a

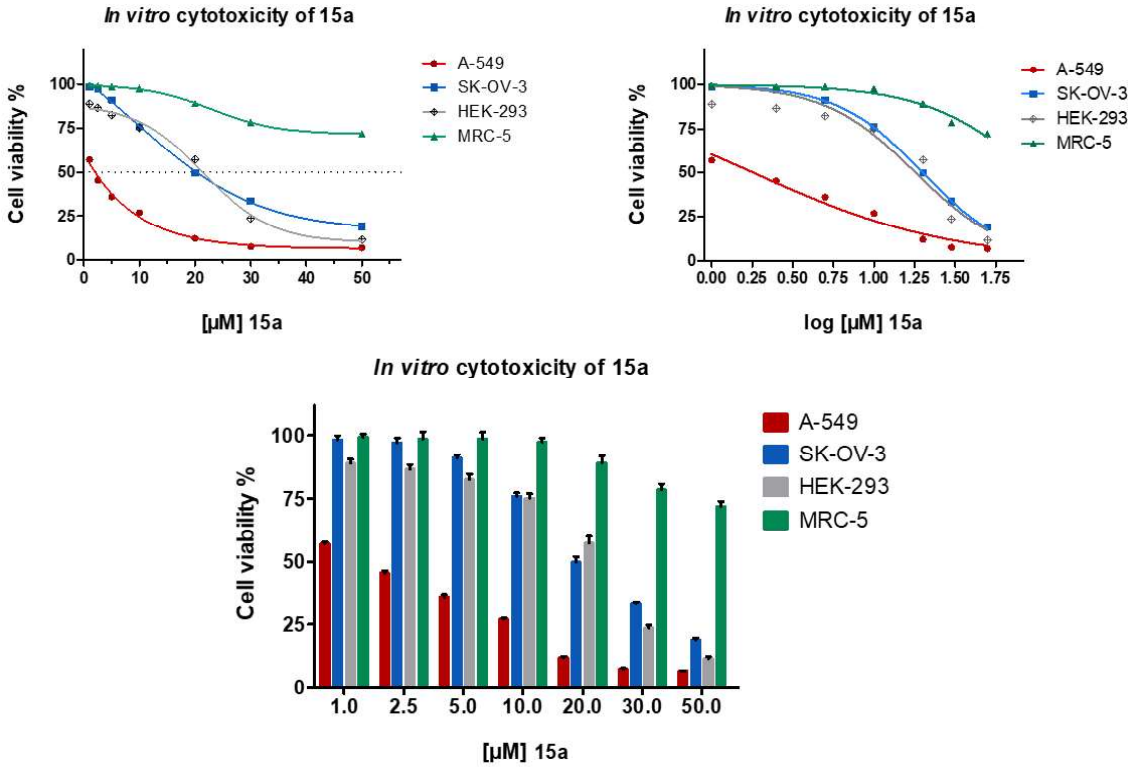

A-549 GI_{50}: 1.96 ± 0.24 µM

SK-OV-3 GI_{50}: 21.12 ± 3.84 µM

HEK-293 GI_{50}: 21.71± 2.19 µM

MRC-5 GI_{50}: > 50 µM

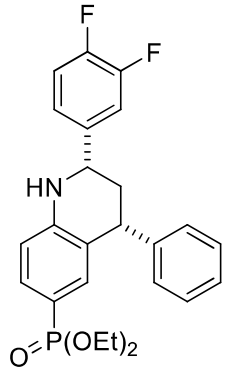

15b

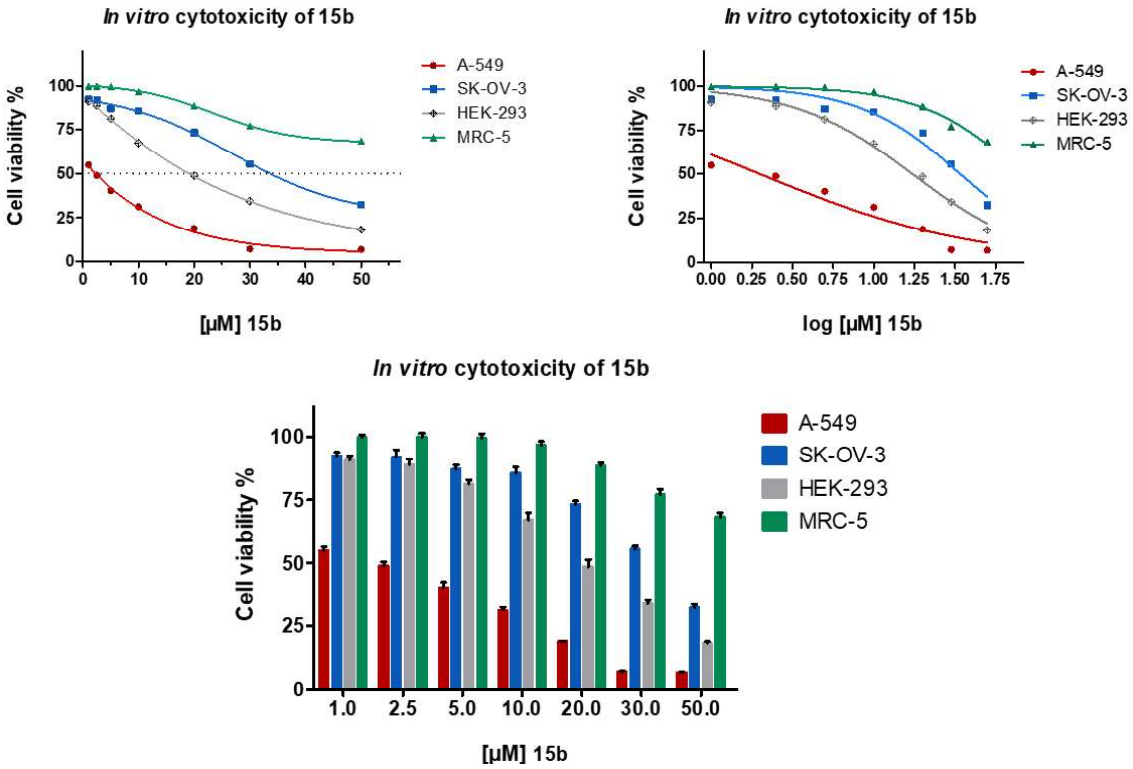

A-549 GI_{50}: 2.21 ± 0.96 µM

SK-OV-3 GI_{50}: 34.84 ± 6.15 µM

HEK-293 GI_{50}: 18.96 ± 2.95 µM

MRC-5 GI_{50}: > 50 µM

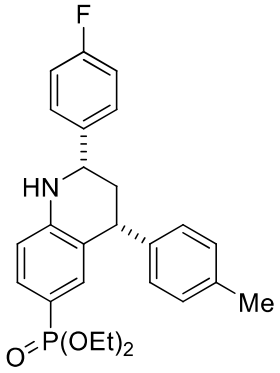

15c

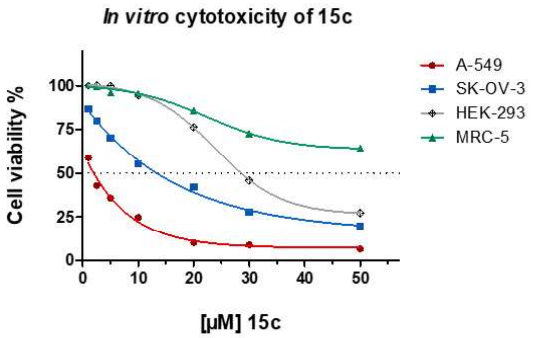

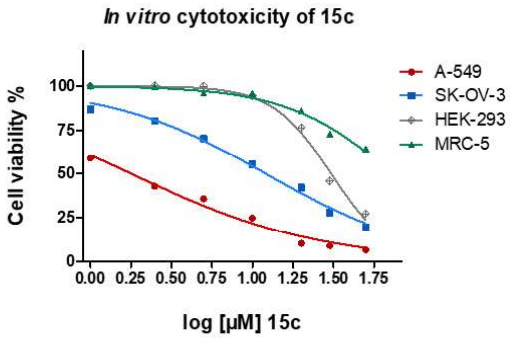

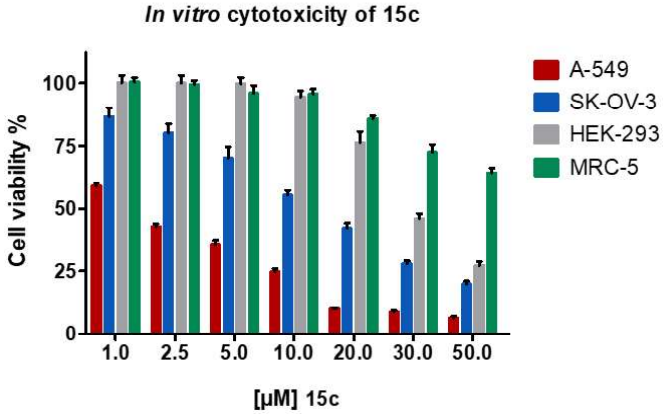

A-549 GI_{50}: 2.51 ± 0.15 µM

SK-OV-3 GI_{50}: 14.23 ± 1.81 µM

HEK-293 GI_{50}: 29.46 ± 6.28 µM

MRC-5 GI_{50}: > 50 µM

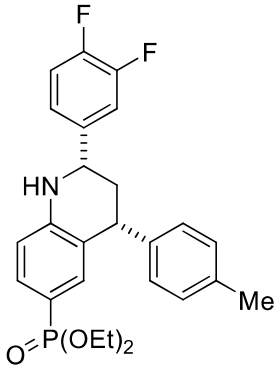

15d

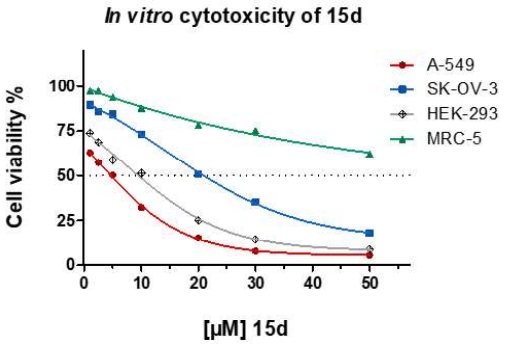

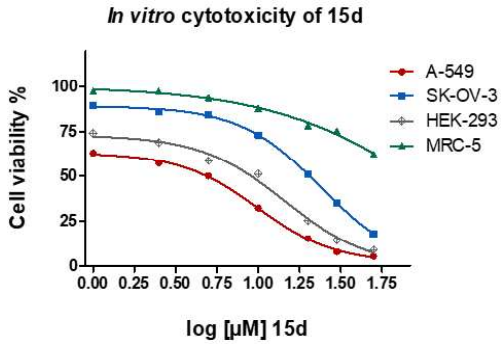

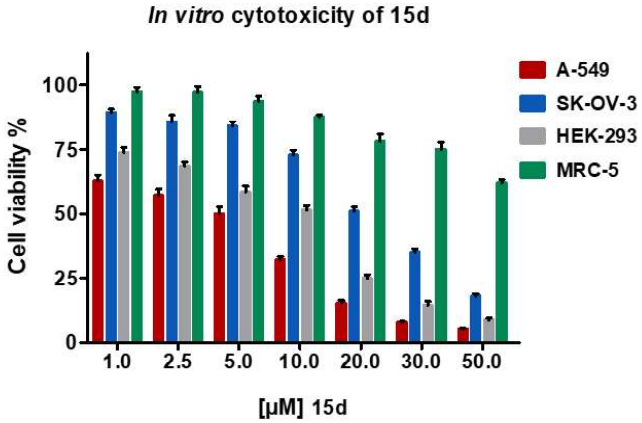

A-549 GI_{50}: 5.28 ± 0.69 µM

SK-OV-3 GI_{50}: 21.55 ± 2.07 µM

HEK-293 GI_{50}: 11.99 ± 2.02 µM

MRC-5 GI_{50}: > 50 µM

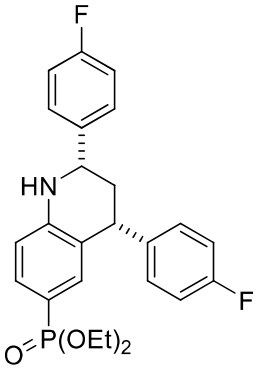

15e

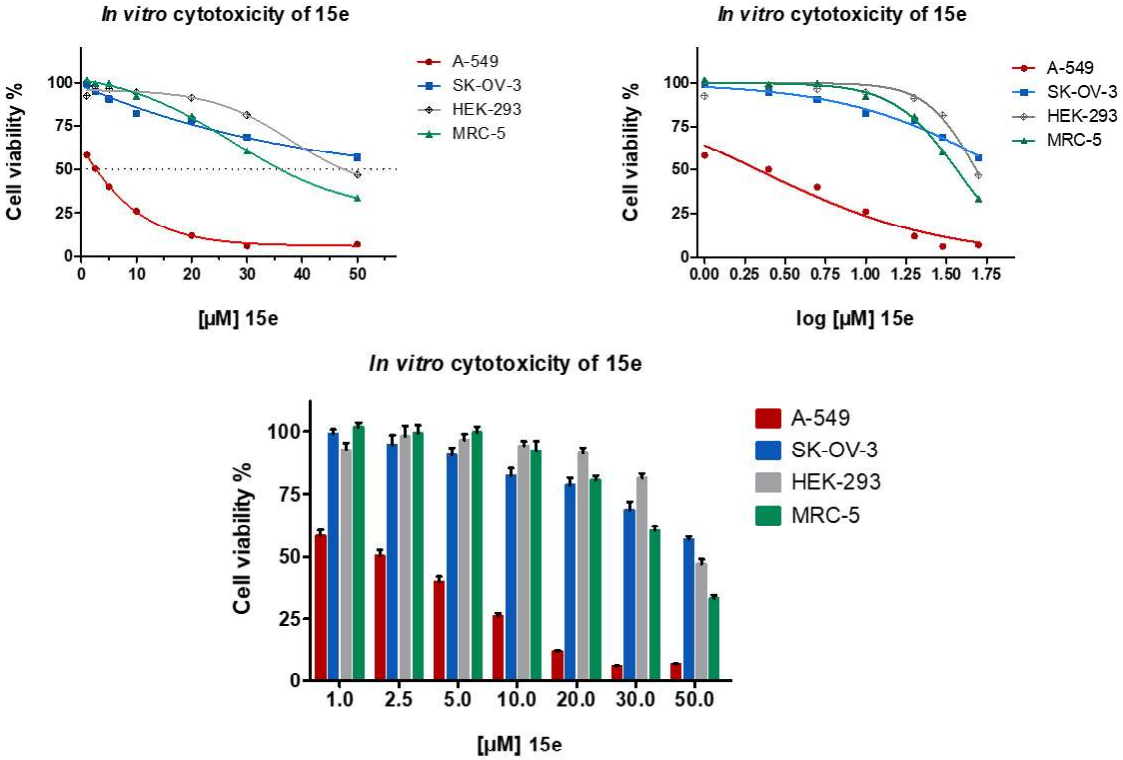

A-549 GI_{50}: 2.50 ± 0.83 µM

SK-OV-3 GI_{50}: > 50 µM

HEK-293 GI_{50}: 47.77 ± 11.86 µM

MRC-5 GI_{50}: 36.96 ± 2.93 µM

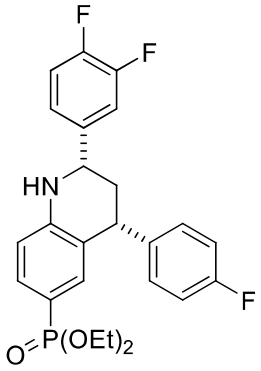

15f

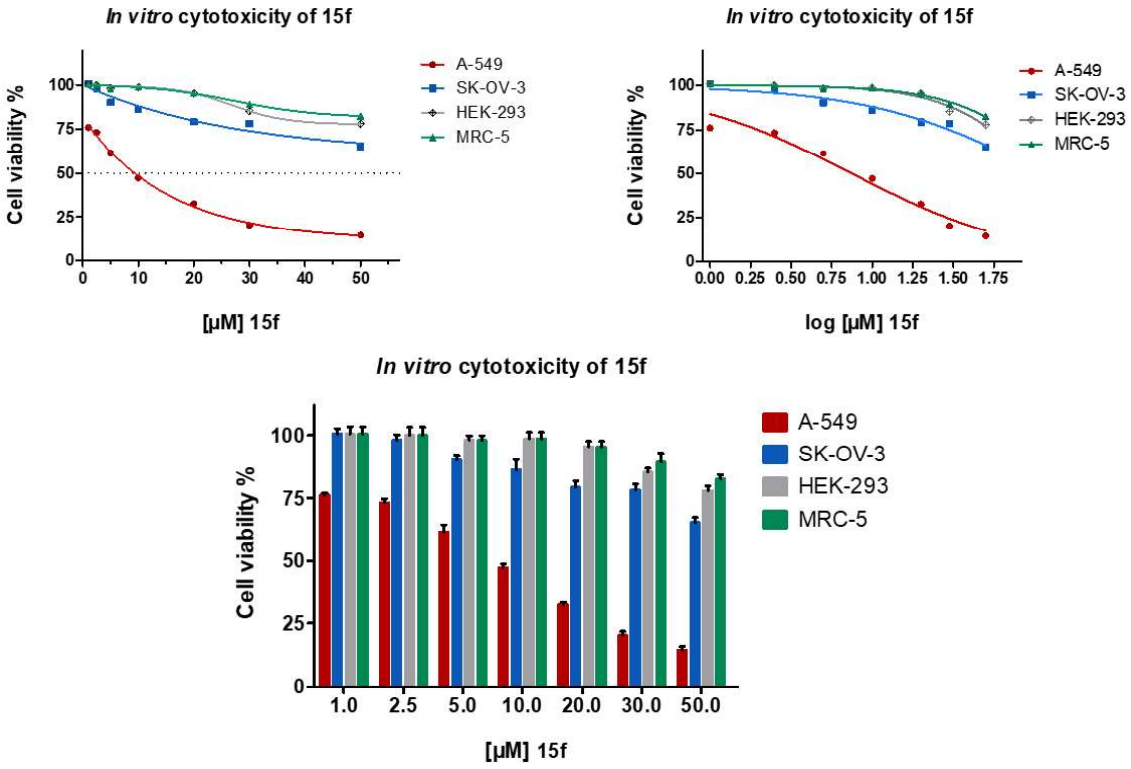

A-549 GI_{50}: 9.52 ± 0.62 μM

SK-OV-3 GI_{50}: > 50 μM

HEK-293 GI_{50}: > 50 μM

MRC-5 GI_{50}: > 50 μM

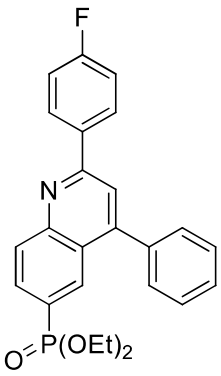

16a

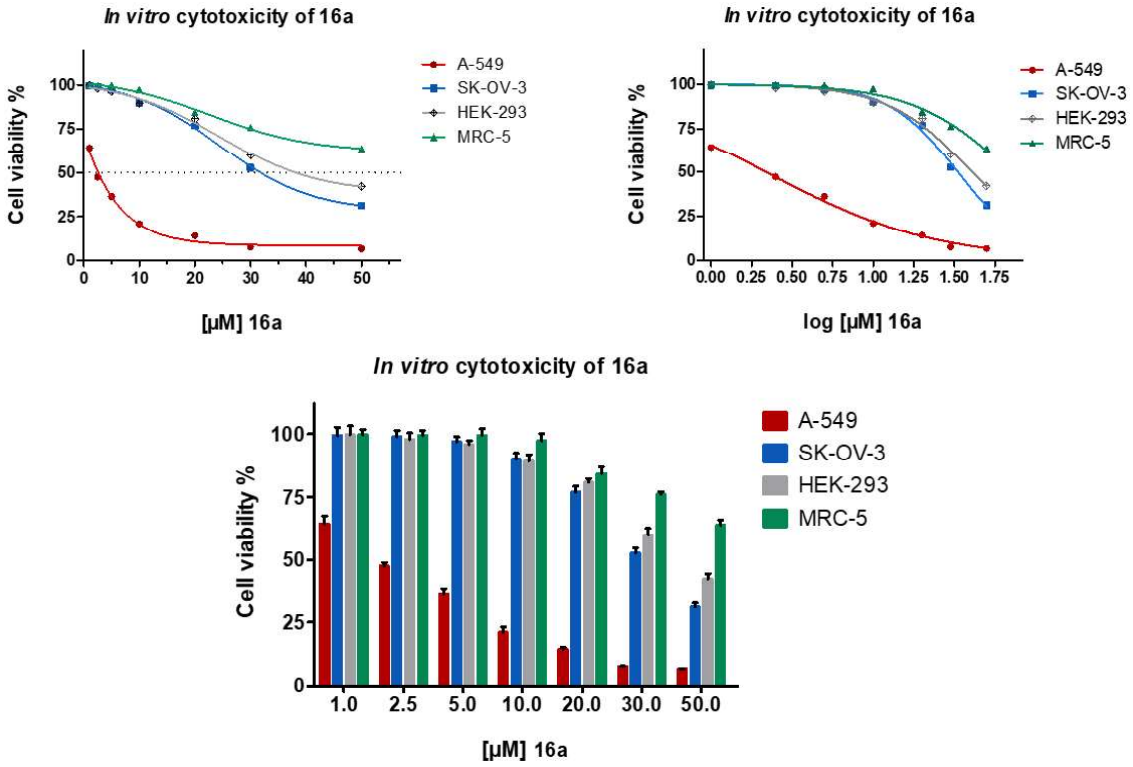

A-549 GI_{50}: 2.80 ± 1.24 µM

SK-OV-3 GI_{50}: 31.03 ± 9.96 µM

HEK-293 GI_{50}: 36.86 ± 8.06 µM

MRC-5 GI_{50}: > 50 µM

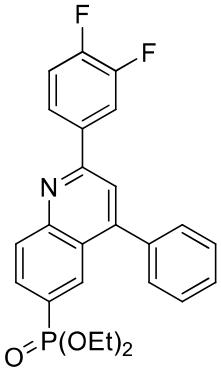

16b

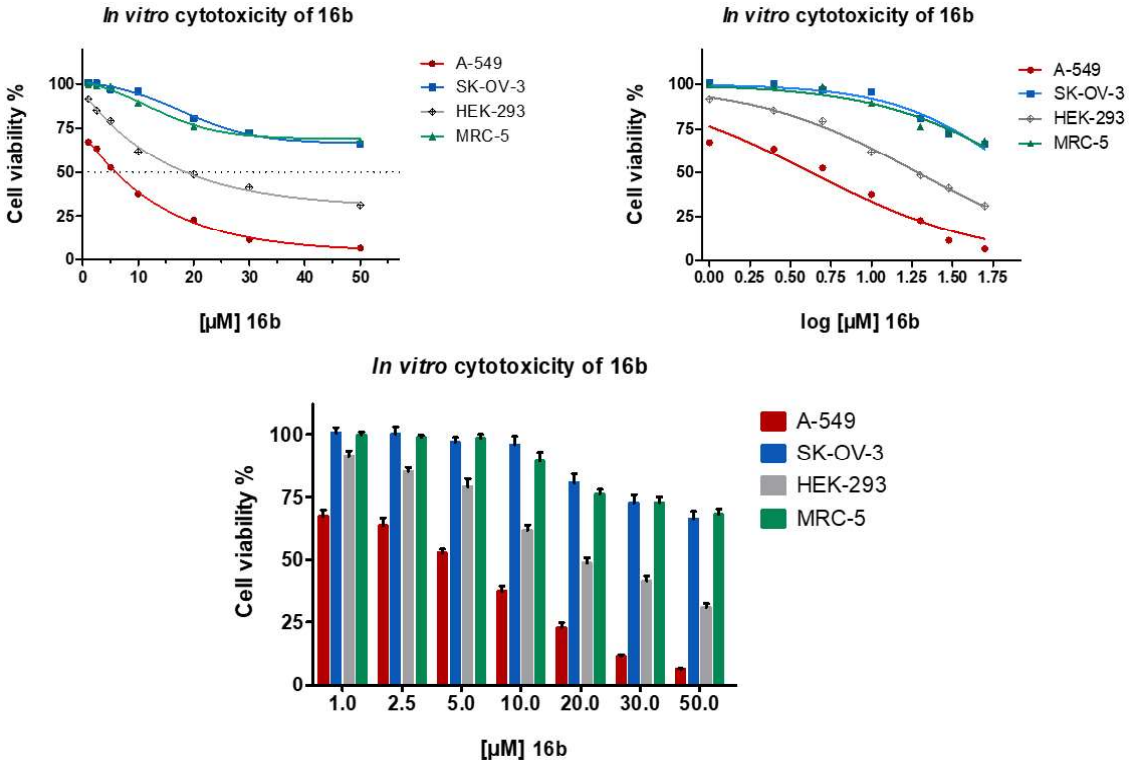

A-549 GI_{50}: 6.19 ± 0.67 µM

SK-OV-3 GI_{50}: > 50 µM

HEK-293 GI_{50}: 19.18 ± 1.13 µM

MRC-5 GI_{50}: > 50 µM

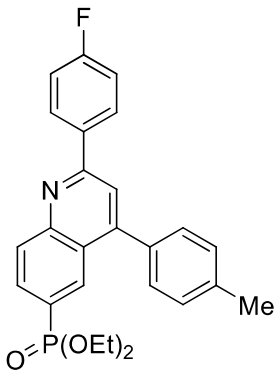

16c

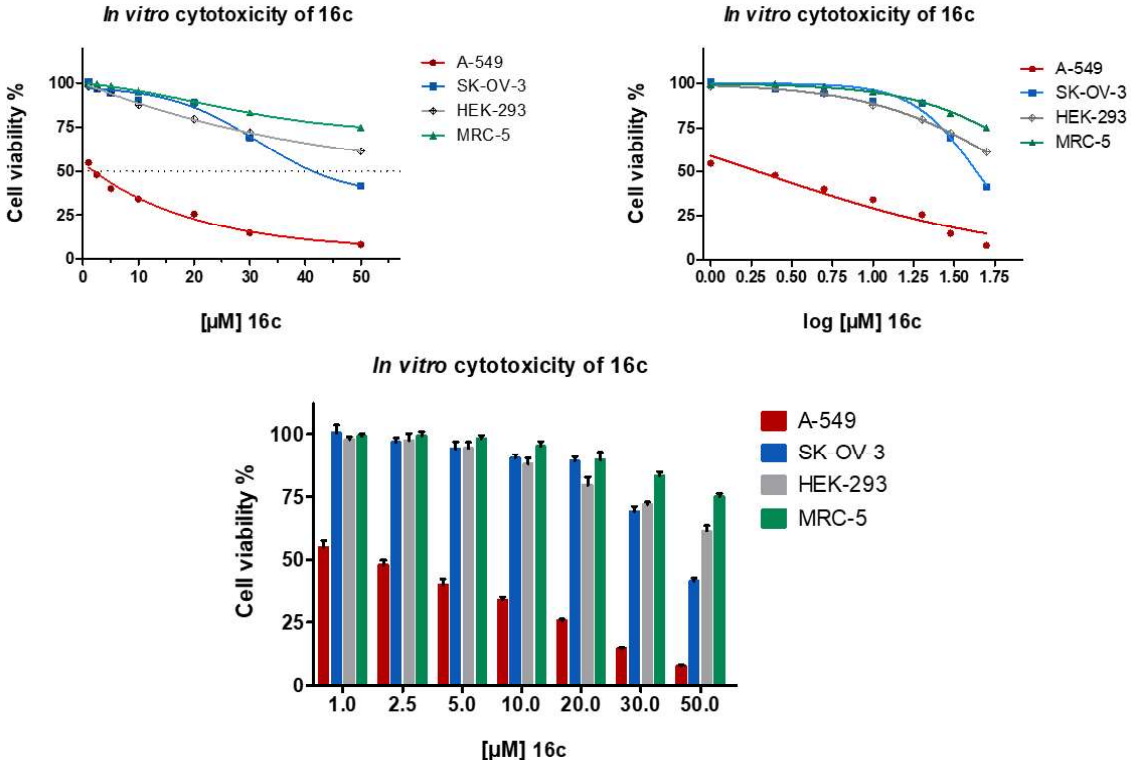

A-549 GI_{50}: 1.91 ± 0.33 µM

SK-OV-3 GI_{50}: 41.61 ± 10.01 µM

HEK-293 GI_{50}: > 50 µM

MRC-5 GI_{50}: > 50 µM

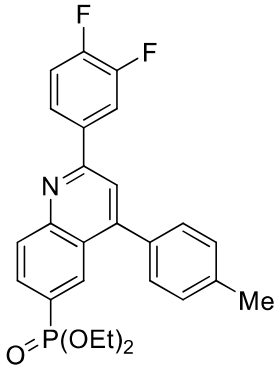

16d

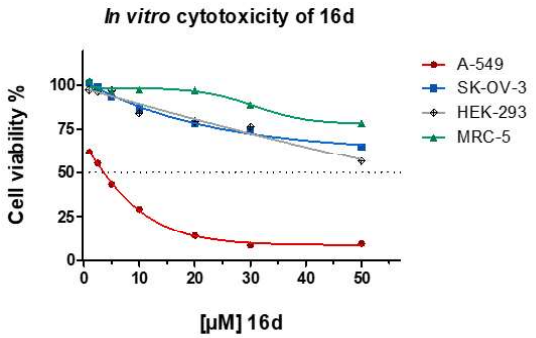

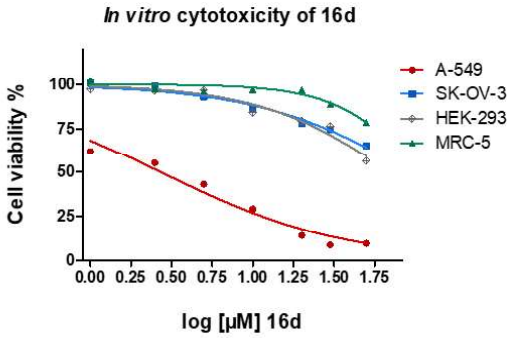

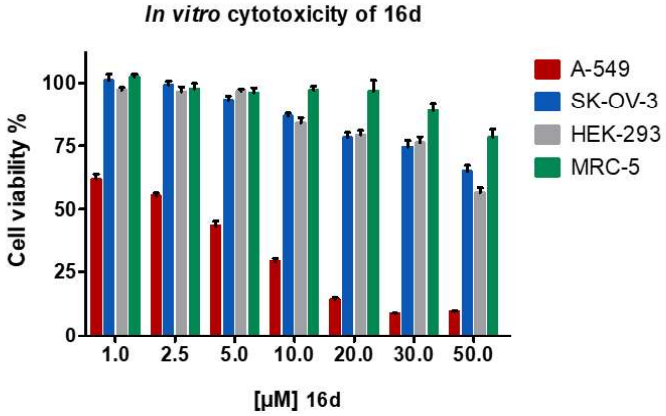

A-549 GI_{50}: 3.05 ± 0.86 µM

SK-OV-3 GI_{50}: > 50 µM

HEK-293 GI_{50}: > 50 µM

MRC-5 GI_{50}: > 50 µM

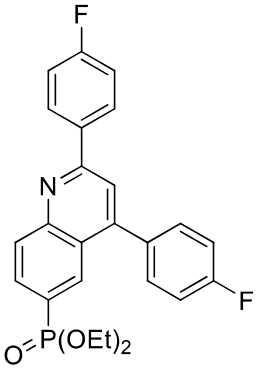

16e

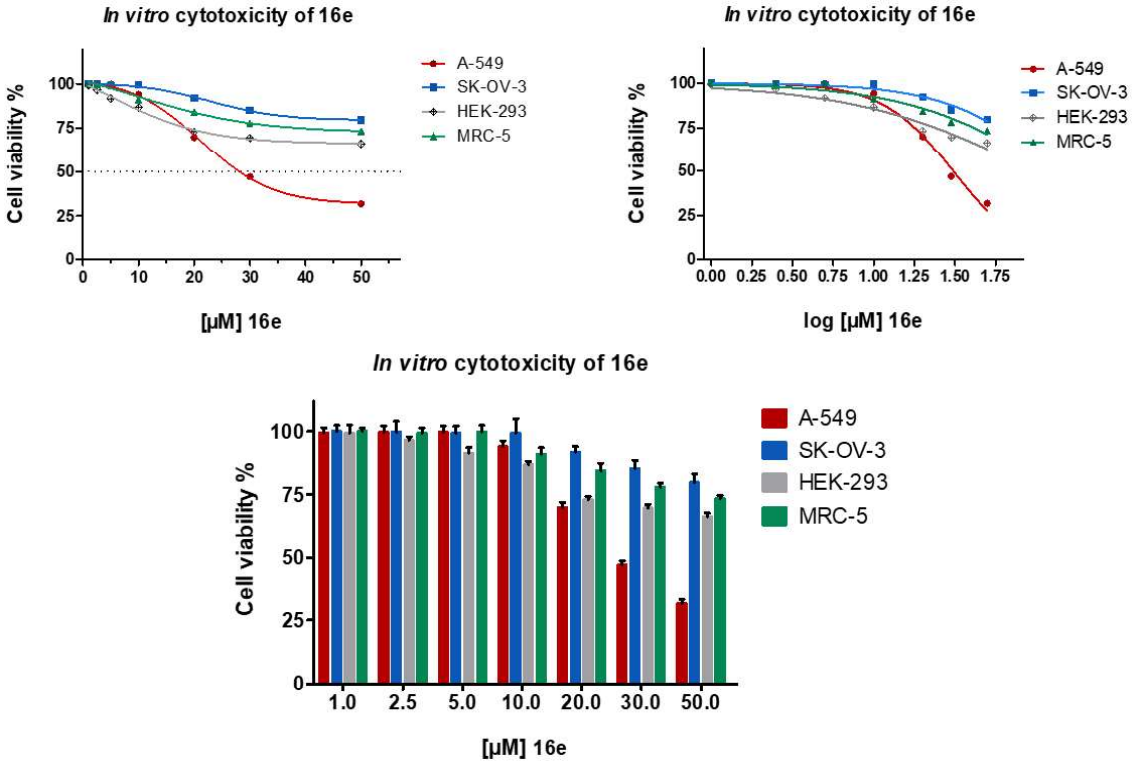

A-549 GI_{50}: 27.85 ± 4.26 µM

SK-OV-3 GI_{50}: > 50 µM

HEK-293 GI_{50}: > 50 µM

MRC-5 GI_{50}: > 50 µM

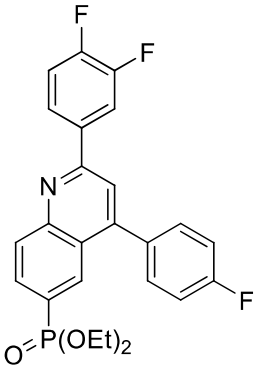

16f

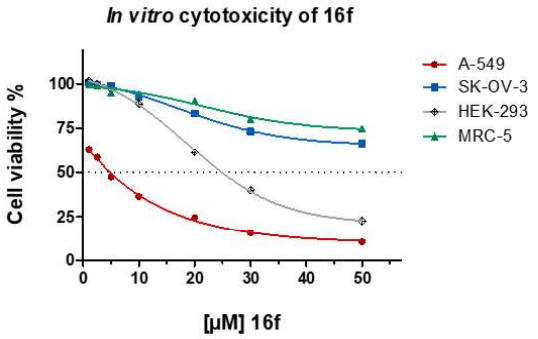

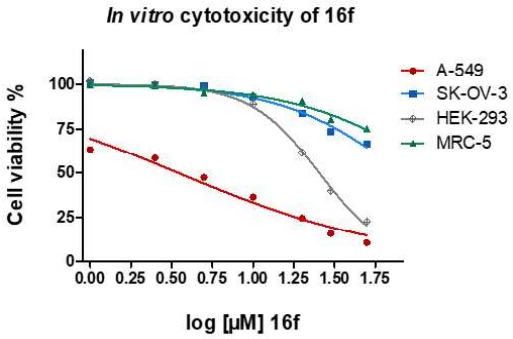

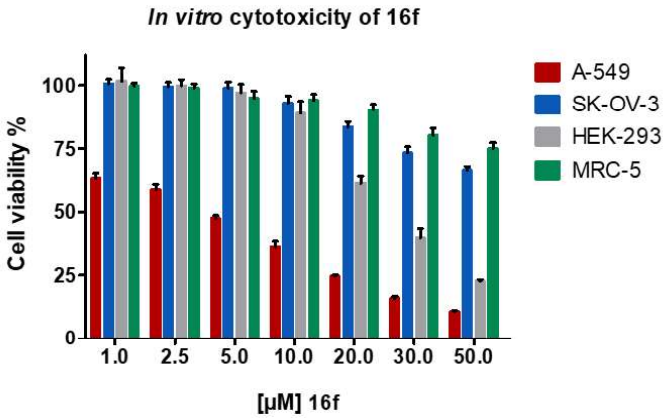

A-549 GI_{50}: 4.33 ± 01.11 µM

SK-OV-3 GI_{50}: > 50 µM

HEK-293 GI_{50}: 25.72 ± 6.34 µM

MRC-5 GI_{50}: > 50 µM

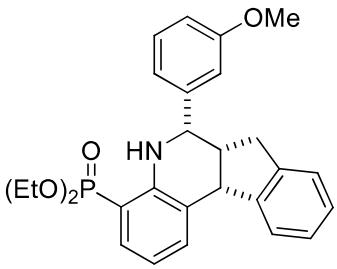

19a

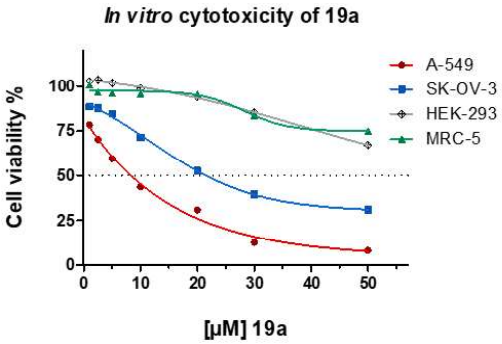

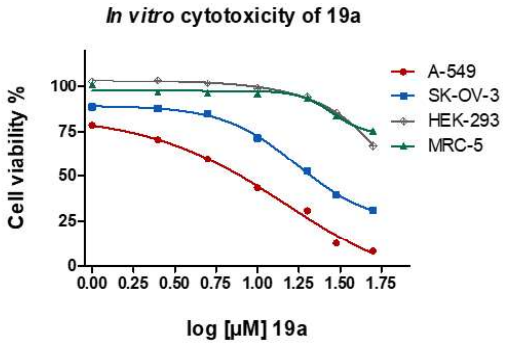

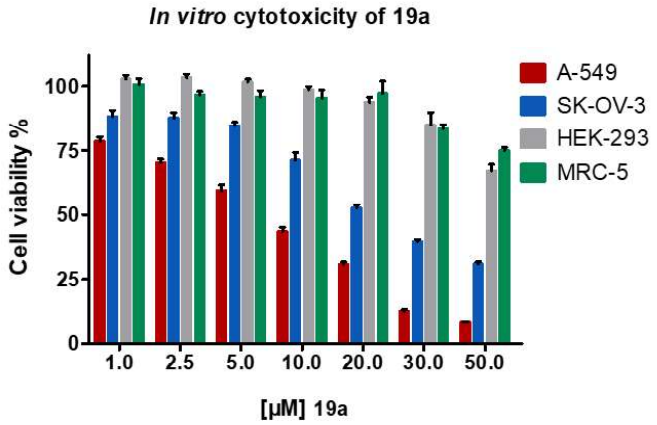

A-549 GI_{50}: 8.71 ± 0.50 µM

SK-OV-3 GI_{50}: 20.95 ± 1.88 µM

HEK-293 GI_{50}: > 50 µM

MRC-5 GI_{50}: > 50 µM

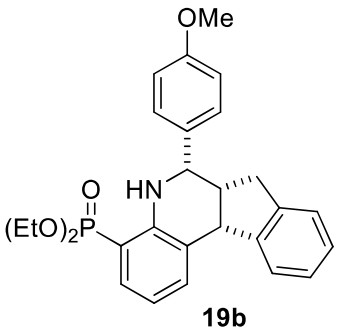

19b

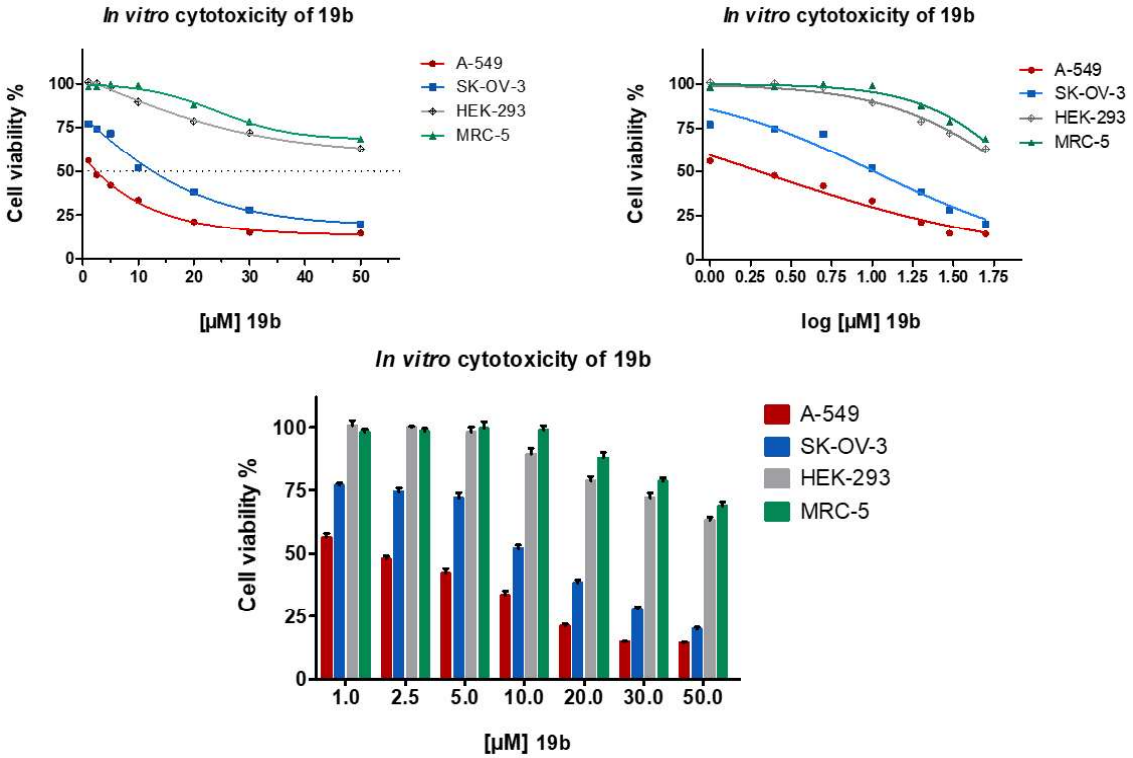

A-549 GI_{50}: 2.10 ± 0.30 µM

SK-OV-3 GI_{50}: 12.62 ± 0.73 µM

HEK-293 GI_{50}: > 50 µM

MRC-5 GI_{50}: > 50 µM

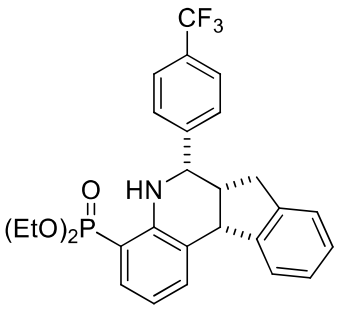

19c

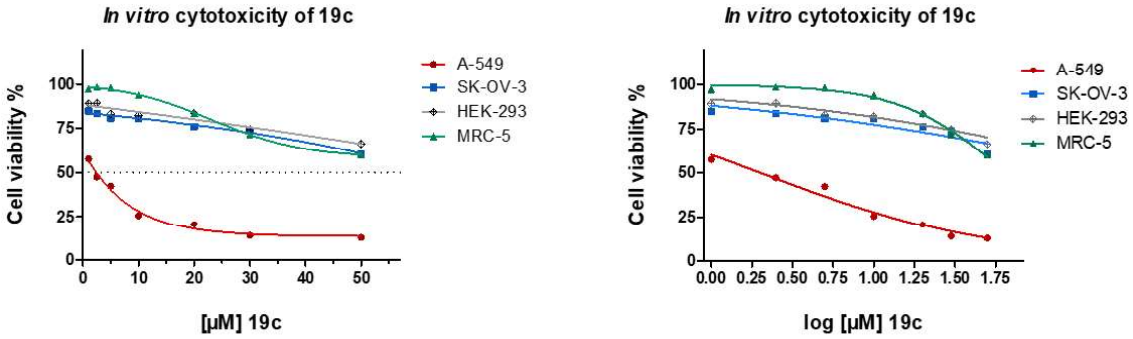

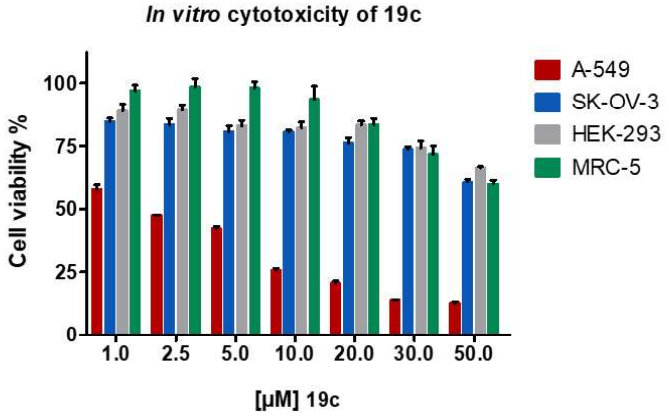

A-549 GI_{50}: 3.39 ± 0.15 µM

SK-OV-3 GI_{50}: > 50 µM

HEK-293 GI_{50}: > 50 µM

MRC-5 GI_{50}: > 50 µM

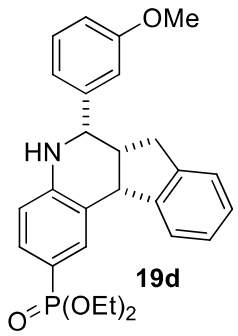

19d

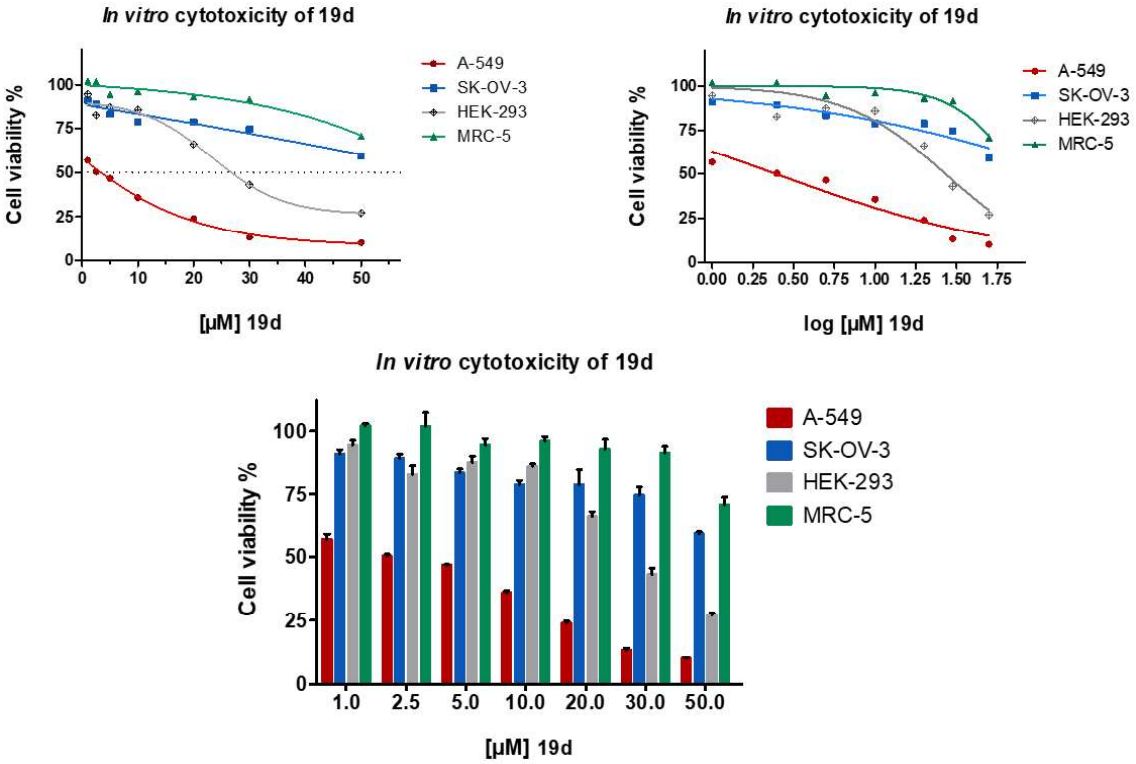

A-549 GI_{50}: 2.07 ± 0.28µM

SK-OV-3 GI_{50}: > 50 µM

HEK-293 GI_{50}: 28.60 ± 3.29 µM

MRC-5 GI_{50}: > 50 µM

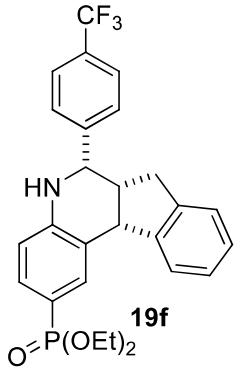

19f

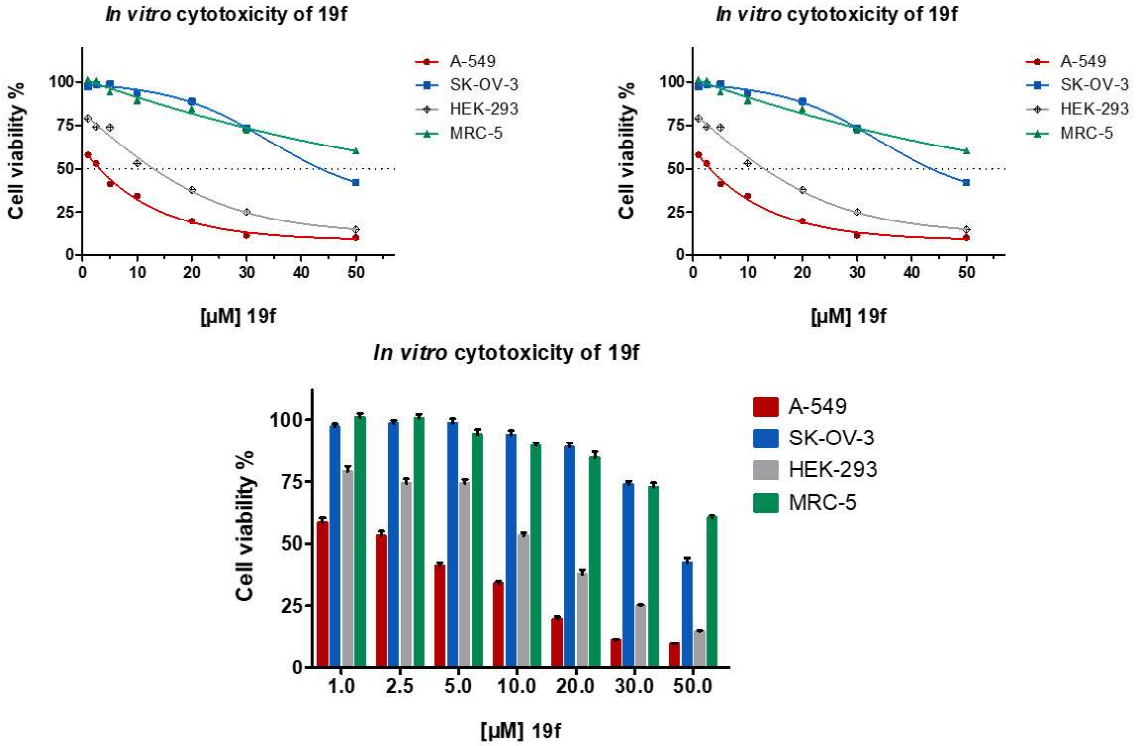

A-549 GI_{50}: 2.91 ± 1.09 µM

SK-OV-3 GI_{50}: 45.53 ± 7.02µM

HEK-293 GI_{50}: 12.51 ± 1.82 µM

MRC-5 GI_{50}: > 50 µM

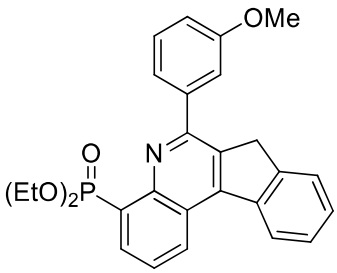

20a

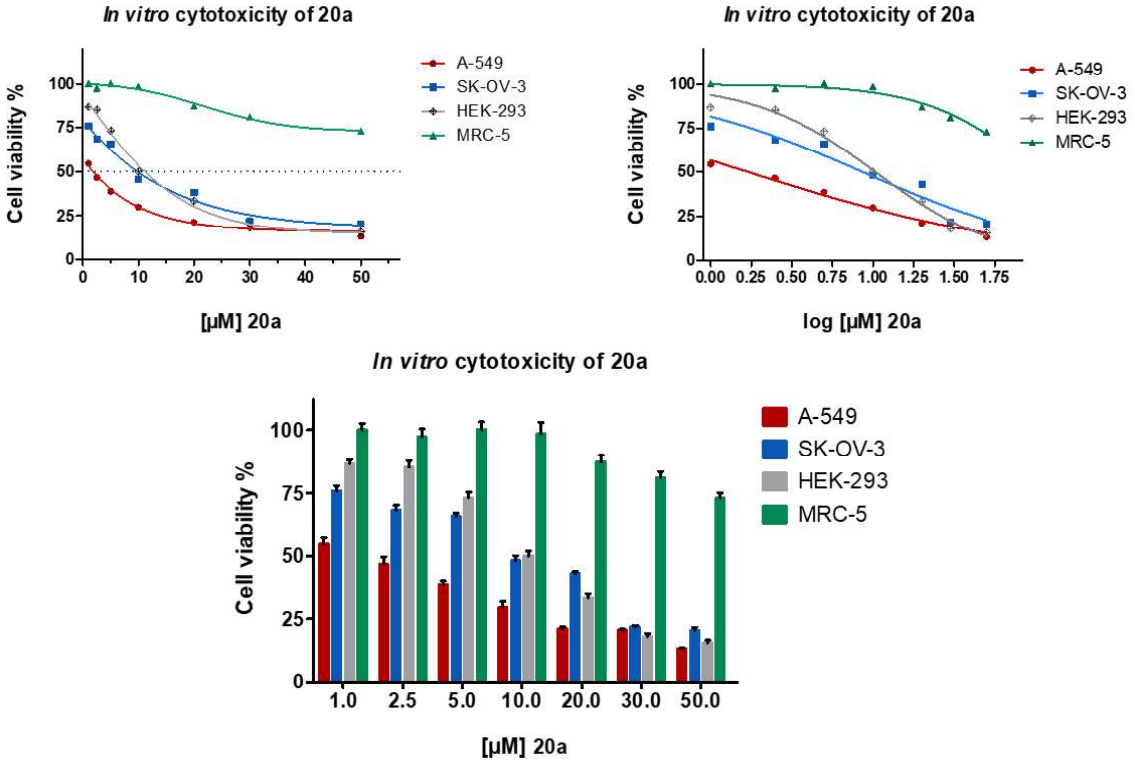

A-549 GI_{50}: 2.91 ± 1.09 μM

SK-OV-3 GI_{50}: 45.53 ± 7.02 μM

HEK-293 GI_{50}: 12.51 ± 1.82 μM

MRC-5 GI_{50}: > 50 μM

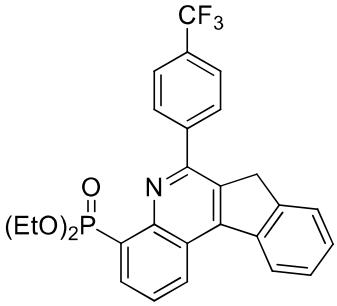

20c

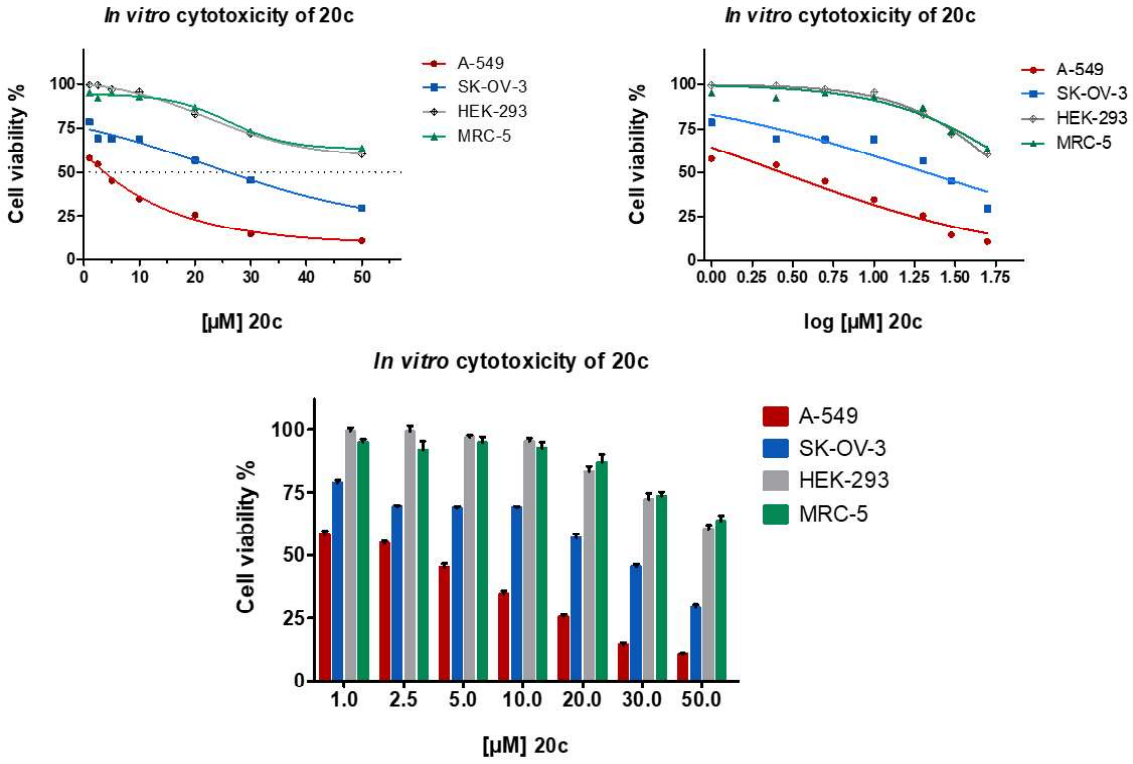

A-549 GI_{50}: 3.14 ± 0.11 µM

SK-OV-3 GI_{50}: 25.70 ± 3.40 µM

HEK-293 GI_{50}: > 50 µM

MRC-5 GI_{50}: > 50 µM

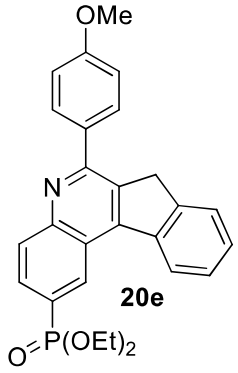

20e

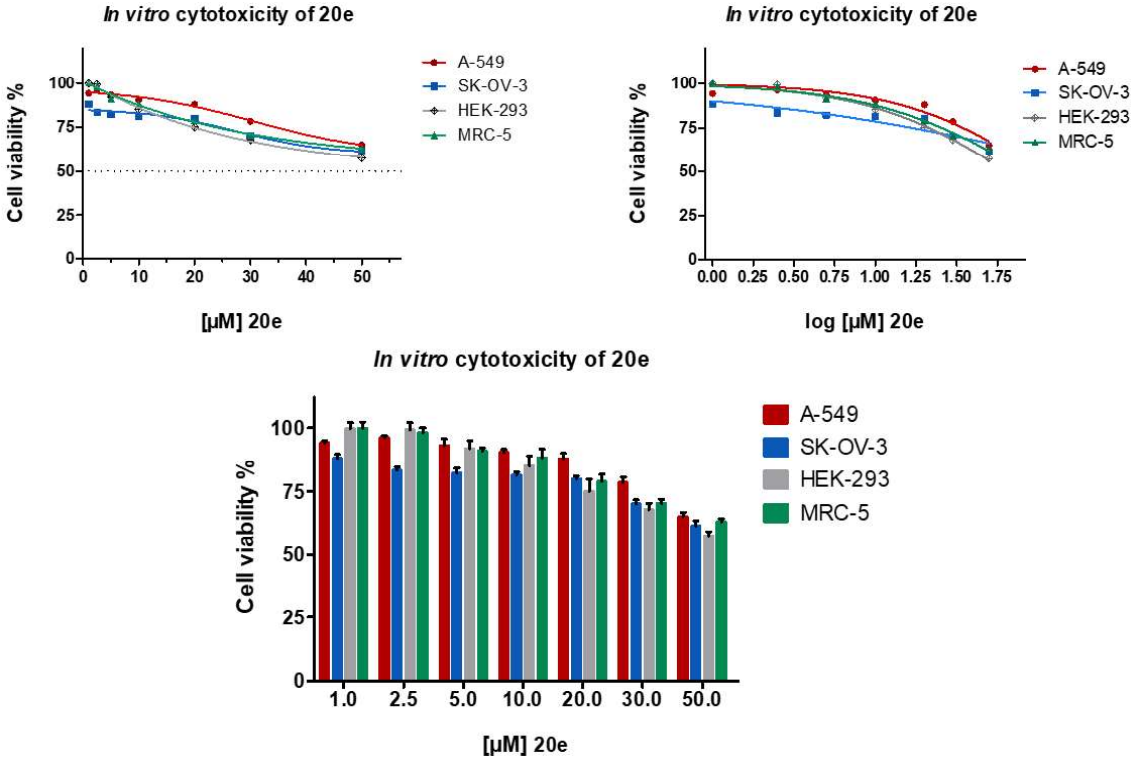

A-549 GI_{50}: > 50 µM

SK-OV-3 GI_{50}: > 50 µM

HEK-293 GI_{50}: > 50 µM

MRC-5 GI_{50}: > 50 µM

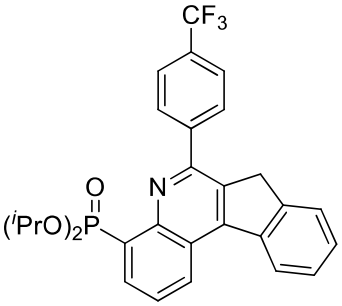

20g

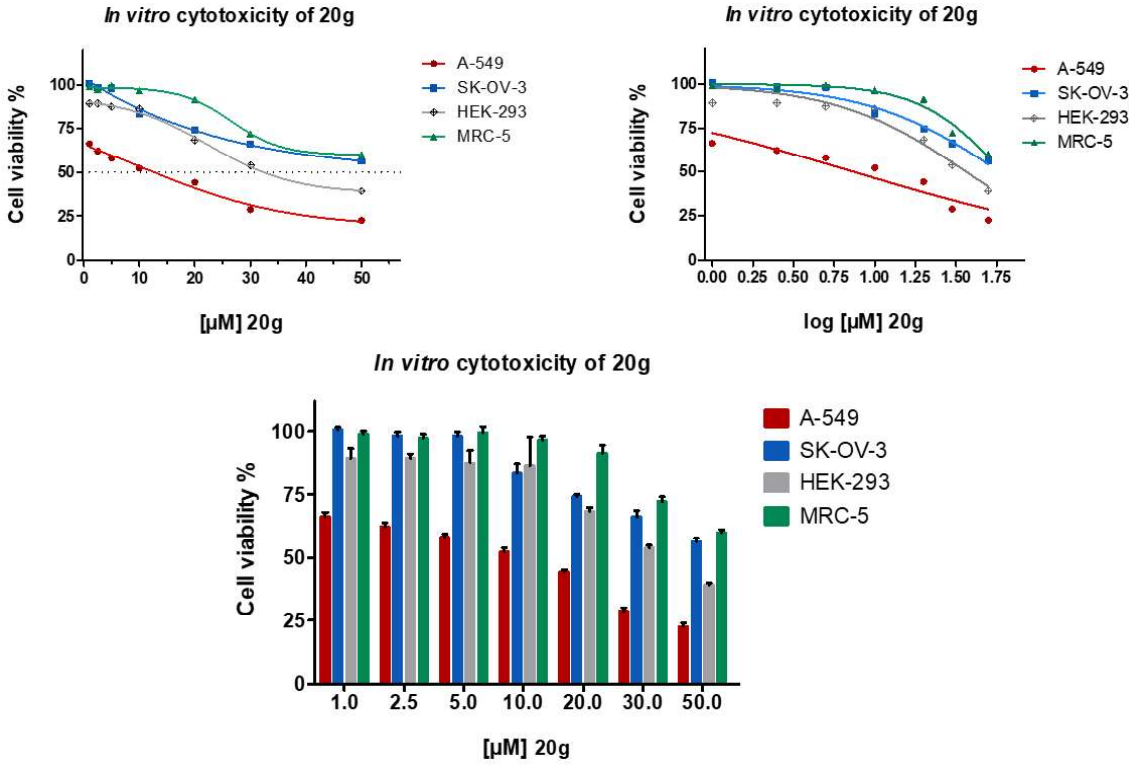

A-549 GI_{50}: 13.50 ± 3.80 µM

SK-OV-3 GI_{50}: > 50 µM

HEK-293 GI_{50}: 31.04 ± 8.73 µM

MRC-5 GI_{50}: > 50 µM

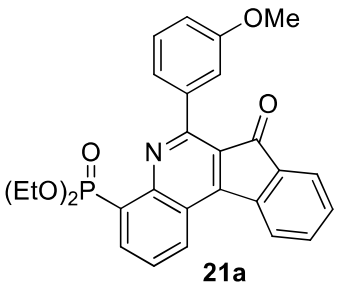

21a

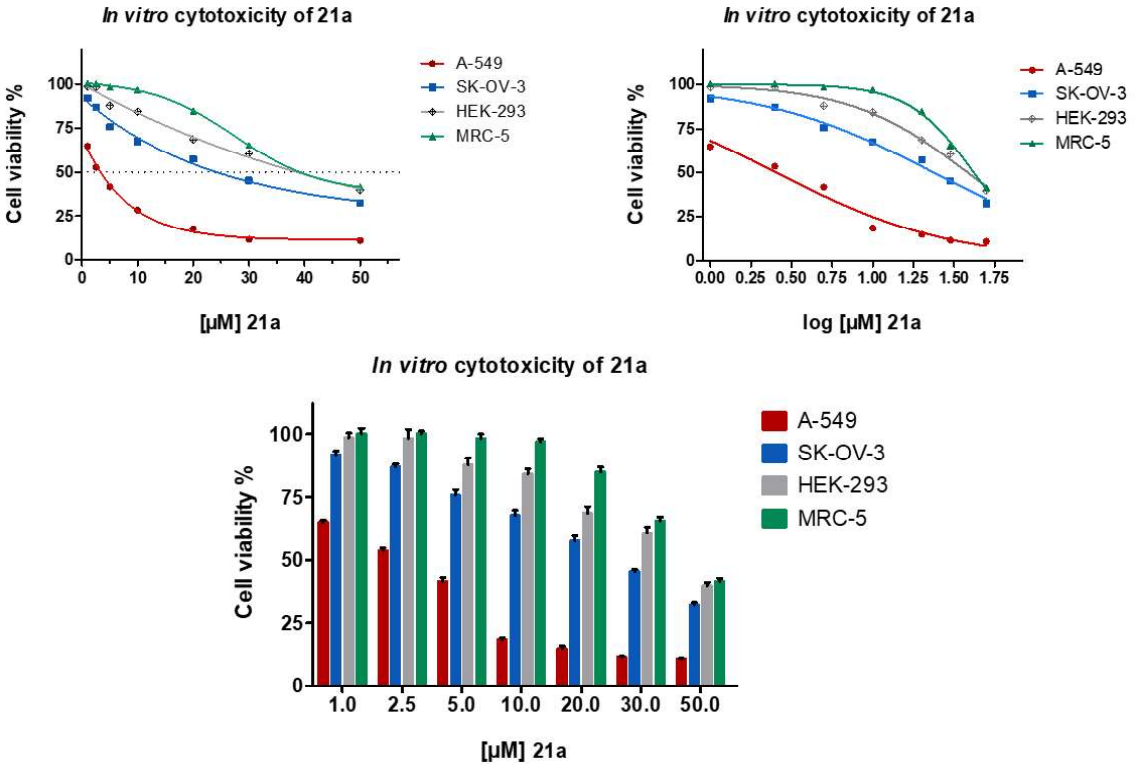

A-549 GI_{50}: 2.58 ± 0.25 μM

SK-OV-3 GI_{50}: 26.82 ± 3.36 μM

HEK-293 GI_{50}: 39.46 ± 5.98 μM

MRC-5 GI_{50}: 39.68 ± 7.37 μM

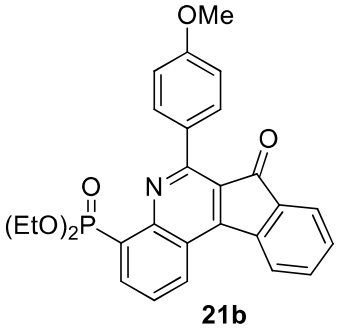

21b

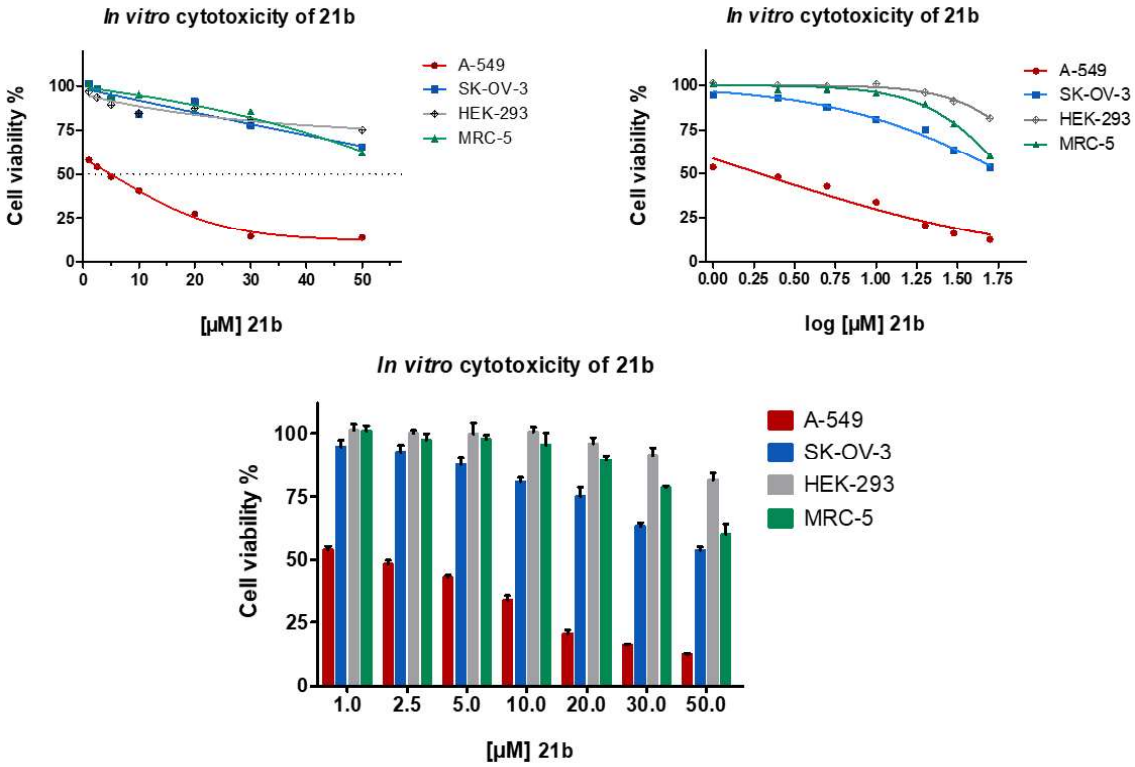

A-549 GI_{50}: 1.51 ± 0.19 µM

SK-OV-3 GI_{50}: > 50 µM

HEK-293 GI_{50}: > 50 µM

MRC-5 GI_{50}: > 50 µM

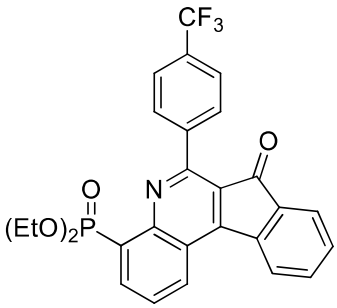

21c

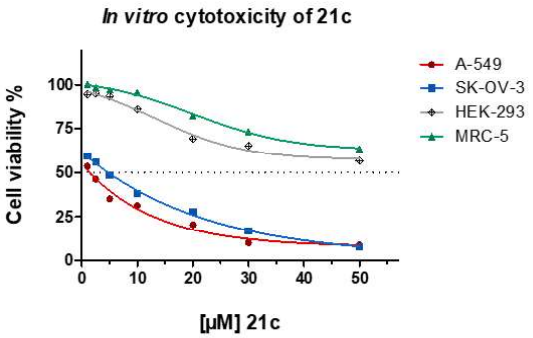

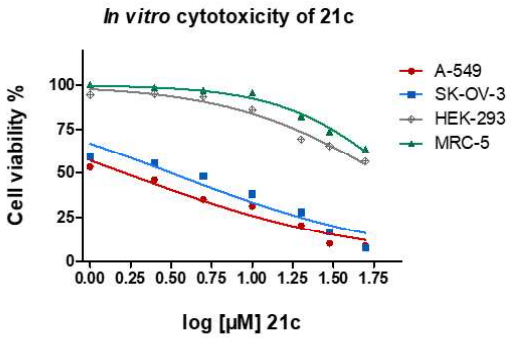

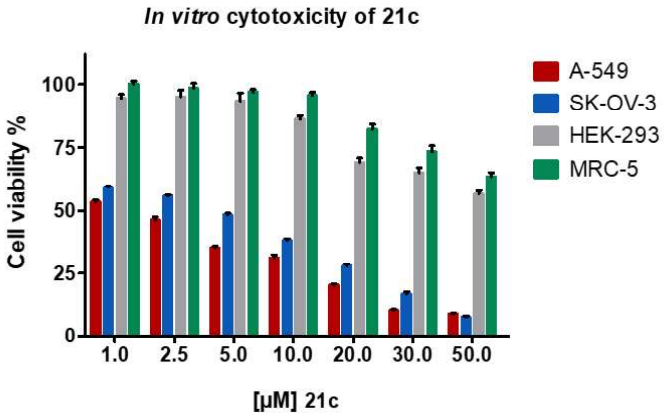

A-549 GI_{50}: 1.53 ± 0.28 µM

SK-OV-3 GI_{50}: 4.55 ± 0.52 µM

HEK-293 GI_{50}: > 50 µM

MRC-5 GI_{50}: > 50 µM

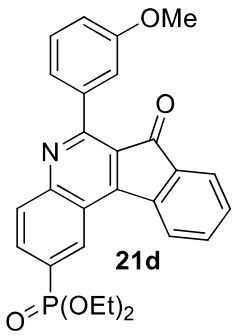

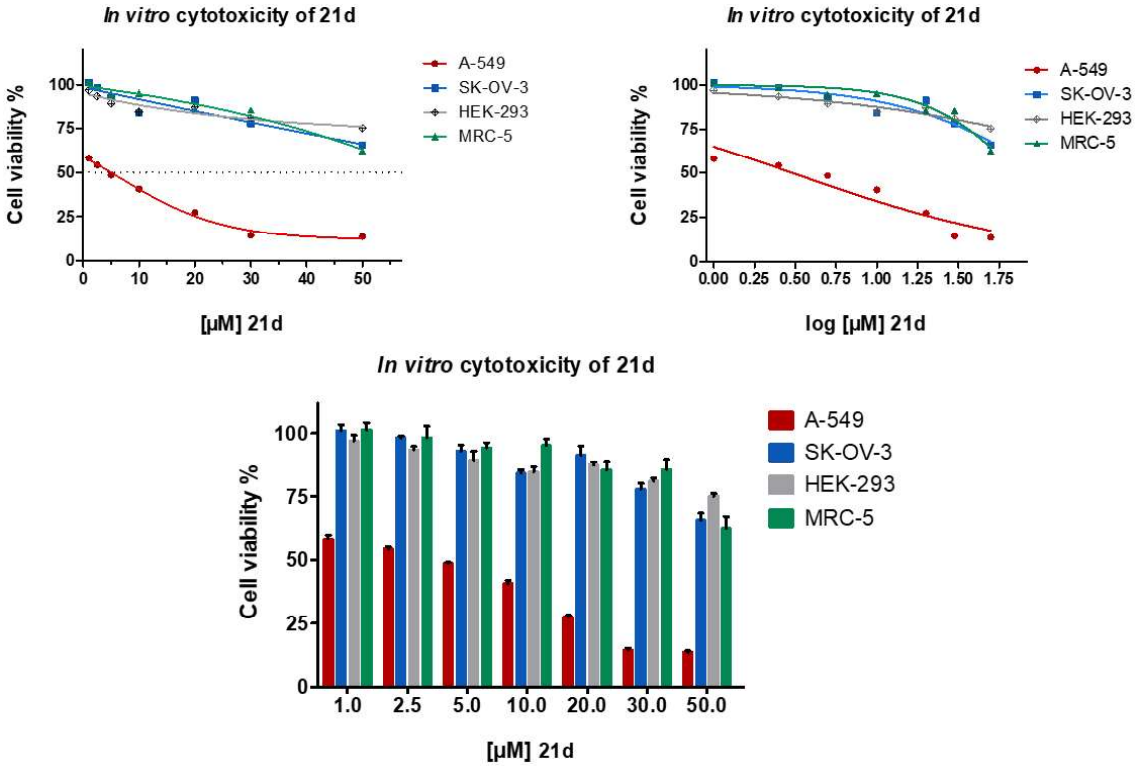

A-549 GI_{50}: 4.41 ± 1.74 µM

SK-OV-3 GI_{50}: > 50 µM

HEK-293 GI_{50}: > 50 µM

MRC-5 GI_{50}: > 50 µM

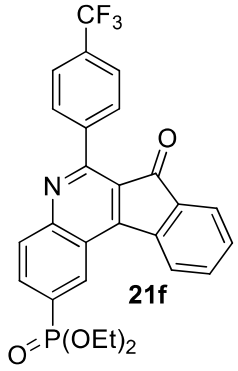

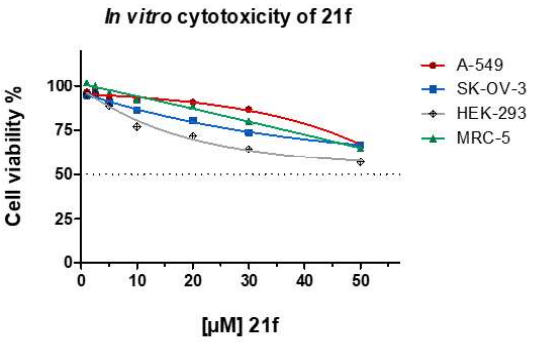

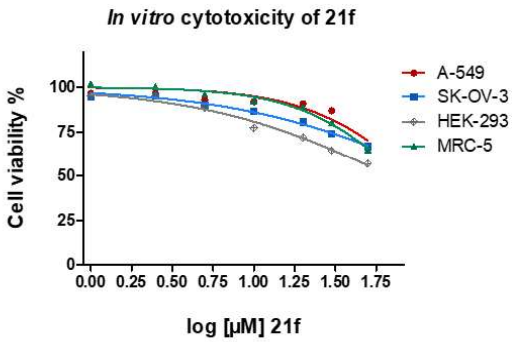

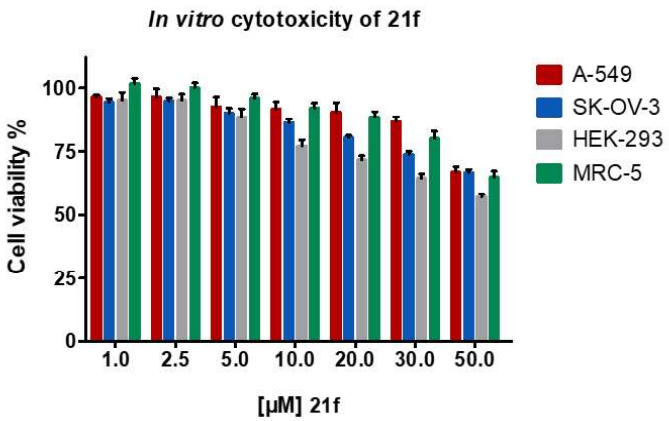

A-549 GI_{50}: > 50 µM

SK-OV-3 GI_{50}: > 50 µM

HEK-293 GI_{50}: > 50 µM

MRC-5 GI_{50}: > 50 µM

VI-3.3. PrestoBlue cell viability assays

The antiproliferative response of the investigated compounds was assessed by using the PrestoBlue cell viability reagent following the supplier´s instructions. 10 mM stock solutions of CPT and the investigated compounds were freshly prepared in 99.9% DMSO and all the derived working dilutions in DMSO were prepared from these stock solutions by serial dilution method. DMSO concentration was corrected to 0.5 % (v/v) in all wells including the controls, and the 0.5 % DMSO-treated cells were considered as 100% viable cells.

A) Cell viability assay with adherent human cell lines (HEK-293 and HEK-293 KD): first 3000 cells/100 µL culture media were seeded into 96-well plates and the cells were incubated under standard mammalian cell-culture conditions (37°C, 5% CO_2, 90% relative humidity). After 24 h of incubation, the old culture media was replaced by fresh medium containing DMSO 0.5% or dilutions of fresh medium with different concentrations of the investigated compounds in 0.5% DMSO (see the cell viability graphs for each concentration-range) and were incubated for another 48 h under standard mammalian cell-culture conditions.

B) Cell viability assay with suspension human cell lines (RPMI-8402 and CPT-K5): first $2 \cdot 10^4$ cells/100 µL culture media (RPMI-8402) or $4 \cdot 10^4$ cells/100 µL culture media (CPT-K5) were plated into 96-well plates with culture medium containing DMSO 0.5% or dilutions of fresh medium with different concentrations of the investigated compounds in 0.5% DMSO (see the cell viability graphs for each concentration-range), and the cells were incubated under standard mammalian cell-culture conditions (37°C, 5% CO_2, 90% relative humidity) for 48 h.

Then (for both **A** and **B** procedures), the Prestoblue reagent was added (10 µL/well) and the plates were incubated in the dark for 15 min before measuring the emitted fluorescence (540 nm excitation/590 nm emission) in an automatic elisa plate reader system (FLUOstar® OPTIMA, BMG Labtech, Ortenberg, Germany). The fluorescence values were processed and plotted using GraphPad Prism 5.01 software to obtain the cell viability graphs and the GI_{50} values (given as the mean ± the SD of the mean from quadruplicate experiments).

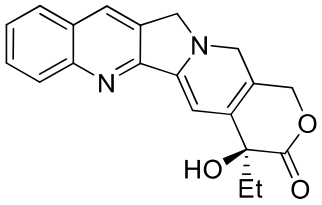

CPT

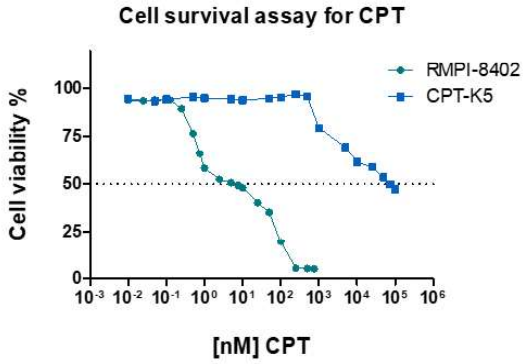

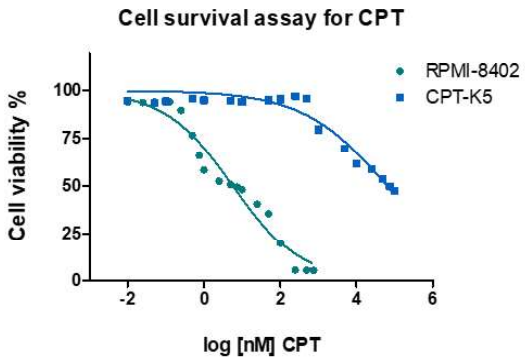

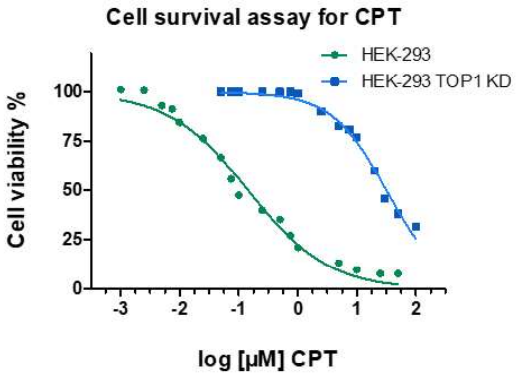

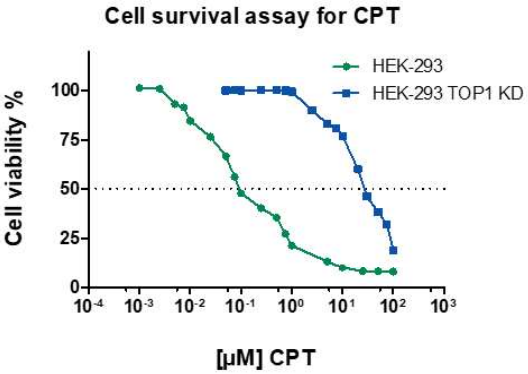

RPMI-8402 GI_{50}: 5.74 ± 0.16 nM

CPT-K5 GI_{50}: 65.67 ± 6.19 µM

HEK-293 GI_{50}: 0.15 ± 0.02 µM

HEK-293 TOP1 KD GI_{50}: 29.49 ± 0.50 µM

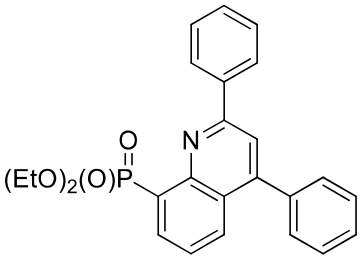

13a

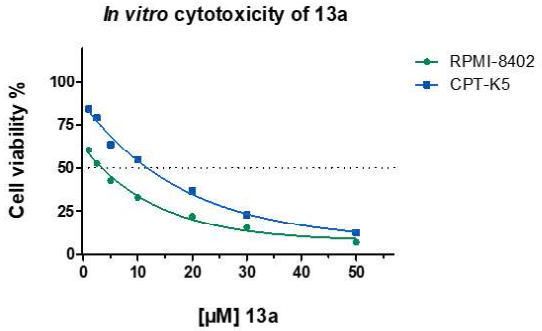

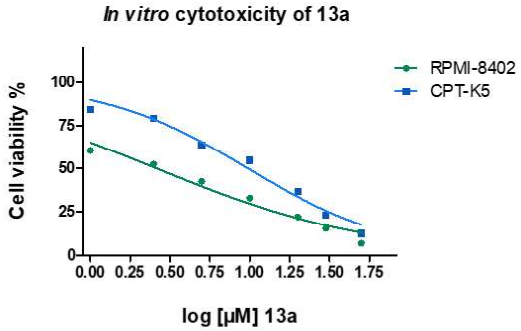

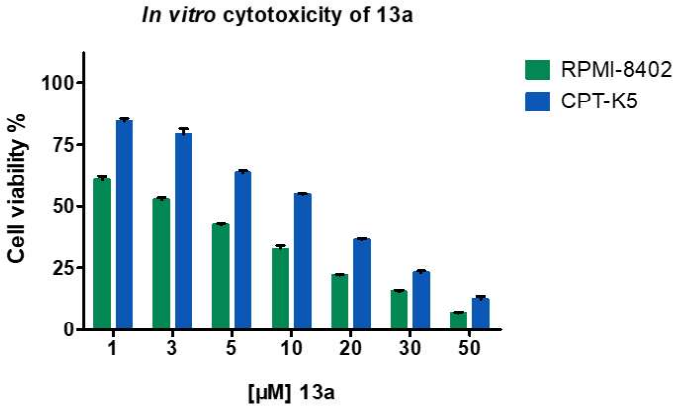

RPMI-8402 GI_{50}: 3.19 ± 0.21 µM

CPT-K5 GI_{50}: 12.27 ± 0.59 µM

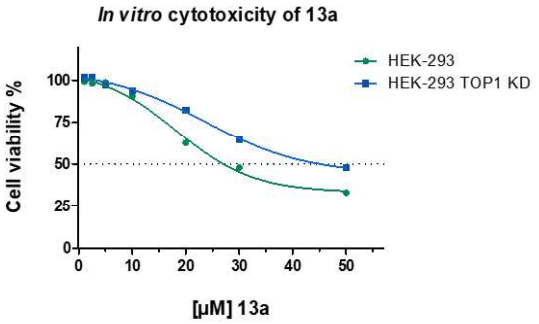

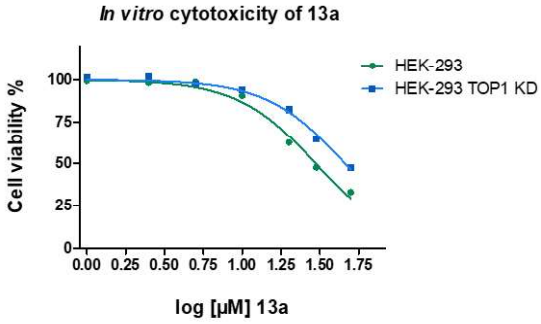

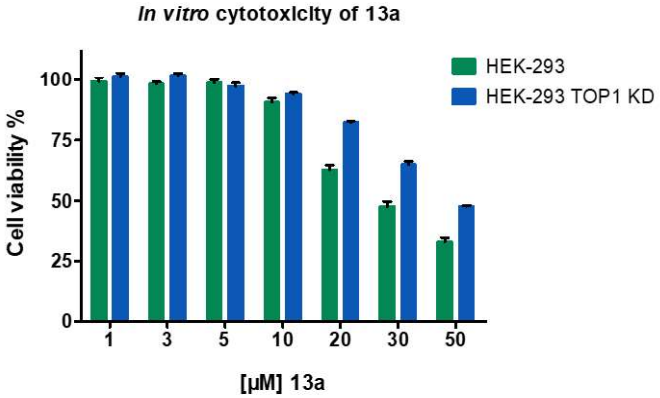

HEK-293 GI_{50}: 27.29 ± 2.22 µM

HEK-293 TOP1 KD GI_{50}: 48.12 ± 1.41 µM

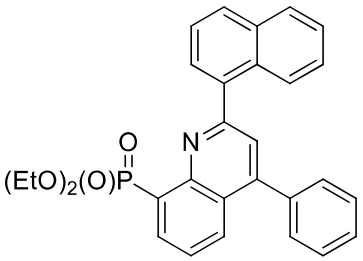

13f

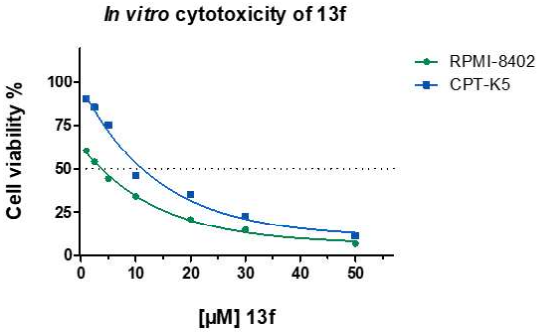

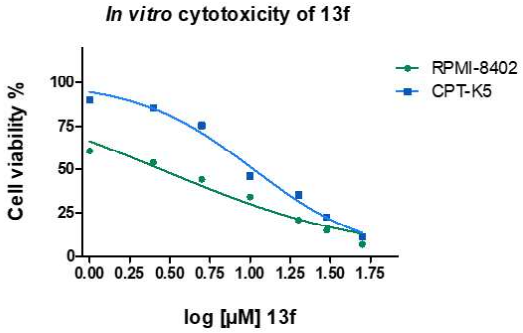

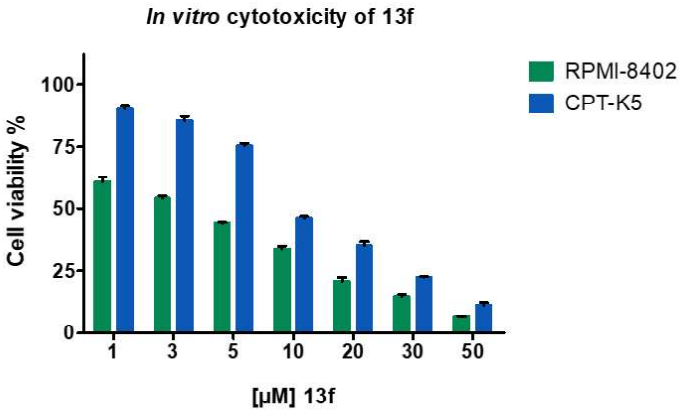

RPMI-8402 GI_{50}: 4.41 ± 0.27 µM

CPT-K5 GI_{50}: 11.83 ± 0.33 µM

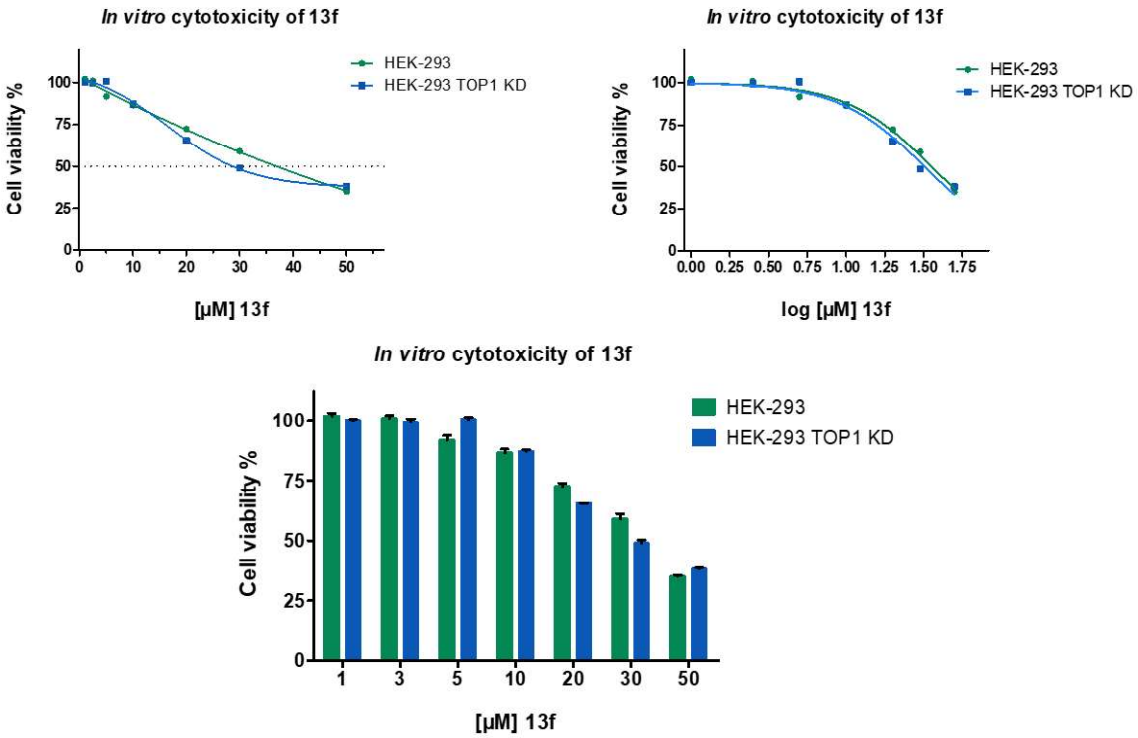

HEK-293 GI_{50}: 35.67 ± 3.13 µM

HEK-293 TOP1 KD GI_{50}: 32.30 ± 1.00 µM

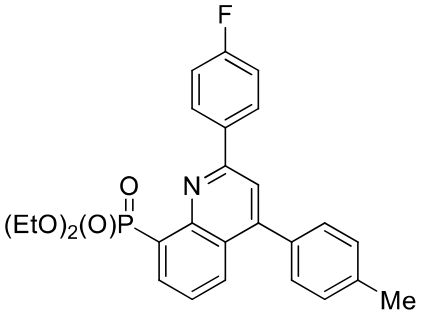

13j

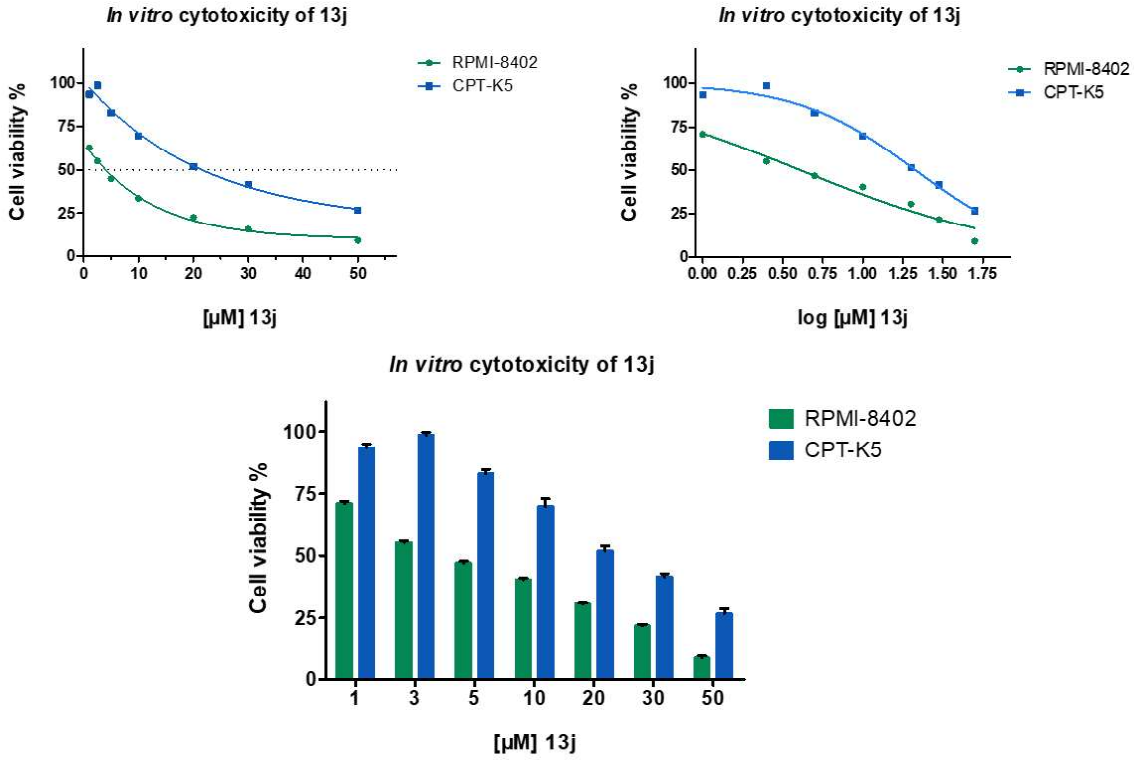

RPMI-8402 GI_{50}: 4.13 ± 0.13 µM

CPT-K5 GI_{50}: 21.58 ± 2.02µM

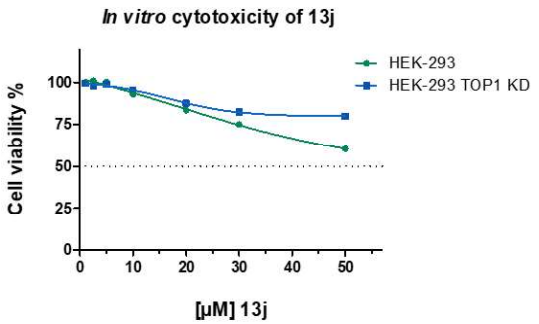

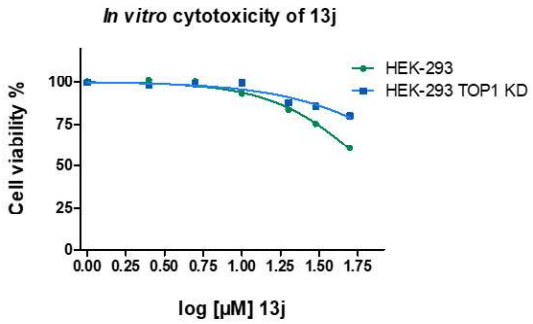

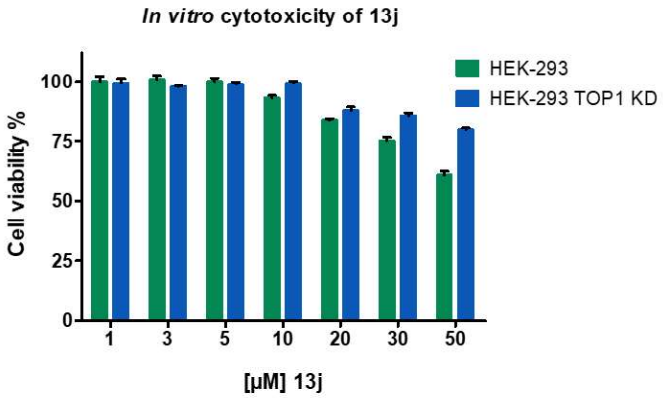

HEK-293 GI_{50}: >50 µM

HEK-293 TOP1 KD GI_{50}: >50 µM

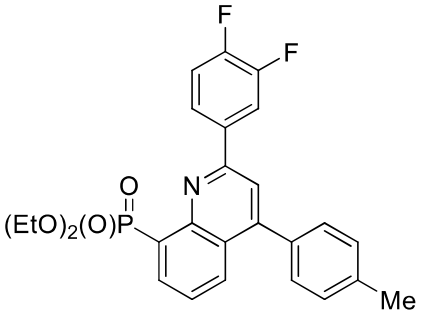

13k

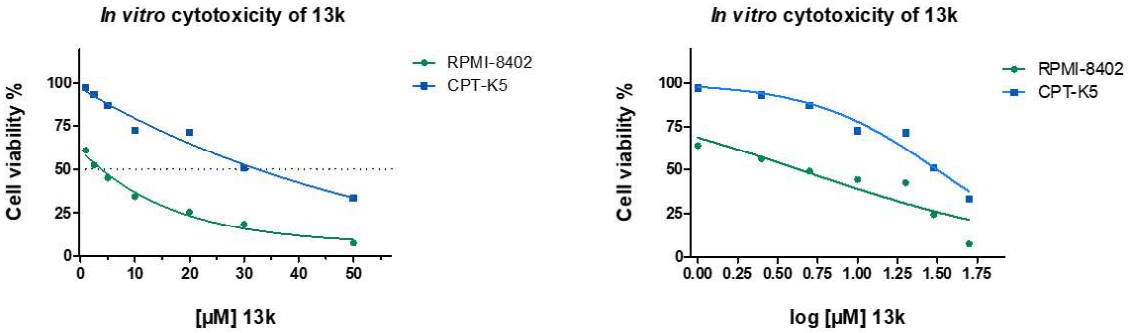

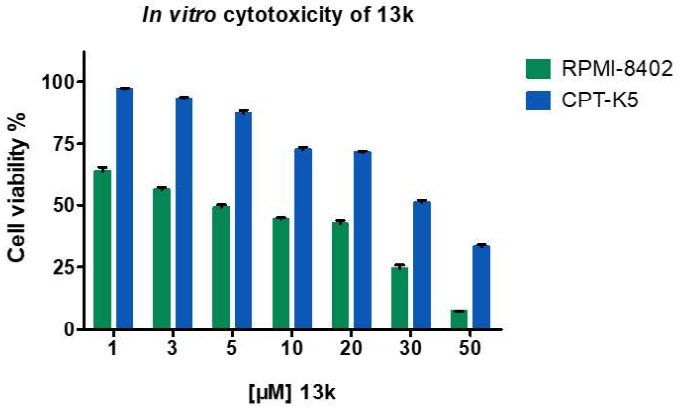

RPMI-8402 GI_{50}: 4.37 ± 0.40 μM

CPT-K5 GI_{50}: 31.53 ± 1.88 μM

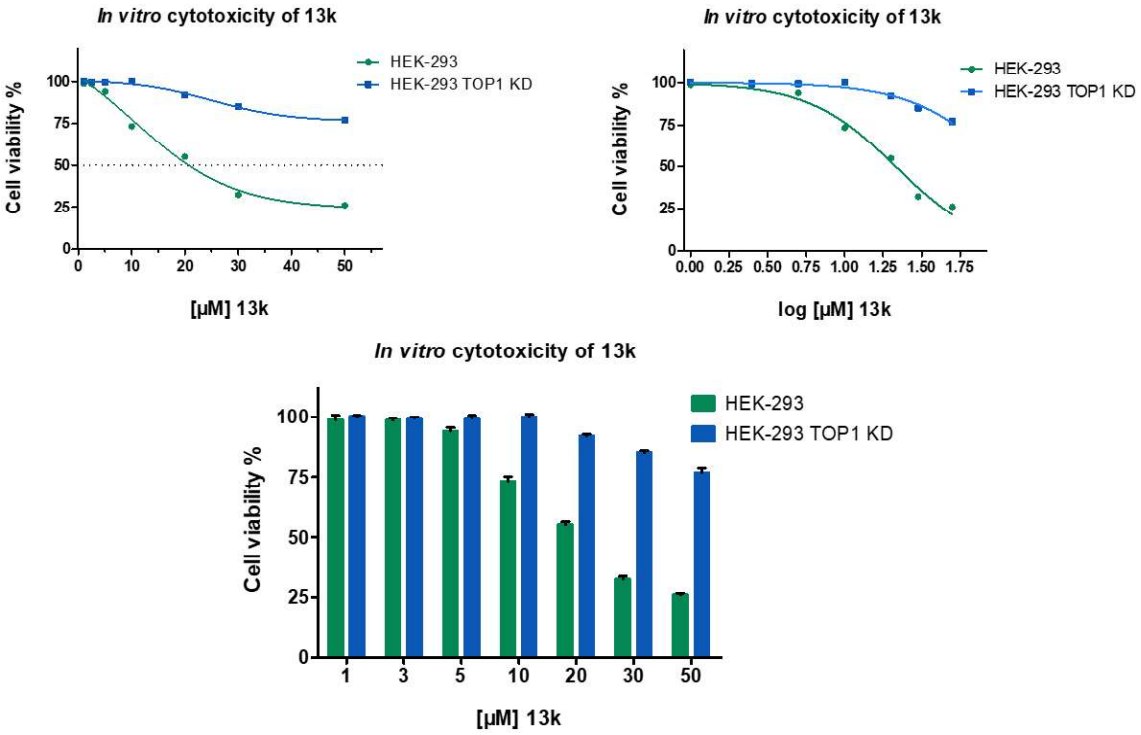

HEK-293 GI_{50}: 22.66 ± 1.36 µM

HEK-293 TOP1 KD GI_{50}: >50 µM

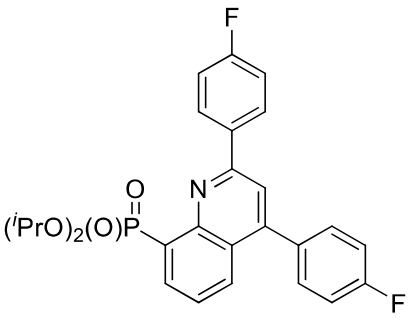

13s

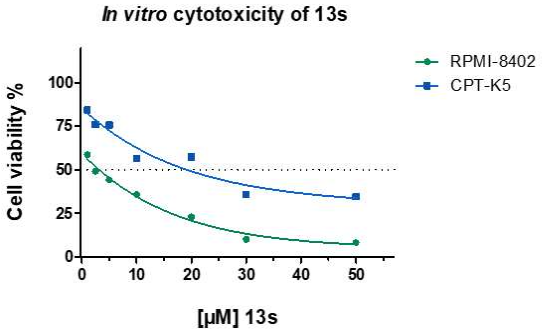

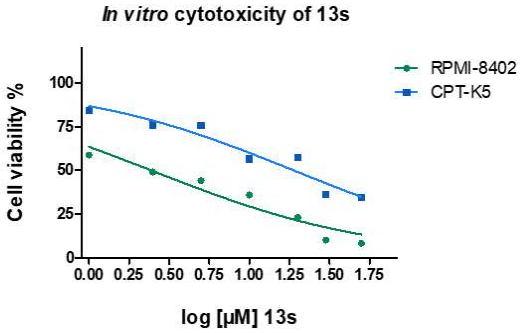

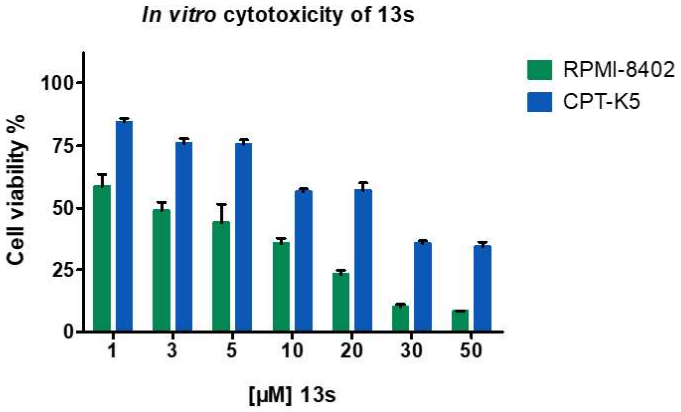

RPMI-8402 GI_{50}: 3.23 ± 0.69 μM

CPT-K5 GI_{50}: 19.19 ± 2.83 μM

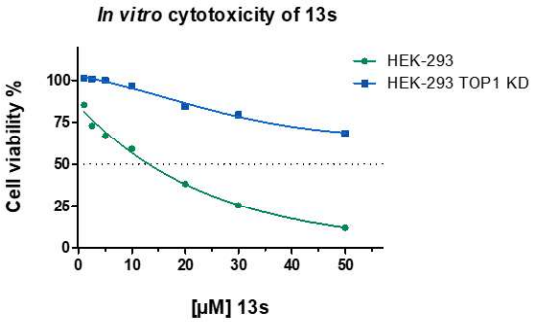

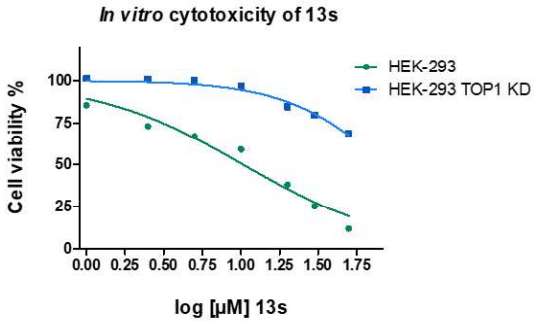

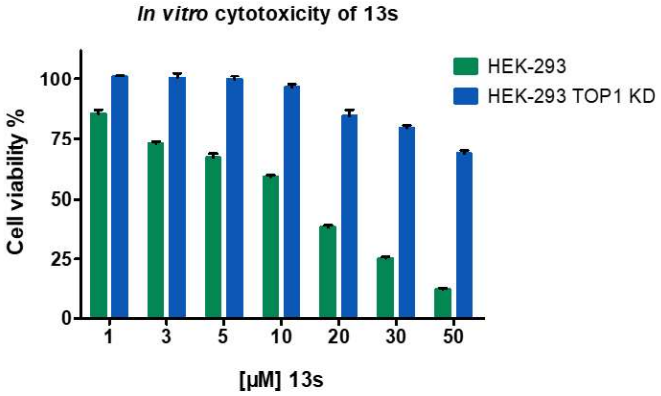

HEK-293 GI_{50}: 15.01 ± 0.99 µM

HEK-293 TOP1 KD GI_{50}: >50 µM

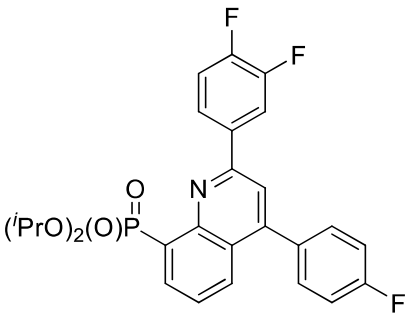

13t

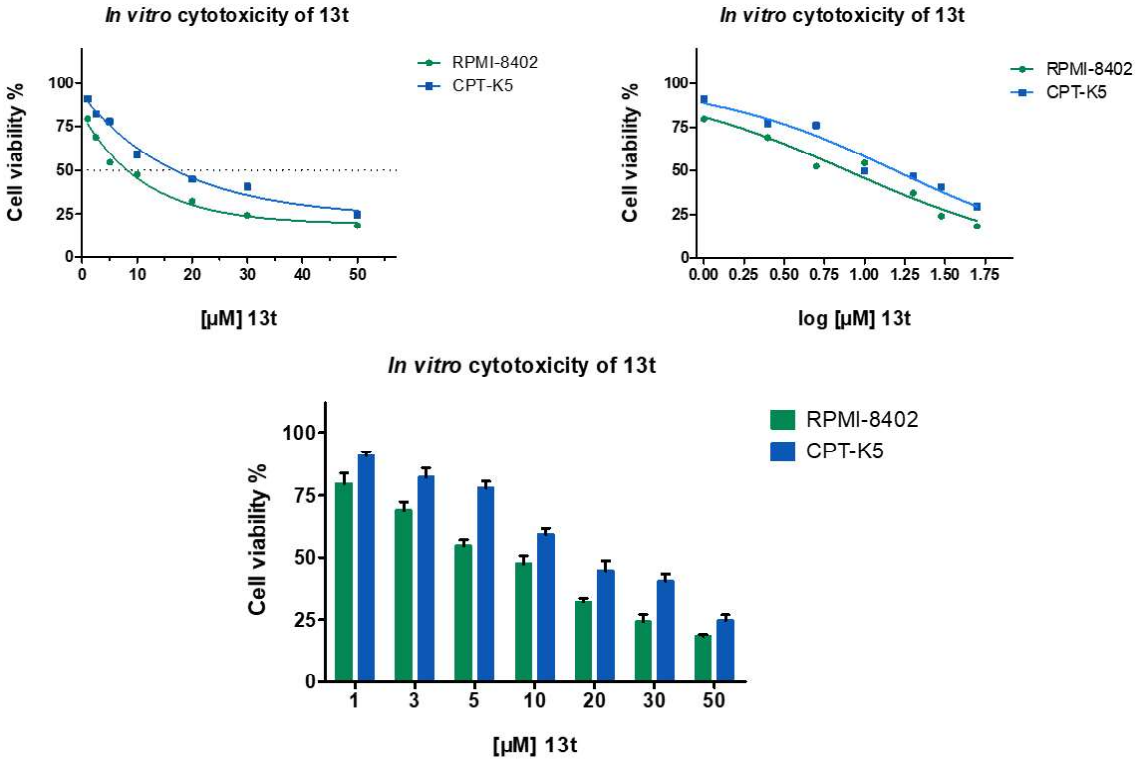

RPMI-8402 GI_{50}: 7.87 ± 0.57 µM

CPT-K5 GI_{50}: 16.85 ± 1.98 µM

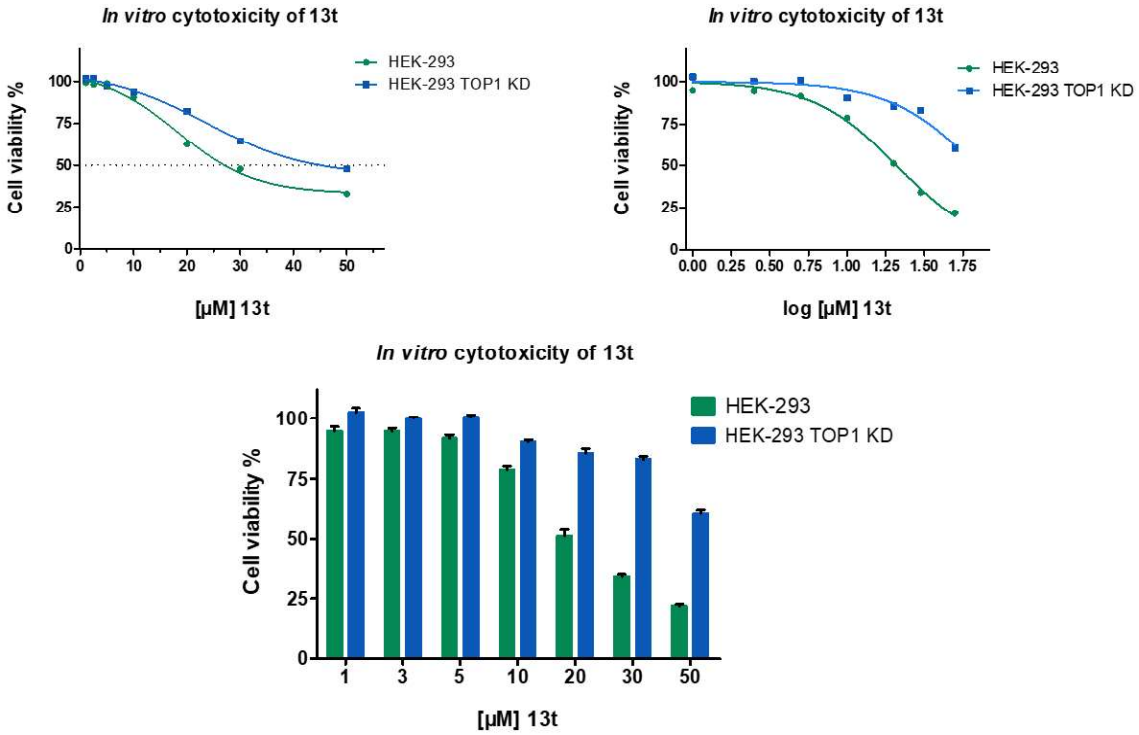

HEK-293 GI_{50}: 21.04 ± 4.05 µM

HEK-293 TOP1 KD GI_{50}: >50 µM

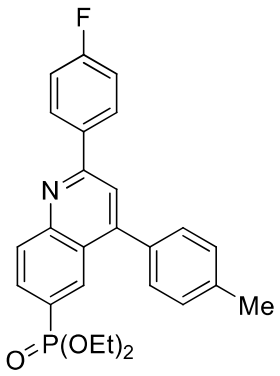

16c

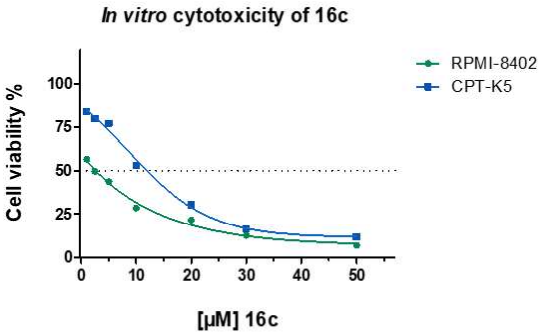

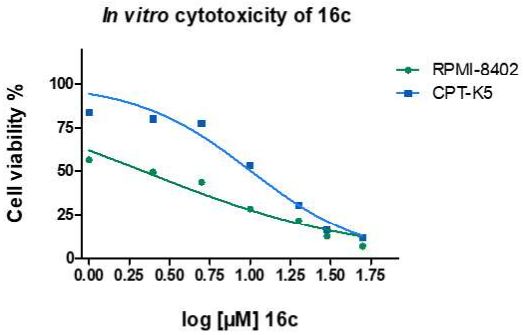

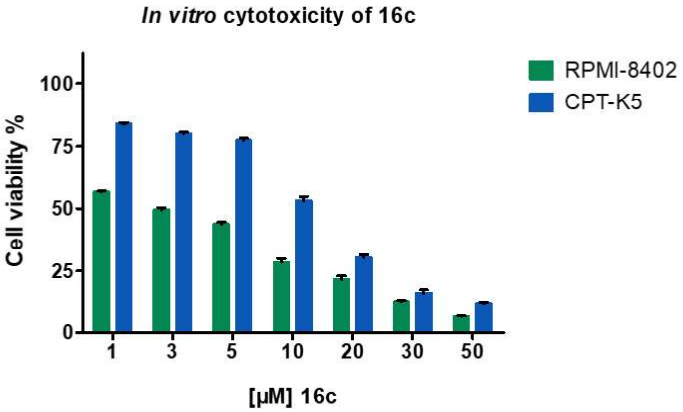

RPMI-8402 GI_{50}: 2.19 ± 0.10 µM

CPT-K5 GI_{50}: 12.11 ± 0.53 µM

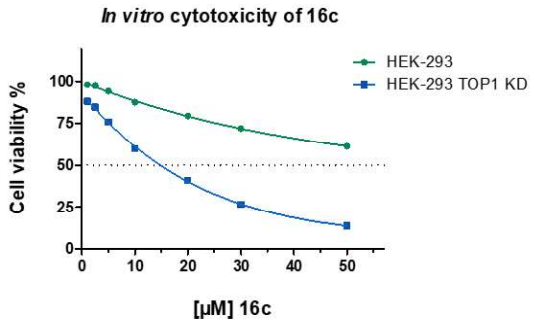

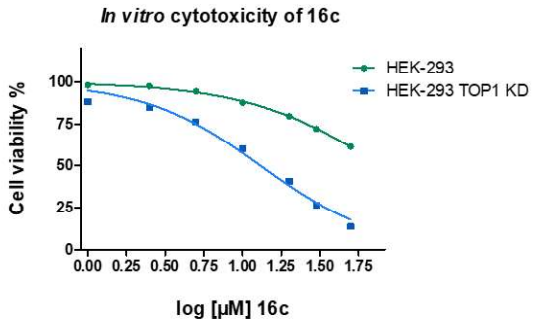

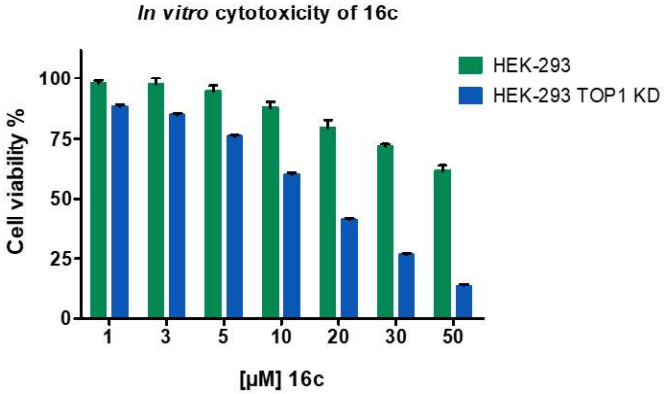

HEK-293 GI_{50}: >50 µM

HEK-293 TOP1 KD GI_{50}: 12.11 ± 0.19 µM

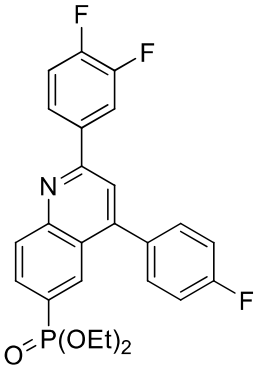

16f

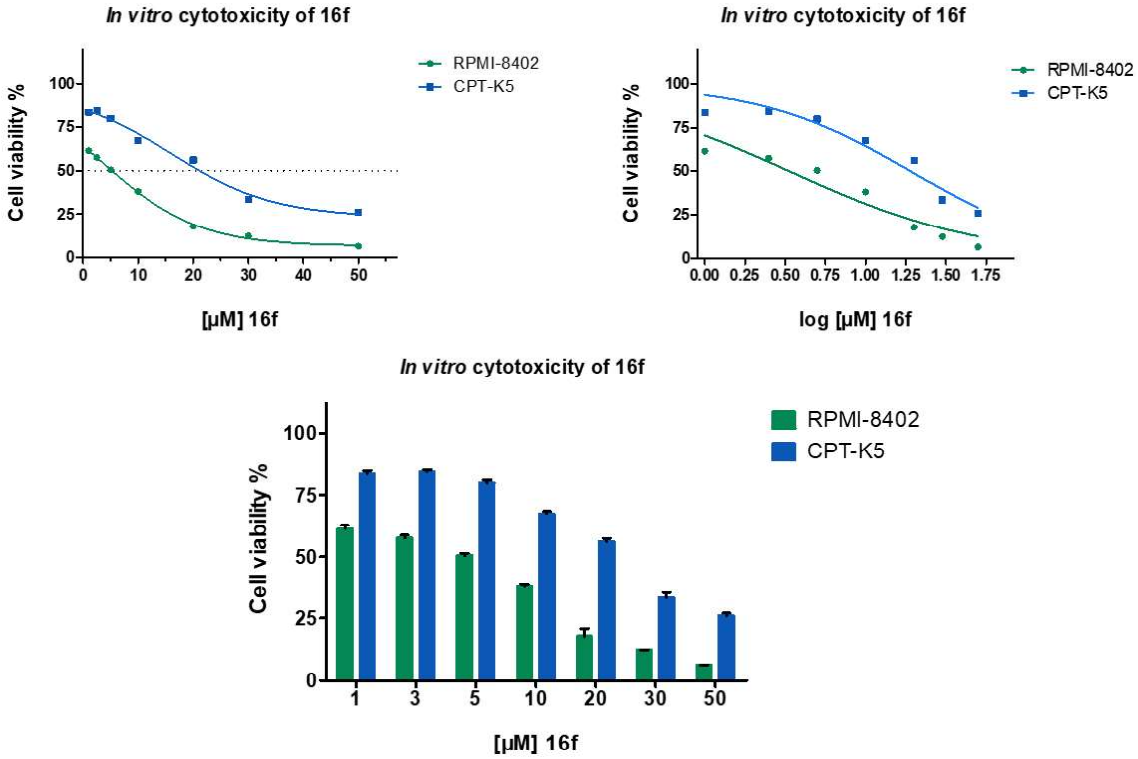

RPMI-8402 GI_{50}: 5.18 ± 0.52 µM

CPT-K5 GI_{50}: 21.18 ± 1.13 µM

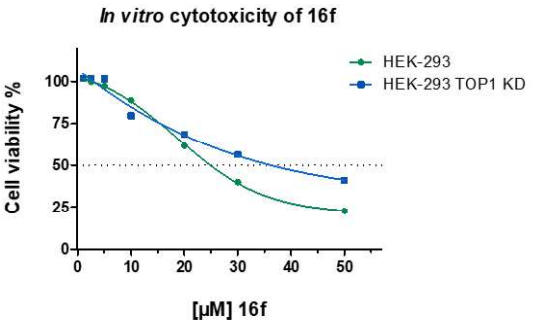

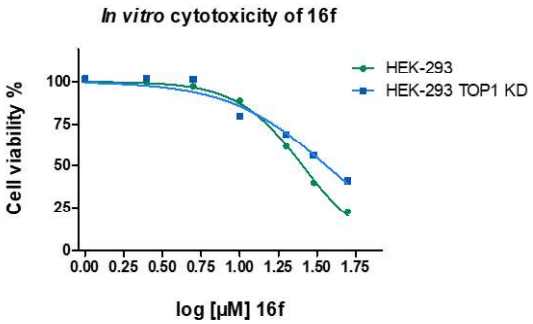

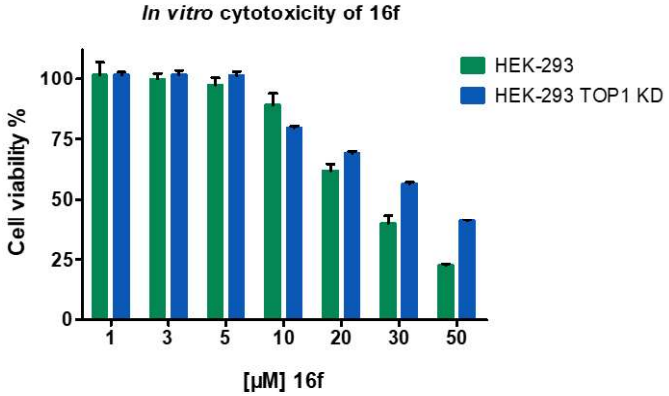

HEK-293 GI_{50}: 25.72 ± 6.34 µM

HEK-293 TOP1 KD GI_{50}: 36.44 ± 1.12 µM

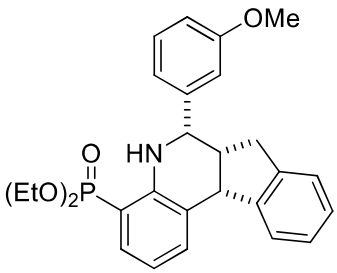

19a

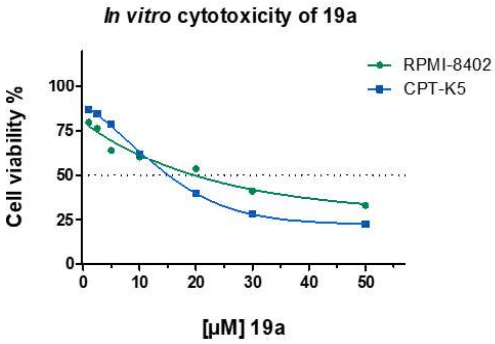

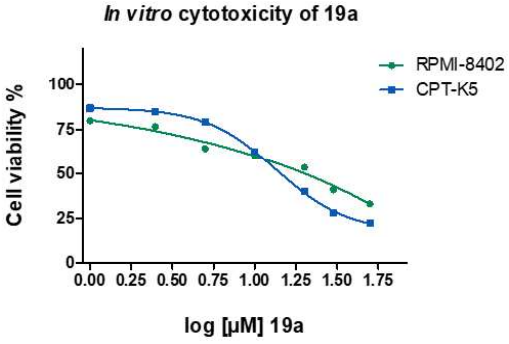

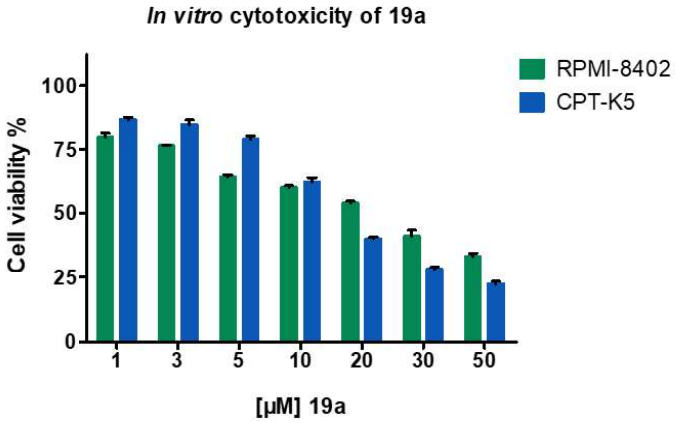

RPMI-8402 GI_{50}: 20.31 ± 1.06 µM

CPT-K5 GI_{50}: 15.13 ± 0.72 µM

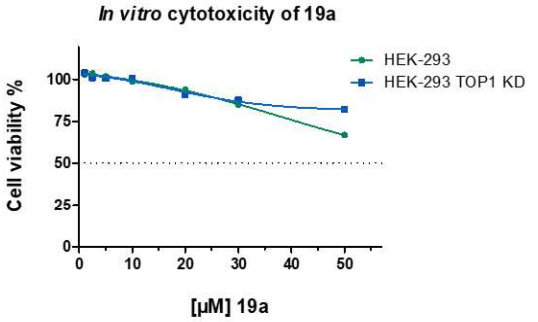

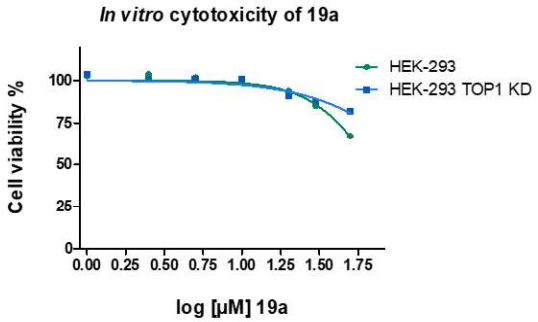

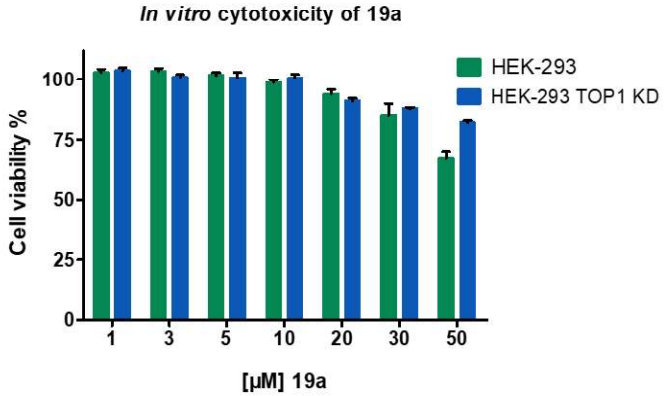

HEK-293 GI_{50}: >50 µM

HEK-293 TOP1 KD GI_{50}: >50 µM

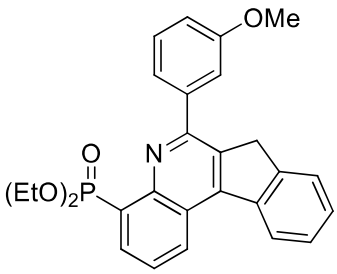

20a

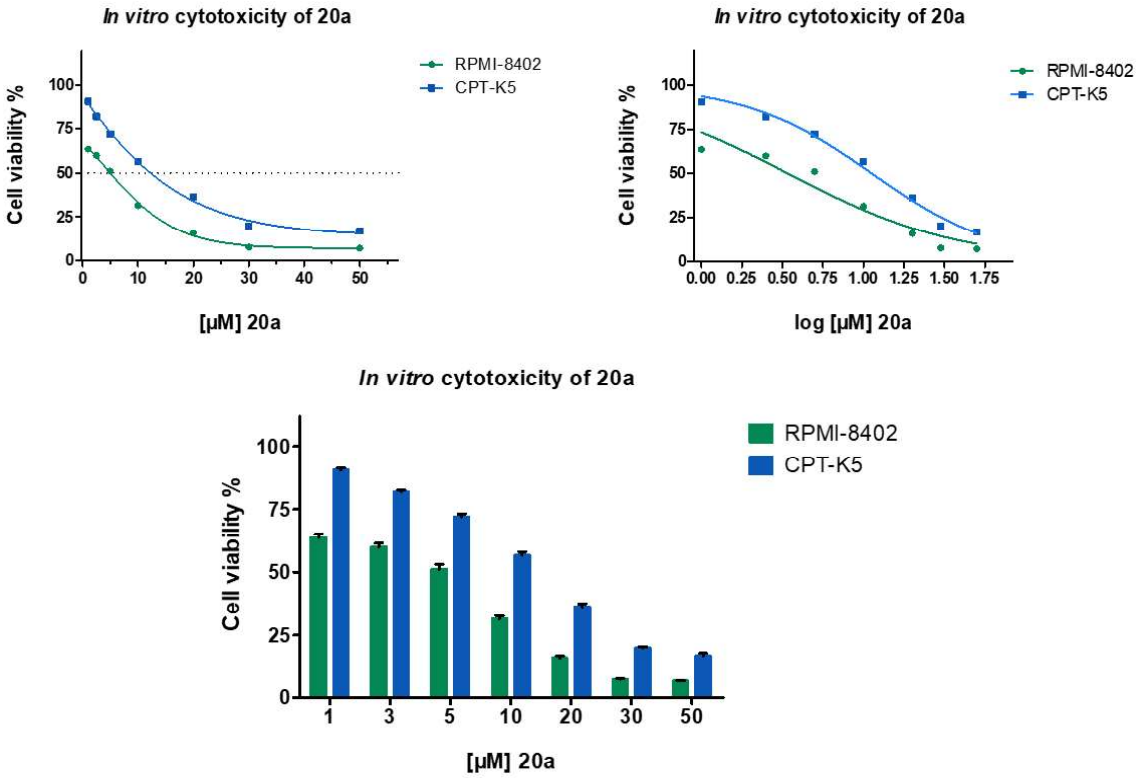

RPMI-8402 GI_{50}: 5.04 ± 0.58 µM

CPT-K5 GI_{50}: 12.07 ± 0.38 µM

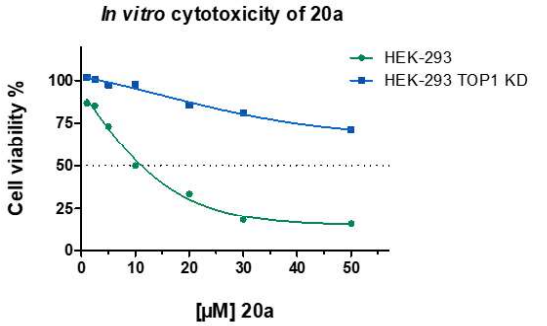

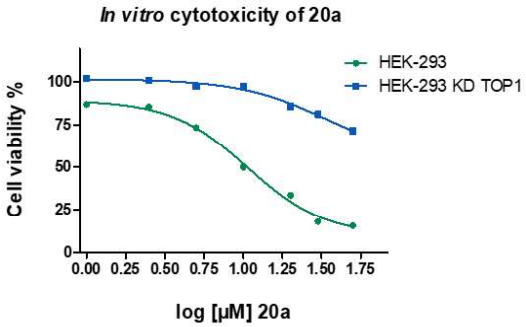

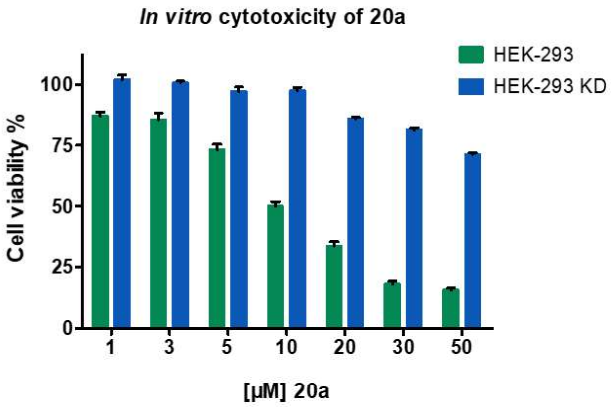

HEK-293 GI_{50}: 11.80 ± 0.97 µM

HEK-293 TOP1 KD GI_{50}: >50 µM

VI-3.4. siRNA mediated TOP1 knockdown in HEK-293 cell line

Cell culture and siRNA transfection of HEK-293: $7.5 \cdot 10^5$ HEK-293 cells were plated into cell-culture dishes in 10 mL DMEM cell-culture medium supplemented with 10% fetal bovine serum without any antimicrobial agent and incubated under standard mammalian cell-culture conditions (37°C, 5% CO_2, 90% relative humidity) for 24 h.

A) TOP1 knockdown: TOP1 down-regulation was induced by transfecting HEK-293 cells with a cocktail of four siRNAs ($siRNA_{TOP1}$) specifically targeting human TOP1 (Hs_TOP1_6 FlexiTube siRNA, Hs_TOP1_7 FlexiTube siRNA, Hs_TOP1_8 FlexiTube siRNA and Hs_TOP1_9 FlexiTube siRNA obtained from Qiagen) according to the lipofectamine transfection method.

B) Scrambled control: scrambled siRNA (AllStars negative control siRNA, #SI03650318, Qiagen) was used to transfect HEK-293 cells according to the lipofectamine transfection method.

C) Mock control: ddH_2O was used instead of any siRNA when following the lipofectamine transfection method.

Lipofectamine transfection method: upon 24 h of incubation, a mixture of 1 mL of OptiMEM (Gibco) and 20 µL of lipofectamine RNAiMAX (Thermo Fischer) mixed with 12 µL of 10 µM siRNATOP1 mix (**A**)/ 10 µM scrambled siRNA (**B**)/ddH_2O (**C**) was incubated at room temperature for 15 min and subsequently added dropwise to the corresponding HEK-293 cell culture by gently stirring the cell-culture dish.

72 h after transfection, cell cultures were harvested by the aforementioned trypsin treatment and a fraction of $1 \cdot 10^6$ cells was saved as cell pellets, which were flash frozen and conserved at -80°C until the forthcoming western blot analysis. The rest of harvested cells were used straightforward in cell viability assays.

VI-3.5. Western blot analysis of HEK-293 cells transfected with $siRNA_{TOP1}$, scrambled siRNA and mock control

Cell extractions: whole cell extractions from TOP1 knockdown/scrambled control/mock control transfected HEK-293 cells were prepared by resuspending a $1 \cdot 10^6$ cell pellet in 100 µL lysis buffer (1 mM Tris-HCl pH 7.5, 0.1 mM EDTA supplemented with PMSF (phenylmethanesulfonyl fluoride), 19 mM NaFl, 1 mM beta glycerophosphate and Roche proteases and phosphatases inhibitors cocktail, EDTA free). The cells were maintained during 10 minutes in the lysis buffer on ice bath and the cells extracts were separated by centrifugation at 9000 × g at 4°C for 10 min.

Western blotting: whole cell extracts prepared from HEK 293 cells (TOP1 knockdown, scrambled and mock) were mixed with SDS loading buffer (250 mM Tris-HCl pH 6.8, 10% SDS, 30% glycerol, 0.02% bromophenol blue) and analyzed by 10% SDS-polyacrylamide gel-electrophoresis ran in 1× SDS running buffer (25 mM Tris, 192 mM glycine, 0.1% SDS) at 200 V for 1.5 h. Proteins were transferred onto a nitrocellulose membrane (Cytiva´s Whatman™ 0.34 mm CHR #3030-917) in 1 × Tris-SDS transfer buffer (25 mM Tris, 192 mM glycine, 0.1% SDS) at 100 V, 4 ◦C for 1 h and 10 min. The membrane was blocked in 5% milk in 1x TBST (20 mM Tris-HCl, 0.5 M NaCl, 0.0225% Tween20) for 1 h at room temperature followed by incubation with 1:3000 rabbit anti-hTOP1 primary antibody (Bethyl, #A302-590A), or 1:2000 mouse anti-TBP primary antibody (Abcam, ab818) diluted in 5% milk in 1xTBST buffer for 1 h at room temperature. Then, the membrane was washed in 5% milk and incubated with 1:2000 polyclonal goat anti-Rabbit Ig/HRP secondary antibody (Dako, #P0448) or polyclonal goat anti-mouse Ig/HRP secondary antibody (Dako, #P0447) diluted in 5% milk in 1xTBST buffer for 1 h at room temperature. The membrane was developed by adding the western blot detection mixture (ECL western blotting detection reagents, Cytiva, #RPN2236) and the signals were subsequently visualized with a CCD (charge-coupled devide) camera (Amersham Imager 600).